

LOW-TEMPERATURE THERMOCHRONOLOGY OF THE NORTHERN CARLIN
TREND: EVIDENCE FOR LATE CRETACEOUS EXHUMATION OF NORTHERN
CENTRAL NEVADA AND SHORT DURATION OF CARLIN ORE-FORMING
HYDROTHERMAL SYSTEMS

by

Moira Cruickshanks

MSci, Imperial College London, 2008

A THESIS SUBMITTED IN PARTIAL FULFILLMENT OF
THE REQUIREMENTS FOR THE DEGREE OF

MASTER OF SCIENCE

in

THE FACULTY OF GRADUATE STUDIES

(Geological Sciences)

THE UNIVERSITY OF BRITISH COLUMBIA

(Vancouver)

September 2012

© Moira Cruickshanks, 2012

Abstract

Samples were collected from Jurassic intrusions in the northern Carlin Trend to determine the thermal history of the region that was strongly affected by Late Cretaceous exhumation and Eocene hydrothermal fluid flow. Low-temperature apatite fission track and apatite and zircon (U-Th)/He thermochronology of the northern Carlin Trend records 3-4 km exhumation since the Late Jurassic. At least 1-2 km exhumation occurred during a phase of rapid exhumation between 85-60 Ma that is coincident with extensional collapse of the overthickened hinterland of the Sevier orogeny. Late Cretaceous exhumation ages provide a background against which ~40 Ma thermal anomalies associated with the formation of the Carlin-type Au deposits can be observed. In the northern Carlin Trend, a thermal halo defined by apatite fission track resetting was observed up to 400 m out from major fluid flow conduits around the Goldstrike Stock that is immediately south of the multi-million ounce Betze-Post deposit. A lack of hydrothermal alteration within the stock shows that Eocene hydrothermal fluid flow was concentrated around its edge, and that heating of the stock was predominantly conductive. Finite element modelling and forward modelling of time-temperature paths constrain the duration of a hydrothermal fluid event to on order of 10 kyr. Multiple phases of this duration of fluid flow are possible, but were either thermally isolated or were shorter-lived. The high rates of fluid flux associated with short fluid flow durations are similar to those observed in hydrothermal systems driven by forced convection or pressure-driven flow, suggesting fluid flow responsible for the formation of Carlin-type Au deposits was driven by a magmatic source or seismicity rather than free convection.

Table of Contents

Abstract	ii
Table of Contents	iii
List of Tables.....	ix
List of Figures	x
Acknowledgements.....	xiv
Chapter 1: Introduction	1
1.1 Thesis goals and fundamental concepts.....	1
1.1.1 Background exhumation study	4
1.1.2 Thermal mapping.....	5
1.1.3 Apatite as a chemical indicator of hydrothermal fluid flow	6
1.2 Thesis structure	6
Chapter 2: Geological background to Carlin-type Au deposits.....	10
2.1 Introduction.....	10
2.2 Geological setting of the northern Carlin Trend.....	10
2.2.1 Stratigraphy of the northern Carlin Trend	10
2.2.2 Igneous geology.....	11
2.2.3 Structure.....	12
2.2.4 Geological history.....	13
2.3 Carlin-type mineralization in the northern Carlin Trend	16
2.4 Alteration in the northern Carlin Trend	17
2.5 Characteristics and source of mineralizing fluids.....	18
2.6 Ore deposit formation models	19

Chapter 3: Thermochronology overview	24
3.1 Principles of low-temperature thermochronology	24
3.2 Apatite fission track dating	26
3.2.1 Annealing.....	27
3.2.2 Fission track length distribution	28
3.2.3 AFT age calculation.....	29
3.2.3.1 EDM and single grain age calculation.....	29
3.2.3.2 LA-ICP-MS and single grain age calculation.....	30
3.2.3.3 Sample AFT ages	31
3.3 (U-Th)/He dating	32
3.3.1 Diffusion behaviour of helium	33
3.3.2 Crystal size and shape.....	33
3.3.3 Alpha-ejection corrections.....	34
3.3.4 Zoning.....	36
3.3.5 Radiation damage	37
Chapter 4: Late Cretaceous exhumation of northern central Nevada: evidence from low-temperature apatite and zircon (U-Th)/He and apatite fission track thermochronology	50
4.1 Introduction.....	50
4.1.1 Tectonic setting of northern central Nevada.....	52
4.1.1.1 Cretaceous contraction and synconvergent extension	52
4.1.1.2 Cenozoic extension.....	53
4.1.2 Metallogeny of northern central Nevada	55
4.1.3 Local geology of the northern Carlin Trend	56

4.2	Previous thermochronology of the northern Carlin Trend	58
4.3	Methods	59
4.3.1	Sampling	59
4.3.2	(U-Th)/He dating	61
4.3.3	Apatite Fission Track (AFT) dating	62
4.3.4	HeFTy modelling.....	64
4.4	Results	67
4.4.1	Apatite and zircon yields	67
4.4.2	Apatite fission track results	67
4.4.2.1	Apatite fission track data analysis	67
4.4.2.2	Apatite fission track ages.....	68
4.4.2.3	Apatite fission track lengths and length distribution	69
4.4.3	(U-Th)/He results.....	71
4.4.3.1	Intrasample variation	71
4.4.3.2	Zircon (U-Th)/He ages	72
4.4.3.3	Apatite (U-Th)/He ages	73
4.4.4	Zircon fission track data	74
4.4.5	HeFTy inverse modelling	74
4.5	Interpretation.....	76
4.5.1	Assumptions	76
4.5.2	Time-temperature-depth histories.....	78
4.5.2.1	Little Boulder Basin Stock	78
4.5.2.2	Vivian Sill.....	82
4.5.2.3	Goldstrike Stock	82

4.5.2.4	Central Tuscarora regional samples	86
4.5.3	Interpreted timing and motion on the Post Fault	87
4.5.4	Interpreted exhumation of the northern Carlin Trend.....	90
4.6	Discussion.....	91
4.6.1	Timing of exhumation	91
4.6.2	Accommodation of eroded material from the northern Carlin Trend.....	94
4.6.3	Motion on the Post Fault	95
4.6.4	Implications for the formation of Carlin-type Au deposits	96
4.7	Conclusions	97
Chapter 5: Thermal halos around Carlin-type Au deposits		125
5.1	Introduction.....	125
5.1.1	Low-temperature thermochronology	126
5.1.2	Carlin-type deposits in the northern Carlin Trend.....	128
5.2	Previous thermochronology studies.....	129
5.3	Methods	131
5.3.1	Sample collection and rock descriptions	131
5.3.2	U-Pb dating.....	132
5.3.3	AFT and (U-Th)/He thermochronology methods.....	133
5.3.4	HeFTy modelling.....	134
5.4	Results	135
5.4.1	Characterisation of alteration.....	135
5.4.2	Thermochronology	138
5.4.3	HeFTy modelling.....	140
5.5	Interpretation of thermochronology data	141

5.5.1	Temporal and spatial patterns in thermochronology data.....	141
5.5.2	Thermochronological constraints on the duration of fluid flow	142
5.5.2.1	Constraints from altered samples - advection-dominated heating.....	143
5.5.2.2	Constraints from unaltered samples - conductive heating.....	144
5.6	Heat flow modelling	145
5.6.1	Numerical modelling of heat flow across the Goldstrike Stock.....	146
5.7	Interpreted duration of hydrothermal fluid flow responsible for formation of Au-deposits in the northern Carlin Trend	149
5.8	Interpreted hydrothermal fluid flux in the northern Carlin Trend	150
5.9	Limitations of the heat flow model.....	152
5.10	Discussion.....	153
5.10.1	Implications for ore deposit formation	156
5.10.2	Potential of low-temperature thermochronology for exploration.....	157
5.11	Conclusions	157
Chapter 6: Compositional and morphological variation in apatite from the northern Carlin Trend, Nevada: an investigation of the effects of hydrothermal fluid flow on apatite.....		182
6.1	Introduction.....	182
6.2	Sample descriptions	183
6.3	Analytical methods	184
6.4	Apatite fission track (AFT) data	186
6.5	Results	186
6.5.1	Major elements	186
6.5.2	Trace elements	187

6.5.3	Morphology and texture	189
6.6	Interpretation and discussion	191
6.6.1	Compositional variation, substitutions	191
6.6.2	Eu anomalies.....	195
6.6.3	Textures	196
6.6.4	Dpar and composition.....	198
6.7	Conclusions	199
6.8	Further work	200
Chapter 7: Thesis conclusions.....		215
References		217
Appendices		236
Appendix A	Mineral separation procedures	237
Appendix B	Sample descriptions, XRD data, whole rock geochemistry data	239
B.1	XRD analysis	239
B.2	Whole rock geochemistry	239
Appendix C	Thermochronology data	257
Appendix D	U-Pb dating analytical techniques	349

List of Tables

Table 3.1 Factors A1 and A2 for calculating FHe for apatite and zircon	49
Table 3.2 Calculations for volume and surface area of apatite and zircon for calculating FHe	49
Table 4.1 AFT data.....	119
Table 4.2 ZHe data	121
Table 4.3 AHe data.....	123
Table 4.4 Closure isotherms at different geothermal gradients	124
Table 5.1 AFT data from the northern Carlin Trend.....	175
Table 5.2 ZHe data from the northern Carlin Trend	177
Table 5.3 AHe data from the northern Carlin Trend.....	179
Table 5.4 Modelling parameters.....	180
Table 5.5 Fluid flux and volumes.....	181
Table 6.1 Major element composition of apatite determined by EMPA	213
Table 6.2 Trace element concentrations determined by LA-ICP-MS.....	214
Table B1 Sample characterisation.....	241
Table B2 Alteration summary	247
Table B3 Whole rock geochemistry.....	248
Table C1 AFT single grain ages LA-ICP-MS method.....	258
Table C2 AFT single grain ages EDM method.....	288
Table C3 AFT fission track lengths	297
Table D1 U-Pb data.....	352

List of Figures

Figure 1.1	Location map of the Carlin Trend.....	8
Figure 1.2	Regional AFT anomalies	9
Figure 2.1	Stratigraphy of the northern Carlin Trend	21
Figure 2.2	Summarised geological history of northern central Nevada.....	22
Figure 2.3	Simplified tectonostratigraphic map of the western United States.....	23
Figure 3.1	Closure temperatures of select thermochronometers combined for a single sample.....	38
Figure 3.2	Schematic illustration of the thermal structure of the shallow crust.....	39
Figure 3.3	The effect of cooling rate on closure temperature	40
Figure 3.4	Variation in mean track length downhole in deep Otway Basin drillholes ...	41
Figure 3.5	Example thermal histories and idealised, non-projected fission track length distributions	42
Figure 3.6	The external detector method (EDM).....	43
Figure 3.7	Example radial plot of single grain AFT ages	44
Figure 3.8	Schematic plot of Arrhenius relationship between temperature and diffusion rate	45
Figure 3.9	Closure temperature in apatite as a function of cooling rate and crystal size	46
Figure 3.10	Schematic diagram of alpha ejection correction.....	47
Figure 3.11	Age bias effects of normal alpha ejection corrections applied to zoned zircons	48
Figure 4.1	Map of the northern Carlin Trend showing the location of the Goldstrike and Little Boulder Basin Stocks.....	99

Figure 4.2 Interpreted geological cross section A-A' across across the Goldstrike Stock, Little Boulder Basin and Vivian Sill	100
Figure 4.3 Location of central Tuscarora Mountains regional samples	101
Figure 4.4 Regional cross section through northern Carlin Trend and Tuscarora Mountains	102
Figure 4.5 Map of the northern Carlin Trend showing pooled AFT ages	103
Figure 4.6 Central Tuscarora Mountains AFT ages	104
Figure 4.7 Probability plot for pooled AFT sample ages from this study	105
Figure 4.8 Interpreted geological cross section A-A' with AFT, ZHe and ZHe data	106
Figure 4.9 Age-elevation plots of AHe, AFT and ZHe data for the Little Boulder Basin Stock and Goldstrike Stock	107
Figure 4.10 AFT ages and modelled t-T histories for selected Central Tuscaroras regional samples	108
Figure 4.11 AFT and ZHe age correlation with northern in the Central Tuscarora samples	109
Figure 4.12 HeFTy models and fission track length distributions for representative Goldstrike, Little Boulder Basin and Vivian samples	110
Figure 4.13 Correlations between MTL, age, elevation and Dpar for Little Boulder Basin, Goldstrike and Vivian Sill samples	111
Figure 4.14 CL images of zoned zircons in GS-1765C-782	112
Figure 4.15 Map of the northern Carlin Trend showing ZHe and AHe ages	113
Figure 4.16 Schematic diagram of Little Boulder Basin Stock drill holes	114
Figure 4.17 Single sample t-T histories based on combined ZHe, AFT and AHe data in the Little Boulder Basin Stock	115

Figure 4.18 Alternative t-T paths to explain observed Little Boulder Basin Stock ZHe and AFT ages	116
Figure 4.19 The effect of isothermal hold time on resetting of AHe, AFT, AHe and AFT	117
Figure 4.20 Proposed tectonic model for the Late Cretaceous to early Eocene evolution of the Sevier Orogen	118
Figure 5.1 Conceptual development of physicochemical halos around a fluid conduit	159
Figure 5.2 Thermochronometric data for samples out from a dike.....	160
Figure 5.3 Distribution of Au mineralization in the northern Carlin Trend and location of samples.....	161
Figure 5.4 Distribution of Au mineralization in the northern Carlin Trend and AFT ages	162
Figure 5.5 Photomicrographs of fresh and altered lamprophyre dikes	163
Figure 5.6 Major element ration plot of $(2Ca+Na+K)/Al$ vs K/Al for samples in this study	164
Figure 5.7 HeFTy models of t-T histories of representative samples from the northern Carlin Trend	165
Figure 5.8 ZHe and AHe ages in the northern Carlin Trend.....	166
Figure 5.9 Effect of isothermal hold time and constraints on the duration of heating..	167
Figure 5.10 Cross section through the West Banshee deposit	168
Figure 5.11 Size of the conductive thermal halo in AFT data in the Goldstrike Stock	169
Figure 5.12 Temperatures into the modelled Goldstrike Stock	170
Figure 5.13 Time-temperature paths at distances into the model Goldstrike Stock	171
Figure 5.14 t-T path of theoretical sample in the Goldstrike Stock	172

Figure 5.15 Maximum duration of heating by 180°C and 240°C fluids	173
Figure 5.16 Fluid flux responsible for Au mineralization around the Goldstrike Stock	174
Figure 6.1 Photomicrographs of apatite associations in thin section	202
Figure 6.2 Relative F, OH and Cl content of individual apatite crystals	203
Figure 6.3 Chondrite normalised apatite REE plots.....	204
Figure 6.4 Examples of zoning or absence of zoning in apatite in CL	205
Figure 6.5 Ternary diagram showing substitutions on the Ca site by Na and REE	206
Figure 6.6 Apatite SiO ₂ vs P ₂ O ₅	207
Figure 6.7 Apatite F decreases with increasing SiO ₂ content	208
Figure 6.8 Sr _{melt} vs Sr _{ap}	209
Figure 6.9 Sr-Y plot to determine host rock type.....	210
Figure 6.10 Apatite halogen content and kinetic parameter D _{par}	211
Figure 6.11 Apatite Fe, Mn, ΣREE content	212
Figure B1 Classification of granodiorites	240
Figure D1 U-Pb concordia plots.....	351

Acknowledgements

My first thanks go to my supervisor Ken Hickey for his guidance and mentorship throughout this MSc project, as an unending source of ideas and thought-provoking questions. My thanks also to my committee members Greg Dipple and Leslie Smith. Completing this project was made easier and even enjoyable by advice and instruction from Jim Mortensen, Mati Raudsepp, Shaun Barker, Thomas Bissig, Farhad Bouzari, Jenni Lai at UBC, Ray Donelick and Paul O'Sullivan at Apatite to Zircon, Inc., and Peter Reiners and Stefan Nicolescu at the University of Arizona.

I'm grateful to everyone in the Barrick Goldstrike exploration department in Nevada for their cooperation and assistance in making this project logistically possible, in particular Richard Hipsley, Zach Hibdon, Dave Grey, Ellen Lander and Nina Cambra, and to Richard Tsosie and Erik Hoekstra for putting up with my never ending requests and providing me with music, good chats and snacks in the core shed. My thanks also to Joe Becker and Rachel Burgess at Newmont for providing geology data.

This project was part of the MDRU Carlin Footprints Project, financially supported by Barrick, Newmont, Teck, and NSERC. A student fellowship grant from the SEG made living on a MSc student salary a little easier.

I'd also like to thank fellow Carlin Project students Ayesha Ahmed, Will Lepore, Trent Newkirk and Jeremy Vaughan for illuminating research related discussion, as well as more than a few Vancouver-Nevada road trip adventures along the way. My thanks to Dan Woodell for his patient explanation of and assistance with Matlab. I'm grateful to friends at both UBC and the University of Arizona for so much discussion and distraction. Lastly, I want to thank my parents and Lorna, Jared, Jack and Leanne for their never failing support and encouragement.

Chapter 1: Introduction

1.1 Thesis goals and fundamental concepts

The Carlin Trend in northern Nevada is the world's fourth largest Au-producing region, producing 157 metric tons of Au in 2009, approximately 70% of annual US gold production (Price, 2010). Despite the region's large Au endowment, the submicron-scale, disseminated nature of gold in Carlin-type deposits and lack of extensive visual alteration make discovery of new deposits in the region challenging, especially as exploration is driven to greater depths (Kelley et al., 2006). Production in the area is currently concentrated in several large deposits, e.g., Barrick Gold Corp.'s Goldstrike deposits, including Betze-Post and Meikle, that produced 1.09 Moz in 2011 (Barrick production figures) and Cortez Hills deposit, 1.42 Moz (Barrick 2011 production), and Newmont's Leeville and Gold Quarry (~2 Moz in 2010, Muntean, 2010). Deposit locations are shown in Figure 1.1. Typical grades vary from less than 1 g/t to around 40 g/t, forming deposits of 0.5 to over 1,500 t Au (Bettles, 2002; Cline et al., 2005). A detailed overview of Carlin-type Au-deposits is provided in Chapter 2.

Exploration for hydrothermal mineral deposits is traditionally based on patterns of physical or chemical alteration around mineralization (Hawkes and Webb, 1962; Eilu and Groves, 2001; Goldberg et al., 2003; Kelley et al., 2006). Alteration is the result of fluid-rock interaction (Giggenbach, 1984). The intensity and nature of alteration is controlled by fluid-rock ratios and the thermal and chemical disequilibrium between a hydrothermal fluid and the host rock (Reed, 1997). Greater disequilibrium results in stronger mineral alteration, often zoned away from the core of the hydrothermal system as fluids are progressively buffered by the host rocks (Reed, 1997). In Carlin-type deposits, formed in a low-temperature hydrothermal environment, visual alteration (decarbonatisation, silicification, argillisation) is subtle and limited in spatial extent (Hofstra and Cline, 2000; Cline et al., 2005). Where

alteration is visible, its intensity is not directly proportional to Au grade (Cline et al., 2005; de Almeida et al., 2010). Due to the subtle and irregular nature of alteration, zoning is not easily or consistently identifiable, and therefore has limited application in exploration for new Carlin-type deposits (Kuehn and Rose, 1992; Hofstra and Cline, 2000; Cline et al., 2005). Trace element enrichment and depletion patterns, e.g., As, Hg, Tl, Cu, Te, S and Sb, have been identified (e.g., Albino, 1994; Hofstra and Cline, 2000), however these are not consistently zoned in the way often observed in other types of deposits (e.g., Ewers and Keays, 1977; Jones, 1992), and so are also of limited use for vectoring to new deposits.

Heat is also transferred from hydrothermal fluid to host rock but does not produce a visible manifestation of hydrothermal fluid flow. The thermal halo that forms around hydrothermal mineral deposits is less often investigated than chemical halos. The size of the thermal halo is primarily a function of the duration of hydrothermal fluid flow, the temperature difference between the fluid and host rock, and the density, size and geometry of the fluid conduits (Cathles, 1997). Apatite and zircon, both common accessory minerals in igneous and sedimentary rocks, are used extensively in apatite fission track (AFT) and (U-Th)/He thermochronology and record the low-temperature cooling history of a rock (Green et al., 1986; Zeitler et al., 1987; Wolf et al., 1997; Farley, 2002; Reiners et al., 2002). In addition to its thermal sensitivity, apatite also records chemical changes resulting from interaction with hydrothermal fluids (Bouzari, 2011). Apatite and zircon, ubiquitous in host rocks across the Carlin Trend, are therefore potential thermal and chemical indicators of hydrothermal fluid flow in and around Carlin-type deposits.

The research presented in this thesis is part of a larger study at the Mineral Deposit Research Unit (MDRU) at the University of British Columbia (UBC). The ultimate goal of that larger study is to identify the physicochemical manifestations of hydrothermal fluid flow

responsible for the formation of Carlin-type Au-deposits, e.g., halos of trace element anomalies, clay mineral zoning, isotope depletion and thermal resetting around deposits. The project also aims to determine the size of these "footprints" of the hydrothermal system responsible for Au-deposit formation, and their spatial association with mineralization, in order to assess potential of each physicochemical manifestation of hydrothermal fluid flow as a vector for future mineral exploration. In addition to the MSc thesis presented here, the project includes one other MSc, concentrating on clay mineral zoning (Ahmed, 2010a), and one PhD thesis, investigating trace element zoning and C and O isotopic depletion around fluid flow paths (Vaughan, 2010; in prep).

This MSc builds on earlier thermal mapping work that identified a spatial association of thermal anomalies with Eocene Carlin-type Au-mineralization on a regional scale around the Carlin Trend (Figure 1.2). That regional study used AFT thermochronology to identify areas thermally reset as a result of the Eocene hydrothermal system (e.g. Hickey, 2005; Hickey, 2007).

The overall goal of this MSc research is to assess the effects of hydrothermal fluid flow on apatite and zircon as thermal and chemical indicators of hydrothermal fluid flow that formed the giant Carlin-type Au-deposits. One focus is a thermochronology study developing on the thermal mapping work of Hickey (2005, 2007) to define the spatial extent of the thermal halo associated with mineralization on the scale of individual deposits using the thermal resetting of apatite and zircon in the northern Carlin Trend (Chapter 5). As a background to thermal halo mapping, a study of the tectonic history of the northern Carlin Trend was conducted using thermochronology (Chapter 4). The other focus is a study of apatite chemistry and morphology to, 1. determine how the mineral is affected by Carlin-type hydrothermal fluids, e.g., changes in chemistry and morphology of primary igneous apatite, and 2. to

distinguish between primary and secondary hydrothermal apatite (Chapter 6). The three main aspects of this thesis are discussed briefly in the following paragraphs and more thoroughly in the remaining chapters of this thesis.

1.1.1 Background exhumation study

In order to assess the thermal effects of the Carlin hydrothermal system the background thermal history must be determined. The regional thermal footprint mapping of Hickey (2007) and Hickey et al. (2005) noted Cretaceous AFT ages away from mineralization and Eocene aged anomalies around the main mineralization trends. The Mesozoic history of the northern Carlin Trend is poorly constrained. Low-temperature thermochronology is therefore used to investigate the background thermal history of the area, building on tectonic studies of the development of northern central Nevada. Studies of the Paleozoic geology (e.g. Roberts, 1958; Stewart, 1972; Miller et al., 1984) and Cenozoic extension (e.g. Wernicke et al., 1982; Wernicke, 1992; Snow and Wernicke, 2000; Haynes, 2003; Colgan et al., 2008; Henry, 2008; Colgan et al., 2010), have led to a reasonably well-constrained history of northern Nevada during those times. However, studies of the Mesozoic history, e.g., the Sonoma Orogeny (Silberling and Roberts, 1962; Gabrielse et al., 1983; Trexler et al., 2004) and Sevier Orogeny (Armstrong, 1972; Miller and Gans, 1989), have focused primarily on neighbouring regions. Knowledge of the timing and scale of Mesozoic tectonic events is critical to the interpretation of data related to subsequent events and Eocene mineralization, so an investigation of the tectonic history of the northern Carlin Trend region using thermochronology is presented in Chapter 4.

1.1.2 Thermal mapping

Earlier thermal mapping work by Hickey (2005, 2007) identified areas of Eocene AFT ages larger than the spatial extent of Eocene Au mineralization in and around the Carlin Trend. These Eocene thermal anomalies stand out against the older Cretaceous ages observed regionally, away from mineralization. The timing of Au mineralization is constrained to between 36 and 42 Ma (Tretbar et al., 2000; Arehart et al., 2003b; Chakurian et al., 2003; Cline et al., 2005). Hickey et al. (2005) interpreted these Eocene ages to be the product of thermal resetting, and inferred that the thermal footprint is therefore an expression of heat flow beyond the extent of hydrothermal fluid flow. Heat flow occurs in two ways: 1. by advection: heat transfer by direct contact with a hydrothermal fluid, which may or may not be associated with mass transfer, e.g., alteration, mineralization; 2. by conduction: transfer of heat alone beyond the path of fluid flow. The large thermal footprint observed therefore defines the limit of heating to temperatures high enough to reset AFT, extending well beyond areas where there is evidence of fluid flow. The size of the footprint is a product of both advective heating within abundant hydrothermal fluid flow conduits (faults, lithological boundaries, favorable stratigraphic horizons) (Bickle and McKenzie, 1987; Cathles, 1997; Hofstra and Cline, 2000), as well as conductive heating, which extends beyond fluid conduits and forms the most distal manifestation of hydrothermal fluid flow. Figure 1.2 shows the spatial association of mapped thermal anomalies with Au mineralization around the Carlin Trend.

Chapter 5 examines the spatial extent of thermal anomalies on a deposit scale to give an indication of how far from a deposit a thermal footprint can be detected, assessing the distance over which thermal mapping might be effective as an exploration tool. Multiple thermochronometers (apatite fission track, apatite and zircon (U-Th)/He dating, see Chapter 2) are combined to define halos corresponding to different temperatures of resetting. These

different temperature thermal halos are potentially concentric and could be used to vector towards ore, assuming temperatures were highest at the heart of the mineralizing system where ore is concentrated. Knowledge of the size of the thermal halo resulting from Carlin-type hydrothermal systems also allows the duration, temperature and volume of fluid flow to be estimated.

1.1.3 Apatite as a chemical indicator of hydrothermal fluid flow

Knowledge of the composition of apatite is of particular importance in AFT dating, in particular the halogen (F, Cl, OH) content, which affects the rate of annealing of fission tracks (Carlson et al., 1999; Barbarand et al., 2003; Donelick et al., 2005). Determining the composition of apatite in the samples analysed for low-temperature thermochronology allows more thorough evaluation of the age data collected. Compositional and textural observations may also allow distinction between primary (igneous) and secondary (hydrothermal) apatite, reflecting differences in melt and hydrothermal fluid chemistries and sources, as well as any changes due to apatite-fluid interaction (Pan and Breaks, 1997; Piccoli and Candela, 2002).

1.2 Thesis structure

This thesis is presented in three research chapters, each focusing on a different aspect of the effects of hydrothermal fluid flow associated with Carlin-style mineralization. Chapter 4 is a background tectonic study to the subsequent investigation of the thermal footprint in Chapter 5, and concentrates on refining the tectonic history of northern central Nevada using low-temperature thermochronology to determine the extent and rate of exhumation prior to the Eocene mineralizing hydrothermal event. Chapter 5 explores the thermal expression of mineralizing hydrothermal fluid flow. This includes results of mapping using low-temperature

thermochronology to determine the size of thermal halos around deposits in the northern Carlin Trend, and what this reveals about the duration and volume of flow and temperature of hydrothermal fluids. Chapter 6 examines the effects of hydrothermal fluid flow on apatite, a key mineral in low-temperature thermochronology, providing further information on hydrothermal processes. Overviews of Carlin-type Au-deposits and (U-Th)/He and AFT thermochronology are presented in Chapters 2 and 3.

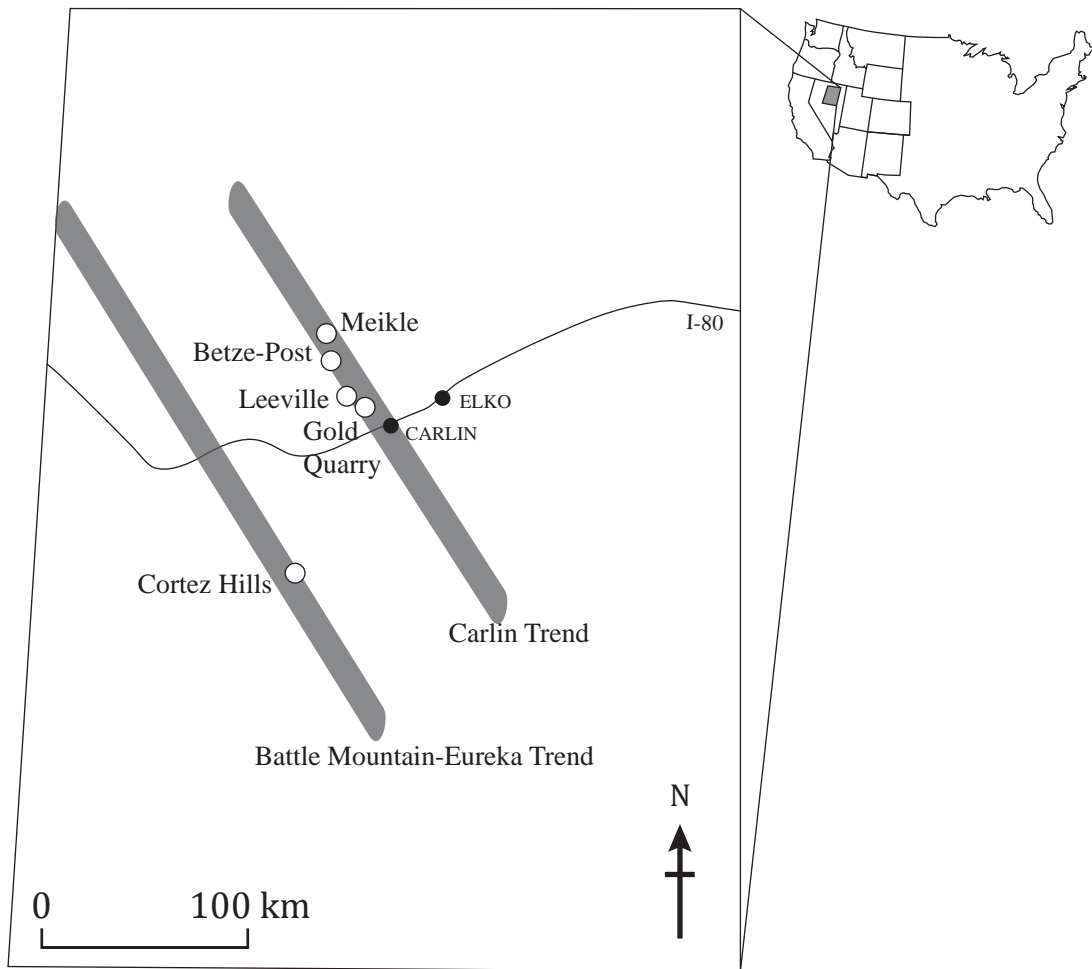


Figure 1.1 Map showing the location of the Carlin Trend and Battle Mountain-Eureka Trend in Nevada, USA. Locations of major deposits mentioned in the test are also shown.

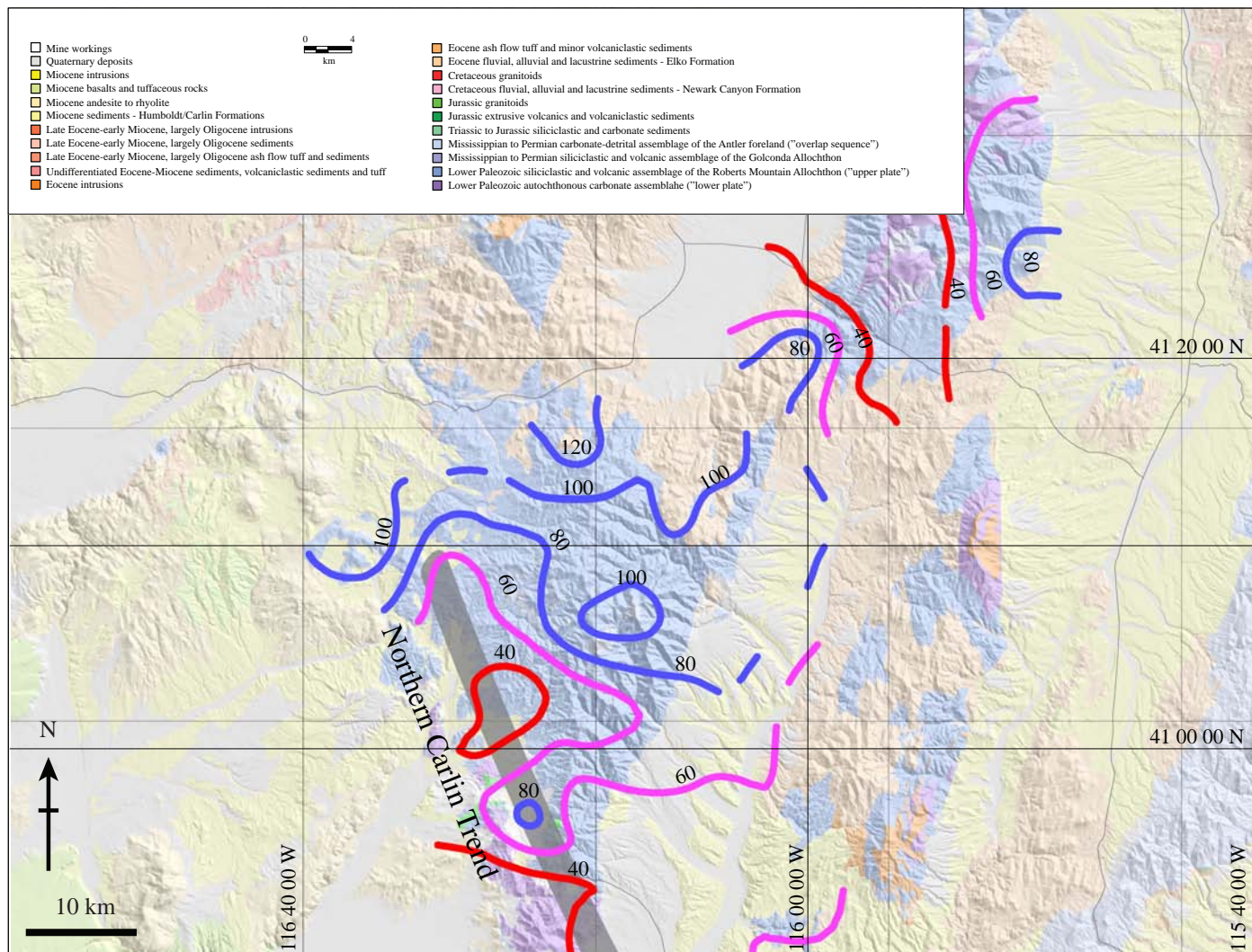


Figure 1.2 Regional association of thermal anomalies defined by AFT resetting with major mineral trends in northern central Nevada, based on data from Hickey (2003, 2005, unpub data) and Chakurian et al. (2003). The northern Carlin Trend (shown in grey) is the focus of this study. The Battle Mountain-Eureka Trend to the west is also shown, as are the Twin Creeks and Getchell districts. Contours are of thermal ages at 20 Myr intervals based on pooled AFT ages. Warm colours are younger ages, more recently thermally reset. Cooler colours correspond to older ages in areas that have remained below $\sim 75^{\circ}\text{C}$ for a longer period of time.

Chapter 2: Geological background to Carlin-type Au deposits

2.1 Introduction

Carlin-type Au deposits are located in northern Nevada, within the Great Basin. The deposits lie along two main north-northwest-striking trends (Figure 1.1), the Carlin Trend and the Battle Mountain-Eureka Trend. The northern Carlin Trend, the focus of this study and this review, is approximately 20 km long and contains over 6 000 t Au (Muntean et al., 2011).

Carlin-type deposits are characterised by submicron scale, disseminated Au in decarbonatised carbonate host rocks. Mineralization is structurally and stratigraphically controlled and hosted predominantly in Paleozoic carbonate sediments, as well as around Jurassic and Eocene sills and dikes (Ressel et al., 2000; Hofstra et al., 2003; Cline et al., 2005).

2.2 Geological setting of the northern Carlin Trend

2.2.1 Stratigraphy of the northern Carlin Trend

The stratigraphy of the northern Carlin Trend comprises two Paleozoic marine packages overlain by Miocene volcanoclastic sediments (Figure 2.1). The Paleozoic "Lower Plate" package consists of carbonate sediments that were deposited on the slope of a passive margin. The Lower Plate carbonate package forms the footwall to the Roberts Mountains Thrust, a significant regional fault that separates the Lower Plate from the overlying siliciclastic "Upper Plate" hanging wall package. The Upper Plate consists of deeper water siliciclastic sediments deposited contemporaneously with the carbonate package on the same passive margin but farther west, and farther offshore (Dickinson, 1978; Stevens, 1991; Armstrong, 1998; Lund, 2008). The Upper Plate is up to 1 km thick and consists of the Ordovician Vinini Formation, overlain at the northern end of the study area by the Silurian Elder Formation (Volk, 2001; Bettles, 2002). In the northern Carlin Trend, the Lower Plate, up to 700 m thick, comprises

(from oldest to youngest) the Ordovician-Silurian Hanson Creek Formation, Devonian-Silurian Roberts Mountains Formation and Bootstrap Limestone, the Devonian Popovich Formation and Devonian Rodeo Creek Formation (see Figure 2.1).

The Upper Plate is overlain by the subhorizontal to gently-dipping units of the Miocene Carlin Formation. The formation consists mainly of unconsolidated sand, silt and gravels (Jory, 2002). Ichnofossils within the sediments suggest that deposition occurred in a lacustrine environment (Theodore et al., 1998). Air fall tuffs and ash deposits that occur within the formation have been dated at 15.1-14.4 Ma using $^{40}\text{Ar}/^{39}\text{Ar}$ dating (Fleck et al., 1998). The Carlin Formation fills narrow pull-apart basins that are up to 800 m deep, evidence of Miocene extension in the region, although low dip angles indicate extension was relatively minor, ~10% (Wallace et al., 2008). Normal faults that offset air fall tuff layers by up to 1.5 m have been observed (Theodore et al., 1998), indicating extension continued, at least locally, post-Miocene.

2.2.2 Igneous geology

Jurassic (157-158 Ma) and Eocene (36-42 Ma) intrusions are common in the northern Carlin Trend (Mortensen et al., 2000; Ressel et al., 2000; Ressel and Henry, 2006). Cretaceous (~112 Ma) intrusions have also been identified, e.g., the granite Richmond Stock to the south of the study area (Ressel and Henry, 2006) and more regionally ~106 Ma, e.g., Gold Acres, Ruby Hill area (Mortensen et al., 2000). Jurassic intrusions include the granodiorite Goldstrike and Little Boulder Basin Stocks that are now separated by the Post-Gen fault system but are interpreted as intruded as a single intrusive body (Chakurian et al., 2003; Ressel and Henry, 2006). Associated with these large felsic-intermediate intrusions are ~157 Ma lamprophyre and porphyritic rhyodacite dikes and sills that fill pre-existing high-angle normal faults. The

Jurassic dikes are commonly altered and host Au-mineralization. (Bettles, 2002; Ressel and Henry, 2006; Ressel et al., 2000).

Eocene rhyolite and dacite dikes dated at 36-42 Ma are present throughout the northern Carlin Trend, also exploiting existing faults and lithological contacts (Arehart et al., 2003a; Ressel and Henry, 2006). Although commonly altered, Eocene dikes are not significant ore hosts (Ressel et al., 2000). The contemporaneous Eocene Tuscarora volcanic field is found to the north of the study area (Henry, 2008).

Miocene rhyolite lavas locally overlie older stratigraphy around the northern Carlin Trend. The lavas were erupted from volcanic centres to the north west, west and south of the northern Carlin Trend around 15 Ma (Ressel and Henry, 2006). Ash-fall tuffs of the same age have been dated in Miocene sedimentary basins (Wallace et al., 2008). No Miocene intrusions are recognised in the northern Carlin Trend itself (Ressel and Henry, 2006).

2.2.3 Structure

The structure of the northern Carlin Trend is complex, resulting from repeated reactivation of existing structures during multiple phases of extension and contraction that began in the Paleozoic and continue today (Miller et al., 1984; Wernicke et al., 1987; Allmendinger, 1992; Miller et al., 1992; DeCelles, 2004). The relative timing of the development of structures is constrained in places by Jurassic and Eocene intrusions, which often exploited existing faults, and by the overlying Miocene Carlin Formation (Emsbo et al., 2006; Muntean et al., 2007). Several fault orientations are present: high-angle north-northwest- to north-northeast-striking faults that dip east or west, low-angle north-northwest to north-northeast-striking faults and northeast-striking, east- or west-dipping faults. Normal, reverse

and oblique motion is evident on most faults, again highlighting the complexity of the area (Teal and Jackson, 2002; Heitt et al., 2003).

Faults are significant ore controls, with high Au grades often found at fault intersections (Heitt et al., 2003; Cline et al., 2005; Mickelthwaite, 2010). Fault densities are greatest around large intrusions, such as the Goldstrike Stock, where rheological contrast between the rigid granodiorite pluton and the host carbonates have resulted in complex fracture networks in the weaker carbonate rock (Heitt et al., 2003; Cline et al., 2005). Gold grades are elevated in these areas of increased fracture density and permeability (Hofstra and Cline, 2000). Antiforms are also centres for Au-deposition, acting as traps to mineralizing fluids. Folds generally have a northwest trend and limbs are commonly offset by subsequent faulting (Volk, 2001).

2.2.4 Geological history

The geological history of northern central Nevada is summarised in Figure 2.2. Neoproterozoic east-west continental rifting laid the underlying tectonic framework that has influenced subsequent structural and tectonic evolution of the region (Dickinson, 1978; Lund, 2008). Many younger faults and folds, including the Post Fault, have north-northwest strikes similar to the strike of the rifted margin. The Carlin Trend and Battle Mountain-Eureka Trend mineral belts are also north-northwest-trending (Figure 1.1). Discontinuities in geophysical properties coincident with these trends are considered evidence of deep crustal scale faults (Rodriguez, 1998). Late Proterozoic rifting led to the development of a passive margin sequence on the western edge of the ancient North American continent that persisted throughout the Paleozoic (Stewart, 1972; Miller et al., 1984; Tosdal et al., 2000; Timmons et al., 2001; Lund, 2008). Following the deposition of Paleozoic shelf carbonate and slope

siliciclastic sediments, which later became the Lower Plate and Upper Plate packages, the region underwent several phases of contraction that are outlined in the following paragraphs.

The Late Devonian-Mississippian Antler Orogeny was responsible for east-verging thrusting and transportation of the internally-deformed Roberts Mountains allochthon (RMA, Figure 2.3) along the Roberts Mountains Thrust (RMT) to its current position above the Lower Plate carbonate package (Roberts, 1958; Burchfiel and Davis, 1972). Internal deformation, such as imbricate thrusts and reverse faults, has been described within both the allochthon and the underlying carbonate package (Miller et al., 1984; Trexler et al., 2004). Contraction was ongoing throughout the Paleozoic, as deformation in northern central Nevada locally records. Folds with northeast-trending axes described in northern central Nevada in Carlin Canyon are considered evidence of northwest-southeast contraction constrained to Pennsylvanian-Early Permian time (Trexler et al., 2004). Towards the northern end of the Carlin Trend, the north-dipping Coyote Thrust and associated imbricate thrusts and folding are considered evidence of a north-south compressive event that occurred in the Pennsylvanian (Theodore et al., 1998). Because of subsequent tectonism, the extent of Pennsylvanian contraction is uncertain but was significant in the tectonic history of northern central Nevada and is evidence of ongoing compression throughout the Late Paleozoic (Trexler et al., 2004).

During the Early Triassic, east-dipping subduction of the Farallon Plate was initiated and continued throughout the Mesozoic (Dickinson, 2008). The Sierra Nevada batholith in western Nevada is a remnant of the magmatic arc associated with subduction (Chen and Moore, 1982). The Late Permian-Triassic Sonoma Orogeny involved east-west folding and faulting of the deep marine sediments of the Golconda allochthon (Silberling and Roberts, 1962; Gabrielse et al., 1983; Miller et al., 1984; Riley et al., 2000), also shown in Figure 2.3. The eastward transportation of the allochthon along the Golconda Thrust to its present position west of the

northern Carlin Trend is widely believed to have occurred during the Sonoma Orogeny, although Ketner (2008) proposed that development of and transport along the east-verging Golconda Thrust occurred as a result of Jurassic east-west contraction that also caused west-verging thrusting in northwestern Nevada.

As subduction and compression continued throughout the Mesozoic, the Cretaceous-Paleocene Sevier Orogeny affected the entire western margin of North America, extending as far east as central Utah (Miller and Gans, 1989; DeCelles, 2004). The Sevier Fold-Thrust Belt front (shown in Figure 2.3) lies ~400 km east of the study area. The Cretaceous-Eocene Laramide Orogeny affected the continental interior east of the Sevier fold-thrust belt front, and was not a major tectonic event in the area of the northern Carlin Trend or the Great Basin (Dickinson, 1978; Engebretson et al., 1984; DeCelles, 2004).

By the Early Eocene, compression had ceased due to removal of the Farallon slab and gravity-driven collapse of thickened continental lithosphere in northern central Nevada (Humphreys, 1995; McGrew et al., 2000). This led to regional extension that exploited north-northwest-striking faults once again. Eocene dikes intruded along many of these faults (Ressel and Henry, 2006), as magmatism swept back westward with steepening subduction and slab rollback (Dickinson, 2006). Metamorphic core complexes, such as the Ruby Mountain metamorphic core complex to the east of the Carlin Trend, record two main phases of exhumation in their P-T histories, one in the Eocene and one more pronounced phases in the Miocene (Wernicke, 1992; McGrew et al., 2000; Howard, 2003; Colgan et al., 2010). Around 17 Ma, more typical Basin-and-Range style block faulting became the dominant extensional mechanism, with localised extension varying 10-100 % (Wernicke et al., 1987; Muntean et al., 2001; Colgan et al., 2008; Wallace et al., 2008). Post Miocene extension is characterised by the development of broad flat valleys bounded by uplifted blocks that formed the ranges that still

dominate the region's topography (Gilbert, 1928; Eaton, 1982; Wernicke, 1992; Dickinson, 2008; Wallace et al., 2008).

Volcanic centres developed to the north and west of the northern Carlin Trend, associated with the NNW-striking northern Nevada Rift (Zoback et al., 1994; Ressel and Henry, 2006), a 500 km long feature approximately 50 km west of the northern Carlin Trend that developed in the Mid Miocene. Rhyolitic and basaltic eruptions occurred between 16 and 14 Ma and contributed volcanoclastic and air fall material to the Carlin Formation (Zoback et al., 1994; John, 2000; Wallace et al., 2008).

2.3 Carlin-type mineralization in the northern Carlin Trend

The microscopic Au of Carlin-type deposits is found in arsenian pyrite rims on disseminated pre-ore pyrite (Cline et al., 2005; de Almeida et al., 2010). The variety of ore body sizes and morphologies (e.g., tabular, strata-bound, irregular, T-shaped) reflects the interplay of several controlling features, namely the intersection of favourable stratigraphic horizons (mostly in the Devonian Popovich Formation) and high- and low-angle faults, which locally increase permeability and porosity (Hofstra and Cline, 2000). Contacts with intrusions were either exploited as fluid conduits (Teal and Jackson, 2002), or acted as aquitards where pre-ore clay alteration reduced permeability and forced precipitation of Au in the surrounding sediments (Emsbo et al., 2003; Cline et al., 2005). Gold mineralization occurs predominantly in Lower Plate rocks (Cline and Hofstra, 2000). The lack of Upper Plate Au-mineralization is considered the result of the lower permeability of the siliciclastic package, or is simply due to the absence of suitably reactive host rocks (i.e. carbonates) in the Upper Plate (Ahmed, 2010a).

The timing of mineralization has been constrained by dating cross-cutting dikes, which have biotite $^{40}\text{Ar}/^{39}\text{Ar}$ ages (Arehart et al., 1993b; Ressel et al., 2000) and zircon and titanite U-

Pb ages (Mortensen et al., 2000; Ressel and Henry, 2006) of ~37-40 Ma. Rb/Sr dating of syn-mineralization galkhaite, an Hg sulfosalt, also yielded an Eocene age of 38-40 Ma (Getchell, Tretbar et al., 2000; Carlin Trend, Arehart et al., 2003a). K/Ar and $^{40}\text{Ar}/^{39}\text{Ar}$ dating of sericite by numerous studies has yielded a range of ages ~100-120 Ma (Kuehn, 1989; Arehart et al., 1993b), however different types of sericite (detrital, deuteritic or magmatic, hydrothermal) are often overprinted and mixed, so ages do not necessarily relate to Au mineralization (Arehart et al., 2003a). Re-Os dating of ore-stage realgar, orpiment and pyrite has been unsuccessful due to the low concentrations of Re and Os in the small mineral grains (Arehart et al., 2003a; J. Vaughan, pers. comm.). AFT cooling ages 36-42 Ma are also coincident with Eocene mineralization and have been interpreted to record a thermal resetting event of pre-existing apatite in igneous and sedimentary host rocks (Chakurian et al., 2003; Hickey, 2005; Arehart and Donelick, 2006).

2.4 Alteration in the northern Carlin Trend

Alteration of host rocks is characterised by decarbonatisation, argillisation and variable silicification and sulfidation; carbonate host rocks were dissolved and sulfidised by acidic auriferous fluids (Kuehn and Rose, 1992). Collapse breccias developed where dissolution was extreme, increasing permeability and porosity and leading to formation of high-grade deposits, e.g., Meikle (Emsbo et al., 2003; Cline et al., 2005).

Argillisation is most apparent in pre-ore intrusions, where acidic fluids reacted with aluminosilicate minerals to form illite±kaolinite±dickite±smectite (Hofstra and Cline, 2000; Ahmed, 2010a). Carbonate host rocks lack abundant aluminosilicates and are therefore minimally argillised.

Silicification occurred locally, and where most pervasive, resulted in the formation of jasperoids (Hofstra and Cline, 2000; Cline et al., 2005). Quartz is found as drusy quartz in vugs or less commonly in veinlets (Cline et al., 2005). The extent of silicification is not proportional to Au grade and is therefore an unreliable indicator of economic mineralization (Cline et al., 2005). Quartz precipitation is a temperature-sensitive process caused by fluid cooling to the point of silica saturation (Holland and Malinin, 1979). The lack of spatial association between Au mineralization and quartz suggests that Au mineralization was not controlled by temperature (Hofstra and Cline, 2000).

Mineralization is associated with sulfidation of host rock (Hofstra and Cline, 2000). Ore fluids liberated Fe from carbonate minerals, triggering pyrite growth that utilised S in the ore fluids, which in turn destabilised Au and As bisulfide complexes in the fluid, causing simultaneous precipitation of Au within As-rich pyrite rims on pre-ore pyrite (Kesler et al., 2003; Barker et al., 2009).

2.5 Characteristics and source of mineralizing fluids

Fluid inclusion data and mineral assemblage studies have shown that the ore fluid was aqueous, low temperature (180-240°C), low to moderate salinity (<6 wt% NaCl equivalent), and moderately acidic (pH 4-6). Fluids contained CO₂ <4 mol %, CH₄ (<0.4 mol %) and H₂S (10⁻¹-10⁻² m) (Hofstra et al., 1991; Hofstra and Cline, 2000; Emsbo et al., 2003; Cline et al., 2005).

The fluid source is a topic of debate due to conflicting $\delta^{18}\text{O}$, δD and $\delta^{34}\text{S}$ isotopic evidence. Very negative $\delta\text{D}_{\text{H}_2\text{O}}$ values, typical of meteoric fluids, have been obtained from fluid inclusion and clay mineral studies of many Carlin-type deposits (Hofstra et al., 1999; Emsbo et al., 2003). There is also variation from deposit to deposit, e.g., the Getchell and Deep

Star deposits have higher, positive δD_{H_2O} values than other deposits, more consistent with a magmatic fluid source (Cline and Hofstra, 2000; Heitt et al., 2003). Other studies yielded higher δD_{H_2O} values that may suggest evolved meteoric fluids or fluid mixing (Hofstra et al., 1999; e.g. Emsbo et al., 2003; Lubben, 2004). $\delta^{34}S$ studies have yielded mixed results, as most suggest a sedimentary source for the majority of Carlin-type deposits (Arehart et al., 1993a; Hofstra, 1997; Emsbo et al., 2003), while some indicate a probable magmatic source (e.g. Screamer, Kesler et al., 2003).

The source of Au remains uncertain but may be derived from a sedimentary or magmatic source (Barker et al., 2009). Emsbo et al. (2003) identified Devonian base- and precious-metal sedimentary exhalative mineralization in the Meikle area and suggested Au may have been concentrated in the region prior to the Eocene Carlin-type mineralization event. In any case, Au cannot have been sourced from greater depths than S (Cline et al., 2005), since Au was transported by bisulfide complexing.

2.6 Ore deposit formation models

Several models for ore deposit formation have been proposed. The two most viable models (Cline et al., 2005) are a meteoric model and a deep source magmatic and/or metamorphic model for fluid source. An epizonal intrusion model has also been proposed (Ressel et al., 2000; Heitt et al., 2003), relating Carlin-type deposits to a distal porphyry deposit, but there is no evidence of such a system nearby and no evidence of boiling in Carlin-type deposits, a characteristic feature of epithermal deposits related to deeper porphyry deposits (Cooke and Simmons, 2000; Cline et al., 2005). A meteoric model involves leaching metals from pre-existing deposits (e.g., Devonian SEDEX deposits described by Emsbo, 1999; Emsbo et al., 2003) or from the deep crust as fluids circulate to deep crustal levels (Seedorff,

1991; Ilchik and Barton, 1997; Person et al., 2008). However, a meteoric model does not account for the deep isotopic signatures observed in some deposits (e.g., Getchell, Cline and Hofstra, 2000; Cline, 2003). Ressel and Henry (2006) propose abundant coeval intrusions are an indication of a larger, deeply concealed pluton, and therefore suggest a deep magmatic source for fluids and metals, as well as heat that drove the ascent of hydrothermal fluids (Muntean et al., 2011; Ressel and Henry, 2006). A deep metamorphic source also explains some of the isotopic data but no Eocene metamorphism is reported (Cline et al., 2005).

Cline et al. (2005) propose a composite model of meteoric fluids circulating and mixing with deep sourced magmatic (or meteoric) fluids that scavenged metals from Neoproterozoic rocks. They observe that Au was transported in bisulfide complexes, and suggest that reactions between pyrite-bearing carbonate host rocks and ascending fluids may have increased H₂S concentrations in the fluid, increasing its capacity to scavenge Au along its path. Extension of the overthickened upper crust facilitated ascent of fluids along reactivated faults. Fluids accumulated in areas of reduced stress at the boundaries of older intrusive stocks, in structural culminations and at boundaries between strata of contrasting permeability. Mildly acidic fluids decarbonatised and argillised carbonate host rocks, enhancing permeability and releasing sedimentary Fe for sulfidation. Sulfidation destabilised the Au bisulfide complexes, resulting in precipitation of Au in submicron scale pyrite rims.

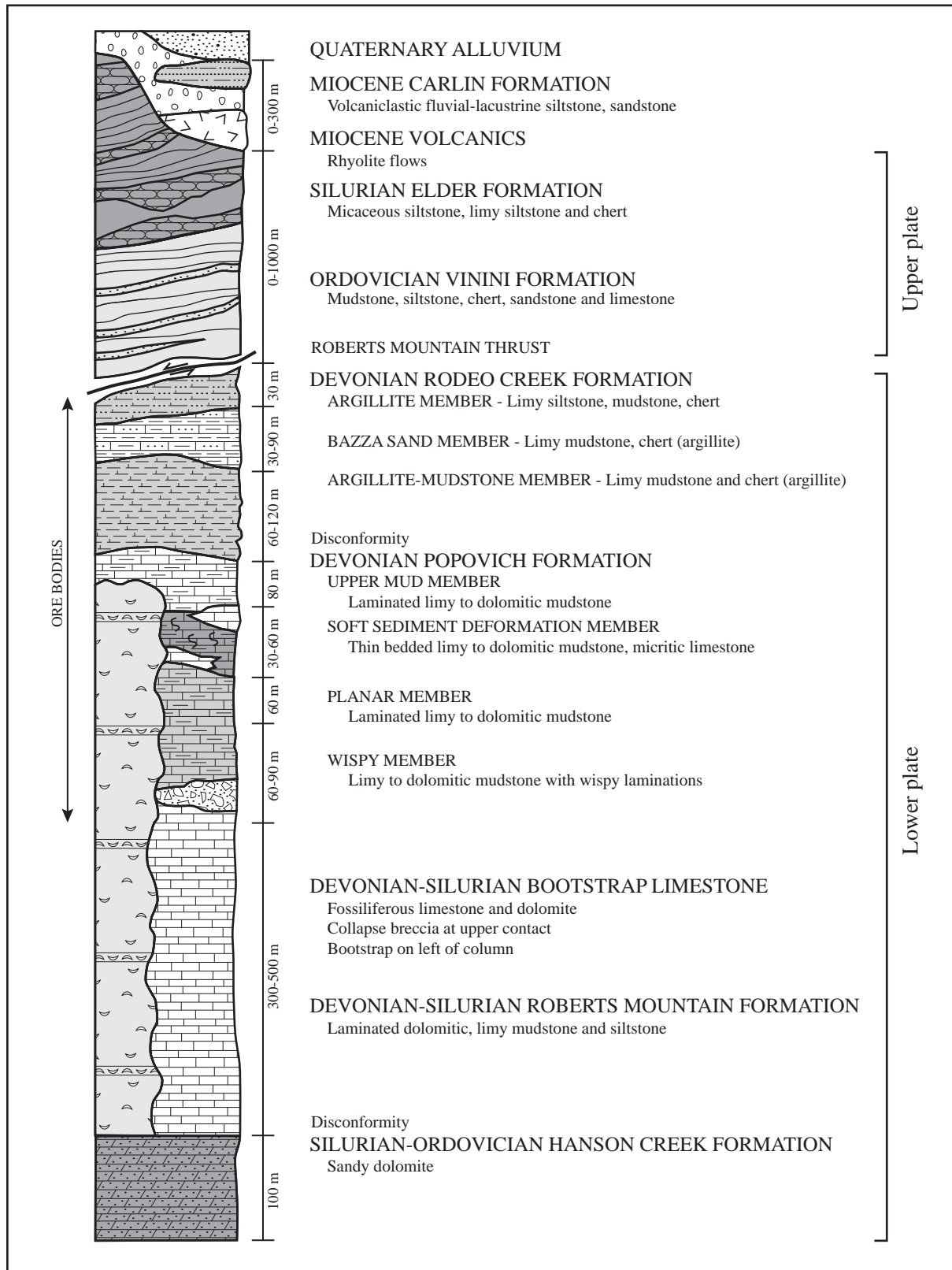


Figure 2.1 Summary stratigraphic column at the Goldstrike property in the northern Carlin Trend. Not to scale. Range of positions of ore bodies is also shown. After from Volk et al. (2001) and Bettles (2002).

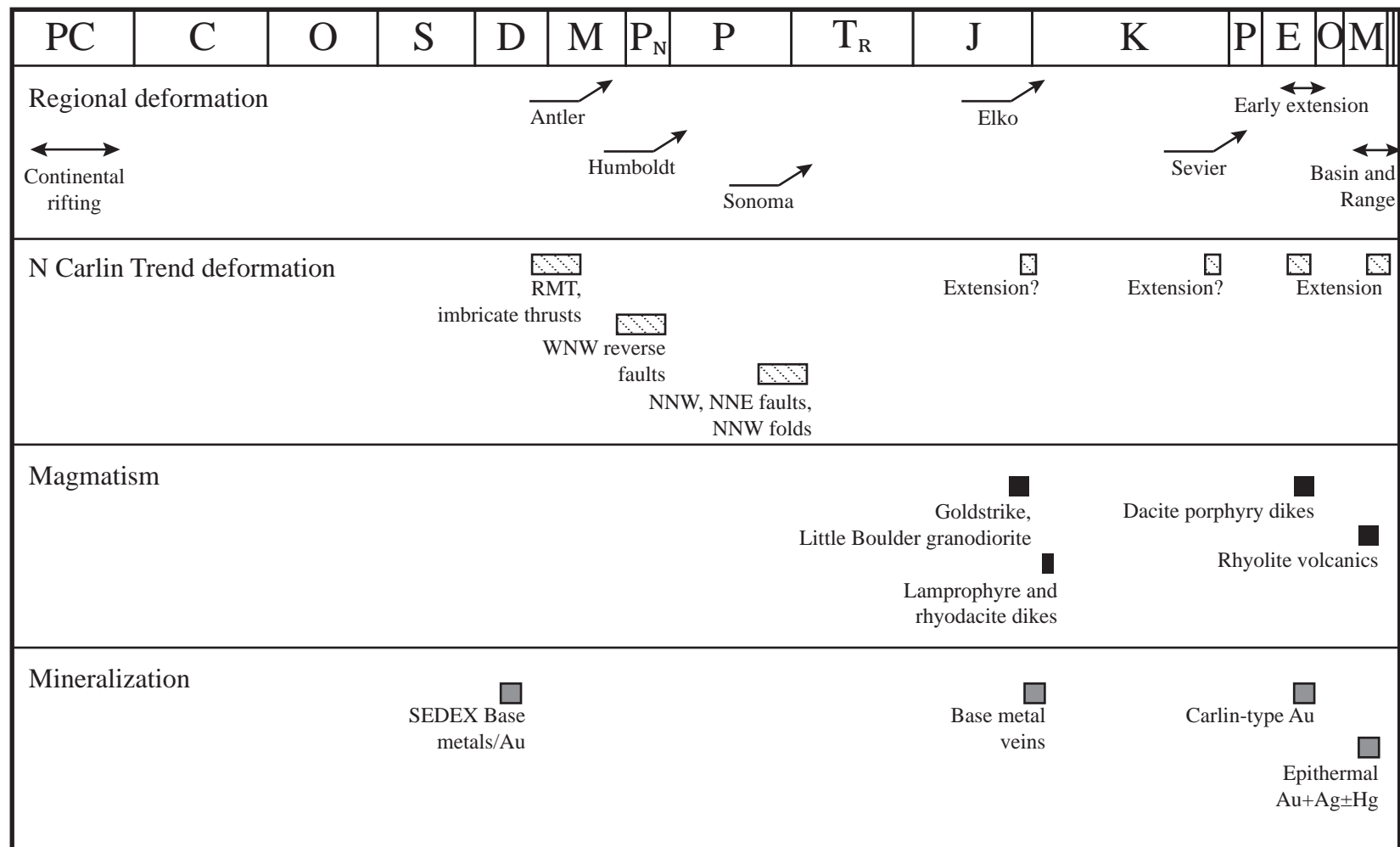


Figure 2.2 Summarised geological history of northern central Nevada, showing the timing of key deformational, magmatic and mineralization events that affected the northern Carlin Trend. Modified from Hofstra and Cline (2000) and Bettles (2002).

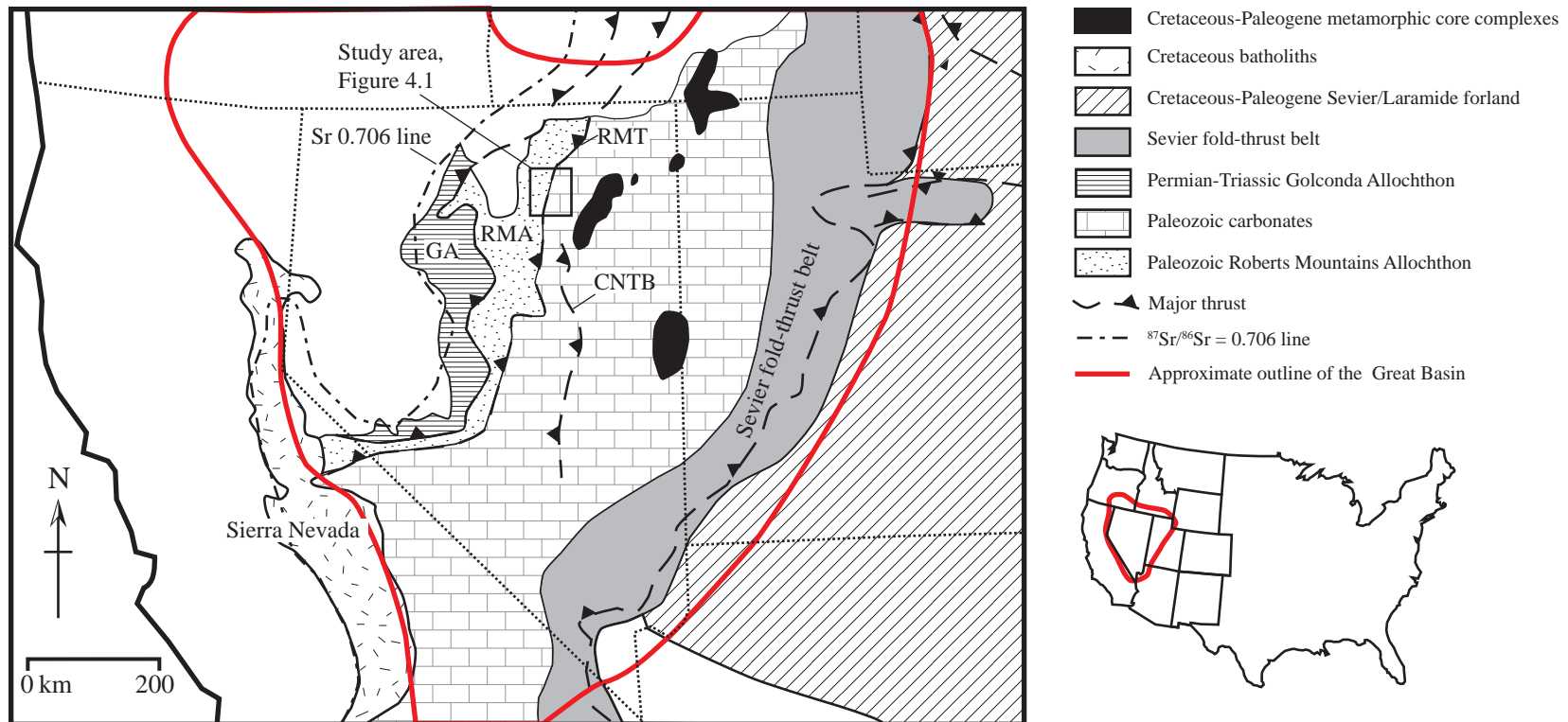


Figure 2.3 Map of the Great Basin showing main tectonostratigraphic regions discussed in the text. The study area in the box is shown in greater detail in Figure 4.1. The $^{87}\text{Sr}/^{86}\text{Sr} = 0.706$ line marks the edge of the Precambrian North American continent. RMT - Roberts Mountains Thrust, RMA - Roberts Mountains Allochthon, both features of the Late Devonian-Mississippian Antler Orogeny. GA - Golconda Allochthon, transported eastward to its present position during the Late Permian-Triassic Sonoma Orogeny. CNTB - the Early Cretaceous Central Nevada Thrust Belt. Based on Dickinson (2006) and Druschke et al. (2011).

Chapter 3: Thermochronology overview

Thermochronology has numerous applications in studies of timing and rate of tectonic events, landscape evolution and ore deposit formation. Thermochronometers record the cooling age of a rock, the time of cooling to below the closure temperature, T_c , of the thermochronometer system. Thermochronometers used in this study were apatite and zircon (U-Th)/He (AHe and ZHe respectively) and apatite fission track (AFT). Others include zircon fission track (ZFT) and $^{40}\text{Ar}/^{39}\text{Ar}$ dating. Thermochronometers can be combined with geochronometers such as U-Pb dating to describe the thermal history of a single rock sample from crystallization to the present day, as shown in Figure 3.1. Thermochronometers can also be combined to infer the exhumation history of a rock, as each system's cooling age records the timing of cooling through its respective closure isotherm (Figure 3.2).

3.1 Principles of low-temperature thermochronology

Thermochronology is based on the principle of radioactive decay, described by Rutherford in the early twentieth century as:

$$d = d_0 + N (e^{\lambda t} - 1)$$

where d and d_0 are the present day and original number of daughter nuclides, N is the present day number of parent nuclides, and λ is the decay constant of the parent nuclide. In thermochronology, d_0 is usually taken to be 0, since the abundance of daughter nuclides results only from decay that occurs after the mineral formed.

(U-Th)/He and fission track dating are based on radioactive alpha decay of ^{238}U that produces ^4He , and on spontaneous fission, which forms damage trails, referred to as fission tracks, in the crystal lattice. In (U-Th)/He dating, relative concentrations of ^{238}U and ^4He are measured to calculate a thermal age of apatite, zircon or titanite crystals (Farley et al., 1996;

Reiners et al., 2002; Harrison and Zeitler, 2005). In fission track dating, the ^{238}U content is measured and the number of fission tracks are counted as equivalents to daughter product (Gleadow and Duddy, 1981; Green et al., 1986; Donelick et al., 1990; Donelick et al., 2005). Importantly, thermochronology also relies on the thermally-sensitive removal of the daughter product from the crystal: ^4He escapes from the crystal by diffusion and fission tracks are thermally annealed. The rates of diffusion and annealing are largely a function of temperature.

In the case of U-Pb dating, the ratio of Pb to U is used to calculate the age of a mineral based on the assumption that all radiogenic Pb is retained in the host crystal. In thermochronology, the daughter products of decay are lost through thermally-sensitive processes (annealing and diffusion, discussed in sections 3.2.1 and 3.3.1), and so the age only represents time passed since the crystal cooled below a certain temperature, the T_c of the system.

The T_c of a system is defined as "its temperature at the time corresponding to its apparent age" (Dodson, 1973, p.259):

$$T_c = R/[E_a \ln (A\tau D_0/a^2)]$$

where R is the gas constant, E_a is activation energy, A is a numerical constant dependent on the geometry and decay constant of the parent, D_0 is the diffusion coefficient and a is the diffusion domain size. The time constant, τ , is related to cooling rate by:

$$\tau = R/(E_a dT^{-1}/dt) = -RT^2/(E_a dT/dt)$$

The T_c is therefore dependent on cooling rate, as well as grain size. The T_c falls within the partial retention zone, PRZ, the temperature range between open and closed system behaviour. At the high temperature limit of the PRZ, all daughter products are lost as they are produced and the system is open. At the low temperature limit, all daughter products are

retained and the system is closed and the amount of daughter product corresponds to the duration of accumulation. Between the upper and lower temperature limits, partial retention of daughter products occurs. The upper bound is equivalent to 10 % retention, at higher temperatures, and the lower bound equivalent to 90 % retention, at lower temperatures (and shallower crustal depth). In practice, the PRZ is collapsed to approximate the T_c to facilitate the interpretation of thermal history of a sample (Reiners and Brandon, 2006). An increase in cooling rate raises the T_c , as Figure 3.3a shows for apatite. Zircon displays similar behaviour (Reiners, 2005). Figure 3.3b shows the PRZ of apatite and zircon (U-Th)/He and AFT thermochronometers. At cooling rates of 1-10°C/Myr, T_c ranges ~50-60°C, 90-110°C and 160-180°C for AHe, AFT and ZHe respectively.

3.2 Apatite fission track dating

Fission track dating is most commonly applied to apatite (AFT) and zircon (ZFT). Many of principals of fission track dating apply to both apatite and zircon, however as only AFT was used in this study, only AFT dating is discussed here in detail. Details of ZFT thermochronology can be found in reviews by Tagami and O'Sullivan (2005) and Tagami (2005).

Fission tracks are damage trails in a crystal lattice formed by spontaneous fission of ^{238}U (and ^{232}Th and ^{147}Sm). In apatite, new fission tracks are typically less than 20 μm long and 6-10 nm wide (Paul and Fitzgerald, 1992). Tracks form at a constant rate but are shortened over time by the thermally-sensitive process of annealing. In apatite this occurs over a range of 20-150°C on geological timescales ($>10^6$ Ma) (Gleadow and Duddy, 1981; Donelick et al., 1990). The number of fission tracks is related to the time passed since fission track formation and the

rate of annealing. Heating to sufficient temperature removes fission tracks and resets the AFT age of an apatite crystal (Naeser and Faul, 1969; Gleadow and Duddy, 1981).

3.2.1 Annealing

Annealing of fission tracks is controlled dominantly by temperature. A study of down hole annealing behaviour in a deep drill hole in the Otway Basin, Victoria, Australia, showed that fission track annealing in apatites increases with temperature and follows an Arrhenius relationship (Gleadow and Duddy, 1981). Figure 3.4 shows data from that study, with track length reduction with increasing temperature (and increasing depth).

Annealing is also controlled by crystallographic orientation and kinetic properties of the crystal. Studies by Donelick et al. (1999) and Ketcham (2003) have shown that annealing is more rapid parallel to the c-axis in apatite. Track lengths are commonly reprojected to an equivalent c-axis parallel length to reduce scatter in track length data following models of Donelick et al. (1999) and Ketcham (2003).

Kinetic properties are controlled by apatite chemistry, in particular relative F, Cl, OH content and to a lesser extent Mn, Fe and possibly REE content (Carlson et al., 1999; Barbarand et al., 2003). The most commonly measured kinetic parameters are Cl wt% (or Cl apfu) and Dpar, the fission track etch pit diameter parallel to the crystallographic c-axis at the apatite surface (Donelick, 1993b; Donelick et al., 2005). Apatites with a high Cl content (>1-2 wt%) typically anneal more slowly than those with lower Cl content, although very high concentrations of Mn, Fe and or OH may cause this to vary (Carlson et al., 1999). Apatite composition was investigated as part of this study to observe any variations in chemistry within single samples and from sample to sample, and to assess the effect these variations might have on the AFT data collected. This work is presented as part of Chapter 6, which also explores the

possible effects of hydrothermal fluids on apatite in the Jurassic intrusions of the northern Carlin Trend.

Dpar is not a proxy for Cl wt%, although there is usually a positive correlation between Dpar and Cl wt% and OH%, and a negative correlation between Dpar and F wt% (Donelick, 1993a; Burtner, 1994; Donelick et al., 2005). Low Dpar ($\leq 1.75 \mu\text{m}$) apatites tend to anneal rapidly (Carlson et al., 1999). Apatites with higher Dpar ($> 1.75 \mu\text{m}$) anneal more slowly.

3.2.2 Fission track length distribution

Examining fission track length distributions allows more detailed interpretation of the thermal history of a sample than the fission track age alone. Figure 3.5 shows several fission track length distributions and their inferred thermal histories described in Galbraith (2005). Rapid cooling from high to low temperature typically produces a unimodal, symmetrical length distribution of long fission track lengths ($\geq 15 \mu\text{m}$). Slow cooling generates a unimodal, asymmetrical distribution around a lower mean length (Galbraith, 2005). Older tracks have experienced more heating so are shorter than more recently-formed (and therefore longer) tracks, which results in an asymmetric fission track length distribution. Shorter track lengths, e.g., Figure 3.5c, suggest gradual heating until the present day, maintaining a typical symmetrical track length distribution but around a lower mean length. A bimodal distribution (Figure 3.5d) results from multiple heating and cooling events: tracks formed prior to reheating are partially annealed but those that formed since reheating are not significantly annealed because they have remained below the lower bound of the PRZ for most of their existence. Modelling software packages such as AFTSolve (Ketcham, 2000) and HeFTy (Ketcham, 2005; Ketcham, 2009) have been developed to incorporate fission track length, single grain age and kinetic data to facilitate interpretation of possible thermal histories of a sample.

In the present study, fission track lengths were projected as c-axis parallel lengths, which has been shown to reduce the spread and asymmetry of fission track lengths in a sample (Donelick et al., 1999; Ketcham, 2003). Projection removes the effects of anisotropic annealing, which occurs fastest parallel to the c-axis, thus removing variation that is due to anisotropic track length reduction and allowing better interpretation of track length distributions as related to the thermal history of the sample (Donelick et al., 1999; Ketcham et al., 1999; Ketcham et al., 2009).

3.2.3 AFT age calculation

The age of a single apatite crystal is calculated based on the density of fission tracks (i.e., number of fission tracks per unit area) as the daughter product, and the concentration of ^{238}U as the parent. Fission tracks are counted using an optical microscope at 1500-1600x magnification in 20-40 crystals per sample, yielding 10s-100s of counted spontaneous tracks, N_s . The concentration of ^{238}U is determined by measurement of ^{235}U and the constant $^{238}\text{U}/^{235}\text{U}$ ratio. The concentration of ^{235}U is measured in one of two ways, 1. by the external detector method (EDM) or 2. by laser ablation inductively coupled plasma mass spectrometry (LA-ICP-MS).

3.2.3.1 EDM and single grain age calculation

EDM involves thermal irradiation of a sample, which induces fission of ^{235}U and leaves damage trails in an external detector, a muscovite plate in direct contact with the internal polished face of the apatite crystal being dated (Figure 3.6). The number of induced fission tracks, N_i , on the external detector is counted as a proxy for ^{235}U content. EDM was used to generate some pre-existing data used as a background to this study in Chapter 4 (e.g.

Chakurian et al., 2003; Hickey, 2005, 2007). A thorough review of EDM is given in Tagami (2005) and Galbraith (2005).

The single grain age, t_i , of an apatite crystal dated using the EDM is given by:

$$t_i = \frac{1}{\lambda_d} \ln \left(1 + \lambda_d \xi g \rho_d \frac{\rho_{s,i}}{\rho_{i,i}} \right)$$

where i is grain i , λ_d is the decay constant of ^{238}U , ξ is a calibration factor based on EDM of fission track standards, g is a geometry factor, ρ_d is the induced fission track density for a U standard irradiated with the sample, $\rho_{s,i}$ is the spontaneous fission track density in grain i based on the number of spontaneous fission tracks counted (N_s) over area Ω_i , and $\rho_{i,i}$ is the induced fission track density in the corresponding Ω_i in the external detector in which induced fission tracks (N_i) are counted.

The symmetrical error, σ_i , of the EDM single grain AFT age is a function of the number of spontaneous fission tracks, analytical error and normal Poissonian variation on the N_i . The σ_i of the EDM single grain AFT age is calculated as:

$$\sigma_i = \left[\frac{1}{N_{s,i}} + \frac{1}{N_{i,i}} + \frac{1}{N_d} + \left(\frac{\sigma_\xi}{\xi} \right)^2 \right]^{1/2}$$

where N_d is the number of fission tracks counted to determine ρ_d in the single grain age calculation.

3.2.3.2 LA-ICP-MS and single grain age calculation

The alternative method for ^{238}U measurement is by volume concentration by LA-ICP-MS, which allows direct measurement of ^{238}U (Hasebe et al., 2004; Donelick et al., 2005). This method was used for samples dated during this study.

The single grain age, t_i , of an apatite crystal dated using LA-ICP-MS is given by:

$$t_i = \frac{1}{\lambda_d} \ln \left(1 + \lambda_d \xi_{MS} g \frac{\rho_{s,i}}{P_i} \right)$$

where ξ_{MS} is a calibration factor and $P_i = (^{238}\text{U}/^{43}\text{Ca})$ for grain i .

The symmetrical error, σ_i , of the LA-ICP-MS single grain AFT age is a function of the number of spontaneous fission tracks and the analytical error in determining ^{238}U concentration, and is calculated as:

$$\sigma_i = \left[\frac{1}{N_{s,i}} + \left(\frac{\sigma_{P_i}}{P_i} \right)^2 + \left(\frac{\sigma_{\xi_{MS}}}{\xi_{MS}} \right)^2 \right]^{1/2}$$

3.2.3.3 Sample AFT ages

A sample AFT age is calculated by combining the ages of a population of single grains. A single grain age has a relative standard error (RSE) of around 12% in zircon and 50% in apatite, but ages are combined to give a statistically valid pooled age with a reduced RSE of 5-10% (Reiners and Brandon, 2006). The pooled age assumes there is a single population of grains (in terms of source and kinetics) with a common age and common thermal history. Variation in single grain ages in a single population results from Poissonian probability of fission track-forming events in a crystal (Galbraith, 2005). The χ^2 test is routinely applied to evaluate a sample's homogeneity. A χ^2 probability ≥ 0.01 signifies a concordant population, i.e. a normal Poissonian variation in grain ages is observed, suggesting the sample is consistent with a single population sharing a common age. A χ^2 probability < 0.01 suggests the single grain ages are discordant, i.e. more than one population is present in the sample. A χ^2 probability < 0.01 may also occur if insufficient data is available, e.g., track counts are low or only a few grains were available for analysis. Initial examination of AFT track and grain counts quickly reveals if this is the case. Multiple populations are common in detrital samples,

where grains have been transported from several different sources. Multiple populations are also possible in igneous samples, where variation arises not from the source of crystals but from the kinetic properties of crystals within a single sample. Even within a single hand sample, significant chemical, and therefore kinetic, variability can be observed (O'Sullivan and Parrish, 1995).

Dispersal can also be examined graphically using a radial plot, which allows comparison of data with different precisions, in this case individual grain ages with different precisions (Galbraith, 1990; Galbraith, 1994). An example radial plot is shown in Figure 3.7.

3.3 (U-Th)/He dating

(U-Th)/He dating is used to date both apatite and zircon, and is based on the principal of radioactive decay of naturally-occurring ^{238}U and ^{232}Th by alpha decay. Alpha decay involves the release of an alpha particle, equivalent to a ^4He atom, during each decay event. Typical U concentration is 20-200 ppm in apatite and 100s to 1000s ppm in zircon (Harrison and Zeitler, 2005).

The ^4He produced by alpha decay is trapped within the host apatite or zircon. The ratio of ^4He to ^{238}U and ^{232}Th within an individual crystal reflects the time passed since ^4He accumulation began. The amount of ^4He produced in a given time, t , is dependent on the decay constants of ^{238}U ($1.55125 \times 10^{-10} \text{ yr}^{-1}$), ^{235}U ($9.8485 \times 10^{-10} \text{ yr}^{-1}$) and ^{232}Th ($4.916 \times 10^{-11} \text{ yr}^{-1}$) (Steiger and Jäger, 1977), and is described by (Farley, 2002) as:

$$^4\text{He} = 8^{238}\text{U}(e^{\lambda_{238}t} - 1) + 7\left(\frac{^{235}\text{U}}{137.88}\right)(e^{\lambda_{235}t} - 1) + 6^{232}\text{Th}(e^{\lambda_{232}t} - 1)$$

Retention of ^4He is a temperature-sensitive process controlled predominantly by diffusion. If the temperature of the crystal exceeds the T_c , ^4He diffuses out of the crystal, resetting the system (Dodson, 1973).

3.3.1 Diffusion behaviour of helium

The diffusion rate of ^4He is temperature dependent, increasing at higher temperatures. The effect of temperature on diffusion rate follows an Arrhenius relationship in both apatite and zircon (Zeitler et al., 1987; House et al., 1999; Farley, 2002; Reiners, 2005), as shown in Figure 3.8.

$$D = D_o e^{-E_a/RT} \quad (4)$$

where D is He diffusivity and other parameters are defined above. Simple He diffusion results in a linear plot of $\ln D/a^2$ as a function of $1/T$. A non-linear plot indicates that more complex diffusion behaviour is occurring, resulting from multiple diffusion mechanisms or multiple diffusion domains (Farley, 2002). In the earliest stages of heating, zircon displays non-Arrhenius behaviour, with excessive diffusivity possibly resulting from localised zones of high diffusivity, crystallographic anisotropy or inhomogeneous distribution of He (Reiners et al., 2004). In addition to temperature, the ^4He loss from a crystal also depends on crystal size and shape (Farley, 2002; Reiners, 2005), ejection of alpha particles, and U and Th content and distribution of radiation damage, each described below.

3.3.2 Crystal size and shape

Step heating experiments by (Farley, 2000) showed that diffusivity decreases with increasing grain size, suggesting the whole grain is the effective diffusion domain. This is

unlike $^{40}\text{Ar}/^{39}\text{Ar}$ dating, which commonly has multiple diffusion domains (Lovera et al., 1991; Lovera et al., 1997; Lovera et al., 2002). Farley (2002) also showed that diffusion of He from apatite is essentially isotropic. Given the hexagonal prism shape of a typical apatite crystal, He loss most significant perpendicular to the crystallographic c-axis, so an infinite cylinder is the most appropriate approximation for shape when estimating He loss (Farley, 2002). The diffusion domain radius, a , can be taken as the half-width of the crystal. Larger grains therefore yield higher T_c estimates. Figure 3.9 shows how T_c varies with cooling rate and half width prism in apatites.

3.3.3 Alpha-ejection corrections

Alpha particles travel approximately 20 μm in an apatite crystal (Farley et al., 1996) and 17-20 μm in zircon (Reiners, 2005). This means that ^4He produced by alpha decay can potentially escape from the outer 20 μm of a crystal (Figure 3.10), or be added by surrounding grains. Experiments by Farley (2002) showed that implantation of ^4He is not a significant factor, except in unusually U or Th-poor crystals, or where surrounding grains are highly radioactive. ^4He loss from the crystal rims is a factor in age calculation, however.

An "alpha-ejection correction" is applied to all raw ages to account for ^4He loss from the crystal rim. The correction depends on the size, shape and U-content of a crystal. Crystal size is important as larger crystals have a greater surface area-to-volume ratio and are less sensitive to alpha ejection. The U and Th content and distribution must also be considered, as more ^4He is trapped from decay of U and Th in the core of a crystal than from decay of U and Th within 20 μm of its edge. Figure 3.10 shows how a crystal rim is relatively depleted in ^4He due to alpha ejection. Farley et al. (2002) modelled the retained fraction of ^4He (F_{He}) in apatites of different sizes assuming an even distribution of U and Th for an idealised hexagonal prism crystal

geometry. F_{He} values are calculated as follows, taking into account crystal morphology, size and Th and U content:

$$F_{\text{He}} = 1 + A_1\beta + A_2\beta^2 \quad (5)$$

Bulk F_{He} for the crystal is calculated by:

$$\hat{F}_{\text{He}} = a_{238} {}^{238}\text{U} F_{\text{He}} + (1 - a_{238}) {}^{231}\text{Th} F_{\text{He}} \quad (6)$$

and

$$a_{238} = (1.04 + 0.245(\text{Th}/\text{U}))^{-1} \quad (7)$$

where factors A_1 and A_2 are experimentally derived values given in Table 3.1 and β is the surface-area-to-volume ratio of the crystal, calculated using the formulas shown in Table 3.2.

The raw, uncorrected He age of a single crystal, t' , is corrected for loss of ${}^4\text{He}$ by ejection to give a corrected age, t , by:

$$t = t' / F_{\text{He}} \quad (8)$$

A sample age is taken as the average corrected age of at least three crystals. Corrections include alpha ejection corrections as well as zoning corrections in the case of zircon (discussed below).

F_{He} values for apatites 75 – 170 μm wide typically range from 0.65-0.85 (Farley, 2002). F_{He} is less for smaller crystals, as almost all of the crystal is within 20 μm of its edge, and so potential for ${}^4\text{He}$ loss is higher. Crystals smaller than 60 μm are therefore avoided. Larger crystals (>300 μm) are rarely examined because total ${}^4\text{He}$ extraction is difficult to ensure because the diffusion domain is so large, and they can be hard to dissolve entirely for U and Th analysis. Alpha ejection corrections are essential, as reported errors are up to 15-33 % when corrections are not applied (Ehlers and Farley, 2003). Other sources of error include mineral inclusions, such as U and Th-bearing minerals zircon or monazite, which contribute ${}^4\text{He}$ to the

crystal but are not dissolved along with apatite during preparation for U and Th analysis. Mineral inclusions therefore contribute "parentless" ^4He to the host apatite crystal without measurement of parent U and Th, leading to an overestimation of cooling ages (Farley, 2002). The presence of mineral inclusions is generally not a problem in ZHe dating, since the zircon dissolution process dissolves any inclusions, so all parents of ^4He are accounted for.

For zircon, the assumed crystal geometry is a tetrahedral prism, with either pinacoidal terminations (Farley, 2002) or pyramidal terminations (Hourigan et al., 2005). Farley (2002) assumes a tetragonal prism with pinacoidal terminations simplified to a prolate sphere, whereas Hourigan et al. (2005) require measurement of zircon tips, which are more commonly bipyramidal, and so produce more realistic estimates of volume and surface area. F_{He} values for crystals 75-170 μm have a similar range to apatites (Hourigan et al., 2005). For the same reasons that apply to apatites, crystals smaller than 60 μm and larger than 300 μm are avoided.

3.3.4 Zoning

Dispersed single grain ages are commonly observed within a single sample. There are several reasons why this variation may occur, including the size of the crystals, presence of inclusions, radiation damage and compositional zoning (Reiners, 2005). Hourigan et al. (2005) investigated the effects of U and Th zoning in ZHe dating. They found that alpha correction, which does not take zoning into account, can bias an age calculation by up to ~30%. Figure 3.11 shows age bias calculated by Hourigan et al. (2005) for zircon crystals with different size rims and different relative enrichment and depletion of rim to core. Zoning effects in apatite have been recognised for the AHe dating system, but have not been quantified as for ZHe dating (Farley et al., 1996).

3.3.5 Radiation damage

Ideally, crystals with obvious signs of radiation damage e.g., discoloration, are avoided. Radiation damage can be imaged using Raman spectroscopy, cathodoluminescence (CL) and back-scattered electron (BSE) imaging (Nasdala et al., 2006). Nasdala et al. (2004) reported that radiation damage only becomes significant in high U zircon, when radiation doses are over $2.5\text{--}3.0 \times 10^{18} \alpha/\text{g}$ and a crystal is held at low enough temperatures for long periods of time to preclude annealing. Zircons that have significant radiation damage experience greater He loss than those with similar thermal histories but less damage (Nasdala et al., 2004).

Radiation damage has been shown to impede He diffusion in apatite, resulting in calculation of anomalously old ages and an increase in T_c (Shuster et al., 2006; Flowers et al., 2009; Shuster and Farley, 2009). Radiation damage can form He traps, which increase retention rather than provide escape pathways as fractures may do (Shuster et al., 2006). The amount of radiation damage in a crystal changes with time, as it is a temperature-sensitive processes involving thermal annealing and recovery of crystal lattice, the same process that is responsible for the annealing of fission tracks (Flowers et al., 2009; Shuster and Farley, 2009). At high temperatures, radiation damage is therefore removed, restoring normal diffusive properties to the crystal.

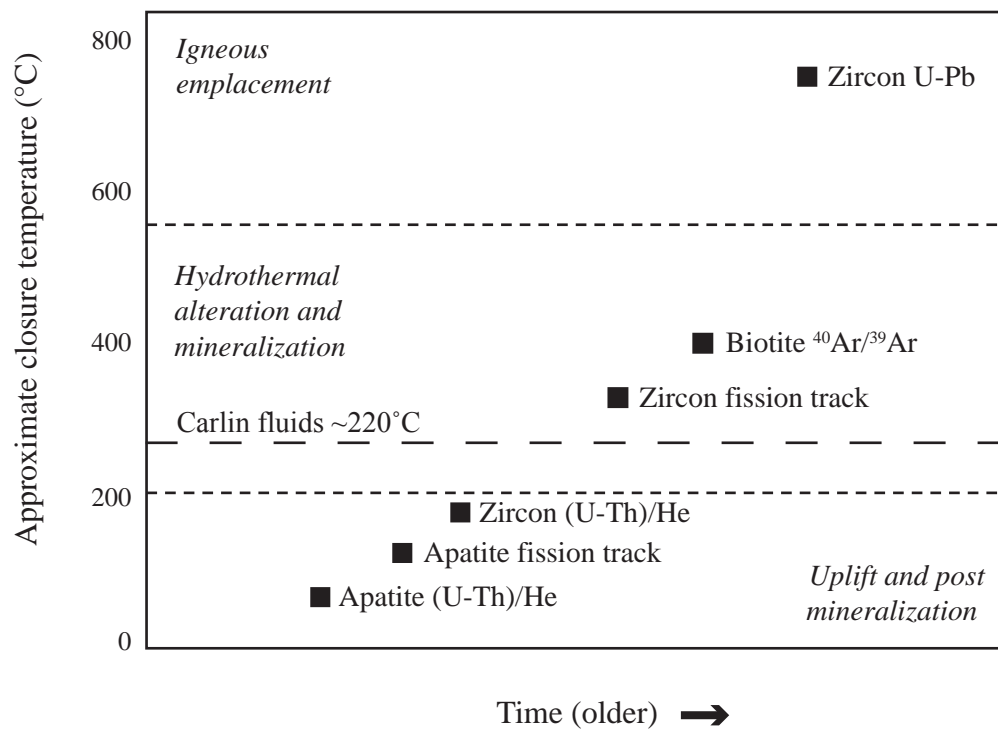


Figure 3.1 Approximate closure temperatures of select thermochronometers. Different thermochronometers have different closure temperatures so combining them allows reconstruction of a thermal history of a single sample. Based on McInnes et al. (2005).

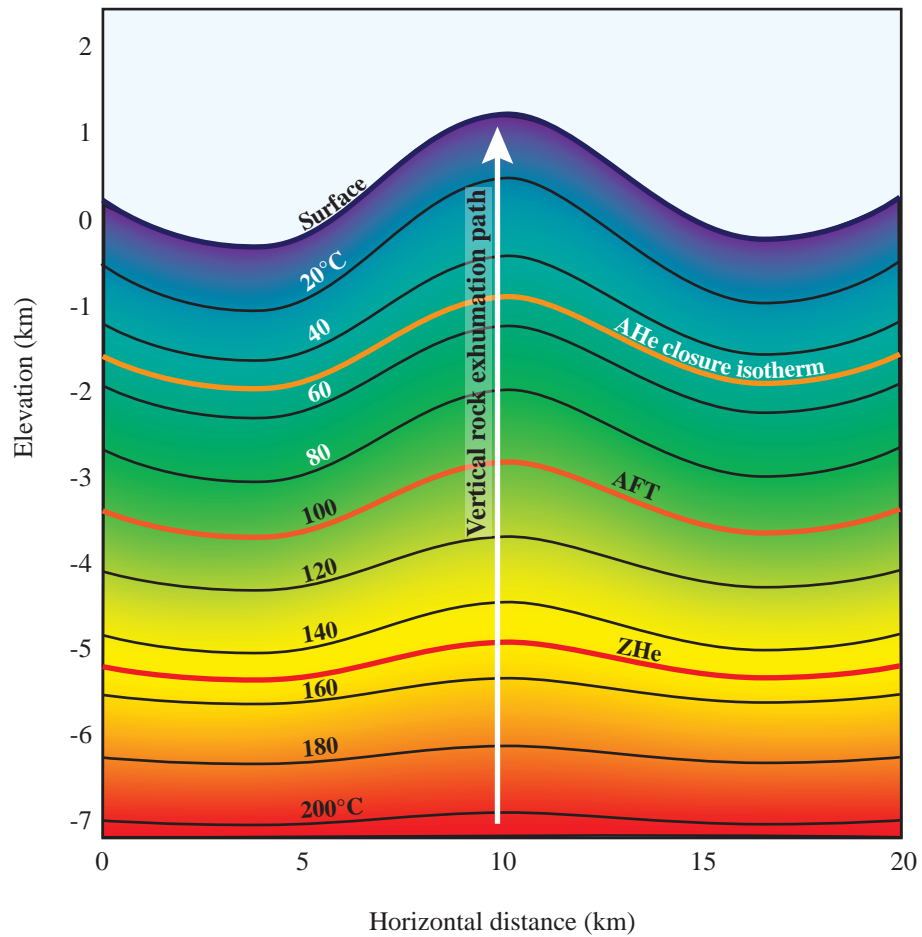


Figure 3.2 Schematic illustration of the thermal structure of the shallow crust showing isotherms and closure isotherms for AHe, AFT and ZHe. Closure isotherms are the isotherm at the closure temperature, T_c , of each thermochronometer, in this case shown for slow cooling rates of $1^\circ\text{C}/\text{Myr}$. The depth of each closure isotherm depends on the geothermal gradient, in this illustration $30^\circ\text{C}/\text{km}$. Estimates for the Cretaceous geothermal gradient in northern central Nevada range $30\text{--}60^\circ\text{C}/\text{km}$. A higher geothermal gradient results in shallower and closer-spaced closure isotherms. As a rock is exhumed towards the surface, it cools and passes through each closure isotherm. The age of that system records the time when the rock passed through that closure isotherm. The wavelength of topography determines the depth to which isotherms are disturbed. After Reiners and Shuster (2009).

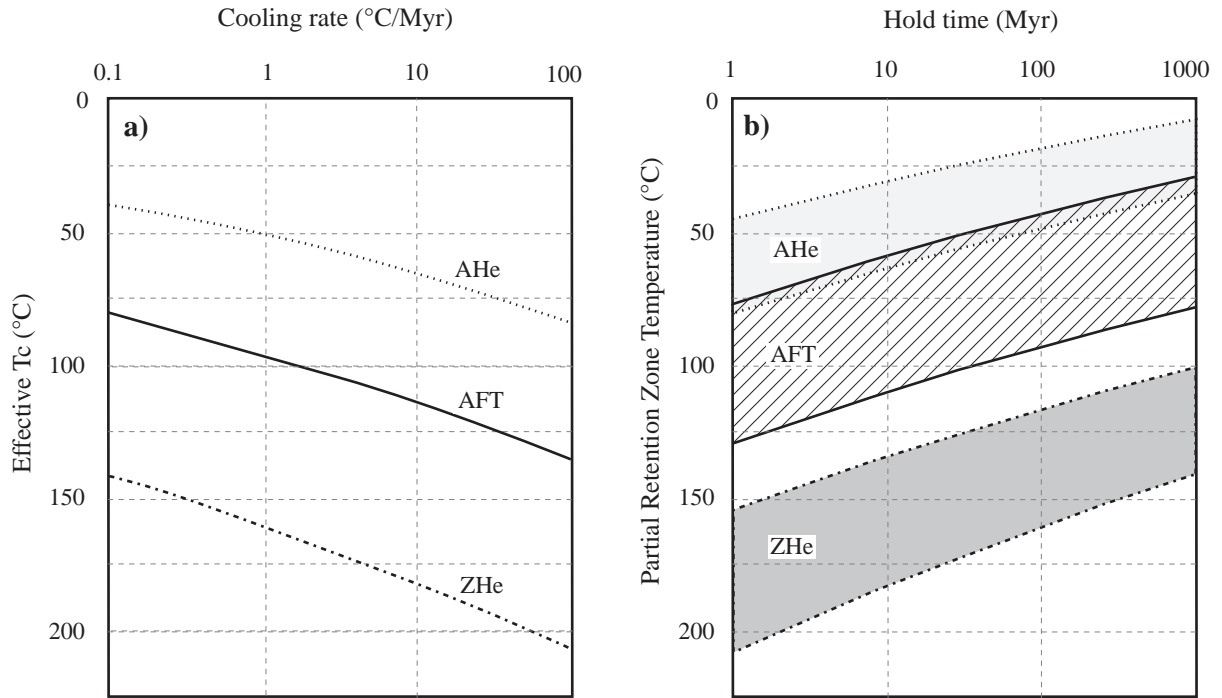


Figure 3.3 a) The effect of cooling rate on closure temperature (T_c) for apatite (AHe) and zircon (ZHe) (U-Th)/He and AFT ages. A higher cooling rate results in an increase in T_c . Modified from Reiners and Brandon (2006). **b)** Temperature range of the Partial Retention Zone (PRZ) changes with hold time for AHe, AFT and ZHe. Longer hold times require lower temperatures to cause resetting. The higher temperature limit for each thermochronometer defines the temperature required to cause 90% resetting, the lower temperature limit defines 10% resetting. Modified from Reiners and Brandon (2006).

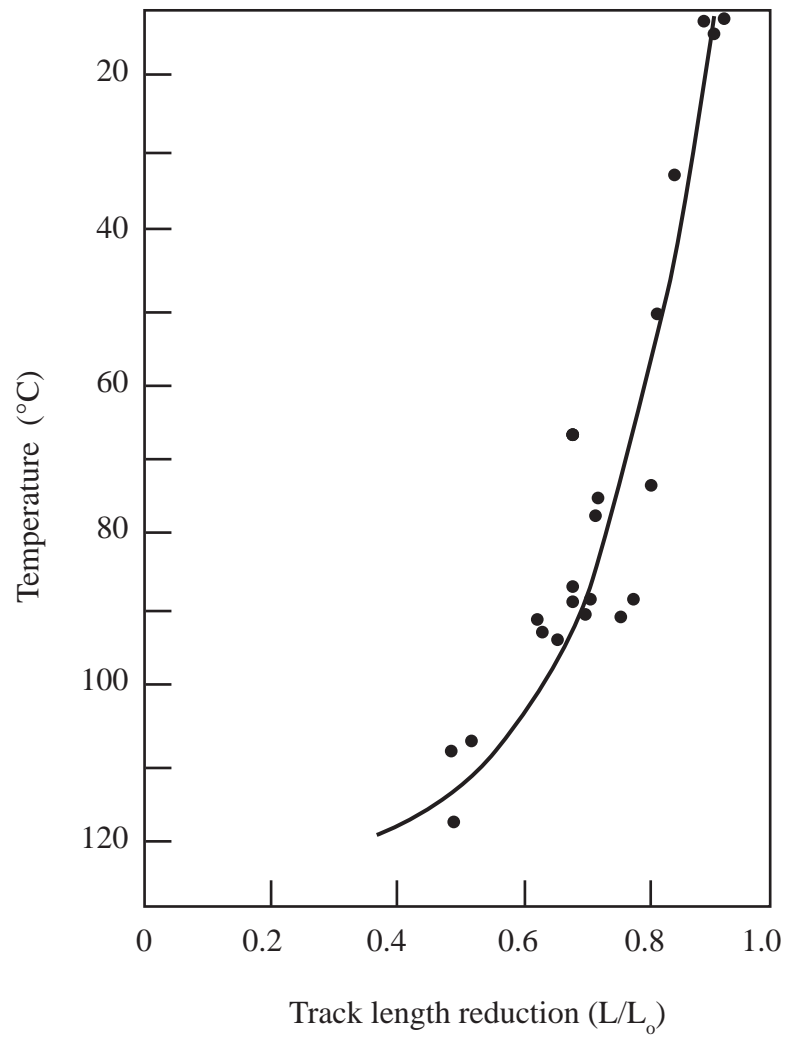


Figure 3.4 Variation in mean track length downhole in deep Otway Basin drillholes. MTL decreases downhole as depth and temperature increase. The rate of fission track annealing increases with temperature. Mean track length, L , is expressed as a fraction of L_0 , the mean length of induced fission tracks, which have not been shortened by annealing. From Gleadow and Duddy (1981).

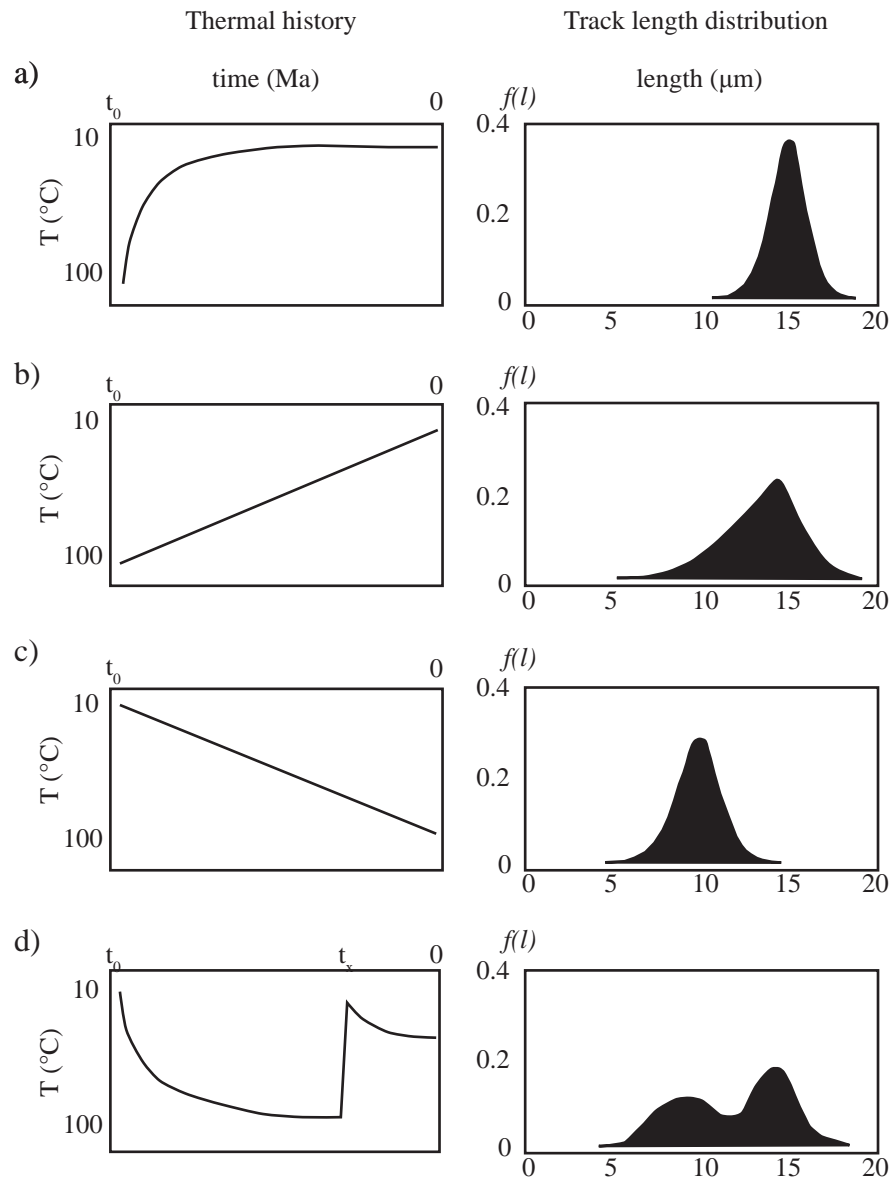
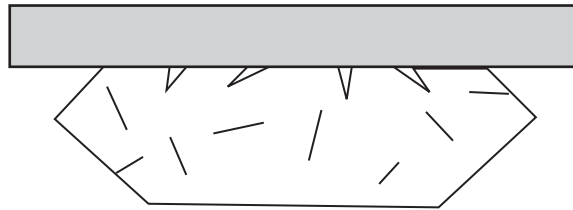
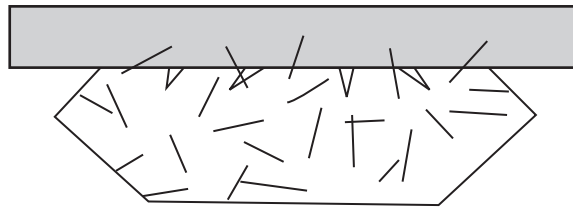


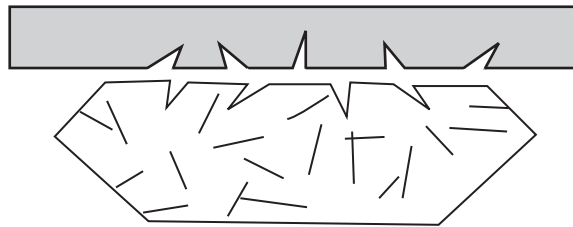
Figure 3.5 Example thermal histories and idealised, non-projected fission track length distributions. a) Rapid cooling to present day temperature, T ; symmetrical around relatively long fission track length. b) Slow cooling to present T ; asymmetric distribution. c) Slow heating to maximum T at present, symmetrical around shorter fission track length. d) Reheating to high T at time t_x followed by rapid cooling and subsequent reheating; bimodal fission track length distribution. $f(l)$ is relative frequency of fission track lengths. After Laslett et al. (1994) and Glabraith (2005).



Muscovite external detector (ED) is attached to the polished, etched internal surface on an apatite crystal.



The ED and apatite crystal are irradiated together to induce fission of ^{235}U , creating new fission tracks in both the ED and apatite crystal.



The induced tracks are etched to increase visibility and ρ_s and ρ_i are measured

Figure 3.6 The external detector method (EDM) involves irradiation of a muscovite external detector (ED) and polished, etched apatite crystal in direct contact with one another. Spontaneous fission of ^{235}U forms new, induced FTs. Modified from Tagami and O'Sullivan (2005).

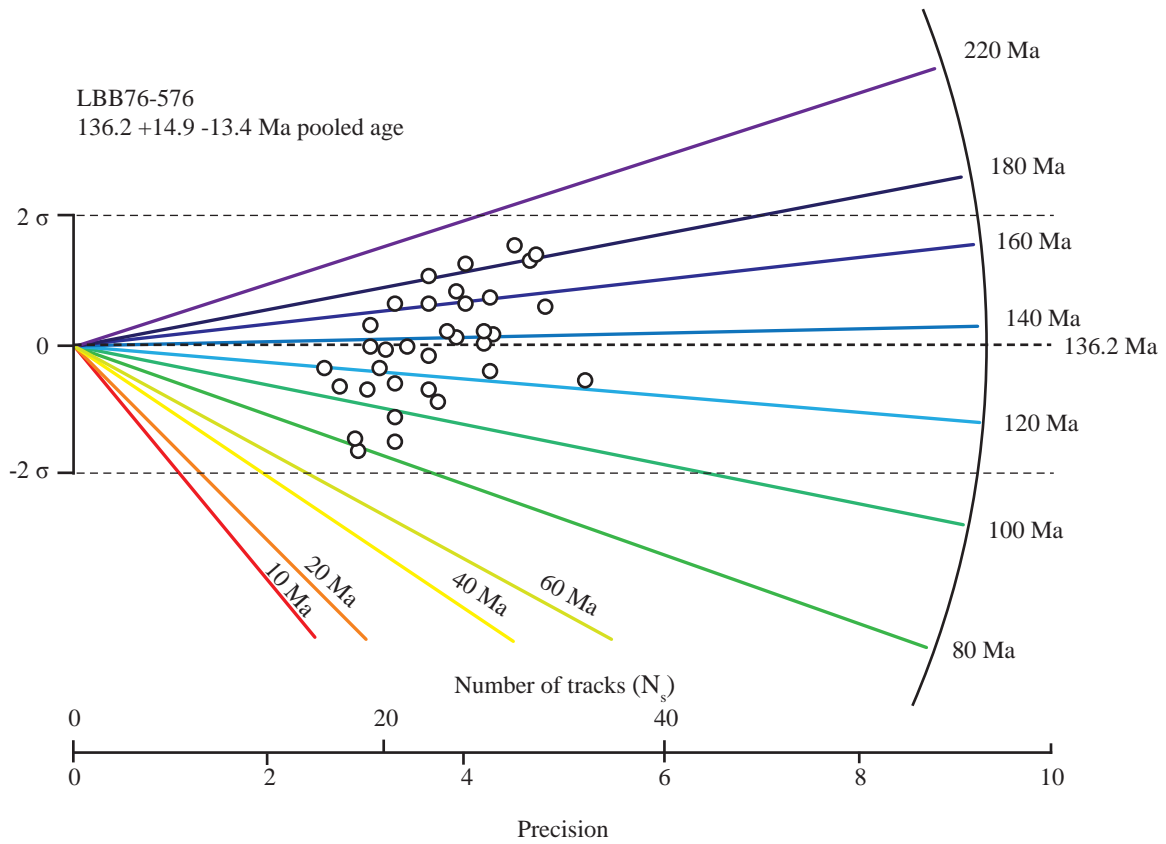


Figure 3.7 Example radial plot of single grain AFT ages. Ages are read by extrapolating a line from 0,0 through a plotted point to the age scale. An increased number of tracks (N_s) increases precision. In this case all points lie between -2σ and $+2\sigma$, so this sample is not overdispersed and all single grain ages are consistent with a concordant pooled age of 136.2 Ma.

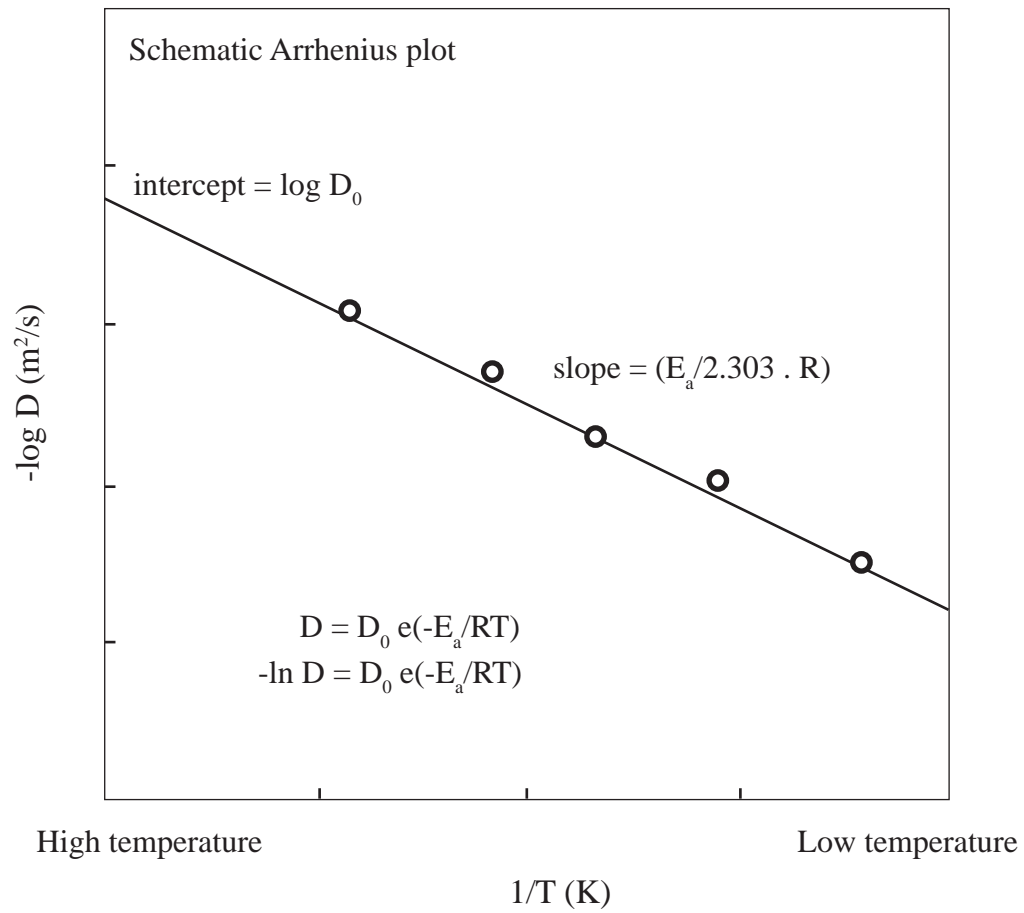


Figure 3.8 Schematic plot showing the Arrhenius relationship between temperature and diffusion rate based on experimental data. D is the diffusion coefficient, D_0 is the diffusion coefficient at infinite temperature, E_a is the molar activation energy, a is the length scale of the diffusion domain (usually the size of the whole crystal), R is the gas constant, and T is absolute temperature. From Harrison and Zeitler (2005)

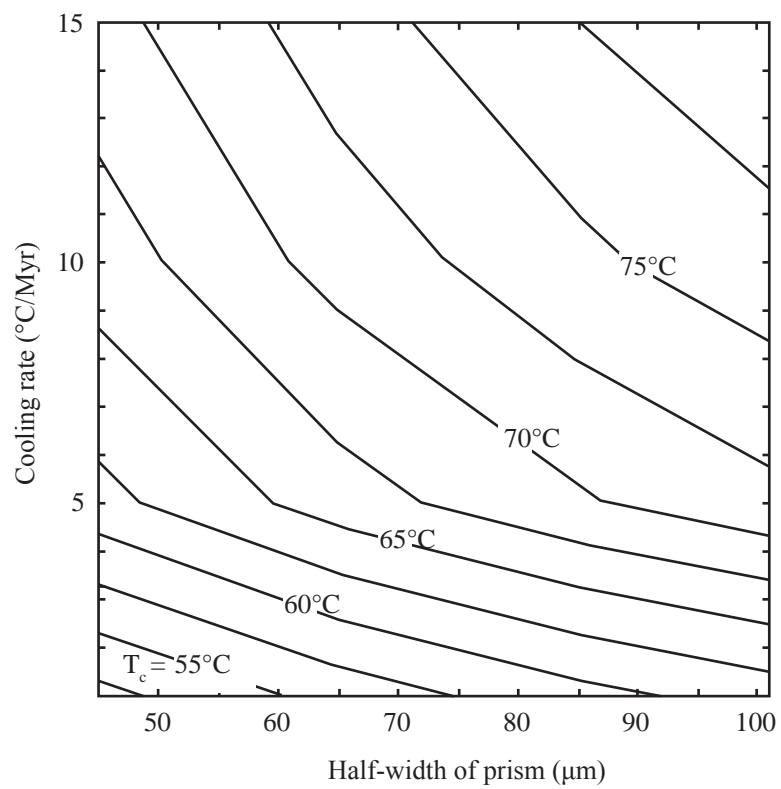


Figure 3.9 T_c in apatite as a function of cooling rate and crystal size assuming $E_a = 138$ kJ/mol and $D_o = 50$ cm²/s. Based on Farley (2000, 2002).

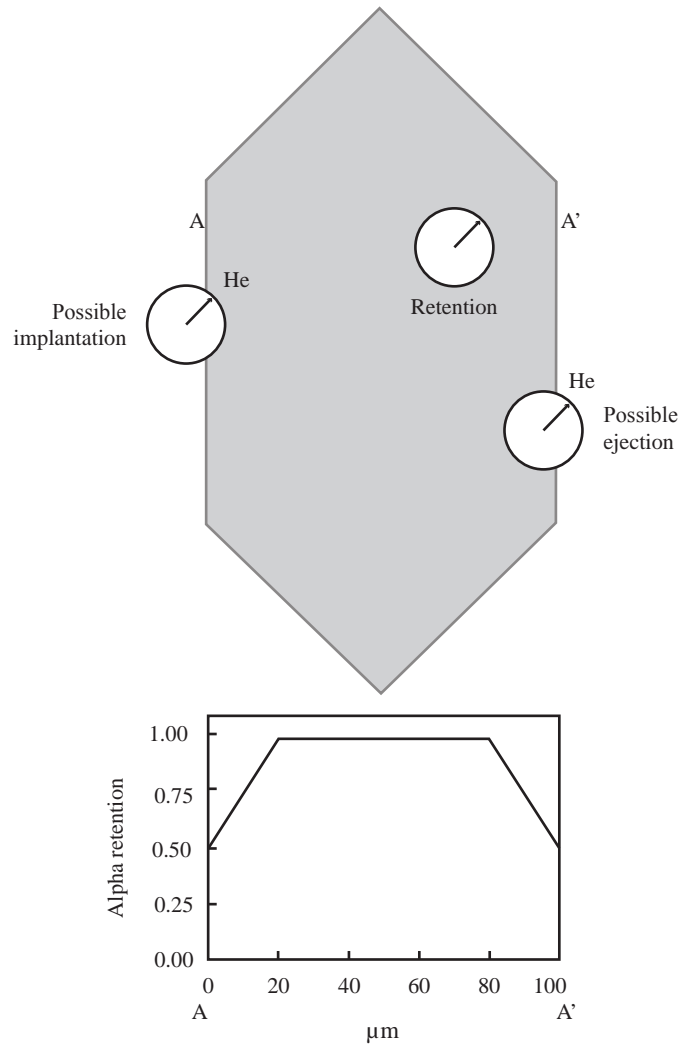


Figure 3.10 Schematic diagram of alpha ejection and ^4He concentration across an apatite crystal. ^4He produced in the outer 20 μm of an apatite crystal ($\sim 17 \mu\text{m}$ in zircon) may be lost by alpha ejection. ^4He produced away from the edge of the crystals will be retained within the crystal. Zoning of U-Th affects where ^4He is produced. In a crystal with a U-Th-rich rim, for example, the majority of ^4He is produced in the edge, increasing the likelihood of ^4He loss. From Dunai (2005) and Farley (2002).

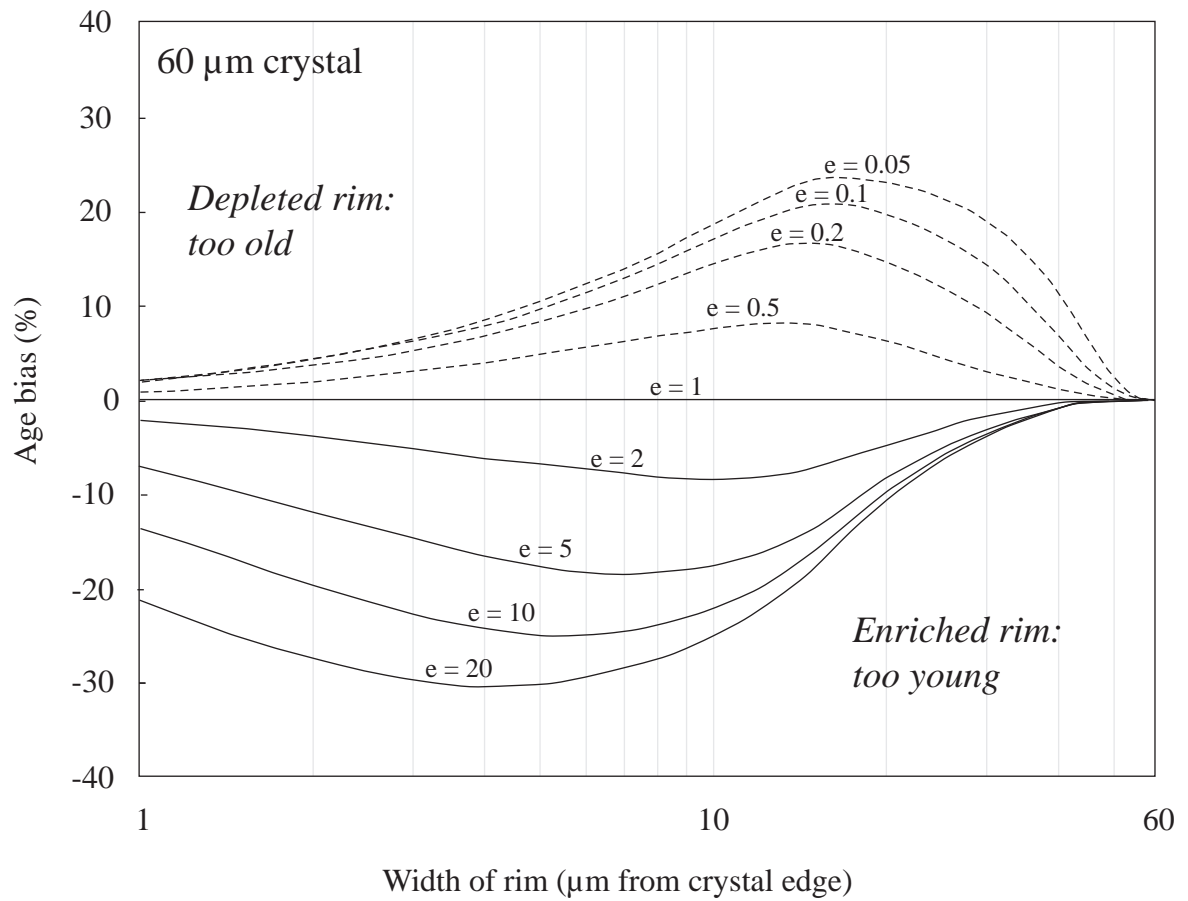


Figure 3.11 Age bias effects of normal alpha ejection corrections applied to zoned zircons. Age bias is shown in per cent for relative enrichment ($e > 1$) and depletion ($e < 1$) values of U in different rim sizes calculated by Hourigan et al. (2005). Normal alpha ejection corrections applied to zircons with relatively U-enriched rims lead to underestimation of (U-Th)/He age. Corrections applied to zircons with relatively U-depleted rims result in overestimation of age. Modified from Hourigan et al. (2005).

Table 3.1 Factors A_1 and A_2 for calculating F_{He} for apatite and zircon for different crystal shapes for ^{238}U and ^{232}Th . Compiled from Farley (2002) and Hourigan et al. (2005). * denotes used in this study.

Crystal geometry	Decay series	A_1	A_2
Apatite hexagonal prism (Farley, 2002)	^{238}U	-5.13	6.78
	^{232}Th	-5.90	8.99
Zircon tetrahedral prism, pinacoidal terminations (Farley, 2002)	^{238}U	-4.31	4.92
	^{232}Th	-5.00	6.80
Zircon tetrahedral prism, pinacoidal terminations (Hourigan et al., 2005)	^{238}U	-4.35	4.57
	^{232}Th	-4.94	6.88
Zircon tetrahedral prism, pyramidal terminations (Hourigan et al., 2005)*	^{238}U	-4.28	4.37
	^{232}Th	-4.87	5.61

Table 3.2 Calculations for volume and surface area of apatite and zircon for calculating F_{He} . Value β is the ratio of surface area to volume. Compiled from Reiners (2005) and Weisstein (2011). * denotes used in this study.

Crystal geometry	Volume	Surface Area
Apatite hexagonal prism	$V_{hex} = \frac{3}{2}\sqrt{3}l^3$	$SA_{hex} = 3(2 + \sqrt{3})a^2$
Zircon tetrahedral prism, pinacoidal terminations	$V_{ps} = \frac{2}{3}\pi r^2 l$	SA_{ps} $= 2\pi r^2 + \left[\frac{2\pi r(l/2)^2}{\sqrt{(l/2)^2}} \right] \sin^{-1} \left[\frac{(l/2)^2 - r^2}{(l/2)} \right]$
Zircon tetrahedral prism, pyramidal terminations *	$V_z = 4r_1 r_2 \left[(l - h_1 - h_2) + \frac{1}{3}(h_1 + h_2) \right]$	$SA_z = 4(l - h_1 - h_2)(r_1 + r_2) + 2r_1 a + 2r_2 a$ $a = \sqrt{h_1^2 + r_2^2} \sqrt{h_2^2 + r_2^2}$ $b = \sqrt{h_1^2 + r_1^2} \sqrt{h_2^2 + r_1^2}$

Chapter 4: Late Cretaceous exhumation of northern central Nevada: evidence from low-temperature apatite and zircon (U-Th)/He and apatite fission track thermochronology

4.1 Introduction

The northern Carlin Trend of northern central Nevada is a major Au-producing region, containing >90 Moz Au (Hofstra, 2010). The northern Carlin Trend lies within the present day Great Basin, an area now characterised by Cenozoic to Recent Basin-and-Range-style extension. Prior to this, northern central Nevada had a long history of contraction and crustal thickening throughout the Late Paleozoic and Mesozoic, culminating in the Late Cretaceous Sevier thrusting seen to the east in Utah. The main tectonostratigraphic features of the western USA are shown in Figure 2.3. Previous workers have proposed that during the Cretaceous, northern central Nevada was an overthickened hinterland to the Sevier fold and thrust belt to the east (Armstrong, 1972; Allmendinger, 1992; DeCelles, 2004). They propose that the latest stage of Sevier thrusting was coincident with gravitational collapse and thinning of the crust in Nevada, based on evidence of mid crustal depressurisation and cooling (Wells et al., 1990; Hodges and Walker, 1992; Camilleri and Chamberlain, 1997; Wells and Hoisch, 2008). There is relatively little evidence for the surface expression of extensional collapse in northern central Nevada, although Cretaceous sedimentary basins are documented in other parts of the state (Biglow, 1986; Suydam, 1988; Vandervoort and Schmitt, 1990; Druschke et al., 2009b) and surface-breaking faults have been described in Cretaceous-Paleocene basins to the south of the northern Carlin Trend (Druschke et al., 2009a; Druschke et al., 2009b).

Low-temperature thermochronology has been widely applied in tectonic studies to determine timing and rates of exhumation (e.g. Reiners et al., 2002; Stockli et al., 2002; Colgan et al., 2010). In the present study, new apatite fission track (AFT) and apatite and zircon (U-Th)/He (AHe and ZHe) data from deep drill holes in Jurassic stocks from the northern Carlin

Trend are used to assess whether there is evidence for exhumation related to extensional collapse preserved in the cooling history of the upper crust. The data also provide temporal constraints for the tectonic evolution of the region, and define the background thermal age against which thermal halos associated with Eocene Au mineralization can be identified (discussed in Chapter 5).

The Post Fault system is an east-dipping, north-northwest-striking normal fault system that at shallow depths defines the eastern limit of Au mineralization in the northern Carlin Trend (Figure 4.1). Timing of Post Fault movement is uncertain, although cross-cutting relationships with the Roberts Mountains Thrust of the Late Devonian-Mississippian Antler Orogeny do show that the fault was active post-Mississippian (Moore, 2002). The Post Fault system has been reactivated multiple times (Volk, 2001), although the timing of displacement episodes is poorly constrained. Current estimates of total offset are 800-1600 m since the Mississippian based on geological and geophysical observations (Bettles, 2002). The Post Fault separates the compositionally similar Jurassic Goldstrike and Little Boulder Basin Stocks, both intruded at around 158 Ma (Morton, 1977; Arehart et al., 1993b; Mortensen et al., 2000; Ressel and Henry, 2006), leading workers to suggest that they were originally emplaced as a single intrusive body that has subsequently been offset by faulting (Chakurian et al., 2003). How much of the total Post Fault offset was post-Jurassic is not well constrained. Samples used in this study were collected from both sides of the Post Fault, from the Goldstrike Stock in the footwall and the Little Boulder Basin Stock in the hanging wall, to determine the timing and amount of motion that occurred on the Post Fault since emplacement of the stocks, to further constrain Cretaceous cooling and exhumation in the Sevier hinterland.

4.1.1 Tectonic setting of northern central Nevada

4.1.1.1 Cretaceous contraction and synconvergent extension

Throughout the Mesozoic, ongoing subduction of the Farallon Plate beneath the western edge of the North American continent resulted in roughly east-west compression of the developing US Cordillera (DeCelles, 2004). Mesozoic contraction in northern central Nevada was dominated by the Cretaceous-Paleogene Sevier Orogeny (Armstrong, 1972; Miller and Gans, 1989; DeCelles, 2004), although Triassic-Jurassic compression did result in gradual crustal thickening. During the Cretaceous, northern central Nevada lay within the Sevier hinterland (Camilleri and Chamberlain, 1997; Druschke et al., 2011), to the west of the Sevier fold and thrust front that deformed parts of what is now Utah, Colorado and Wyoming (Figure 2.3). The Sevier hinterland has been interpreted as a high-elevation (>3 km), low-relief orogenic plateau similar to the present-day Andean Altiplano-Puna Plateau (Armstrong, 1972; Allmendinger, 1992; DeCelles, 2004). Estimates of total crustal thickness are ~ 45 -70 km, enough to cause metamorphism and partial melting at depth (Coney and Harms, 1984; Colgan et al., 2006; DeCelles and Coogan, 2006). Metamorphic core complexes exhumed in the Cenozoic, such as the Ruby-East Humboldt metamorphic core complex, record evidence of burial up to 13-18 km based on thermobarometry studies of peak metamorphism mineral assemblages (Miller and Gans, 1989; Hudec, 1992). Estimates of timing of peak metamorphism and maximum crustal thickness vary from Late Jurassic to Late Cretaceous (Miller and Gans, 1989; Hudec, 1992; Camilleri and Chamberlain, 1997; McGrew et al., 2000).

Attainment of maximum crustal thickness was followed by gravity-driven collapse and extension of overthickened Sevier hinterland crust beginning in the Late Cretaceous (Wells et al., 1990; Hodges and Walker, 1992; Camilleri and Chamberlain, 1997; DeCelles, 2004). Extension was facilitated by delamination of mantle lithosphere below the thickened Sevier

hinterland crust; subsequent upwelling of hot asthenosphere buoyed the overlying crust and caused uplift, erosion and extension (Wells and Hoisch, 2008; Wells et al., 2012). Removal of the lithospheric mantle beneath the Sevier hinterland permitted a shallowing of the subduction angle of the Farallon slab beneath North America. Shallowing of the Farallon slab resulted in an eastward migration of magmatism across the region during the Late Cretaceous and Earliest Paleogene (Dickinson, 2006).

4.1.1.2 Cenozoic extension

Cenozoic extension was dominated by the evolution of the Miocene to Recent Basin-and-Range topography that characterises northern central Nevada today. Minor extension also occurred in the Eocene and Oligocene (Potter et al., 1995; DeCelles, 2004; Cline et al., 2005; Wallace et al., 2008). Eocene sedimentation occurred predominantly in lacustrine basins that formed in paleovalleys up to 1.5 km deep behind dams that were temporarily created by volcanic flows or normal faulting that resulted from extension (Cline et al., 2005; Henry, 2008; Colgan and Henry, 2009). Eocene extension is coincident with regional intrusive magmatism and volcanism ~42-36 Ma (Cline et al., 2005; Henry, 2008). In the northern Carlin Trend, intermediate-felsic dikes exploited pre-existing north-northwest striking faults. Magmatism in northern central Nevada was part of the southwestward migration of magmatism that occurred through the Early Eocene to Early Miocene as subduction of the Farallon slab steepened and eventually ceased (Dickinson, 2006). Slab rollback resulted in renewed contact between the asthenosphere and overlying crust, once again causing heating and an increase in buoyancy and uplift (Dickinson, 2006; Wells and Hoisch, 2008).

There is no evidence of large magnitude regional extension in northern central Nevada during the Eocene and Oligocene, although McGrew et al. (2000) infer significant cooling and

exhumation of up to 7 km in parts of the Ruby Mountain metamorphic core complex between the Late Cretaceous and Oligocene. Many workers suggest the Ruby Mountain metamorphic core complex underwent a prolonged period of cooling and uplift in the Late Eocene-Early Miocene, involving a total of up to 30 km exhumation to its present position (McGrew and Snee, 1994; McGrew et al., 2000). However other workers have recently suggested exhumation of the southern Ruby Mountain metamorphic core complex was rapid and occurred primarily in the Mid Miocene, reinterpreting older Oligocene thermochronometric constraints on cooling as partially reset ages (Colgan et al., 2010).

Major Basin-and-Range-style extension in northern central Nevada began in the Mid Miocene (Zoback et al., 1981; Wernicke et al., 1982; Colgan et al., 2006). Extension was facilitated by a change in tectonic regime at the western plate margin of North America, from compressional to transtensional strike-slip as the San Andreas Fault system developed following delamination of the Farallon slab (Colgan et al., 2006; Dickinson, 2006). Estimates of extension vary across the Basin-and-Range province, in some parts of the southern Great Basin as much as 300 % (Zoback et al., 1981). In northern central Nevada, however, extension was more modest, varying from ~10 % in the area of the northern Carlin Trend to ~110 % in the Caetano Caldera fill between the Cortez Mountains and Fish Creek Mountains to the south (Colgan et al., 2008). Extension was highly localised and partitioned between high-strain domains that were extended 50-100 % but separated by largely unextended blocks (Colgan and Henry, 2009). Cross-cutting relationships, low-temperature thermochronology and dating of widespread clastic deposits in extensional basins constrain the timing of major extension in northern central Nevada to ~16-10 Ma (Zoback et al., 1994; Colgan et al., 2008; Wallace et al., 2008; Colgan and Henry, 2009; Colgan et al., 2010). Since ~10 Ma, movement on wide-spaced

(>5 km) normal faults has led to the definition of the basins and ranges that are characteristic of the region today (Colgan et al., 2008).

Major Mid Miocene regional extension was coincident with regional volcanism, with volcanic centres to the north, south and west of the Carlin Trend. Existing basins, such as the Carlin and Ivanhoe Basins around the northern Carlin Trend, are partially filled with 14-16 Ma air-fall tuff deposits that are interlayered with fluviolacustrine sediments. Regional low dip angles of those sediments are evidence that the northern Carlin Trend was an area of minimal Miocene to Recent extension (Wallace et al., 2008).

4.1.2 Metallogeny of northern central Nevada

Hydrothermal mineralization has occurred at several times during the evolution of northern central Nevada. Emsbo (1999) described features consistent with a SEDEX deposit that formed during the Devonian, when host rocks were being deposited in a passive margin environment. The giant Carlin Au deposits formed coincident with minor extension and regional magmatism during the Eocene. Cross-cutting relationships with Eocene dikes and Rb/Sr dating of ore-stage galkhaite constrain the timing of Carlin Au deposits to 36-42 Ma (Hofstra et al., 1999; Tretbar et al., 2000; Ressel and Henry, 2006). Magmatism has been invoked as a potential source of heat and hydrothermal fluids (Ressel and Henry, 2006; Muntean et al., 2011), and extension as a driving force for hydrothermal circulation (Ilchik and Barton, 1997), although the formation of these large submicron-scale disseminated deposits remains enigmatic (Hofstra and Cline, 2000; Cline et al., 2005). Small-scale epithermal Au+Ag±Hg deposits formed in the Miocene-Early Pliocene associated with localised geothermal activity and volcanism (John, 2001), and minor Au mineralization hosted in the

Miocene Carlin Formation has been described in the vicinity of the northern Carlin Trend (Fleck et al., 1998).

4.1.3 Local geology of the northern Carlin Trend

The geology of the northern Carlin Trend is dominated by two Paleozoic sedimentary packages: the siliciclastic Upper Plate that forms the hanging wall to the Roberts Mountains Thrust, and the Lower Plate carbonate package in the footwall. These are described in further detail in Chapter 2, and in Figure 2.1 in particular. Gold mineralization is generally confined to the Lower Plate (Hofstra and Cline, 2000), although exceptions do occur (e.g. Elder Creek, Ahmed, 2010b). In the immediate vicinity of the northern Carlin Trend, Mesozoic sedimentary deposits are scarce. Eocene cover (dominated by volcanoclastic sediments) is found only towards the northern end of the Tuscarora Mountains that form the northernmost boundary of the present study area. Miocene sedimentation along the northern Carlin Trend is dominated by the Carlin Formation that consists of lacustrine, alluvial and volcanoclastic air fall deposits dated to 14-16 Ma (Fleck et al., 1998; Wallace et al., 2008). Quaternary alluvial deposits locally overlie Miocene, Eocene and Paleozoic stratigraphy.

The northern Carlin Trend was intruded by the granodiorite Jurassic Goldstrike and Little Boulder Basin Stocks around ~158 Ma, based on hornblende and biotite $^{40}\text{Ar}/^{39}\text{Ar}$ (Arehart et al., 1993b), K/Ar (Morton, 1977) and zircon U-Pb dating (Mortensen et al., 2000; Ressel and Henry, 2006). The petrologic similarity of the stocks and their positions either side of the Post Fault system has led workers to conclude they were originally intruded as a single igneous body (Chakurian et al., 2003; Ressel and Henry, 2006). The Vivian Sill, to the east of the Little Boulder Basin Stock, is also petrologically similar and therefore probably an extension of the same intrusive body, now also offset by younger faulting. Lamprophyre and rhyodacite dikes

of similar Jurassic age are found across the northern Carlin Trend, commonly along pre-existing north-northwest-striking faults, and are important hosts to Au-mineralization in some deposits (e.g. Banshee, Barker et al., 2009). Magmatism also affected the northern Carlin Trend during the Eocene, evidenced by abundant intermediate-felsic dikes dated at ~36-42 Ma (Ressel et al., 2000; Ressel and Henry, 2006). It has been proposed that the Eocene intrusions are linked to a larger felsic pluton that is concealed at depth (Ressel and Henry, 2006). More recently, Miocene felsic volcanism produced rhyolite lavas found south and west of the northern Carlin Trend and air fall deposits in the Carlin Formation.

The northern Carlin Trend has a complex structure that results from multiple phases of contraction and extension that repeatedly reactivated pre-existing faults (Teal and Jackson, 2002; Heitt et al., 2003; Muntean et al., 2007; Mickelthwaite, 2010). The study area is dominated by steeply-dipping north-northwest-striking faults and north-northeast-striking faults, and lower-angle west-northwest-striking faults. The Post fault system is part of the larger Post-Gen fault system that consists of numerous high-angle normal faults, with two main segments each ~5-7 km long, the Post Fault to the north and the Gen Fault to the south, with a stepover across the granodiorite Goldstrike-Little Boulder Basin Stocks (Heitt et al., 2003; Mickelthwaite, 2010)(Figures 4.1). Kinematic indicators are complex and display evidence of normal, oblique dextral-normal and sinistral-normal and apparent strike-slip movement (Teal and Jackson, 2002; Heitt et al., 2003). The presence of Jurassic dikes locally filling Post-Gen system faults shows the initiation of the system pre-dates Jurassic magmatism, however post-158 Ma motion has also offset apophyses of the Goldstrike Stock (Heitt et al., 2003). Sediments of the Miocene Carlin Formation in the Little Boulder Basin have also been offset by up to 100 m since 15 Ma (Thoreson, 1993; Moore and Norby, 2002). Total estimates of offset on the Post Fault range 800-1600 m based on displacement of Paleozoic stratigraphy

(Bettles, 2002). The Post-Gen fault system was a major conduit for hydrothermal fluids and exerted significant structural control on the formation and distribution of Carlin-type Au deposits of the northern Carlin Trend. Gold mineralization is concentrated in broad shallow scallops of mineralization within the footwall of the Post-Gen fault system and at greater depth at the tips of the fault system, the stepover and in the hanging wall (Mickelthwaite, 2010).

4.2 Previous thermochronology of the northern Carlin Trend

A study by Chakurian et al. (2003) investigated the timing of Carlin-type Au mineralization and the timing and amount of offset of the Post Fault using AFT, $^{40}\text{Ar}/^{39}\text{Ar}$ and AHe thermochronology. That study produced pooled AFT ages for 20 samples from the Carlin Trend, including samples from the Goldstrike and Little Boulder Stocks. A weighted mean AFT age of 37.3 ± 1.5 to 41.6 ± 1.6 Ma for samples from the Betze-Post and Carlin East deposits led Chakurian et al. (2003) to infer that Au mineralization occurred at 37-42 Ma, consistent with the estimates of Arehart et al. (2003b) and Tretbar et al. (2000). Two AHe ages, 21.4 ± 1.3 Ma from the Goldstrike Stock, and 31.0 ± 1.9 Ma from Carlin East, and an AFT age 18.6 ± 4.5 Ma also from Carlin East led the authors to conclude that localised hydrothermal activity took place subsequent to formation of the Carlin-type deposits, possibly associated with Miocene volcanism. They also suggested that those young ages may record the hydrothermal event responsible for local Au mineralization of the Miocene Carlin Formation described by Fleck et al. (1998) near the Gold Quarry and Betze-Post deposits. Chakurian et al. (2003) also obtained downhole AFT ages from the ST7 hole in the Goldstrike Stock, 58.0-80.4 Ma, and from the LBB-76 hole in the Little Boulder Basin Stock, 62-129 Ma. Based on those AFT data, those authors estimated that the Little Boulder Basin Stock was $\sim 35^\circ\text{C}$ cooler than the Goldstrike Stock around 40 Ma. Whether this was due to a difference in depth (~ 1 km

assuming a geothermal gradient of $40 \pm 10^\circ\text{C}/\text{km}$), or due to mineralization-related heating, was not determined but both were considered possibilities. Hickey et al. (2003; 2005), Cline et al. (2005) and Hickey (2007) used AFT dating to identify regional thermal anomalies around the Carlin Trend, including the northern Carlin Trend, shown in Figure 1.2. They determined that young (20-40 Ma) AFT ages were spatially coincident with Au deposit trends, and that these ages were the result of heating associated with Eocene hydrothermal activity that formed the giant Au deposits. The thermal anomalies were distinct against older, >60 Ma, regional background AFT ages that they proposed record regional exhumation in the Cretaceous.

4.3 Methods

4.3.1 Sampling

Low-temperature thermochronology is commonly used to interpret the cooling history of a sample and infer the exhumation history of an area (Reiners and Brandon, 2006). Thermochronometers, e.g., AHe, AFT, ZHe, can be combined to determine the cooling history of a single sample because each has a different closure temperature, T_c . The age recorded by progressively lower-temperature thermochronometers gives the timing of cooling through each T_c (see Figure 3.1). A suite of samples collected from a vertical transect, i.e. over a range of depths, allows construction of an age-elevation profile, the slope of which indicates the rate of cooling of that suite of samples. Changes in slope represent changes in cooling rate, generally considered to represent changes in exhumation rate linked to tectonic activity. A goal of the present study is to determine the exhumation history of the northern Carlin Trend, both regionally and on either side of the Post Fault. Samples forming a vertical section were therefore required for dating by AHe, AFT and ZHe to construct age-elevation profiles to

examine the timing and rates of cooling and exhumation. Use of multiple thermochronometers allows interpretation of cooling over a greater temperature range than a single dating method.

Samples were collected from drill core and surface locations in the Goldstrike (n=14) and Little Boulder Basin (n=15) granodiorite stocks and from the surface in the Vivian Sill (n=1). Goldstrike Stock GS-1845CW series (n=5) and 50-series (n=2) and Little Boulder Basin Stock and Vivian Sill samples were collected by K. Hickey. Granodiorite was sampled to increase apatite and zircon yields, as these minerals are more abundant in intrusive material than in the host carbonate rocks that surround the intrusions. Samples were collected at various depths up to 1.3 km downhole in selected drill holes in both stocks, hole GS-1845C in the Goldstrike Stock and holes LBB-76, LBB-100 and LBB-102 in the Little Boulder Basin Stock. Samples were also collected from drill holes laterally spaced across the Goldstrike Stock in a roughly northwest-southeast transect at depths 100-450 m. Additional data from downhole samples of Chakurian et al. (2003), ST7 (n=5) from the Goldstrike Stock and LBB-76 (n=4) from the Little Boulder Basin Stock, and the Vivian Sill (n=1) are also used in this study. LBB-76 samples from Chakurian et al. (2003) are similar intervals to those collected for this study from the same drill hole. Locations of Little Boulder Basin Stock, Goldstrike Stock and Vivian Sill samples are shown in Figure 4.1.

More distal regional surface (S-series) samples of Upper Plate sandstone were collected and dated by Hickey and presented in Cline et al. (2005) in a reconstruction of Eocene paleolandscape around the time of Au mineralization. A subset of these (n=16) from the central Tuscarora Mountains to the north of the northern Carlin Trend were incorporated in this study to provide AFT data from a larger area and greater range in elevation, important in interpreting the thermal structure and evolution of a region. The location of these samples is shown in

Figure 4.3 and in the cross section in Figure 4.4. ZHe ages were obtained for five of those sixteen samples.

Full sample descriptions of samples collected for this study are provided in Appendix B. Samples from the Goldstrike and Little Boulder Basin Stocks and Vivian Sill were of fine-medium grained, granodioritic material. A study of alteration minerals revealed that most granodiorite samples are only mildly altered, with 5-15% chlorite±sericite±smectite alteration of whole rock samples (see Chapter 5). Sample GS-1814C-1595 from the Goldstrike Stock is more pervasively altered, with almost total replacement of feldspars by sericite and mafic phases strongly altered to chlorite±smectite. Samples are unmineralized, with Au content typically <0.001 ppm.

4.3.2 (U-Th)/He dating

Mineral separation for (U-Th)/He dating was carried out by the author at the University of British Columbia using conventional mechanical, density and magnetic separation methods following recommendations in Donelick et al. (2005). Separation methods are fully described in Appendix A.

Apatite and zircon picking and (U-Th)/He dating were carried out by the author at the Arizona Radiogenic Helium Dating Laboratory (ARHDL) at University of Arizona, Tucson, following the methods described in Reiners (2005). Where available, three apatite crystals and three zircon crystals were chosen for each sample, selecting those that were at least 60 µm across and were inclusion-free, whole crystals. Width and length dimensions for mass and volume calculations of picked crystals were measured in two orientations on digital photomicrographs using a Leica MX16 microscope before packing each crystal into its own 500 µm diameter Nb tube. Helium liberation was achieved by laser heating using a 1064-nm

Nd:YAG laser. Released He gas was analysed by a Balzers gas quadrupole mass spectrometer (QMS). Crystals were then dissolved in nitric acid (for apatite) or hydrofluoric acid (for zircon) and U, Th (and Sm in apatite) analysis was carried out using dissolution ICP-MS on a Finnigan Element2 ICP-MS. Fish Canyon Tuff zircon and Durango apatite were used as standards, running a standard for every 4-5 sample analyses. Ages were calculated based on the relative abundance of ^4He and ^{238}U , ^{232}Th and in the case of apatite also ^{147}Sm . Alpha ejection corrections were applied to account for excessive ^4He loss from crystal rims (Farley, 2002; Reiners, 2005). Sample ages were calculated from the average single crystal ages. Further details and age calculations are given in Chapter 3. ZHe and AHe dating was attempted for all Goldstrike Stock samples collected by this study and for five samples from the Little Boulder Basin Stock.

4.3.3 Apatite Fission Track (AFT) dating

AFT dating and sample preparation were carried out by Apatite to Zircon, Inc using the LA-ICP-MS method described in Donelick et al. (2005) modified from Hasebe et al. (2004), see Chapter 3. Apatite separates for AFT dating were prepared by Apatite to Zircon, Inc for each sample following conventional separation methods modified after Donelick et al. (2005). Apatites were mounted in epoxy resin, polished and then etched for 20 s in 5.5 M HNO_3 at 21°C to reveal and enlarge natural spontaneous fission tracks within the apatite crystals for counting. Counting was done using an optical microscope at 1562.5x dry magnification at Apatite to Zircon, Inc using non-polarised transmitted light on a Nikon Optiphot2 microscope. D_{par} , the mean fission-track etch pit diameter parallel to the crystallographic c-axis, was measured for each apatite as an indicator of susceptibility to annealing. Fission tracks in low

Dpar apatites typically anneal more readily than in high Dpar apatites (Carlson et al., 1999; Donelick et al., 2005).

U, Th and Sm concentrations were calculated from measurement on a 20 µm spot using LA-ICP-MS at the Washington State University Geoanalytical Laboratory, Pullman, using a New Wave YAG 213 nm laser ablation system in line with a Finnigan Element2 magnetic sector ICP-MS. Durango apatite was used as a standard. During each LA-ICP-MS session 25 spots were analysed from the standard near the beginning and end of the session for purposes of calibrating $^{238}\text{U}/^{43}\text{Ca}$, used as a background signal check for ^{238}U and ^{43}Ca . Single grain and pooled sample ages were calculated using equations in Chapter 3. AFT dating was attempted for all samples collected in this study. Only samples that yielded ≥ 15 datable grains are presented in the text as representative pooled ages. Data from all samples dated is included in Appendix C.

A χ^2 test was applied to pooled ages to determine whether single grain ages in a sample are concordant (χ^2 probability, $p, \geq 0.01$) or discordant ($p < 0.01$) (Galbraith, 2005). Discordance can arise due to the presence of multiple populations of apatite grains or where insufficient data is available, e.g., limited apatite recovery from a sample or low track counts (N_s) in single grains (O'Sullivan and Parrish, 1995; Galbraith, 2005).

Fission track lengths were also measured to allow interpretation of the thermal history of each sample. Confined, horizontal fission track lengths were measured following ^{252}Cf irradiation (to enlarge fission tracks in a controlled manner) using 1562.5x magnification as above. Lengths were measured digitally and the angle of each measured fission track relative to the crystallographic c-axis was noted for c-axis projection of lengths for modelling (see below). Annealing is influenced by the angle to c-axis as well as inherent kinetic properties of the apatite crystal that are a complex function of apatite chemistry (Donelick et al., 1990;

Donelick et al., 1999; Ketcham, 2003). C-axis projection has been found to significantly reduce the variability in fission track lengths that arises from anisotropic annealing and etching of fission tracks, which occurs slowest parallel to the c-axis (Carlson et al., 1999; Donelick et al., 1999; Barbarand et al., 2003; Ketcham et al., 2007). C-axis projection helps reduce variation in track length data that arises from analytical factors such as etch conditions, microscope calibration and optics, determination of fission track tips for measurement and analyst bias towards measurement of longer lengths (Laslett et al., 1982; Ketcham et al., 2009).

4.3.4 HeFTy modelling

Fission tracks thermally anneal over time. Annealing is a gradual process that involves the progressive shortening of fission tracks (Naeser and Faul, 1969; Fleischer et al., 1975). Fission tracks form continuously in a crystal and are either retained, or fully or partially annealed depending on the thermal conditions of the host apatite. The length distribution therefore provides information on the thermal history of the sample. Laboratory experiments and drill hole studies have investigated the relationship between temperature, duration of heating and track length (Gleadow and Duddy, 1981; Green et al., 1986; Laslett et al., 1987; Donelick et al., 1990; Carlson et al., 1999; Donelick et al., 1999; Ketcham et al., 1999). Several modelling software packages have been developed using these empirical observations on annealing behaviour to allow the possible thermal histories of a sample to be generated and evaluated (Ehlers et al., 2005). In this study the software package HeFTy (v1.7.3), developed by Ketcham (2005), was used for this purpose.

HeFTy was used to inversely model fission track length and single grain age data. Time-temperature paths are generated using a constrained Monte-Carlo scheme, the constraints determined by the user based on known age of crystallization, present-day temperature and

cooling or heating events to be tested. The user specifies regions of time-temperature space through which all paths must pass. The user can also specify the complexity of the paths between those regions, by defining whether path segments between regions must be monotonic, i.e. only cooling or only heating, or variable, allowing both cooling and heating to occur between regions. The randomly-generated paths produce model fission track lengths and single grain ages that are evaluated by combining multiple statistical tests and classified by the software as "good" or "acceptable" fit to the observed input data. Goodness of fit (GOF) to track length data is assessed using Kuiper's statistic. GOF to single grain age data is measured comparing the model age to measured age as described in Ketcham (2005). "Good" models have a GOF value of 0.50 or higher, "acceptable" models 0.05 or higher. Ketcham (2009, p.4-3) suggests that "a good result implies the time-temperature path is supported by the data, while an acceptable time-temperature path is not ruled out by the data".

Other definable parameters include kinetic parameters and experimental conditions. In this study D_{par} was the kinetic parameter. D_{par} correlates positively with resistance of an apatite crystal to annealing (Carlson et al., 1999). In this study ^{252}Cf irradiation was used prior to track length measurement to systematically enlarge fission tracks for improved resolution and accuracy of measurement (Carlson et al., 1999). C-axis projection was applied to measured fission track lengths in this study to account for the preferential etching and annealing of fission tracks at a high angle to the c-axis described in numerous studies (e.g. Laslett et al., 1982; Green et al., 1986; Laslett et al., 1994; Donelick et al., 1999; Barbarand et al., 2003).

Possible t-T histories were generated for each sample collected from the northern Carlin Trend with constraints based on suspected geological events that would affect the cooling or heating of a sample, e.g., Cretaceous cooling due to exhumation, or Eocene reheating by hydrothermal fluids, as well as constraints from measured ZHe and AHe ages. Models were

allowed to run until at least 30 good fit paths were found. A set of constraints was considered improbable if fewer than 30 good paths were found after ~12 hours running. If no good paths were found after ~12 hours, the tested constrained t-T history was ruled out. In the case where >30 good paths were found in different models for the same sample, the modelled T-t of surrounding samples was considered and used to evaluate the more representative model. In some cases, a preferred model could not be produced.

Single grain ages are typically obtained for 20-40 individual apatite crystals from a sample. Large variation in single grain ages from a single sample can cause the pooled sample age to fail a X^2 test of sample age concordance (Galbraith, 2005). In sedimentary samples this commonly arises due to multiple sources of apatite, which have different chemical and kinetic characteristics (Green et al., 1986; Carlson, 1990). In igneous samples, variation in kinetic parameters may reflect compositional variation of the host melt and apatite (O'Sullivan and Parrish, 1995). Single grain ages from a sample can therefore sometimes be divided into multiple populations based on annealing properties, which can be inferred from Dpar measurements, as Dpar is a kinetic parameter that correlates positively with resistance to annealing. These populations can be modelled simultaneously in HeFTy, which quantitatively relates Dpar to annealing. Modelling multiple populations improves interpretation of a t-T history because each population constrains the thermal history of a sample in different ways depending on its kinetic properties (Ketcham, 2005; Ketcham, 2009). In this study multiple populations were identified in both igneous and sedimentary samples. Where present, multiple populations were modelled simultaneously to analyse the thermal history of the sample they occur in.

4.4 Results

4.4.1 Apatite and zircon yields

Of the thirty samples collected from the Little Boulder Basin Stock, Goldstrike Stock and Vivian Sill for this study, only twenty-four yielded sufficient apatite of acceptable quality for AFT dating, and only six of twelve attempted for AHe dating. Initially, mechanical mineral separation was carried out at UBC using a jaw crusher and disc grinder, but was modified for later batches of samples following recommendations in Donelick et al. (2005) to omit grinding to reduce fragmentation. Yields of apatite were better in samples that were prepared without use of the disc grinder, although still not sufficient in all cases as small crystal size and presence of inclusions remains a common feature in apatite from the northern Carlin Trend. Other studies around the Carlin Trend also report low apatite yields, e.g., Arehart et al. (1993b), Chakurian et al. (2003), Colgan et al. (2010). Zircon is more resistant than apatite and so less prone to fragmentation. Zircon yields for ZHe dating were low due predominantly to small crystal size but sufficient to allow dating of all but one of the selected subset of sixteen samples.

4.4.2 Apatite fission track results

4.4.2.1 Apatite fission track data analysis

Eleven of the twenty-four new (Little Boulder Basin Stock $n = 5$, Vivian Sill $n = 1$, Goldstrike Stock $n = 5$) AFT pooled ages were discordant when X^2 tested ($p < 0.01$), a possible indication of multiple populations of apatite crystals. As all samples are igneous, this is more likely an indication of populations with different kinetic properties than different sources. However, an examination of Dpar values (described below) does not reveal multiple populations based on that kinetic parameter, as the range in Dpar values is essentially

continuous in all samples. In all cases, omission of one or two outliers results in concordant ($p>0.01$) pooled ages that were still within error of the original pooled ages for each sample. Both pooled and concordant ages and X^2 probabilities (Q) are shown in Table 4.1. The concordant ages are used from this point onwards, and are considered representative AFT ages corrected for obvious outliers.

4.4.2.2 Apatite fission track ages

AFT ages generated in this study ($n=24$) and from Chakurian et al. (2003) ($n=10$) are presented in Table 4.1 and in the map in Figure 4.5. Data from a subset of samples from the central Tuscarora Mountains ($n=16$) collected by K. Hickey and published in Cline et al. (2005) are also shown in Table 4.1 and in Figure 4.6. AFT ages range from $20.9 +15.6 -8.9$ Ma to $136.2 +14.9 -13.9$ Ma (2σ) among granodiorite samples and from $70.3 +15.6 -12.9$ Ma to $145.9 +29.2 -24.3$ Ma among the central Tuscarora sandstone samples. AFT ages fall roughly into three main groups, shown in Figure 4.7: 1. >85 Ma, observed predominantly in the central Tuscarora and Vivian Sill samples and upper portions of the Little Boulder Basin Stock at elevations >1400 m, 2. 60-80 Ma, observed in deep drill hole samples from both the Little Boulder Basin and Goldstrike Stocks, and 3. $\leq \sim 40$ Ma, recorded near the edges of the Goldstrike Stock and in the Betze-Post pit, just north of the Goldstrike Stock (Figure 4.8).

Where the same intervals were dated by this study and Chakurian et al. (2003), new AFT ages for deep drill hole LBB76 samples overlap with AFT ages obtained over the same intervals by Chakurian et al. (2003) at the 2σ level. The same drill holes were not sampled from the Goldstrike Stock, however, the AFT ages in deep drill hole GS-1845CW from this study is similar to the AFT ages in deep drill hole ST7 of Chakurian et al. (2003), ~ 60 Ma in both holes.

Among deep drill hole samples, which were collected to observe vertical patterns in cooling ages in both the Little Boulder Basin and Goldstrike Stocks, AFT ages correlate with elevation, with the oldest ages at higher elevations (Figure 4.9). In the Little Boulder Basin Stock, the oldest ages, >120 Ma, are recorded in the highest elevation samples, LBB76-343, at 1647 m and LBB76-576, at 1584 m. At high elevations the Little Boulder Basin Stock AFT age-elevation profile has a shallow slope, but below ~1400 m, ages are ~70 Ma and the age-elevation profile is near vertical (Figure 4.9a). In the Goldstrike Stock, AFT ages from downhole samples in deep drill holes GS-1845CW and ST7 are consistently ~60 Ma, with no increase in AFT age with elevation (Figure 4.9b). Samples within ~400 m of the edge of the Goldstrike Stock do not show a correlation with elevation, and, with AFT ages ≤ 40 Ma, are younger than samples from the centre of the stock. The youngest AFT age of 20.9 Ma was obtained for sample RM91-22C-1460 at the edge of the stock.

Only two samples were dated from the Vivian Sill, so no meaningful age-elevation profile can be constructed. Vivian Sill samples Viv-A and Viv-B are the same sample dated twice. Viv-A a pooled AFT age of $131.3 \pm 19.8 - 17.2$ Ma that overlaps at the 2σ level with Viv-B, $124.7 \pm 14.2 - 16.1$ Ma. Chakurian et al. (2003) also obtained an AFT age for the Vivian Sill of $91.6 \pm 13.0 - 11.4$ Ma for sample V1 at at 1920 m.

Among the central Tuscarora samples, no correlation with elevation is observed. A north-south trend is seen, with the oldest AFT ages towards the north (Figure 4.10, Figure 4.11). At the northern end of the section, Eocene cover unconformably overlies Upper Plate rocks along a contact now tilted $\sim 30^\circ$ to the northeast (K. Hickey, pers. comm.).

4.4.2.3 Apatite fission track lengths and length distribution

Mean c-axis projected fission track lengths (MTL) range from 12.42 ± 3.09 to 14.92 ± 1.63 μm among granodiorite samples, displaying similar ranges of variation within the Little

Boulder Basin and Goldstrike Stock and the Vivian Sill separately. Fission track length distributions are bimodal in the Vivian Sill, upper Little Boulder Basin Stock (LBB76-343 and -576) and most Goldstrike Stock samples (Figure 4.12). Most Little Boulder Basin Stock samples (LBB76-762 at 1533 m and below) and samples RM98-04C-459, GS-1814C-1595, GS-1845C-1 and GS-1845CW-5 from the Goldstrike Stock are unimodal (Figure 4.12). In the Goldstrike Stock, the distribution of fission track lengths does not relate to elevation or distance from the stock's edge.

Within Little Boulder Basin Stock samples and Vivian Sill samples, MTL correlates inversely with AFT age (Figure 4.13a), which is expected as tracks in younger samples formed more recently than in older samples and have not experienced the same amount of annealing. MTL in Goldstrike Stock samples does not correlate systematically with AFT age or elevation (Figure 4.13b). In the deep drill holes, LBB76, -100, -102, GS-1845CW, MTL correlates inversely with Dpar (Figure 4.13c), surprising since higher Dpar apatites are typically more resistant to annealing than lower Dpar apatites. However, this may be linked to susceptibility to resetting, so that readily reset, low Dpar apatites were reset more recently than higher Dpar ones, and so have only been accumulating fission tracks for a short period of time, and so have not experienced as much annealing and track length reduction as more resistant, higher Dpar apatites that were not reset by more recent heating.

Dpar values for granodiorite samples range from 1.85 ± 0.12 to 2.56 ± 0.14 μm , and like MTL, display similar ranges within each of the Little Boulder Basin Stock, Goldstrike Stock and Vivian Sill. Within individual samples, continuous distributions of Dpar values are observed, suggesting single apatite crystals within each sample share similar kinetic properties and can be considered single populations. Dpar does not correlate with age (Figure 4.13d), and only with elevation in LBB102, where higher Dpar values are observed at lower elevations

(Figure 4.13e). This suggests Dpar, an indication of resistance to annealing, is not a source for variation in AFT ages, since there is no systematic relationship between Dpar and elevation as there is between AFT age and elevation.

MTL values for central Tuscarora samples are slightly higher than granodiorite samples, ranging 14.33 ± 1.22 to 15.03 ± 0.93 μm . Overall, the Tuscarora samples have unimodal fission track length distributions (Figure 4.10). Dpar ranges 1.81 ± 0.21 to 2.21 ± 0.41 μm . There is no correlation between Dpar and MTL, single or pooled age, elevation or northing. Dpar values within each samples typically occur over a single continuous range rather than as multiple populations as might commonly be expected from a sediment with multiple sources of material and multiple compositions and kinetic properties. Most samples have concordant AFT ages.

4.4.3 (U-Th)/He results

4.4.3.1 Intrsample variation

ZHe ages are typically taken as the average of all single grain ages. However, significant intrasample single zircon age variation was observed in nine of the seventeen ZHe dated samples. These are marked in Table 4.2. In most cases, two ages within error of one another and the third significantly older or younger. Variation may result from by compositional zoning of U and Th described in Chapters 3, 5 and 6 and shown in Figure 4.14. Sample ZHe ages presented here are therefore based on the mean of the zoning-adjusted single grain ages. Adjustments were based on recommendations by Hourigan et al. (2005) summarised in Figure 3.11 as discussed in Chapter 3. In three cases (GS-1765C-782, GS-1814C-1595, GS-1818C-1000) a zoning adjustment could not bring the third zircon to within error of the other two, so a sample age based on only the two ages in agreement was calculated. Zoning may be more

complex in these samples, and oscillatory U zoning was observed in zircons in GS-1765C-782 under cathodoluminescence (Figure 4.14).

Similar variation is observed in AHe data, and while zoning may influence the accuracy of alpha-ejection corrections, no recommended zoning corrections are published for AHe. Variation in AHe ages is more likely to arise from the presence of mineral inclusions and radiation damage, (see Chapter 3, section 3.3) although inclusion-bearing apatite crystals were avoided during picking and the U and effective U (eU) content of the apatite in this study is not abnormally high, as would be expected in radiation damaged crystals (Table 4.3). Where variation is observed and two single apatite ages were within error of the other and the third was significantly younger or older, the sample age was taken as the average of the two grains that are within error of one another. Otherwise, sample AHe ages are the average of three single grain ages.

4.4.3.2 Zircon (U-Th)/He ages

ZHe ages obtained for the Little Boulder Basin and Goldstrike Stocks are shown in Table 4.2 and Figures 4.8 and 4.14. ZHe ages range 66.9 ± 2.1 to 154.1 ± 14.8 Ma (2σ). Overall ZHe ages are older in the Little Boulder Stock ($>\sim 85$ Ma) than in the Goldstrike Stock ($\leq \sim 80$ Ma). ZHe ages obtained for five of the central Tuscarora samples by K. Hickey (unpub. data) are older than the granodiorite ZHe ages, with highly variable Paleozoic or older ages. Central Tuscarora samples display significant variation both within single samples and from sample to sample. Individual grain ages range from 318.9 ± 6.9 to 1298.4 ± 44.2 Ma .

An age-elevation correlation similar to that seen in AFT ages is observed in the Little Boulder Basin Stock and Goldstrike Stock ZHe data (Figure 4.9). In the Little Boulder Basin Stock the oldest samples are at the highest elevations and samples below ~ 1400 m forming a

steep age-elevation slope around 85 Ma. Only one zircon was dated from the lowest sample, LBB102-6090, yielding an age of 66.7 ± 1.2 Ma. Although this fits the age-elevation correlation pattern observed in the Little Boulder Basin Stock, no interpretation can be made solely on this sample given the variation seen in other samples. In the Goldstrike Stock, ZHe ages in deep drill hole GS-1845CW are ~ 70 Ma with no increase in age with elevation (Figure 4.9b). Unlike AFT ages, ZHe ages in the Goldstrike Stock are essentially consistent across the stock, regardless of proximity to the edge or centre.

Central Tuscarora ZHe ages do not correlate with elevation. However, as seen in the AFT data for the region, there is a north-south trend. Overall, ZHe ages get younger further north, the opposite to AFT ages (Figure 4.11). The age of the Upper Plate rocks is Ordovician-Silurian, and most single grain ages are >416 Ma. With the exception of the three youngest grains with ages 318.7 ± 8.7 Ma, 362.6 ± 8.9 Ma and 374.7 ± 7.8 Ma which are from three different samples. The pre-416 Ma ZHe ages are therefore considered detrital ages, retaining their original, pre-deposition cooling ages. The younger grains may be evidence of Devonian-Mississippian sedimentation, suggesting the "Upper Plate" rocks to the north may be slightly younger than in the immediate vicinity of the northern Carlin Trend, where they are considered Ordovician-Silurian.

4.4.3.3 Apatite (U-Th)/He ages

Six new AHe ages are shown in maps in Figures 4.8 and 4.16 and in Table 4.3. Two AHe ages obtained for the Little Boulder Stock are 69.7 ± 1.4 and 67.0 ± 1.4 Ma at 1457 m, although the latter is based on dating a single apatite only. The four AHe ages from the Goldstrike Stock are younger, ranging 20.3 ± 0.7 Ma to 32.3 ± 6.5 Ma but are mostly ~ 30 Ma. GS-1845CW downhole samples were not AHe dated owing to a lack of sample material remaining following

earlier AFT and ZHe dating procedures. Chakurian et al. (2003) reported an AHe age 21.4 ± 1.3 Ma for sample ST7-D at 994 m elevation. It is not known how many apatite crystals were dated to obtain that age. The limited number of AHe analyses precludes construction of age-elevation profiles for the Little Boulder Basin and Goldstrike Stocks.

4.4.4 Zircon fission track data

In addition to AFT, ZHe and AHe data, two zircon fission track (ZFT) dates have been obtained for samples GS-1845CW1-5 and 5029 with ages 138.2 ± 14.2 (2σ) and 131.0 ± 12.2 Ma respectively (Hickey, pers. comm.). These are similar to ZFT ages obtained in Goldstrike Stock samples by Arehart et al. (1993b) of 132 ± 16 Ma (GSS-1), 169 ± 42 Ma (FTZ-2) and 133 ± 14 Ma (FTZ-3), interpreted as post-emplacement cooling ages that have not subsequently been affected by low-temperature Carlin fluids. ZFT dating follows the same principals as AFT dating but has a much higher $T_c > 320^\circ\text{C}$ (Rahn et al., 2004; Tagami and O'Sullivan, 2005).

4.4.5 HeFTy inverse modelling

HeFTy models of AFT data generated for representative samples are shown in Figure 4.12. Earlier higher temperature histories are poorly constrained and therefore display a wide range of possible "good fit" paths. Interpretation of AFT data therefore focuses on the parts of the models below 100°C , typically younger than ~ 100 Ma.

HeFTy models show that most Little Boulder Basin Stock, Goldstrike Stock and Vivian Sill samples experienced a major cooling phase at ~ 80 - 60 Ma. In the Little Boulder Stock, models of all samples with unimodal fission track length distributions (all except LBB76-343 and -576 and LBB102-1035) suggest a single-stage cooling history that involved rapid cooling from $> 110^\circ\text{C}$ to present day temperatures between 80 - 60 Ma.

Little Boulder Basin Stock sample LBB76-343 and -576 and LBB102-1035 and Vivian Sill samples, which have bimodal fission track length distributions, support two-stage model cooling histories. The Late Cretaceous rapid cooling is present in models for these samples, but is preceded by a rapid post-emplacement cooling phase complete by ~140 Ma and an intervening period of residence within a paleo PRZ, with little appreciable heating or cooling between ~140 and 100 Ma. Within the PRZ, fission tracks are partially annealed, as a sample lies within the temperature range between total loss and total retention, ~80-100°C (see Chapter 3). In the Vivian Sill, the rapid Late Cretaceous cooling phase is slightly earlier than in the upper Little Boulder Stock samples, ~100-80 Ma rather than 80-60 Ma. The first cooling stage in sample V-1 is poorly constrained due to the small number of single grain ages (n=12), which permit a wide range of t-T paths to be "good" paths.

Goldstrike Stock sample HeFTy models reveal a more complex thermal history than seen in the Little Boulder Basin Stock and Vivian Sill samples. Two main stages of cooling can be identified in the t-T models for Goldstrike Stock samples, one at 60-80 Ma, and a second at ~40 Ma. The t-T history between the two main cooling events is largely unconstrained. Models permit a heating event, such as one associated with a phase of major hydrothermal activity, immediately prior to Eocene cooling. Prior to Eocene reheating, cooling could have been either to near present-day temperatures during the Late Cretaceous, or to within the paleo PRZ temperature range. Despite the range of sample AFT ages recorded across the Goldstrike Stock, models show the same main cooling events affected all Goldstrike Stock samples at 80-60 Ma and ~40 Ma. However, in sample around the edge of the stock, the 40 Ma reheating event was sufficiently hot and sustained to totally reset AFT ages (Figure 4.12a). In samples near the centre of the stock, 40 Ma reheating is recorded but was not of sufficient temperature

and/or duration to cause significant resetting (Figure 4.12b). No 40 Ma cooling is noted in HeFTy models for the Little Boulder Basin Stock and Vivian Sill.

HeFTy models for a subset of central Tuscarora samples show that in most samples cooling was gradual, but with a more rapid phase in the Cretaceous between ~130 Ma and ~80 Ma. The timing of rapid cooling varies between samples. Models for all samples show gradual cooling since the Late Cretaceous.

4.5 Interpretation

4.5.1 Assumptions

The cooling rate of a sample is constrained by the timing of cooling through the effective T_c of the ZHe, AFT and AHe systems, calculated by dividing the difference in T_c between two systems by the difference in cooling ages. The rate of exhumation is then estimated by dividing the cooling rate by an assumed geothermal gradient (discussed below). The T_c of a thermochronometer is defined as "its temperature at the time corresponding to its apparent age" (Dodson, 1973, p.259). The T_c lies within the temperature range of the PRZ, which is the transition zone between all daughter products being retained and all being lost. In practice, the PRZ can be collapsed to a single effective T_c to allow more straightforward interpretation of cooling ages (Reiners and Brandon, 2006). The effective T_c is dependent on cooling rate, taken as 150-170°C, 100-110°C and 45-60°C for ZHe, AFT and AHe respectively for cooling rates of 1-10°C/Myr. T_c for AHe and ZHe was calculated using the software program Closure (Brandon et al., 1998; Ehlers et al., 2005).

The assumption of a geothermal gradient is critical to estimating exhumation rates. Typical geothermal gradients for continental crust are 25-30°C/km (Dumitru, 1990; Foster and John, 1999; Moore and England, 2001). In modern settings, the geothermal gradient can be

measured directly by deep drilling. In the modern Basin-and-Range, gradients are highly variable, in some geothermal wells exceeding 100°C/km (Sass, 1999). However, estimates of paleo geothermal gradients become more difficult further back in time. Estimates of Miocene gradients before Basin-and-Range extension range ~15-50°C/km (Foster et al., 1991; Foster and John, 1999). Published estimates of the Cretaceous geothermal gradient around the time of maximum crustal thickness are high, up to $70 \pm 30^\circ\text{C}/\text{km}$, but probably $\sim 50^\circ\text{C}/\text{km}$ based on metamorphic thermobarometry studies (Miller and Gans, 1989). A range of geothermal gradients was evaluated for this study from 30-60°C/km (Table 4.4), however the Cretaceous gradient that best matched geological observations was $\sim 50^\circ\text{C}/\text{km}$. The geothermal gradient can change over time in response to rapid exhumation, leading to isothermal compression until thermal equilibrium can be re-established (Moore and England, 2001; Reiners and Brandon, 2006). In this study, however, the geothermal gradient assumed constant throughout the Cretaceous for simplicity. A geothermal gradient of 50°C/km puts the closure isotherms of AHe, AFT and ZHe at ~1, ~2 and ~3 km respectively.

The rate of exhumation and cooling can also change over time as a result of changes in rate of erosion or tectonic denudation, e.g., normal faulting, that disturb thermal equilibrium. Sampling from a vertical transect can improve estimates of a cooling rate. The difference in cooling age between the top and bottom samples records how rapidly the height of the section cooled through a particular closure isotherm. The effect of pre-, syn- and post-extensional Basin-and-Range geothermal gradients was not taken into account in this study because all samples had cooled through the T_c of ZHe, AFT and AHe systems prior to the onset of Miocene Basin-and-Range extension.

4.5.2 Time-temperature-depth histories

4.5.2.1 Little Boulder Basin Stock

AHe, AFT and ZHe data from the Little Boulder Basin Stock are combined to determine the thermal histories of single samples, as well as the composite vertical section to determine the thermal history of the stock as a whole. The absence of nearby younger intrusions, hydrothermal alteration or mineralization, and the simple cooling paths supported by HeFTy modelling suggest the thermal history of the Little Boulder Basin Stock was determined predominantly by exhumation and related cooling.

Samples from deep drill holes in the Little Boulder Basin Stock were collected to create a composite vertical transect through the stock to allow construction of an age-elevation profiles to aid interpretation of the timing of major cooling and exhumation events (Figure 4.9a). Samples were collected assuming a continuous section could be constructed, and that no material had been added or lost from the ~1.3 km vertical sample profile. However, detailed examination of ZHe, AFT and AHe in combination suggests that this may not have been the case, as some material does appear to have been removed from the vertical section. The distribution of ages and suspected loss intervals are summarised in Figure 4.16. The uppermost sample, LBB76-343 at 1647 m, has a ZHe age of 154.1 ± 14.8 Ma, that records cooling through the ZHe closure isotherm, ~150°C, shortly after emplacement at ~158 Ma. Assuming the geothermal gradient was 50°C/km (as discussed above) and surface temperature was 10°C, the depth of the ZHe closure isotherm was at ~3 km. LBB76-343 has an AFT age of $121.6 +14.2 - 12.8$ Ma, which records cooling through the AFT closure isotherm, ~100°C, at ~2 km. The next sample with a ZHe age is LBB76-1038 at 1457 m, which has a ZHe age of 107.3 ± 2.3 Ma and an AFT age of $74.3 +9.5 - 8.5$ Ma. These cooling ages indicate LBB76-1038 cooled through 150°C at ~3 km by ~107 Ma and through 100°C at ~2 km by ~68 Ma. LBB76-343 and

LBB76-1038 currently lie 200 m apart vertically, differing in ambient temperature by $<10^{\circ}\text{C}$. If sample LBB76-343 was <2 km at ~ 121 Ma, then sample LBB76-1038 should also have been ≤ 2 km and record a similar AFT age to LBB76-343. However, ZHe data indicates LBB76-1038 was still $>150^{\circ}\text{C}$, 3 km, until 107 Ma. If sample LBB76-343 cooled to $<100^{\circ}\text{C}$ by 121 Ma, then sample LBB76-1038 just 200 m, $<10^{\circ}\text{C}$, below should have a similar AFT age rather than its observed AFT age of ~ 74 Ma, and should have a ZHe age older than 121 Ma. The apparent difference of ~ 1 km during the Cretaceous suggests faulting may have caused displacement of samples LBB76-343 and LBB76-576 relative to sample LBB76-762 and below since 107 Ma.

An alternative explanation for the observed ZHe-AFT relationship is a Cretaceous reheating event that totally reset AFT age in the Little Boulder Basin Stock ~ 75 Ma and partially reset the ZHe system in all but the uppermost sample, which retains its post-emplacement cooling age ~ 154 Ma. Forward modelling t-T paths using HeFTy shows that reheating could have reset AFT ages and partially reset ZHe ages in deeper Little Boulder Basin Stock samples, as the paths in Figure 4.18 show. Heating is most commonly caused by hydrothermal activity or emplacement of younger intrusions, however there is no evidence of hydrothermal activity in the Little Boulder Basin Stock in the drill holes sampled. The stock in this drill hole is unmineralized and only minimally altered, and no Cretaceous intrusions have been described in the northern Carlin Trend. Another cause of heating is burial. Although burial could occur by thrusting in a compressive setting such as the Sevier Orogeny, there is no evidence of Cretaceous thrusting or significant sedimentation in the northern Carlin Trend.

Further evidence of different cooling histories for upper and bulk portions of the Little Boulder Basin Stock is recorded in the distribution of fission track lengths. The distribution of fission track lengths differs between the two samples, with bimodal distribution in LBB76-343

and a unimodal distribution in LBB76-1038. HeFTy models of LBB76-343 support a two-stage cooling history over temperatures 100-20°C at ~150 Ma and 80-60 Ma, whereas models of LBB76-1038 and deeper samples show that a single dominant cooling event ~80-60 Ma is more plausible for those deeper samples from the bulk of the stock. No ZHe ages were obtained for AFT samples LBB76-567 or LBB76-762, which lie at 1584 m and 1533 m, between LBB76-343 and LBB76-1038. Sample LBB76-567 has a similar bimodal track length distribution and two-stage cooling "good fit" HeFTy model paths to the upper sample, LBB76-343. Sample LBB76-762 has a similar unimodal track length distribution and HeFTy model to LBB76-1038. Any material lost was therefore from between samples LBB76-576 and LBB76-762 (Figure 4.16). A similar difference in track length distribution, AFT age and t-T model paths suggests material may also have been removed from between samples LBB102-1035 and LBB-1940, although the lack of ZHe age for LBB102-1035 makes this less constrained.

The most feasible explanation for removal of the intervening material is a fault that moved LBB76-343 and -576 down 1 km relative to their present position ~200 m above the other Little Boulder Basin samples. The orientation of such a fault is uncertain, but could have a similar north-northwest strike to the Post Fault system and dip steeply to the west or east, or cut roughly northeast as shown in Figure 4.17. A fault is noted in the drill log for hole LBB76-343 at around 1560 m elevation and one is shown in the cross-sections of Moore and Norby (2002) that shows faults within the stock. The similar AHe ages of samples LBB76-343 (above the proposed fault) and LBB76-1038 (below the fault) of ~65 Ma suggest that displacement occurred prior to or at this time, and that both samples cooled to <50°C, <1 km, at the same time.

The bulk of the Little Boulder Basin Stock (LBB76-762 and deeper samples, ~900 m vertical section) was emplaced at >150°C, equivalent to >3 km and was slowly exhumed and

cooled to bring sample LBB76-1038 through the ZHe closure isotherm at ~3 km around 107 Ma. ZHe ages of deeper samples, LBB102-1940 and LBB102-3900, record a pulse of rapid cooling ~85 Ma that resulted from exhumation of the remaining 900 m of the transect through the ZHe closure isotherm. By ~65 Ma all samples in the 1.1 km section had also cooled through the AFT closure isotherm, 100°C, ~2 km in another rapid pulse at ~70-65 Ma. Sample LBB76-1038 had cooled through the AHe closure isotherm ~50°C, <1 km below the surface by 65 Ma. No AHe data was obtained for deeper samples in the Little Boulder Basin Stock, so it cannot be determined how much of the stock was exhumed to <1 km in that exhumation event. Either just the upper samples, the top 0.2 km of the section, which have AHe ages, were <1 km, and the rest of the section was deeper, or the entire sampled bulk of the stock was exhumed to <1 km and brought to near its present position where upper samples are within a few hundred meters of the surface. In the former case, where only the top 0.2 km of the section was <1 km, total cooling between 85 and 65 Ma was ~100°C at an average rate of 5°C/Myr. Total exhumation was therefore ~2 km, from ~3 km to ~1 km, at a rate of 0.1 km/Myr assuming a steady rate of exhumation. If the entire bulk of the stock was exhumed to <1 km, exhumation over the same 20 Myr period was ~3 km, at a rate of 0.15 km/Myr. However, exhumation is unlikely to have proceeded at a constant rate throughout the 20 Myr period 85-65 Ma, and instead probably occurred in several more rapid phases, one at ~85 Ma as recorded in the steep ZHe age-elevation profile, and a second at 70-65 Ma, recorded in the AFT data. In the case of episodic exhumation, rates were feasibly up to 1 km/Myr if the whole vertical section was exhumed through the closure isotherm within ~1 Myr.

The stock has not been buried to a depth greater than ~1 km since 65 Ma, as the AHe dates have not been reset since exhumation through the AHe closure isotherm. The Little Boulder Basin Stock is currently buried below ~0.1-0.2 km of Miocene Carlin Formation. The

present thickness of cover is not enough to affect the thermal history of the stock at present geothermal gradients of $\leq 30^{\circ}\text{C}/\text{km}$.

4.5.2.2 Vivian Sill

The Vivian Sill is at a higher elevation than the Little Boulder Basin Stock and records a shallower thermal history extension of the Little Boulder Basin age-elevation profile, although abundant faults likely caused relative displacement of the stock and the sill. The upper Vivian Sill sample, Viv-A, B at 1989 m, cooled through the AFT closure isotherm $\sim 100^{\circ}\text{C}$, ~ 2 km, by ~ 130 Ma. Sample V-1 of Chakurian et al. (2003) at 1920 m cooled through $\sim 100^{\circ}\text{C}$, ~ 2 km at ~ 92 Ma. All dated Vivian samples have bimodal track length distributions and "good fit" two-stage model cooling histories. The Vivian Sill is therefore interpreted to have spent significant time within a paleo PRZ between emplacement at ~ 158 Ma and ~ 90 Ma, when the sill was exhumed enough to cool the lower elevation sample to below $\sim 100^{\circ}\text{C}$. Viv-A, B, presently only 70 m above V-1, could have sat just above the paleo PRZ after 130 Ma, while V-1 remained within it. However, as 70 m is the equivalent of only $3\text{--}4^{\circ}\text{C}$, it is likely that faulting on one or more of the numerous faults around the sill has also removed material from between the Vivian Sill samples.

4.5.2.3 Goldstrike Stock

Examination of AFT ages from the Goldstrike Stock shows that samples around the edge of the stock have cooling ages of ≤ 40 Ma, younger than samples in the centre of the stock, ~ 60 Ma. The samples around the edge therefore cooled later than samples in the stock's centre. ZHe ages, however, are consistent across the stock, suggesting the observed difference is not related to exhumation. The thermal history of the Goldstrike Stock therefore appears to have been

complicated by reheating by hydrothermal fluids that deposited Au around the outside of the stock in the Eocene. Samples from the edge of the Goldstrike Stock typically have AFT ages ~40 Ma, coincident with the timing of Au mineralization, and are therefore interpreted as totally reset by heating from hydrothermal fluids. Abundant good fit paths in HeFTy support this interpretation, showing rapid heating and cooling ~40 Ma was possible.

The age-elevation profile and overall t-T history of the Goldstrike Stock is dominated by ZHe and AFT cooling at 80-60 Ma, similar to the Little Boulder Basin Stock (Figure 4.9, 4.11). Downhole samples from drill holes GS-1845CW from this study and ST7 of Chakurian et al. (2003) from the centre of the stock have AFT ages ~60 Ma and ZHe ages ~75-80 Ma, and record rapid cooling through the ZHe and AFT closure isotherms, through ~150-100°C in ~20 Myr at an average cooling rate of 2.5°C/Myr. The effective T_c correspond to exhumation through depths of ~3 and ~2 km between 80 and 60 Ma, assuming a geothermal gradient of 50°C/km, at an average exhumation rate of 0.05 km/Myr. Cooling and exhumation may have continued to shallower depths and cooler temperatures, however subsequent Eocene heating would have removed thermal evidence of this. Exhumation was potentially from >3 km to approaching 1 km depth. If 2 km exhumation occurred over 20 Myr, the cooling and exhumation rates were up to 5°C/km and 0.1 km/Myr respectively. Inverse modelling of fission track data in HeFTy cannot constrain the pre-Eocene heating temperature because of the extent of reheating ~40 Ma. Cooling was not through the AHe closure isotherm, because AHe ages not do record Eocene cooling ages similar to AFT ages of samples around the edge of the stock.

Although the Goldstrike Stock downhole ages are younger than the Little Boulder Basin Stock, HeFTy modelling of AFT data suggests the same major cooling occurred at 80-60 Ma in both stocks. A heating event ~40 Ma can also be modelled in HeFTy in central stock samples,

however heating was insufficient to cause total resetting of the AFT system, and models do not permit as much heating as totally reset edge samples do. Heating by ~180-240°C Carlin fluids was insufficient over the duration of the hydrothermal system to cause total resetting of AFT in samples across the entire stock. Instead, Eocene hydrothermal activity only raised the temperature across the stock enough to partially reset samples away from its edge, resulting in AFT ages that are typically slightly younger than in the Little Boulder Basin Stock. Alternatively, partial resetting was minimal in the centre of the stock and the AFT ages do represent exhumational cooling ages through the AFT closure isotherm ~100°C at ~2 km, which occurred 5-10 Myr later in the Goldstrike Stock than the Little Boulder Basin Stock. HeFTy models cannot be used to distinguish whether cooling occurred nearer 70 or 60 Ma, as the fission track data supports either.

ZHe ages in the Goldstrike Stock are ~75-80 Ma, also slightly younger than the Little Boulder Basin Stock. While it is possible for the ZHe system to be partially reset, the lower temperature limit of the ZHe PRZ is higher than that of the AFT upper temperature PRZ limit (Figure 4.19) and so is more resistant than AFT to partial resetting by Carlin fluid temperatures. Heating that would partially reset the ZHe system would therefore totally reset the AFT system, which is not observed. ZHe ages are fairly consistent across the Goldstrike Stock, similar in both edge samples that have totally reset Eocene AFT ages, and central samples that have Late Cretaceous-Paleocene AFT ages. If partial resetting of the ZHe system did occur, edge samples should have younger ZHe ages than central samples, which is not observed. This suggests that the ZHe system was not partially reset by Eocene hydrothermal heating, and therefore that the Goldstrike Stock was exhumed through the ZHe closure isotherm ~3 km deep 5-10 Myr later than the Little Boulder Basin Stock. Exhumation of the

Goldstrike Stock through the AFT closure isotherm was therefore likely also 5-10 Myr later than the Little Boulder Basin Stock.

The AHe ~ 30 Ma ages in the Goldstrike Stock can be explained in two ways. They may record Cenozoic exhumation through the AHe closure isotherm, $\sim 50^\circ\text{C}$, the equivalent of ~ 1 km depth. Alternatively, the ~ 30 Ma AHe ages record reheating by localised hydrothermal heating, which would also explain the $20.9 +15.6 -8.9$ Ma AFT age obtained in sample RM91-22C-1460 and the 20.3 ± 0.5 Ma AHe age of sample RM94-03C-459 on the northern edge of the stock. Localised post-Eocene hydrothermal activity that has been documented around the northern Carlin Trend (Fleck et al., 1998)

Chakurian et al. (2003) obtained an AHe age of 21.4 ± 1.3 Ma for central downhole sample ST7-D at 994 m, ~ 350 m below the ~ 30 Ma ages. ST7-D is near the centre of the Goldstrike Stock and not expected to be affected by hydrothermal heating around the outside of the stock. The ~ 21.4 Ma age could therefore record cooling through the AHe isotherm ~ 10 Myr after other AHe samples that are 350 m shallower. If Goldstrike AHe ages do record exhumation, then ~ 1 km material has been eroded from above the stocks since ~ 30 Ma, at a rate < 0.04 km/Myr. Additional AHe data from downhole samples in the Goldstrike Stock and deeper in the Little Boulder Basin Stock would elucidate whether AHe ages are related to exhumation or to local hydrothermal heating. Post-Oligocene exhumation and associated cooling of the stocks was below the T_c of AHe, and therefore too low temperature to be recorded with the methods used in this study. However, if the AHe ages record local hydrothermal heating, then the Goldstrike Stock was already shallower than the AHe isotherm, ~ 1 km, and near its present depth as early as the Late Cretaceous, similar to the Little Boulder Basin Stock.

4.5.2.4 Central Tuscarora regional samples

Central Tuscarora samples are detrital samples collected over a small vertical range and large lateral extent, so it is not possible to construct a meaningful age-elevation profile. Neoproterozoic to Mississippian ZHe ages are detrital ages, and record the time at which the source rocks were exhumed through the ZHe closure isotherm, prior to their erosion and subsequent deposition as the sampled passive margin sediments. The preservation of old ZHe ages indicates the samples have not been heated to above 150°C over geological timescales 10^7 - 10^8 years since deposits, so have not been buried to ≥ 3 km. The younging of ZHe ages to the north reflects input from more recently exhumed source rocks and does not record the thermal history of the central Tuscarora Mountains.

In contrast, AFT ages are Cretaceous, indicating that the central Tuscarora samples were heated to $>100^\circ\text{C}$, the AFT T_c , erasing earlier Mississippian-Neoproterozoic ages. Following deposition in the Ordovician, the samples were buried to >2 km, where they were heated and AFT ages were thermally reset. Pre-Cretaceous geothermal gradients were probably lower than $50^\circ\text{C}/\text{Myr}$, so burial could have been >3 km. HeFTy modelling shows samples were $>80^\circ\text{C}$ and typically $>100^\circ\text{C}$ prior to ~ 160 Ma before gradual cooling to present day temperatures began between 130 and 80 Ma. Most samples had already cooled through the AFT closure isotherm, through $\sim 100^\circ\text{C}$, ~ 2 -3 km, by 80 Ma and so have older, Cretaceous, AFT ages. However, HeFTy models of the majority of samples do show some cooling ~ 80 Ma, coincident with exhumation-related cooling observed in the Little Boulder Basin and Goldstrike Stocks.

The timing of cooling, inferred to be related to exhumation, varies between samples. The variation in the timing of cooling periods may be attributable to abundant localised faulting in the area that offset samples in different fault blocks (Theodore et al., 2003), localised heating e.g., by hydrothermal activity, intrusions, or variations in depth relative to the Jurassic-

Cretaceous paleosurface. Samples towards the northern end of the section were nearer to the Cretaceous paleosurface than samples further south, so cooled earlier, and therefore have older AFT ages than samples further south. Samples towards the southern end of the section have AFT ages similar to the Little Boulder Basin Stock, Goldstrike Stocks and Vivian Sill, and so were $>100^{\circ}\text{C}$, ~ 2 km deep, until exhumation in the Late Cretaceous.

The younging of AFT ages towards the south in the Tuscarora section may be evidence of tilting throughout the Mesozoic, or of greater Mesozoic exhumation of the area around the northern Carlin Trend than of the central Tuscaroras to the north. The Eocene sediments that unconformably overlie the Ordovician Vinini Formation to the north presently dip $\sim 30^{\circ}$ to the north (K. Hickey, pers. comm.). Tilting must have occurred subsequent to the deposition of the sediments, perhaps during Miocene Basin-and-Range faulting.

4.5.3 Interpreted timing and motion on the Post Fault

Overall, the Goldstrike Stock has a similar exhumation history to the Little Boulder Basin Stock but major exhumation occurred ~ 5 - 10 Myr later in the Goldstrike Stock than the Little Boulder Basin Stock. With the exception of upper Little Boulder Basin Stock samples LBB76-343 and -576, samples from both stocks were emplaced at $>150^{\circ}\text{C}$, equivalent to >3 km. The onset of rapid cooling is recorded in the ZHe ages in both the Little Boulder Basin and Goldstrike Stocks, and occurred at ~ 85 Ma and ~ 75 - 80 Ma respectively. Rapid cooling continued to $<100^{\circ}\text{C}$ by ~ 65 Ma, as recorded in downhole AFT data, indicating that both ~ 1 km vertical sample profiles had been exhumed to $<\sim 2$ km by the Late Cretaceous. If Little Boulder Basin AHe data of ~ 65 Ma are included, rapid cooling of the uppermost Little Boulder Basin samples continued through $\sim 50^{\circ}\text{C}$, the AHe T_c , suggesting those upper samples had been exhumed to within ~ 1 km of the Late Cretaceous paleosurface.

The ~5-10 Myr difference in cooling through the ZHe and possibly AFT closure isotherms between the Little Boulder Basin Stock, in the hanging wall of the Post fault system, and Goldstrike Stock, in the footwall, implies some motion occurred on the Post Fault around the time of cooling through 150-100°C, between 3-2 km. The amount of offset between the stocks can be estimated based on examination of their age-elevation profiles (Figure 4.9). The upper part of the bulk Little Boulder Basin Stock age-elevation profile has a shallower slope where higher elevation samples have older AFT and ZHe ages than deeper samples. This shallow slope is not present in the Goldstrike Stock samples collected over a similar elevation range to Little Boulder Basin samples. The shallow slope part of the age-elevation curve in the Little Boulder Basin Stock can be interpreted as a record of slower cooling, either due to a period of residence in a paleo PRZ, or to slower exhumation prior to the phase of Late Cretaceous rapid cooling and exhumation. The absence of this shallow slope part of the Goldstrike Stock age-elevation profile suggests that stock has been exhumed further than the Little Boulder Basin Stock, and the shallow part of the age-elevation profile that was once preserved in the upper portions of the Goldstrike Stock has been eroded. The minimum difference in exhumation is therefore the difference between the elevation of the inflection point in the Little Boulder Basin Stock profile and the elevation of the uppermost Goldstrike Stock sample, which could have been just below the now-removed inflection point in the Goldstrike age-elevation profile. In the Little Boulder Basin Stock the inflection point is ~1400 m in both AFT and ZHe age-elevation profiles, ~250 m below the highest elevation Goldstrike Stock sample that was not reset by Eocene hydrothermal heating. The Post Fault therefore accommodated at least 250 m vertical displacement, and possibly more if more Goldstrike material was removed between the uppermost Goldstrike sample and the eroded age-elevation

inflection point. Displacement occurred since exhumation of both the Goldstrike and Little Boulder Basin Stocks had been exhumed through the AFT closure isotherm.

The proposed timing of fault motion is coincident with the main phase of exhumation, ~80-60 Ma. Offset did not occur prior to this, or the Little Boulder Basin and Goldstrike ZHe and AFT ages would be the same. Based on the ~5-10 Myr difference between the stocks passing through the ZHe closure isotherm, ~150°C, at ~3 km, and the estimated average exhumation rate of 0.05-0.1 km/Myr during the rapid exhumation phase, the Goldstrike Stock was exhumed 0.25-1 km further than the Little Boulder Basin Stock, 0.05-0.1 km every Myr for a period of 5-10 Myr. The stocks are now at similar elevations, so the Goldstrike Stock must originally have been ~0.25-1 km deeper than the Little Boulder Basin Stock. The upper estimate of ~1 km offset on the Post Fault is within the estimated 0.8-1.6 km separation on the Post Fault described in the literature (Bettles, 2002). Examination of the published geology in Moore and Norby (2002) and Heitt et al. (2003) shows ~1 km offset of the RMT across the Post Fault system and ~1 km offset on opposite sides of the Little Boulder Basin Stock in the vicinity of the study area, potentially accommodated by the inferred Little Boulder Basin Fault.

The timing of fault motion could also have occurred since exhumation of both stocks through the ZHe and AFT closure isotherms. At the very latest, offsetting therefore occurred before the Mid Miocene, before deposition of the overlying Carlin Formation which contains basal gravels that include weathered granodiorite clasts (Jory, 2002), suggesting the stocks were at one point exposed at surface prior to Carlin Formation deposition.

Up to 1 km material appears to have been lost from Little Boulder Basin Stock between samples LBB76-576 and LBB76-762. Uppermost samples LBB76-343 and LBB76-576 were emplaced at ≤ 3 km, constrained by the ZHe age of LBB76-343, ~154 Ma, which is almost the same as the emplacement age, ~158 Ma. A proposed fault caused up to 1 km relative motion.

The AHe age of samples LBB76-343 above the fault and LBB76-1038 below the fault are both ~65 Ma, indicating the offset occurred prior to that time.

4.5.4 Interpreted exhumation of the northern Carlin Trend

The Little Boulder Basin and Goldstrike Stocks record exhumation from >3-4 km, from emplacement to their present depths within 0.1 km of the surface. The Tuscarora samples are presently ~1 km higher elevation, and record 2-3 km exhumation in total. The Tuscarora samples record gradual Early-Mid Cretaceous cooling through the AFT closure isotherm, ~100°C, which assuming a geothermal gradient of 50°C/km, is equivalent to a depth of ~2 km. The uppermost part of the Little Boulder Basin Stock (LBB76-343 and -576) and the Vivian Sill were shallower than the Goldstrike Stock and main bulk of the Little Boulder Basin Stock and also record Mid Cretaceous cooling and exhumation. A major exhumation event took place in the Late Cretaceous between ~85 and 60 Ma, and involved at least 2-3 km exhumation of the stocks. During the same event, movement on the Post Fault could have exhumed the Goldstrike Stock ~1 km relative to the Little Boulder Basin Stock to its present position. A similar amount of offset is inferred on a proposed fault in the Little Boulder Basin Stock that brought the bulk of the stock ~1 km up to its present position just below the uppermost LB section samples, LBB76-343 and -576. Regional Tuscarora samples do not record these Late Cretaceous ages because they had already been exhumed through the AFT closure isotherm. AHe data suggests the Little Boulder Basin Stock was within 1 km of the surface at the end of the Cretaceous, and possibly at surface, as a result of average exhumation rates of >0.1 km/Myr and as high as 1 km/Myr is exhumation occurred in rapid pulses at ~85 Ma and at 70-65 Ma. AHe ages in the Goldstrike Stock are 30-20 Ma, and are interpreted as cooling ages resulting from more gradual exhumation at a rate <0.04 km/Myr since the major

phase of exhumation ended ~60 Ma. Goldstrike AHe ages may have recorded Late Cretaceous cooling through the higher temperature AHe closure isotherm 60°C at ~1 km for, but would have been reset by Eocene hydrothermal heating and so instead record cooling through the lower temperature closure isotherm, 50°C, <1 km. In total, >4 km exhumation is recorded in ZHe, AFT and AHe thermochronology data from the Goldstrike and Little Boulder Basin Stocks, the majority of which occurred in one or more rapid pulses between 85 and 60 Ma.

4.6 Discussion

4.6.1 Timing of exhumation

Major Late Cretaceous cooling between ~85-60 Ma is recorded in ZHe, AFT and AHe data and is attributed to 3-4 km of exhumation. The amount of total exhumation is based on the assumption of a constant Late Cretaceous geothermal gradient of 50°C/km. A lower geothermal gradient would require a greater amount of total exhumation to cause the observed pattern of cooling ages, e.g., at 30°C/km total exhumation would be ~4-5 km. The period of exhumation is coincident with published phases of regional cooling and exhumation. The Late Cretaceous has been identified as a period of regional extension across northern Nevada associated with the collapse of overthickened Sevier hinterland (Vandervoort and Schmitt, 1990; Wells et al., 1990; Livaccari, 1991; Hodges and Walker, 1992; Camilleri and Chamberlain, 1997; Wells and Hoisch, 2008; Druschke et al., 2009b). Studies of metamorphic assemblages, which suggest maximum crustal thickness and peak metamorphism were attained in the Late Cretaceous by 84 Ma, and extensional collapse of the thickened crust began soon after, sometime between 84 and 75 Ma (Camilleri and Chamberlain, 1997). Based on Lu-Hf garnet and U-Th monazite dating, Wells et al. (2012) proposed that a decompression event

occurred between 86 and 65 Ma, resulting from regional extension in the Sevier hinterland at that time.

Exhumation results from removal of overlying material, denudation, that can be erosional, tectonic, or a combination of the two (Ring et al., 1999). Tectonic denudation occurs in the footwall of a low-angle normal fault by removing overlying hanging wall rocks, as normal slip uplifts and exposes the footwall. Erosion requires removal of material by air or water (or gravity in the case of rockfall) and is driven primarily by topographic relief. As surface uplift proceeds, drainage systems incise deeper into the surface to maintain drainage equilibrium relative to a base level, such as the ocean or lake (Burbank and Anderson, 2011). In the area around the northern Carlin Trend, there is no reported evidence of Cretaceous low-angle faulting. Exhumation around the northern Carlin Trend therefore results from either tectonic exhumation on high-angle normal faults, across the Post Fault system, or from erosional denudation as the gradually uplifted surface was stripped by integrated large scale drainage that transported material to distant basins.

Although Sevier contraction was ongoing, many workers have described evidence on syn-orogenic extension in the Sevier hinterland. Evidence of extension includes retrograde metamorphic assemblages dated to ~85-65 Ma interpreted to signify a period of regional decompression (Wells et al., 1990; Camilleri and Chamberlain, 1997; Wells and Hoisch, 2008; Wells et al., 2012) as well as surface-breaking syn-sedimentary normal faults (Druschke et al., 2009b). Widespread, large-scale Cretaceous sedimentary basins have not been identified, but Cretaceous sediments have been described across northern Nevada, now fragmented by Cenozoic Basin-and-Range extension (Vandervoort and Schmitt, 1990; Crafford, 2007; Druschke et al., 2009a; Druschke et al., 2009b; Druschke et al., 2011).

Synconvergent extension has been recognised in similar tectonic settings to the Sevier hinterland. Examples include the Tibetan Plateau in the Himalayas (Hodges et al., 1992) and the Andean Altiplano-Puna Plateau (Allmendinger et al., 1997). Proposed mechanisms for synconvergent extension are highly debated (Coney and Harms, 1984; Platt, 1986; England and Houseman, 1989; Allmendinger, 1992). Proposed mechanisms in the Sevier hinterland include slab rollback, which slows convergence and reduces horizontal compressive stress (Royden, 1993; Collins, 2002; Saleeby, 2003), or convective removal or delamination of the dense lithospheric mantle, which result in an increase in elevation and gravitational potential energy that leads to collapse and extension. Geological and modelling evidence indicates the Farallon slab shallowed rather than steepened in the Late Cretaceous, so slab rollback is unlikely to have occurred at that time (Coney and Harms, 1984; Engebretson et al., 1984; Wells et al., 2012). The preferred model for the Sevier Orogeny is delamination of lithospheric mantle and decoupling of the crust from the mantle by lower crustal heating, hydration and partial melting (Figure 4.20) (Bird, 1979; England and Houseman, 1989; DeCelles, 2004; Wells and Hoisch, 2008; Wells et al., 2012). Extension is accompanied by crustal thinning and normal faulting, which results in tectonic exhumation as deeper rocks are brought to the surface, as well as denudational exhumation as rocks in the hanging wall are eroded. Figure 4.20c shows how uplift occurs following delamination, initiated by removal of dense lithospheric mantle that increase in crustal buoyancy and isostatic rebound, in turn increasing rates of erosion.

Estimates of maximum crustal thickness of the Cretaceous Sevier hinterland vary from 45-70 km (Coney and Harms, 1984; Miller and Gans, 1989; Colgan et al., 2006; DeCelles and Coogan, 2006), thinning to as little as 38 km following Late Cretaceous extension and collapse (Colgan et al., 2006). Estimates of total exhumation are also highly variable but many workers

have suggested values of ~7-15 km (Hudec, 1992; Colgan et al., 2006; Wells and Hoisch, 2008). Data from the Little Boulder Basin and Goldstrike Stocks, Vivian Sill and central Tuscarora Mountains record exhumation through a total of ~4 km, less than the lower limit estimate of total exhumation. However, larger estimates are based on studies of metamorphic core complexes exhumed on large detachment faults from depths of 20-30 km (Hudec, 1992; Camilleri and Chamberlain, 1997; Colgan et al., 2010) throughout the Cenozoic (Coney and Harms, 1984; McGrew et al., 2000; Howard, 2003; Colgan et al., 2010). These record a deeper exhumation history than the relatively shallow vertical range sampled in this study.

4.6.2 Accommodation of eroded material from the northern Carlin Trend

Cretaceous synconvergent extension was for some time considered confined to mid crustal levels (Hodges and Walker, 1992). Decoupling between shallow and mid crust has also been invoked to explain extension at mid crustal levels only (Hodges and Walker, 1992). However, Druschke et al. (2009b) described syn-extensional faulting and surface breaking normal faults with up to 4 km throw in the Cretaceous Sheep Pass Formation south of the present study area, evidence that extension did occur at shallow crustal and surface levels during the Cretaceous. Druschke et al. (2009b) constrained formation of the extensional basin and sedimentation in the Sheep Pass Formation to 81-66 Ma using ZHe and U-Pb dating, and determined paleo drainage was to the south. Similar Cretaceous basins have been identified across Nevada (Vandervoort and Schmitt, 1990), including the Newark Canyon Formation, also to the south of the study area near the Cortez Range. A zircon U-Pb date of 125-127 Ma was obtained for a basal conglomerate sample of that formation (K. Hickey, written comm.), showing basin formation and sedimentation occurred over a significant time period in the Cretaceous. Paleo drainage studies show drainage was to the south in the Newark Canyon

Formation (Biglow, 1986; Suydam, 1988). Southward drainage suggests material was being shed from high ground to the north, potentially from the northern Carlin Trend area, although provenance of basin material has not been conclusively determined. Sources include Paleozoic sediments, which are ubiquitous in northern central Nevada, as well as Jurassic and Early Cretaceous material (Vandervoort and Schmitt, 1990). Despite their fragmented distribution, the existence of Cretaceous-Paleogene sedimentary basins across northern Nevada is evidence of regional extension and topographic relief, and also provides potential depocentres for material eroded from the northern Carlin Trend area during exhumation in the Late Cretaceous. In his study of Eocene paleo valleys, Henry (2008) suggests Eocene drainage was roughly east-west, with rivers flowing east to the Uinta Basin in Utah or west to the Pacific Ocean, which was in California's Great Valley at the time. If these large drainage systems were established earlier, sediment could have been removed to distal depocentres in either direction.

4.6.3 Motion on the Post Fault

Between 250 m and 1 km normal throw occurred on the Post Fault towards the end of the main exhumation phase in the Late Cretaceous. This is within the estimated 0.8-1.6 km based on geological and geophysical observation (Bettles, 2002). It is possible that offsetting occurred subsequent to the main Late Cretaceous exhumation phase, for example during the Eocene as invoked by Micklethwaite (2010) as a primary control on Au mineralization distribution. Eocene fault motion is also a potential driving force for hydrothermal fluids flow, which is addressed further in Chapter 5. It is therefore possible that motion occurred over a longer period of time subsequent to the rapid exhumation of the northern Carlin Trend area. The overlying Miocene Carlin Formation is offset by up to 100 m around the Meikle deposit, evidence of post-Miocene motion, however the presence of weathered clasts in the basal

gravels of the Carlin Formation suggests erosion of the paleo PRZ portion of the Goldstrike Stock occurred prior to Miocene deposition.

The presence of another fault, within the Little Boulder Basin Stock, is inferred based on discrepancies within the Little Boulder Basin ZHe and AFT data that require up to 1 km offset. Although not described anywhere, a fault is shown in cross sections of the northern Carlin Trend, and would explain the apparent 1 km stratigraphic offset observed on the east and west sides of the Little Boulder Basin Stock. Any motion on the proposed fault occurred prior to 65 Ma, the AHe age of samples above and below the fault.

4.6.4 Implications for the formation of Carlin-type Au deposits

Approximately 1 km exhumation of the northern Carlin Trend has occurred of the Goldstrike Stock since the Late Cretaceous. The depth of major Au ore bodies is currently 0.2-0.3 km (Bettles, 2002). Estimates of exhumation in this study therefore suggest that Eocene Au mineralization occurred at a depth of ~1.2-1.3 km. This is in keeping with previous estimates of depth of mineralization of 0.3-3 km based on reconstructions of Eocene paleo landscape, ore-fluid phase equilibria, and textural observations in coeval intrusions and jasperoids (Hofstra and Cline, 2000; Hickey, 2003; Nutt and Hofstra, 2003; Cline et al., 2005).

Although the major phase of exhumation occurred in the Late Cretaceous, ~25 Myr prior to hydrothermal activity responsible for Au mineralization, exhumation may have contributed to the formation of Au deposits in the northern Carlin Trend. It has been shown that faults were active during Late Cretaceous exhumation, maintaining motion on deep north-northwest trending faults such as the Post Fault, that were important conduits to hydrothermal fluids in the Eocene. Motion on the Post Fault up to 1 km may have increased Eocene fluid flow into favorable carbonate host rocks in shallow crustal levels, by placing very low permeability

Upper Plate siliciclastic rocks of the hanging wall against Lower Plate carbonate host rocks in the footwall.

4.7 Conclusions

New AFT, ZHe and AHe data presented in this study combined with existing thermochronology data from the northern Carlin Trend show a major period of exhumation affected the area in the Late Cretaceous. An estimated 3-4 km exhumation occurred between ~85-60 Ma at rates of up to 1 km/Myr at an average of ~0.1 km/Myr. Eroded material is not preserved in the immediate area, but Cretaceous basins, now fragmented by more recent Basin-and-Range topography, were present. Cretaceous basins south of the study area record southward drainage, so may have accommodated material from the Carlin Trend area. Larger scale drainage could also have removed large volumes of overlying material and deposited them in distant basins far to the east and west. The timing of rapid exhumation is in keeping with proposed gravitational collapse of overthickened Cretaceous Sevier hinterland crust by mid and shallow crustal levels. Since ~60 Ma, ~1 km further exhumation has brought the Jurassic Little Boulder Basin and Goldstrike Stocks to present subsurface levels. Estimates of rate of this slower exhumation are <0.04 km/Myr, and are inferred to be controlled predominantly by erosion.

Regional AFT data from the central Tuscarora Mountains to the north of the northern Carlin Trend record exhumation from depths 2-3 km, less than proposed around the main study area around the Little Boulder Basin and Goldstrike Stocks. Samples were never buried to the depths at which the stocks were emplaced, but a younging to the south trend suggests exhumation was greater around the stocks than across the Tuscarora Mountains to the north.

New thermochronology data from deep drill holes in the Little Boulder Basin and Goldstrike Stocks record up to 1 km throw across the Post Fault, and ~1 km on an inferred fault within the Little Boulder Basin Stock. The timing of motion on both faults occurred during or at the end of the major phase of exhumation, 85-60 Ma.

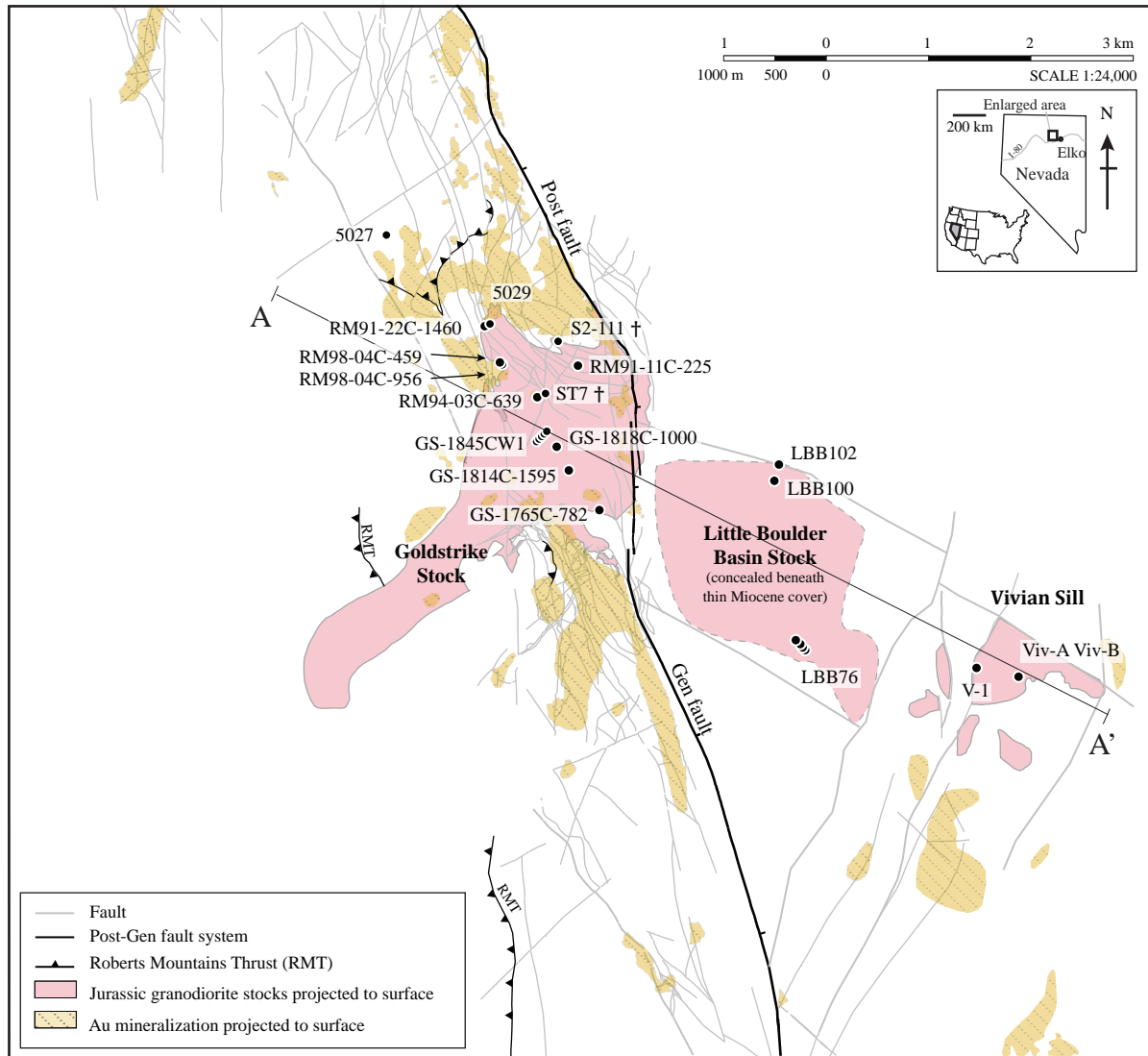


Figure 4.1 Map of the study area in the northern Carlin Trend showing the location of the Goldstrike and Little Boulder Stocks, Vivian Sill and samples used in this study. Samples marked † are from Chakurian et al. (2003). The surface projection of Au mineralization, Post-Gen fault system and Roberts Mountains Thrust are also shown. Section A-A' is shown in Figure 4.2. Geology after Teal and Jackson (2002), Moore (2002) and Heitt et al. (2003).

Section A-A'

Cross section across Goldstrike Stock, Little Boulder Stock, Vivian Sill

Looking 025 NNE

No vertical exaggeration

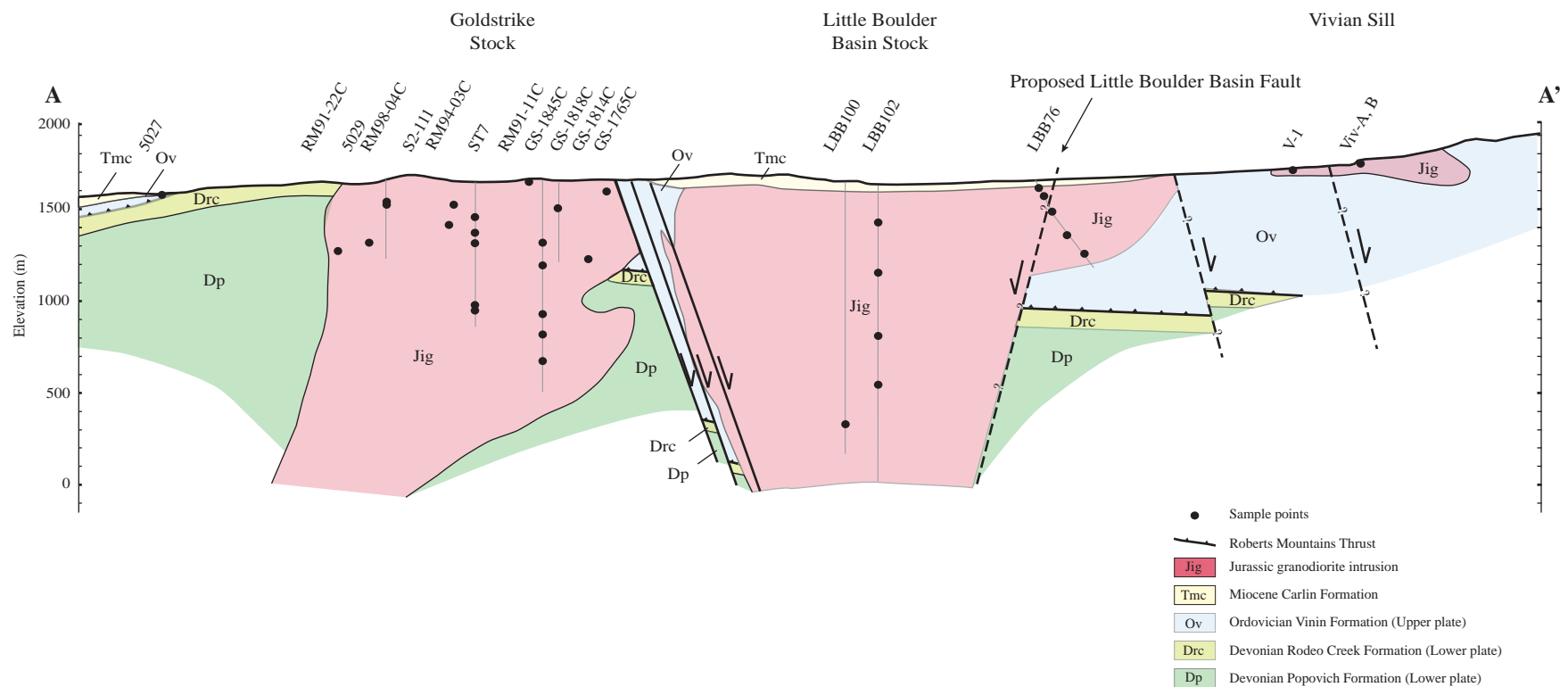


Figure 4.2 Interpreted geological cross section A-A' across Goldstrike Stock, Little Boulder Basin Stock and Vivian Sill with projected drill hole and sample locations Section line shown in Figure 4.1. Geology modified from Moore and Norby (2002) and Heitt et al. (2003).

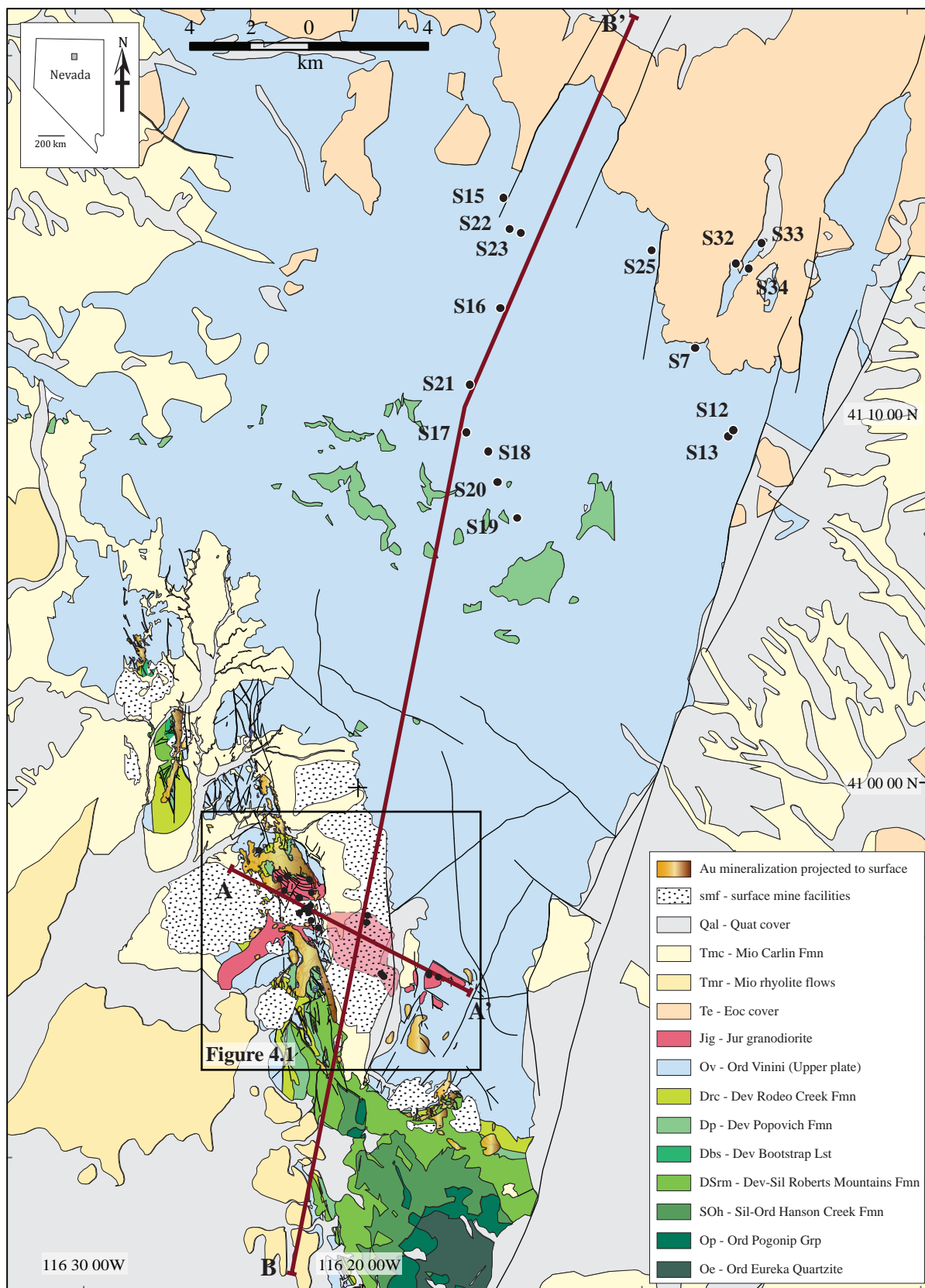


Figure 4.3 Location of Central Tuscarora Mountains regional samples relative to the main study area shown in Figure 4.1 (box). Section lines A-A', B-B' are also shown. Geology after Moore (2002) and Crafford (2007).

Section B-B'

Regional cross section through northern Carlin Trend and Tuscarora Mountains
Two times vertical exaggeration

Looking 280 WNW

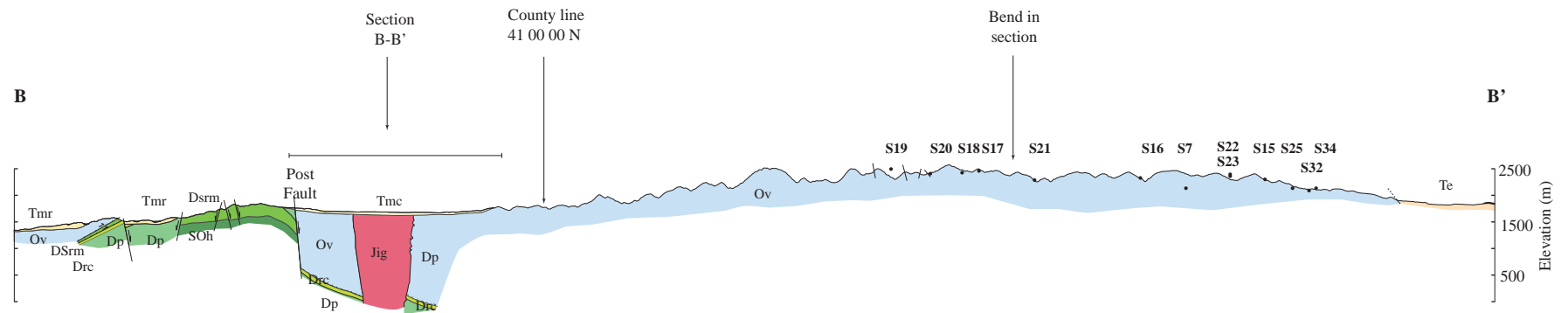


Figure 4.4 Regional cross section through northern Carlin Trend and Tuscarora Mountains showing location of Tuscarora (S-) samples. Locations of Little Boulder Basin Stock samples are also shown. Geology compiled from Moore and Norby (2002), Crafford (2007) and Theodore et al. (2003).

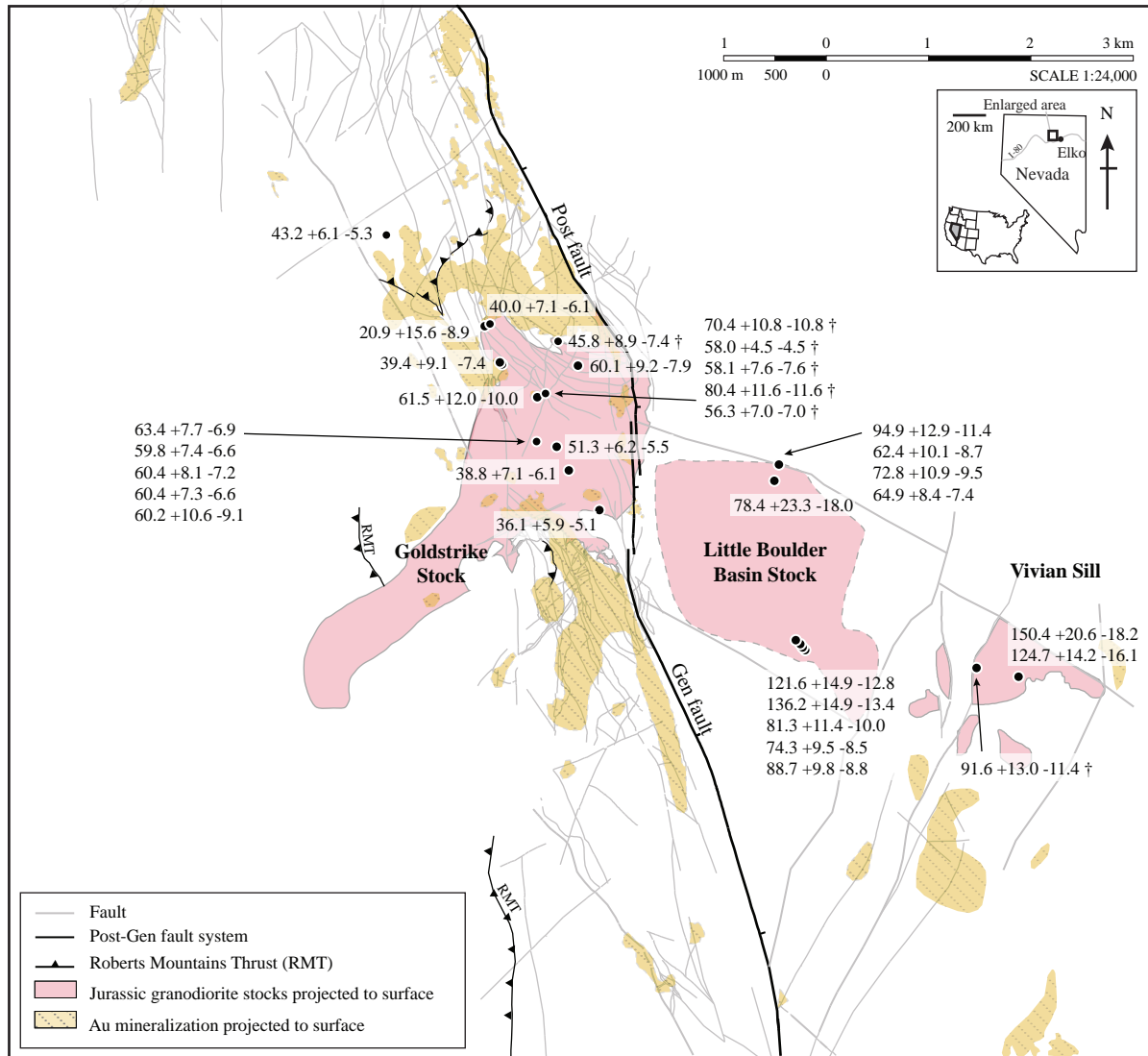


Figure 4.5 Map of the study area in the northern Carlin Trend showing pooled AFT ages used in this chapter. Samples marked † are from Chakurian et al. (2003). AFT ages of Chakurian et al. (2003) from the Little Boulder Basin Stock are not shown; they are within error of LBB76 samples dated over the same intervals.

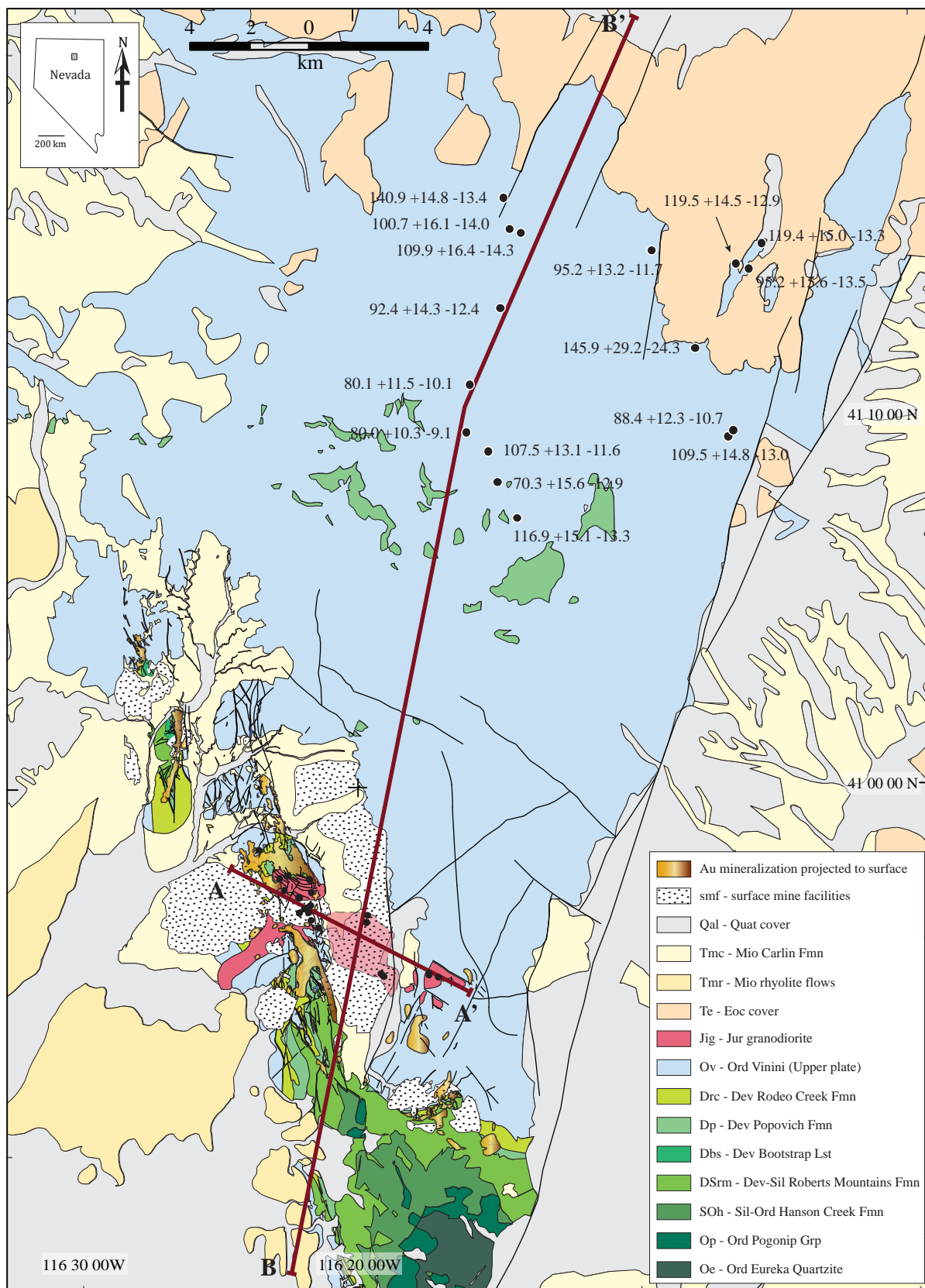


Figure 4.6 Central Tuscarora Mountains AFT ages. Section lines A-A' and B-B' are also shown. Geology after Moore (2002) and Crafford (2007).

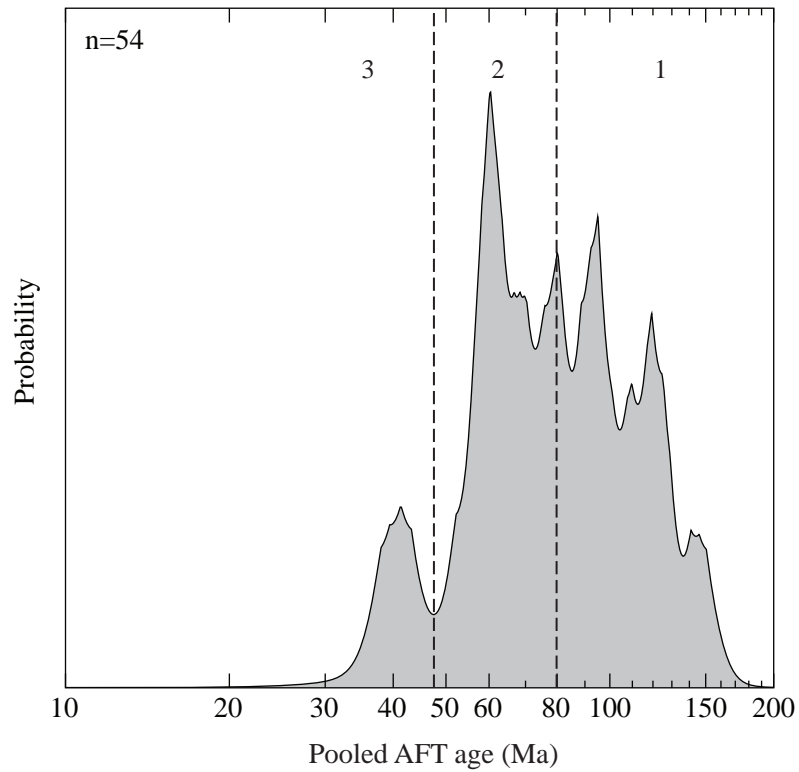


Figure 4.7 Probability plot for pooled AFT sample ages from this study. Main peaks are at 40 Ma, 60 Ma, 80 Ma, 100 Ma and 120 Ma. (1) Ages ≥ 100 Ma are from high elevation samples in the Little Boulder Stock, Vivian Sill and central Tuscarora Mountains. (2) Peaks at 80 Ma and 60 Ma record Late Cretaceous exhumation through the AFT closure isotherm. (3) The peak at 40 Ma comprises ages proximal to Au mineralization and records resetting by hydrothermal heating associated with the formation of the Carlin Au deposits.

Section A-A'

Cross section across Goldstrike Stock, Little Boulder Stock, Vivian Sill

Looking 025 NNE

No vertical exaggeration

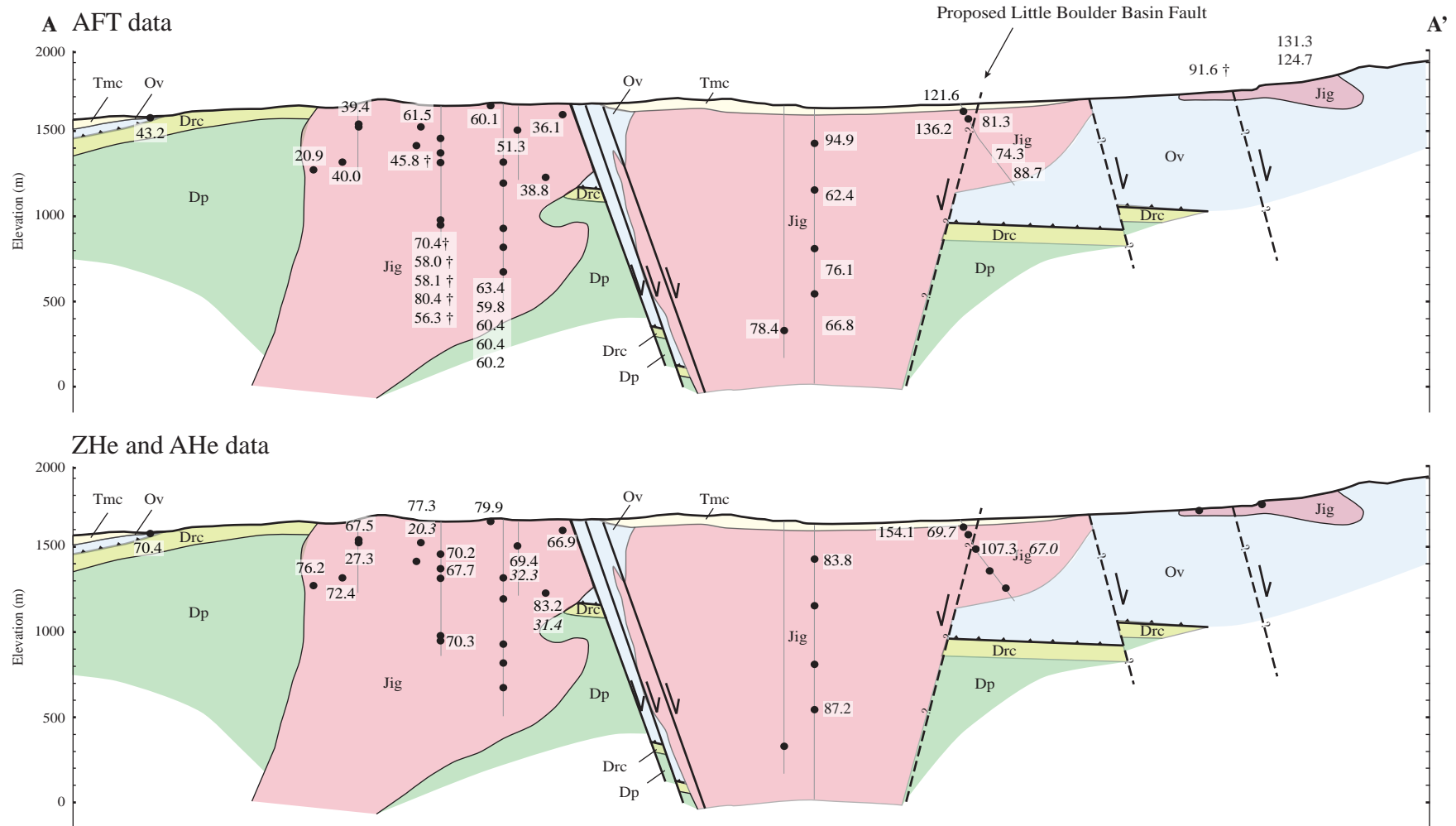


Figure 4.8 Interpreted geological cross section A-A' across Goldstrike Stock, Little Boulder Basin Stock and Vivian Sill with projected drill hole and sample locations and AFT, ZHe and AHe data. ' denotes AFT data from Chakurian et al. (2003). Section line shown in Figure 4.1. Geology after Moore and Norby (2002) and Heitt et al. (2003) as shown in Figure 4.2..

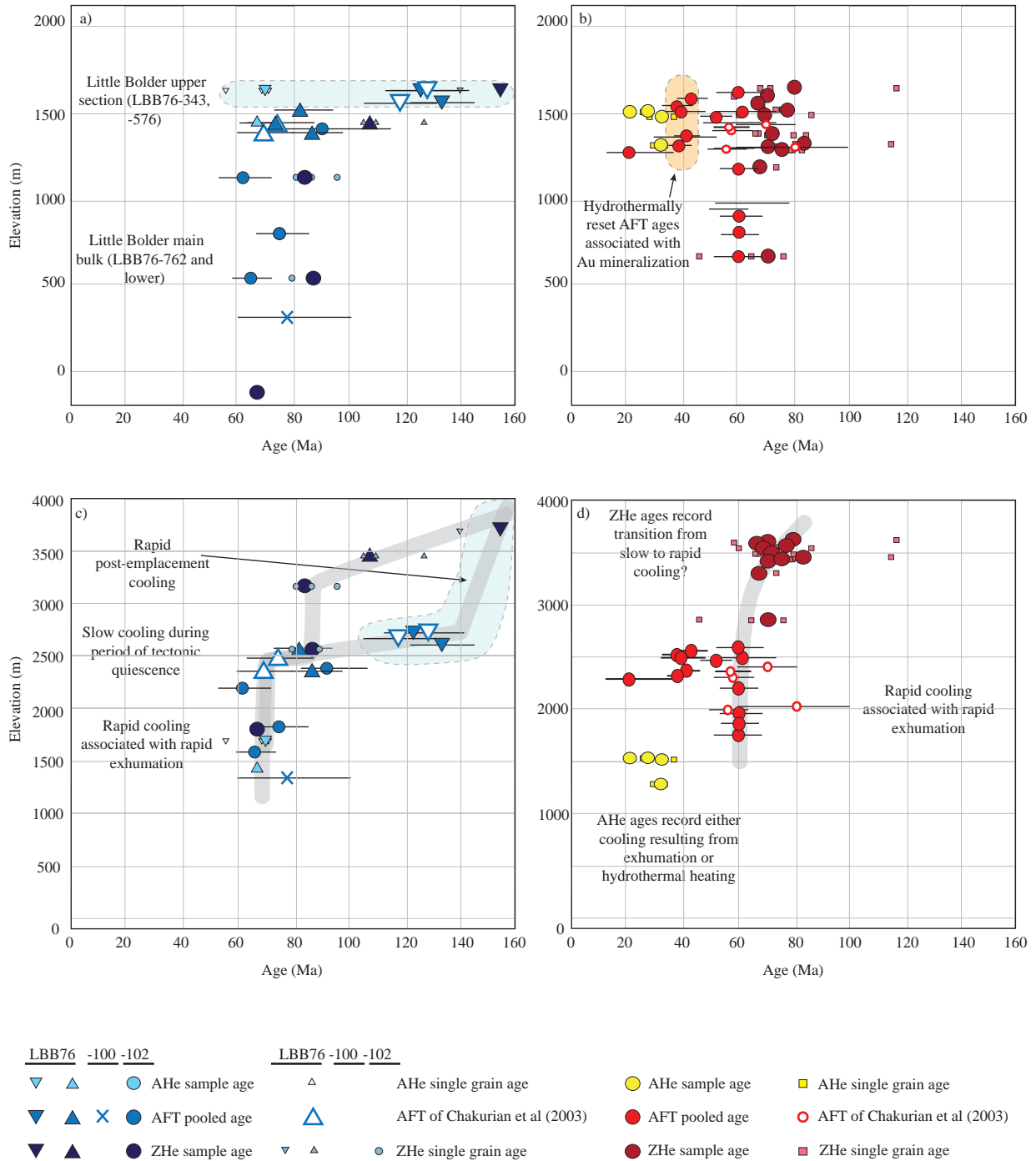


Figure 4.9 Age-elevation plots of AHe, AFT and ZHe data for the Little Boulder Basin Stock (a) and Goldstrike Stock (b). Pseudo-elevation plots are also shown for the Little Boulder Basin Stock (c) and Goldstrike Stock (d). In pseudo-elevation plots, AHe ages are shown at their measured elevation and AFT and ZHe data are offset upwards from their measured elevation by a height equal to the difference in depth to the respective closure isotherms following procedure in Reiners and Brandon (2006). The T_c of AFT is 50°C hotter than AHe, so assuming a geothermal gradient of 50°C/km, AFT data are offset upwards by 1 km relative to AHe. The T_c of ZHe is 100°C hotter than AHe, so ZHe data are offset upwards by 2 km relative to AHe.

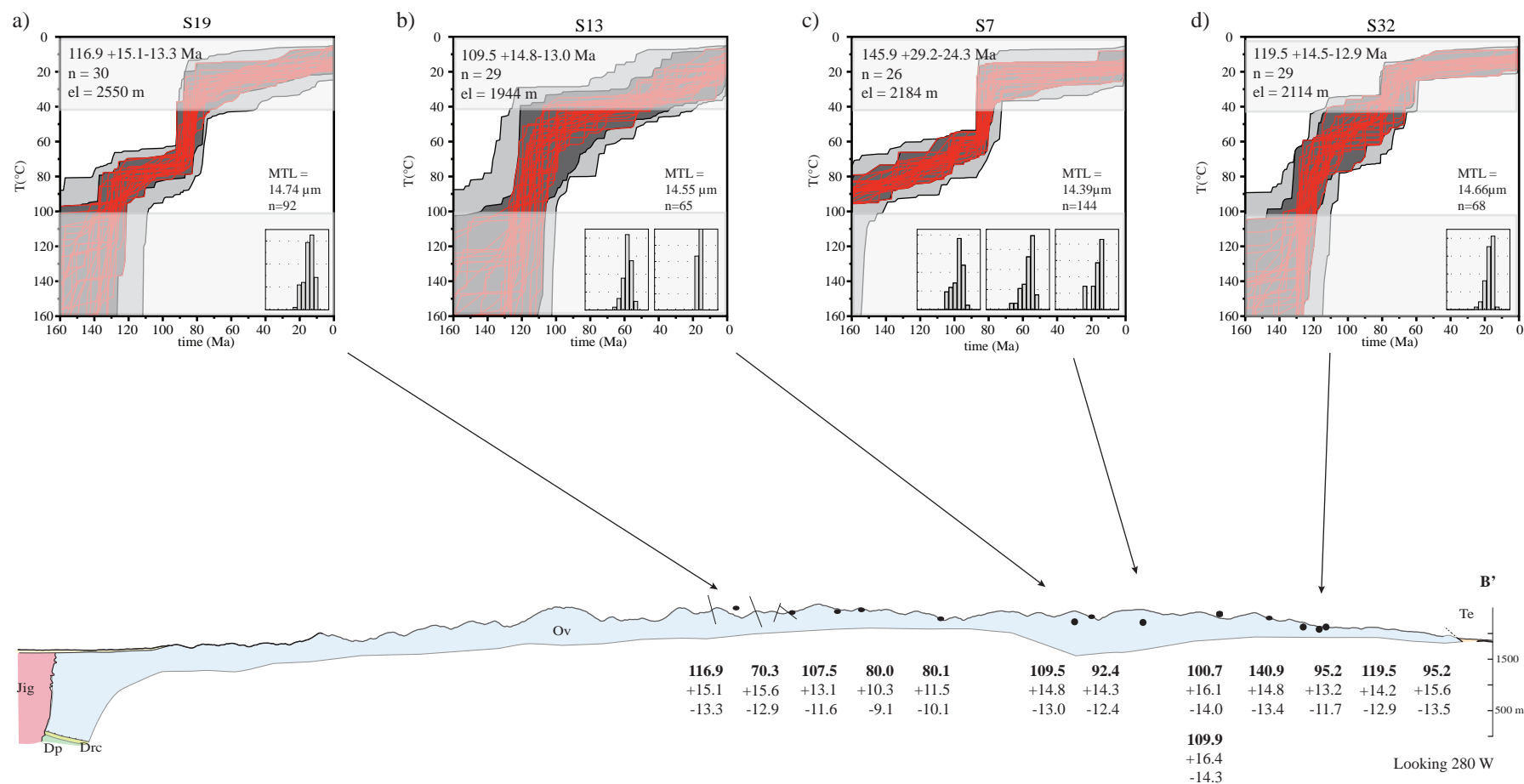


Figure 4.10 AFT ages and modelled t-T histories for selected Central Tuscarora regional samples along part of section A-A'. Models show more gradual cooling paths over the temperature range 100-40°C than the granodiorite intrusions at the southern end of the section (Figure 4.11). All but S13 (b) also show a component of rapid cooling around 80 Ma. Track length distributions are unimodal in whole samples and subpopulations (shown). Shaded regions of HeFTy models cover temperature ranges poorly constrained by AFT data alone.

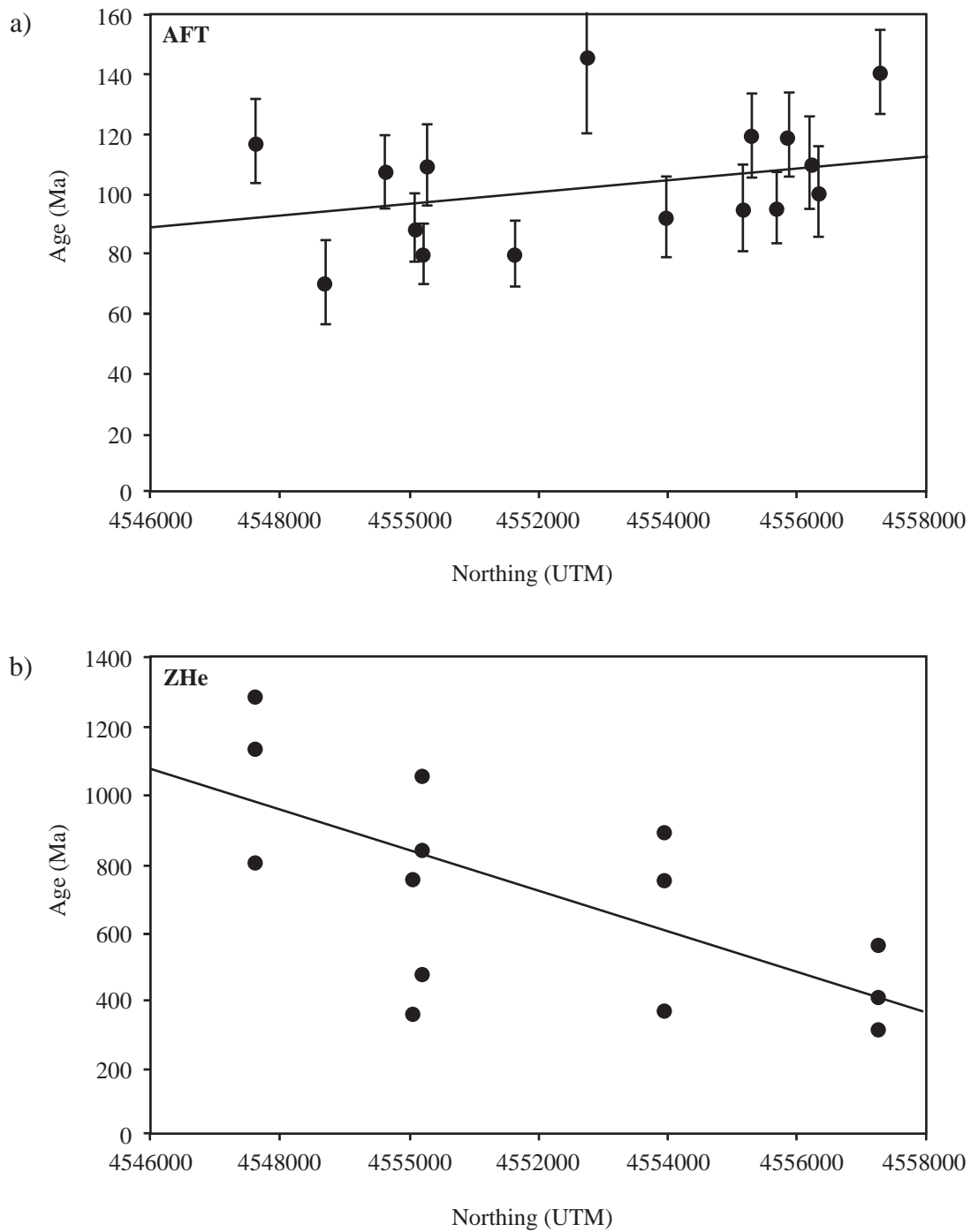


Figure 4.11 AFT (a) and ZHe (b) ages correlate with northing among Central Tuscarora samples. AFT pooled sample ages increase further north, ZHe single grain ages decrease. ZHe ages are interpreted as detrital ages due to their age and intra-sample variation. ZHe errors are smaller than symbol size.

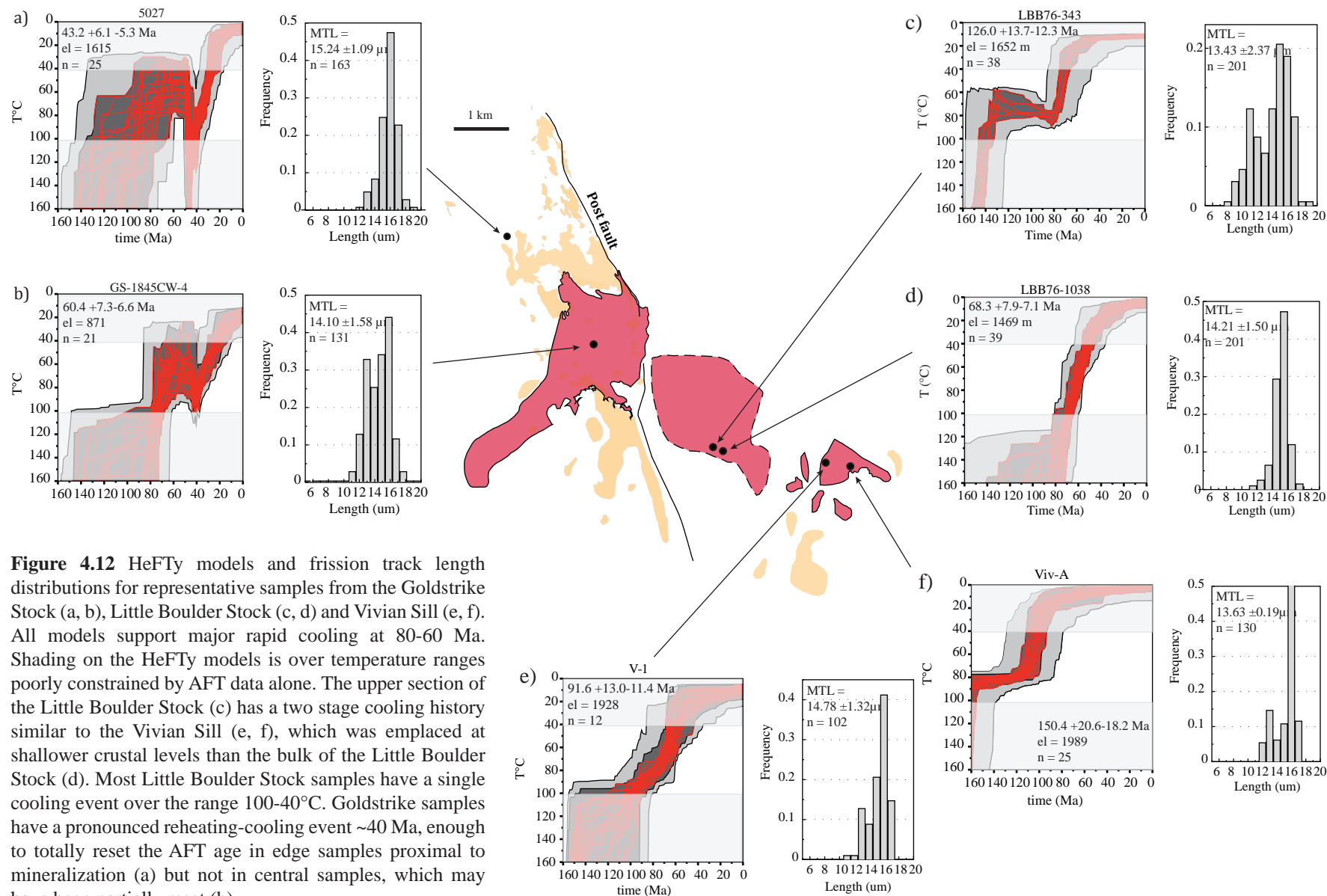


Figure 4.12 HeFTy models and fission track length distributions for representative samples from the Goldstrike Stock (a, b), Little Boulder Stock (c, d) and Vivian Sill (e, f). All models support major rapid cooling at 80-60 Ma. Shading on the HeFTy models is over temperature ranges poorly constrained by AFT data alone. The upper section of the Little Boulder Stock (c) has a two stage cooling history similar to the Vivian Sill (e, f), which was emplaced at shallower crustal levels than the bulk of the Little Boulder Stock (d). Most Little Boulder Stock samples have a single cooling event over the range 100-40°C. Goldstrike samples have a pronounced reheating-cooling event ~40 Ma, enough to totally reset the AFT age in edge samples proximal to mineralization (a) but not in central samples, which may have been partially reset (b).

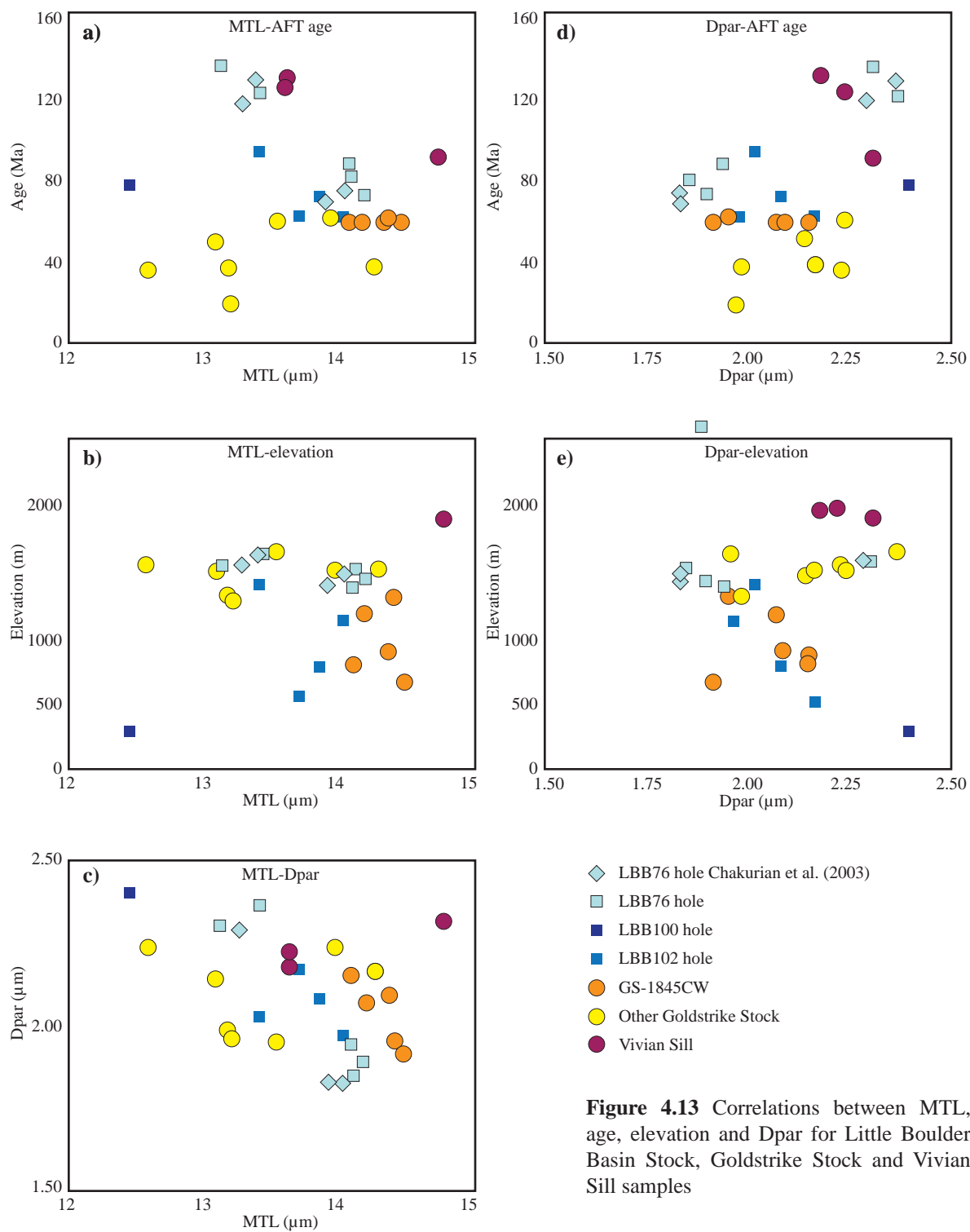


Figure 4.13 Correlations between MTL, age, elevation and Dpar for Little Boulder Basin Stock, Goldstrike Stock and Vivian Sill samples

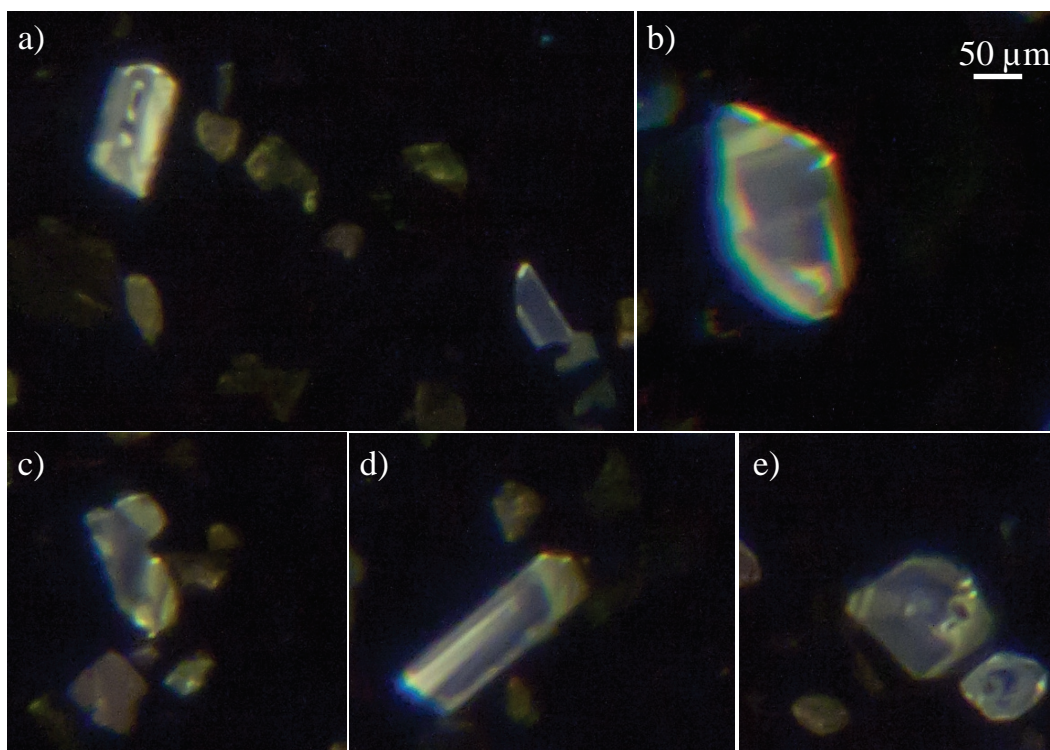


Figure 4.14 CL images of zoned zircons in GS-1765C-782. Darker areas indicate higher U content, brighter areas indicate lower U. Most zircons observed are zoned. U-rich inclusions are also observed (a). U zoning within a crystal can result in overestimation of age if the core is U-rich, or underestimation of age if the rim is U-rich.

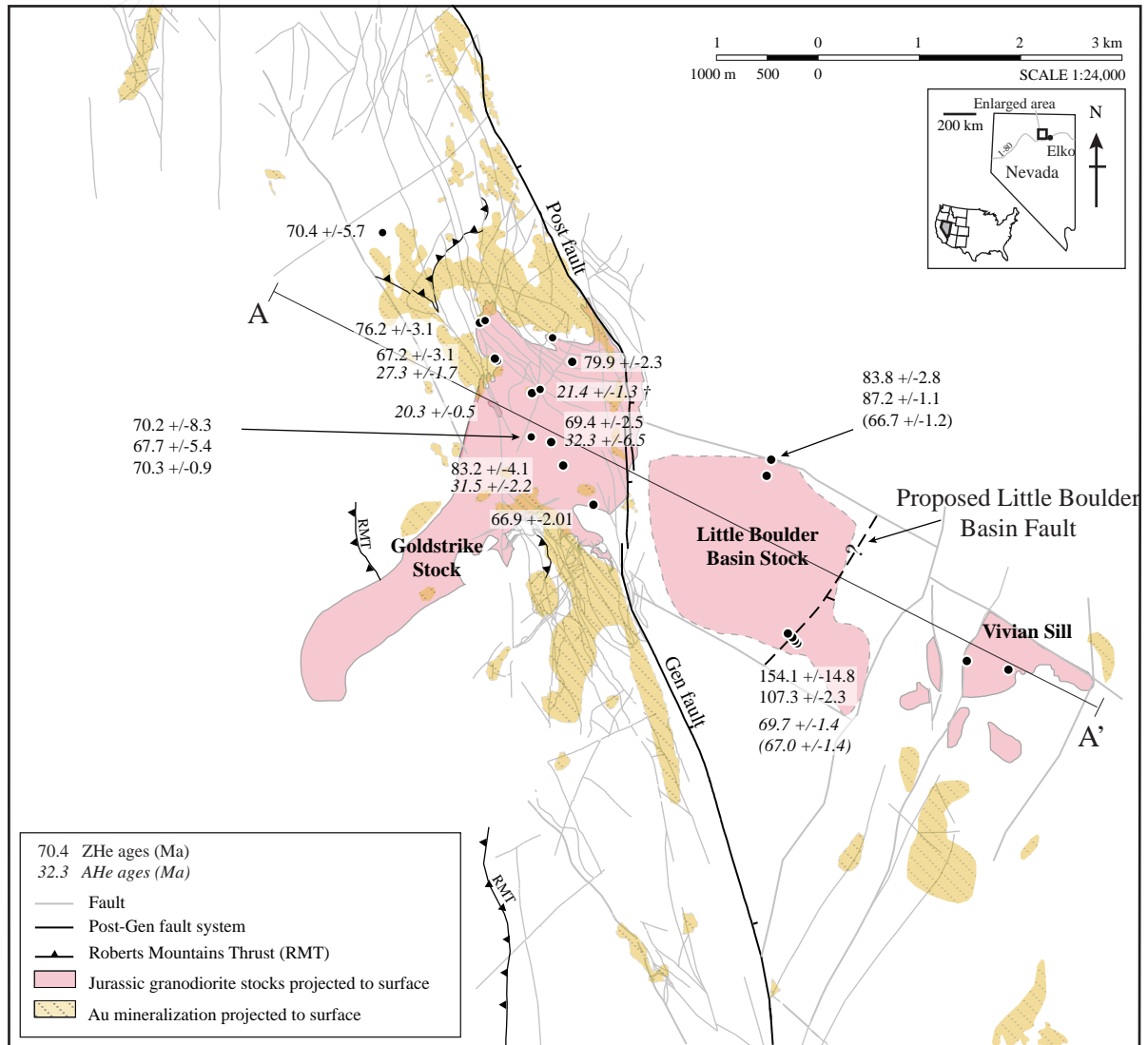


Figure 4.15 Map of the northern Carlin Trend showing ZHe and AHe (italics) ages used in this chapter. Samples in parentheses are based on a single He age. Samples marked † are from Chakurian et al. (2003). A proposed fault in the Little Boulder Basin Stock is also shown.

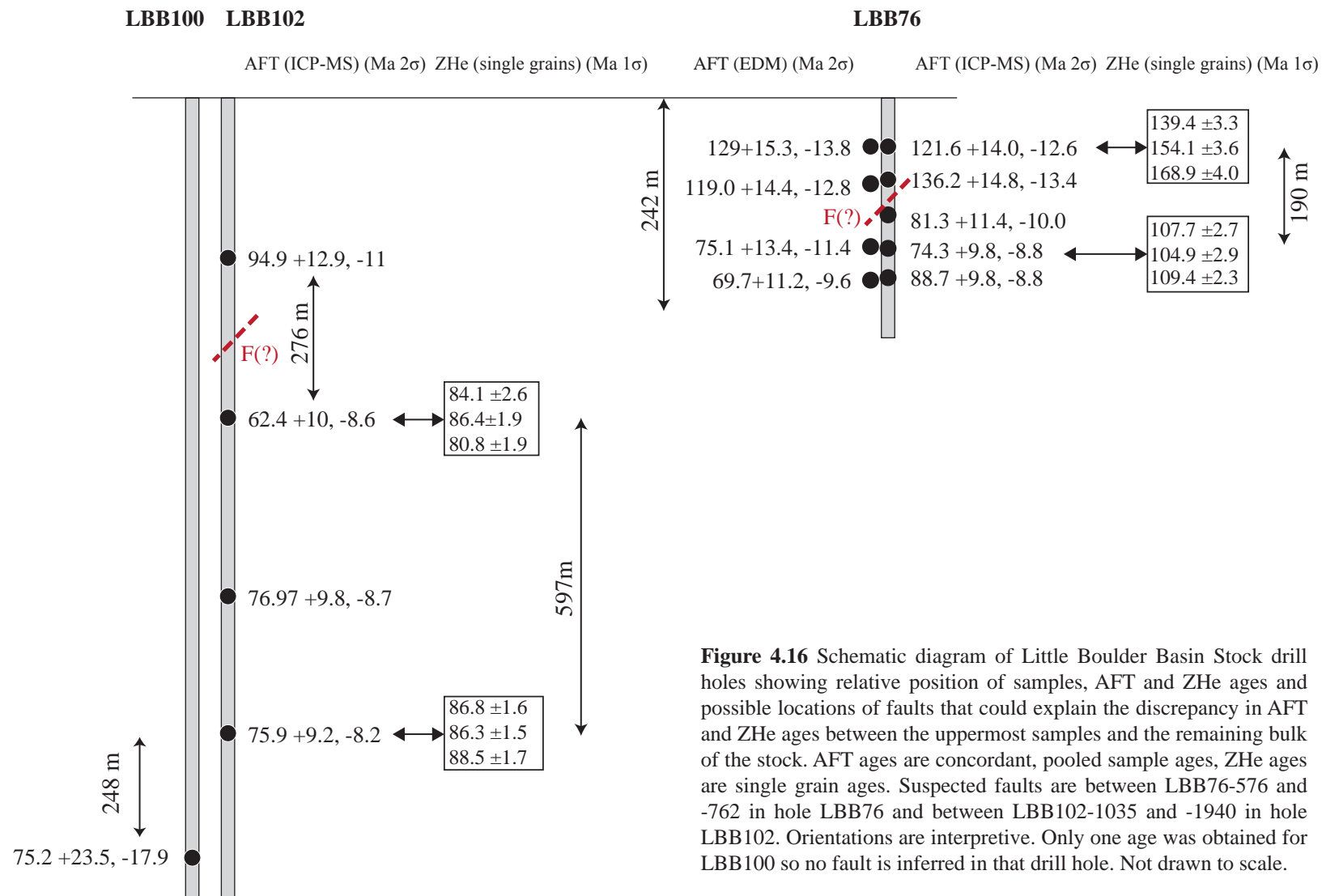


Figure 4.16 Schematic diagram of Little Boulder Basin Stock drill holes showing relative position of samples, AFT and ZHe ages and possible locations of faults that could explain the discrepancy in AFT and ZHe ages between the uppermost samples and the remaining bulk of the stock. AFT ages are concordant, pooled sample ages, ZHe ages are single grain ages. Suspected faults are between LBB76-576 and -762 in hole LBB76 and between LBB102-1035 and -1940 in hole LBB102. Orientations are interpretive. Only one age was obtained for LBB100 so no fault is inferred in that drill hole. Not drawn to scale.

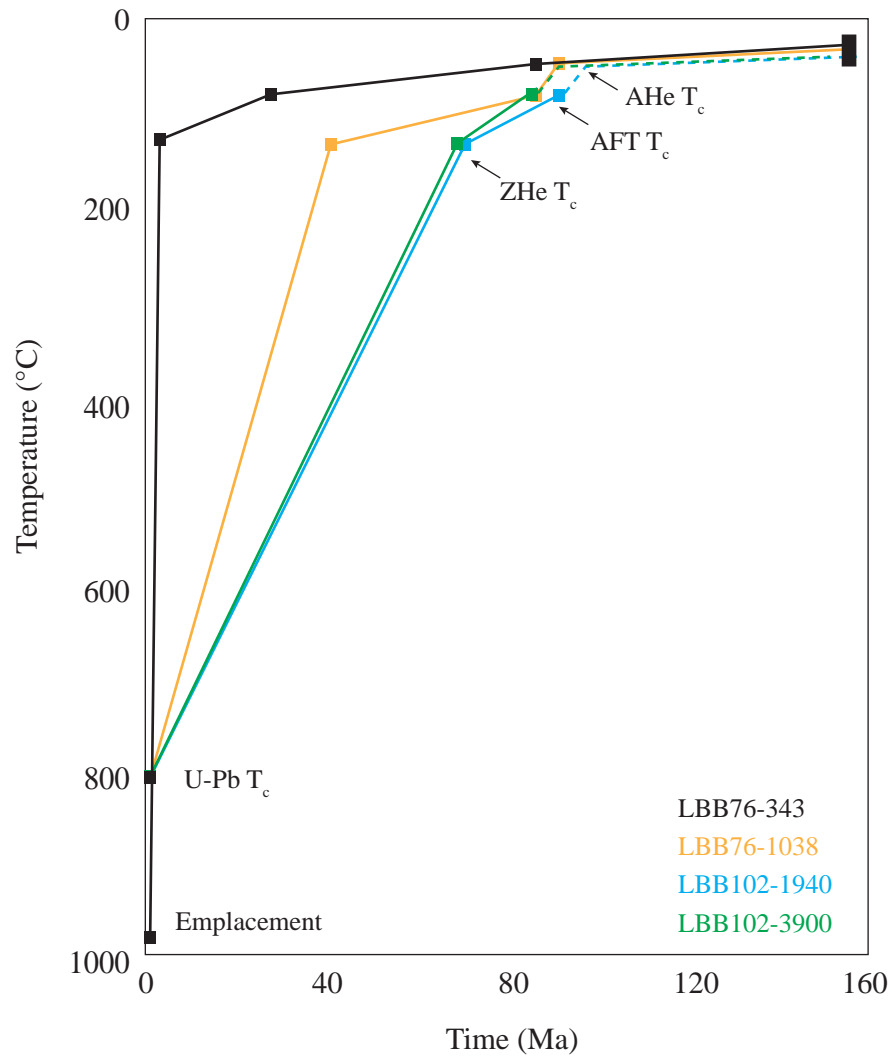
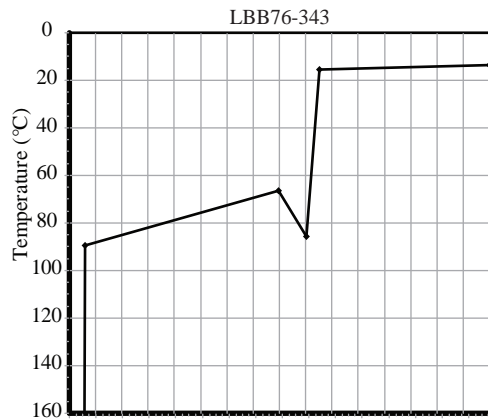
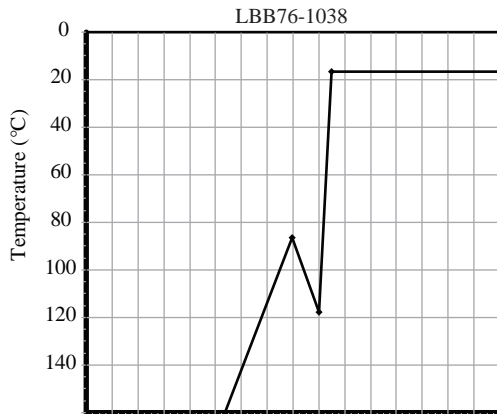


Figure 4.17 Single sample t-T histories based on combined ZHe, AFT and AHe data from four samples in the Little Boulder Basin Stock. LBB76-343 was emplaced into country rocks cooler than the ZHe T_c, ~150°C, so has a ZHe age of 154 Ma, similar to the crystallization age of the stock, ~158 Ma. Lower elevation samples LBB76-1038, LBB102-1940 and LBB-3900 were emplaced into country rocks hotter than the ZHe T_c and cooled more gradually to below 150°C. LBB76-343 cooled through the AFT T_c, ~100°C than the other samples, ~121 Ma compared to ~65-70 Ma. Both LBB76-343 and LBB76-1038 cooled through the AHe T_c, ~50°C at ~65 Ma and share a common t-T history since that time.



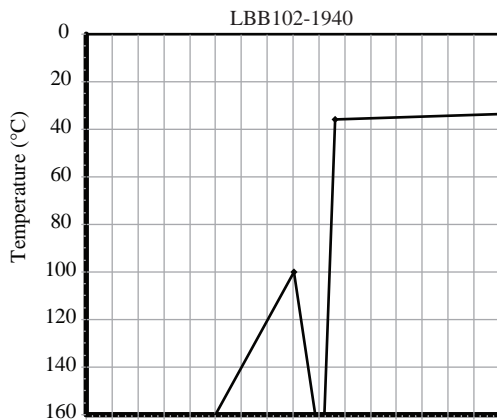
Model
ZHe 153.4 Ma
AFT 126.0 Ma

Measured
ZHe 154.4 Ma
AFT 121.6 Ma



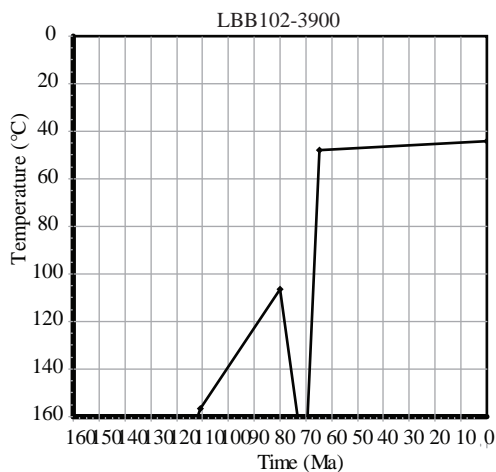
Model
ZHe 107.7 Ma
AFT 70.2

Measured
ZHe 107.3 Ma
AFT 74.3 Ma



Model
ZHe 86.3 Ma
AFT 63.5 Ma

Measured
ZHe 83.79 Ma
AFT 62.5 Ma



Model
ZHe 85.1 Ma
AFT 61.8 Ma

Measured
ZHe 87.24 Ma
AFT 64.9 Ma

Figure 4.18 Alternative t-T paths to explain observed Little Boulder Basin Stock ZHe and AFT ages. Reheating around 80-70 Ma is sufficient to totally reset AFT and partially reset ZHe ages. Causes for reheating include emplacement of younger intrusions, hydrothermal heating or burial. No evidence for these has been described in the northern Carlin Trend at 80-70 Ma.

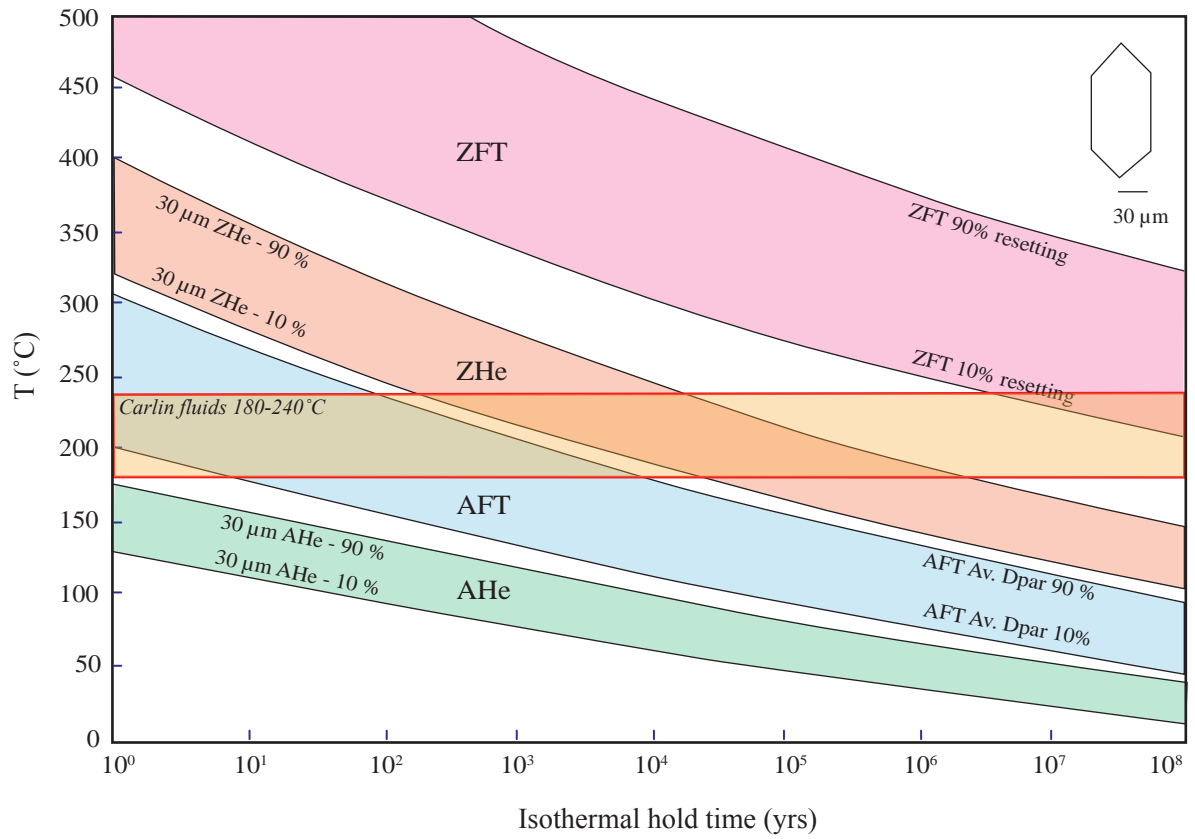


Figure 4.19 The effect of isothermal hold time on resetting of AHe, AFT, ZHe and ZFT. Temperatures calculated using Closure (Brandon et al. 1998; Ehlers et al. 2005). AHe and ZHe limits were calculated based on 30 μm equivalent radii, as observed in picked apatite and zircon crystals, using models of Farley (2000) and Reiners et al. (2004) respectively. AFT temperatures were calculated for apatite of average composition after Ketcham et al. (1999). ZFT temperatures were calculated after Rahn et al. (2004).

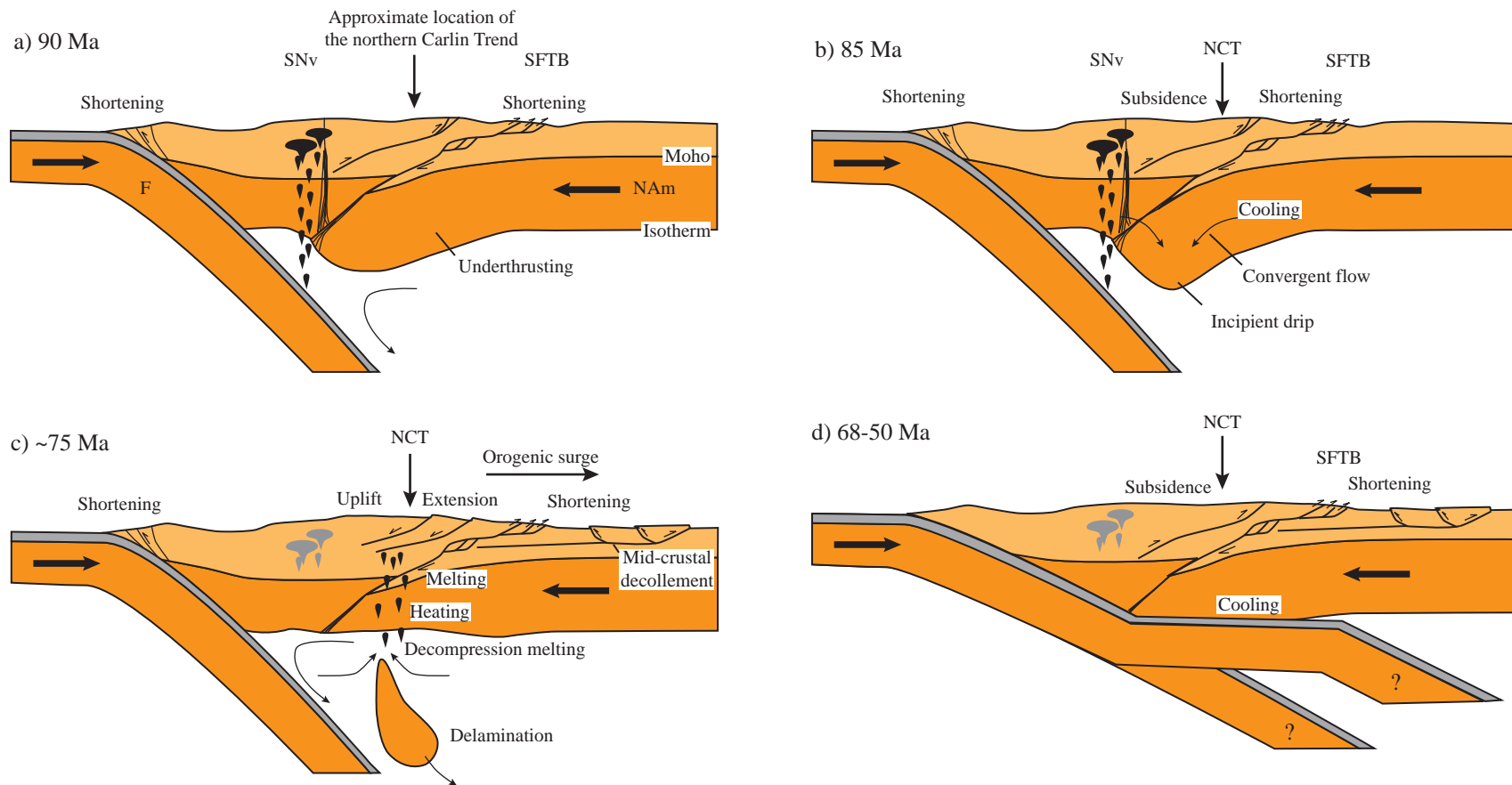


Figure 4.20 Proposed tectonic model for the Late Cretaceous to early Eocene evolution of the Sevier Orogen of Wells et al. (2012). (a) A thick lithospheric root developed during plate convergence, accompanied by shortening, underthrusting and crustal thickening. (b) The thickened lithospheric root becomes gravitationally unstable and convergent flow of weak lithosphere initiates incipient drip. Convergent flow and gravitational instability cause isostatic subsidence, cooling and further shortening. Panel (c) shows how syn-orogenic extension could have occurred in the Sevier hinterland around the time of major cooling and exhumation identified in the ZHe, AFT and AHe data of the present study. Delamination of the dense mantle drip from the overlying continental lithosphere causes isostatic uplift, decompression melting. Isostatic uplift results in extension. (d) The angle of subduction of the Farallon slab cools the lithospheric mantle below the Sevier hinterland, causes subsidence and renews shortening. The approximate location of the northern Carlin Trend is marked by the yellow circle. F, Farallon slab; NA, North American plate; NCT, northern Carlin Trend; SFTB, Sevier fold-thrust belt; SNv, Sierra Nevada magmatic arc. Inactive magmatism shown in grey.

Table 4.1 AFT ages obtained using LA-ICP-MS method, unless italicised where EDM was used

Sample name	East	North	Elev (m)	Tracks meas'd	Mean length (μm)	1σ (μm)	Grains	N _s	Dpar _A (μm)	Dpar 1σ (μm)	Area analyzed (cm ²)	Σ (PΩ) (cm ²)	1σ Σ(PΩ) (cm ²)	ξ _{MS}	1σ ξ _{MS}	Q (X ² prob)	Pooled FT age (Ma)	+ (Ma) 2σ	- (Ma) 2σ	Conc pooled age	+ (Ma) 2σ	- (Ma) 2σ	Lith
											ρ _s (10 ⁶ tracks/cm ²)	ρ _i (10 ⁶ tracks/cm ²)	N _i	ρ _d (10 ⁶ tracks/cm ²)	N _d								
Little Boulder Stock																							
LBB76-343	555488	4533058	1647	201	13.43	2.37	38	537	2.37	0.13	9.63E-04	4.09E-05	2.12E-07	19.3275	0.5584	0.0002	126.0	13.7	12.3	121.6	14.2	12.8	gdiO
LBB76-576	555514	4533032	1584	203	13.12	2.48	38	624	2.31	0.15	1.11E-03	6.28E-05	6.80E-07	19.2460	0.5423	0.0000	94.9	9.9	9.0	136.2	14.9	13.4	gdiO
LBB76-762	555534	4533012	1533	203	14.12	1.59	35	279	1.85	0.12	6.63E-04	3.27E-05	1.93E-07	19.1645	0.5262	0.0260	81.3	11.4	10.0	81.3	11.4	10.0	gdiO
LBB76-1038	555563	4532983	1457	201	14.21	1.50	39	426	1.89	0.20	8.10E-04	5.85E-05	6.32E-07	18.8384	0.4609	0.0000	68.3	7.9	7.1	74.3	9.5	8.5	gdiO
LBB76-1228	555584	4532962	1405	200	14.10	1.33	40	471	1.94	0.30	9.19E-04	4.97E-05	3.84E-07	18.8251	0.4584	0.0138	88.7	9.8	8.8	88.7	9.8	8.8	gdiO
LBB100-4346	555045	4534988	418	insufficient data			0																
LBB100-4568	555045	4534988	351	insufficient data			0																
LBB100-4679	555045	4534988	311	8	12.42	3.09	15	61	2.40	0.84	1.15E-04	7.28E-06	1.08E-07	18.8152	0.4566	0.5614	78.4	23.3	18.0	78.4	23.3	18.0	dike
LBB100-5400	555045	4534988	97	insufficient data			14																
LBB102-1035	555003	4534762	1422	147	13.40	2.11	37	288	2.01	0.18	3.52E-04	2.83E-05	2.15E-07	18.7983	0.4535	0.0852	94.9	12.9	11.4	94.9	12.9	11.4	gdiO
LBB102-1940	555003	4534762	1146	149	14.06	1.73	32	202	1.97	0.18	3.06E-04	3.03E-05	3.85E-07	18.7850	0.4510	0.1675	62.4	10.1	8.7	62.4	10.1	8.7	gdiO
LBB102-3050	555003	4534762	808	155	13.88	1.93	36	317	2.08	0.19	4.39E-04	3.89E-05	4.77E-07	18.7716	0.4485	0.0000	76.1	10.0	8.9	72.8	10.9	9.5	gdiO
LBB102-3900	555003	4534762	549	200	13.72	1.49	34	454	2.17	0.41	7.88E-04	6.34E-05	7.31E-07	18.7583	0.4461	0.0001	66.8	7.6	6.8	64.9	8.4	7.4	gdiO
LBB102-6090	555003	4534762	-119	insufficient data			6																
LBB102-6148	555003	4534762	-131	insufficient data			0																
LBB76-A †	555489	4533057	1648	200	13.4	2.45	37	711	2.37	0.16	0.570	0.856	1068	3.439	4062	0.7490	129.0	15.3	13.8	129.0	15.3	13.8	gdiO
LBB76-B †	555518	4533028	1577	202	13.29	2.53	25	559	2.29	0.13	0.495	1.442	1629	6.153	4065	0.2290	119.0	14.4	12.8	119.0	14.4	12.8	gdiO
LBB76-C †	555560	4532986	1476	200	14.07	1.82	24	203	1.83	0.24	0.410	1.908	944	6.172	4065	0.0210	75.1	13.4	11.4	75.1	13.4	11.4	gdiO
LBB76-D †	555586	4532960	1411	200	13.92	1.52	33	288	1.83	0.13	0.481	1.355	811	3.468	4062	0.0670	69.7	11.2	9.6	69.7	11.2	9.6	gdiO
Vivian Sill																							
Viv-A	557373	4532939	1989	130	13.63	0.19	25	302	2.18	0.11	3.27E-04	1.55E-05	5.14E-08	15.6781	0.4734	0.0000	150.4	20.6	18.2	131.3	19.8	17.2	gdiO
Viv-B	557373	4532939	1989	173	13.64	2.38	38	329	2.23	0.12	6.14E-04	7.97E-03	2.82E-07	17.0915	0.3299	0.3407	124.7	14.2	16.1	124.7	14.2	16.1	gdiO
V-I †	556760	4532960	1920	102	14.78	1.32	12	352	2.31	0.15	1.632	6.060	1307	6.02	4065	0.0111	91.6	13.0	11.4	91.6	13.0	11.4	gdiO
Goldstrike Stock																							
GS-1765C-782	553414	4534581	1572	160	12.57	2.82	38	329	2.23	0.18	6.14E-04	3.60E+00	6.19E-07	17.0915	0.3299	0.0050	37.9	6.0	5.2	36.1	5.9	5.1	gdiO
GS-1814C-1595	553170	4534818	1334	183	13.18	2.18	40	192	1.98	0.15	7.81E-04	1.06E-04	7.24E-06	13.7986	0.2363	0.0123	38.8	7.1	6.1	38.8	7.1	6.1	gdiO
GS-1818C-1000	553084	4535070	1505	210	13.07	2.57	38	395	2.14	0.12	2.96E-04	5.53E-05	9.66E-07	14.6241	0.2652	0.0088	52.0	6.2	5.5	51.3	6.2	5.5	gdiO
RM91-11C-225	553173	4535757	1657	148	13.54	2.54	39	209	1.96	0.16	5.05E-04	4.69E-05	6.65E-07	17.0781	0.3339	0.0000	60.1	9.2	7.9	60.1	9.2	7.9	gdiO
RM91-22C-1460	552124	4536211	1300	48	13.19	2.75	15	13	1.96	0.17	1.15E-04	4.61E-06	1.33E-07	14.8372	0.2682	0.9922	20.9	15.6	8.9	20.9	15.6	8.9	gdiO
RM94-03C-639	552751	4535590	1535	159	13.98	2.22	32	138	2.24	0.16	4.16E-04	1.68E-05	3.37E-07	15.0503	0.2711	0.0169	61.5	12.0	10.0	61.5	12.0	10.0	gdiO
RM98-04C-459	552280	4535823	1534	141	14.29	1.63	35	99	2.17	0.15	4.67E-04	1.78E-05	3.49E-07	14.2083	0.2682	0.7264	39.4	9.1	7.4	39.4	9.1	7.4	gdiO
5027**	551377	4537158	1615	163	15.24	1.09	25	261	1.97	0.13	6.52E-04	4.18E-05	4.98E-07	13.8922	0.3067	0.0208	43.2	6.1	5.3	43.2	6.1	5.3	lamp
5029**	552363	4536299	1395	192	15.61	0.99	40	342	2.56	0.14	6.26E-04	5.68E-05	5.85E-07	13.7383	0.3070	0.0001	41.3	5.1	4.6	40.0	7.1	6.1	gdiO
GS1845C 1**	552767	4535055	1319	132	14.42	1.40	20	372	1.95	0.12	2.34E-04	2.70E-05	3.27E-07	9.2674	0.2363	0.0798	63.4	7.7	6.9	63.4	7.7	6.9	gdiO
GS1845CW1 2**	552789	4535070	1198	135	14.21	1.41	23	359	2.07	0.18	2.68E-04	2.78E-05	3.11E-07	9.2944	0.2358	0.3285	59.8	7.4	6.6	59.8	7.4	6.6	gdiO
GS1845CW1 3**	552942	4535192	921	133	14.38	1.47	24	296	2.09	0.19	3.85E-04	2.27E-05	2.88E-07	9.3214	0.2354	0.0300	60.4	8.1	7.2	60.4	8.1	7.2	gdiO
GS1845CW1 4**	553042	4535245	803	131	14.10	1.58	25	373	2.15	0.16	4.61E-04	2.87E-05	3.31E-07	9.3485	0.2349	0.0129	60.4	7.3	6.6	60.4	7.3	6.6	gdiO
GS1845CW1 5**	553150	4535306	679	135	14.50	1.25	21	165	1.91	0.19	4.19E-04	1.28E-05	1.56E-07	9.3755	0.2345	0.4509	60.2	10.6	9.1	60.2	10.6	9.1	gdiO

Table 4.1 cont. AFT ages obtained using LA-ICP-MS method, unless italicised where EDM was used

Sample name	East	North	Elev (m)	Tracks meas'd	Mean length (μm)	1σ (μm)	Grains	N _s	Dpar _A (μm)	Dpar 1σ (μm)	Area	Σ (PΩ)	1σ	ξ _{MS}	1σ ξ _{MS}	Q (X ² prob)	Pooled FT age (Ma)	+ (Ma) 2σ	- (Ma) 2σ	Conc pooled age	+ (Ma) 2σ	- (Ma) 2σ	Lith
											analyzed (cm ²)	Σ (PΩ) (cm ²)	Σ(PΩ) (cm ²)										
											ρ _s (10 ⁶ tracks/cm ²)	ρ _i (10 ⁶ tracks/cm ²)	N _i		ρ _d (10 ⁶ tracks/cm ²)								
Goldstrike Stock cont.																							
S2-111 †	553111	4536180	1404	135	13.27	2.59	40	177	1.92	0.31	0.242	1.023	747	3.41	4062	0.0000	45.8	8.2	8.2	45.8	8.2	8.2	gdio
ST7-980 †	552794	4535585	1468	198	14.28	1.46	20	88	1.97	0.16	0.988	4.921	1200	6.19	4065	0.2140	70.4	10.8	10.8	70.4	10.8	10.8	gdio
ST7-1250 †	552794	4535585	1386	139	14.46	1.45	21	99	2.09	0.16	0.587	1.902	840	15.00	4062	0.6590	58	4.5	4.5	58.0	4.5	4.5	gdio
ST7-1480 †	552794	4535585	1316	200	14.51	1.44	14	49	1.89	0.12	0.971	3.175	1455	3.35	4062	0.0000	58.1	7.6	7.6	58.1	7.6	7.6	gdio
ST7-2535 †	552794	4535585	994	136	14.45	1.42	18	159	1.95	0.2	0.538	2.352	1263	6.21	4065	0.0000	80.4	11.6	11.6	80.4	11.6	11.6	gdio
ST7-2660 †	552794	4535585	956	196	14.04	1.43	39	432	2.12	0.14	0.899	3.058	1470	3.38	4062	0.1290	56.3	7.0	7.0	56.3	7.0	7.0	gdio
Tuscarora Mountains																							
S7*	565489	4552746	2184	144	14.39	1.30	26	198	2.21	0.42	0.530	1.046	391	5.12	4119	0.4028	145.9	29.2	24.3	145.9	29.2	24.3	sst
S12*	566488	4550087	1882	88	14.54	1.02	33	413	2.06	0.33	1.253	3.207	1057	4.01	4101	0.0315	88.4	12.3	10.7	88.4	12.3	10.7	sst
S13*	566643	4550271	1944	65	14.55	0.96	29	432	1.92	0.23	1.133	2.983	1138	5.11	4119	0.1079	109.5	14.8	13.0	109.5	14.8	13.0	sst
S15*	559711	4557274	2314	186	14.48	1.29	39	902	1.89	0.21	2.002	4.084	1840	5.11	4119	0.0132	140.9	14.8	13.4	140.9	14.8	13.4	sst
S16*	559611	4553939	2336	98	14.50	1.29	21	302	1.82	0.23	1.229	3.833	942	5.10	4119	0.2385	92.4	14.3	12.4	92.4	14.3	12.4	sst
S17*	558606	4550206	2418	61	15.03	0.90	36	484	1.86	0.2	1.238	3.503	1370	4.01	4101	0.0289	80.0	10.3	9.1	80.0	10.3	9.1	sst
S18*	559250	4549627	2407	91	14.92	1.05	37	566	1.92	0.23	1.388	3.714	1514	5.10	4119	0.4741	107.5	13.1	11.6	107.5	13.1	11.6	sst
S19*	560123	4547604	2550	92	14.74	1.14	30	496	1.92	0.23	1.435	3.524	1218	5.09	4119	0.0830	116.9	15.1	13.3	116.9	15.1	13.3	sst
S20*	559531	4548685	2413	34	14.90	0.99	23	133	1.81	0.17	0.805	3.301	545	5.09	4119	0.0284	70.3	15.6	12.9	70.3	15.6	12.9	sst
S21*	558694	4551632	2291	48	15.03	0.93	23	366	1.96	0.21	1.277	3.613	1036	4.01	4101	0.0074	80.1	11.5	10.1	80.1	11.5	10.1	sst
S22*	559909	4556332	2370	46	14.78	1.12	21	305	2.06	0.31	1.366	3.071	686	4.01	4101	0.0000	100.7	16.1	14.0	100.7	16.1	14.0	sst
S23*	560235	4556207	2392	128	14.84	1.13	23	370	1.86	0.2	1.705	3.512	762	4.01	4101	0.2572	109.9	16.4	14.3	109.9	16.4	14.3	sst
S25*	564184	4555682	2109	50	14.40	1.36	26	388	1.88	0.2	1.304	3.928	1169	5.08	4119	0.0384	95.2	13.2	11.7	95.2	13.2	11.7	sst
S32*	566722	4555288	2114	68	14.66	0.95	29	581	1.81	0.21	1.838	4.397	1390	5.07	4119	0.0375	119.5	14.5	12.9	119.5	14.5	12.9	sst
S33*	567513	4555843	2134	38	14.52	1.11	19	531	1.81	0.17	2.014	4.816	1270	5.07	4119	0.0021	119.4	15.0	13.3	119.4	15.0	13.3	sst
S34*	567304	4555147	2169	24	14.33	1.22	24	268	1.79	0.19	0.771	2.316	805	5.06	4119	0.0025	95.2	15.6	13.5	95.2	15.6	13.5	sst

* from Hickey (in Cline et al. 2005)

† from Chakurian et al. (2003), EDM ages

Table 4.2 ZHe ages for samples from the Goldstrike Stock, Little Boulder Stock and Tuscarora Mountains. Bold ages are **sample ZHe** ages.

Sample name	East	North	Elevation (m)	F _{He} corrected age (Ma)	Is (Ma)	Zoning adjusted age (Ma)	Is (Ma)	mass (μg)	mwar (μm)	U (ppm)	Th (ppm)	He (ncc/mg)	F _{He}	eU (ppm)
GS-1765C-782_Z1				68.3	1.6	68.3		7.16	48.25	573.38	184.34	29.01	0.79	616.70
GS-1765C-782_Z2				65.4	1.5	65.4		2.48	30.75	551.58	209.24	8.24	0.70	600.75
GS-1765C-782_Z3				114.7	12.1	-		3.74	33.00	358.54	236.51	15.49	0.72	414.12
GS-1765C-782**	553414	4534581	1572	82.8	5.1	66.9	2.1	4.46	37.33	494.50	210.03	17.58	0.74	543.86
GS-1814C-1595_Z1				80.3	1.5	80.3		2.46	31.39	222.90	179.48	4.41	0.69	265.07
GS-1814C-1595_Z2				60.1	1.1	-		1.67	31.01	257.32	147.91	2.40	0.67	292.08
GS-1814C-1595_Z3				86.0	1.5	86.0		3.72	47.63	95.87	90.05	3.44	0.76	117.04
GS-1814C-1595**	553170	4534818	1334	75.5	1.4	83.2	4.1	2.62	36.68	192.03	139.15	3.41	0.71	224.73
GS-1818C-1000_Z1				116.6	2.4	-		1.90	32.50	310.74	344.70	7.27	0.69	391.74
GS-1818C-1000_Z2				67.7	1.5	67.7		2.09	33.50	121.51	92.70	1.71	0.70	143.30
GS-1818C-1000_Z3				71.2	1.6	71.2		2.42	36.00	246.16	108.77	4.07	0.72	271.72
GS-1818C-1000**	553084	4535070	1505	85.2	1.8	69.4	2.5	2.14	34.00	226.14	182.06	4.35	0.70	268.92
RM91-11C-225_Z1				79.1	1.6	79.1		4.42	35.50	151.36	108.11	5.53	0.74	176.76
RM91-11C-225_Z2				82.5	1.7	82.5		1.81	34.00	99.49	88.57	1.51	0.69	120.30
RM91-11C-225_Z3				78.1	1.6	78.1		5.39	47.00	90.63	65.05	4.16	0.77	105.91
RM91-11C-225	553173	4535757	1657	79.9	1.7	79.9	2.3	3.87	38.83	113.82	87.25	3.73	0.73	134.33
RM91-22C-1460_Z1				75.7	1.3	75.7		15.88	60.08	1046.31	1269.58	457.24	0.83	1344.67
RM91-22C-1460_Z2				73.4	1.3	73.4		4.89	35.58	944.94	1120.06	352.27	0.73	1208.15
RM91-22C-1460_Z3				68.5	1.2	79.4		14.71	58.32	1074.20	1068.26	406.67	0.83	1325.24
RM91-22C-1460*	552124	4536211	1300	72.5	1.3	76.2	3.1	11.83	51.33	1021.82	1152.63	405.39	0.80	1292.69
RM94-03C-639_Z1				75.4	1.4	75.4		2.66	32.54	126.61	117.56	44.43	0.70	154.24
RM94-03C-639_Z2				83.9	1.6	83.9		4.32	39.61	119.25	105.28	48.69	0.74	143.99
RM94-03C-639_Z3				79.7	1.5	79.7		1.97	29.16	166.45	113.85	56.18	0.67	193.21
RM94-03C-639_Z4				70.3	1.3	70.3		2.38	29.23	145.50	132.79	45.81	0.68	176.71
RM94-03C-639	552751	4535590	1535	77.3	1.4	77.3	5.8	2.83	32.63	139.45	117.37	48.78	0.70	167.04
RM98-04C-956_Z1				58.4	1.2	67.7		0.89	26.14	161.23	147.25	37.90	0.61	195.83
RM98-04C-956_Z2				68.9	1.3	68.9		1.09	27.14	363.43	258.07	100.29	0.63	424.07
RM98-04C-956_Z3				65.9	1.3	65.9		0.75	23.56	263.59	229.96	66.92	0.59	317.63
RM98-04C-956*	552280	4535823	1385	64.4	1.2	67.5	1.5	0.91	25.61	262.75	211.76	68.37	0.61	312.51
5027_Z1				67.1	5.4	67.1		3.70	na	123.20	122.70	904.00	0.72	152.03
5027_Z2				73.7	5.9	73.7		2.20	na	1194.60	451.50	8184.80	0.70	1300.70
5027	551377	4537158	1615	70.4	5.7	70.4	5.7	2.20		658.90	287.10	4544.40	0.71	726.37
5029_Z1				71.1	5.7	71.1		3.10	na	441.70	184.70	3115.20	0.74	485.10
5029_Z2				73.7	5.9	73.7		2.10	na	965.50	424.80	6853.10	0.71	1065.33
5029	552363	4536299	1395	72.4	5.8	72.4	5.8	2.60		703.60	304.75	4984.15	0.73	775.22
GS-1845C-1_Z1				64.3	0.9	64.3		na	na	773.28	932.25	5.00	0.65	992.36
GS-1845C-1_Z2				46.0	0.8	-		na	na	685.08	342.84	2.49	0.58	765.64
GS-1845C-1_Z3				76.1	1.1	76.1		na	na	673.08	769.04	4.61	0.58	853.80
GS-1845C-1	552767	4535055	1319	62.1	0.9	70.2	8.3			710.48	681.38	4.03	0.60	870.60
GS1845CW1 2_Z1				249.2	19.9	-		3.2	na	318.50	263.20	8537.60	0.73	380.35
GS1845CW1 2_Z2				67.7	5.4	67.7		4.7	na	90.80	41.60	650.80	0.78	100.58
GS-1845CW1-2	553150	4535306	1198	67.7	5.4	67.7	5.4	3.95		204.65	152.40	4594.20	0.76	240.46
GS-1845CW1-5_Z1				64.7	1.0	70.6		na	na	465.54	298.89	3.15	0.75	535.78
GS-1845CW1-5_Z2				71.0	1.1	71.0		na	na	404.72	326.30	3.02	0.73	481.40
GS-1845CW1-5_Z3				69.4	1.1	69.4		na	na	433.41	250.66	3.09	0.75	492.31
GS-1845CW1-5	553150	4535306	679	68.4	1.1	70.3	0.9			434.56	291.95	3.09	0.74	503.16
LBB76-343_Z1				139.4	3.3	139.4		9.68	54.00	350.15	334.69	57.07	0.81	428.80
LBB76-343_Z2				154.1	3.6	154.1		2.16	31.50	1347.75	1559.34	48.09	0.69	1714.20
LBB76-343_Z3				168.9	4.0	168.9		2.83	34.50	1024.72	1020.93	52.72	0.71	1264.64
LBB76-343**	555488	4533058	1647	154.1	3.6	154.1	14.8	4.89	40.00	907.54	971.65	52.63	0.74	1135.88
LBB76-1038_Z1				126.7	2.7	107.7		11.68	56.75	148.96	86.75	25.07	0.82	169.34
LBB76-1038_Z2				104.9	2.9	104.9		4.33	37.50	190.86	136.80	9.14	0.74	223.01
LBB76-1038_Z3				109.4	2.3	109.4		5.54	41.50	271.33	163.25	17.46	0.76	309.70
LBB76-1038*	555563	4532983	1457	113.7	2.6	107.3	2.3	7.19	45.25	203.72	128.93	17.22	0.78	234.02
LBB102-1940_Z1				95.6	2.6	84.1		2.39	31.00	434.69	179.70	9.24	0.70	476.92
LBB102-1940_Z2				86.4	1.9	86.4		1.46	28.75	661.75	282.37	7.39	0.66	728.11
LBB102-1940_Z3				80.8	1.9	80.8		2.87	36.00	323.09	112.53	7.13	0.72	349.54
LBB102-1940*	555003	4534762	1146	87.6	2.1	83.8	2.8	2.24	31.92	473.18	191.53	7.92	0.69	518.19
LBB102-3900_Z1				86.9	1.6	86.9		3.53	31.24	413.49	287.66	12.66	0.71	481.09
LBB102-3900_Z2				79.2	1.5	86.3		2.00	30.51	151.00	108.04	2.32	0.68	176.38
LBB102-3900_Z3				88.5	1.7	88.5		2.74	33.54	469.38	194.61	10.83	0.71	515.11
LBB102-3900*	555003	4534762	549	84.9	1.6	87.2	1.1	2.76	31.76	344.62	196.77	8.60	0.70	390.86
LBB102-6090_Z1				66.7	1.2	66.7		3.04	33.83	135.23	98.27	2.79	0.72	158.32
LBB102-6090	555003	4534762	-119	66.7	1.2	66.7	1.2	3.04	33.83	135.23	98.27	2.79	0.72	158.32

* denotes zoning-corrected ** zoning could not account for variation

Table 4.2 cont.

Sample name	East	North	Elevation (m)	F _{He} corrected age (Ma)	1s (Ma)	Zoning adjusted age (Ma)	1s (Ma)	mass (μg)	mwar (μm)	U (ppm)	Th (ppm)	He (ncc/mg)	F _{He}	eU (ppm)
S12_Z1	566488	4550087	1882	756.1	16.7	-		na	na	na	na	43.19	0.73	na
S12_Z2	566488	4550087	1882	362.6	8.9	-						4.90	0.64	
S15_Z1	559711	4557274	2314	414.8	8.6	-		na	na	na	na	27.38	0.78	na
S15_Z2	559711	4557274	2314	318.9	6.9	-		na	na	na	na	20.89	0.76	na
S15_Z3	559711	4557274	2314	568.4	12.6	-						66.37	0.83	
S16_Z1	559611	4553939	2336	374.7	7.8	-		na	na	na	na	53.20	0.79	na
S16_Z2	559611	4553939	2336	899.3	18.9	-		na	na	na	na	820.46	0.89	na
S16_Z3	559611	4553939	2336	753.3	24.0	-						166.14	0.84	
S17_Z1	558606	4550206	2418	482.3	15.3	-		na	na	na	na	41.78	0.81	na
S17_Z2	558606	4550206	2418	1061.2	34.7	-		na	na	na	na	106.01	0.87	na
S17_Z3	558606	4550206	2418	846.6	26.9	-						52.00	0.81	
S19_Z1	560123	4547604	2550	1143.0	38.6	-		na	na	na	na	89.17	0.82	na
S19_Z2	560123	4547604	2550	1298.4	44.2	-		na	na	na	na	81.92	0.85	na
S19_Z3	560123	4547604	2550	814.6	25.6	-						48.02	0.81	
								na	na	na	na			na

* denotes zoning-corrected ** zoning could not account for variation

Table 4.3 AHe ages for samples from the Goldstrike Stock, Little Boulder Stock and Tuscarora Mountains. Bold ages are **sample AHe** ages.

Sample name	East	North	Elevation (m)	F _{He} corrected age (Ma)	Is (Ma)	mass (ug)	mwar (um)	U ppm	Th ppm	Sm ppm	% Sm contrib to age	He (ncc/g)	F _{He}	eU (ppm)
GS-1814C-1595_A	553170	4534818	1333	31.5	0.5	3.41	49.38	30.63	46.56	154.21	0.45	0.40	0.73	41.57
GS-1814C-1595_A	553170	4534818	1333	29.2	0.5	1.80	39.59	29.48	53.11	255.35	0.73	0.18	0.65	41.96
GS-1814C-1595_A	553170	4534818	1333	33.7	0.6	1.46	36.12	41.08	85.53	102.08	0.20	0.23	0.62	61.18
GS-1814C-1595	553170	4534818	1333	31.5	2.2	2.22	41.70	33.73	61.73	170.55	0.46	0.27	0.67	48.23
GS-1818C-1000_A	553084	4535070	1504	27.7	0.7	0.72	32.64	55.43	41.77	304.73	0.56	0.09	0.57	65.25
GS-1818C-1000_A	553084	4535070	1504	36.9	0.7	1.22	32.37	49.13	33.81	347.44	0.73	0.19	0.60	57.07
GS-1818C-1000	553084	4535070	1504	32.3	6.5	0.97	32.51	52.28	37.79	326.08	0.65	0.14	0.58	61.16
RM94-03C-639_A1	552751	4535590	1525	20.7	0.5	1.13	34.77	45.76	24.21	118.55	0.28	0.09	0.61	51.45
RM94-03C-639_A2	552751	4535590	1525	20.4	1.1	1.76	39.86	8.66	12.67	113.69	1.17	0.03	0.67	11.64
RM94-03C-639_A3	552751	4535590	1525	19.7	0.4	1.11	35.15	52.27	9.83	495.89	1.09	0.09	0.61	54.58
RM94-03C-639	552751	4535590	1525	20.3	0.5	1.33	36.59	35.56	15.57	242.71	0.84	0.07	0.63	39.22
RM98-04C-459_A1	552280	4535823	1531	25.4	0.4	6.41	72.87	11.23	16.69	182.94	1.44	0.24	0.77	15.15
RM98-04C-459_A2	552280	4535823	1531	28.1	0.5	3.57	46.83	22.52	32.46	362.18	1.43	0.27	0.72	30.14
RM98-04C-459_A3	552280	4535823	1531	28.5	0.5	0.89	27.71	28.93	33.84	381.52	1.23	0.06	0.55	36.88
RM98-04C-459	552280	4535823	1531	27.3	1.7	3.62	49.14	20.89	27.66	308.88	1.37	0.19	0.68	27.39
LBB76-343_A1	555488	4533058	1652	68.7	1.5	1.64	37.75	18.03	43.37	332.44	1.40	0.26	0.65	28.22
LBB76-343_A2	555488	4533058	1652	70.7	1.6	2.00	41.50	11.59	28.52	271.73	1.76	0.22	0.69	18.29
LBB76-343_A3	555488	4533058	1652	55.5	1.3	2.60	41.50	20.94	31.64	227.67	0.96	0.35	0.69	28.38
LBB76-343	555488	4533058	1652	69.7	1.4	1.82	39.63	14.81	35.95	302.09	1.58	0.24	0.67	23.26
LBB76-1038_A1	555563	4532983	1469	67.0	1.4	4.97	53.50	15.68	45.81	332.11	1.49	0.81	0.75	26.44
LBB76-1038	555563	4532983	1469	67.0	1.4	4.97	53.50	15.68	45.81	332.11	1.49	1.49	0.75	26.44

Table 4.4 Estimates of depth to closure isotherm for different geothermal gradients and cooling rates of 1°C/Myr and 10°C/Myr. Assumed surface temperature 10°C

	°C/Myr	T _c (°C)	30°C/km	40°C/km	50°C/km	60°C/km
AHe	1	50	1.3	1.0	0.8	0.7
	10	60	1.7	1.3	1.0	0.8
AFT	1	100	3.0	2.3	1.8	1.5
	10	110	3.3	2.5	2.0	1.7
ZHe	1	150	4.7	3.5	2.8	2.3
	10	170	5.3	4.0	3.2	2.7

Chapter 5: Thermal halos around Carlin-type Au deposits

5.1 Introduction

Carlin-type deposits are the product of an Au-bearing hydrothermal system. Hydrothermal systems involve transfer of heat and mass. Fluid-rock interaction results in mass transfer (Giggenbach, 1984; Reed, 1997), physicochemical manifestations of which include mineralization, chemical alteration and trace element and isotopic enrichment or depletion. Heat transfer between fluid and rock occurs either by movement of the hot fluid medium through a rock, advection, or of heat through the rock mass, conduction (Figure 5.1). A hydrothermal deposit (the product of mass transfer) should also have an associated thermal halo (Cathles, 1997; Cathles and Shannon, 2007). The conductive thermal halo is usually the most distal expression of a hydrothermal system, extending well beyond the manifestations of fluid-rock interaction (Bickle and McKenzie, 1987; Cathles, 1997). The size of the halo is determined by the duration of the hydrothermal fluid flow, the thermal gradient between the fluid and the host rock, the thermal diffusivity of the rock, the magnitude of fluid flux, and the density and geometry of fluid conduits that hydrothermal fluids travel along (Cathles, 1997). Determining the size of a thermal halo therefore facilitates understanding of the hydrothermal system responsible for formation of an ore deposit. Traditional mineral exploration makes use of chemical alteration and trace element anomalies to identify new ore deposit targets (Giggenbach, 1984; Reed, 1997; Kelley et al., 2006). Thermal mapping therefore also has potential as a tool for locating undiscovered deposits in future exploration.

Carlin-type deposits are sedimentary rock-hosted deposits that occur primarily in carbonate host rocks in northern central Nevada. Characteristic submicron scale, disseminated Au mineralization is rarely a visual expression of the hydrothermal system. Manifestations of Carlin hydrothermal fluid-rock interaction include mineral alteration (argillisation,

silicification, decarbonatisation) of host rocks (Kuehn and Rose, 1992; Hofstra and Cline, 2000; Heitt et al., 2003; Kesler et al., 2003), trace element enrichment and $\delta^{18}\text{O}$ isotope depletion halos (Hofstra and Cline, 2000; Nutt and Hofstra, 2003; Vaughan, 2010). An apatite fission track (AFT) study by Hickey (2005) identified a thermal anomaly spatially coincident with Au mineralization on a regional scale around the northern Carlin Trend (Figure 1.2). However, the size of a thermal halo, which is a function of fluid temperature, fluid volume and the size and spacing of fluid conduits, is not well constrained for individual Carlin-type deposits. The northern Carlin Trend has a complex network of faults and fractures, permeable strata and lithological contacts, all of which may have acted as conduits for hydrothermal fluid flow (Hofstra and Cline, 2000; Jory, 2002; Cline et al., 2005; Emsbo et al., 2006; Mickelthwaite, 2010). The duration of flow and magnitude of fluid flux, however, are not well constrained at present (Arehart et al., 2003a; Cline et al., 2005; Hickey et al., 2011). In the present study, AFT thermochronology is combined with apatite and zircon (U-Th)/He dating (AHe and ZHe respectively) to determine the size of conductive thermal halos around Au-mineralization at the deposit scale in the northern Carlin Trend. Knowledge of the size of the conductive thermal halo is then used to model the duration of hydrothermal fluid flow and the fluid flux responsible for the formation of these world-class Au deposits. Knowledge of the duration and fluid flux can be used to infer the primary driving mechanism of a hydrothermal system, i.e. forced convection, free convection or seismic pumping.

5.1.1 Low-temperature thermochronology

A full review of low-temperature thermochronology is provided in Chapter 3. Thermochronology is based in the principles of radioactive decay and the tendency of thermochronometer minerals, including apatite and zircon, to lose the daughter products of

decay through thermally-sensitive processes. Uranium and Th are present in trace amounts in most apatite and zircon crystals and decay radioactively over time. Spontaneous fission produces fission tracks; alpha decay results in production of ^4He . At low temperatures, daughter product fission tracks and ^4He accumulate over time within the host crystal. Retention of fission tracks or ^4He is temperature-sensitive. Heating at sufficient temperature or duration results in annealing and removal of fission tracks, or in diffusive loss of ^4He . Loss of fission tracks or ^4He causes resetting of an apatite or zircon crystal. Fission tracks and ^4He are only retained below a certain temperature, the closure temperature, T_c . The fission track or (U-Th)/He age of a crystal therefore records the amount of time passed since a crystal last cooled to below the T_c , 50°C, 100° and 150°C for AHe, AFT and ZHe thermochronometers respectively over geological timescales (10^6 - 10^7 yrs).

Mapping a thermal halo around a mineral deposit can be achieved using low-temperature thermochronometers that record resetting by heat associated with a hydrothermal system. Resetting of the highest T_c thermochronometer, in this case ZHe, defines the smallest thermal halo around mineralization and AHe, with the lowest T_c , should define the largest halo. An example of resetting profiles of multiple thermochronometers from around a dike is shown in Figure 5.2. A similar pattern might be expected around a major hydrothermal fluid conduit, with nested halos from highest T_c proximal to the deposit to lowest T_c halo most distal. Heat is conductively transferred beyond the limit of the thermal halo, which defines the limit of heating to sufficient temperature to cause total resetting of the thermochronometer in question. The size of the thermal halo around a hydrothermal fluid conduit is a function of fluid temperature, fluid volume and the size of the conduit and the duration of fluid flow and resultant heating.

5.1.2 Carlin-type deposits in the northern Carlin Trend

The northern Carlin Trend contains more than 90 Moz Au (Cline et al., 2005) in numerous deposits, including the Betze-Post, Meikle, and Banshee deposits. Average grade in the northern Carlin Trend is 5.86 g/t (Cline et al., 2005) but locally can exceed 400 g/t in the high-grade Meikle deposit (Emsbo et al., 2003). The location of these deposits and distribution of Au mineralization is shown in Figure 5.3. In the Betze-Post deposit, Au mineralization is concentrated at lithological boundaries such as the one between the Jurassic granodiorite Goldstrike Stock and the surrounding Paleozoic carbonate package. Elsewhere in the study area, mineralization is also commonly hosted in Jurassic lamprophyre and rhyodacite dikes, e.g., in the Meikle, Banshee and Golden April deposits.

Gold occurs in rims on microscopic disseminated pyrite in carbonate host rocks or Jurassic lamprophyre dikes (Kuehn, 1989; Arehart et al., 1993a; Barker et al., 2009). Previous authors have identified at least two phases of Au-bearing rim growth on pyrites in the northern Carlin Trend (Arehart et al., 1993a; Barker et al., 2009). Alteration includes silicification (locally forming jasperoid), argillisation (dominated illite±kaolinite±dickite), sulfidation and decarbonatisation. Alteration is neither consistently spatially associated with mineralization nor does its intensity correlate with Au grade (Kuehn and Rose, 1992; Arehart et al., 1993a; Yigit and Hofstra, 2003; Yigit et al., 2006), although illite intensity has been shown to correlate with Au concentration at some deposits (e.g. Getchell, Cail and Cline, 2001; Banshee, J. Vaughan, in prep). Deposits formed as fluids moved along permeable carbonate strata reacting with Fe in the host rocks that destabilised H₂S-Au complexes in the ore fluid and led to formation of Au-bearing pyrite (Cline and Hofstra, 2000; Hofstra and Cline, 2000). Permeability was enhanced by dissolution of carbonate rocks by mildly acidic (pH 4-6) hydrothermal fluids, enough to cause almost complete carbonate dissolution in places (Emsbo et al., 2003; Heitt et al., 2003).

Fluid inclusion studies have shown ore fluids contained CO₂ (<4 mol %), CH₄ (<0.4 mol %) and enough H₂S to transport Au (10⁻¹-10⁻² m) (Hofstra et al., 1991; Cline and Hofstra, 2000; Emsbo et al., 2003; Lubben, 2004). Fluid temperatures were 180-240°C, relatively low-temperature, but similar to temperatures observed in modern geothermal systems (White, 1974; Struhsacker, 1980; Cline and Hofstra, 2000; Hofstra and Cline, 2000; Simmons and Browne, 2000; Emsbo et al., 2003).

Eocene intrusions dated at 36-42 Ma cross cut Carlin-type Au mineralization and constrain the timing of mineralization to that time interval (Arehart et al., 2003b). Rb-Sr dating of galkhaite, an ore-stage sulfosalt, also yielded an Eocene age of mineralization (Tretbar et al., 2000). AFT anomalies of the same age have also been identified around Au trends in northern Nevada (Chakurian et al., 2003; Hickey, 2005; Arehart and Donelick, 2006; Hickey, 2007). Carlin-type deposits in Nevada therefore formed some time in a ~6 Myr interval in the Eocene. However, the duration of the hydrothermal events that formed them is undetermined.

5.2 Previous thermochronology studies

Arehart et al. (1993b) obtained zircon fission track (ZFT) ages for the Goldstrike Stock. ZFT dating is based on the same principles as AFT dating, but the closure temperature of the ZFT system is much higher, >250°C at cooling rates 10°C/Myr (Rahn et al., 2004). ZFT ages in that study obtained for fresh, weakly altered and highly altered samples of the Goldstrike Stock were 132 ±16 Ma (2σ) (GSS-1), 169 ±42 Ma (FTZ-2) and 133 ±14 Ma (FTZ-3), all only slightly younger than or within 2σ of the crystallization age of the stock, ~158 Ma. Any subsequent thermal event therefore caused insufficient heating to even partially reset ZFT.

A zone of AFT ages of ~40-20 Ma that is spatially coincident with the Carlin Trend was identified by regional AFT sampling by Hickey (2003; 2005) (Figure 1.2). The thermal

anomaly is considered a zone of pervasive annealing by hydrothermal fluids responsible for Au mineralization at ~36-42 Ma, although the distribution is less pervasive towards the northern end of the trend, around the Betze-Post and Meikle deposits (Hickey et al., 2003; Cline et al., 2005). The spatial relationship is not entirely consistent, as some large deposits lie outside of the annealed area, but in other places the zone extends laterally beyond the extent of the Carlin Trend. It has been suggested that flow of auriferous fluids was focused along the Carlin Trend but that hydrothermal fluid flow did extent beyond the trend (Cline et al., 2005).

Chakurian et al. (2003) obtained AFT and AHe ages for the Goldstrike and Little Boulder Basin Stocks and Carlin deposit to the southeast of the present study area. They determined that the Little Boulder Basin Stock and bulk of the Goldstrike Stock had been largely unaffected by Eocene hydrothermal activity that formed the Carlin-type deposits, based on AFT ages ~60 Ma in those stocks. They did observe that samples proximal to mineralization, around the edge of the Goldstrike Stock and in the Carlin deposit, have ages ~40 Ma, coincident of the timing of mineralization, and considered those ages further supporting evidence of an Eocene mineralization age. Two AHe ages were determined in that study, 21.4 ± 1.3 Ma for the centre of the Goldstrike Stock and 31.0 ± 1.9 Ma for the Carlin deposit. Chakurian et al. (2003) concluded those AHe ages may record localised heating associated with younger, localised hydrothermal activity. In Chapter 4 it is suggested that in the Goldstrike Stock at least, the age of 21.4 ± 1.3 Ma may record the timing of exhumation through ~ 1 km depth during gradual Cenozoic exhumation of the northern Carlin Trend.

As discussed in Chapter 4, AFT data from deep drillholes around the Goldstrike Stock and Little Boulder Basin Stocks have AFT ages ~60-70 Ma, considered the exhumation age of the stocks and much of the northern Carlin Trend, and record the time that the studied portions of the stocks cooled to <100°C. Samples from the edge of the stock, proximal to Au deposits,

have ages ~40 Ma, and were interpreted as thermally reset by hydrothermal fluids also responsible for Eocene Au mineralization. Data from those samples were presented in Chapter 4 and are included again here with additional new AFT, AHe and ZHe data to assess the duration of heat flow into the Goldstrike Stock and at Meikle, Banshee, Golden April and the Post area.

5.3 Methods

5.3.1 Sample collection and rock descriptions

Sample locations are shown in the map in Figure 5.3 and were collected for this study from Jurassic granodiorite, lamprophyre and rhyodacite intrusions in drill core from the Little Boulder Basin (n=15) and Goldstrike Stocks (n=14), Banshee deposit (n=4), Meikle-Golden April section (n=5) and Post Fault area (n=10). Samples were collected only from igneous material to increase the likelihood of obtaining sufficient apatite and zircon yields, both minerals that are of limited abundance in carbonate host rocks. Samples were selected at a range of distances from suspected fluid flow zones, e.g., across the Goldstrike Stock, a large intrusion that does not appear to have been penetrated by hydrothermal fluids, to observe the limit of thermal resetting in AFT, ZHe and AHe. Samples range from minimally chemically altered, distal samples (~5% alteration of mafic minerals to smectite±chlorite) to pervasively argillised (>80% argillised lamprophyre dikes) in main fluid flow paths. Sample spacing was limited by the distribution of intrusions, drill spacing and extensive alteration of some intrusions. Existing AFT ages of Chakurian et al. (2003) from the Goldstrike Stock was also incorporated into the present study and are included in Figure 5.4.

Petrologic, whole rock geochemistry and X-Ray Diffraction (XRD) methods were used to characterise the mineralogy and alteration of samples dated in this study. Details of

geochemical analytical methods and XRD methods and spectra can be found in Appendix B. Full petrological descriptions can be found in Table B1. Whole rock geochemistry data is included in Table B3.

5.3.2 U-Pb dating

A single lamprophyre sample, GA-34C-1280, was dated to confirm its emplacement age. Reported hornblende $^{40}\text{Ar}/^{39}\text{Ar}$ ages for lamprophyre dikes in the northern Carlin Trend are 158.9 ± 0.2 to 167.4 ± 2.4 Ma (Emsbo et al., 1996; Orobona, 1996). Other dike samples would also have been dated, however the lack of zircon in the lamprophyre dikes meant this was not possible and hornblende or biotite separates were not obtained during the mineral separation process. Although enough zircon was obtained for ZHe dating of U16-H07-68 and EX-29C, both rhyodacite dikes, not enough remained to confirm the assumed Jurassic age of those samples. The age of the granodiorite Goldstrike and Little Boulder Basin Stocks has previously been established as ~157-158 Ma using U-Pb dating (Mortensen et al., 2000) and K/Ar dating (Morton, 1977; Mortensen et al., 2000).

Zircon separates were prepared and picked by the author. A subset of these (n=6) were processed for CA-TIMS dating by the Pacific Centre for Isotopic and Geochemical Research (PCIGR) at UBC. Details of analytical methods and U-Pb data are provided in Appendix D. Data reduction and age interpretation were also carried out by the PCIGR. Standard concordia diagrams were constructed (see Appendix D) and regression intercepts and weighted averages calculated using Isoplot (Ludwig, 2003), yielding an age of 160.76 ± 0.25 Ma (2σ), within the range of previously published lamprophyre ages.

5.3.3 AFT and (U-Th)/He thermochronology methods

AFT and (U-Th)/He dating of apatite and zircon were carried out using the methods described in Chapter 4. In summary, mineral separates of apatite and zircon were prepared using conventional mechanical, gravity and magnetic techniques. AFT dating was carried out by Apatite to Zircon, Inc. Separated apatite crystals were mounted in epoxy resin. Mounts were then polished and etched in 5.5 M HNO₃ at 21°C for 20s to enlarge fission tracks for counting. Fission tracks were counted in 20-40 apatite crystals using an optical microscope at 1650x magnification. U and Th concentrations were determined using the LA-ICP-MS method of Hasebe et al. (2004). Dpar, the mean etch pit diameter parallel to the c-axis, was measured as an indicator of kinetic behaviour and annealing properties. Mounts were then ²⁵²Cf irradiated to further enlarge fission tracks for track length measurement. Fission track lengths and their angle to c-axis were measured digitally for modelling of t-T histories of individual samples. Samples AFT ages were calculated as pooled single grain ages from each sample using equations provided in Chapter 3.

Apatite and zircon (U-Th)/He dating was carried out at the University of Arizona. Three apatite and three zircon crystals per sample were picked, measured and packed into 500 µm diameter Nb tubes. Crystals were picked based on the following criteria: crystals must be whole crystals, at least 60 µm on their shortest axis, and inclusion free. The latter is of particular importance in AHe dating because apatite has relatively low U and Th concentrations compared to inclusions, which contribute He to the host apatite crystal, so presence of inclusions can lead to overestimation of a crystal's AHe age (Farley, 2002). Zircon typically has higher U and Th concentrations, so is less sensitive to U- and Th-rich inclusions (Reiners, 2005). He extraction was achieved by laser heating and analysis was carried out by gas quadrupole mass spectrometry. U and Th (and Sm) concentrations were determined using

dissolution ICP-MS following dissolution of each crystal in HF (for zircon) and HNO₃ (for apatite). Alpha ejection corrections were applied to each crystal. A sample age was calculated from the average of the crystals from that sample using equations given in Chapter 3.

5.3.4 HeFTy modelling

Fission track length and single grain age data were inversely modelled using the software package HeFTy (as described in Chapter 4) to establish possible t-T histories for each sample. Constraints were placed at the start (158 Ma, >200°C) and end of each history (0 Ma, 10-30°C based on present depth), as well as a period of cooling around 90-60 Ma from >120°C to at ≤60°C that resulted from Late Cretaceous regional exhumation (see Chapter 4). Modelled t-T paths are classified as "good fit" if they have a Kuiper's statistic value of 0.50 or higher, which shows the modelled t-T path is supported by the data. Acceptable paths, with Kuiper's values 0.05 or higher, are possible paths that are "not ruled out" by the data (Ehlers et al., 2005; Ketcham, 2009). Each sample was modelled until at least 30 good t-T paths were generated, as this was considered representative of probable t-T histories of the samples. In addition to goodness of fit of t-T histories, HeFTy modelling also calculates the age of the oldest fission track that could be preserved by a modelled t-T history. When the oldest fission track has the same age as the modelled sample age, the sample is considered totally reset. In many cases the oldest fission track is older than the sample age, an indication that some of the sample's earlier history can be interpreted meaningfully. In the following section, this feature is discussed in the context of forward modelling t-T histories to infer the maximum duration of heating of the Goldstrike Stock.

5.4 Results

5.4.1 Characterisation of alteration

Samples from the Goldstrike and Little Boulder Basin Stocks range from gabbro to granodiorite in composition but are mostly diorite-granodiorite (Figure B1). Samples are hypidiomorphic, equigranular, phaneritic, fine-medium grained and are composed of plagioclase and K feldspar, quartz, hornblende and biotite (Figure 5.5a). Samples are minimally altered by hydrothermal fluids (<15% argillisation of rock). Alteration of the Goldstrike and Little Boulder Basin Stocks is dominated by alteration of feldspar cores to sericite and mafic minerals to chlorite (Figure 5.5a). XRD analysis shows alteration minerals are mostly interlayered chlorite+smectite \pm sericite (sericite refers to fine-grained white mica), typical of deuteric style alteration.

Lamprophyre samples are porphyritic with phenocrysts of hornblende, or less commonly biotite, in a fine grained groundmass of plagioclase (or K-feldspar with biotite phenocrysts). Alteration of lamprophyre samples is typically more pervasive and more variable than that of granodiorite samples, from essentially unaltered (Figure 5.5b) to ~85 % argillised (Figure 5.5c). Mafic phenocrysts are commonly totally argillised or chloritised. XRD analysis shows the main alteration assemblage at Golden April is illite+smectite \pm chlorite, with 50-85% alteration of lamprophyre whole rock samples. Chlorite and illite represent different alteration stages, since chlorite typically forms in higher temperature settings than illite. Chlorite is not described in mineralized samples that are strongly illitised, further evidence that chlorite is not related to the mineralizing hydrothermal system. The dominant alteration assemblage at Meikle and along the Post Fault is illite+kaolinite, with samples 88-90% and 50-95% altered respectively. Banshee sample U16-H07-34C-537 is considered "fresh" lamprophyre with only

minor chloritisation of hornblende (Figure 5.5b). Banshee rhyodacite sample U16-H07-68-247 is dominated by illite, which thin section examination shows has replaced ~85% of the sample.

Figure 5.6 summarises alteration of samples from the northern Carlin Trend. Mass transfer of Na, Ca, K is observed using a K/Al and (2Ca + Na + K)/Al molar ratio plot after Warren et al. (2007). Granodiorite samples are only minimally altered, plotting within the normal felsic-mafic range and showing no major loss or gain of K, Na or Ca. Goldstrike granodiorite sample GS-1818C-1000 falls outside of the normal trend, probably reflecting analysis of calcite vein material and higher K-feldspar content rather than addition of Ca and K, as the sample appears only minimally altered in thin section (Figure 5.5a). Lamprophyre and rhyodacite samples display more variation, with significant loss of Na and Ca and minor addition or loss of K compared to fresh sample U16-H07-34-537. Na and Ca loss are associated with illite alteration, and occur as feldspars are broken down by mildly acidic fluids. Mg and Fe are also released from mafic phases, resulting in breakdown of hornblende to chlorite and in some cases chlorite+pyrite as S is added to the rock by the hydrothermal fluid. Pseudomorphic replacement of hornblende by chlorite+pyrite was observed in thin section in samples U10-P05-06-319, U12-P05-16-814 and GA-52C-1585.

The degree of illitisation of samples increases with proximity to Au mineralization and zones of high fluid flow and high fluid-rock ratios. Illite is considered a low-temperature alteration mineral, forming where fluid temperatures are <250°C (Seedorff et al., 2005). Sericite is typically considered an indicator of hydrothermal fluid temperatures >250°C (Seedorff et al., 2005; Tosdal et al., 2009). It is found in the granodiorite samples but is a function of deuteric alteration during igneous cooling rather than high temperature hydrothermal alteration.

Kaolinite is considered evidence of acidic fluids and is observed proximal to major fluid conduits, e.g., at Meikle and in the Post Fault area, where large volumes of mildly acidic fluids interacted with host rocks (Cline et al., 2005). Smectite forms in cool, near neutral pH environments. More distal samples contain smectite instead of kaolinite, as a result of buffering and neutralisation of fluids moving away from main fluid conduits. This pattern of kaolinite proximal to fluid conduits zoned outward to illite±smectite is described in several deposits in the Carlin Trend (Carlin, Kuehn and Rose, 1992; Betze-Post, Arehart et al., 1993a; Deep Star, Heitt et al., 2003), although illite is the most consistently associated with Au mineralization (Cail and Cline, 2001; Vaughan, in prep). Kaolinite could also indicate alteration involving meteoric fluids, downwelling along faults. Whether kaolinite is supergene (downwelled, meteoric fluids) or hypogene (ascending hydrothermal fluids) can be determined by $\delta\text{H}_2\text{O}$ studies (Taylor, 1997), however this was beyond the scope of the present study.

Granodiorite samples are characterised by minor chloritisation of mafic phases and argillisation of feldspars. Alteration of this kind is evidence of limited hydrothermal fluid-rock interaction in the main Goldstrike and Little Boulder Basin Stocks, most likely occurring during late stages of igneous cooling as a result of deuteritic alteration, and/or low-temperature groundwater interaction. Lamprophyre samples are more pervasively altered as a result of reaction with greater volumes of fluids. The clay mineral assemblage in altered lamprophyres is dependent on fluid temperature and acidity. More proximal samples have been altered by higher temperature, acidic fluids and so are dominated by illite+kaolinite argillisation. More distal samples interacted with cooler, buffered fluids that resulted in less pervasive argillisation dominated by illite+smectite. Overall, the argillic alteration observed in the northern Carlin Trend is typical of a low-temperature, weakly acidic hydrothermal system, consistent with

published estimates of fluid temperature 180-240°C and pH 4-6 (Hofstra and Cline, 2000; Emsbo et al., 2003; Cline et al., 2005).

5.4.2 Thermochronology

Overall, yields of apatite and zircon of sufficient size and quality were low, particularly in lamprophyre samples. Of 50 samples processed for AFT dating, only 35 yielded sufficient apatite to calculate pooled AFT ages. Nine samples yielded fewer than 15 single grain ages and are not presented here, however they are included in Appendix C. Six samples yielded no single grain apatite ages at all. Attempts were made to date a subset of 31 samples using AHe (omitting some samples from the Little Boulder Basin Stock), but only 11 yielded sufficient sufficiently large, whole, inclusion-free apatite. Limited apatite recovery has been reported in several studies of the northern Carlin Trend (e.g. Arehart et al., 1993b; Arehart et al., 2003a; Chakurian et al., 2003) and is discussed in Chapter 4. Suitable zircon for ZHe dating was obtained for only 12 samples of 24 selected samples. Zircon recovery from lamprophyres was particularly poor, but not surprising given the mafic composition of lamprophyre melts.

AFT ages generated by this study are shown with previously published data in Table 5.1. AFT ages range 20.4 +3.3-2.9 Ma to 136.2 +14.9 -13.4 Ma (2σ), with most around 30-40 Ma proximal to mineralization or >60 Ma in more distal samples (Figure 5.3). AFT ages in the Little Boulder Basin Stock, away from mineralization, are 62.4 +10.1 -8.7 to 136.2 +14.9 -13.4 Ma. Within deep drill holes in the Little Boulder Basin and Goldstrike Stocks, age correlates with elevation, and records the exhumation history of the stocks discussed in detail in Chapter 4. Most samples have concordant single grain ages, usually an indication of a single population of apatite in each sample. Discordance in igneous samples, which typically have a single source of apatite, may arise from low track counts (N_s) or chemical variability (correlates with

Dpar variability, see Chapter 6) within the host intrusion and is neither uncommon, nor necessarily implies bad quality data (O'Sullivan and Parrish, 1995; Galbraith, 2005). Measured values of the kinetic parameter Dpar in samples from this study range 1.85 ± 0.12 to 2.66 ± 0.54 μm . The range of Dpar is similar in lamprophyre and granodiorite samples, indicating little variation in resistance to annealing between rock types in this study. Mean c-axis projected track lengths range 12.42 ± 3.09 to 15.61 ± 0.99 μm (1σ). Fission track distributions from Golden April, Meikle, Banshee and the Little Boulder Basin Stock are mostly unimodal (Figure 4.12 and 5.7). Distributions from Post Fault samples and the Goldstrike Stock are mostly bimodal (see Figure 4.12 and 5.7).

ZHe ages are shown in Table 5.2 and Figure 5.8. ZHe ages across the study area are 66.7 ± 1.2 Ma to 154.1 ± 14.8 Ma (1σ), with the exception of U16-H07-68-247 and EX-29C-1783, which have Eocene ZHe ages 45.2 ± 2.0 Ma and 34.7 ± 1.7 Ma respectively. The latter samples are proximal to mineralization and are highly altered. Individual zircon ages were corrected for alpha ejection. Zoning was observed in Goldstrike sample GS-1765C-782 (Figure 4.14) during a CL investigation of apatite described in Chapter 6, so zircons from other parts of the same stock are also potentially compositionally zoned. Single zircon ages in samples with dispersed single grain ages were corrected for zoning if appropriate by multiplying by a correction factor typically 5-15% to account for suspected relative enrichment or depletion of the rim (Hourigan et al., 2005), Figure 3.11. In many samples two of three single zircon ages were within error of one another and the third age was older or younger; zoning corrections applied to the third age brought that crystal to within error of the other two ages. Where a reasonable zoning correction could not be applied, the sample age was calculated as the average of the two similar ages. Sample U16-H07-34-537 has three distinct ages, 130.1 ± 2.88 , 171.1 ± 3.7 and 250.4 ± 5.2 Ma, which could not be accounted for by simple zoning, but are near or older than the

crystallization age of the host dike, ~158 Ma. Radiation damage can result in widely dispersed ages (Reiners et al., 2002; Nasdala et al., 2004), however sufficiently high U, Th concentrations (>1000 ppm) were not observed in samples in this study (Table 5.2).

AHe ages are shown in Table 5.3 and Figure 5.8. AHe ages range from 3.6 ± 0.2 to 69.7 ± 1.6 Ma. AHe ages are oldest in the Little Boulder Basin Stock, ~68 Ma. AHe ages in the Goldstrike Stock range 20-30 Ma. AHe ages of samples near the Golden April and Meikle deposits, and within the Post Fault system, are 3.6 ± 0.2 to 23.0 ± 0.5 Ma (1σ). Single AHe grain age variation greater than 2σ was observed within 2 samples, GS-1818C-1000 and LBB76-343, but no quantified correction values have been published to correct for zoning as for ZHe dating, so no correction was applied.

5.4.3 HeFTy modelling

HeFTy models for selected representative samples are shown in Figure 5.7. HeFTy models of samples away from mineralization, i.e. the Little Boulder Basin Stock samples, support a simple cooling history dominated by a major phase of cooling at 85-60 Ma to near present-day temperature (see Chapter 4). Modelling of all other samples supports t-T histories involving Cretaceous cooling followed by reheating at $\leq \sim 40$ Ma. In samples from Meikle, Golden April and the edge of the Goldstrike Stock, Eocene heating was sufficient to cause total resetting at ~40 Ma. Samples at the centre of the Goldstrike Stock, which have AFT ages 60-70 Ma, show a t-T history dominated by Late Cretaceous cooling followed by a lesser degree of Eocene heating than samples proximal to major fluid flow zones, indicating that Eocene heating was not enough to cause total resetting of AFT ages in the centre of the stock. Models of AFT data from Post Fault samples, which have AFT ages ~20-30 Ma, are dominated by rapid cooling between 20 and 30 Ma. Models allow an earlier rapid Late Cretaceous cooling

and allow Eocene reheating and cooling prior to a 20-30 Ma reheating and cooling, however this is not well constrained (Figure 5.7c). The last cooling event from $>100^{\circ}\text{C}$ can only be constrained to sometime between 20 and 30 Ma.

5.5 Interpretation of thermochronology data

5.5.1 Temporal and spatial patterns in thermochronology data

Several thermal events are recorded in the thermochronology data presented in this study (Figure 4.7). Regional Late Cretaceous exhumation, discussed in Chapter 4, is recorded in ZHe ages ranging ~60-95 Ma in samples across the entire study area. Similar Late Cretaceous AFT ages in the Goldstrike and Little Boulder Basin Stocks and sample U16-H07-34-537 from the Banshee deposit also record exhumation-related cooling. For the purposes of this chapter, Late Cretaceous regional exhumation ages are considered "background" ages, against which younger thermal anomalies related to hydrothermal heating can be identified. Existing and new U-Pb zircon data obtained for samples in this study indicate that all samples in this study were emplaced at ~161-157 Ma. Samples therefore record the thermal history of the area since the Jurassic.

AFT ages within 400 m of the edge of the Goldstrike Stock and up to 200 m around the Golden April and Meikle deposits are ~40 Ma, coincident with the timing of Carlin-type Au mineralization. These ages are younger than the Late Cretaceous exhumation age constrained by the background samples that are more distal to mineralization. The ~40 Ma AFT ages of samples close to mineralization are therefore attributed to hydrothermal heating, the duration of which is the main focus of this chapter (see heat flow modelling below).

Younger hydrothermal events are recorded in AHe data <30 Ma, as well as Post Fault sample RM91-22C-1460 that has an AFT age of $20.9 \pm 15.6 - 8.9$ Ma. Sample AHe ages around

Au deposits are variable, ranging 3.6 ± 0.2 to 32.3 ± 0.7 Ma, suggesting AHe data is not recording a single widespread event. Instead, AHe ages are interpreted as recording localised hydrothermal fluid flow that occurred around the Golden April deposit 3-23 Ma, in the Post Fault area ~10 Ma and around the edge of the Goldstrike Stock ~20 Ma. AHe ages of ~30 Ma in the Goldstrike Stock may be related to exhumation and cooling (see Chapter 4), but could also result from hydrothermal heating. Post Fault area AFT ages 20-30 Ma are not exhumation-related because the entire area had cooled through the AFT closure isotherm by ~60 Ma as a result of exhumation to <2 km. Instead, the young Post area AFT ages record hydrothermal fluid flow that was focused along the Post Fault in the Oligocene-Miocene. The Post Fault samples are highly altered, probably as a result of multiple hydrothermal fluid flow events along the fault system, a major fluid conduit in the northern Carlin Trend.

5.5.2 Thermochronological constraints on the duration of fluid flow

Although a thermal resetting halo can only be identified in AFT data, the obtained ZHe and AHe ages can also help constrain the duration of the Carlin hydrothermal system. ZHe ages are consistently >60 Ma across the study area, an indication that the Eocene hydrothermal system that was responsible for total resetting of AFT ages around fluid conduits was too short-lived to noticeably affect the ZHe system at known Carlin fluid temperatures of 180-240°C. In contrast, AHe ages are highly variable but consistently younger than the Carlin mineralizing hydrothermal system. The AHe system has a much lower T_c , ~50°C, so has been reset by localised hydrothermal events that occurred subsequent to the main Eocene Carlin hydrothermal system and no longer relates spatially to Carlin-type Au mineralization.

Samples in the study can be divided into two groups - those that are altered, and those that are not. Samples that are altered include those from the Post Fault area, the Golden April

and Meikle deposits, and sample U16-H07-68-247 from the Banshee deposit. Alteration in those areas is pervasive, affecting 50-85 % of the bulk rock in each sample. Chemical alteration results from interaction with a hydrothermal fluid, so these samples were at some point within a fluid flow path. These samples were therefore heated primarily by advective heating. In contrast, unaltered samples were outside of fluid flow paths so any heating was purely conductive. Both altered and unaltered samples provide constraints for the duration of heating.

5.5.2.1 Constraints from altered samples - advection-dominated heating

Altered samples were within a hydrothermal fluid flow path and were directly heated by the hydrothermal fluids. The altered samples are typically lamprophyre dikes that are hosted in carbonate rocks. The carbonate host rocks are highly fractured and have a higher fluid conduit density and effective permeability than the dikes or granodiorite stocks. The dike samples are therefore more proximal to fluid flow conduits (e.g., fractures) than samples within the essentially impermeable Goldstrike or Little Boulder Basin Stocks (permeability $<10^{-14}$ - 10^{-15} cm² (Bear, 1988)). Heating of a sample within a fluid flow path is assumed to be isothermal, i.e. the sample was consistently heated by the hydrothermal fluid at fluid temperature for the duration of the fluid flow event. Altered samples in this study typically have AFT ages of ~40 Ma, coincident with the timing of Carlin mineralization, so are considered to have been thermally reset by heating associated with that ~40 Ma hydrothermal system. A small number have ~20-30 Ma AFT ages and record more localised Oligocene and Miocene hydrothermal activity. The majority of altered samples with Eocene AFT ages have ZHe ages of >60 Ma that are interpreted to record exhumation-related cooling. The preservation of background ZHe ages in 40 Ma AFT samples indicates that the ZHe system, which has a higher T_c than the AFT

system, was not affected by heating by 180-240°C fluids over the duration of Carlin hydrothermal fluid flow. Figure 5.9 shows the relationship between temperature, duration of heating and resetting of AHe, AFT, ZHe and ZFT thermochronometers for the size of apatite and zircon analysed in this study. The diagram shows that the maximum duration of isothermal heating by 180°C fluids that totally reset AFT without affecting the ZHe system was on the order of 10^4 years. For a higher temperature fluid, e.g., 240°C, this estimate is even lower, on the order of 10^2 years. Two samples, EX-29C-1783 and U16-H07-68-247, both highly altered samples, have Eocene ZHe ages. Resetting of the ZHe system by Carlin temperature fluids can be achieved in 10^4 - 10^6 years. Although it is possible that these samples represent more sustained, longer-lived hydrothermal fluid flow, they may also be evidence of higher temperature parts of the Carlin hydrothermal system. Isothermal heating over 10^4 years by a 240°C fluid would also be sufficient to reset ZHe. At the Banshee deposit (Figure 5.10), the proximity of sample U16-H07-34-537, with a background Late Cretaceous AFT age of 62.9 ± 14.3 - 11.7 Ma, to sample U16-H07-68-247 that has an Eocene ZHe age of 45.2 ± 2.0 Ma, may be evidence of localised short-lived higher temperature fluid flow that was sufficient to reset the ZHe system proximal to fluid flow but not ~150 m away (Figure 5.10).

5.5.2.2 Constraints from unaltered samples - conductive heating

Samples from the Goldstrike Stock are unaltered, yet show a range of AFT ages from ~40 Ma around the edge of the stock to ~60 Ma at its centre (Figure 5.11). The background exhumation age in the northern Carlin Trend was established as ~60 Ma, so central samples were not reset by the Eocene heating that caused total resetting of AFT ages proximal to Au mineralization and hydrothermal fluid flow. The lack of hydrothermal alteration in the Goldstrike Stock samples suggests that the heating responsible for total resetting the AFT ages

of samples up to 400 m into the stock was purely conductive, and involved no advective transfer of heat or mass from fluid to rock. HeFTy modelling of fission track data from samples nearer the centre of the Goldstrike Stock does show that heating of central samples around 40 Ma was possible, but not to sufficient temperatures or for long enough to reset AFT (Figure 5.7e).

Heating outside of the fluid flow path is not isothermal, as there is a long period of heating until fluid temperatures are attained. The duration of conductive heating to produce the observed 400 m AFT total resetting halo was therefore investigated further using finite element modelling.

5.6 Heat flow modelling

In hydrothermal systems, heat is transferred from fluid to rock advectively within the fluid flow path by direct fluid-rock interaction, or conductively beyond the fluid conduit through the host body of rock. Whether heat transfer is dominantly advective or conductive depends on fluid flux and the time and length scales considered (Bickle and McKenzie, 1987; Cathles, 1997). This study focuses on conductive (diffusional) heat transfer, which is governed by Fourier's law:

$$q = -k \cdot \nabla T \quad (1)$$

where q is heat flux in W/m^2 , k is thermal conductivity in W/m K , and ∇T is the thermal gradient.

In order to determine how long a single pulse of hydrothermal heating lasted in the northern Carlin Trend, modelling of heat flow and the effects of heating on the AFT system in the Goldstrike Stock was undertaken. The Goldstrike Stock was chosen because AFT data is

available at a range of distances across the stock, from the edge into the centre of the stock, and because no fluid flow has occurred within the stock, as the lack of hydrothermal alteration of Goldstrike Stock samples shows. The temperature in fluid conduits around the outside of the stock can be considered isothermal over the duration of hydrothermal fluid flow. Fluid flow around the outside of the stock is therefore considered a consistent source for heat that is conductively transferred into the body of the stock.

Inverse modelling using HeFTy supports heating of the entire stock around 40 Ma (Figure 5.7d), with greatest heating in samples around the edge of the stock, enough to totally reset AFT ages within ~400 m of the stock edge (Figure 5.11). Samples from the centre of the stock retain Late Cretaceous-Paleocene ages but may also have been affected by Eocene reheating and cooling (Figure 5.7e). Conductive heat flow therefore raised the temperature of the entire stock but not to sufficiently high temperatures for long enough to totally reset samples greater than 400 m from the stock's edge. Modelling of the temperature attained in across the stock with increasing duration of heating was modelled using the finite element method (FEM) using the Matlab® Partial Differential Equation Toolbox™ (PDE Toolbox) extension. The maximum duration of heating was then determined by forward modelling theoretical t-T histories of the stock in HeFTy to determine the maximum duration of heating without totally resetting samples greater than 400 m from the edge of the stock.

5.6.1 Numerical modelling of heat flow across the Goldstrike Stock

The FEM was used to model conductive heating of the Goldstrike Stock. FEM is a numerical method used to find approximate solutions to partial differential equations, such as the heat equation (Equation 5.2). A complex geometry, in this case the Goldstrike Stock, approximated as a cylinder, is discretised into a number of smaller simple geometric objects to

form a mesh. In PDE Toolbox the mesh consists of triangles, the vertices of which are nodes. Using the FEM, a PDE is converted to simpler algebraic equations solved for each node. The solutions on each node are combined to generate an approximate solution for the whole cylinder.

Heat transfer is described by the parabolic partial differential equation:

$$\rho C \frac{\partial T}{\partial t} - \nabla(k \nabla T) = Q + h(T_{ext} - T) \quad (2)$$

where ρ is rock density, C is the heat capacity of the stock and $\nabla(k \nabla T)$ is the heat flux gradient, $k \nabla T$, where k is the conductive heat coefficient, the thermal conductivity of the stock, and ∇T is the thermal gradient. Q is the heat source, h is convective heat transfer coefficient and T_{ext} is the external temperature. In this case Q is zero because there is no heat source in the already crystallized stock. Heat generated by decay of radioactive elements within the stock is not considered a significant source of heat over the timescales investigated in this study, and therefore not accounted for. Convective heat transfer, h , is zero because there is no convective heat transfer in this purely conductive heating model. $T_{ext} - T$ describes transversal heat transfer from a body to its surroundings, so is also zero in this case. The modelled equation therefore becomes:

$$\rho C \frac{\partial T}{\partial t} - \nabla(k \nabla T) = 0 \quad (3)$$

Parameters are defined in Table 5.4. The modelled stock density, ρ , was 2700 kg/m³. Heat capacity, C , 780 J/kg K, and coefficient of thermal conductivity, k , 2.7 W/m K, were taken from published studies of granodiorite thermal properties (Arndt et al., 1997). The thermal conductivity, k , does decrease with increasing temperatures (Sass et al., 1992) but was assumed to be constant over the temperature range and timescales investigated in this study. The stock geometry was approximated as a cylinder of infinite length with a radius of 800 m.

A mesh was generated automatically using PDE Toolbox consisting of triangles with vertices 50-70 m. The stock's starting temperature was set to 30°C. Starting temperatures of 20°C and 40°C were also tested, but the difference in stock temperature after models were run was minimal and so not investigated further. The heated perimeter of the stock was set at either 180 or 240°C, the temperature range of Carlin ore fluids determined by fluid inclusion studies (Cline and Hofstra, 2000; Emsbo et al., 2003). Fluid heating temperatures were assumed constant for the duration of heating, and no cooling period following cessation of hydrothermal fluid flow was accounted for.

Boundary conditions can be of Dirichlet or Neumann-type. On Dirichlet-type boundaries, a constant temperature can be specified, in this case the temperature of hydrothermal fluids around the outside of the stock, 180-240°C. Dirichlet-type boundary conditions were specified on the heated side(s) of the stock, i.e. on all sides when the entire perimeter of the stock was heated, or for the heated 1/2 or 1/4 of the stock when only part of the stock's perimeter was heated. Unheated parts of the stock's perimeter were set as Neumann-type boundary conditions, where heat flux, $n(k\nabla T) + qT = g$, can be specified, in this case as generalised Neumann type conditions, $n(k\nabla T) + qT = g = 0$, as the flux from the heated stock into the surrounding country rock as the model proceeded was not known.

Models were run up to 1 Myr for fluid temperatures of 180°C and 240°C heating the entire perimeter of the cylindrical stock to observe the temperature reached inside the stock after increasing time intervals. Heating on all sides raises the entire stock to fluid temperature within 10 kyr (Figure 5.12). The temperature at 50, 100, 200, 400, 600 and 800 m into the stock was extracted to generate idealised t-T path at increasing distance into the stock (Figure

5.13). The effect of heating 1/2 and 1/4 of the stock's perimeter was also modelled (Figure 5.13). Fluid temperature was reached across the stock within 50 kyr and 100 kyr respectively.

5.7 Interpreted duration of hydrothermal fluid flow responsible for formation of Au-deposits in the northern Carlin Trend

Durations of heating are best estimated using AFT data, as this thermochronometer is susceptible to resetting by hydrothermal fluid temperatures (unlike ZHe) but has not been widely reset by younger, more localised fluid flow (as AHe is). The thermal history of a sample is recorded in the density and distribution of fission track lengths (Gleadow et al., 1986; Corrigan, 1991; Ketcham et al., 1999). A rise in temperature increases the rate of shortening and removal of fission tracks, ultimately total annealing removes all existing tracks and resets the AFT age of a sample (Naeser and Faul, 1969; Gleadow and Duddy, 1981; Green et al., 1986; Laslett et al., 1987; Carlson et al., 1999). Fission track data can be inversely modelled to determine possibly t-T histories of a given sample (see Chapter 4, and HeFTy modelling above). In this section, proposed t-T paths were forward modelled to determine the duration of heating that would result in total annealing of all fission tracks that existed prior to the period of modelled heating. The Matlab-generated heating t-T path of each theoretical sample was spliced at 40 Ma into the best fit HeFTy t-T path of sample GS-1845C-1 from the centre of the Goldstrike Stock (Figure 5.14).

Forward modelling in HeFTy calculates the age of the oldest fission track that could be preserved by the modelled t-T path (Ketcham, 2005). The age of the oldest track denotes the total time span over which the t-T history can be inferred by the fission track data (Willett, 1997). An oldest track age of 40 Ma, the age of reheating, indicates total annealing by the 40 Ma reheating event. An older age shows some information about the earlier t-T history is

preserved. The background AFT age in the area is ~70-60 Ma, as a result of regional exhumation (see Chapter 4). Estimates of maximum duration of heating were based on forward modelling t-T paths of increasing duration until the model sample was totally reset. The modelled sample was considered totally reset when the age of the oldest track fell from ~70 to 40 Ma, when the last "old" fission track was removed.

Figure 5.15 shows the maximum duration of heating in the modelled cylindrical stock heated on all, 1/2 and 1/4 of its perimeter. If heated on all sides simultaneously, the modelled maximum duration of heating to reset samples up to 400 m into the stock is 2.1 kyr (240°C fluids) to 3.5 kyr (180°C fluids). Heating for any longer period of time would reset in a larger AFT reset thermal halo than is observed, e.g., heating for 3.2 kyr (240°C fluids) to 4.6 kyr (180°C fluids) would result in total resetting of samples at the centre of the stock. Heating 1/2 of the stock's perimeter yields a maximum duration of 2.1 kyr (240°C fluids) to 4.5 kyr (180°C fluids) at 400 m in, and central samples would be reset within 5.6 kyr (240°C fluids) to 10.5 kyr (180°C fluids). Heating 1/4 yields a maximum duration of 4.6 kyr (240°C fluids) to 10 kyr (180°C fluids) at 400 m, and central samples would be reset within 12 kyr (240°C fluids) to 30 kyr (180°C fluids).

5.8 Interpreted hydrothermal fluid flux in the northern Carlin Trend

The magnitude of fluid flux required to form the Au deposits around the Goldstrike Stock can be estimated from Au content of the deposits and proposed duration of Au-bearing hydrothermal fluid flow. Deposits around the Goldstrike Stock contain approximately 40 Moz Au (Bettles, 2002). Figure 5.16 shows the range of fluid flux values for the durations inferred from heat flow modelling. These first order estimates of fluid flux are based on the assumption that all 40 Moz was deposited during a single hydrothermal event and that the system was

turned on and off rapidly, without significant heating and cooling. Fluid flux and total volume of fluid for durations 2.1 kyr to 10 kyr are summarised in Table 5.5. The Au content of mineralizing fluids is uncertain, although based on measurement of fluid inclusion salinity, H₂S content and Au saturation, previous studies suggest it was as high as 200 ppb at the Pipeline deposit in the Cortez area (Blamey, 2000) and 200-1700 ppb in the Jerritt Canyon deposit (Hofstra et al., 1991). For 180°C fluids, flux ranges from 20 kg/s for a high Au (200 ppb) fluid over a duration of 10 kyr (heating 1/4 of the stock) to 1125 kg/s for a low Au (10 ppb) fluid over 3.5 kyr (heating all of the stock's perimeter at once). Flux in a higher temperature system, i.e. with 240°C fluids, ranges 43 kg/s for a 200 ppb Au fluid over 4.6 kyr (heating 1/4 of the stock) to 1876 kg/s for a 10 ppb fluid over 2.1 kyr (heating all of the stock's perimeter). Figure 5.16 shows how these estimates compare to other hydrothermal and geothermal systems. Based on comparison with fluid flux in modern geothermal systems, a reasonable estimate of fluid flux is on the order 100 kg/s. If Au concentration is 100-200 ppb, estimates of fluid and Au flux are in agreement with short durations of hydrothermal fluid flow of 2.1-10 kyr.

The total volume of fluids involved in depositing 40 Moz Au around the Goldstrike Stock can be estimated based on duration and fluid flux, or total Au and fluid Au concentration. Assuming Au content of the fluids was between 100 and 200 ppb, the total volume of auriferous fluid involved in formation of Carlin-type deposits around the Goldstrike Stock was between ~125 km³ and ~62 km³ respectively.

The above estimates of fluid and Au flux are made assuming all Au was deposited in a single event. However, studies of Au-bearing pyrite have identified at least two distinct episodes of Au precipitation, recorded in hydrothermal growth rims on arsenian pyrite from the Carlin Trend (Arehart et al., 1993a; Barker et al., 2009). If the formation of Au deposits

occurred in multiple phases, the fluid and Au flux would be lower than proposed here, as not all 40 Moz Au were in fact deposited during a single hydrothermal event. Estimates of the maximum duration of fluid flow are not affected if individual pulses are temporally and thermally distinct, as the thermal effects of individual pulses on the AFT system are the same, regardless of the amount of Au precipitated. However, multiple pulses that overlap temporally without cooling back to ambient temperatures have a cumulative effect. Cumulative heating by multiple pulses cannot have exceeded the maximum estimated duration of ~10 kyr in total, or a larger AFT reset halo would be observed. Temporally and spatially overlapping pulses must therefore each have been shorter than 10 kyr.

5.9 Limitations of the heat flow model

Heat flow models were kept simple to provide first-order estimates of the duration of hydrothermal fluid flow. Only a single heating phase was considered, whereas in reality Carlin Au deposits were probably formed by many shorter lived pulses (Barker et al., 2009; Hickey et al., 2011). Unless temporally and thermally isolated, the effects of multiple heating pulses are cumulative. The model durations are therefore estimates of the maximum duration of either a single, thermally isolated pulse, or of the cumulative duration of multiple short-lived pulses. However, models did not account for cooling once hydrothermal fluid flow had ceased or for the effects of multiple fluid flow and heating events. During a cooling period, samples are still at elevated temperatures compared to pre-heating ambient temperatures, so fission track annealing continues to proceed at a higher rate.

The role of heat transfer from the stock to the country rock when only 1/2 or 1/4 of the stock was heated was also not accommodated in the finite element models of stock heating. The heat flux between stock and country rock would have changed over time as the stock and

country rock were heated. If heat was lost from the unheated sides of the stock, the duration of permissible heating would increase, as it would take longer to heat the stock to temperatures capable of causing total annealing. An increase in fluid flow duration requires lower rates of fluid flux than proposed for the high fluid Au concentrations published. At low fluid Au concentrations, ~10 ppb, fluid flux is still similar to modern geothermal systems.

Although there are several factors that may mean the actual duration of hydrothermal heating is higher or lower than proposed in this study, the order of magnitude is not changed. Hydrothermal fluid flow responsible for the formation of Carlin-type deposits was short-lived and required high rates of fluid flux.

5.10 Discussion

The estimated duration of hydrothermal heating in the northern Carlin Trend is short, <10 kyr. Greater durations would result in the formation of an AFT reset halo larger than the observed 400 m into the Goldstrike Stock. The duration calculated in this study do not necessarily constrain the duration of the entire hydrothermal system, but instead defines the maximum duration of a single, thermally isolated heating event that affected the Goldstrike Stock. The timing of Carlin-type Au deposit formation in the northern Carlin Trend has been constrained to a period of 6 Myr, from ~36 to 42 Ma, based on previous thermochronology and cross-cutting relationships (Arehart et al., 2003a; Ressel and Henry, 2006). Continuous heating over 6 Myr by 180-240°C fluids would totally reset AFT, and even ZHe, across the entire study area (Figure 5.9). However, hydrothermal fluid flow likely did not pervasively affect the whole length of the trend for the entire 6 Myr period, as flow could have been concentrated in a few areas at any given time. Even around the Goldstrike Stock, heating of just a portion of the stock, i.e., 1/4, is considered more likely than heating the entire perimeter at once. Episodic

fluid flow is a commonly described feature of modern geothermal systems (Bibby et al., 1995; Arehart et al., 2002; Rowland and Simmons, 2012), with individual pulses of flow feasibly lasting as little as 1 kyr (You and Bickle, 1998; Rowland and Simmons, 2012). Hydrothermal fluid flow paths are transient, affected by seismicity as well as mineral deposition and dissolution as a hydrothermal system evolves over time. Carbonate host rocks in the northern Carlin Trend were subject to changes in permeability and porosity as carbonate dissolution, dolomitisation and silicification progressed, and intrusive hosts and faults became argillised (Kuehn and Rose, 1992; Hofstra and Cline, 2000; Emsbo and Hofstra, 2003; Heitt et al., 2003). The total volume of rock affected by hydrothermal heating at any given time is therefore small compared to the overall volume of rock hosting the hydrothermal system (Rowland and Simmons, 2012).

Ressel and Henry (2006) proposed the emplacement of intrusions was the driving heat source for forced fluid circulation that formed the Carlin-type deposits. Cathles et al. (1997) estimated the maximum duration of hydrothermal fluid flow sustained by a single intrusion is ~800 kyr. Eocene intrusions in the northern Carlin Trend are volumetrically smaller than those modelled by Cathles et al. (1997), so a single intrusion would sustain fluid flow for less than 800 kyr. Even an inferred large intrusion at depth would not sustain heating for 6 Myr. Emplacement of multiple volumetrically small intrusions could therefore potentially have induced hydrothermal fluid flow for 1-10 kyr. An alternative mechanism for episodic fluid flow is seismicity, which involves very rapid pressure-driven flow along faults (Cox, 2005). In the northern Carlin Trend, the Post Fault system could have facilitated tapping of fluids from as deep as 15 km (Mickelthwaite, 2010). A free circulation model was proposed by Person et al. (2008), suggesting hydrothermal fluid flow resulted from deep circulation up to 6-8 km, where fluid flow was driven by buoyancy changes in fluids heated along the existing

geothermal gradient. The estimated duration of fluid flow based on free buoyancy-driven convection was sustained over ~170 kyr, significantly longer than shown possible here. Based on the short duration of fluid flow proposed in the present study, free convection is not a viable mechanism for driving hydrothermal fluid flow in the northern Carlin Trend.

Although the estimated duration of hydrothermal fluid flow around the Goldstrike Stock is short, it is in agreement with other proposed durations of hydrothermal systems. Overall durations range from ~1 kyr for individual pulses of fluid flow (e.g. Taupo Volcanic Zone, Rowland and Simmons, 2012), to 1-3 Myr for the overall duration of the geothermal system at Steamboat Springs in western Nevada (White, 1974). Simmons and Brown (2006) proposed the 38 Moz Ladolam Au deposit in Indonesia could have formed in <55 kyr at rates of Au and fluid flux of 24 kg/yr and 50 kg/s respectively. Similar estimates of ore-forming hydrothermal systems are <500 kyr (Arribas et al., 1995; Ronacher et al., 2002), but those do not propose durations of individual pulses. Existing estimates of Carlin hydrothermal activity range from <10 kyr to 1 Myr based on thermochronology data (Hofstra et al., 1999) but it is not clear whether they describe individual pulses or the whole system.

Proposed fluid flux in this study is 40-188 kg/s are also similar to modern geothermal systems in New Zealand (Simmons and Brown, 2007) and Iceland (Hardardóttir et al., 2009) and the Ladolam deposit (Simmons and Brown, 2006). The necessary Au flux in the northern Carlin Trend is higher than many modern geothermal systems, >100 kg/yr compared to typically 1-40 kg/yr (Figure 5.16). Very high fluid Au concentrations exceeding 100 ppb have been inferred based on thermodynamic modelling of proposed fluid compositions of Carlin deposits, so high Au flux is not unreasonable. If Au was deposited around the Goldstrike Stock in more than one episode of fluid flow and heating, the Au and fluid flux would be lower, and more in keeping with described geothermal flux rates.

Due to the complexity and density of fluid conduits outside of the Goldstrike Stock, and limited sample availability, definition of a conductive thermal halo was not possible in other parts of the study area. Dating of more distal samples to mineralization may provide sufficient data needed to define an AFT resetting halo around carbonate-hosted deposits beyond the limit of advective heating and advective mass transfer. Samples within 200 m of the Golden April deposit were reset at the time of mineralization by advective heating, so the size of the conductive halo must be greater than 200 m.

5.10.1 Implications for ore deposit formation

Estimates of fluid flux are similar to modern geothermal systems, which result from forced convection driven by a magmatic heat source (Ingebritsen et al., 2006). Magmatic heating lowers the density and increases the buoyancy of fluids, "forcing" the ascent of hydrothermal fluids. Ressel and Henry (2006) and Muntean et al. (2011) suggested that the coincidence of Eocene magmatism and Carlin deposit formation indicated magmatic heating of hydrothermal fluids. High fluid flux is also characteristic of pressure-driven fluid flow associated with fault seismicity, which has also been proposed as a mechanism for driving hydrothermal fluid flow along the Post-Gen fault system (Mickelthwaite, 2010). Free convection, as proposed by Person et al. (2008) typically involves lower fluid flux and longer durations of hydrothermal fluid flow. Based on comparison of short hydrothermal fluid flow duration and high fluid flux estimates, the present study suggests Carlin-type deposits were formed by a hydrothermal system driven by either forced convection or pressure-driven flow.

5.10.2 Potential of low-temperature thermochronology for exploration

In terms of exploration tools, the ZHe thermochronometer has too high a T_c to be reset by Carlin fluids over the inferred durations, except proximal to major fluid conduits and mineralization as at Meikle. ZHe dating is therefore not considered an appropriate tool in exploration for deposits formed by low-temperature systems. ZHe may have potential in exploring for higher temperature deposits, such as porphyries. AHe was also used in this study, but with a $T_c < 60^\circ\text{C}$, is too readily reset by lower magnitude hydrothermal events to define a thermal halo formed by a single hydrothermal system such as the one that formed Eocene Au deposits of the northern Carlin Trend. For exploration of deposits formed by Carlin temperature systems, AFT is therefore considered the most appropriate thermochronometer. Even so, AFT may be of limited use in green fields exploration where significant cover exists, as younger material will not record an older hydrothermal event in its thermal history. A preliminary calibration study would be required to determine the background thermal age. AFT has potential in exploration to determine whether the full potential of a deposit has been explored, or whether undetected mineralization may be present up to 400 m away.

5.11 Conclusions

Using AFT thermochronology, the size of a thermal halo on a deposit scale has been defined extending 400 m into the Goldstrike Stock. The stock is essentially unaltered, suggesting heating was predominantly conductive. Modelling using the finite element method was used to determine that the temperature across the stock reaches Carlin fluid temperature within 100 kyr. Forward modelling of AFT data and t-T paths shows that to form a 400 m halo, the maximum duration of conductive heating of a granodiorite stock by 180-240°C fluids is 2.1-10 kyr. Associated estimates of fluid flux range 40-188 kg/s, assuming all Au was

deposited in a single event and that Au content of the fluid was very high, 100-200 ppb. However, the short duration of hydrothermal heating is similar to proposed durations of episodic fluid flow pulses at other hydrothermal and geothermal systems. The short duration of flow and observations of other authors indicating multiple phases of alteration and Au precipitation are therefore considered evidence that the Au deposits of the northern Carlin Trend were formed by multiple hydrothermal pulses that were highly localised, short-lived and temporally and spatially distinct within a larger, more sustained hydrothermal system that persisted for several million years. Comparison with modern geothermal systems suggests Carlin-type deposits were formed by hydrothermal fluid flow driven by forced convection or pressure-driven flow rather than by free convection.

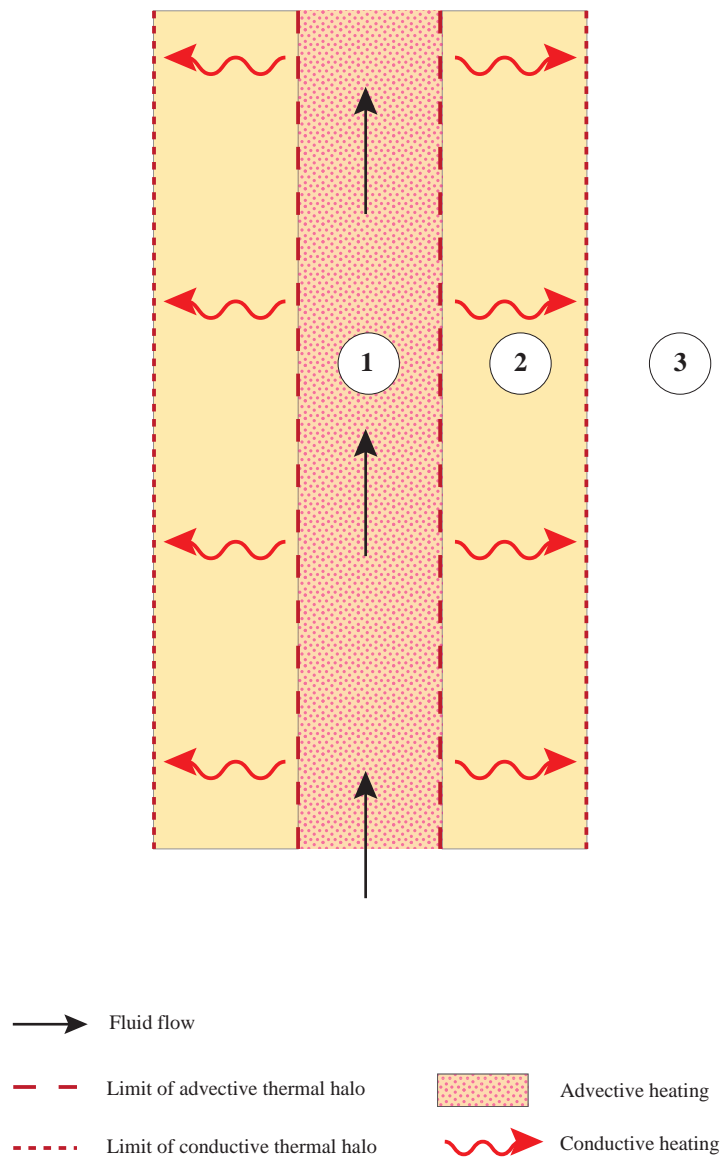


Figure 5.1 Conceptual development of thermal halos around a fluid conduit. (1) In the fluid pathway the rock is altered and mineralized by direct fluid-rock interaction. Rocks in the pathway are rapidly heated to the fluid temperature by advection and temperatures across the conduit are essentially isothermal. (2) A conductive halo is the most distal expression of fluid flow around a conduit. Barren rock (3) is thermally and chemically unaffected by heat or mass transfer from the passing hydrothermal fluid.

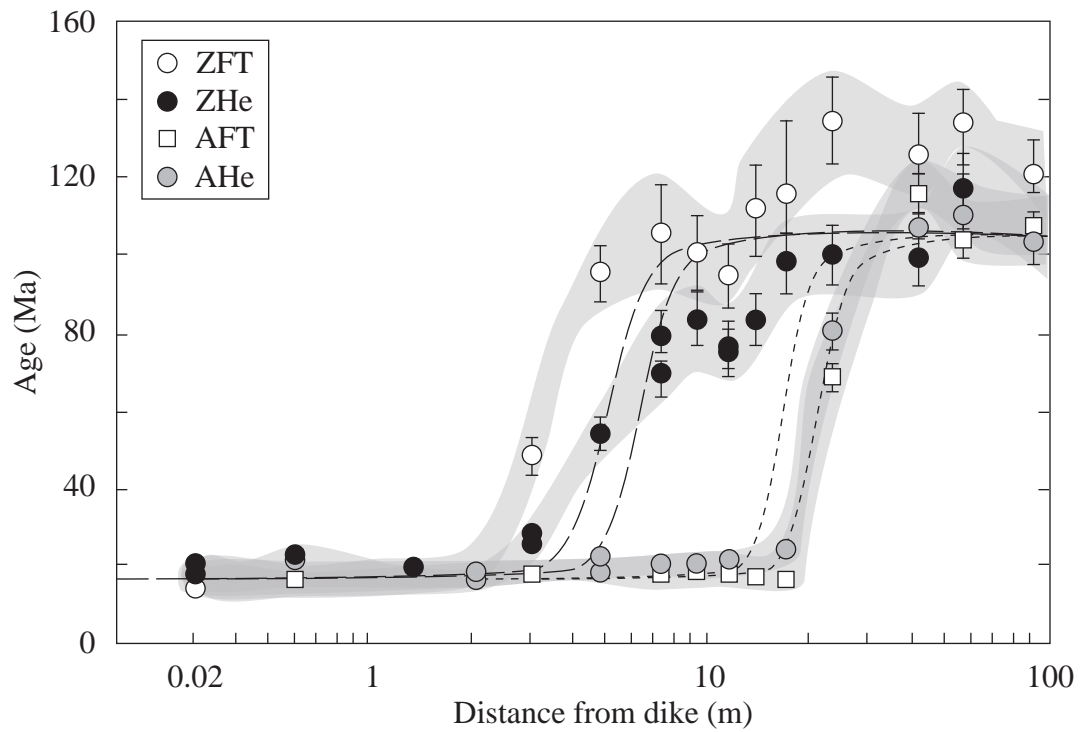


Figure 5.2 Thermochronometric data for samples out from a ~10 m wide dike of the Columbia River Basalt Group, in the Wallowa Mountains of northeastern Oregon from Reiners (2005). Dashed lines are predicted apatite and zircon ages. All thermochronometers are reset at 17 Ma within 2 m of the dike. The largest “halo” is recorded in the lowest temperature system, the AHe system, and is reset up to 11 m from the dike. Systems with higher closure temperatures, ZFT, ZHe and AFT, are not reset as far from the dike.

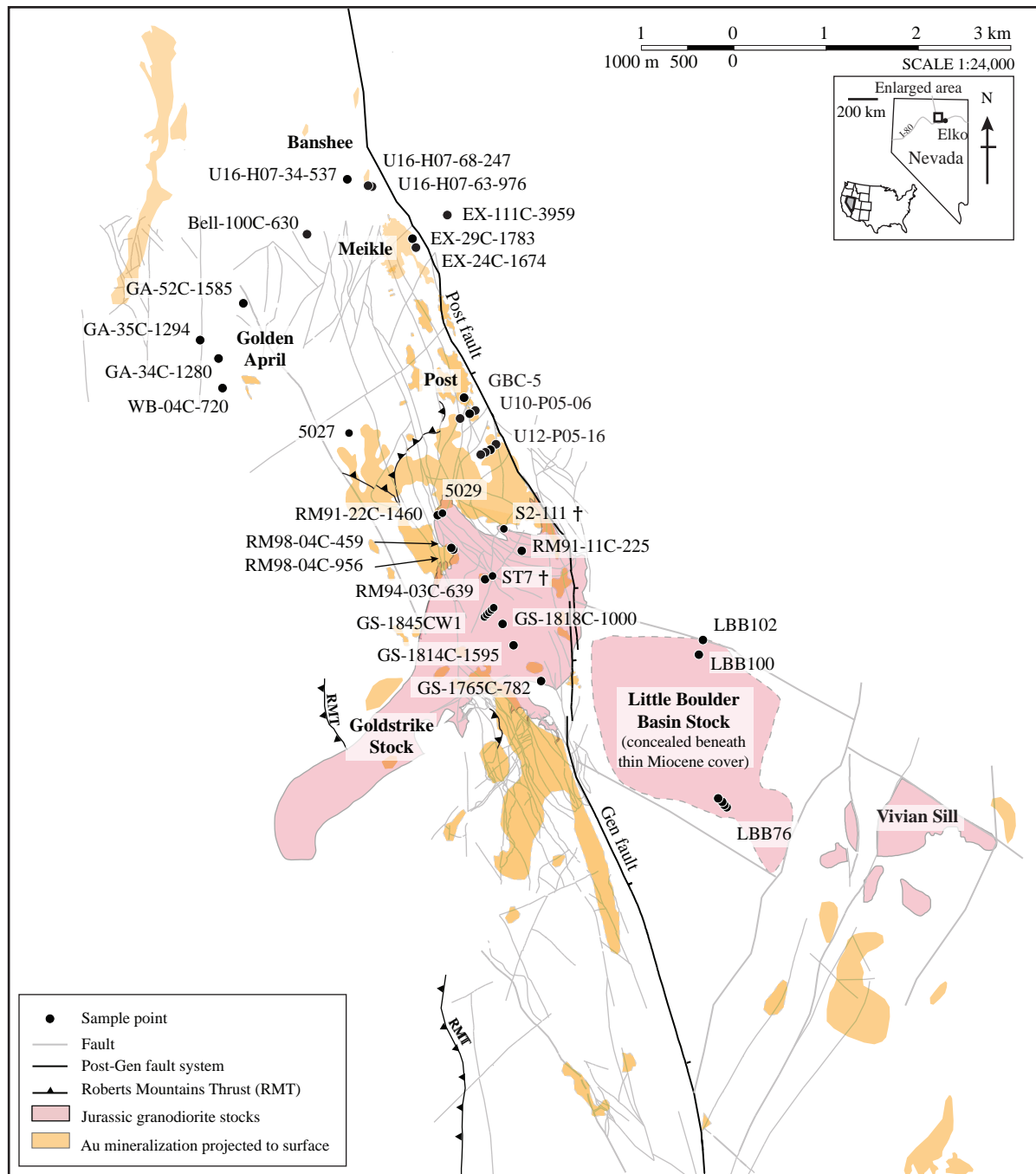


Figure 5.3 Distribution of Au mineralization in the northern Carlin Trend and location of major deposits, faults and samples referred to in this study. Geology after Teal and Jackson (2002), Moore (2002) and Heitt et al. (2003).

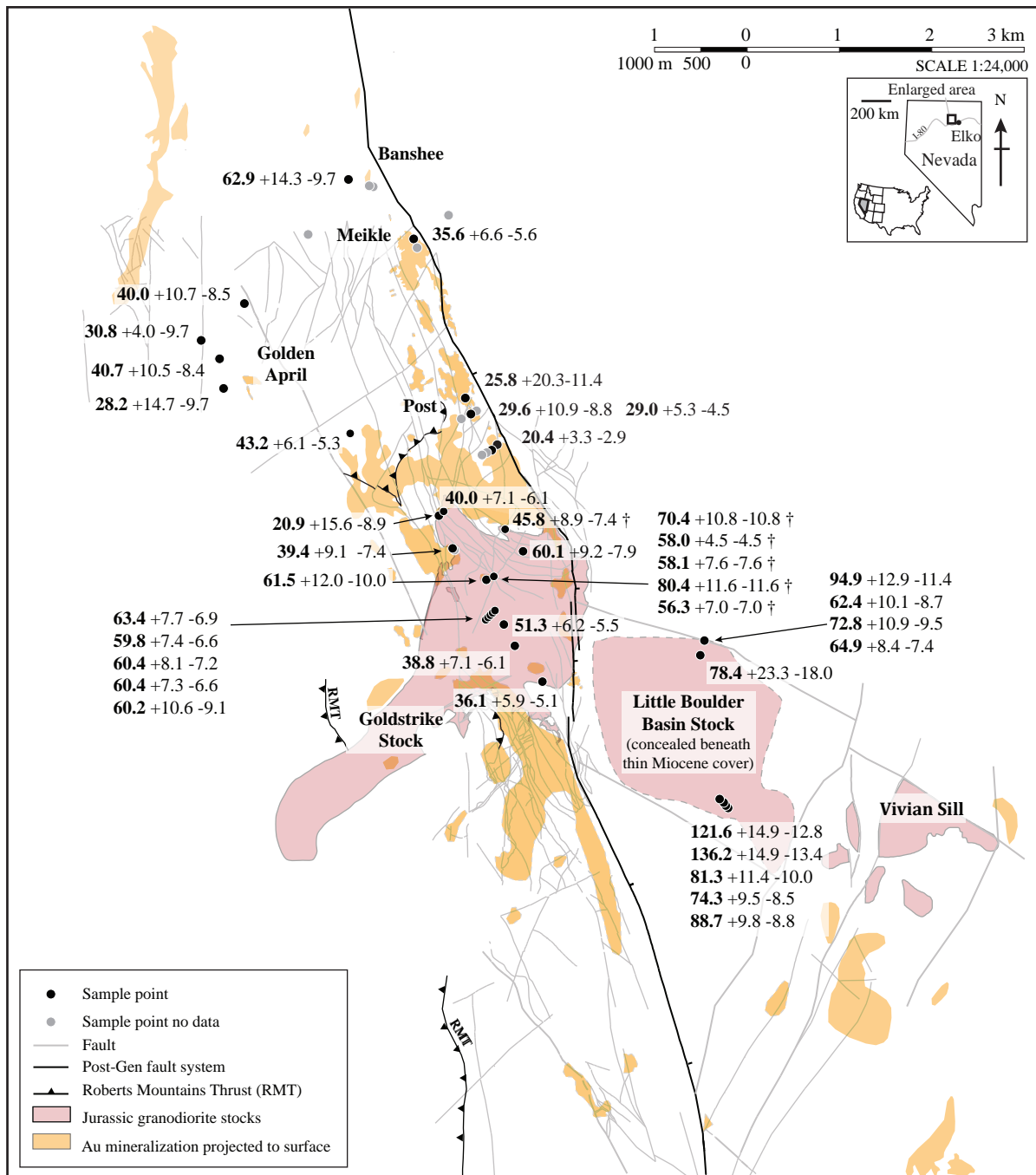


Figure 5.4 AFT ages obtained for samples shown in Figure 5.3. Ages in the Little Boulder Basin Stock and Goldstrike Stock are typically over 60 Ma. AFT ages for samples proximal to Au mineralization around Golden April, Meikle and the edge of the Goldstrike Stock are ~30-40 Ma. AFT ages for samples in the Post area are 20-30 Ma. Geology after Teal and Jackson (2002), Moore (2002) and Heitt et al. (2003).

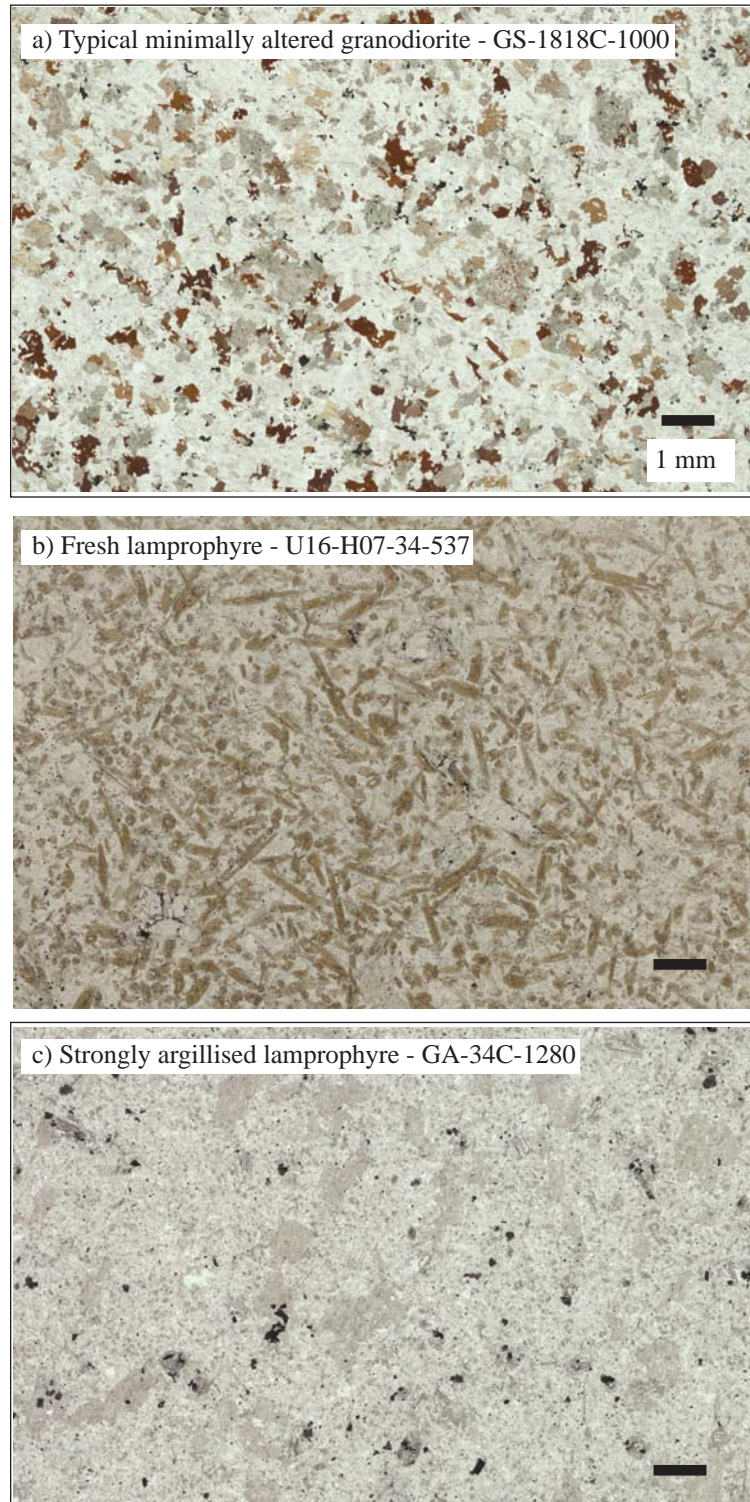


Figure 5.5 Photomicrographs of (a) typical granodiorite sample, minimal alteration of feldspars to sericite and mafic phases to chlorite±smeectite, (b) fresh hornblende lamprophyre from Banshee and (c) highly altered lamprophyre from Golden April. Alteration of lamprophyre samples is characterised by illite±smeectite.

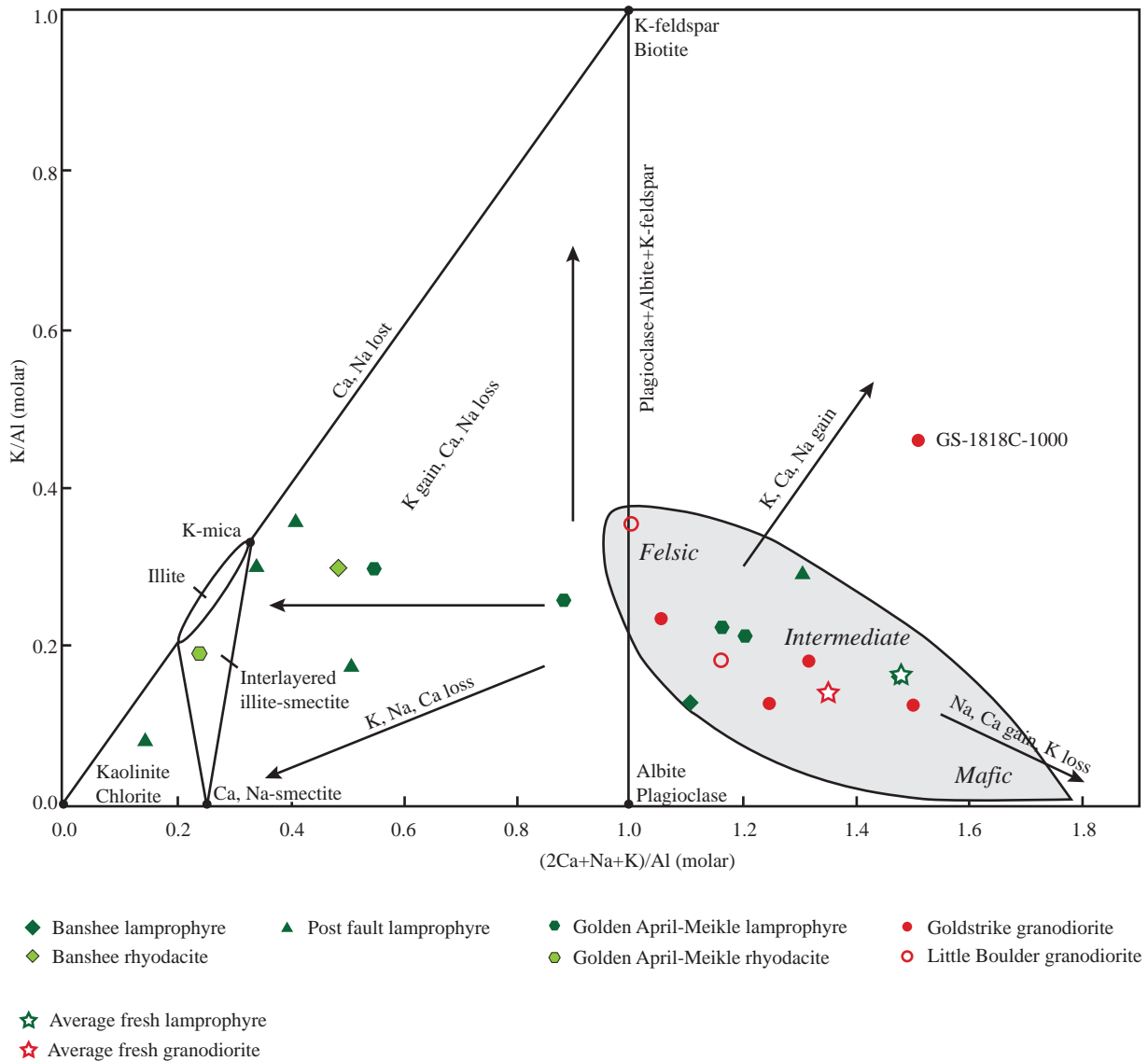


Figure 5.6 Molar element ratio plot of $(2Ca+Na+K)/Al$ vs K/Al for samples analysed in this study. Addition and loss of mobile elements K, Ca and Na is indicated by arrows vectoring towards alteration minerals. Fresh samples are indicated by stars (lamprophyre - green, granodiorite - red) and sit to the right on the plagioclase+albite+K-feldspar line. Granodiorite samples are relatively unaltered, with no significant gain in K or loss Na, Ca other than normal felsic-mafic compositional trends, in keeping with observed compositional variation in the Goldstrike and Little Boulder Basin Stocks. Lamprophyre samples from both Banshee and Golden April-Meikle section show systematic loss of Na, Ca from fresh towards more altered samples more proximal to Au mineralization. K addition or loss is minor. Post samples show strong Na, Ca loss and variable K. No fresh rhyodacite samples were collected. Both rhyodacite samples lie left of the $(2Ca+Na+K)/Al = 1$ line, so have probably lost Na and Ca relative to a hypothetical fresh sample.

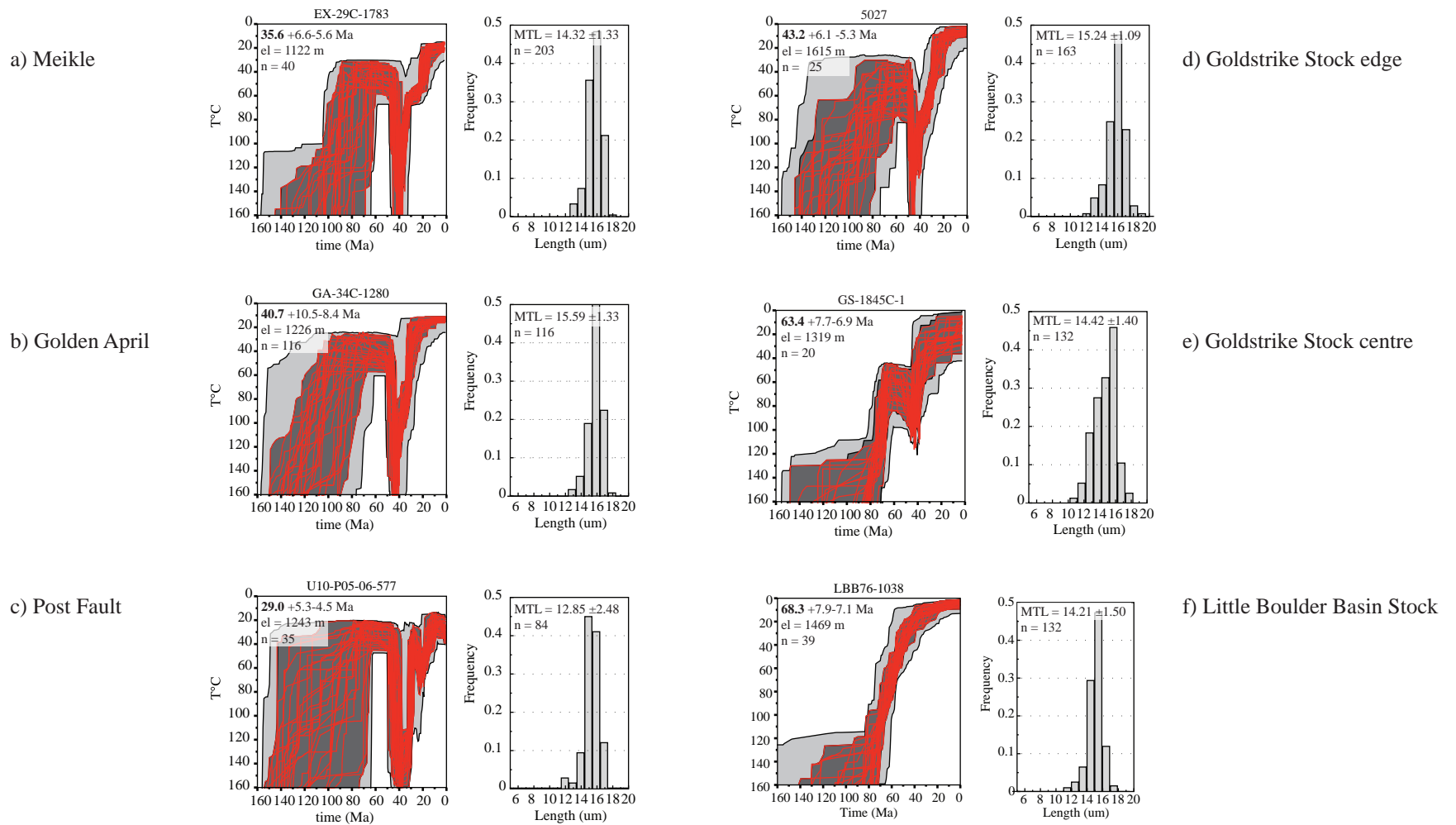


Figure 5.7 HeFTy models of t-T histories of representative samples from the northern Carlin Trend based on fission track length data. Samples cooled to near-present day temperatures by 60 Ma as a result of regional exhumation. Samples west of the Post Fault (a-e) then underwent heating associated with Au mineralization around 40 Ma. With the exception of the central Goldstrike Stock sample (e), Eocene heating was sufficient to reset AFT (a-d). The centre of the Goldstrike Stock (e) was heated but not enough to reset AFT so ~60 Ma exhumation ages are retained. The Little Boulder Basin Stock (f) is the the east of the Post Fault, away from mineralization and was not affected by Eocene hydrothermal fluid flow or associated heating.

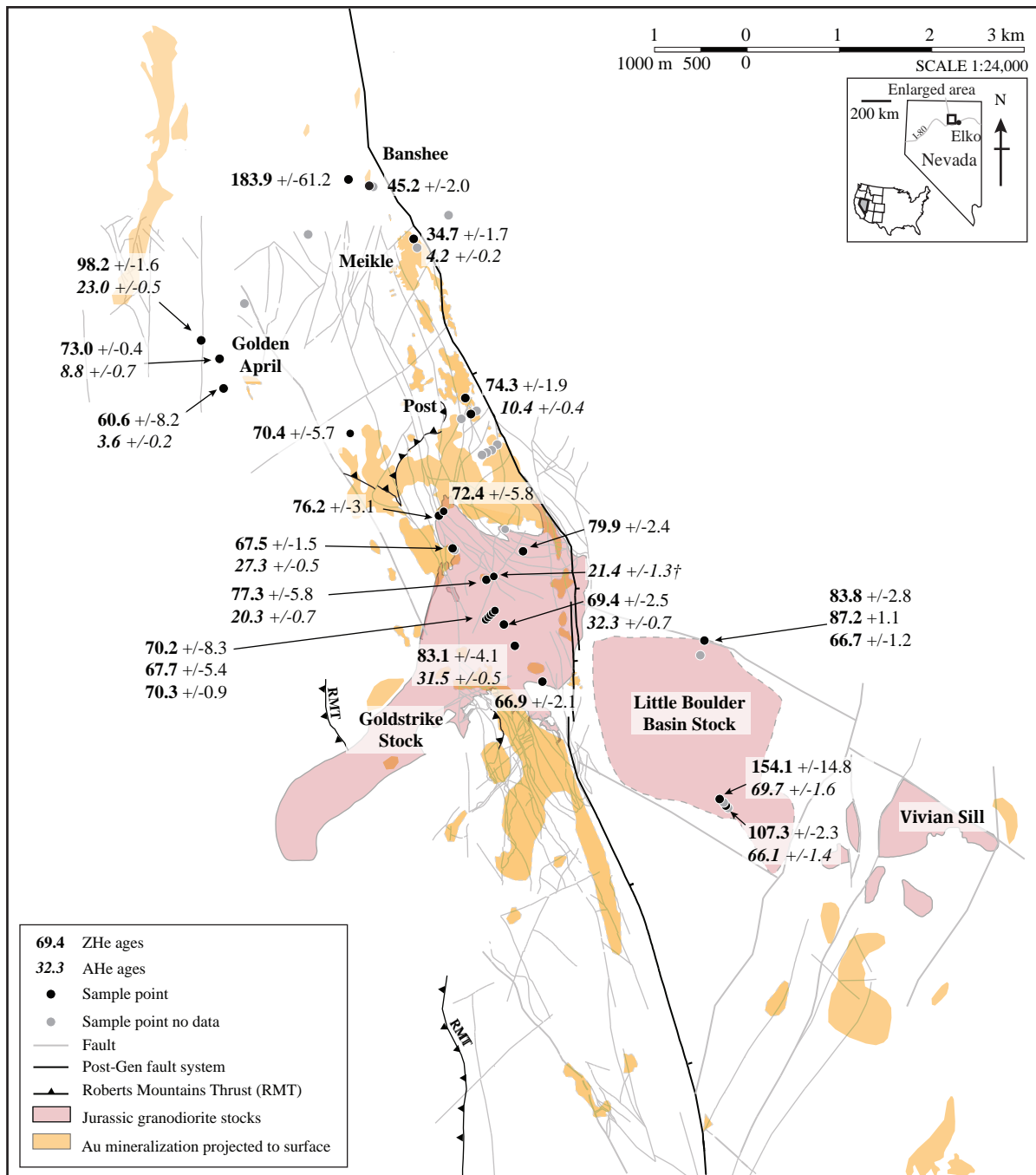


Figure 5.8 (U-Th)/He ages obtained for samples shown in Figure 5.3. ZHe ages across the study area typically over 70 Ma, with the exception of Banshee sample U16-H07-68-247 and Meikle sample EX-29C-1783, which have Eocene ZHe ages. AHe ages are more variable, ~65 Ma in the Little Boulder Basin Stock samples, 20-30 Ma in the Goldstrike Stock, ~4-23 Ma at Golden April and Meikle, and ~10 Ma in the Post area. No AHe ages were obtained for Banshee samples. Geology after Teal and Jackson (2002), Moore (2002), Heitt et al. (2003).

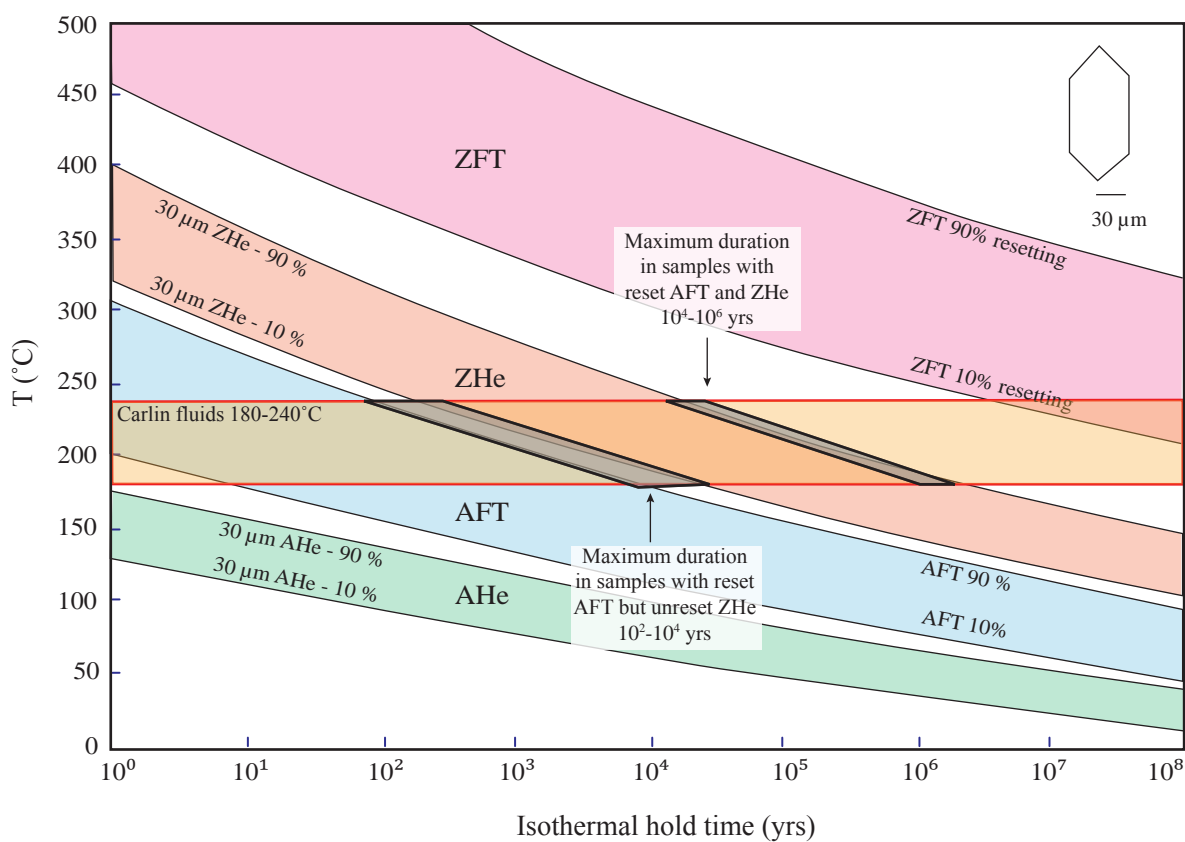


Figure 5.9 The effect of isothermal hold time on resetting of AHe, AFT, ZHe and ZFT. Temperatures calculated using Closure (Brandon et al. 1998; Ehlers et al. 2005). AHe and ZHe limits were calculated based on 30 μm equivalent radii, as observed in picked apatite and zircon crystals, using models of Farley (2000) and Reiners et al. (2004) respectively. AFT and ZFT temperatures were also calculated using Closure after Ketcham et al. (1999) and Rahn et al. (2004).

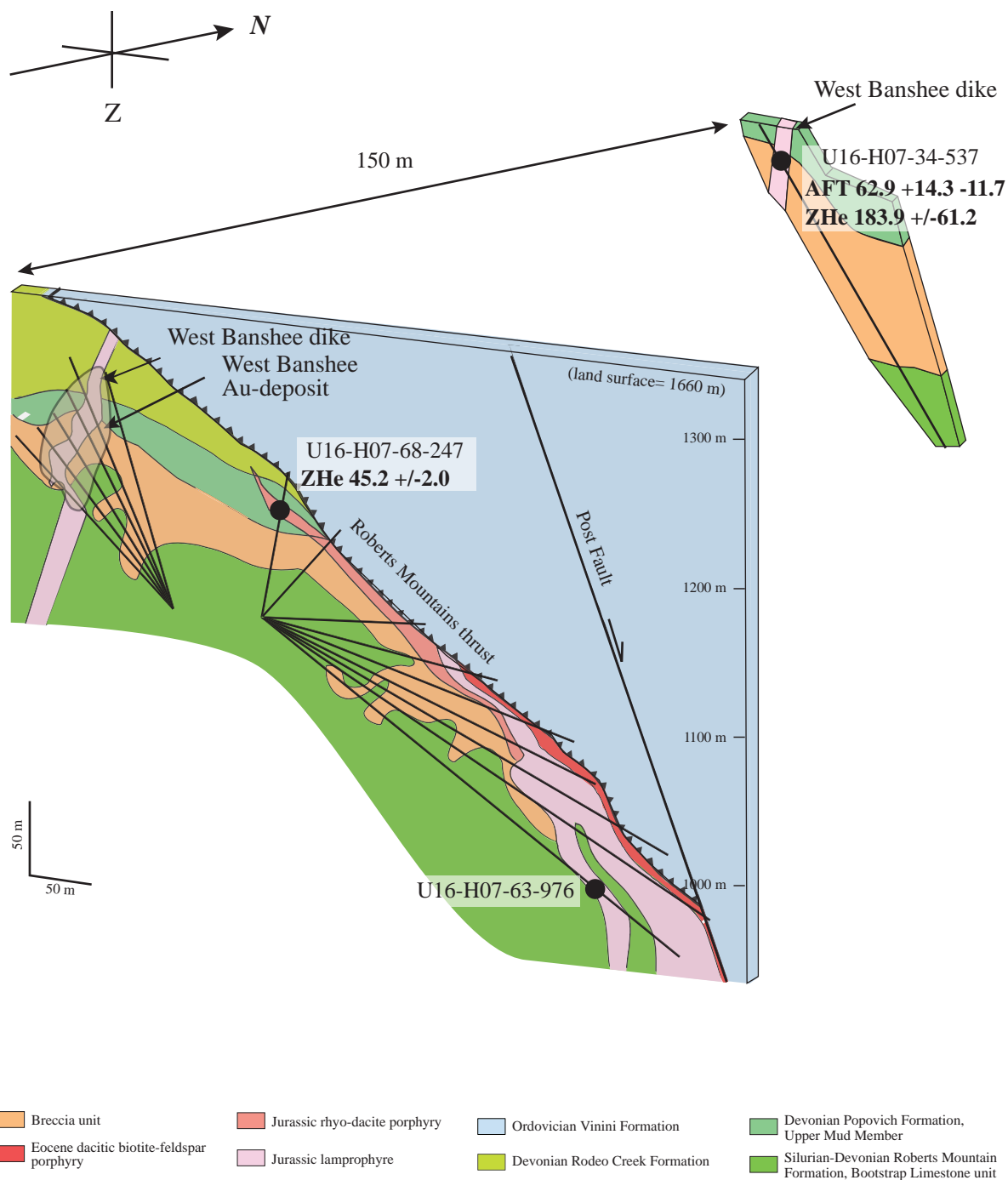


Figure 5.10 Projected cross sections through the West Banshee deposit showing location of samples and AFT and ZHe ages. Sample U16-H07-68-247 has an Eocene ZHe age whereas U16-H07-34-537 150 m to the north has a Cretaceous AFT age unaffected by Eocene hydrothermal fluid flow. Distance between sections not to scale. Geology modified from Vaughan (in prep.).

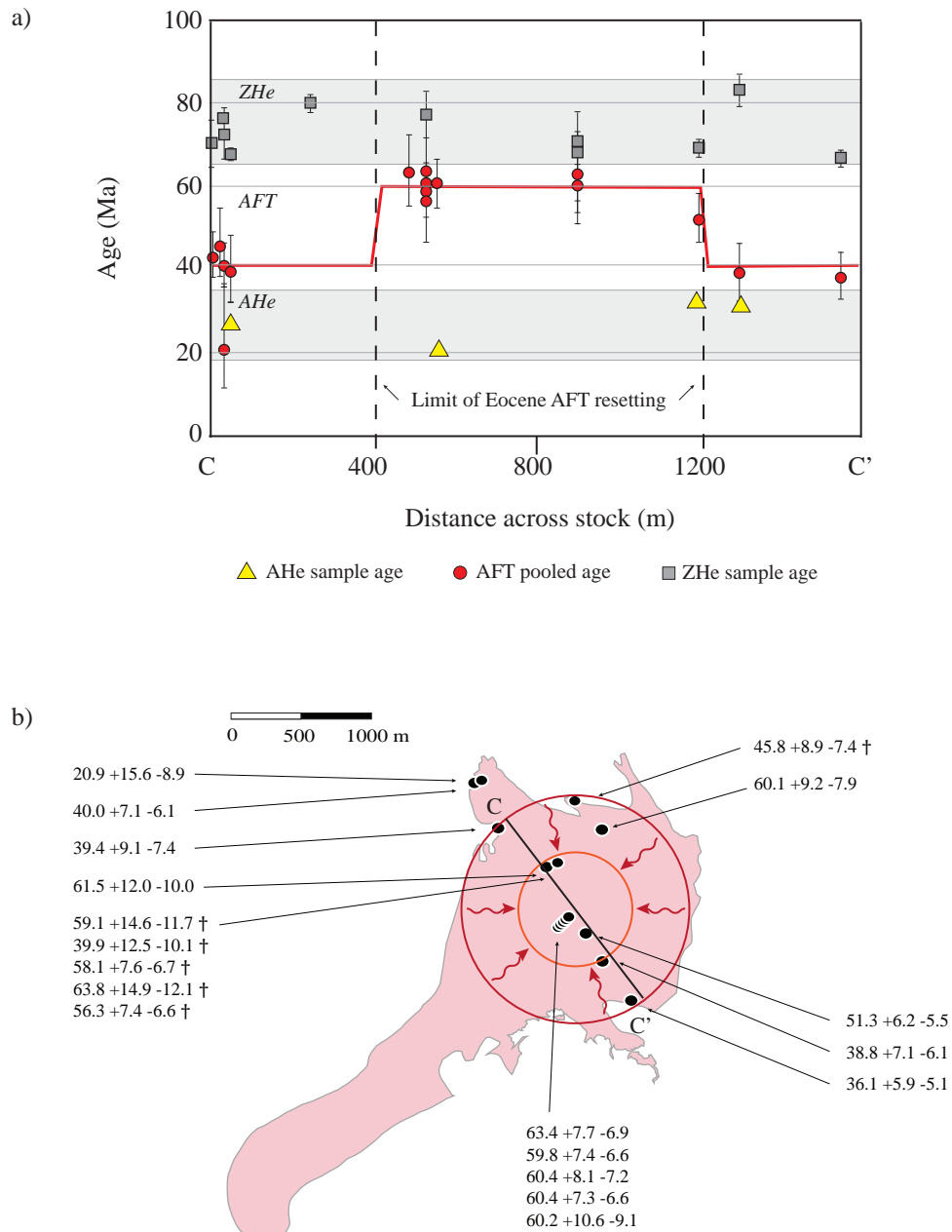
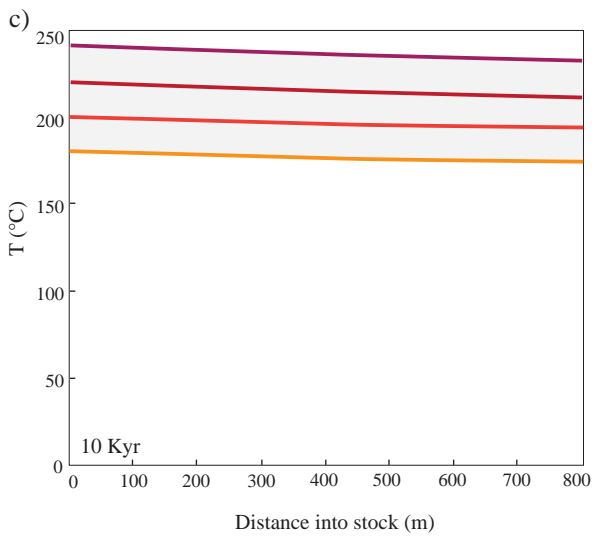
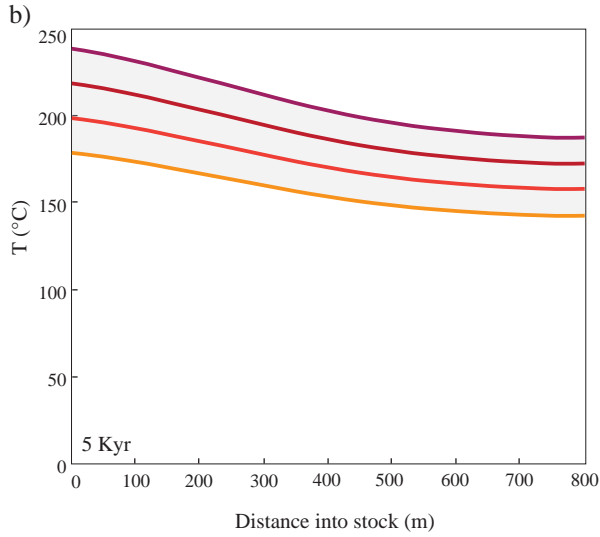
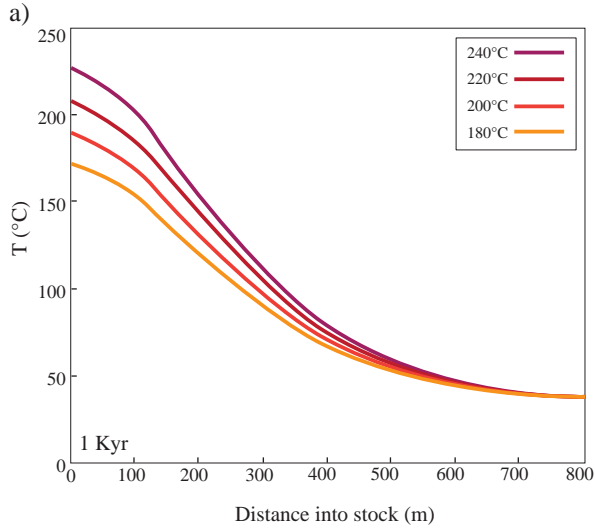
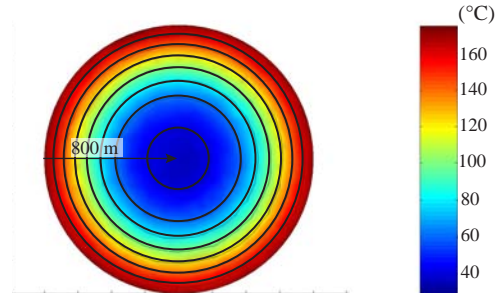


Figure 5.11 Size of the conductive thermal halo observed in AFT data in the Goldstrike Stock. (a) ZHe, AFT and AHe data in a NNW transect C-C' across the stock; ZHe ages are ~70-80 Ma across the stock and not affected by younger heating; AFT ages are ~60 Ma at the centre but samples within ~400 m of the edge of the stock have ~40 Ma ages reset by hydrothermal heating; AHe ages record younger hydrothermal heating or possibly exhumation through ~1 km depth. (b) Location of samples and AFT ages obtained from the Goldstrike Stock. AFT ages marked † are from Chakurian et al (2003).

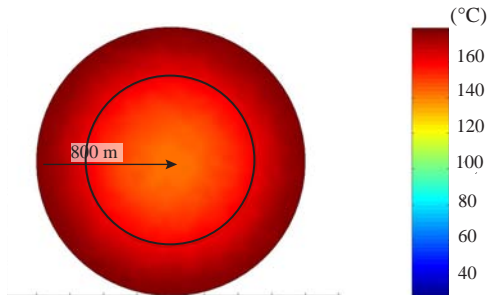


d) $T_n = 180^\circ\text{C}$



Temperature as a result of conductive heating after 1 kyr by 180°C fluids around the stock's perimeter

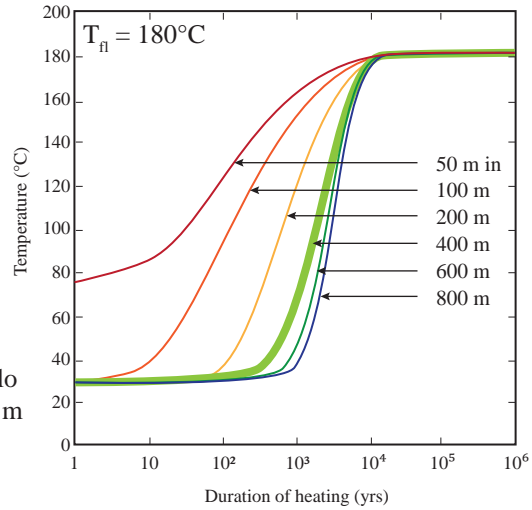
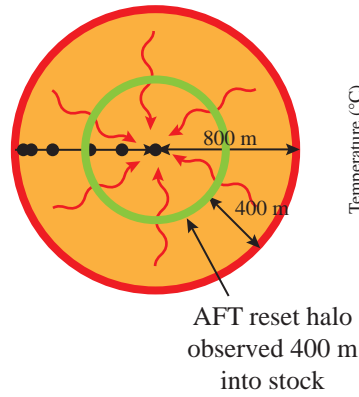
e) $T_n = 180^\circ\text{C}$



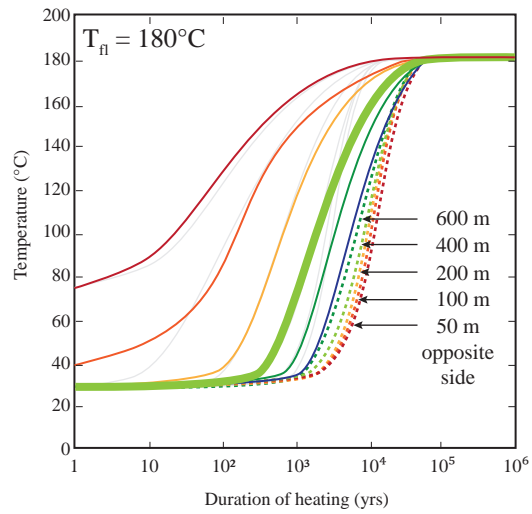
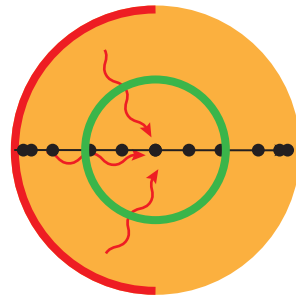
Temperature as a result of conductive heating after 5 kyr by 180°C fluids around the stock's perimeter

Figure 5.12 (a)-(c): Temperature into the modelled Goldstrike Stock after 1 Kyr, 5 Kyr and 10 Kyr resulting from heating on all sides by $180\text{--}240^\circ\text{C}$ fluids around the edge of the stock. (d), (e): Modelled temperature across the Goldstrike Stock after conductive heating by 180°C fluids for 1 kyr (d) and 5 kyr (e). Contour spacing in (d) and (e) 20°C .

a) Heating on all sides



b) Heating 1/2



c) Heating 1/4

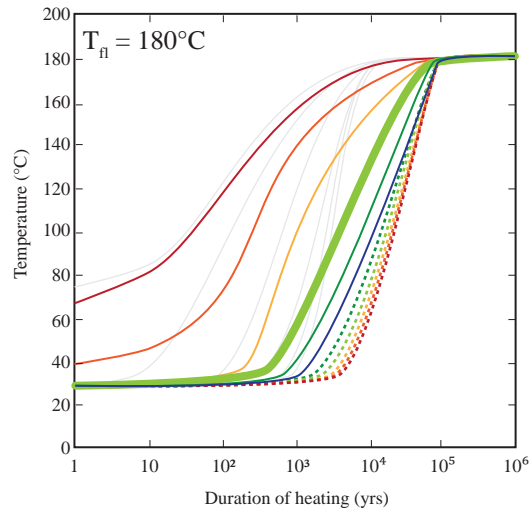
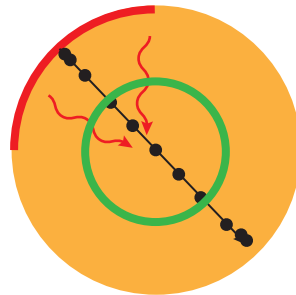


Figure 5.13 Time-temperature paths at distances 50, 100, 200, 400, 600 and 800 m into the centre of the model Goldstrike Stock cylinder heated by 180°C fluids around its perimeter. a) Heating on all sides of the stock, fluid temperature attained across the stock within 10 kyr. b) Half the perimeter of the stock is heated, fluid temperature attained within 50 kyr. c) Quarter of the stock is heated, fluid temperature attained within 100 kyr. Time-temperature paths for opposite sides to heated are also shown (dashed lines).

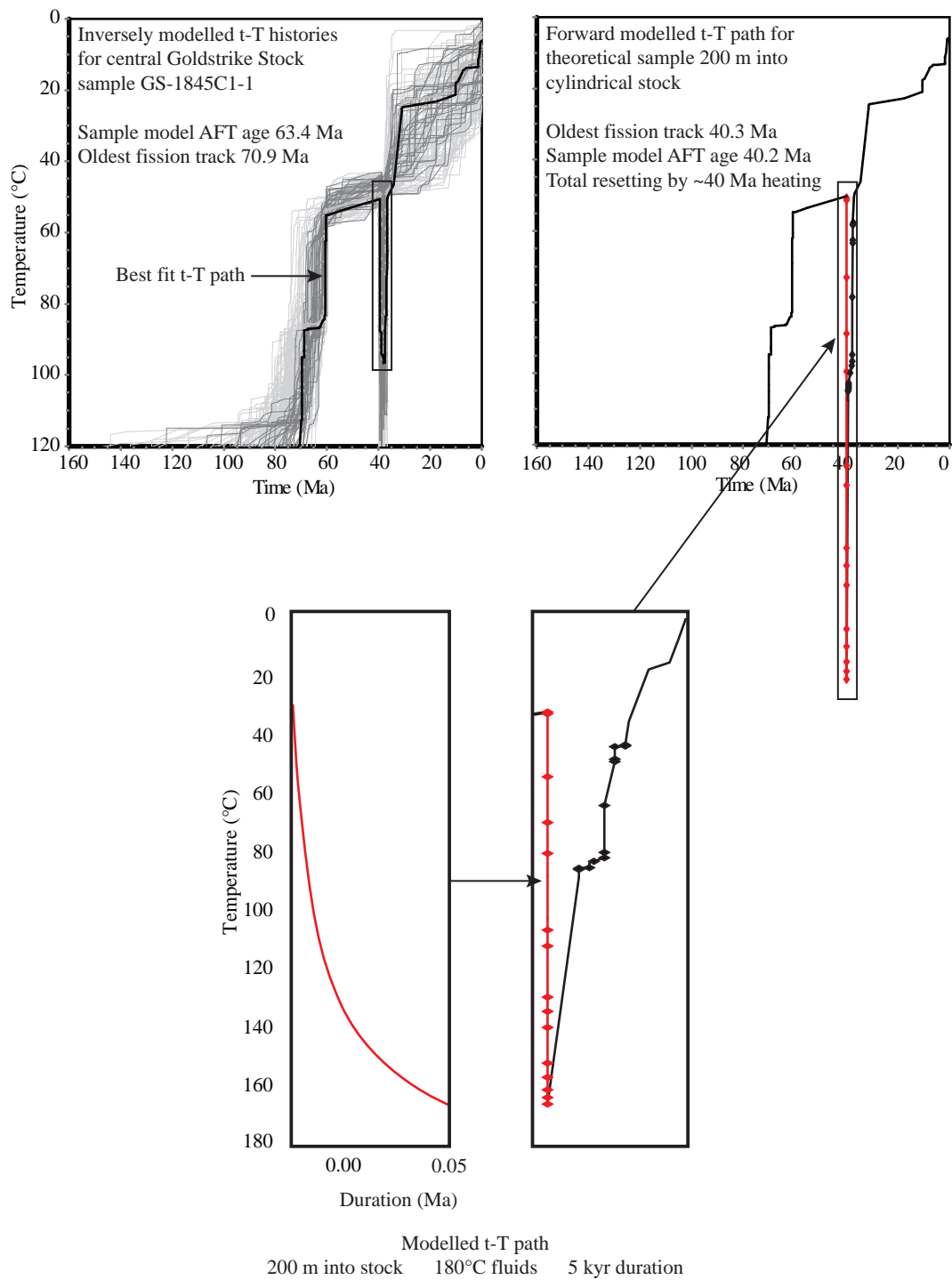


Figure 5.14 t-T path of a theoretical sample from the model Goldstrike Stock (red line) is spliced into a best fit t-T path of an actual Goldstrike Stock sample (black line) and forward modelled using HeFTy. Different durations of heating were forward modelled until the maximum duration was determined, the duration at which the sample is totally reset and the age of the oldest fission track equals the sample model AFT age. The example shows a t-T heating path of a theoretical sample 200 m into the stock conductively heated for 5 kyr by 180°C fluids around the outside of the stock.

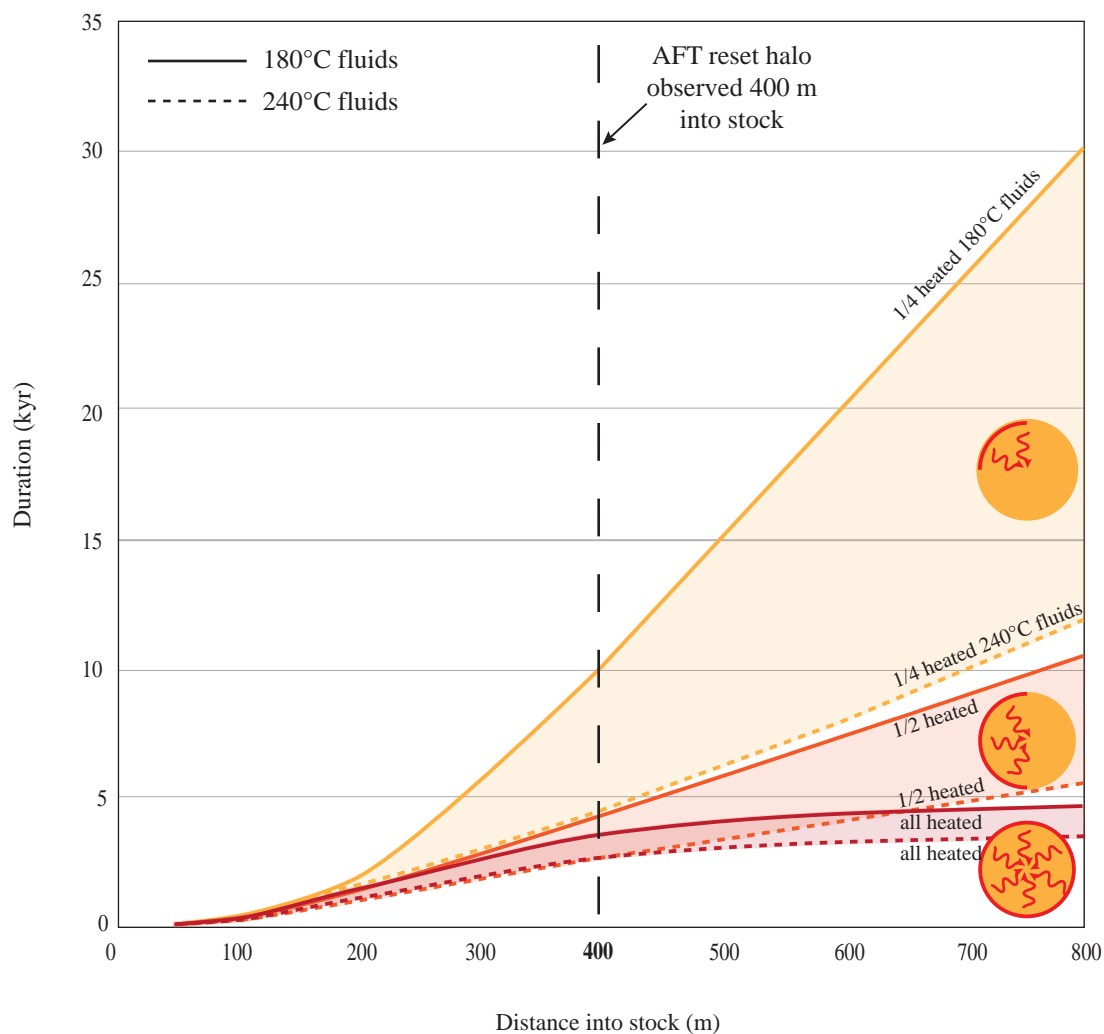


Figure 5.15 Maximum duration of heating by 180°C and 240°C fluids without causing total resetting of samples at increasing distance into an idealised cylindrical stock. Modelled cylinder radius was 800 m, equivalent to the granodiorite Goldstrike Stock. Distances are from the heated edge toward the centre of the stock. Heating on the opposite side would result in greater durations to totally reset samples.

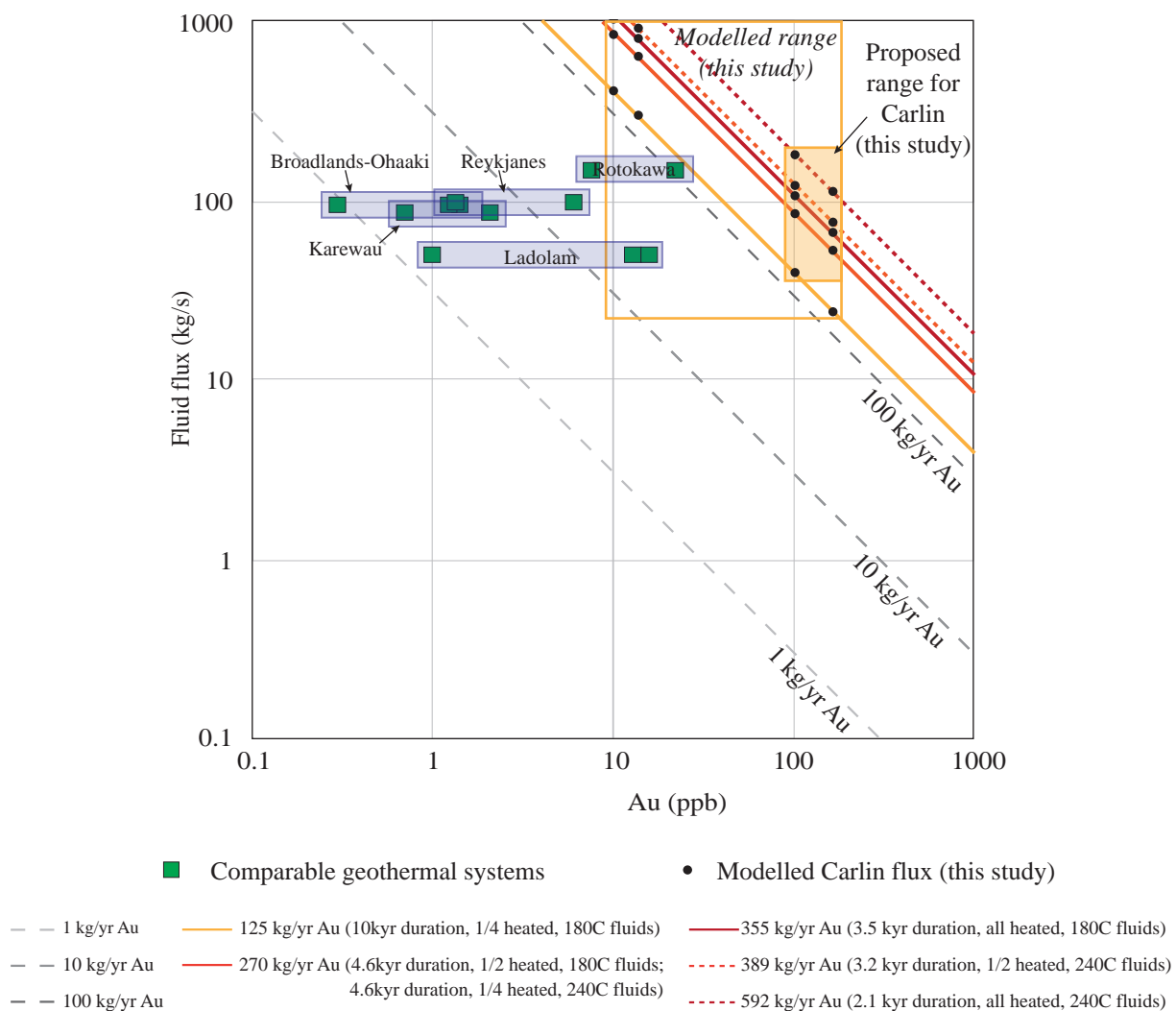


Figure 5.16 Fluid flux responsible for Au mineralization around the Goldstrike Stock in the northern Carlin Trend in comparison with active Au-bearing geothermal systems and the Ladolam Au deposit. The Au content of Carlin hydrothermal fluids is unknown but upper and lower estimates are 10-200 ppb. The Au flux required to deposit ~40 Moz Au is shown for different durations of hydrothermal fluid flow. Modified from Simmons and Brown (2007).

Table 5.1 AFT ages obtained using LA-ICP-MS method unless indicated

Sample name	East	North	Elev (m)	Tracks meas'd	Mean length (μm)	1σ (μm)	Grains	N _s	Dpar _A (μm)	Dpar 1σ (μm)	Area analyzed (cm ²)	Σ (PΩ) (cm ²)	1σ Σ(PΩ) (cm ²)	ξ _{MS}	1σ ξ _{MS}	Q (X ² prob)	Pooled FT age (Ma)	+ (Ma) 2σ	- (Ma) 2σ	Conc pooled age	+ (Ma) 2σ	- (Ma) 2σ	Lith
											ρ _i (10 ⁶ tracks/cm ²)	ρ _d (10 ⁶ tracks/cm ²)	N _i	ρ _d (10 ⁶ tracks/cm ²)	N _d								
Golden April-Meikle section lamprophyre, rhyodacite																							
GA-34C-1280	550153	4537827	1223	116	14.59	1.29	26	23	2.19	0.21	3.35E-04	6.97E-06	1.65E-07	17.1179	0.3220	0.8226	40.7	10.5	8.4	40.7	10.5	8.4	lamp
GA-35C-1295	550045	4538027	1219	195	13.86	0.9	38	432	1.89	0.14	0.00128	1.05E-04	8.78E-07	15.0486	0.5672	0.0478	30.8	4.0	3.6	30.8	4.0	3.6	lamp
WB-04C-720	550157	4537501	1384	10	14.56	1.24	39	340	2.09	0.32	7.32E-04	7.76E-05	1.16E-07	17.1289	0.3186	1.0000	28.2	14.7	9.7	28.2	14.7	9.7	lamp
GA-52C-1585	550481	4538654	1201	115	14.19	1.12	38	75	2.41	0.16	9.86E-04	1.34E-05	2.83E-07	14.3174	0.2690	0.7831	40.0	10.7	8.5	40.0	10.7	8.5	lamp
EX-24C-1674	552095	4539151	1156	insufficient data			1															rhyod	
EX-29C-1783	552027	4539222	1124	203	14.32	1.33	40	153	2.70	0.21	1.67E-03	5.75E-05	7.63E-07	13.7986	0.2363	0.6703	35.6	6.6	5.6	35.6	6.6	5.6	rhyod
EX-111C-3959	552597	4539358	1628	insufficient data			0															lamp	
Banshee lamprophyre																							
Bell-100-630	551029	4539151	1156	insufficient data			0															lamp	
U16-H07-34-537	551714	4539813	1259	51	14.49	1.43	25	107	2.39	0.54	2.41E-04	1.43E-05	5.92E-07	17.0543	0.3410	0.1609	62.9	14.3	11.7	62.9	14.3	11.7	lamp
U16-H07-63-976	551773	4539737	965	insufficient data			4															lamp	
U16-H07-68-247	551772	4539736	1211	insufficient data			4															rhyod	
Post Fault lamprophyre																							
GBC5-751	552789	4537599	1408	insufficient data																			
GBC5-928-938	552789	4537599	1355	16	13.50	1.48	31	12	1.91	0.41	4.93E-04	3.32E-06	1.00E-07	14.2918	0.2607	0.0066	25.8	20.3	11.4	25.8	20.3	11.4	lamp
GBC5-1444	552788	4537599	1199	insufficient data			5															lamp	
U10-P05-06-319	552601	4537263	1255	73	14.33	1.30	37	42	2.66	0.37	7.37E-04	9.58E-06	1.75E-07	13.5549	0.2505	0.9825	29.6	10.9	8.0	29.6	10.9	8.0	lamp
U10-P05-06-577	552664	4537311	1243	84	13.80	1.58	35	159	2.13	0.15	5.60E-04	3.78E-05	7.38E-07	13.8439	0.2545	0.2156	29.0	5.3	4.5	29.0	5.3	4.5	lamp
U10-P05-06-440	552645	4537294	1249	insufficient data			0															lamp	
U10-P05-06-1055	552784	4537400	1220	insufficient data			7															lamp	
U12-P05-16-271	553047	4537045	1188	insufficient data			13															lamp	
U12-P05-16-814	553402	4537130	1105	insufficient data			1															lamp	
U12-P05-16-1303	553531	4537196	1029	101	13.28	2.14	38	203	2.39	0.20	3.15E-04	6.56E-05	1.38E-06	13.2299	0.2460	0.0033	20.4	3.3	2.9	20.4	3.3	2.9	lamp
Little Boulder Basin Stock granodiorite																							
LBB76-343	555488	4533058	1647	201	13.43	2.37	38	537	2.37	0.13	9.63E-04	4.09E-05	2.12E-07	19.3275	0.5584	0.0002	126.0	13.7	12.3	121.6	14.2	12.8	gdiol
LBB76-576	555514	4533032	1584	203	13.12	2.48	38	624	2.31	0.15	1.11E-03	6.28E-05	6.80E-07	19.2460	0.5423	0.0000	94.9	9.9	9.0	136.2	14.9	13.4	gdiol
LBB76-762	555534	4533012	1533	203	14.12	1.59	35	279	1.85	0.12	6.63E-04	3.27E-05	1.93E-07	19.1645	0.5262	0.0094	81.3	11.4	10.0	81.3	11.4	10.0	gdiol
LBB76-1038	555563	4532983	1457	201	14.21	1.50	39	426	1.89	0.20	8.10E-04	5.85E-05	6.32E-07	18.8384	0.4609	0.0000	68.3	7.9	7.1	74.3	9.5	8.5	gdiol
LBB76-1228	555584	4532962	1405	200	14.10	1.33	40	471	1.94	0.30	9.19E-04	4.97E-05	3.84E-07	18.8251	0.4584	0.0033	88.7	9.8	8.8	88.7	9.8	8.8	gdiol
LBB100-4346	555045	4534988	418	insufficient data			0																
LBB100-4568	555045	4534988	351	insufficient data			0																
LBB100-4679	555045	4534988	311	8	12.42	3.09	15	61	2.40	0.84	1.15E-04	7.28E-06	1.08E-07	18.8152	0.4566	0.5614	78.4	23.3	18.0	78.4	23.3	18.0	dike
LBB100-5400	555045	4534988	97	insufficient data			14																
LBB102-1035	555003	4534762	1422	147	13.40	2.11	37	288	2.01	0.18	3.52E-04	2.83E-05	2.15E-07	18.7983	0.4535	0.0377	94.9	12.9	11.4	94.9	12.9	11.4	gdiol
LBB102-1940	555003	4534762	1146	149	14.06	1.73	32	202	1.97	0.18	3.06E-04	3.03E-05	3.85E-07	18.7850	0.4510	0.1233	62.4	10.1	8.7	62.4	10.1	8.7	gdiol
LBB102-3050	555003	4534762	808	155	13.88	1.93	36	317	2.08	0.19	4.39E-04	3.89E-05	4.77E-07	18.7716	0.4485	0.0000	76.1	10.0	8.9	72.8	10.9	9.5	gdiol
LBB102-3900	555003	4534762	549	200	13.72	1.49	34	454	2.17	0.41	7.88E-04	6.34E-05	7.31E-07	18.7583	0.4461	0.0001	66.8	7.6	6.8	64.9	8.4	7.4	gdiol
LBB102-6090	555003	4534762	-119	insufficient data			6																
LBB102-6148	555003	4534762	-131	insufficient data			0																

Table 5.1 cont. AFT ages obtained using LA-ICP-MS method unless indicated

Sample name	East	North	Elevation (m)	Thickness (mm)	Mean length (μm)	1σ (μm)	Grains (dmm)	N _s	Dpar _A (μm)	1σ (μm)	Area analyzed (cm ²)	Σ (PΩ) (cm ²)	1σ Σ(PΩ) (cm ²)	ξ _{MS}	1σ ξ _{MS}	Q (X ² prob)	Pooled FT age (Ma)	+ (Ma) 2σ	- (Ma) 2σ	Conc pooled age	+ (Ma) 2σ	- (Ma) 2σ	Lith
Goldstrike Stock granodiorite																							
GS-1765C-782	553414	4534581	1572	160	12.57	2.82	38	329	2.23	0.18	6.14E-04	1.55E-02	6.19E-07	17.0915	0.3299	0.0050	37.9	6.0	5.2	36.1	5.9	5.1	gdi
GS-1814C-1595	553170	4534818	1334	183	13.18	2.18	40	192	1.98	0.15	7.81E-04	1.06E-04	7.24E-06	13.7986	0.2363	0.0000	38.8	7.1	6.1	38.8	7.1	6.1	gdi
GS-1818C-1000	553084	4535070	1505	210	13.07	2.57	38	395	2.14	0.12	2.96E-04	5.53E-05	9.66E-07	14.6241	0.2652	0.0088	52.0	6.2	5.5	51.3	6.2	5.5	gdi
RM91-11C-225	553173	4535757	1657	148	13.54	2.54	39	209	1.96	0.16	5.05E-04	4.69E-05	6.65E-07	17.0781	0.3339	0.0000	60.1	9.2	7.9	60.1	9.2	7.9	gdi
RM91-22C-1460	552124	4536211	1300	48	13.19	2.75	15	13	1.96	0.17	1.15E-04	4.61E-06	1.33E-07	14.8372	0.2682	0.9922	20.9	15.6	8.9	20.9	15.6	8.9	gdi
RM94-03C-639	552751	4535590	1535	159	13.98	2.22	32	138	2.24	0.16	4.16E-04	1.68E-05	3.37E-07	15.0503	0.2711	0.0169	61.5	12.0	10.0	61.5	12.0	10.0	gdi
RM98-04C-459	552280	4535823	1534	141	14.29	1.63	35	99	2.17	0.15	4.67E-04	1.78E-05	3.49E-07	14.2083	0.2682	0.7264	39.4	9.1	7.4	39.4	9.1	7.4	gdi
5027**	551377	4537158	1615	163	15.24	1.09	25	261	1.97	0.13	6.52E-04	4.18E-05	4.98E-07	13.8922	0.3067	0.0208	43.2	6.1	5.3	43.2	6.1	5.3	lamp
5029**	552363	4536299	1395	192	15.61	0.99	40	342	2.56	0.14	6.26E-04	5.68E-05	5.85E-07	13.7383	0.3070	0.0001	41.3	5.1	4.6	40.0	7.1	6.1	gdi
GS1845C 1**	552767	4535055	1319	132	14.42	1.40	20	372	1.95	0.12	2.34E-04	2.70E-05	3.27E-07	9.2674	0.2363	0.0798	63.4	7.7	6.9	63.4	7.7	6.9	gdi
GS1845CW1 2**	552789	4535070	1198	135	14.21	1.41	23	359	2.07	0.18	2.68E-04	2.78E-05	3.11E-07	9.2944	0.2358	0.3285	59.8	7.4	6.6	59.8	7.4	6.6	gdi
GS1845CW1 3**	552942	4535192	921	133	14.38	1.47	24	296	2.09	0.19	3.85E-04	2.27E-05	2.88E-07	9.3214	0.2354	0.0300	60.4	8.1	7.2	60.4	8.1	7.2	gdi
GS1845CW1 4**	553042	4535245	803	131	14.10	1.58	25	373	2.15	0.16	4.61E-04	2.87E-05	3.31E-07	9.3485	0.2349	0.0129	60.4	7.3	6.6	60.4	7.3	6.6	gdi
GS1845CW1 5**	553150	4535306	679	135	14.50	1.25	21	165	1.91	0.19	4.19E-04	1.28E-05	1.56E-07	9.3755	0.2345	0.4509	60.2	10.6	9.1	60.2	10.6	9.1	gdi
												EDM: ps (10 ⁶ tracks/cm ²)	EDM: pi (10 ⁶ tracks/cm ²)	EDM: N _i	EDM: pd (10 ⁶ tracks/cm ²)	EDM: N _d							
Goldstrike Stock granodiorite EDM samples																							
S2-111 †	553111	4536180	1404	135	13.27	2.59	40	177	1.92	0.31	0.242	1.023	747	3.41	4062	0.0000	45.8	8.2	8.2	45.8	8.2	8.2	gdi
ST7-980 †	552794	4535585	1468	198	14.28	1.46	26	241	2.13	0.16	0.988	4.921	1200	6.191	4065	0.2140	70.4	10.8	10.8	70.4	10.8	10.8	gdi
ST7-1250 †	552794	4535585	1386	139	14.46	1.45	40	259	1.94	0.16	0.587	1.902	840	3.324	4062	0.6590	58	4.5	4.5	58	4.5	4.5	gdi
ST7-1480 †	552794	4535585	1316	200	14.51	1.44	38	445	1.93	0.12	0.971	3.175	1455	3.353	4062	0.0000	58.1	7.6	7.6	58.1	7.6	7.6	gdi
ST7-2535 †	552794	4535585	994	136	14.45	1.42	33	289	2.17	0.2	0.538	2.352	1263	6.21	4065	0.0000	80.4	11.6	11.6	80.4	11.6	11.6	gdi
ST7-2660 †	552794	4535585	956	196	14.04	1.43	39	432	2.12	0.14	0.899	3.058	1470	3.381	4062	0.1290	56.3	7.0	7.0	56.3	7.0	7.0	gdi

** from Hickey (unpub data)

† from Chakurian et al. (2003), EDM ages

Table 5.2 ZHe ages for samples from the northern Carlin Trend. Bold ages are sample Z He ages

Sample name	East	North	Elevation (m)	F _{He} corrected age (Ma)	1s (Ma)	Zoning adjusted age (Ma)	1s (Ma)	mass (μg)	mwar (μm)	U (ppm)	Th (ppm)	He (ncc/mg)	F _{He}	eU (ppm)
GS-1765C-782_Z1				68.3	1.6	68.3		7.16	48.25	573.38	184.34	29.01	0.79	616.70
GS-1765C-782_Z2				65.4	1.5	65.4		2.48	30.75	551.58	209.24	8.24	0.70	600.75
GS-1765C-782_Z3				114.7	12.1	-		3.74	33.00	358.54	236.51	15.49	0.72	414.12
GS-1765C-782**	553414	4534581	1572	82.8	5.1	66.9	2.1	4.46	37.33	494.50	210.03	17.58	0.74	543.86
GS-1814C-1595_Z1				80.3	1.5	80.3		2.46	31.39	222.90	179.48	4.41	0.69	265.07
GS-1814C-1595_Z2				60.1	1.1	-		1.67	31.01	257.32	147.91	2.40	0.67	292.08
GS-1814C-1595_Z3				86.0	1.5	86.0		3.72	47.63	95.87	90.05	3.44	0.76	117.04
GS-1814C-1595**	553170	4534818	1334	75.5	1.4	83.2	4.1	2.62	36.68	192.03	139.15	3.41	0.71	224.73
GS-1818C-1000_Z1				116.6	2.4	-		1.90	32.50	310.74	344.70	7.27	0.69	391.74
GS-1818C-1000_Z2				67.7	1.5	67.7		2.09	33.50	121.51	92.70	1.71	0.70	143.30
GS-1818C-1000_Z3				71.2	1.6	71.2		2.42	36.00	246.16	108.77	4.07	0.72	271.72
GS-1818C-1000**	553084	4535070	1505	85.2	1.8	69.4	2.5	2.14	34.00	226.14	182.06	4.35	0.70	268.92
RM91-11C-225_Z1				79.1	1.6	79.1		4.42	35.50	151.36	108.11	5.53	0.74	176.76
RM91-11C-225_Z2				82.5	1.7	82.5		1.81	34.00	99.49	88.57	1.51	0.69	120.30
RM91-11C-225_Z3				78.1	1.6	78.1		5.39	47.00	90.63	65.05	4.16	0.77	105.91
RM91-11C-225	553173	4535757	1657	79.9	1.7	79.9	2.3	3.87	38.83	113.82	87.25	3.73	0.73	134.33
RM91-22C-1460_Z1				75.7	1.3	75.7		15.88	60.08	1046.31	1269.58	457.24	0.83	1344.67
RM91-22C-1460_Z2				73.4	1.3	73.4		4.89	35.58	944.94	1120.06	352.27	0.73	1208.15
RM91-22C-1460_Z3				68.5	1.2	79.4		14.71	58.32	1074.20	1068.26	406.67	0.83	1325.24
RM91-22C-1460*	552124	4536211	1300	72.5	1.3	76.2	3.1	11.83	51.33	1021.82	1152.63	405.39	0.80	1292.69
RM94-03C-639_Z1				75.4	1.4	75.4		2.66	32.54	126.61	117.56	44.43	0.70	154.24
RM94-03C-639_Z2				83.9	1.6	83.9		4.32	39.61	119.25	105.28	48.69	0.74	143.99
RM94-03C-639_Z3				79.7	1.5	79.7		1.97	29.16	166.45	113.85	56.18	0.67	193.21
RM94-03C-639_Z4				70.3	1.3	70.3		2.38	29.23	145.50	132.79	45.81	0.68	176.71
RM94-03C-639	552751	4535590	1535	77.3	1.4	77.3	5.8	2.83	32.63	139.45	117.37	48.78	0.70	167.04
RM98-04C-956_Z1				58.4	1.2	67.7		0.89	26.14	161.23	147.25	37.90	0.61	195.83
RM98-04C-956_Z2				68.9	1.3	68.9		1.09	27.14	363.43	258.07	100.29	0.63	424.07
RM98-04C-956_Z3				65.9	1.3	65.9		0.75	23.56	263.59	229.96	66.92	0.59	317.63
RM98-04C-956*	552280	4535823	1385	64.4	1.2	67.5	1.5	0.91	25.61	262.75	211.76	68.37	0.61	312.51
5027_Z1				67.1	5.4	67.1		3.70	na	123.20	122.70	904.00	0.72	152.03
5027_Z2				73.7	5.9	73.7		2.20	na	1194.60	451.50	8184.80	0.70	1300.70
5027	551377	4537158	1615	70.4	5.7	70.4	5.7	2.20		658.90	287.10	4544.40	0.71	726.37
5029_Z1				71.1	5.7	71.1		3.10	na	441.70	184.70	3115.20	0.74	485.10
5029_Z2				73.7	5.9	73.7		2.10	na	965.50	424.80	6853.10	0.71	1065.33
5029	552363	4536299	1395	72.4	5.8	72.4	5.8	2.60		703.60	304.75	4984.15	0.73	775.22
GS-1845C-1_Z1				64.3	0.9	64.3		na	na	773.28	932.25	5.00	0.65	992.36
GS-1845C-1_Z2				46.0	0.8	-		na	na	685.08	342.84	2.49	0.58	765.64
GS-1845C-1_Z3				76.1	1.1	76.1		na	na	673.08	769.04	4.61	0.58	853.80
GS-1845C-1	552767	4535055	1319	62.1	0.9	70.2	8.3			710.48	681.38	4.03	0.60	870.60
GS1845CW1_2_Z1				249.2	19.9	-		3.2	na	318.50	263.20	8537.60	0.73	380.35
GS1845CW1_2_Z2				67.7	5.4	67.7		4.7	na	90.80	41.60	650.80	0.78	100.58
GS-1845CW1-2	553150	4535306	1198	67.7	5.4	67.7	5.4	3.95		204.65	152.40	4594.20	0.76	240.46
GS-1845CW1-5_Z1				64.7	1.0	70.6		na	na	465.54	298.89	3.15	0.75	535.78
GS-1845CW1-5_Z2				71.0	1.1	71.0		na	na	404.72	326.30	3.02	0.73	481.40
GS-1845CW1-5_Z3				69.4	1.1	69.4		na	na	433.41	250.66	3.09	0.75	492.31
GS-1845CW1-5	553150	4535306	679	68.4	1.1	70.3	0.9			434.56	291.95	3.09	0.74	503.16
LBB76-343_Z1				139.4	3.3	-		9.68	54.00	350.15	334.69	57.07	0.81	428.80
LBB76-343_Z2				154.1	3.6	-		2.16	31.50	1347.75	1559.34	48.09	0.69	1714.20
LBB76-343_Z3				168.9	4.0	-		2.83	34.50	1024.72	1020.93	52.72	0.71	1264.64
LBB76-343**	555488	4533058	1647	154.1	3.6	154.1	14.8	4.89	40.00	907.54	971.65	52.63	0.74	1135.88
LBB76-1038_Z1				126.7	2.7	107.7		11.68	56.75	148.96	86.75	25.07	0.82	169.34
LBB76-1038_Z2				104.9	2.9	104.9		4.33	37.50	190.86	136.80	9.14	0.74	223.01
LBB76-1038_Z3				109.4	2.3	109.4		5.54	41.50	271.33	163.25	17.46	0.76	309.70
LBB76-1038*	555563	4532983	1457	113.7	2.6	107.3	2.3	7.19	45.25	203.72	128.93	17.22	0.78	234.02
LBB102-1940_Z1				95.6	2.6	84.1		2.39	31.00	434.69	179.70	9.24	0.70	476.92
LBB102-1940_Z2				86.4	1.9	86.4		1.46	28.75	661.75	282.37	7.39	0.66	728.11
LBB102-1940_Z3				80.8	1.9	80.8		2.87	36.00	323.09	112.53	7.13	0.72	349.54
LBB102-1940*	555003	4534762	1146	87.6	2.1	83.8	2.8	2.24	31.92	473.18	191.53	7.92	0.69	518.19
LBB102-3900_Z1				86.9	1.6	86.9		3.53	31.24	413.49	287.66	12.66	0.71	481.09
LBB102-3900_Z2				79.2	1.5	86.3		2.00	30.51	151.00	108.04	2.32	0.68	176.38
LBB102-3900_Z3				88.5	1.7	88.5		2.74	33.54	469.38	194.61	10.83	0.71	515.11
LBB102-3900*	555003	4534762	549	84.9	1.6	87.2	1.1	2.76	31.76	344.62	196.77	8.60	0.70	390.86
LBB102-6090_Z1				66.7	1.2	66.7		3.04	33.83	135.23	98.27	2.79	0.72	158.32
LBB102-6090	555003	4534762	-119	66.7	1.2	66.7	1.2	3.04	33.83	135.23	98.27	2.79	0.72	158.32

* denotes zoning-corrected ** zoning could not account for variation

Table 5.2 continued ZHe ages for samples from the northern Carlin Trend. Bold ages are sample Z He ages

Sample name	East	North	Elevation (m)	F _{He} corrected age (Ma)	1s (Ma)	Zoning corrected age (Ma)	1s (Ma)	mass (μg)	mwar (μm)	U (ppm)	Th (ppm)	He (ncc/mg)	F _{He}	eU (ppm)
GA-34C-1280_Z1				88.5	1.6	72.6		3.27	29.61	204.58	167.59	80.99	0.69	243.96
GA-34C-1280_Z2				73.0	1.3	73.0		4.80	51.17	208.66	192.00	77.49	0.77	253.78
GA-34C-1280_Z4				73.5	1.4	73.5		1.73	31.49	180.76	111.38	55.82	0.68	206.93
GA-34C-1280*	550153	4537827	1223	78.3	1.4	73.0	0.4	3.27	37.42	198.00	156.99	71.43	0.71	234.89
GA-35C-1294_Z1				96.3	1.9	96.3		4.09	40.87	1167.75	302.10	486.40	0.75	1238.74
GA-35C-1294_Z2				85.4	1.7	99.1		2.86	31.20	1521.64	446.63	530.39	0.70	1626.60
GA-35C-1294_Z3				99.2	1.7	99.2		1.04	22.43	1496.32	1361.20	582.84	0.60	1816.21
GA-35C-1294*	550045	4538027	1219	93.6	1.8	98.2	1.6	2.66	31.50	1395.24	703.31	533.21	0.68	1560.52
WB-04C-720_Z1				68.1	1.4	-		1.25	29.28	131.63	76.89	36.04	0.65	149.70
WB-04C-720_Z2				51.8	1.0	-		1.45	28.97	138.45	111.95	30.29	0.66	164.76
WB-04C-720_Z3				61.8	1.2	-		2.25	29.35	132.68	105.74	35.67	0.68	157.53
WB-04C-720**	550157	4537501	1384	60.6	1.2	60.6	8.2	1.65	29.20	134.25	98.19	34.00	0.66	157.33
EX-29C-1783_Z1				33.8	0.7	33.8		3.91	51.10	130.22	55.72	19.95	0.76	143.32
EX-29C-1783_Z2				36.7	0.7	36.7		2.21	32.32	292.98	121.54	44.42	0.70	321.55
EX-29C-1783_Z3				33.7	0.7	33.7		1.60	29.61	231.10	114.93	31.32	0.67	258.10
EX-29C-1783	552027	4539222	1124	34.7	0.7	34.7	1.7	2.57	37.68	218.10	97.39	31.90	0.71	240.99
U16-H07-34-537_Z1				130.1	2.9	-		5.28	49.00	96.07	37.44	57.76	0.78	104.87
U16-H07-34-537_Z2				250.4	5.2	-		3.24	33.00	45.89	32.79	52.50	0.71	53.59
U16-H07-34-537_Z3				171.1	3.7	-		4.21	40.25	78.25	40.32	61.43	0.75	87.72
U16-H07-34-537**	551714	4539813	1259	183.8	3.9	183.8	61.2	4.24	40.75	73.40	36.85	57.23	0.75	82.06
U16-H07-68-247_Z1				46.2	1.0	46.2		2.53	34.00	125.35	49.84	24.39	0.71	137.06
U16-H07-68-247_Z2				42.9	1.0	42.9		12.87	67.50	106.86	38.69	22.42	0.83	115.95
U16-H07-68-247_Z3				61.2	1.7	46.5		8.19	52.25	194.50	85.11	57.03	0.80	214.50
U16-H07-68-247*	551772	4539736	1211	50.1	1.2	45.2	2.0	7.86	51.25	142.24	57.88	34.62	0.78	155.84
GBC5-751_Z1				72.5	1.5	72.5		0.42	20.91	628.77	209.19	140.85	0.53	677.93
GBC5-751_Z2				63.9	1.3	74.1		1.65	30.02	1015.97	277.73	252.69	0.68	1081.24
GBC5-751_Z3				76.3	1.5	76.3		0.69	25.04	817.66	383.34	221.09	0.59	907.75
GBC5-751*	552789	4537599	1408	70.9	1.5	74.3	1.9	0.92	25.32	820.80	290.09	204.88	0.60	888.97

* denotes zoning-corrected ** zoning could not account for variation

Table 5.3 AHe ages for samples from the northern Carlin Trend. Bold ages are sample A He ages

Sample name	East	North	Elevation (m)	F_{He} corrected age (Ma)	$1s$ (Ma)	mass (μg)	mwar (μm)	U ppm	Th ppm	Sm ppm	% Sm contrib to age	He (ncc/g)	F_{He}	eU (ppm)
Golden April-Meikle lamprophyre and rhyodacite dikes														
GA-34C-1280_A1				9.69	0.74	1.04	33.58	6.92	25.73	243.25	2.21	0.01	0.58	12.97
GA-34C-1280_A2				7.84	0.59	1.37	36.19	6.16	21.28	189.34	2.00	0.01	0.64	11.17
GA-34C-1280	550153	4537827	1223	8.76	0.66	1.21	34.89	6.54	23.51	216.29	2.11	0.01	0.61	12.07
GA-35C-1294_A1				22.42	0.46	0.74	30.66	26.81	49.93	243.80	0.76	0.04	0.55	38.55
GA-35C-1294_A2				23.62	0.48	1.37	36.50	29.10	36.86	214.28	0.68	0.09	0.63	37.76
GA-35C-1294	550045	4538027	1219	23.02	0.47	1.06	33.58	27.96	43.40	229.04	0.72	0.07	0.59	38.15
WB-04C-720_A1				2.35	0.17	1.32	26.55	10.59	38.45	273.61	1.65	0.00	0.56	19.63
WB-04C-720_A2				3.99	0.28	1.35	33.35	6.53	24.42	176.28	1.70	0.01	0.62	12.27
WB-04C-720_A3				4.61	0.23	1.03	29.43	6.84	56.54	179.62	1.06	0.01	0.57	20.12
WB-04C-720	550157	4537501	1384	3.65	0.23	1.23	29.78	7.99	39.80	209.84	1.47	0.01	0.58	17.34
EX-29C-1783_A1				4.54	0.20	2.06	36.12	9.33	29.40	268.14	1.95	0.01	0.64	16.24
EX-29C-1783_A2				3.88	0.14	2.79	41.63	5.09	14.16	149.08	2.09	0.01	0.68	8.42
EX-29C-1783	552027	4539222	1124	4.21	0.17	2.42	38.88	7.21	21.78	208.61	2.02	0.01	0.66	12.33
Post lamprophyre dikes														
U10-P05-06-577_A1				10.97	0.59	1.13	39.79	25.57	32.28	175.20	0.63	0.03	0.65	33.15
U10-P05-06-577_A2				10.35	0.24	1.57	37.35	15.15	38.11	194.10	0.96	0.03	0.65	24.11
U10-P05-06-577_A3				9.71	0.22	2.10	42.08	18.55	26.52	206.95	1.00	0.04	0.70	24.78
U10-P05-06-577	552664	4537311	1243	10.34	0.35	1.60	39.74	19.76	32.30	192.09	0.86	0.04	0.67	27.35
Little Boulder Stock granodiorite														
LBB76-343_A1				68.72	1.51	1.64	37.75	18.03	43.37	332.44	1.40	0.26	0.65	28.22
LBB76-343_A2				70.71	1.63	2.00	41.50	11.59	28.52	271.73	1.76	0.22	0.69	18.29
LBB76-343_A3				55.54	1.26	2.60	41.50	20.94	31.64	227.67	0.96	0.35	0.69	28.38
LBB76-343	555488	4533058	1647	69.72	1.57	1.82	39.625	14.81	35.945	302.085	1.58	0.24	0.67	23.255
LBB76-1038_A1				66.97	1.41	4.97	53.50	15.68	45.81	332.11	1.49	0.81	0.75	26.44
LBB76-1038	555563	4532983	1457	66.97	1.41	4.97	53.50	15.68	45.81	332.11	1.49	1.49	0.75	26.44
Goldstrike Stock granodiorite														
GS-1814C-1595_A1				31.50	0.53	3.41	49.38	30.63	46.56	154.21	0.45	0.40	0.73	41.57
GS-1814C-1595_A2				29.22	0.52	1.80	39.59	29.48	53.11	255.35	0.73	0.18	0.65	41.96
GS-1814C-1595_A3				33.66	0.55	1.46	36.12	41.08	85.53	102.08	0.20	0.23	0.62	61.18
GS-1814C-1595	553170	4534818	1334	31.46	0.54	2.22	41.70	33.73	61.73	170.55	0.46	0.27	0.67	48.23
GS-1818C-1000_A1				27.69	0.66	0.72	32.64	55.43	41.77	304.73	0.56	0.09	0.57	65.25
GS-1818C-1000_A2				36.85	0.74	1.22	32.37	49.13	33.81	347.44	0.73	0.19	0.60	57.07
GS-1818C-1000	553084	4535070	1505	32.27	0.70	0.97	32.51	52.28	37.79	326.08	0.65	0.14	0.58	61.16
RM94-03C-639_A1				20.73	0.50	1.13	34.77	45.76	24.21	118.55	0.28	0.09	0.61	51.45
RM94-03C-639_A2				20.35	1.15	1.76	39.86	8.66	12.67	113.69	1.17	0.03	0.67	11.64
RM94-03C-639_A3				19.70	0.41	1.11	35.15	52.27	9.83	495.89	1.09	0.09	0.61	54.58
RM94-03C-639	552751	4535590	1535	20.26	0.69	1.33	36.59	35.56	15.57	242.71	0.84	0.07	0.63	39.22
RM98-04C-459_A1				25.44	0.41	6.41	72.87	11.23	16.69	182.94	1.44	0.24	0.77	15.15
RM98-04C-459_A2				28.14	0.46	3.57	46.83	22.52	32.46	362.18	1.43	0.27	0.72	30.14
RM98-04C-459_A3				28.45	0.54	0.89	27.71	28.93	33.84	381.52	1.23	0.06	0.55	36.88
RM98-04C-459	552280	4535823	1534	27.34	0.47	3.62	49.14	20.89	27.66	308.88	1.37	0.19	0.68	27.39

Table 5.4 Parameters used to model the duration of heating

<i>Parameter</i>	Definition	Value/units	Comments or reference
C	Stock heat capacity	780 J/kg K	Arndt et al. (1997)
g	Heat flux on Neumann-type boundary condition	0 W/m ²	Time-dependent
h	Coefficient of convection	0 W/m K	No convection within the model stock
k	Thermal conductivity	2.7 W/m K	Arndt et al. (1997)
n	Outward normal unit on Neumann condition	0	Time-dependent
q	Heat flux	W/m ²	
Q	Heat source	0	
r	Radius of stock	800 m	Observed
t	Time	s	
T_{fluid}	Fluid temperature	180-240°C	Cline et al. (2005)
T_{stock}	Stock ambient temperature	20-40°C	Estimated from depth of samples and geothermal gradient of 20-40°C/km
∇T	Thermal gradient between fluid and rock	°C, K	Time-dependent
x	Distance into stock	50-800 m	Observed
κ	Thermal diffusivity	1.28x10 ⁻⁶ m ² /s	Calculated in model by $\kappa = k/\rho C$
ρ	Stock density	2700 kg/m ³	Arndt et al. (1997)

Table 5.5 Fluid flux and total fluid volume of hydrothermal fluids responsible for 40 Moz Au around the Goldstrike Stock

	2.1 kyr duration		3.2 kyr duration		3.5 kyr duration		4.6 kyr duration		10 ky duration	
°C	<u>240</u>				<u>180, 240</u>		<u>180</u>			
Heated	all		1/2		all, 1/4		1/2		1/4	
ppb	flux (kg/s)	volume (km ³)	flux (kg/s)	volume (km ³)	flux (kg/s)	volume (km ³)	flux (kg/s)	volume (km ³)	flux (kg/s)	volume (km ³)
10	1876	124	1233	124	1125	124	856	124	396	124
20	938	62	616	62	562	62	428	62	198	62
100	188	124	123	124	112	124	86	124	40	124
200	94	62	62	62	56	62	43	62	20	62

Chapter 6: Compositional and morphological variation in apatite from the northern Carlin Trend, Nevada: an investigation of the effects of hydrothermal fluid flow on apatite

6.1 Introduction

Chapter 5 investigated the effects of heat transfer during hydrothermal fluid flow. The present chapter assesses the effects of hydrothermal fluids on apatite chemistry and morphology. Apatite, $\text{Ca}_5(\text{PO}_4)_3(\text{OH}, \text{F}, \text{Cl})$, is the most abundant phosphate mineral in the Earth's crust and is a common accessory mineral in igneous, metamorphic and sedimentary rocks (Hughes and Rakovan, 2002). Apatite chemistry, in particular halogen, trace element and REE content, varies depending on petrology and conditions of the host rock and melt that it crystallized from (Fleischer and Altschuler, 1986; Sha and Chappell, 1999; Piccoli and Candela, 2002).

Apatite chemistry reflects the composition, temperature and $f\text{O}_2$ of the host melt, and of hydrothermal fluids that have interacted with the apatite post-crystallization (Piccoli and Candela, 2002). The chemistry can also reveal the existence of multiple populations of apatite, for example a primary, igneous phase and a secondary, hydrothermal phase, which can be further compared by morphological studies of apatite present in the samples.

In this chapter, backscattered electron (BSE), electron microprobe analysis (EMPA), laser ablation inductively-coupled plasma mass spectrometry (LA-ICP-MS) and cathodoluminescence (CL) are used to characterise the apatite in granodiorite and lamprophyre samples from the northern Carlin Trend. The area has undergone several phases of hydrothermal activity, at least one involving Au mineralization, so one objective is to identify any chemical and textural evidence of hydrothermal fluid flow in apatite. Examples of this include precipitation of overgrowths or growth of new, hydrothermal, apatite. This study builds

on the apatite fission track (AFT) investigation of the area discussed in Chapters 4 and 5. Apatite composition affects the susceptibility of apatite to thermal annealing, the removal of fission tracks that are fundamental to AFT dating. A second objective is therefore to observe how apatite compositional variation influences parameter D_{par} , an etch pit length measured in AFT dating that is an indicator of resistance to annealing.

6.2 Sample descriptions

Granodiorite samples GS-1765C-782, GS-1818C-1000 and LBB76-343 are from the Goldstrike (GS) and Little Boulder Basin (LBB) stocks. These are believed to be part of the same intrusion but are now separated by the Post Fault system (Figure 4.1). Granodiorite samples are fine-medium grained, hypidiomorphic, consisting predominantly of euhedral polysynthetically twinned plagioclase with euhedral-subhedral K-feldspar, quartz, biotite and hornblende. Samples are minimally altered, with mild sericitisation of feldspar cores and chloritisation of mafic phases. Apatite occurs as acicular and stubby crystals up to but typically less than 100 μm in length, mostly as single grains or as clusters within quartz (Figure 6.1a-c), but are sometimes included within biotite and hornblende. Zircon is also present as an accessory phase.

Lamprophyre samples are more variable. GA-34C-1280 and GA-52C-1585 from the Golden April deposit, and U16-H07-34-537 from Banshee are highly porphyritic, with 2-5% euhedral hornblende phenocrysts in a fine plagioclase-dominated groundmass. Alteration of Golden April samples includes sericitisation of feldspars and chloritisation of hornblende and affects ~80% GA-34C-1280 and ~50% GA-52C-1585. Alteration of Banshee sample U16-H07-34-537 is minimal. Apatite crystals are small (<100 μm long) and occur mostly as isolated crystals in quartz or rarely in hornblende (Figure 6.1d, e, g). Lamprophyre GBC-5-928 from

the Post Fault system is very fine and almost totally argillised. Apatite may be present in the wall rock but was only observed as very small ($<20\ \mu\text{m}$) stubby crystals in quartz veinlets that cross cut the sample (Figure 6.1f).

6.3 Analytical methods

Mineral separation was carried out following standard mechanical, density and magnetic separation procedures described in Appendix A. Apatite crystals were mounted in epoxy using techniques described in Donelick et al. (2005) for AFT dating. Mounts were then polished and etched for 20 s in 5.5 M HNO_3 at 21°C to reveal fission tracks for AFT dating. Fission tracks were counted and U and Th concentrations were measured using LA-ICP-MS after Donelick et al. (2005) and Hasebe et al. (2004) described in Chapter 3. Compositional analysis of apatite in this study was subsequently carried out on these AFT mounts.

EMPA was used to measure F, Cl, Ca, P, Si, S, Mn and Fe. EMPA was carried out using a fully automated wavelength-dispersive Cameca SX-50 at the University of British Columbia. Operating conditions were 15 kV, with a beam current of 10 nA and a spot diameter of $10\ \mu\text{m}$. For Ca, P, Si, Fe and Mn, peak count time was 20 s and background count was 10s. For F, Cl and S, peak count time was 40 s and background count time was 20 s. Typical detection limits were 0.02 - 0.05 wt%. Precision, based on the standard deviation of an in-house standard, s421, run twice at the start and once at the end of each session, ranges 0.02-0.63 wt%. Only apatite crystals aligned with their crystallographic c-axis perpendicular to the beam were analysed. This was done to reduce the effects anisotropic diffusion of F ions attracted to the electron beam that result in overestimation of F content; diffusion is greatest parallel to the c-axis (Stormer et al., 1993). The low beam current also minimised elevated F diffusion. Average values were calculated from 2-4 spot analyses on each of 8-14 apatite crystals per sample.

Trace elements were measured using LA-ICP-MS with a 23 μm spot at 5 Hz for 20-45 s per spot. Typical detection limits were <1 ppm and precision, calculated from the standard deviation of a standard run every 4 samples, was typically <0.1%. The 30-40 AFT-dated apatite crystals were the ones analysed for trace element content using LA-ICP-MS. EMPA were carried out on different apatite crystals because of potential damage and F loss caused by earlier LA-ICP-MS analysis of U and Th for AFT dating that was carried out prior to this apatite study. Average compositions for each sample were by calculated combining EMPA and LA-ICP-MS data. Some elements (Si, Mn and Fe) were measured using both methods, which allowed comparison of data from the different methods and allowed further investigation of correlations of F, Cl, S, Ca, P with trace element and rare earth element (REE) data.

Thin sections from each sample were examined to determine apatite texture and morphology as well as mineral associations, which are known to affect apatite chemistry (e.g., the association with biotite or hornblende, both hydrous phases, affect OH content of apatite (Stormer and Carmichael, 1971). Apatite morphology and texture were further observed using scanning electron microscopy (SEM) on both grain mounts and thin sections.

Optical CL was employed to observe any internal textures such as overgrowths or compositional zoning. The colour of minerals in CL results from their composition. Luminescence results from activator elements in the apatite crystal, predominantly Mn^{2+} , Sm^{3+} , Dy^{3+} , Eu^{2+} and Eu^{3+} . Inhibitors include Fe^{2+} and Fe^{3+} , which reduce luminescence. A pure end-member apatite crystal without activator substitutes or vacancies does not display luminescence (Roeder et al., 1987; Mitchell et al., 1997). CL has been used as a quantitative tool in apatite analysis (e.g. Roeder et al., 1987; Barbarand and Pagel, 2001; Kempe and Götze, 2002), however here it was used primarily as a qualitative tool to observe compositional zoning, overgrowths and general apatite chemistry, which are identifiable from variations in

colour. Optical CL was completed after EMPA as the method is destructive and would potentially have affected measurement of F and Cl. Beam conditions were 17-19kV at 300-350 μm using a Citl CLmk4. Images were captured using a Canon 20C camera at 25 s exposure and 1600 ISO.

6.4 Apatite fission track (AFT) data

AFT dating was carried out prior to this chemical investigation. Results can be found in Table 5.1. Dpar, the mean fission-track etch pit diameter parallel to the crystallographic *c*-axis, is considered a kinetic parameter that correlates with fission track annealing kinetics in apatite (see Chapter 3). Greater Dpar values indicate greater resistance to annealing (fission track removal). AFT ages of 36.1 ± 5.9 -5.1, 51.3 ± 6.2 -5.5 and 121.6 ± 13.7 -12.3 Ma (2σ) were obtained for granodiorite samples GS-1765C-782, GS-1818C-1000 and LBB76-343. Dpar values are 1.96 ± 0.17 , 2.14 ± 0.12 and 2.37 ± 0.13 μm respectively. AFT ages in lamprophyre samples are 25.8 ± 20.3 -11.4, 40.0 ± 10.7 -8.5, 40.7 ± 10.5 -8.4 and 62.9 ± 14.2 -12.8 Ma for GBC-5-928, GA-52C-1585, GA-34C-1280 and U16-H07-34-537. Dpar values are 1.91 ± 0.41 , 2.41 ± 0.15 , $2.19 \pm$ and 2.37 ± 0.54 μm respectively.

6.5 Results

Apatite compositions determined by EMPA and LA-ICP-MS are shown in Tables 6.1 and 6.2.

6.5.1 Major elements

Calcium and P are consistently 51-53 wt% CaO and 38-40 wt% P₂O₅ in all samples. Halogen (F, Cl, OH) contents are presented in terms of relative mole fraction of F (XFAp), Cl

(XClAp) and OH (XOHAp). Estimates of F are high, and probably overestimated due to attraction of F to the electron beam during EMPA. High Fe concentrations can also lead to overestimation of F because Fe and F share an identifying k peak in EMPA spectral data. Analyses with F content >3.75 wt% were discounted as anomalously high and attributed to attraction of F to the electron beam. Relative F-Cl-OH contents are shown in the ternary diagram in Figure 6.2. OH content was calculated based on assumption of 2 ions on the halogen site occupied by F, Cl or OH only ($2-F-Cl = OH$). Based on F, Cl, OH content, GS-apatites are near end-member fluorapatites (0.93-0.94 XFAP), with the exception of LBB76-343, which has a significant Cl content (0.14 XClAp). Goldstrike Cl content is 0.06-0.07 XClAp. OH content of granodiorite apatite is negligible.

Lamprophyre XFAP is similar to the Goldstrike samples but XOHAp is greater at 0.02-0.06. XClAp varies 0.01 (GBC5-928) to 0.08 (GA34C-1280), and is typically less than granodiorite apatite. Overall lamprophyre apatites can be considered fluorapatites, with XFAP ranging 0.85-0.99 XFAP. The exception is U16-H07-34-537, which has a significantly lower F content, at 0.61 XFAP and a variable but significant OH content up to 0.57 XOHAp.

6.5.2 Trace elements

Granodiorite apatites have the highest proportion of Σ REE in trace element content. Based on REE patterns, all three granodiorite samples have single populations of apatite, where the chondrite-normalised La-Gd ratio, $(La/Gd)_{cn}$, is >1 (5-6) (Figure 6.3a). Si is also a significant trace element, especially in the GS- samples (0.42, 0.46 wt% SiO₂) and in the LBB sample (0.29 wt%). Na is similar in the GS- samples (0.38, 0.46 wt% Na) and lower in LBB76-343 at 0.11 wt% Na. Mn, Sr and Fe are low in all granodiorite samples, at <0.1 wt%. S is more variable, low in LBB76-343 and GS-1765C-782 (0.02, 0.07 wt% SO₃ respectively) and higher

in GS-1818C-1000 at 0.19 wt%. Concentrations of U and Th, important for AFT dating, are 42-220 ppm in Goldstrike apatite and 36-42 ppm in Little Boulder Basin Stock apatite.

Lamprophyre apatite composition is more variable. Samples GA-34C-1280 and GA-52C-1585 have very similar single REE patterns but different trace element chemistry overall. GA-34C-1280 has a Σ REE of 0.61 wt%, higher than that of GA-52C-1585 at 0.37 wt%. GA-34C-1280 has 0.2 wt% MnO, 0.13 wt% Sr and 0.05 wt% Na. GA-52C-1585 has higher Sr and Na, 0.24 wt% and 0.41 wt%, and lower Mn, 0.06 wt% MnO. SiO₂ is 0.24 wt% in both samples. S and Fe content are almost 1:1 ratios in both samples, around 0.3 wt% each in both samples. U is 21 ppm in GA-34C-1280 and 8 ppm in GA-52C-1585. Th is 31 ppm in GA-34C-1280 and 14 ppm in GA-52C-1585.

Samples GBC-5-928 and U16-H07-34-537 have at least two populations of apatite based on REE pattern (Figure 6.3). In both cases the populations can be distinguished by their (La/Gd_{cn}) ratio, with population 1 (La/Gd_{cn}) >1 (LREE>HREE) and population 2 (La/Gd_{cn}) <1 (concave-down). Overall population 1 has a higher trace element content, although both populations of apatites have very low total trace element contents (1.44 wt% average total). GBC-5-928 Σ REE is 0.35 wt% in population 1 and 0.17 wt% in population 2, and Na concentration is 0.29 wt% and 0.13 wt% respectively. Both GBC-5-928 populations of apatite have low Si, Mn, Fe and S (<~0.1 wt%) but are characterised by high Sr, at 0.42 and 0.49 wt% Sr, higher than any other sample. U is 8 ppm in population 1 and 22 ppm in population 2. Th is 12 ppm in population 1 and 15 ppm in population 2. U16-H07-34-537 trace element content is higher in population 1 apatites ((La/Gd)_{cn} >1) than in population 2 ((La/Gd)_{cn} <1). Na and Σ REE are both high at ~0.6 wt% in population 1 compared to 0.23 and 0.15 wt% in population 2. Fe, S and Sr are also higher in population 1 (0.31 vs 0.05 wt% FeO, 0.7 vs 0.1 wt% SO₃ and 0.25 vs 0.12 wt% Sr). SiO₂ is 0.1 wt% in population 1 and 0.15 wt% in population 2. Mn is

similar in both populations of apatite, ~0.15 wt% MnO. S is 0.7 wt% SO₃ in population 1 and 0.1 wt% in population 2. U is 36 ppm in population 1 and 134 ppm in population 2. Th is 52 ppm in population 1 and 42 ppm in population 2.

6.5.3 Morphology and texture

In granodiorite sample GS-1765C-782, apatite morphology is generally acicular but with varying length-width ratios (Figure 6.1a). Apatite crystals associated with biotite are generally shorter than those associated with quartz or feldspar. In the other granodiorite samples, LBB76-343 and GS-1818C-1000, apatite is stubbier with hexagonal prism morphology (Figure 6.1b and 6.1c). Separated apatites are generally clear, prismatic inclusion-free apatites, with no evidence of zoning or overgrowths in thin section.

Lamprophyre GA-52C-1585 apatites observed in thin section are acicular, whereas GA-34C-1280 apatite is stubby. Again, there was no visual indication of secondary growth or alteration of apatite in thin section. Apatite in GBC-5-928 was only identified in quartz veinlets, where it occurs as small, stubby crystals (Figure 6.1f). Apatite in U16-H07-34-537 is acicular in quartz, extremely elongate in some cases, but shorter when associated with hornblende.

BSE imaging did not show compositional zoning in the samples as would be expected if the distribution of high atomic number elements REE or U and Th were heterogeneous (Tepper and Kuehner, 1999). However, most studies of apatite zoning have examined apatite crystals >200 µm on their shortest axis (Jolliff et al., 1989; Rakovan and Reeder, 1994; Tepper and Kuehner, 1999), compared to <50 µm typically observed in this study. The small crystal size and limited resolution of the optical CL hindered observation of zoning. However, under CL compositional variation was seen in a small number of crystals in GS-1765C-782, GS-1818C-

1000, GA-34C-1280 and GBC-5-928. GS- apatites display igneous growth zoning (Figure 6.4a, b) whereas several apatites from GA-34C-1280 and GBC-5-928 have embayed cores (Figure 6.4d, f). The infrequency of occurrence of zoned crystals among hundreds of grains suggests compositional zoning is not a distinguishing feature among the apatites from this area. Further work on a cold SEM-based CL would allow unequivocal assessment of zoning. Zoning was not identified in any of the apatites analysed using EMPA or LA-ICP-MS, so the variation seen in composition and REE patterns is not a function of zoning (as far as identified here).

In apatite, CL activators include Mn, which produces bright yellow-green CL colours, and REEs, which typically have violet or dark green CL colours. Fe acts as an inhibitor, reducing luminescence. Granodiorite apatites are predominantly pale violet in CL or, less commonly, yellow-green (GS- samples only), indicating high REE/Fe and high Mn/Fe ratios. Apatite from lamprophyre samples is most commonly pale yellow, with a small proportion of bright yellow-green apatites, again suggesting high Mn/Fe ratios. GBC-5-928 contains near equal abundances of yellow-green and violet crystals, as well as a small number of dark green crystals, which can indicate a high MREE/Fe ratio. Concentric zoning was observed in several violet apatites in GBC-5-928 (Figure 6.4g).

Zoning of U and Th was not observed in BSE or CL. The distribution of fission tracks, which form when a U or Th atoms undergoes spontaneous fission, is directly linked to the distribution of U and Th in a crystal (Knutson et al., 1985). Fission track distribution was homogenous in apatite crystals in this study, further evidence that U and Th is not zoned.

6.6 Interpretation and discussion

6.6.1 Compositional variation, substitutions

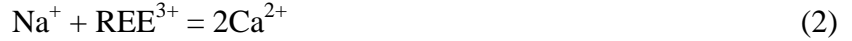
A number of substitutions are observed in apatites in this study, all common in naturally-occurring apatites (Watson and Capobianco, 1981; Watson and Green, 1981; Ronsbo, 1989; Hughes et al., 1991a; Hughes et al., 1991b; Sha and Chappell, 1999; Pan and Fleet, 2002). Substitutions are generally determined by melt composition.

Substitution of F by Cl and OH is observed in this study. OH is essentially absent from granodiorite apatites but is highly variable in lamprophyres, which are characteristically hydrous melts (Rock, 1987). Variation in X_F and X_{Cl} arises from variation in volatile content in different parts of the crystallizing melt. The granodiorite melt had a higher Cl content, reflected in the greater Cl content in apatite in those samples, especially LBB76-343. In Chapter 4 it was shown that LBB76-343 crystallized at a shallower depth than the Goldstrike samples (now at approximately the same elevation due to motion on the Post Fault). Elevated Cl content in apatite is commonly seen in intrusions due to the greater volatility of Cl than F in melts, so Cl tends to rise and become concentrated in phases shallower in the magma body (Boudreau and Kruger, 1990), as observed in the GS-LBB Stock.

Ca^{2+} in apatite has two sites, a nine-coordinated Ca(1) site and a seven-coordinated Ca(2) site. Common substitutions are Na^+ and Mn^{2+} , which prefer the larger Ca(1) site, and Sr^{2+} and REE^{3+} , preferring the smaller Ca(2) site (Hughes et al., 1991a; Hughes et al., 1991b). Fe substitutes into both sites, although there is evidence that in high concentrations, Fe preferentially substitutes into the Ca(1) site (Pan and Fleet, 2002). Substitutions for Ca^{2+} by cations are commonly by:



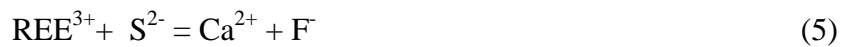
where M^{2+} is Mn^{2+} , Sr^{2+} or Fe^{2+} (or other divalent metal cations). In this study, high Na and REE contents are seen in the granodiorite apatites, suggesting the following substitution is important:



In lamprophyre samples GA-52C-1585, GBC-5-928 and U16-H07-34-537, the REE/Na ratio is ~ 1 (Figure 6.5). However, granodiorite and lamprophyre GA-34C-1280 apatites have ratios $\gg 1$, suggesting the substitution of Ca by trivalent REE^{3+} s is not always coupled with monovalent Na^{+} as in substitution (2). In this study, REE substitution is therefore also inferred to occur in apatites by:



Substitution may also be coupled with Si or S in these samples, which would account for slight variation in P contents observed. Substitution of P^{5+} is also common, typically by Si^{4+} or S^{6+} (Pan and Fleet, 2002). Here a negative correlation is seen between SiO_2 and P_2O_5 (Figure 6.6), so it is assumed that P is in fact being substituted by Si^{4+} (Equation 4). S shows a negative correlation with F content, evidence that (5) is a substitution mechanism in these apatites, most notably in the lamprophyre samples, which have higher S content than granodiorite samples (Figure 6.7).



Fe and Mn are relatively low in granodiorites, reflecting the lower concentration of these elements in the host melt. The low Sr values are characteristic of more fractionated melts such as granodiorites (Belousova et al., 2002). Sr may also be outcompeted by REEs that substitute for the same Ca(2) site (Watson and Green, 1981).

Sr in lamprophyre apatites is highly variable but relatively high in GBC-5-928. GBC-5-928 has low trace element content overall, so substitution in this sample is dominated by Sr substitution onto the Ca(2) site. Apatite Sr concentration should approximately equal the concentration of Sr in the melt (approximated by whole rock Sr content)(Sha and Chappell, 1999). Figure 6.8 shows that while apatite Sr does equal melt Sr in most samples, in GBC-5-928, a highly altered sample, apatite Sr is ~10 times greater than melt Sr. Similarly, apatite Sr in GA-34C-1280, also strongly altered, apatite Sr is ~30 times that of the melt. Vaughan et al. (in prep) describe loss of Sr from altered lamprophyre samples in the northern Carlin Trend, and conclude that alteration by hydrothermal fluids removes Sr from host rocks. The apparently elevated apatite Sr content in altered samples of this study is therefore inferred to represent original Sr content of the melt, and evidence that Sr is not removed from apatite by hydrothermal fluids.

Belousova et al. (2002) proposed a discrimination diagram for apatite source rock based on Sr and Y content (Figure 6.9). The granodiorites from this study fall into the granitoid field. A lamprophyre field, not previously included on the diagram, has been added here. Lamprophyres fall between granitoids and carbonatites on the diagram, not surprising since they are more mafic than granitoids and have some affinity with carbonatites (Rock, 1987).

REE values are lower in lamprophyre apatite and Mn, Fe and Sr are higher, again as expected from more mafic, less fractionated melts. Na in lamprophyres is similar to granodiorite samples. REE patterns for natural apatites are determined by the partition coefficient (D_{REE}), as well as melt REE content and other REE-bearing mineral phases present. The highest D is for Nd (Hughes et al., 1991b), so the most common REE pattern for apatite is concave down, with greatest MREE and lower LREE and HREE contents. In this study the

concave-down pattern was observed (in lamprophyres GBC-5-928, U16-H07-34-537), but a pattern LREE>>HREE was also present (all samples).

Granodiorite samples display consistent Σ REE, typical of an intermediate-felsic melt (Belousova et al., 2002; Piccoli and Candela, 2002). The REE pattern is also very consistent, with high relative enrichment of LREE compared to HREE and a pronounced negative Eu anomaly. The LREE/HREE ratio is strongly affected by the presence of other REE-bearing minerals such as monazite, xenotime and allanite (Sha and Chappell, 1999). Zircon, a common REE-bearing phase, was observed in thin section in the GS- and LB samples. Zircon has a lower D_{LREE} and higher D_{HREE} than apatite, so preferentially incorporates HREE as it crystallises (Sha and Chappell, 1999). In the presence of abundant zircon, the melt is depleted in HREE that would otherwise partition into apatite. Apatite that crystallises after zircon therefore crystallised from a melt relatively rich in LREE but poor in HREE, imparting a LREE>>HREE pattern to those apatites. The presence of zircon most likely resulted in the apatite REE pattern observed in granodiorite apatites, which also indicates that apatite crystallised after zircon, and relatively late.

Lamprophyre Σ REE are lower due to a lower concentration of REE in more mafic melts (Belousova et al., 2002; Piccoli and Candela, 2002). Apatites from samples GA-34C-1280 and GA-52C-1585, both altered samples, display consistent single REE patterns with LREE>HREE and a negative Eu anomaly. Again, the presence of zircon (or other REE-bearing phases) may explain the pattern. Other lamprophyre apatites have a LREE>HREE pattern (where $(\text{La}/\text{Gd})_{\text{cn}} > 1$) as well as a concave-down pattern (where $(\text{La}/\text{Gd})_{\text{cn}} < 1$).

There are several possible reasons that explain the existence of multiple populations of apatites in highly altered sample GBC-5-928 and minimally altered sample U16-H07-34-537. These include different association with REE-bearing minerals or multiple stages of apatite

crystallization, or different sources of apatite. Zircon preferentially takes up HREE, leading to a relative LREE enrichment in later stage apatites. Conversely, monazite partitions LREE as it crystallizes, leading to relative enrichment of HREEs (Sha and Chappell, 1999). Although this could explain the concave down patterns, no monazite was observed in these samples, and there are other potential explanations for variation in REE pattern. U16-H07-34-537 REE populations are influenced by the crystallization history of the lamprophyre dike as well as mineral associations, as apatite was observed within mafic phases and within later stage interstitial quartz. A large range of halogen contents was also observed in this sample, so the effect of mineral association is also likely, since biotite preferentially incorporates F, resulting in a higher Cl or OH content in apatite associated with biotite. GBC-5-928 is the only sample with apatite observed in quartz veinlets. This suggests one of the observed populations is either hydrothermal, precipitated from the same hydrothermal fluids that formed the quartz veinlet, or it is entrained from another igneous source. Although the sample is too fine grained to see apatite in the wall rock, the variation seen in REE patterns suggests there is at least one wall rock population. The large range in trace element compositions but similar Σ REE makes distinction difficult.

U and Th also vary with melt composition. U and Th are both incompatible elements, becoming increasingly concentrated as a melt is fractionated, so felsic melts (e.g., granodiorites) have higher U and Th contents than more mafic melts (lamprophyres).

6.6.2 Eu anomalies

A negative Eu anomaly is observed in all granodiorite apatites and in lamprophyre apatites from GA-34C-1280, GA-52C-1585 and U16-H07-34-537. Eu exists as Eu^{2+} and Eu^{3+} depending on the oxidation state of the host melt. Eu^{3+} is more compatible in apatite than Eu^{2+} ,

substituting for the smaller Ca(2) site (Hughes et al., 1991b). Eu^{2+} is also preferentially partitioned into plagioclase due to the similar ionic radius of Eu^{2+} and Ca^{2+} , a major constituent in plagioclase (Watson and Green, 1981; Fleischer and Altschuler, 1986; Bau, 1991). The presence of plagioclase in a reduced melt results in development of a negative Eu anomaly in the REE pattern, as seen in the granodiorite apatites of this study. Apatite that crystallises early, before plagioclase, tends not to have a negative Eu anomaly, whereas apatite that crystallises later is affected by partitioning of Eu^{2+} . Comparison of apatite REE with whole rock REE (Figure 6.3) shows that the apatite in this study is affected by Eu partitioning, since Eu anomalies are not strongly developed in whole rock REE. The GA- apatites have a negative Eu anomaly that is less pronounced than in granodiorite apatites, as would be expected in lamprophyres that characteristically contain less plagioclase than granodiorites, as is consistent with petrographic observations. In the lamprophyre samples with two populations, one population has an Eu anomaly and the other does not, an indication that population 1 either crystallised before the onset of plagioclase crystallisation, or that population 1 was isolated from the increasingly partitioned melt, e.g., by biotite or hornblende.

6.6.3 Textures

Concentric zoning was consistently observed in zircons (Figure 5.5) but not in other commonly zoned minerals, e.g., plagioclase. Some variation in trace element composition is therefore possible, so zoning in apatites could be the result of fluctuations in melt trace element chemistry, although why it is not seen in the majority of crystals is uncertain. It also remains a possibility that higher resolution CL work would reveal more subtle zoning or overgrowths.

Simple igneous growth zoning was observed in some apatites from GS-1765C-782 and GS-1818C-1000, recording at least three stages of igneous growth (Figure 6.4). These zones

were not analysed, as they were not identified prior to chemical analysis, and so cannot explain the chemical variation seen, especially in REE pattern. Relative abundances can be observed, however. The cores and outer rim have a higher Mn/Fe, REE/Fe ratio than the intervening zone, which has a greater relative Fe content that suppresses luminosity in that zone.

Unaltered samples LBB76-343 and U16-H07-34-537 did not display any compositional zoning or contain any evidence of overgrowths. GA-52C-1585 is altered but did not show zoning. GA-34C-1280 is highly altered, and does contain a small number of crystals that to have embayed cores with a high Mn/Fe ratio, and darker, lower Mn/Fe ratios in the rim. The overall morphology of these apatites remains prismatic and stubby. If this is the result of hydrothermal activity, the morphology suggests the apatite has not been dissolved or precipitated, but that fluids have either added Fe or removed Mn from the core. Embayment likely reflects uneven penetration of the crystals by the fluids.

Barker et al. (2009) identified at least one hydrothermal zone in altered apatites from the Carlin Trend, and up to four in Au-bearing apatites. Most apatites in this study do not show zoning, igneous or hydrothermal. Only the most altered samples, GA-34C-1280 and GBC-5-928, displayed irregular zoning that may record hydrothermal alteration of apatite. In GA-34C-1280, a small number of apatites have bright yellow-green high Mn/Fe embayed cores and darker lower Mn/Fe rims. In GBC-5-928, cores have high REE/Fe and rims have high Mn/Fe. The altered apatites retain their primary prismatic shape, suggesting precipitation of new apatite is not occurring. Instead, the chemistry of these apatites is being subtly modified by hydrothermal fluids that either removed Mn or added Fe (or other suppressors). Other workers have reported chemical alteration of apatites in porphyry systems, involving addition or loss of Na, S, Mn, Fe, REEs (Bouzari, 2011). However, this may not be a dominant feature in the samples in this study since the hydrothermal fluids involved in Carlin-type Au mineralization

were much lower temperature and less acidic at 180-240°C and pH 4-6 (Cline et al., 2005) than fluids typical of porphyry systems (Tosdal et al., 2009).

The different chemical character of the rims in GA-34C-1280 and GBC-5-928 indicate the hydrothermal fluids affecting these samples were different. This may arise from different fluid sources simultaneously involved in Eocene hydrothermal event (related to mineralization) or to different hydrothermal events. The AFT age of GA-34C-1280 records a hydrothermal event at 40.7 ± 10.5 -8.4 Ma, so the alteration observed in the small number of apatites may record that event, which is coincident with the age of Au mineralization in the area. Eocene fluids may have removed Mn or added Fe to apatite. GBC-5-928 has an AFT age 25.8 ± 20.3 -11.4 Ma, recording a younger heating event. The chemical alteration of apatite from that sample, which lies proximal to the Post Fault, a major fluid conduit, may result from a different hydrothermal fluid flow event, or a different fluid composition during the same Eocene event. This cannot be determined by data collected in this study. Neither sample is mineralized (<0.001 ppm and 0.009 ppm Au in GA-34C-1280 and GBC-5-928 respectively), so compositional differences do not relate to differences in Au-bearing vs barren hydrothermal fluids.

6.6.4 Dpar and composition

Dpar values are more variable in the lamprophyre samples than in granodiorite samples. Lamprophyre samples also display more chemical variation, in XOHAp in particular. The positive correlation in XOHAp and Dpar suggests OH increases resistance to annealing (Figure 6.10). Similarly, within the granodiorite samples XClAp is greatest in the highest Dpar sample, LBB76-343, so higher Cl content makes a crystal more resistant. This agrees with published findings that pure end-member FAp anneals the fastest, and that high F content relative to other

halogens, Cl and OH, lowers resistance to thermal annealing. Sample GBC-5-928 has the highest XFAP at 0.99 and has the lowest Dpar value 1.41 μm .

A more subtle correlation between ΣREE and Dpar and Mn and Dpar can also be seen (Figure 6.11), which has also been described by other workers (Carlson et al., 1999; Barbarand et al., 2003; Donelick et al., 2005). The possible effects of REE and Mn zoning on Dpar were not investigated, as no zoned apatites were analysed. The granodiorite samples are minimally altered, displaying only mild H^+ metasomatism. The composition of apatite in these samples displays little variation and they share a common REE pattern. Apatite from these samples is therefore considered primary igneous apatite. The REE pattern of GA-34C-1280 and GA-52C-1585 is similar to that of the granodiorites, despite both samples being strongly argillised. The absence of overgrowths and zoning suggest these lamprophyre apatites are also primary, and that fluids responsible for alteration were not chemically different enough, or hot enough or acidic enough to affect the REE in those apatites. However, hydrothermal fluids may have affected the Mn/Fe ratio of apatites that do show non-igneous zoning. Lamprophyre apatite major element and other trace element chemistry is within the normal range of compositions observed in this study.

6.7 Conclusions

Intergrain variation in trace element content in apatite is common, and results from very localised changes in melt composition as apatite crystallises (Jolliff et al., 1989). This variation is especially evident if there is an early and a late stage of apatite crystallisation (Sha and Chappell, 1999). Although there are multiple populations of apatites in some of the lamprophyre samples, there is no consistent distinction in their chemistry other than REE patterns, which can be explained by mineral associations and crystallization history. The single

REE patterns in two strongly altered samples GA-34C-1280 and GBC-5-928 and similarity of their chemistry to apatite from other lamprophyres suggests they also contain primary apatite that overall is not strongly affected by the hydrothermal fluids that altered the host rock. It is possible that the different patterns reflect a later magmatic, or a hydrothermal event, but the prismatic morphology and size of apatites in the samples suggest all apatite observed is igneous, or that hydrothermal fluids induced chemical change only, without dissolution and reprecipitation or formation of overgrowths. Textural evidence from CL supports this.

Dpar does correlate positively with Cl and OH and negatively with F, in agreement with other published studies (e.g. Carlson et al., 1999; Barbarand et al., 2003). A positive correlation was also observed between Dpar and REE and possibly Mn, although these relationships are more subtle than with the halogens. There is no evidence that Dpar has been strongly affected by hydrothermal fluid flow.

6.8 Further work

In situ analysis of apatite would elucidate the relationship between mineral association and apatite composition. This was not carried out in this study due to the lack of suitably oriented apatite crystals that are necessary for accurate determination of F content, which requires analysis of apatites oriented c-axis perpendicular to the electron beam. Although halogen zoning is uncommon, measurement of F, Cl, and OH contents of zones could also improve interpretation of AFT data.

EMPA and LA-ICP-MS analysis of zones and higher resolution CL imaging would also provide a better understanding of the crystallization history of igneous apatite in the granodiorite samples and unaltered lamprophyre samples, and of the chemistry of hydrothermal fluids in the altered apatites from highly altered samples GA-34C-1280 and

GBC-5-928. Analysis of a larger sample set of fresh to altered samples of the same rock type, e.g., granodiorite, would also improve interpretation of hydrothermal processes affecting apatites in the northern Carlin Trend.

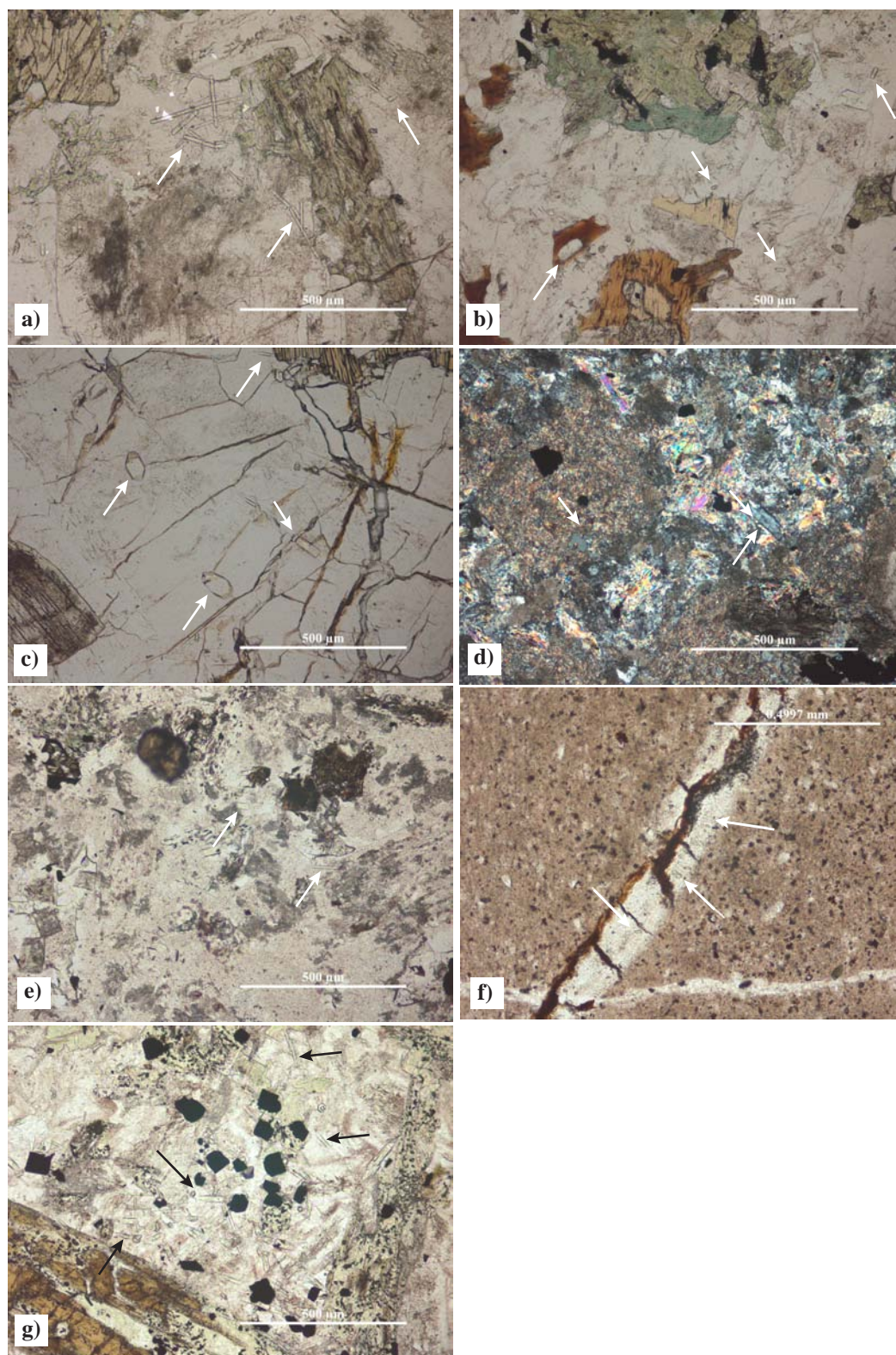


Figure 6.1 Photomicrographs of apatite associations in thin section from this study. Apatite is acicular and quartz-hosted in granodiorite samples GS-1765C-782 (a), GS-1818C-1000 (b) and LBB76-343 (c). Apatite was also less frequently observed in biotite (b). Apatite is stubbier in altered lamprophyre samples GA-34C-1280 (d) and GA-52C-1585 (e) and found in quartz and sericitised feldspars. Tiny stubby apatite crystals were observed in quartz veinlets in GBC-5-928. Apatite in lamprophyre U16-H07-34-537 is acicular, seen in quartz (g).

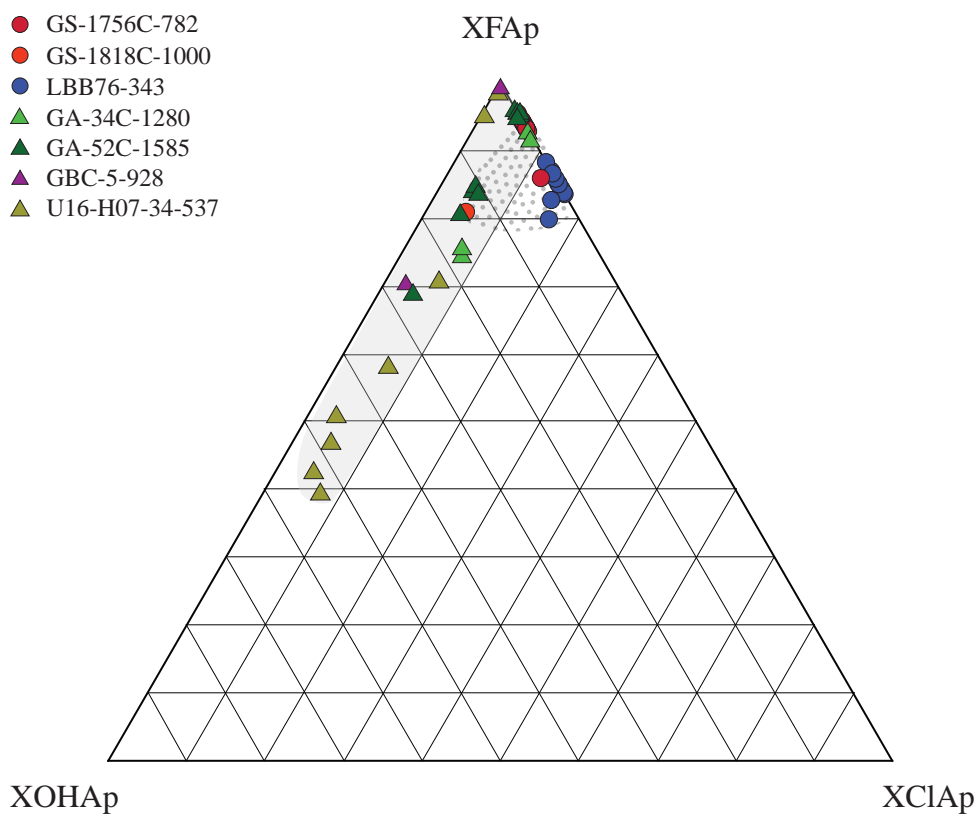


Figure 6.2. Relative F, OH and Cl content of individual apatite crystals of granodiorite (circles, stippled area) and lamprophyre (triangles, shaded area) samples in this study. Granodiorites are near end-member FAp, except LBB73-343, which has an elevated Cl content. Lamprophyres contain little Cl but variable low to high OH.

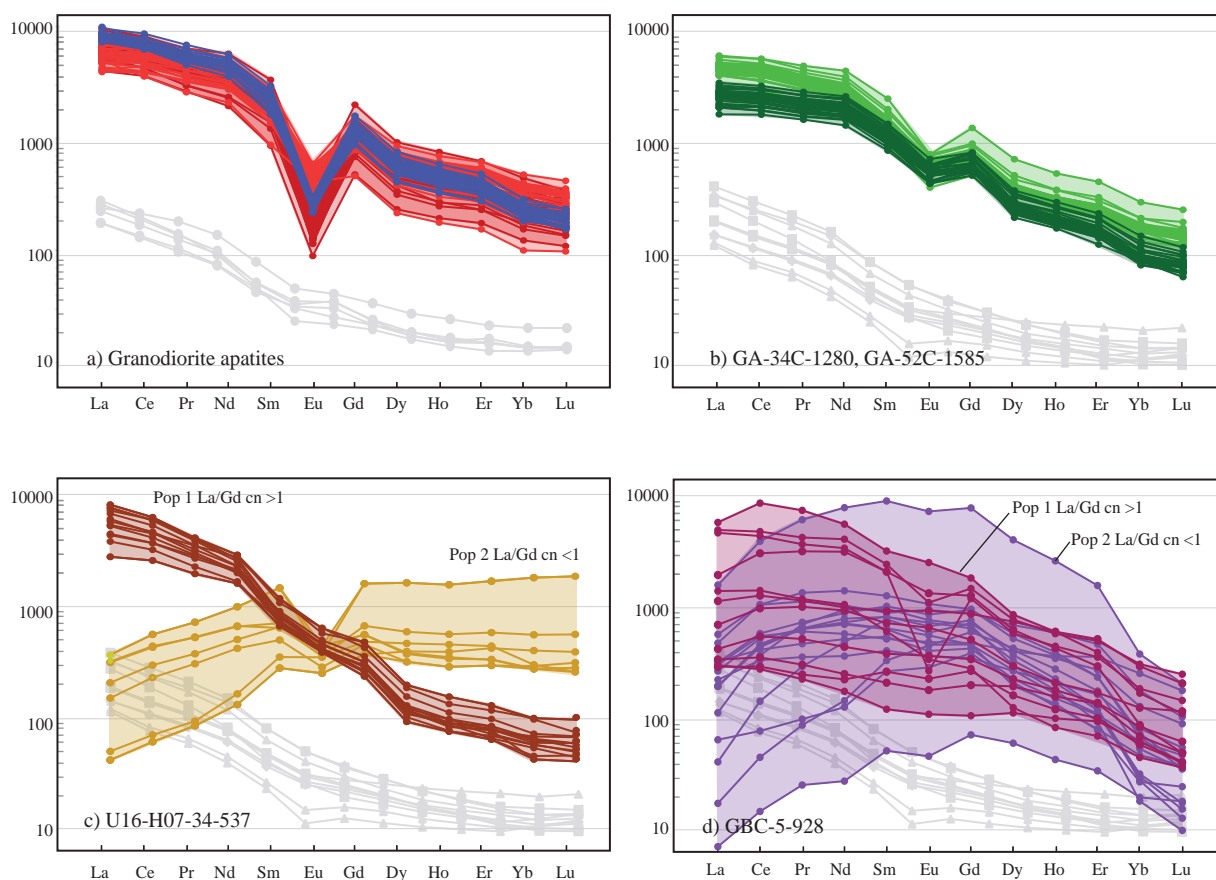


Figure 6.3 Chondrite normalised REE plots for granodiorite (a) and lamprophyre samples (b-d) show apatite REE character and define REE populations within samples. Whole rock REE shown in grey. a) REE patterns are very similar for all granodiorite samples (LBB76-343 blue, GS-1756C-782 dark red, GS-1818C-1000 light red), with a distinct negative Eu anomaly. b) lamprophyres GA-34C-1280 (light green) and GA-52C-1585 (dark green) have consistent REE patterns with a weaker negative Eu anomaly. Lamprophyre samples U16-H07-34-537 (c), and GBC-5-928 (d) have at least 2 populations of apatite based on REE pattern. U16-H07-34-537 has a consistent population (La/Gd) $_{cn} > 1$ (brown), which has no Eu anomaly; population (La/Gd) $_{cn} < 1$ (tan) has a characteristic concave-down pattern and negative Eu anomaly. GBC-5-928 REE populations (La/Gd) $_{cn} > 1$ (magenta) and (La/Gd) $_{cn} < 1$ (purple) are both highly variable in abundance; neither displays an Eu anomaly. Chondrite normalisation after Sun and McDonough (1995).

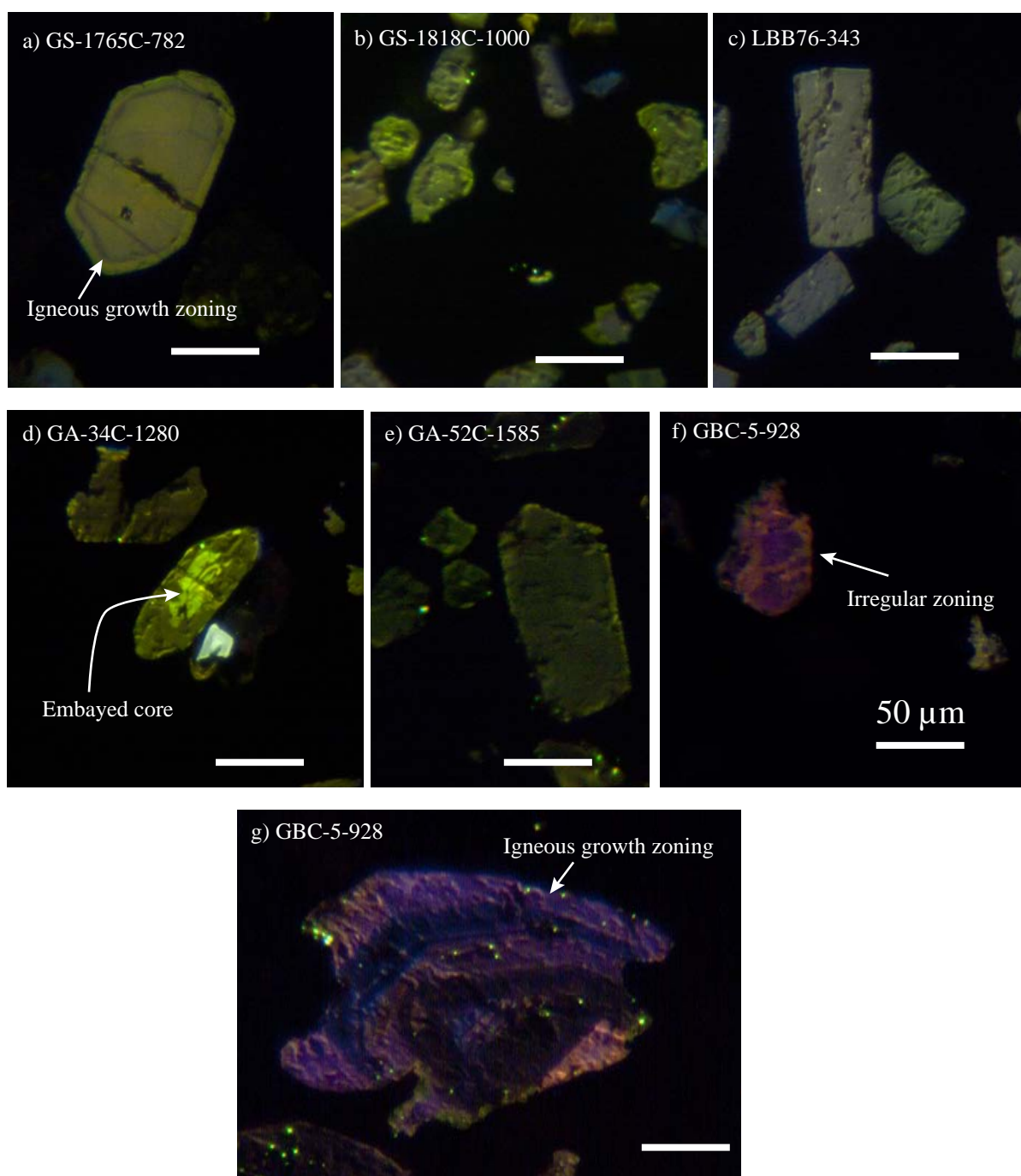


Figure 6.4 Examples of zoning, or absence of zoning, in CL images of apatite. GS-1765C-782 (a) and GS-1818C-1000 (b) contain a small number of apatites with bright cores and bright outer rims. LBB76-343 (c), and GA-52C-1585 (e) contain no zoned apatites. GA-34C-1280 (d) contains a small number of apatites with darker rims; brighter cores are embayed. GBC-5-928 contains apatites patchy hydrothermal alteration (f) and with igneous zoning (g). U16-H07-34-537 apatite is not shown; no zoning was observed in that sample.

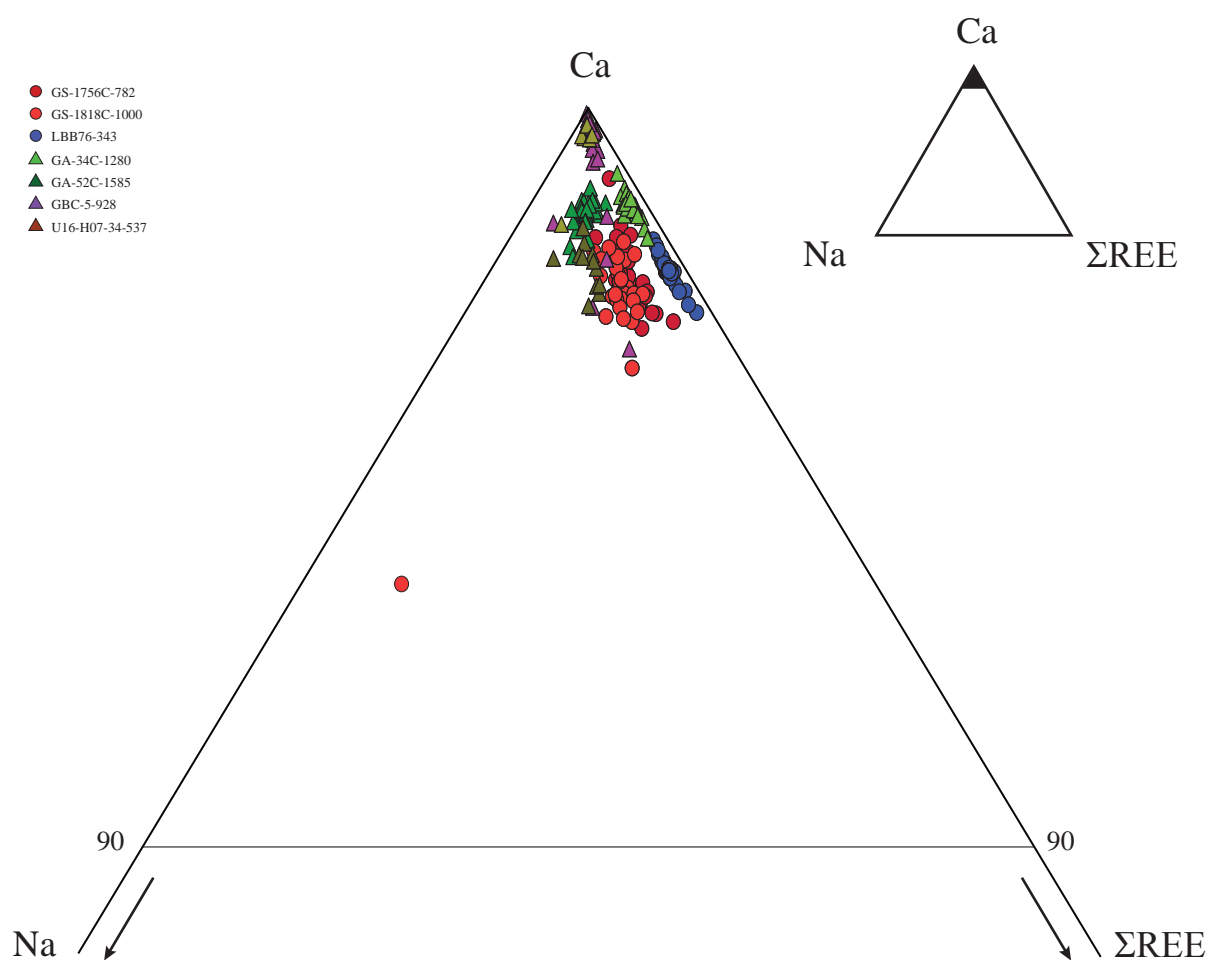


Figure 6.5 Ternary diagram showing substitutions on the Ca site by common substituting elements, Na and REE.

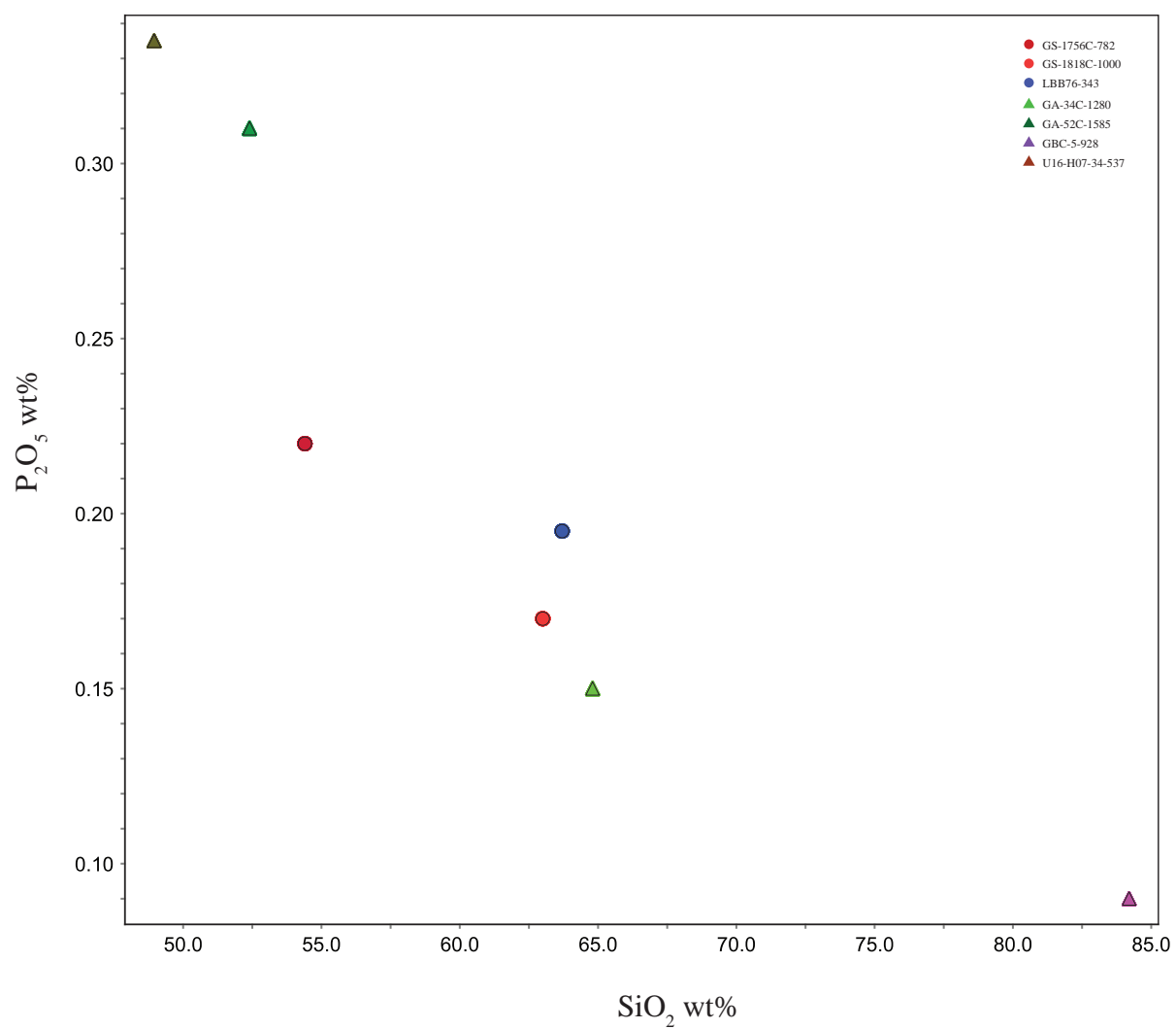
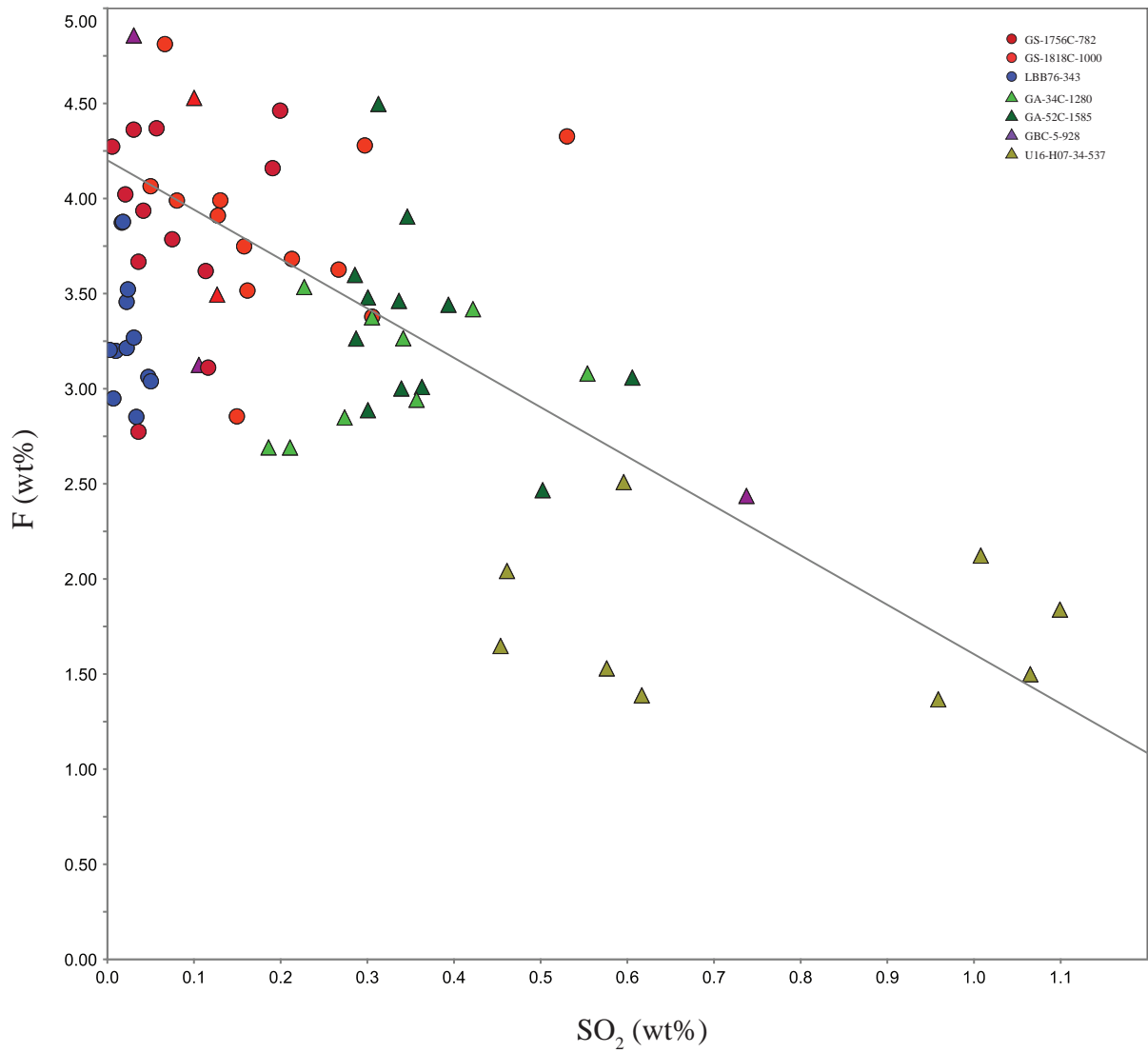


Figure 6.6 Apatite SiO_2 vs P_2O_5 . P_2O_5 decreases with increasing SiO_2 content.



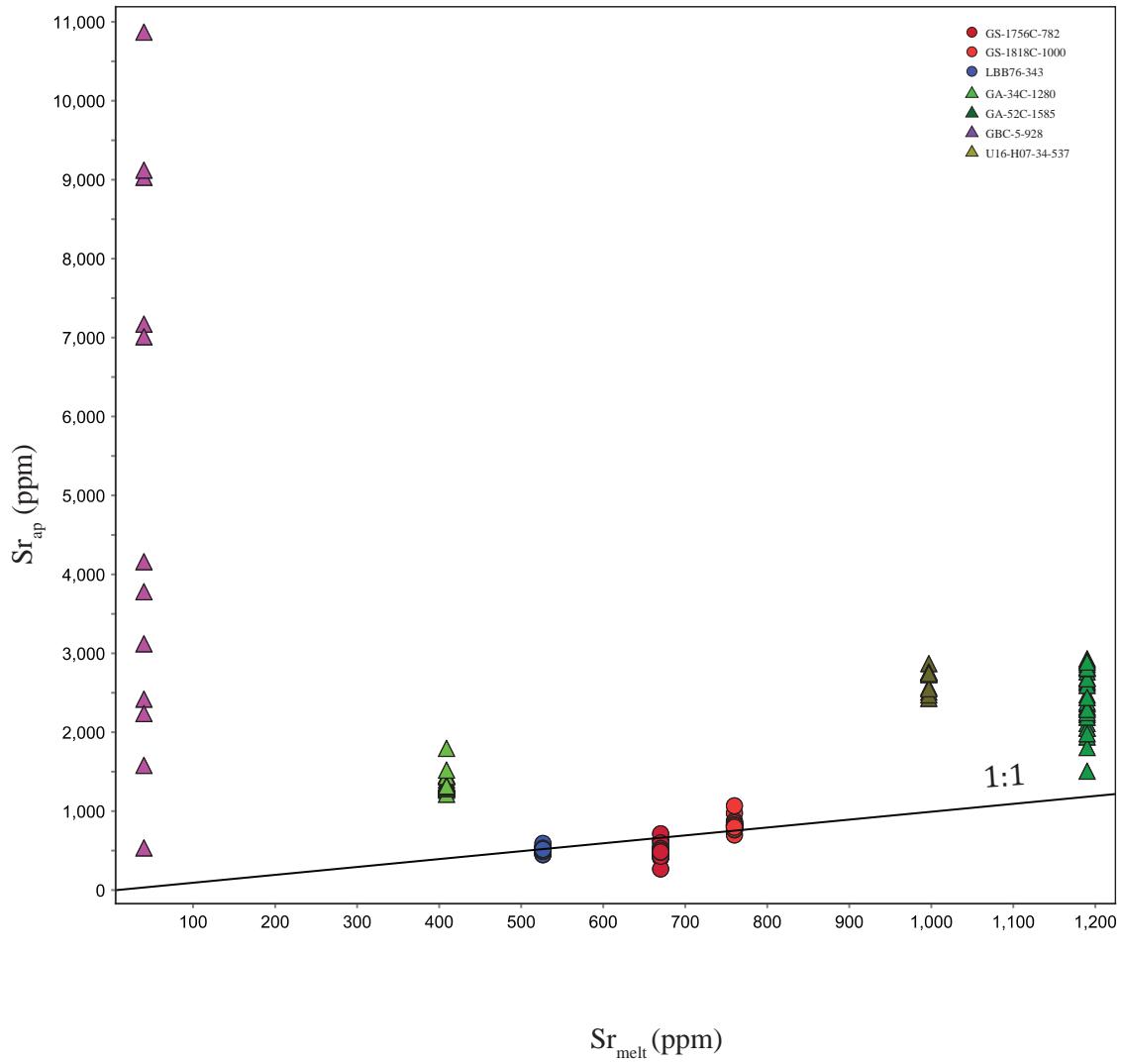


Figure 6.8 Sr_{melt} vs Sr_{ap} for granodiorite (circles) and lamprophyre (triangles) apatite and host melt. Sr is approximately 1:1. In altered samples GBC-5-928, GA-34C-1280 and U16-H07-34-537. Sr_{ap} is higher than Sr_{melt} suggesting Sr has been removed from the host rock by hydrothermal alteration. GBC-5-928 Sr_{ap} is highly variable.

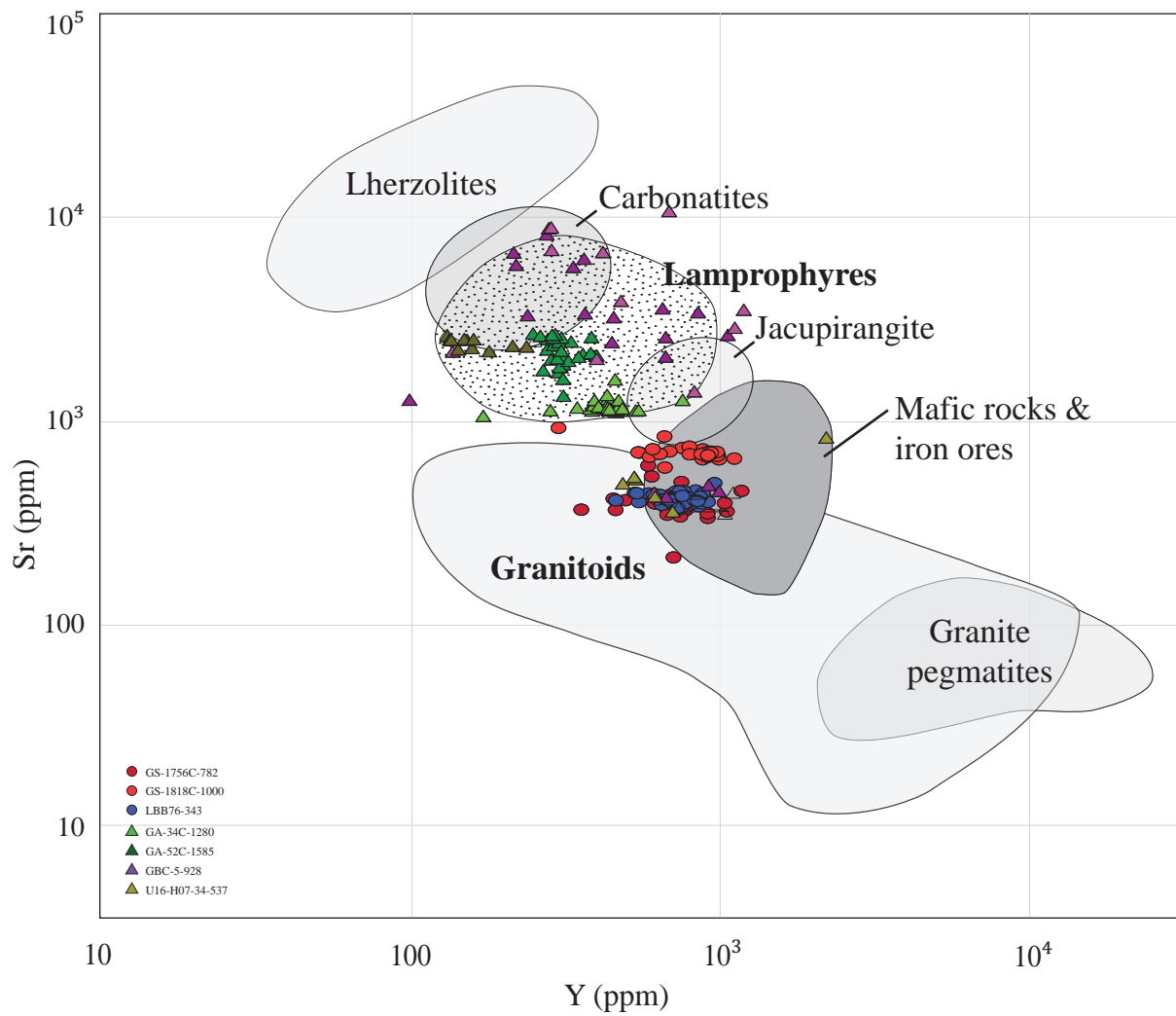


Figure 6.9 Sr-Y plot to determine host rock type, after Belousova et al. (2002) with addition of lamprophyre field from this study.

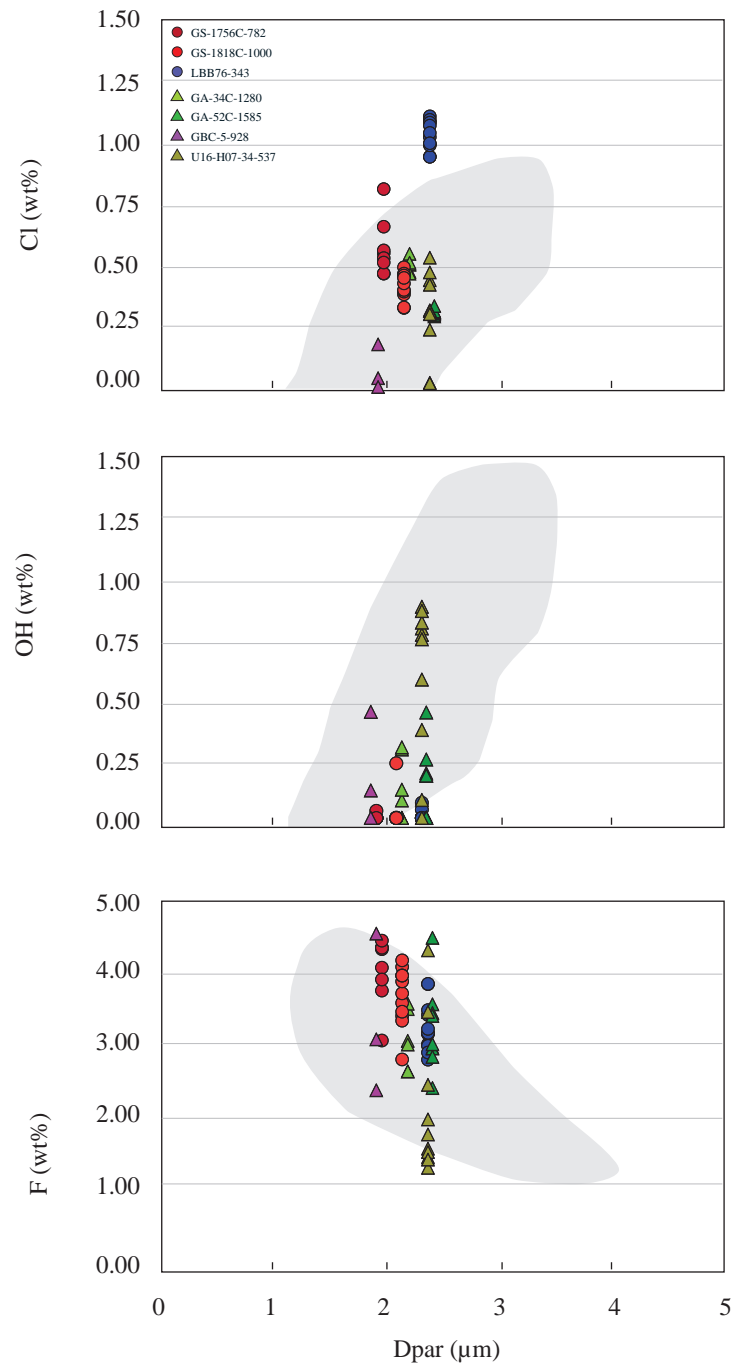


Figure 6.10 Apatite halogen content and kinetic parameter Dpar. Dpar increases with OH or Cl content and decreases with increasing F content. Shaded areas are the range in Dpar-halogen values from Donelick et al. (2005).

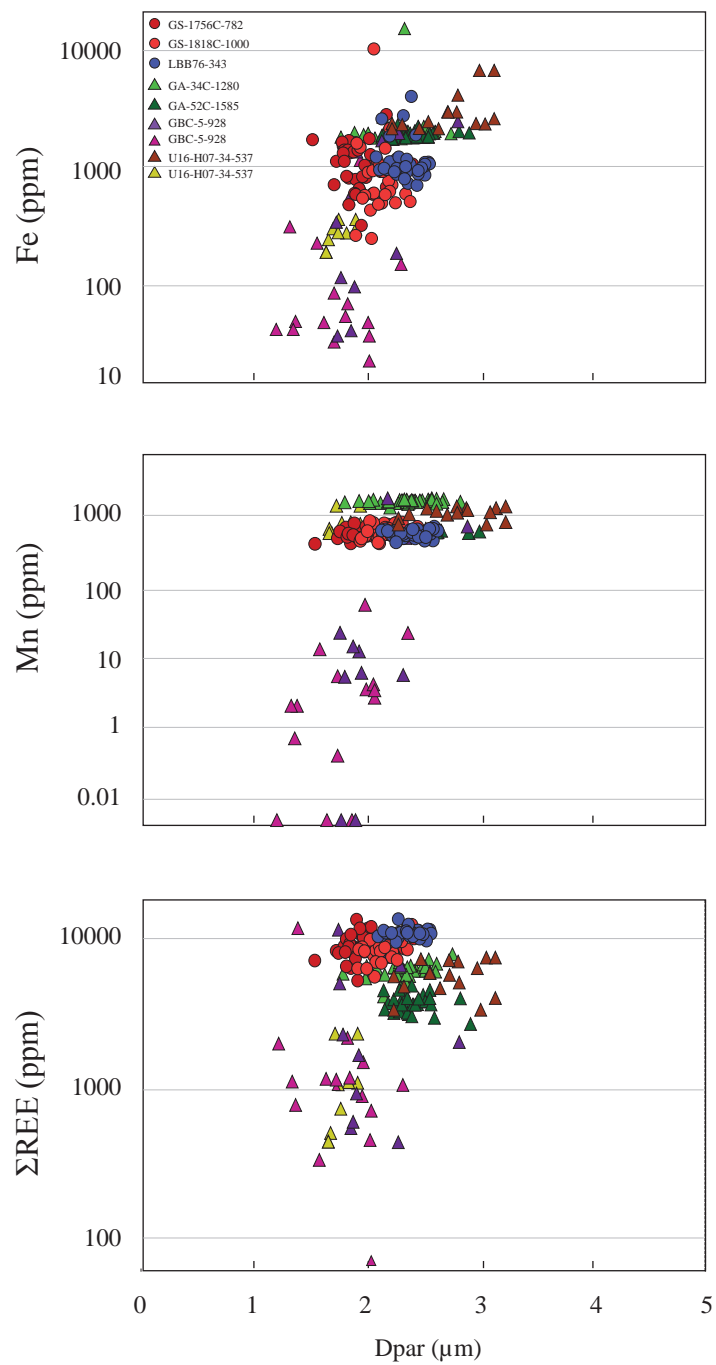


Figure 6.11 Apatite Fe, Mn, Σ REE content and kinetic parameter Dpar. Overall Dpar increases with increasing Fe, Mn and Σ REE content.

Table 6.1 Major and select trace element composition of apatite determined by EMPA

	GS1765C-782		GS1818C-1000		LBB76-343		GA34C-1280		GA52C-1585		GBC5-928		U16-H07-34-537	
F	4.06	± 0.45	3.70	± 0.39	3.29	± 0.33	3.11	± 0.39	3.33	± 0.58	3.37	± 1.08	2.19	± 0.98
SiO₂	0.42	0.37	0.46	0.25	0.29	0.07	0.24	0.04	0.25	0.06	0.20	0.12	0.39	0.18
P₂O₅	39.28	0.41	38.89	0.77	39.38	0.57	39.28	0.62	39.19	0.30	38.67	1.34	39.49	1.50
SO₃	0.07	0.06	0.19	0.13	0.02	0.01	0.31	0.12	0.37	0.10	0.30	0.38	0.64	0.35
Cl	0.58	0.12	0.43	0.06	1.04	0.06	0.51	0.03	0.32	0.01	0.08	0.09	0.31	0.18
CaO	53.74	0.28	52.76	0.70	53.11	0.40	53.43	0.28	53.68	0.43	51.70	1.98	52.50	0.93
MnO	0.09	0.04	0.07	0.04	0.06	0.04	0.20	0.05	0.06	0.03	0.07	0.06	0.10	0.03
FeO	0.15	0.07	0.10	0.07	0.15	0.05	0.30	0.05	0.31	0.05	0.28	0.27	0.23	0.11
REE*	0.61	0.17	0.84	0.14	1.08	0.14	0.61	0.07	0.37	0.05	0.24	0.31	0.39	0.25
Sr*	0.05	0.01	0.08	0.01	0.05	0.00	0.13	0.01	0.24	0.04	0.45	0.28	0.19	0.10
Na*	0.38	0.06	0.46	0.10	0.11	0.01	0.10	0.02	0.41	0.09	0.20	0.27	0.45	0.23
	99.44	0.72	98.17	1.33	98.58	0.91	98.13	0.59	98.54	0.67	97.46	3.75	96.84	2.67
O=F	1.84	0.17	1.66	0.17	1.62	0.15	1.43	0.17	1.48	0.25	1.44	0.44	0.99	0.38
Total	97.60	0.67	96.52	1.27	96.96	0.84	96.70	0.67	97.06	0.59	96.02	3.48	95.84	1.41
Numbers of ions on the basis of 26 (O,OH,F,Cl)														
Si	0.08	5.88	0.08	5.88	0.05	5.92	0.04	5.94	0.04	5.88	0.03	5.94	0.07	6.05
P	5.80		5.77		5.86		5.87		5.79		5.85		5.89	
S	0.01		0.03		0.00		0.03		0.05		0.05		0.08	
Ca	10.01	10.26	9.91	10.21	10.01	10.17	10.04	10.22	10.03	10.33	9.91	10.12	9.94	10.24
Mn	0.01		0.01		0.01		0.03		0.01		0.01		0.01	
Fe	0.02		0.02		0.02		0.04		0.05		0.04		0.04	
REE	0.04		0.06		0.07		0.04		0.02		0.02		0.03	
Sr	0.01		0.01		0.01		0.02		0.03		0.05		0.02	
Na	0.17		0.21		0.05		0.05		0.19		0.09		0.21	
F	2.16	2.33	2.13	2.25	1.83	2.14	1.69	2.00	1.84	2.00	2.03	2.06	1.15	2.00
OH	0.00		0.00		0.00		0.16		0.07		0.00		0.75	
Cl	0.17		0.13		0.31		0.15		0.09		0.03		0.10	
Ca/P	1.73		1.72		1.71		1.71		1.73		1.69		1.69	
XFap	0.93		0.94		0.86		0.85		0.92		0.99		0.57	
XOHap	0.00		0.00		0.00		0.08		0.03		0.00		0.38	
XClap	0.07		0.06		0.14		0.07		0.05		0.01		0.05	
Dpar (µm)	1.96	0.17	2.14	0.12	2.37	0.13	2.19	0.21	2.41	0.15	1.91	0.41	2.37	0.54
AFT (Ma)	37.9	2.8	52.0	2.9	126.0	7.0	40.7	4.7	40.0	4.8	25.8	7.0	62.9	6.9

*from LA-ICP-MS

Table 6.2 Trace element concentrations determined by LA-ICP-MS

	GS-1765C-782	GS-1818C-1000	LBB76-343	GA-34C-1280	GA-52C-1585	GBC-5-928		U16-H07-34-537	
	<i>Single REE population per sample</i>					<i>La/Gd_{cn} >1</i>	<i>La/Gd_{cn} <1</i>	<i>La/Gd_{cn} >1</i>	<i>La/Gd_{cn} <1</i>
Na	3772	4591	1098	987	4062	2901	1339	5839	2140
Mg	197	179	377	1325	2425	402	513	3041	99
Si	2302	1995	2039	2622	1210	1551	951	2193	1014
Sc	0.5	0.6	0.9	0.8	1.2	3.5	3.5	0.7	0.6
Mn	526	566	529	1472	551	253	7	1011	769
Fe	1126	1156	1254	2313	1940	803	190	3184	276
As	14.8	28.4	21.8	23.2	8.2	16.4	7.6	7.6	8.2
Rb	0.2	0.2	0.2	1.0	0.5	0.4	0.2	0.2	0.2
Sr	490	816	509	1334	2423	4896	4212	2656	642
Y	749	850	762	449	303	602	710	155	1018
Ba	1.7	1.6	2.3	15.0	14.1	14.4	12.2	62.3	1.4
La	1749	1483	2164	1118	621	478	74	1315	50
Ce	4116	3673	4821	2682	1527	1465	405	2744	185
Pr	465	456	571	334	203	198	85	289	36
Nd	1806	1924	2316	1406	919	854	501	1018	236
Sm	303	331	374	230	166	178	178	124	103
Eu	11	28	17	36	31	42	57	26	20
Gd	231	252	272	159	126	153	210	64	146
Dy	144	167	156	98	69	107	145	33	166
Ho	25	31	27	17	12	18	22	6	35
Er	67	79	65	41	27	41	43	14	107
Yb	47	58	40	28	16	22	15	11	106
Lu	6.0	7.6	5.0	3.7	2.1	2.5	1.4	1.5	16.4
Hg	0.7	2.1	0.9	1.1	0.9	1.1	0.9	1.3	1.8
Pb	5.2	8.8	6.1	5.6	2.3	5.2	3.7	4.8	9.5
Th	47	49	36	31	14	12	15	52	42
U	92	220	42	21	8	8	22	36	134
Total REE	8903	8411	10763	6112	3691	3516	1693	5618	1104
Eu/Eu*	0.12	0.30	0.15	0.55	0.63	0.83	0.91	0.80	0.63
La/Gd _{cn}	6.55	5.12	6.78	5.94	4.13	2.40	0.36	18.26	0.33
A Dpar (µm)	1.96	2.14	2.36	2.32	2.41	2.04	1.75	2.73	1.77

Chapter 7: Thesis conclusions

A study of apatite composition and texture determined that there is no consistent chemical or morphological evidence of hydrothermal fluid flow affecting the composition or morphology of apatite from Jurassic intrusions of the northern Carlin Trend. Apatite from granodiorite and lamprophyre samples is near end-member calcian fluorapatite and displays common minor substitutions. In keeping with published studies, substitutions by Cl and OH for F, and Mn and REE for Ca, were seen to increase D_{par} , a kinetic parameter related to annealing used in AFT dating. Apatite analysed in this study is primary igneous apatite that crystallized with the host intrusion and therefore records the post-emplacement thermal history of the host rock, including exhumation-related cooling and the thermal effects of hydrothermal fluid flow.

Northern central Nevada underwent a major phase of exhumation in the Late Cretaceous between ~85-60 Ma that is recorded in ZHe, AFT and AHe data from the Jurassic Little Boulder Basin Stock, Goldstrike Stock and Vivian Sill. The stocks record 3-4 km exhumation from emplacement depths to present subsurface positions. Exhumation resulted from a combination of tectonic and erosional denudation as the thickened Sevier hinterland was eroded as the surface uplift occurred and extension led to normal faulting and denudation of footwall rocks. Rates of exhumation as high as 1 km/Myr are inferred. Rapid Late Cretaceous exhumation was preceded by more gradual exhumation over ~140-90 Ma that is recorded in the central Tuscarora Mountains to the north of the northern Carlin Trend. Rapid Late Cretaceous exhumation is coincident with a period of decompression and mid- to upper-crustal extension in the Sevier hinterland.

The size and shape of the AFT resetting thermal halo associated with the Eocene Carlin mineralizing system is defined against the Late Cretaceous exhumation background ages. The

size of the thermal halo around Carlin-type deposits is best defined using AFT thermochronology. The ZHe system has too high a T_c to be affected by Carlin-temperature fluids and the AHe system, with a lower T_c , is too readily reset by younger hydrothermal events. A 400 m conductive thermal halo has been defined using AFT resetting in the Goldstrike Stock, an unaltered, unmineralized granodiorite intrusion otherwise unaffected by hydrothermal fluid flow. Outside of the stock, within carbonate host rocks, the fluid conduit geometry is complex and the resulting thermal halo more difficult to define, since it was formed by overlapping thermal halos around variably spaced fluid conduits. The conductive thermal halo identified in this study is the most distal expression of the Carlin hydrothermal system, extending beyond other physicochemical manifestations of fluid flow such as isotopic depletion, trace element zones and mineral alteration.

The maximum duration of heating by 180°C fluids to produce a 400 m halo is 10 kyr, or ~2 kyr by 240°C fluids. Multiple pulses are not ruled out, but must be temporally distinct or shorter-lived to produce the observed AFT resetting halo. Estimated fluid flux to deposit Au hosted in rocks around the Goldstrike Stock over 10 kyr is on the order of 100 kg/s, similar to modern geothermal systems at the Ladolam Au deposit in Papua New Guinea and in the Taupo Volcanic Zone, New Zealand. These modern geothermal systems are a product of magmatically-driven forced convection. The short durations of fluid flow proposed for Carlin hydrothermal systems suggests the deposits may be the result of vigorous fluid flow driven by magmatic heating or pressure-driven fluid flow rather than free convection.

References

- Ahmed, A. D., 2010a, Beyond the confines of the ore deposit : mapping low temperature hydrothermal alteration above, within, and beneath Carlin-type Gold deposits: Unpub. M.Sc thesis, University of British Columbia.
- Ahmed, A. D., 2010b, The Elder Creek Deposit: An Upper Plate Expression of an Auriferous Carlin-type hydrothermal system, GSN Symposium: Reno.
- Albino, G. V., 1994, Geology and lithogeochemistry of the Ren gold prospect, Elko County, Nevada -- the role of rock sampling in exploration for deep Carlin-type deposits: *Journal of Geochemical Exploration*, v. 51, p. 37-58.
- Allmendinger, R., 1992, Fold and thrust tectonics of the western United States exclusive of the accreted terranes: The Cordilleran Orogen: Conterminous US: Boulder, Colorado, Geological Society of America, *Geology of North America*, v. 3, p. 583–607.
- Allmendinger, R. W., Jordan, T. E., Kay, S. M., and Isacks, B. L., 1997, The Evolution of the Altiplano-Puna Plateau of the Central Andes: *Annual Review of Earth & Planetary Sciences*, v. 25, p. 139.
- Arehart, G., Chakurian, A., Tretbar, D., Christensen, J., McInnes, B., and Donelick, R., 2003a, Evaluation of radioisotope dating of Carlin-type deposits in the Great Basin, western North America, and implications for deposit genesis: *Economic Geology*, v. 98, p. 235-248.
- Arehart, G. B., Chakurian, A. M., Tretbar, D. R., Christensen, J. N., McInnes, B. A., and Donelick, R. A., 2003b, Evaluation of Radioisotope Dating of Carlin-Type Deposits in the Great Basin, Western North America, and Implications for Deposit Genesis: *Economic Geology*, v. 98, p. 235-248.
- Arehart, G. B., Christenson, B. W., Wood, C. P., Foland, K. A., and Browne, P. R. L., 2002, Timing of volcanic, plutonic and geothermal activity at Ngatamariki, New Zealand: *Journal of Volcanology and Geothermal Research*, v. 116, p. 201-214.
- Arehart, G. B., Chrysosoulis, S. L., and Kesler, S. E., 1993a, Gold and arsenic in iron sulfides from sediment-hosted disseminated gold deposits; implications for depositional processes: *Economic Geology*, v. 88, p. 171-185.
- Arehart, G. B., and Donelick, R. A., 2006, Thermal and isotopic profiling of the Pipeline hydrothermal system: Application to exploration for Carlin-type gold deposits: *Journal of Geochemical Exploration*, v. 91, p. 27-40.
- Arehart, G. B., Foland, K. A., Naeser, C. W., and Kesler, S. E., 1993b, $^{40}\text{Ar}/^{39}\text{Ar}$, K/Ar, and fission track geochronology of sediment-hosted disseminated gold deposits at Post-Betze, Carlin Trend, northeastern Nevada: *Economic Geology*, v. 88, p. 622-646.
- Armstrong, A. K., Theodore, T.G., Oscarson, R.L., Kotlyar, B.B, Harris, A.G, Bettles, K.H., Lauha, E.A., Hipsley, R.A. ,Griffin, G.L., Abbott, E.W., and Cluer, J.K., 1998, Preliminary facies analysis of Silurian and Devonian autochthonous rocks that host gold along the Carlin trend, Nevada, *in* Tosdal, R. M., ed., *CONTRIBUTIONS TO THE GOLD METALLOGENY OF NORTHERN NEVADA*, USGS Open-File Report 98-338.

- Armstrong, R. L., 1972, Low-angle (denudation) faults, hinterland of the Sevier orogenic belt, eastern Nevada and western Utah: *Geological Society of America Bulletin*, v. 83, p. 1729-1754.
- Arndt, J., Bartel, T., Scheuber, E., and Schilling, F., 1997, Thermal and rheological properties of granodioritic rocks from the Central Andes, North Chile: *Tectonophysics*, v. 271, p. 75-88.
- Arribas, A., Hedenquist, J. W., Itaya, T., Okada, T., Concepcion, R. A., and Garcia, J. S., 1995, CONTEMPORANEOUS FORMATION OF ADJACENT PORPHYRY AND EPITHERMAL CU-AU DEPOSITS OVER 300 KA IN NORTHERN LUZON, PHILIPPINES: *Geology*, v. 23, p. 337-340.
- Barbarand, J., Carter, A., Wood, I., and Hurford, T., 2003, Compositional and structural control of fission-track annealing in apatite: *Chemical Geology*, v. 198, p. 107-137.
- Barbarand, J., and Pagel, M., 2001, Cathodoluminescence study of apatite crystals: *American Mineralogist*, v. 86, p. 473-484.
- Barker, S. L. H., K. A.; Dipple, G. M.; Layne, G., 2009, Apatite as a paleohydrothermal fluid recorder in Carlin-type gold deposits: Joint Assembly: The Meeting of the Americas. American Geophysical Union, Spring Meeting., Toronto, Ontario, Canada, 2009.
- Barker, S. L. L., Hickey, K. A., Cline, J. S., Dipple, G. M., Kilburn, M. R., Vaughan, J. R., and Longo, A. A., 2009, UNCLOAKING INVISIBLE GOLD: USE OF NANOSIMS TO EVALUATE GOLD, TRACE ELEMENTS, AND SULFUR ISOTOPES IN PYRITE FROM CARLIN-TYPE GOLD DEPOSITS: *Economic Geology*, v. 104, p. 897-904.
- Bau, M., 1991, Rare-earth element mobility during hydrothermal and metamorphic fluid-rock interaction and the significance of the oxidation state of europium: *Chemical Geology*, v. 93, p. 219-230.
- Bear, J., 1988, *Dynamics of fluids in porous media*, Dover publications.
- Belousova, E. A., Griffin, W. L., O'Reilly, S. Y., and Fisher, N. I., 2002, Apatite as an indicator mineral for mineral exploration: trace-element compositions and their relationship to host rock type: *Journal of Geochemical Exploration*, v. 76, p. 45-69.
- Bettles, K., 2002, Exploration and geology, 1962 to 2002, at the Goldstrike Property, Carlin Trend, Nevada: *Economic Geology Special Publication 9*, p. 275-298.
- Bibby, H. M., Caldwell, T. G., Davey, F. J., and Webb, T. H., 1995, Geophysical evidence on the structure of the Taupo Volcanic Zone and its hydrothermal circulation: *Journal of Volcanology and Geothermal Research*, v. 68, p. 29-58.
- Bickle, M. J., and McKenzie, D., 1987, The transport of heat and matter by fluids during metamorphism: *Contributions to Mineralogy and Petrology*, v. 95, p. 384-392.
- Biglow, C. C., 1986, Startigraphy and sedimentology of the Cretaceous Newark Canyon Formation in the Cortez Mountains, North-Central Nevada: Unpub. MSc thesis, Eastern Washington University.
- Bird, P., 1979, Continental delamination and the Colorado Plateau: *J. geophys. Res.*, v. 84, p. 7561-7571.
- Blamey, N. J. F., 2000, The evolution of hydrothermal fluids at the Pipeline gold mine, Lander County, Nevada: Unpub. PhD thesis, New Mexico Institute of Mining and Technology.

- Boudreau, A. E., and Kruger, F. J., 1990, Variation in the composition of apatite through the Merensky cyclic unit in the western Bushveld Complex: *Economic Geology*, v. 85, p. 737-745.
- Bouzari, F., Hart, C.J.R., Barker, S., and Bissig, T., 2011, Porphyry Indicator Minerals (PIMS): A new exploration tool for concealed deposits in south-central British Columbia: *Geoscience BC*, v. Report 2011-17.
- Brandon, M. T., Roden-Tice, M. K., and Garver, J. I., 1998, Late Cenozoic exhumation of the Cascadia accretionary wedge in the Olympic Mountains, northwest Washington State: *Geological Society of America Bulletin*, v. 110, p. 985-1009.
- Burbank, D. W., and Anderson, R. S., 2011, *Tectonic geomorphology*, Wiley-Blackwell.
- Burchfiel, B. C., and Davis, G. A., 1972, Structural framework and evolution of the southern part of the Cordilleran orogen, western United States: *American Journal of Science*, v. 272, p. 97-118.
- Burtner, R. L., Nigrini, A. and Donelick, R.A. , 1994, Thermochronology of lower Cretaceous source rocks in the Idaho–Wyoming thrust belt.: *Am. Assoc. Pet. Geol. Bull.*, v. 78, p. 1613-1636.
- Cail, T. L., and Cline, J. S., 2001, Alteration Associated with Gold Deposition at the Getchell Carlin-Type Gold Deposit, North-Central Nevada: *Economic Geology*, v. 96, p. 1343-1359.
- Camilleri, P. A., and Chamberlain, K. R., 1997, Mesozoic tectonics and metamorphism in the Pequop Mountains and Wood Hills region, northeast Nevada: Implications for the architecture and evolution of the Sevier orogen: *Geological Society of America Bulletin*, v. 109, p. 74.
- Carlson, W. D., 1990, Mechanisms and kinetics of apatite fission-track annealing: *American Mineralogist*;(United States), v. 75.
- Carlson, W. D., Donelick, R. A., and Ketcham, R. A., 1999, Variability of apatite fission-track annealing kinetics; I, Experimental results: *American Mineralogist*, v. 84, p. 1213.
- Cathles, L., 1997, Thermal aspects of ore formation: *Geochemistry of hydrothermal ore deposits*, v. 3, p. 125-190.
- Cathles, L. M., Erendi, A. H. J., and Barrie, T., 1997, How long can a hydrothermal system be sustained by a single intrusive event?: *Economic Geology*, v. 92, p. 766-771.
- Cathles, L. M., and Shannon, R., 2007, How potassium silicate alteration suggests the formation of porphyry ore deposits begins with the nearly explosive but barren expulsion of large volumes of magmatic water: *Earth and Planetary Science Letters*, v. 262, p. 92-108.
- Chakurian, A. M., Arehart, G. B., Donelick, R. A., Zhang, X., and Reiners, P. W., 2003, Timing Constraints of Gold Mineralization along the Carlin Trend Utilizing Apatite Fission-Track, $^{40}\text{Ar}/^{39}\text{Ar}$, and Apatite (U-Th)/He Methods: *Economic Geology*, v. 98, p. 1159-1171.
- Chen, J. H., and Moore, J. G., 1982, URANIUM-LEAD ISOTOPIC AGES FROM THE SIERRA NEVADA BATHOLITH, CALIFORNIA: *J. Geophys. Res.*, v. 87, p. 4761-4784.
- Cline, J. S., and Hofstra, A. H., 2000, Ore-fluid evolution at the Getchell Carlin-type gold deposit, Nevada, USA: *Eur J Mineral*, v. 12, p. 195-212.

- Cline, J. S., Hofstra, A. H., Muntean, J. M., Tosdal, R. M., and Hickey, K. A., 2005, Carlin-type gold deposits in Nevada: critical geologic characteristics and viable models: SEG 100th Anniversary Volume p. pp. 451–484.
- Cline, J. S., Stuart, F.M., Hofstra, A.H., Premo, W., Riciputi, L., Tosdal, R.M. and Tretbar, D.R., 2003, Multiple sources of ore-fluid components at the Getchell Carlin-type gold deposit, north-central Nevada, USA: Mineral exploration and sustainable development, Rotterdam, 2003, p. 965-968.
- Colgan, J. P., Dumitru, T. A., Reiners, P. W., Wooden, J. L., and Miller, E. L., 2006, Cenozoic Tectonic Evolution of the Basin and Range Province in Northwestern Nevada: American Journal of Science, v. 306, p. 616-654.
- Colgan, J. P., and Henry, C. D., 2009, Rapid middle Miocene collapse of the Mesozoic orogenic plateau in north-central Nevada: International Geology Review, v. 51, p. 920-961.
- Colgan, J. P., Howard, K. A., Fleck, R. J., and Wooden, J. L., 2010, Rapid middle Miocene extension and unroofing of the southern Ruby Mountains, Nevada: Tectonics, v. 29, p. TC6022.
- Colgan, J. P., John, D. A., Henry, C. D., and Fleck, R. J., 2008, Large-magnitude Miocene extension of the Eocene Caetano caldera, Shoshone and Toiyabe Ranges, Nevada: Geosphere, v. 4, p. 107-130.
- Collins, W., 2002, Hot orogens, tectonic switching, and creation of continental crust: Geology, v. 30, p. 535-538.
- Coney, P. J., and Harms, T. A., 1984, Cordilleran metamorphic core complexes: Cenozoic extensional relics of Mesozoic compression: Geology, v. 12, p. 550-554.
- Cooke, D. R., and Simmons, S. F., 2000, Characteristics and genesis of epithermal gold deposits: Reviews in Economic Geology, v. 13, p. 221-244.
- Corrigan, J., 1991, Inversion of apatite fission track data for thermal history information: Journal of geophysical research, v. 96, p. 10347-10,360.
- Cox, S., 2005, Coupling between deformation, fluid pressures, and fluid flow in ore-producing hydrothermal systems at depth in the crust: Economic Geology, 100th Anniversary Volume, p. 39-75.
- Crafford, A. E. J., 2007, Geologic Map of Nevada: U.S. Geological Survey Data Series 249, p. 1 CD-ROM, 46 p., 1 plate.
- de Almeida, C. M., Olivo, G. R., Chouinard, A., Weakly, C., and Poirier, G., 2010, Mineral Paragenesis, Alteration, and Geochemistry of the Two Types of Gold Ore and the Host Rocks from the Carlin-Type Deposits in the Southern Part of the Goldstrike Property, Northern Nevada: Implications for Sources of Ore-Forming Elements, Ore Genesis, and Mineral Exploration: Econ Geol, v. 105, p. 971-1004.
- DeCelles, P. G., 2004, Late Jurassic to Eocene evolution of the Cordilleran thrust belt and foreland basin system, western U.S.A: Am J Sci, v. 304, p. 105-168.
- DeCelles, P. G., and Coogan, J. C., 2006, Regional structure and kinematic history of the Sevier fold-and-thrust belt, central Utah: Geological Society of America Bulletin, v. 118, p. 841-864.
- Dickinson, W. R., 2006, Geotectonic evolution of the Great Basin: Geosphere, v. 2, p. 353-368.
- Dickinson, W. R., 2008, Accretionary Mesozoic-Cenozoic expansion of the Cordilleran continental margin in California and adjacent Oregon: Geosphere, v. 4, p. 329-353.

- Dickinson, W. R., Snyder, W.S., 1978, Plate tectonics of the Laramide orogeny, *in* Matthews, V., ed., Laramide folding associated with basement block faulting in the western United States, Memoir 151, Geological Society of America, p. 355-366.
- Dodson, M. H., 1973, Closure temperature in cooling geochronological and petrological systems: Contributions to Mineralogy and Petrology, v. 40, p. 259-274.
- Donelick, R. A., 1993a, Apatite etching characteristics versus chemical composition.: Nucl. Tracks Radiat. Meas., v. 21, p. 604.
- Donelick, R. A., 1993b, Method of fission track analysis utilizing bulk chemical etching of apatite, Google Patents.
- Donelick, R. A., Ketcham, R. A., and Carlson, W. D., 1999, Variability of apatite fission-track annealing kinetics; II, Crystallographic orientation effects: American Mineralogist, v. 84, p. 1224.
- Donelick, R. A., O'Sullivan, P. B., and Ketcham, R. A., 2005, Apatite fission-track analysis, Low-Temperature Thermochronology: Techniques, Interpretations, and Applications, 58. Reviews in Mineralogy & Geochemistry: Chantilly, Mineralogical Soc America, p. 49-94.
- Donelick, R. A., Roden, M. K., Mooers, J. D., Carpenter, B. S., and Miller, D. S., 1990, Etchable length reduction of induced fission tracks in apatite at room temperature ([approximate] 23°C): Crystallographic orientation effects and "initial" mean lengths: International Journal of Radiation Applications and Instrumentation. Part D. Nuclear Tracks and Radiation Measurements, v. 17, p. 261-265.
- Druschke, P., Hanson, A., and Wells, M., 2009a, Structural, stratigraphic, and geochronologic evidence for extension predating Palaeogene volcanism in the Sevier hinterland, east-central Nevada: International Geology Review, v. 51, p. 743-775.
- Druschke, P., Hanson, A., Wells, M., Gehrels, G., and Stockli, D., 2011, Paleogeographic isolation of the Cretaceous to Eocene Sevier hinterland, east-central Nevada: Insights from U-Pb and (U-Th)/He detrital zircon ages of hinterland strata: Geological Society of America Bulletin, v. 123, p. 1141.
- Druschke, P., Hanson, A. D., Wells, M. L., Rasbury, T., Stockli, D. F., and Gehrels, G., 2009b, Synconvergent surface-breaking normal faults of Late Cretaceous age within the Sevier hinterland, east-central Nevada: Geology, v. 37, p. 447-450.
- Dumitru, T. A., 1990, Subnormal Cenozoic Geothermal Gradients in the Extinct Sierra Nevada Magmatic Arc: Consequences of Laramide and Post-Laramide Shallow-Angle Subduction: J. Geophys. Res., v. 95, p. 4925-4941.
- Eaton, G. P., 1982, The Basin and Range Province: Origin and Tectonic Significance: Annual Review of Earth and Planetary Sciences, v. 10, p. 409-440.
- Ehlers, T. A., Chaudhri, T., Kumar, S., Fuller, C. W., Willett, S. D., Ketcham, R. A., Brandon, M. T., Belton, D. X., Kohn, B. P., and Gleadow, A. J. W., 2005, Computational tools for low-temperature thermochronometer interpretation: Reviews in Mineralogy and Geochemistry, v. 58, p. 589-622.

- Eilu, P., and Groves, D. I., 2001, Primary alteration and geochemical dispersion haloes of Archaean orogenic gold deposits in the Yilgarn Craton: the pre-weathering scenario: *Geochemistry: Exploration, Environment, Analysis*, v. 1, p. 183-200.
- Emsbo, P., 1999, Origin of the Meikle high-grade gold deposit from the superposition of late Devonian sedex and mid-Tertiary Carlin-type gold mineralization, Colorado School of Mines.
- Emsbo, P., Groves, D., Hofstra, A., and Bierlein, F., 2006, The giant Carlin gold province: a protracted interplay of orogenic, basinal, and hydrothermal processes above a lithospheric boundary: *Mineralium Deposita*, v. 41, p. 517-525.
- Emsbo, P., Hofstra, A., Park, D., Zimmerman, J., and Snee, L., 1996, A mid-Tertiary age constraint on alteration and mineralization in igneous dikes on the Goldstrike property, Carlin trend, Nevada: *Geological Society of America Abstracts with Programs*, 1996, p. A476.
- Emsbo, P., and Hofstra, A. H., 2003, Origin and Significance of Postore Dissolution Collapse Breccias Cemented with Calcite and Barite at the Meikle Gold Deposit, Northern Carlin Trend, Nevada: *Economic Geology*, v. 98, p. 1243-1252.
- Emsbo, P., Hofstra, A. H., Lauha, E. A., Griffin, G. L., and Hutchinson, R. W., 2003, Origin of High-Grade Gold Ore, Source of Ore Fluid Components, and Genesis of the Meikle and Neighboring Carlin-Type Deposits, Northern Carlin Trend, Nevada: *Economic Geology*, v. 98, p. 1069-1105.
- Engelbreton, D. C., Cox, A., and Thompson, G. A., 1984, Correlation of plate motions with continental tectonics: Laramide to basin-range: *Tectonics*, v. 3, p. 115-119.
- England, P., and Houseman, G., 1989, Extension during continental convergence, with application to the Tibetan Plateau: *Journal of geophysical research*, v. 94, p. 17,561-17,579.
- Ewers, G. R., and Keays, R. R., 1977, Volatile and precious metal zoning in the Broadlands geothermal field, New Zealand: *Economic Geology*, v. 72, p. 1337-1354.
- Farley, K. A., 2000, Helium diffusion from apatite: General behavior as illustrated by Durango fluorapatite: *J. Geophys. Res.*, v. 105, p. 2903-2914.
- Farley, K. A., 2002, (U-Th)/He dating: Techniques, calibrations, and applications, *in* Porcelli, D., Ballentine, C. J., and Wieler, R., eds., *Noble Gases in Geochemistry and Cosmochemistry*, 47. *Reviews in Mineralogy & Geochemistry*: Washington, Mineralogical Soc America, p. 819-844.
- Farley, K. A., Wolf, R. A., and Silver, L. T., 1996, The effects of long alpha-stopping distances on (U-Th)/He ages: *Geochimica et Cosmochimica Acta*, v. 60, p. 4223-4229.
- Fleck, R. J., Theodore, T. G., Sarna-Wojcicki, A., and Meyer, C. E., 1998, Age and possible source of air-fall tuffs of the Miocene Carlin Formation, northern Nevada: *US Geological Survey Open-File Report*, p. 98-338.
- Fleischer, M., and Altschuler, Z. S., 1986, The lanthanides and yttrium in minerals of the apatite group – an analysis of the available data: *Neues Jahrbuch für Mineralogie Monatshefte*, v. 1986(10), p. 467-480.
- Fleischer, R. L., Price, P. B., and Walker, R. M., 1975, *Nuclear tracks in solids: principles and applications*, University of California Press.

- Flowers, R. M., Ketcham, R. A., Shuster, D. L., and Farley, K. A., 2009, Apatite (U-Th)/He thermochronometry using a radiation damage accumulation and annealing model: *Geochimica et Cosmochimica Acta*, v. 73, p. 2347-2365.
- Foster, D. A., and John, B. E., 1999, Quantifying tectonic exhumation in an extensional orogen with thermochronology: examples from the southern Basin and Range Province: Geological Society, London, Special Publications, v. 154, p. 343-364.
- Foster, D. A., Miller, D. S., and Miller, C. F., 1991, Tertiary extension in the Old Woman Mountains Area, California: Evidence from apatite fission track analysis: *Tectonics*, v. 10, p. 875-886.
- Gabrielse, H., Snyder, W. S., and Stewart, J. H., 1983, Sonoma orogeny and Permian to Triassic tectonism in western North America: *Geology*, v. 11, p. 484-486.
- Galbraith, R., 2005, *Statistics for fission track analysis*, Chapman & Hall.
- Galbraith, R. F., 1990, The radial plot; graphical assessment of spread in ages: *Nuclear Tracks and Radiation Measurements*, v. 17, p. 207-214.
- Galbraith, R. F., 1994, Some Applications of Radial Plots: *Journal of the American Statistical Association*, v. 89, p. 1232-1242.
- Gerstenberger, H., and Haase, G., 1997, A Highly effective emitter substance for mass spectrometric Pb isotopic ratio determinations: *Chemical Geology*, v. 136, p. 309-312.
- Giggenbach, W. F., 1984, Mass transfer in hydrothermal alteration systems--a conceptual approach: *Geochimica et Cosmochimica Acta*, v. 48, p. 2693-2711.
- Gilbert, G. K., 1928, *Studies of basin-range structure*, US Govt. Print. Off.
- Gleadow, A. J. W., and Duddy, I. R., 1981, A natural long-term track annealing experiment for apatite: *Nuclear Tracks*, v. 5, p. 169-174.
- Gleadow, A. J. W., Duddy, I. R., Green, P. F., and Lovering, J. F., 1986, Confined fission track lengths in apatite: a diagnostic tool for thermal history analysis: *Contributions to Mineralogy and Petrology*, v. 94, p. 405-415.
- Goldberg, I. S., Abramson, G. Y., and Los, V. L., 2003, Depletion and enrichment of primary haloes: their importance in the genesis of and exploration for mineral deposits: *Geochemistry: Exploration, Environment, Analysis*, v. 3, p. 281-293.
- Green, P. F., Duddy, I. R., Gleadow, A. J. W., Tingate, P. R., and Laslett, G. M., 1986, Thermal annealing of fission tracks in apatite : 1. A qualitative description: *Chemical Geology: Isotope Geoscience section*, v. 59, p. 237-253.
- Hardardóttir, V., Brown, K., Fridriksson, T., Hedenquist, J., Hannington, M., and Thorhallsson, S., 2009, Metals in deep liquid of the Reykjanes geothermal system, southwest Iceland: Implications for the composition of seafloor black smoker fluids: *Geology*, v. 37, p. 1103-1106.
- Harrison, T. M., and Zeitler, P. K., 2005, Fundamentals of Noble Gas Thermochronometry: *Reviews in Mineralogy and Geochemistry*, v. 58, p. 123-149.

- Hasebe, N., Barbarand, J., Jarvis, K., Carter, A., and Hurford, A. J., 2004, Apatite fission-track chronometry using laser ablation ICP-MS: *Chemical Geology*, v. 207, p. 135-145.
- Hawkes, H. E., and Webb, J. S., 1962, *Geochemistry in Mineral Exploration*: New York, Harper and Row.
- Haynes, S. R., 2003, Development of the Eocene Elko Basin, Northeastern Nevada: Implications for Paleogeography and Regional Tectonism: Unpub. M.Sc thesis, University of British Columbia.
- Heitt, D. G., Dunbar, W. W., Thompson, T. B., and Jackson, R. G., 2003, Geology and geochemistry of the Deep Star gold deposit, Carlin Trend, Nevada: *Economic Geology*, v. 98, p. 1107-1135.
- Henry, C. D., 2008, Ash-flow tuffs and paleovalleys in northeastern Nevada: Implications for Eocene paleogeography and extension in the Sevier hinterland, northern Great Basin: *Geosphere*, v. 4, p. 1-35.
- Hickey, K., Haynes, S., Tosdal, R., and Mortensen, J., 2003, Cretaceous-Paleogene denudation, volcanism and faulting in the Carlin-Jerritt Canyon mining district, northeastern Nevada: Implications for the paleogeographic and tectonic environment of Carlin-type gold deposits: Mineral exploration and sustainable development: Rotterdam, Millpress, p. 685-688.
- Hickey, K. A., 2003, Restoration of the Eocene landscape in the Carlin-Jerritt Canyon mining district: Constraining depth of mineralisation for Carlin-type Au-deposits using low-temperature apatite thermochronology 2003.
- Hickey, K. A., 2007, Thermal footprints - defining the far-field extent of hydrothermal fluid flow using low-temperature thermochronology, Mineral Exploration Roundup07: Vancouver, Association for Mineral Exploration British Columbia.
- Hickey, K. A., Dipple, G. M., and Barker, S. L. L., 2011, The brevity of hydrothermal fluid flow revealed by thermal haloes around giant Au-deposits: GSA Annual Meeting, Minneapolis, 2011, p. 152.
- Hickey, K. A., Tosdal, R.M., Donelick, R.A. and Arehart, G.B., 2005, Apatite fission-track thermal anomalies and the evolution of syn-extensional hydrothermal flow accompanying Au-mineralization along the northern Carlin Trend, Nevada, Geological Society of America, Annual Meeting: Salt Lake City, Geological Association of America.
- Hodges, K., Parrish, R., Housh, T., Lux, D., Burchfiel, B., Royden, L., and Chen, Z., 1992, Simultaneous Miocene extension and shortening in the Himalayan orogen: *Science*, v. 258, p. 1466-1470.
- Hodges, K. V., and Walker, J. D., 1992, Extension in the Cretaceous Sevier orogen, North American Cordillera: *Geological Society of America Bulletin*, v. 104, p. 560-569.
- Hofstra, A. H., 1997, Isotopic composition of sulfur in Carlin-type gold deposits: Implications for genetic models, 1997, p. 119-129.
- Hofstra, A. H., Christiansen, William D., Tousignant, Gilles, 2010, Lithogeochemistry of the Devonian Popovich Formation in the Northern Carlin Trend, Nevada, GSN Symposium: Reno.
- Hofstra, A. H., and Cline, J. S., 2000, Characteristics and Models for Carlin-Type Gold Deposits: Reviews in *Economic Geology*, v. 13, p. 162-220.
- Hofstra, A. H., John, D. A., and Theodore, T. G., 2003, A Special Issue Devoted to Gold Deposits in Northern Nevada: Part 2. Carlin-Type Deposits: *Economic Geology*, v. 98, p. 1063-1067.

- Hofstra, A. H., Leventhal, J. S., Northrop, H. R., Landis, G. P., Rye, R. O., Birak, D. J., and Dahl, A. R., 1991, Genesis of sediment-hosted disseminated-gold deposits by fluid mixing and sulfidization: Chemical-reaction-path modeling of ore-depositional processes documented in the Jerritt Canyon district, Nevada: *Geology*, v. 19, p. 36-40.
- Hofstra, A. H., Snee, L. W., Rye, R. O., Folger, H. W., Phinisey, J. D., Loranger, R. J., Dahl, A. R., Naeser, C. W., Stein, H. J., and Lewchuk, M. T., 1999, Age constraints on Jerritt Canyon and other carlin-type gold deposits in the Western United States; relationship to mid-Tertiary extension and magmatism: *Economic Geology*, v. 94, p. 769-802.
- Holland, H. D., and Malinin, S. D., 1979, The Solubility and Occurrence of Non-Ore Minerals, *in* Barnes, H. L., ed., *Geochemistry of Hydrothermal Ore Deposits*, John Wiley & Sons.
- Hourigan, J. K., Reiners, P. W., and Brandon, M. T., 2005, U-Th zonation-dependent alpha-ejection in (U-Th)/He chronometry: *Geochimica et Cosmochimica Acta*, v. 69, p. 3349-3365.
- House, M. A., Farley, K. A., and Kohn, B. P., 1999, An empirical test of helium diffusion in apatite: borehole data from the Otway basin, Australia: *Earth and Planetary Science Letters*, v. 170, p. 463-474.
- Howard, K. A., 2003, Crustal structure in the Elko-Carlin region, Nevada, during Eocene gold mineralization: Ruby-East Humboldt metamorphic core complex as a guide to the deep crust: *Economic Geology*, v. 98, p. 249-268.
- Hudec, M. R., 1992, Mesozoic structural and metamorphic history of the central Ruby Mountains metamorphic core complex, Nevada: *Geological Society of America Bulletin*, v. 104, p. 1086-1100.
- Hughes, J. M., Cameron, M., and Crowley, K. D., 1991a, Ordering of divalent cations in the apatite structure; crystal structure refinements of natural Mn- and Sr-bearing apatite: *American Mineralogist*, v. 76, p. 1857.
- Hughes, J. M., Cameron, M., and Mariano, A. N., 1991b, RARE-EARTH-ELEMENT ORDERING AND STRUCTURAL VARIATIONS IN NATURAL RARE-EARTH-BEARING APATITES: *American Mineralogist*, v. 76, p. 1165-1173.
- Hughes, J. M., and Rakovan, J., 2002, The Crystal Structure of Apatite, $\text{Ca}_5(\text{PO}_4)_3(\text{F},\text{OH},\text{Cl})$: *Reviews in Mineralogy and Geochemistry*, v. 48, p. 1-12.
- Humphreys, E. D., 1995, Post-Laramide removal of the Farallon slab, western United States: *Geology*, v. 23, p. 987-990.
- Ilchik, R. P., and Barton, M. D., 1997, An amagmatic origin of carlin-type gold deposits: *Economic Geology*, v. 92, p. 269-288.
- Ingebritsen, S. E., Sanford, W. E., and Neuzil, C. E., 2006, *Groundwater in geologic processes*, Cambridge Univ Pr.
- Jaffey, A. H., Flynn, K. F., Glendenin, L. E., Bentley, W. C., and Essling, A. M., 1971, Precision measurement of half-lives and specific activities of ^{235}U and ^{238}U : *Phys. Rev.*, v. C4, p. 1889-1906.

- John, D. A., 2001, Miocene and early Pliocene epithermal gold-silver deposits in the northern Great Basin, western United States: Characteristics, distribution, and relationship to magmatism: *Economic Geology*, v. 96, p. 1827-1853.
- John, D. A., Wallace, A.R., Ponce, D.A., Fleck, R.B., and Conrad, J.E., 2000, New perspectives on the geology and origin of the northern Nevada rift: Geological Society of Nevada, *Geology and Ore Deposits 2000: The Great Basin and Beyond Symposium*, Reno/Sparks, Nevada, May 15–18, 2000, Proceedings, 2000, p. 127–154.
- Jolliff, B. L., Papike, J. J., and Shearer, C. K., 1989, INTER-CRYSTAL AND INTRA-CRYSTAL REE VARIATIONS IN APATITE FROM THE INGERSOLL, BOB PEGMATITE, BLACK HILLS, SOUTH-DAKOTA: *Geochimica et Cosmochimica Acta*, v. 53, p. 429-441.
- Jones, B. K., 1992, Application of metal zoning to gold exploration in porphyry copper systems: *Journal of Geochemical Exploration*, v. 43, p. 127-155.
- Jory, J., 2002, Stratigraphy and Host Rock Controls of Gold Deposits of the Northern Carlin Trend: *NBMG Bulletin* 111, p. 20-34.
- Kelley, D. L., Kelley, K. D., Coker, W. B., Caughlin, B., and Doherty, M. E., 2006, Beyond the Obvious Limits of Ore Deposits: The Use of Mineralogical, Geochemical, and Biological Features for the Remote Detection of Mineralization: *Economic Geology*, v. 101, p. 729-752.
- Kempe, U., and Götze, J., 2002, Cathodoluminescence (CL) behaviour and crystal chemistry of apatite from rare-metal deposits: *Mineral Mag*, v. 66, p. 151-172.
- Kesler, S. E., Fortuna, J., Ye, Z., Alt, J. C., Core, D. P., Zohar, P., Borhauer, J., and Chrysosoulis, S. L., 2003, Evaluation of the Role of Sulfidation in Deposition of Gold, Screamer Section of the Betze-Post Carlin-Type Deposit, Nevada: *Economic Geology*, v. 98, p. 1137-1157.
- Ketcham, R. A., 2003, Observations on the relationship between crystallographic orientation and biasing in apatite fission-track measurements: *American Mineralogist*, v. 88, p. 817.
- Ketcham, R. A., 2005, Forward and Inverse Modeling of Low-Temperature Thermochronometry Data: *Reviews in Mineralogy and Geochemistry*, v. 58, p. 275-314.
- Ketcham, R. A., 2009, HeFTy Version 1.6.7: Manual.
- Ketcham, R. A., Carter, A., Donelick, R. A., Barbarand, J., and Hurford, A. J., 2007, Improved modeling of fission-track annealing in apatite: *American Mineralogist*, v. 92, p. 799-810.
- Ketcham, R. A., Donelick, R. A., Balestrieri, M. L., and Zattin, M., 2009, Reproducibility of apatite fission-track length data and thermal history reconstruction: *Earth and Planetary Science Letters*, v. 284, p. 504-515.
- Ketcham, R. A., Donelick, R. A., and Carlson, W. D., 1999, Variability of apatite fission-track annealing kinetics; III, Extrapolation to geological time scales: *American Mineralogist*, v. 84, p. 1235.
- Ketcham, R. A., Donelick, R.A., Donelick, M.B., 2000, AFTSolve: A program for multi-kinetic modeling of apatite fission-track data. : *Geol Mat Res*, v. 2.

- Ketner, K. B., 2008, The Inskip Formation, the Harmony Formation, and the Havallah Sequence of Northwestern Nevada An Interrelated Paleozoic Assemblage in the Home of the Sonoma Orogeny: US Geological Survey professional paper.
- Knutson, C., Peacor, D. R., and Kelly, W. C., 1985, LUMINESCENCE, COLOR AND FISSION-TRACK ZONING IN APATITE CRYSTALS OF THE PANASQUEIRA TIN-TUNGSTEN DEPOSIT, BEIRA-BAIXA, PORTUGAL: *American Mineralogist*, v. 70, p. 829-837.
- Kuehn, C. A., 1989, Studies of disseminated gold deposits near Carlin, Nevada: Evidence for a deep geologic setting of ore formation, Pennsylvania State Univ., Middletown, PA (USA).
- Kuehn, C. A., and Rose, A. W., 1992, Geology and geochemistry of wall-rock alteration at the Carlin gold deposit, Nevada: *Economic Geology*, v. 87, p. 1697-1721.
- Laslett, G., Galbraith, R., and Green, P., 1994, The analysis of projected fission track lengths: *Radiation Measurements*, v. 23, p. 103-123.
- Laslett, G. M., Green, P. F., Duddy, I. R., and Gleadow, A. J. W., 1987, Thermal annealing of fission tracks in apatite 2. A quantitative analysis: *Chemical Geology: Isotope Geoscience section*, v. 65, p. 1-13.
- Laslett, G. M., Kendall, W. S., Gleadow, A. J. W., and Duddy, I. R., 1982, Bias in measurement of fission-track length distributions: *Nuclear Tracks and Radiation Measurements* (1982), v. 6, p. 79-85.
- Livaccari, R. F., 1991, Role of crustal thickening and extensional collapse in the tectonic evolution of the Sevier-Laramide orogeny, western United States: *Geology*, v. 19, p. 1104-1107.
- Lovera, O. M., Grove, M., and Harrison, T. M., 2002, Systematic analysis of K-feldspar $^{40}\text{Ar}/^{39}\text{Ar}$ step heating results II: Relevance of laboratory argon diffusion properties to nature: *Geochimica et Cosmochimica Acta*, v. 66, p. 1237-1255.
- Lovera, O. M., Grove, M., Mark Harrison, T., and Mahon, K., 1997, Systematic analysis of K-feldspar $^{40}\text{Ar}/^{39}\text{Ar}$ step heating results: I. Significance of activation energy determinations: *Geochimica et Cosmochimica Acta*, v. 61, p. 3171-3192.
- Lovera, O. M., Richter, F. M., and Harrison, T. M., 1991, DIFFUSION DOMAINS DETERMINED BY $\text{AR}-^{39}\text{AR}$ RELEASED DURING STEP HEATING: *Journal of Geophysical Research-Solid Earth and Planets*, v. 96, p. 2057-2069.
- Lubben, J., 2004, Quartz as clues to paragenesis and fluid properties at the Betze-Post deposit, northern Carlin trend, Nevada: Unpub. M.Sc thesis, University of Nevada, 155 p.
- Ludwig, K. R., 2003, Isoplot 3.00, A Geochronological Toolkit for Microsoft Excel, University of California at Berkeley.
- Lund, K., 2008, Geometry of the Neoproterozoic and Paleozoic rift margin of western Laurentia: Implications for mineral deposit settings: *Geosphere*, v. 4, p. 429-444.
- Mattinson, J. M., 2005, Zircon U-Pb chemical abrasion ("CA-TIMS") method: Combined annealing and multi-step partial dissolution analysis for improved precision and accuracy of zircon ages, v. 220, p. 47-66.

- McGrew, A. J., Peters, M. T., and Wright, J. E., 2000, Thermobarometric constraints on the tectonothermal evolution of the East Humboldt Range metamorphic core complex, Nevada: *Geological Society of America Bulletin*, v. 112, p. 45-60.
- McGrew, A. J., and Snee, L. W., 1994, $^{40}\text{Ar}/^{39}\text{Ar}$ thermochronologic constraints on the tectonothermal evolution of the Northern East Humboldt range metamorphic core complex, Nevada: *Tectonophysics*, v. 238, p. 425-450.
- Mickelthwaite, S., 2010, Fault-induced damage controlling the formation of Carlin-type ore deposits, *in* Stieninger, R., and Pennell, B., eds., *Geological Society of Nevada Symposium: Great Basin Evolution and Metallogeny*, 1: Reno, NV, p. 221-231.
- Miller, E. L., and Gans, P. B., 1989, Cretaceous crustal structure and metamorphism in the hinterland of the Sevier thrust belt, western U.S. Cordillera: *Geology*, v. 17, p. 59-62.
- Miller, E. L., Holdsworth, B. K., Whiteford, W. B., and Rodgers, D., 1984, Stratigraphy and structure of the Schoonover sequence, northeastern Nevada: Implications for Paleozoic plate-margin tectonics: *Geological Society of America Bulletin*, v. 95, p. 1063-1076.
- Miller, E. L., Miller, M. M., Stevens, C. H., Wright, J. E., and Madrid, R., 1992, Late Paleozoic paleogeographic and tectonic evolution of the western US Cordillera: The Cordilleran Orogen: Conterminous US: *Geological Society of America, The Geology of North America*, v. 3, p. 57-106.
- Mitchell, R. H., Xiong, J., Mariano, A. N., and Fleet, M. E., 1997, Rare-earth-element-activated cathodoluminescence in apatite: *Can Mineral*, v. 35, p. 979-998.
- Moore, M. A., and England, P. C., 2001, On the inference of denudation rates from cooling ages of minerals: *Earth and Planetary Science Letters*, v. 185, p. 265-284.
- Moore, S., 2002, Geology of the northern Carlin trend, *in* Thompson, T. B., Teal, L. and Meeuwig, R.O., ed., *Gold Deposits of the Carlin Trend*, 111: Nevada Bureau of Mines and Geology.
- Moore, S., and Norby, J. W., 2002, Cross sections for plates 1 and 2, *in* Thompson, T. B., Teal, L. and Meeuwig, R.O., ed., *Gold Deposits of the Carlin Trend*, 111: Nevada Bureau of Mines and Geology.
- Mortensen, J. K., Thompson, J. F. H., and Tosdal, R. M., 2000, U-Pb age constraints on magmatism and mineralization in the northern Great Basin, Nevada, *in* Cluer, J. K., Price, J.G., Struhsacker, E.M., Hardyman, R.F., and Morris, C.L., ed., *Geology and Ore Deposits 2000: The Great Basin and Beyond*: Geological Society of Nevada Symposium, Reno, 2000, Proceedings, p. 419-438.
- Morton, J. L., Silberman, M.L., Bonham, H.F., Garside L.J. and Noble, D.C., 1977, K-Ar ages of volcanic rocks, plutonic rocks, and ore deposits in Nevada and eastern California; determinations run under the USGS-NBMG Cooperative Program: *Isochron/West*, v. 20, p. 19-29.
- Mundil, R., Ludwig, K. R., Metcalfe, I., and Renne, P. R., 2004, Age and timing of the Permian Mass Extinctions: U/Pb Dating of Closed-System Zircons: *Science*, v. 305.
- Muntean, J., Tarnocai, C., Coward, M., Rouby, D., and Jackson, A., 2001, Styles and restorations of Tertiary extension in north-central Nevada: Regional tectonics and structural control of ore: The major gold trends of northern Nevada: *Geological Society of Nevada Special Publication*, v. 33, p. 55-69.

- Muntean, J. L., 2010, The Nevada Mineral Industry 2009 Major Precious-Metal Deposits: Nevada Bureau of Mines and Geology: Special Publication MI-2009, p. 68-100.
- Muntean, J. L., Cline, J. S., Simon, A. C., and Longo, A. A., 2011, Magmatic-hydrothermal origin of Nevada's Carlin-type gold deposits: *Nature Geosci*, v. 4, p. 122-127.
- Muntean, J. L., Coward, M. P., and Tarnocai, C. A., 2007, Reactivated Palaeozoic normal faults: controls on the formation of Carlin-type gold deposits in north-central Nevada: Geological Society, London, Special Publications, v. 272, p. 571-587.
- Naeser, C. W., and Faul, H., 1969, Fission Track Annealing in Apatite and Sphene: *J. Geophys. Res.*, v. 74, p. 705-710.
- Nasdala, L., Kronz, A., Hanchar, J. M., Tichomirowa, M., Davis, D. W., and Hofmeister, W., 2006, Effects of natural radiation damage on back-scattered electron images of single crystals of minerals: *American Mineralogist*, v. 91, p. 1739-1746.
- Nasdala, L., Reiners, P. W., Garver, J. I., Kennedy, A. K., Stern, R. A., Balan, E., and Wirth, R., 2004, Incomplete retention of radiation damage in zircon from Sri Lanka: *American Mineralogist*, v. 89, p. 219-231.
- Nutt, C. J., and Hofstra, A. H., 2003, Alligator Ridge District, East-Central Nevada: Carlin-Type Gold Mineralization at Shallow Depths: *Economic Geology*, v. 98, p. 1225-1241.
- O'Sullivan, P. B., and Parrish, R. R., 1995, The importance of apatite composition and single-grain ages when interpreting fission track data from plutonic rocks: a case study from the Coast Ranges, British Columbia: *Earth and Planetary Science Letters*, v. 132, p. 213-224.
- Orobona, M. J. T., 1996, Structural Setting of the Blue Star Subdistrict: Implications for Origin of the Carlin Trend, Eureka County, Nevada.
- Pan, Y., and Breaks, F. W., 1997, Rare-earth elements in fluorapatite, Separation Lake area, Ontario; evidence for S-type granite-rare-element pegmatite linkage: *Can Mineral*, v. 35, p. 659-671.
- Pan, Y., and Fleet, M. E., 2002, Compositions of the Apatite-Group Minerals: Substitution Mechanisms and Controlling Factors: *Reviews in Mineralogy and Geochemistry*, v. 48, p. 13-49.
- Paul, T. A., and Fitzgerald, P. G., 1992, Transmission electron microscopic investigation of fission tracks in fluorapatite: *American Mineralogist*, v. 77, p. 336-344.
- Person, M., Banerjee, A., Hofstra, A., Sweetkind, D., and Gao, Y., 2008, Hydrologic models of modern and fossil geothermal systems in the Great Basin: Genetic implications for epithermal Au-Ag and Carlin-type gold deposits: *Geosphere*, v. 4, p. 888-917.
- Piccoli, P. M., and Candela, P. A., 2002, Apatite in Igneous Systems: *Reviews in Mineralogy and Geochemistry*, v. 48, p. 255-292.
- Platt, J., 1986, Dynamics of orogenic wedges and the uplift of high-pressure metamorphic rocks: *Geological Society of America Bulletin*, v. 97, p. 1037-1053.

- Potter, C. J., Dubiel, R. F., Snee, L. W., and Good, S. C., 1995, Eocene extension of early Eocene lacustrine strata in a complexly deformed Sevier-Laramide hinterland, northwest Utah and northeast Nevada: *Geology*, v. 23, p. 181-184.
- Price, J. G., 2010, The Nevada Mineral Industry 2009 Overview: Nevada Bureau of Mines and Geology: Special Publication MI-2009, p. 3-26.
- Rahn, M. K., Brandon, M. T., Batt, G. E., and Garver, J. I., 2004, A zero-damage model for fission-track annealing in zircon: *American Mineralogist*, v. 89, p. 473-484.
- Rakovan, J. H. N., and Reeder, R. J., 1994, Differential incorporation of trace elements and dissymmetrization in apatite: The role of surface structure during growth.
- Reed, M. H., 1997, Hydrothermal alteration and its relationship to ore fluid composition: *Geochemistry of hydrothermal ore deposits*, p. 303-365.
- Reiners, P., 2005, Zircon (U-Th)/He thermochronometry: *Reviews in Mineralogy and Geochemistry*, v. 58, p. 151.
- Reiners, P. W., and Brandon, M. T., 2006, USING THERMOCHRONOLOGY TO UNDERSTAND OROGENIC EROSION: *Annual Review of Earth and Planetary Sciences*, v. 34, p. 419-466.
- Reiners, P. W., Farley, K. A., and Hickes, H. J., 2002, He diffusion and (U-Th)/He thermochronometry of zircon: initial results from Fish Canyon Tuff and Gold Butte: *Tectonophysics*, v. 349, p. 297-308.
- Reiners, P. W., Spell, T. L., Nicolescu, S., and Zanetti, K. A., 2004, Zircon (U-Th)/He thermochronometry: He diffusion and comparisons with Ar-40/Ar-39 dating: *Geochimica et Cosmochimica Acta*, v. 68, p. 1857-1887.
- Ressel, M. W., and Henry, C. D., 2006, Igneous Geology of the Carlin Trend, Nevada: Development of the Eocene Plutonic Complex and Significance for Carlin-Type Gold Deposits: *Economic Geology*, v. 101, p. 347-383.
- Ressel, M. W., Noble, D. C., Henry, C. D., and Trudel, W. S., 2000, Dike-Hosted Ores of the Beast Deposit and the Importance of Eocene Magmatism in Gold Mineralization of the Carlin Trend, Nevada: *Economic Geology*, v. 95, p. 1417-1444.
- Riley, B. C. D., Snyder, W. S., and Gehrels, G. E., 2000, U-Pb detrital zircon geochronology of the Golconda allochthon, Nevada: *Geological Society of America Special Papers*, v. 347, p. 65-75.
- Ring, U., Brandon, M. T., Willett, S. D., and Lister, G. S., 1999, Exhumation processes: *Geological Society, London, Special Publications*, v. 154, p. 1-27.
- Roberts, R. J., 1958, Paleozoic rocks of north-central Nevada: *American Association of Petroleum Geologists Bulletin*, v. 42, p. 2813-2857.
- Rock, N. M. S., 1987, The nature and origin of lamprophyres: an overview: *Geological Society, London, Special Publications*, v. 30, p. 191-226.
- Rodriguez, B. D., 1998, Regional crustal structure beneath the Carlin Trend, Nevada based on deep electrical geophysical measurements, *in* Tosdal, R. M., ed., *Contributions to the Gold Metallogeny of Northern Nevada*, Open-File Report 98-338-B, U.S. Geol. Surv., p. 15-19.

- Roeder, P. L., MacArthur, D., Ma, X. P., Palmer, G. R., and Mariano, A. N., 1987, Cathodoluminescence and microprobe study of rare-earth elements in apatite: *American Mineralogist*, v. 72, p. 801.
- Ronacher, E., Richards, J. P., Villeneuve, M. E., and Johnston, M. D., 2002, Short life-span of the ore-forming system at the Porgera gold deposit, Papua New Guinea: laser (40)Ar/(39)Ar dates for roscoelite, biotite, and hornblende: *Mineralium Deposita*, v. 37, p. 75-86.
- Ronsbo, J. G., 1989, COUPLED SUBSTITUTIONS INVOLVING REES AND NA AND SI IN APATITES IN ALKALINE ROCKS FROM THE ILIMAUSSAQ INTRUSION, SOUTH-GREENLAND, AND THE PETROLOGICAL IMPLICATIONS: *American Mineralogist*, v. 74, p. 896-901.
- Rowland, J. V., and Simmons, S. F., 2012, Hydrologic, Magmatic, and Tectonic Controls on Hydrothermal Flow, Taupo Volcanic Zone, New Zealand: Implications for the Formation of Epithermal Vein Deposits: *Economic Geology*, v. 107, p. 427-457.
- Royden, L. H., 1993, The tectonic expression slab pull at continental convergent boundaries: *Tectonics*, v. 12, p. 303-325.
- Saleeby, J., 2003, Segmentation of the Laramide Slab—evidence from the southern Sierra Nevada region: *Geological Society of America Bulletin*, v. 115, p. 655-668.
- Sass, J. H., Lachenbruch, A. H., Moses, T. H., and Morgan, P., 1992, HEAT-FLOW FROM A SCIENTIFIC-RESEARCH WELL AT CAJON PASS, CALIFORNIA: *Journal of Geophysical Research-Solid Earth*, v. 97, p. 5017-5030.
- Sass, J. H., Priest, S. S., Blanton, A.J., Sackett, P.C., Welch, S.L., Walters, M.A., 1999, Geothermal Industry Temperature Profiles from the Great Basin: US Geol. Sur. Open-File Report 99-425, Online version 1.0.
- Schmitz, M. D., and Schoene, B., 2007, Derivation of isotope ratios, errors, and error correlations for U-Pb geochronology using 205Pb-235U-(233U)-spiked isotope dilution thermal ionization mass spectrometric data: *Geochem. Geophys. Geosyst.*, v. 8.
- Scoates, J. S., and Friedman, R. M., 2008, Precise age of the platiniferous Merensky Reef, Bushveld Complex, South Africa, by the U=Pb ID-TIMS chemical abrasion ID-TIMS technique: *Econ Geol.*, v. 103.
- Seedorff, E., 1991, Magmatism, extension, and ore deposits of Eocene to Holocene age in the Great Basin-Mutual effects and preliminary proposed genetic relationships: *Geology and Ore Deposits of the Great Basin, Symposium Proceedings*, Reno, Nevada, 1991, p. 133–178.
- Seedorff, E., Dilles, J., Proffett Jr, J., Einaudi, M., Zurcher, L., Stavast, W., Johnson, D., and Barton, M., 2005, Porphyry deposits: Characteristics and origin of hypogene features: *Economic Geology 100th Anniversary Volume*, v. 29, p. 251-298.
- Sha, L.-K., and Chappell, B. W., 1999, Apatite chemical composition, determined by electron microprobe and laser-ablation inductively coupled plasma mass spectrometry, as a probe into granite petrogenesis: *Geochimica et Cosmochimica Acta*, v. 63, p. 3861-3881.
- Shuster, D. L., and Farley, K. A., 2009, The influence of artificial radiation damage and thermal annealing on helium diffusion kinetics in apatite: *Geochimica et Cosmochimica Acta*, v. 73, p. 183-196.

- Shuster, D. L., Flowers, R. M., and Farley, K. A., 2006, The influence of natural radiation damage on helium diffusion kinetics in apatite: *Earth and Planetary Science Letters*, v. 249, p. 148-161.
- Silberling, N. J., and Roberts, R. J., 1962, Pre-Tertiary stratigraphy and structure of northwestern Nevada: New York, Geological Society of America, 58 p.
- Simmons, S. F., and Brown, K. L., 2006, Gold in magmatic hydrothermal solutions and the rapid formation of a giant ore deposit: *Science*, v. 314, p. 288-291.
- Simmons, S. F., and Brown, K. L., 2007, The flux of gold and related metals through a volcanic arc, Taupo Volcanic Zone, New Zealand: *Geology*, v. 35, p. 1099-1102.
- Simmons, S. F., and Browne, P. R. L., 2000, Hydrothermal minerals and precious metals in the Broadlands-Ohaaki geothermal system: Implications for understanding low-sulfidation epithermal environments: *Economic Geology*, v. 95, p. 971-999.
- Snow, J. K., and Wernicke, B., 2000, Cenozoic tectonism in the central Basin and Range; magnitude, rate, and distribution of upper crustal strain: *Am J Sci*, v. 300, p. 659-719.
- Steiger, R. H., and Jäger, E., 1977, SUBCOMMISSION ON GEOCHRONOLOGY - CONVENTION ON USE OF DECAY CONSTANTS IN GEOCHRONOLOGY AND COSMOCHRONOLOGY: *Earth and Planetary Science Letters*, v. 36, p. 359-362.
- Stevens, C. H., 1991, Summary of Paleozoic paleogeography of western United States, *in* Cooper, J. D., and Stevens, C.H., ed., *Paleozoic paleogeography of the western United States—II: Pacific Section*, SEPM (Society for Sedimentary Geology), p. 1-11.
- Stewart, J. H., 1972, Initial Deposits in the Cordilleran Geosyncline: Evidence of a Late Precambrian (<850 m.y.) Continental Separation: *Geological Society of America Bulletin*, v. 83, p. 1345-1360.
- Stockli, D. F., Surpless, B. E., Dumitru, T. A., and Farley, K. A., 2002, Thermochronological constraints on the timing and magnitude of Miocene and Pliocene extension in the central Wassuk Range, western Nevada: *Tectonics*, v. 21.
- Stormer, J. C., and Carmichael, I. S. E., 1971, Fluorine-hydroxyl exchange in apatite and biotite: A potential igneous geothermometer: *Contributions to Mineralogy and Petrology*, v. 31, p. 121-131.
- Stormer, J. C., Pierson, M. L., and Tacker, R. C., 1993, Variation of F and Cl X-ray intensity due to anisotropic diffusion in apatite during electron microprobe analysis: *American Mineralogist*, v. 78, p. 641-648.
- Struhsacker, E., 1980, *Geology of the Beowawe geothermal system, Eureka and Lander Counties, Nevada*, Utah Univ., Salt Lake City (USA). Research Inst.
- Suydam, J. D., 1988, Sedimentology, provenance, and paleotectonic significance of the Cretaceous Newark Canyon Formation, Cortez Mountains, Nevada: Unpub. MSc thesis, Montana State University.
- Tagami, T., 2005, Zircon Fission-Track Thermochronology and Applications to Fault Studies: *Reviews in Mineralogy and Geochemistry*, v. 58, p. 95-122.
- Tagami, T., and O'Sullivan, P. B., 2005, Fundamentals of Fission-Track Thermochronology: *Reviews in Mineralogy and Geochemistry*, v. 58, p. 19-47.

- Taylor, H. P., 1997, Oxygen and hydrogen isotope relationships in hydrothermal mineral deposits: *Geochemistry of hydrothermal ore deposits*, v. 3, p. 229-302.
- Teal, L., and Jackson, M., 2002, Geologic overview of the Carlin Trend gold deposits, *in* Thompson, T. B., Teal, L. and Meeuwig, R.O., ed., *Gold Deposits of the Carlin Trend*, 111: Nevada Bureau of Mines and Geology, p. 9-19.
- Tepper, J. H., and Kuehner, S. M., 1999, Complex zoning in apatite from the Idaho Batholith; a record of magma mixing and intracrystalline trace element diffusion: *American Mineralogist*, v. 84, p. 581-595.
- Theodore, T. G., Armstrong, A. K., Harris, A. G., Stevens, C., and Tosdal, R., 1998, Geology of the northern terminus of the Carlin trend, Nevada: Links between crustal shortening during the Late Paleozoic Humboldt orogeny and northeast-striking faults: Contributions to the gold metallogeny of northern Nevada: US Geological Survey Open-File Report, p. 98-338.
- Theodore, T. G., Moring, B. C., Harris, A. G., Armstrong, A. K., and Finney, S. C., 2003, Nevada Bureau of Mines and Geology Map 143: Geologic map of the Beaver Peak Quadrangle, Elko and Eureka Counties, Nevada, Nevada Bureau of Mines and Geology.
- Thirlwall, M. F., 2000, Inter-laboratory and other errors in Pb isotope analyses investigated using a ^{207}Pb - ^{204}Pb double spike: *Chemical Geology*, v. 163, p. 299-322.
- Thoreson, R. F., 1993, Geology of the Post Deposit, Eureka County, Nevada, 1993, p. 13-15.
- Timmons, J. M., Karlstrom, K. E., Dehler, C. M., Geissman, J. W., and Heizler, M. T., 2001, Proterozoic multistage (ca. 1.1 and 0.8 Ga) extension recorded in the Grand Canyon Supergroup and establishment of northwest- and north-trending tectonic grains in the southwestern United States: *Geological Society of America Bulletin*, v. 113, p. 163-180.
- Tosdal, R., Wooden, J., and Kistler, R., 2000, Geometry of the Neoproterozoic continental break-up, and implications for location of Nevadan mineral belts: *Geology and ore deposits*, p. 451-466.
- Tosdal, R. M., Dilles, J. H., and Cooke, D. R., 2009, From source to sinks in auriferous magmatic-hydrothermal porphyry and epithermal deposits: *Elements*, v. 5, p. 289.
- Tretbar, D. R., Arehart, G. B., and Christensen, J. N., 2000, Dating gold deposition in a Carlin-type gold deposit using Rb/Sr methods on the mineral galkhaite: *Geology*, v. 28, p. 947-950.
- Trexler, J. H., Cashman, P. H., Snyder, W. S., and Davydov, V. I., 2004, Late Paleozoic tectonism in Nevada: Timing, kinematics, and tectonic significance: *Geological Society of America Bulletin*, v. 116, p. 525-538.
- Vandervoort, D. S., and Schmitt, J. G., 1990, Cretaceous to early Tertiary paleogeography in the hinterland of the Sevier thrust belt, east-central Nevada: *Geology*, v. 18, p. 567-570.
- Vaughan, J. R., Hickey, Kenneth, Barker, Shaun, and Dipple, Gregory, 2010, Isotopic Alteration of Carbonate in Carlin-type Au Deposits: Implications for Fluid Flow: GSN Symposium: Great Basin Evolution and Metallogeny, Reno, NV, USA, 2010.
- Volk, J., Weakley, C., Penick, M., and Lander, A., 2001, Structural geology of the Goldstrike property, north-central Nevada: *Geological Society of Nevada Special Publication* v. 33, p. 361-379.

- Wallace, A. R., Perkins, M. E., and Fleck, R. J., 2008, Late Cenozoic paleogeographic evolution of northeastern Nevada: Evidence from the sedimentary basins: *Geosphere*, v. 4, p. 36-74.
- Warren, I., Simmons, S. F., and Mauk, J. L., 2007, Whole-rock geochemical techniques for evaluating hydrothermal alteration, mass changes, and compositional gradients associated with epithermal Au-Ag mineralization: *Economic Geology*, v. 102, p. 923-948.
- Watson, E. B., and Capobianco, C. J., 1981, Phosphorus and the rare earth elements in felsic magmas: an assessment of the role of apatite: *Geochimica et Cosmochimica Acta*, v. 45, p. 2349-2358.
- Watson, E. B., and Green, T. H., 1981, Apatite/liquid partition coefficients for the rare earth elements and strontium: *Earth and Planetary Science Letters*, v. 56, p. 405-421.
- Wells, M. L., Dallmeyer, R. D., and Allmendinger, R. W., 1990, Late Cretaceous extension in the hinterland of the Sevier thrust belt, northwestern Utah and southern Idaho: *Geology*, v. 18, p. 929-933.
- Wells, M. L., and Hoisch, T. D., 2008, The role of mantle delamination in widespread Late Cretaceous extension and magmatism in the Cordilleran orogen, western United States: *Geological Society of America Bulletin*, v. 120, p. 515-530.
- Wells, M. L., Hoisch, T. D., Cruz-Urbe, A. M., and Vervoort, J. D., 2012, Geodynamics of synconvergent extension and tectonic mode switching: Constraints from the Sevier-Laramide orogen: *Tectonics*, v. 31.
- Wernicke, B., 1992, Cenozoic extensional tectonics of the U.S. Cordillera, *in* Burchfiel, B. C., P.W. Lipman, and M.L. Zoback, ed., *The Cordilleran Orogen: Conterminous U.S., The Geology of North America*, G-3: Boulder, Colorado, Geological Society of America, p. 553-582.
- Wernicke, B., Spencer, J. E., Burchfiel, B. C., and Guth, P. L., 1982, Magnitude of crustal extension in the southern Great Basin: *Geology*, v. 10, p. 499-502.
- Wernicke, B. P., England, P. C., Sonder, L. J., and Christiansen, R. L., 1987, Tectonomagmatic evolution of Cenozoic extension in the North American Cordillera: Geological Society, London, Special Publications, v. 28, p. 203-221.
- White, D. E., 1974, Diverse Origins of Hydrothermal Ore Fluids: *Economic Geology*, v. 69, p. 954-973.
- Willett, S. D., 1997, Inverse modeling of annealing of fission tracks in apatite 1: A controlled random search method: *American Journal of Science*, v. 297, p. 939-969.
- Wolf, R. A., Farley, K. A., and Silver, L. T., 1997, Assessment of (U-Th)/He thermochronometry: The low-temperature history of the San Jacinto mountains, California: *Geology*, v. 25, p. 65-68.
- Yigit, O., and Hofstra, A. H., 2003, Lithogeochemistry of Carlin-type gold mineralization in the Gold Bar district, Battle Mountain-Eureka trend, Nevada: *Ore Geology Reviews*, v. 22, p. 201-224.
- Yigit, O., Hofstra, A. H., Hitzman, M. W., and Nelson, E. P., 2006, Geology and geochemistry of jasperoids from the Gold Bar district, Nevada: *Mineralium Deposita*, v. 41, p. 527-547.
- You, C. F., and Bickle, M. J., 1998, Evolution of an active sea-floor massive sulphide deposit: *Nature*, v. 394, p. 668-671.
- Zeitler, P. K., Herczeg, A. L., McDougall, I., and Honda, M., 1987, U-Th-He dating of apatite: A potential thermochronometer: *Geochimica et Cosmochimica Acta*, v. 51, p. 2865-2868.

- Zoback, M. L., Anderson, R., and Thompson, G., 1981, Cainozoic evolution of the state of stress and style of tectonism of the Basin and Range province of the western United States: Philosophical Transactions of the Royal Society of London. Series A, Mathematical and Physical Sciences, v. 300, p. 407.
- Zoback, M. L., McKee, E. H., Blakely, R. J., and Thompson, G. A., 1994, The northern Nevada rift: Regional tectono-magmatic relations and middle Miocene stress direction: Geological Society of America Bulletin, v. 106, p. 371-382.

Appendices

Appendix A **Mineral separation procedures**

Mineral separation was carried out at UBC using modified separation procedures of the PCIGR and Donelick et al. (2005). Approximately 0.5 – 1.0 kg sample rock was passed through a Rhino jaw crusher several times until enough material of sand size or finer was produced. The first samples to be prepared were then ground using a ceramic plate Bico disk grinder, however this was found to cause fragmentation of large whole apatite crystals, making them useless for (U-Th)/He dating. Following recommendations by Donelick et al. (2005), procedures were modified to preserve apatite, which is commonly damaged using grinding/milling methods. For later samples, crushed material was sieved using 300 μm mesh. The fine fraction was then washed in stainless steel pans to remove clays, and air dried at room temperature. Again, the first samples were not ideally processed, being passed across a Wilfley ripple table instead of washing, however this was found to result in loss of smaller apatites and zircons, so the process was abandoned in favour of pan washing.

Once dried, each sample was separated using heavy liquids. Apatite has a specific gravity of 3.15–3.20 g/cm^3 (Donelick et al., 2005). Zircon has a specific gravity of 4.6 g/cm^3 (Reiners, 2005). In a fume hood, the first batch of samples was separated using methylene iodide (MEI), which has a specific gravity of 3.3 g/cm^3 . Approximately 500 ml MEI was poured into a 750 ml glass separation funnel, the dry sample was added and stirred into the MEI with a glass rod and left to separate. The heavy fraction (e.g., zircon, apatite, pyroxene, sulfides, oxides etc.) settled to the bottom and was released into a filter paper-lined Nalgene funnel in a beaker and rinsed with acetone to remove all traces of MEI. The heavy fraction was allowed to dry and then separated for apatite and zircon using a Frantz magnetic separator.

A second batch of samples was separated using lithium metatungstate (LMT), specific gravity 2.95 g/cm^3 . The dry sample was divided into ~0.5 g batches and placed into 50 ml

Nalgene test tubes, which were filled to 42 ml with LMT and centrifuged for several minutes to speed up the separation of heavy and light minerals. The light fraction was poured off, the heavy fraction poured into a filter paper-lined funnel in a beaker and rinsed clean with distilled water. The dried sample was then passed through a Frantz magnetic separator to produce apatite and zircon fractions.

Details of separation procedures at Apatite to Zircon Inc. can be found in Donelick (2005). Samples separated at Apatite to Zircon Inc are crushed, sieved, washed and dried as described above. A first heavy liquid separation is carried out using LMT and a centrifuge. After drying, a second separation is carried out using MEI to separate the apatite and zircon fractions.

Appendix B Sample descriptions, XRD data, whole rock geochemistry data

Descriptions of samples collected for this study are summarised in Table B1.

B.1 XRD analysis

Approximately 1 g of each whole rock sample was hand ground using a pestle and mortar and mixed with ethanol to prepare individual smear mounts. Each sample was run in a Bruker D8 Focus diffractometer for 28 minutes at 50 rpm from angles of 0-80°. Resulting spectra were interpreted using Eva software. 17 samples required glycolation for further analysis of clay minerals. In some cases, where spectra from nearby samples were the same and from the same area, representative samples were run and used as basis for clay analysis in similar samples. Selected samples were heated with glycol in an oven at 60°C for 4 hours. XRD analysis was then repeated as above. New spectra were compared with those originally obtained to identify and interpret diagnostic shifts in peak positions. XRD spectra are included at the end of Appendix B. A summary of alteration minerals is included in Table B2.

B.2 Whole rock geochemistry

Whole rock geochemistry was carried out on 23 samples by ALS Chemex, Vancouver. Major elements were analysed using lithium metaborate fusion decomposition and inductively coupled plasma - atomic emission spectrometry (ICP-AES), at a detection limit of 0.01 wt%. Fire assay ICP-AES was used to analyse Au content, detection limit 0.001 ppm. Trace elements (Ba, Ce, Cr, Cs, Dy, Er, Eu, Ga, Gd, Hf, Ho, La, Lu, Nb, Pr, Rb, Sn, Sr, Ta, Tb, Th, Tl, Tm, U, V, W, Y, Yb, Zr) were analysed using lithium metaborate fusion and LA-ICP-MS. Trace base metals (Ag, As, Cd, Co, Cu, Mo, Ni, Pb, Zn) were analysed using four acid digestion and ICP-AES, detection limits varying 0.01-10 ppm. Results are in Table B3.

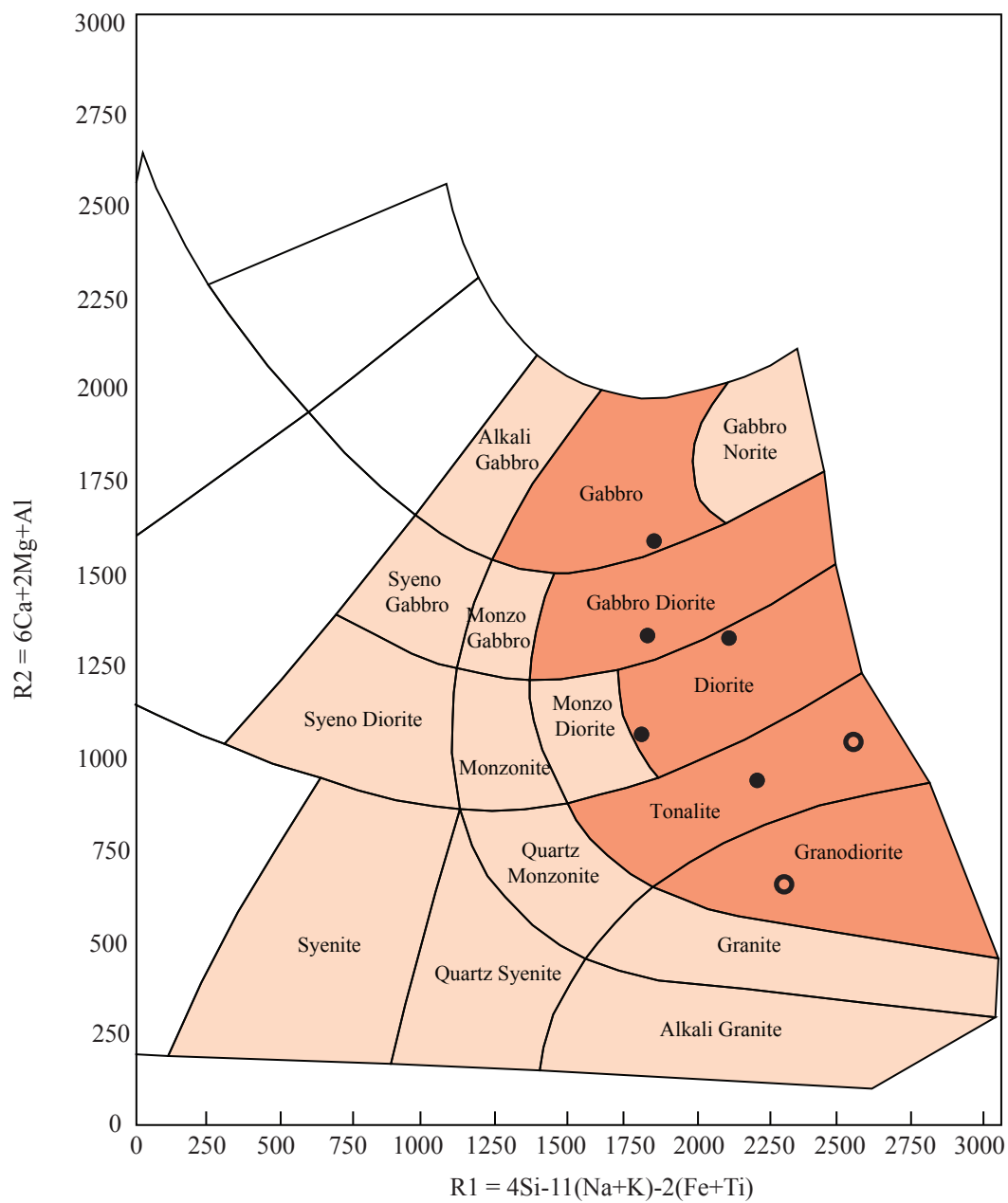


Figure B1 R1-R2 classification of Goldstrike (filled circles) and Little Boulder Stock (open circles) samples based on classification of De La Roche (1980). Although a single intrusion, considerable compositional variation is seen. Goldstrike Stock samples range from gabbro to tonalite, Little Boulder Stock samples from tonalite to granodiorite.

Table B1 Characteristics of samples used in this study


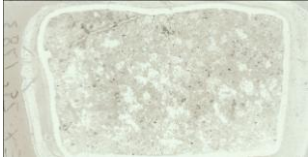



Sample	Area	Thin section	Lithology	Age*	AHe	AFT	ZHe	TS description	Mineralogy	Mineralogy (XRD)	Alteration (XRD)	Treatment	Au (ppm)
Bell-110C-630	Banshee	n/a RC sample	Hbl lamprophyre	~157 Ma	insuff. apatite	insuff. apatite	insuff. zircon	n/a - RC hole	-	Quartz, sanidine, apatite, sericite, chlorite, (smectite?), talc, pyrite, ankerite	Sericite, chlorite?, smectite?, talc	-	0.019
EX-24C-1674	Meikle		Rhyodacite porphyry	~157 Ma	insuff. apatite	insuff. apatite	insuff. zircon	Porphyritic, 1-2mm altered (illite and oxide) phenos (hbl, cpx? From xtal shape) in fine-grained illitised groundmass. Qtz microphenos (smaller than main phenos), pyrite.	5% phenos, 95% groundmass. 1% pyr, 1% oxides, 5% qtz, 93% illite	Quartz, illite	Illite	Glycolated	0.612
EX-29C-1783	Meikle		Rhyodacite porphyry	~157 Ma	4.2 +/- 0.2	35.64 +6.62 - 5.58	34.7 +/- 1.7	Thin section shows plucking, missing sections. Porphyritic, 1 set phenos tabular/laths, replcd by musc(?) cleavage well-preserved. Other phenos more hexagonal x-section, no cleavage preserved, cpx? hbl?. Also cubic oxide rims, cores replaced by arg. TS domiated by v fine arg, some fibrous growth replacing phenos. Qtz microphenos in groundmass. Rel large, whole apatite xtals with inlcusions. Quartz veinlets <1% TS	3% phenos (100% arg), 10% qtz, 1% pyr, 1% oxides, 88% arg	Quartz, illite, kaolinite	Illite, kaolinite	Glycolated	<0.001
GA-34C-1280	Golden April		Hbl lamprophyre	160.76±0.25 Ma (U/Pb Ca-TIMS) (this study)	8.8 +/- 0.7	40.7 +10.5 - 8.4	73.0 +/- 0.5	Porphyritic - phenos 2-3mm, v fine groundmass. Phenos 100% replaced by v fine ser, finer than in groundmass: 1 set tabular, well-defined cleavage replaced by musc (once bio?). other set hexagonal/rhombic replaced by v fine musc (hbl? Cpx?). Carbonate also in groundmass. Most of TS replaced by musc. Pyrite, oxides. Accessory zircon, apatite.	3% phenos (replaced by arg), 5% qtz, 1% pyr, 1% oxides, 5% calcite, 85% arg	Quartz, plag, sanidine, sericite, chlorite, smectite, ankerite	Sericite, chlorite+ smectite	-	<0.001
GA-35C-1265	Golden April		Hbl lamprophyre	~157 Ma	23.0 +/-0.5	30.8 +4.4 - 3.6	98.2 +/-1.6	Porphyritic hbl laths partially altered cores, not extensively altered. Quartz xenoliths. Fine groundmass of plag(?), sericitized cores.	3% hbl phenos, 5% qtz, 1% pyr, 1% oxides, 5% calcite, 15% plag, 70% arg	Quartz, plag, sanidine, phlog/bio, chlorite, (smectite), talc, calcite, dolomite	Chlorite+ smectite, talc	-	-
GA-52C-1585	Golden April		Hbl lamprophyre	~157 Ma	insuff. apatite	40.0 +10.7 - 8.5	insuff. zircon	V fine grained, porphyritic, phenos ≤1 mm. Mafic (hbl? From shape) phenos 100% replaced by ser, qtz, chlorite. Pyrite and oxide mineral associated with former mafic phenos => liberated Fe. Trace apatite. Sample totally overprinted by qtz, ser, arg alt, carbonate, original texture mostly preserved.	45% qtz, 50% arg (ser, arg). 3% chlorite, 2% carbonate. Trace pyr, oxide, apatite	Quartz, plag, apatite, sericite, chlorite, (smectite), dolomite	Sericite, chlorite+ smectite	-	<0.001

Table B1 Characteristics of samples used in this study


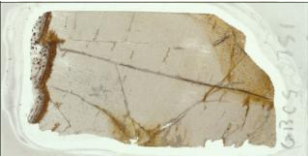
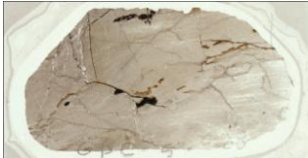
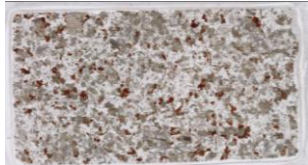
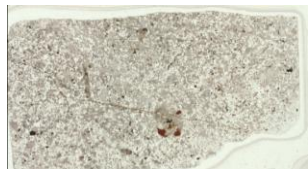
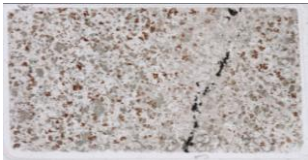
Sample	Area	Thin section	Lithology	Age*	AHe	AFT	ZHe	TS description	Mineralogy	Mineralogy (XRD)	Alteration (XRD)	Treatment	Au (ppm)
GBC-5-1444	Post Fault		Hbl lamprophyre	~157 Ma	insuff. apatite	insuff. apatite	insuff. zircon	Very fine-grained Qtz, carbonate, illite groundmass. Porphyritic, plag(?) laths totally replaced but refl light shows pheno outlines are lathlike, possible remnants of zoning. Patches undulose ext quartz. Musc(?) replacing POSSIBLE hbl phenos? And much of groundmass. Pyrite and arsenopyrite? Some zoning observed...Aspyr core with pyr rim? Accessory rutile. <1% Qtz veinlets up to 1mm wide	15% Qtz, 20% carbonate, 5% pyr/Aspyr, 60% arg (ill) accessory rutile.	Quartz, anatase, illite, ankerite	Illite	Glycolated	0.555
GBC-5-751	Post Fault		Lamprophyre?	~157 Ma	insuff. apatite	insuff. apatite	74.3 +/-1.9	V fine grained. Qtz and arg dom. Microphenos rext Qtz in arg-dom matrix that possibly shows developing fabric?? Fe staining along fractures. See minor offset on fracture (normal motion), infilling by silvery-grey metallic phase in places, multiple stages of vein growth visible (metallic and oxides), selvage around veinlet arg? Veinlets 2-3% TS, <=1mm wide. Disseminated metallic phase. Oxidation on and out from fracture exploiting layering (or fabric)	50% Qtz, 45% arg. 5% metallic, metal oxide and Fe staining	Quartz, sanidine, illite	Illite	Glycolated	0.004
GBC-5-928	Post Fault		Lamprophyre?	~157 Ma	insuff. apatite	25.8 +20.3 - 11.4	insuff. zircon	V fine grained, sed layering or alginment fabric?? Quartz microphenos (rext?) not aligned/oriented. arg (+carbonate??) subtly define fabric. Totally altered by v fine arg/illite. Hematite at veinlet intersections, on veinlets that x-cut Qtz veinlets with selvage. Veinlets 2%? TS<1mm wide	5% hematite, 10% Qtz, 85% arg	Quartz, anatase, illite, ankerite	Illite		0.009
GS-1765C-782	Goldstrike Stock		Granodiorite (gabbro diorite)	~158 Ma	insuff. apatite	36.1 +5.9 - 5.1	66.9 +/-2.1	Fine-medium-grained, equigranular, hypidiomorphic. Chlorite after bio, hbl (greenish in PPL), chl also associated with arg (smect?). Oxidation on edges of bio. Diffuse edges of large plag laths (polysynth twinned, no comp zoning) where surrounded by quartz, sign of minor silicification/resorption? V fine musc replacing plag. Abundant apatite, zircon accessory minerals. Silica veinlets <1mm wide. Arg on HS fracture faces	5% hbl, 3% bio, 5% chl, 12% musc/ser, 15% Qtz, 60% plag (+ksp?)	Quartz, plag, sanidine, hornblende, sericite, chlorite, (smectite), calcite	Sericite, chlorite+ smectite	-	0.009
GS-1814C-1595	Goldstrike Stock		Granodiorite	~158 Ma	31.5 +/- 0.5	23.8 +4.5 - 3.8	83.2 +/-4.1	Very-fine-grained, inequigranular, hypidiomorphic. Rext fine-grained quartz, pervasive sericitization of fsp (no laths remain), fibrous sericite(?) replacing bio, minor chl. Opaques, pyrite as xtals and in veinlets. Accessory apatite assoc with quartz. HS arg (smect, chl, musc?) and Fe-ox stained fracture faces	1% hbl, 1% bio, 1% chl, 1% pyr, 1% oxides, 50% Qtz, 45% arg (musc, smect)	Quartz, plag, orthoclase, hornblende, sericite, chlorite, calcite	Sericite, chlorite+ smectite	-	-
GS-1818C-1000	Goldstrike Stock		Granodiorite (diorite)	~158 Ma	32.3 +/-0.7	51.3 +6.2 - 5.5	69.4 +/- 2.5	Fine-grained, inequigranular, hypidiomorphic. Chl after biotite, chl after hbl (minor phase), range plag lath (lamellar twinning) sizes, partial resorption by quartz, polysynthetic twinning. Oxidation on edges of bio. Fibrous, in some places radial, arg (musc/ser?) after fsp, commonly replacing fsp cores. Calcite in patches. Pyrite as isolated xtals and in veinlets, showing minor comp'l variation (refl light - growth?). Abundant accessory apat and zirc	<1% hbl, 5% bio, 5% chl, 15% arg, 40% plag, 1% pyr, 33% quartz	Quartz, plag, sanidine, hornblende, phlog/bio, chlorite, (smectite), calcite	Chlorite+ smectite	-	0.016

Table B1 Characteristics of samples used in this study



Sample	Area	Thin section	Lithology	Age*	AHe	AFT	ZHe	TS description	Mineralogy	Mineralogy (XRD)	Alteration (XRD)	Treatment	Au (ppm)
LBB100-4679	Little Boulder Basin Stock	n/a sample used up	Granodiorite	~158 Ma	not dated	78.4 +23.3 -18.0	not dated	n/a	-	Quartz, apatite, pyrite, anatase, rutile, sericite, kaolinite, dolomite	Sericite, kaolinite		-
LBB102-1940	Little Boulder Basin Stock	n/a sample used up	Granodiorite	~158 Ma	insuff. apatite	62.4 +10.1 8.9	83.8 +/- 2.8	n/a	-	Quartz, plag, orthoclase, hornblende, phlog/bio, chlorite, smectite, calcite	Chlorite+smectite, sericite	Glycolated	-
LBB102-3050	Little Boulder Basin Stock	n/a sample used up	Granodiorite	~158 Ma	not dated	94.9 +12.9 11.4	not dated	n/a	-				
LBB102-3900	Little Boulder Basin Stock	n/a sample used up	Granodiorite (tonalite)	~158 Ma	insuff. apatite	66.8 +7.6 6.8	87.2 - +/-1.1	n/a	-	Quartz, plag, orthoclase, hornblende, cpx?, phlob/bio, chlorite, pyrophyllite, calcite	Chlorite+smectite, sericite, pyrophyllite	Glycolated	0.016
LBB102-6090	Little Boulder Basin Stock		Granodiorite	~158 Ma	insuff. apatite	insuff. apatite	66.7 +/-1.2 (single xtal only)	V fine gr, porphyritic, euhedral-subhedral. Phenos are qtz cumulates., G/mass very fine, ser? arg? Replacing plag laths	Qtz 15%, 85% arg. Trace cubic pyrite	Quartz, plag, orthoclase, hornblende, cpx?, apatite, chlorite, smectite, calcite	Chlorite+smectite	Glycolated	-
LBB76-1038	Little Boulder Basin Stock	n/a sample used up	Granodiorite	~158 Ma	67.0 +/-1.4	68.3 +7.9 7.1	107.3 - +/-2.3	n/a	-	Quartz, plag, sanidine, sericite, chlorite, (smectite), calcite,	Chlorite+smectite, talc	-	0.16
LBB76-1228	Little Boulder Basin Stock	n/a sample used up	Granodiorite	~158 Ma	not dated	88.7 +9.8 8.8	not dated	n/a	-				
LBB76-343	Little Boulder Basin Stock		Granodiorite	~158 Ma	69.7 +/-1.6	126.0 +13.7 12.3	154.1 - +/-14.8	Medium gr, equigranular, euhedral xtals plag, hbl, bio. Plag xtals polysynthetically twinned. Chl + smect after hbl. Otherwise fresh	Qtz 40%, plag 40% ksp 5%, Hbl 3%, bio 5%, chl 5%, smect 2%	Quartz, plag, sanidine, hornblende, phlogopite/bio, apatite, chlorite, smectite, talc, ankerite	Chlorite+smectite, talc	Glycolated	-

Table B1 Characteristics of samples used in this study




Sample	Area	Thin section	Lithology	Age*	AHe	AFT	ZHe	TS description	Mineralogy	Mineralogy (XRD)	Alteration (XRD)	Treatment	Au (ppm)
LBB76-576.5	Little Boulder Basin Stock	n/a no sample remaining	Granodiorite	~158 Ma	not dated	94.9 +9.9 - 9.0	not dated	n/a	-	Quartz, plag, sanidine, hornblende phlogopite/bio, pyrophanite, chlorite, smectite, talc	Chlorite+ smectite, talc	Glycolated	-
LBB76-762	Little Boulder Basin Stock		Granodiorite	~158 Ma	not dated	81.3 +11.4 - 10.0	not dated	Fine gr, inequigranular, subhedral xtals. All fsp argillized. Qtz (rext?) remains abundant	50% qtz, 50% arg (ser, arg). Trace titanite?ilm?	Quartz, plag, orthoclase, sericite, kaolinite	Sericite, kaolinite	-	-
RM91-11C-225	Goldstrike Stock		Granodiorite (tonalite)	~158 Ma	insuff. apatite	60.1 +9.2 - 7.9	79.9 +/-2.4	Very fine-fine-grained, inequigranular, hypidiomorphic. Chl after biotite (oxidised edges), chl after hbl (greenish in PPL), range plag lath (lamellar twinning, zoning) sizes. V fine arg (musc/ser?) of fsp cores. Magnetite(?) assoc with bio. Interstitial quartz, minor resorption of fsp by qtz. Abundant accessory ap, some accessory zircon	2% hbl, 5% bio, 3% chl, 60% fsp, 15% qtz, 15% arg/ser, <1% mag	Quartz, plag, orthoclase, hornblende, phlog/bio, chlorite, smectite, calcite	Chlorite+ smectite	Glycolated	2.19
RM91-22C-1460	Goldstrike Stock	n/a sample used up	Granodiorite (gabbro)	~158 Ma	insuff. apatite	20.9 +15.6 - 8.9	76.2 +/- 3.1	n/a	-	Quartz, plag, sanidine, hornblende, sericite, chlorite, (smectite), barite, calcite	Sericite, chlorite+ smectite	-	<0.001
RM94-03C-639	Goldstrike Stock	n/a sample used up	Granodiorite (diorite)	~158 Ma	20.3 +/-0.7	61.5 +12.0 - 10.0	77.3 +/-1.4	n/a	-	Quartz, plag, orthoclase, phlog/bio, sericite, chlorite, (smectite), calcite	Sericite, chlorite+ smectite	-	<0.001
RM98-04C-459	Goldstrike Stock		Granodiorite	~158 Ma	27.3 +/- 0.5	39.4 +9.1 - 7.4	not dated	Fine-medium-grained, equigranular, hypidiomorphic, 2% hbl, 3% bio, 5% chl, chl after bio. Twinned, zoned plag, partial replacement by ser/arg, in zoned xtals seems selective in some zones, in fsp tends to be most extensive in cores. Partial resorption of plag laths by quartz. Exsolution(?) of opaque phase in bio. Accessory apatite and zircon.	2% hbl, 5% bio, 5% chl, 10% musc/ser, 15% qtz, 63% plag (+ksp?)	Quartz, plag, orthoclase, hornblende, phlog/bio, sericite, chlorite, (smectite), calcite	Sericite, chlorite+ smectite	-	-

Table B1 Characteristics of samples used in this study

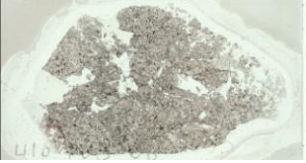
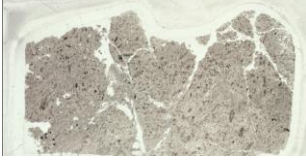




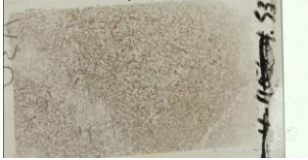



Sample	Area	Thin section	Lithology	Age*	AHe	AFT	ZHe	TS description	Mineralogy	Mineralogy (XRD)	Alteration (XRD)	Treatment	Au (ppm)
RM98-04C-956	Goldstrike Stock	n/a	Granodiorite	~158 Ma	insuff. apatite	not dated	64.4 +/- 1.2	n/a	-	Quartz, plag, orthoclase, hornblende, phlog/bio, sericite, chlorite, (smectite)	Sericite, chlorite+smectite	-	-
U10-P05-06-1055	Post Fault		Lamprophyre	~157 Ma	insuff. apatite	insuff. apatite	insuff. zircon	BX. Clasts mm-scale, subrounded. Comprise rext qtz, calcite, oxides, arg on frags. Disseminated sub-mm pyr, not cubic, not replacing laths.	20% qtz, 20% carbonate, 2% pyr, 58% arg	Quartz, anatase, marcasite, apatite, illite, calcite, ankerite	Illite	-	-
U10-P05-06-319	Post Fault		Hbl lamprophyre	~157 Ma	insuff. apatite	29.6 +10.9 - 8.0	insuff. zircon	BX, clasts cm-scale. Totally arg, possible hint of replaced phenos (hbl? By morph) by brownish arg (kaol, smect+chl?), ser+quartz in groundmass, microphenos plag laths (?) totally ser and arg. Pyrite replacing fibrous min as in U12-814. Minor oxides	5% phenos (once hbl??? Totally arg and pyr replaced), 3% pyr, 20% qtz, 72% ser/arg	Quartz, pyrite, arsenopyrite, anatase, jarosite, sericite, dickite/kaol, chlorite, smectite, calcite, ankerite	Sericite, chlorite (+smectite), kaol/dickite	Glycolated	0.237
U10-P05-06-577	Post Fault		Lamprophyre	~157 Ma	10.3 +/-0.4	29.0 +5.3 - 4.5	insuff. zircon	Large pyrite replacing 1/4 TS, pyrite replacing plag laths throughout TS. Subrounded quartz phenos display undulose extinction, fracturing, some pyr along intracrystal fractures. Large Ksp(?) pheno, 2mm. Groundmass mostly sericite and quartz, very fine grained. No other discernible phenos or texture	30% pyr, 1% ksp, 20% quartz, 49% arg	Quartz, anatase, marcasite, illite, dickite/kaol, jarosite, gypsum	Illite, kaol/dickite	Glycolated	-
U12-P05-16-1303	Post Fault		Lamprophyre	~157 Ma	insuff. apatite	20.4 +3.3 - 2.9	insuff. zircon	BX??clasts mm scale. Subangular clasts 2-5mm comprising fine-med gr rext qtz and arg (some musc, see patches high biref colours). Clasts supported, clasts separated by "veinlets" of arg matrix. Disseminated cubic pyrite <0.1mm through. Minor oxides, more assoc with matrix. Hint of phenos (mafic mins??) totally arg, approx 1mm but not distinct.	2% pyr, 20% quartz, 78% arg	Quartz, illite, kaolinite	Illite, kaolinite	-	-
U12-P05-16-271	Post Fault		Hbl lamprophyre	~157 Ma	insuff. apatite	44.2 +22.7 - 15.0	insuff. zircon	Refl light shows original texture equigranular, tabular plag(?) laths with undulose fine quartz. Plag now sericitised. Pyrite, minor rutile, skinny prismatic apatite as accessories	15% quartz, 3% pyr, 2% oxides, 80% arg	Quartz, rutile, pyrite, sericite, chlorite, kaolinite	Sericite, chlorite+smectite, kaolinite	-	0.012

Table B1 Characteristics of samples used in this study

Sample	Area	Thin section	Lithology	Age*	AHe	AFT	ZHe	TS description	Mineralogy	Mineralogy (XRD)	Alteration (XRD)	Treatment	Au (ppm)
U12-P05-16-814	Post Fault		Hbl lamprophyre	~157 Ma	insuff. apatite	insuff. apatite	insuff. zircon	Refl light shows original texture porphyritic once? tabular plag(?) laths replaced by sericite, carbonate? Groundmass sericite, carbonate with undulose fine quartz. Pyrite replacing hbl, bio? Evidence of S fluid passing through rock? minor rutile, skinny prismatic apatite as accessories	15% quartz, 15% carbonate, 3% pyr, 2% oxides, 65% arg	Quartz, rutile, pyrite, marcasite, apatite, sericite, kaolinite	Sericite, kaolinite	-	-
U16-H07-34-537	Banshee		Hbl lamprophyre	~157 Ma	insuff. apatite	62.9 +14.3 - 11.7	183.9 +/-61.2	Porphyritic. Fresh euhedral 1-2 mm hbl lath phenos, v minor argillization on pheno edges/fractures (minimal). Fine g/mass sub-anhedral fsp (plag?) sericitised cores. Minor silification of g/mass? Hard to determine due to small xt size. Carbonate xenoliths? Accessory needle-like apatite. Trace pyrite.	5% hbl phenos, 95% plag-dominated groundmass. ~60% feldspar xtals	Quartz, plag, hornblende, phlog/bio, chlorite, (smectite), illite, calcite	Chlorite+smectite, illite	-	0.001
U16-H07-63-976	Banshee		Lamprophyre	~157 Ma	insuff. apatite	insuff. apatite	insuff. zircon	Porphyritic, altered phenos <1mm, groundmass very fine-grained. Chlorite and carbonate after hbl phenos, hbl almost entirely replaced. Quartz, sericitised plag laths and calcite make up groundmass. Trace pyr	Phenos 2%, all altered (once hbl)?, 15% chl, 20% qtz, 20% carbonate, 53% arg. Trace pyr	Quartz, plag, actinolite, apatite, rutile, sericite, chlorite, smectite, calcite, ankerite	Sericite, chlorite+smectite	Glycolated	0.006
U16-H07-68-247	Banshee		Rhyodacite porphyry	~157 Ma	insuff. apatite	insuff. apatite	45.2 +/-2.0	Porphyritic, altered phenos 1-2mm 100% replaced by illite+oxides, from morph probably hornblende and fsp. Partial resorption by silica, rext silica rims on some phenos. Groundmass incl microphenos of quartz, dominated by illite. Carbonate patches. Pyrite minor.	3% phenos (totally illitised), 5% quartz, 2% pyr, 5% dolomite, 85% arg (illite)	Quartz, illite, smectite?, dolomite	Illite	-	0.673
Viv-B	Vivian Sill	n/a sample used up	Granodiorite	~158 Ma	not dated	124.7 +14.2 -16.1	not dated	n/a	-	Quartz, plag, hornblende, cpx?, phlog/bio, apatite, zircon	-	-	-
WB-04C-720	Golden April		Lamprophyre?	~157 Ma	3.6 +/-0.2	28.2 +14.7 - 9.7	60.6 +/- 8.2	Porphyritic - phenos 1-2mm, some clustering of phenos. Qtz microphenos 1.5mm, subrounded, undulose extinction. 1 set phenos mica (now musc, good cleavage), 1 set totally replaced by arg. (carbonate?) and minor oxides. Micropheno laths, also totally replaced. Groundmass very fine, argillized (once plag??). Pyrite and oxides present.	5% phenos (100% ser+carb?), 2% qtz microphenos, 5% musc phenos, 1% pyr, 10% carbonate, 77% arg	Quartz, anatase, sericite, smectite, pyrite, ankerite	Illite, smectite	-	0.001

* Age estimates based on:

Granodiorite 157.7 +/-0.4 Ma to 159.1 +/-4.4 Ma (Mortensen et al., 2000)

Lamprophyre ~157 (Ressel and Henry, 2006)

Table B2 Summary of clay alteration minerals identified using XRD

	Illite	Sericite	Kaolinite	Smectite	Chlorite	Talc	Comparative spectrum if not glycolated
GS-1765C		x		i	x		RM91-11C
GS-1814C		x		i	x		RM91-11C
GS-1818C				i	x		RM91-11C
RM91-11C*				x	x		
RM91-22C		x		i	x		RM91-11C
RM94-03C-639		x		i	x		RM91-11C
RM98-04C-459		x		i	x		RM91-11C
RM98-04C-956		x		i	x		RM91-11C
LBB76-343*				x	x		
LBB76-576*				x	x	x	
LBB76-762		x	x				
LBB76-1038		x		i	x		
LBB102-1940*				x	x		
LBB102-3900*				x	x		
LBB102-6090*				x	x		
Viv-B				x	x		
GA-34C	x			x	x		
GA-35C	x			i	x		GA-34C
WB-04C	x						EX-24C
GA-52C	x			x	x		GA-34C
EX-29C*	x		x				
U10-P05-06-319	?		x	x	x		
U10-P05-06-577	x		x				
U12-P05-16-271	?		x				
U12-P05-16-1303	x		x				
GBC5-751*	x						
GBC5-928	x		x				GBC5-751
GBC5-1444	x						GBC5-751
U16-H07-34					x		
U16-H07-68*	x						

* glycolated samples

i inferred present based on comparative treated sample spectrum

Table B3. Whole rock geochemical analyses of Jurassic intrusive rocks in samples from the Northern Carlin Trend

Sample		Average fresh granodiorite	Average fresh lamprophyre	Goldstrike Stock				
				GS-1765C-782*	GS-1818C-1000	RM91-11C-225	RM91-22C-1460*	RM94-03C-639*
Lithology				Granodiorite	Granodiorite	Granodiorite	Granodiorite	Granodiorite
East		-	-	553414	553084	553173	552124	552751
North		-	-	4534581	4535070	4535757	4536211	4535590
Elev	m	-	-	1292	1504	1650	1269	1525
Depth	m	-	-	239	305	69	445	195
SiO ₂	%	53.83	48.20	54.40	63.00	58.30	51.20	55.90
Al ₂ O ₃	%	15.10	13.00	15.40	14.50	14.95	14.60	15.30
Fe ₂ O ₃	%	7.87	8.18	8.20	2.16	6.13	8.28	7.12
CaO	%	7.60	7.53	7.19	6.13	4.89	8.69	6.93
MgO	%	6.17	8.83	5.26	2.47	2.44	7.53	5.72
Na ₂ O	%	2.67	2.09	2.68	2.48	2.04	2.58	2.75
K ₂ O	%	2.01	1.92	2.56	6.16	3.24	1.68	1.79
Cr ₂ O ₃	%	0.03	0.08	0.02	0.01	0.01	0.04	0.03
TiO ₂	%	1.09	1.18	1.12	0.80	0.96	1.22	0.94
MnO	%	0.13	0.11	0.15	0.05	0.09	0.12	0.11
P ₂ O ₅	%	0.25	0.34	0.22	0.17	0.28	0.34	0.20
SrO	%	0.09	0.12	0.08	0.09	0.07	0.10	0.09
BaO	%	0.11	0.28	0.20	0.14	0.13	0.06	0.08
C	%	0.19	1.08	0.19	0.34	0.60	0.21	0.17
S	%	0.17	0.11	0.14	0.05	1.17	0.36	0.02
LOI	%	3.00	6.99	2.45	1.99	4.61	3.84	2.70
Total	%	100.03	98.90	99.90	100.00	98.10	100.50	99.70
Ba	ppm	852	2510	1290	1155	866	570	696
Ce	ppm	98	150	81	117	104	132	83
Cr	ppm	203	540	110	40	30	270	230
Cs	ppm	2.92	3.90	4.81	2.42	17.10	1.84	2.10
Dy	ppm	5.19	5.40	4.26	4.24	4.59	6.72	4.58
Er	ppm	2.73	2.39	2.38	2.44	2.61	3.43	2.38
Eu	ppm	2.03	2.78	1.78	1.86	1.99	2.58	1.72
Ga	ppm	18.6	15.5	19.6	17.2	18.9	18.8	17.3
Gd	ppm	6.43	7.32	6.07	7.02	6.88	8.16	5.05
Hf	ppm	5.7	5.3	6.3	6.6	6.1	5.9	4.9
Ho	ppm	1.02	0.97	0.83	0.83	0.86	1.33	0.91
La	ppm	46.8	76.7	41.8	61.5	53.4	56.7	41.8
Lu	ppm	0.39	0.32	0.34	0.33	0.33	0.50	0.34
Nb	ppm	16.9	19.2	16.2	20.9	16.8	20.9	13.5
Nd	ppm	43.633	63.8	33.6	45.5	42.8	63	34.3
Pr	ppm	11.89	17.60	9.09	12.70	11.65	16.90	9.69
Rb	ppm	69.5	55.5	96.7	212.0	129.5	53.3	58.5
Sm	ppm	8.27	11.95	6.30	7.57	7.66	11.75	6.77
Sn	ppm	1	2	1	2	2	2	1
Sr	ppm	726	964	670	760	629	819	688
Ta	ppm	1.0	1.1	1.0	1.4	1.1	1.1	0.8
Tb	ppm	0.93	1.01	0.78	0.85	0.87	1.22	0.78
Th	ppm	8.23	12.55	9.49	19.70	11.60	6.95	8.25
Tl	ppm	<0.5	0.6	<0.5	<0.5	1.5	<0.5	<0.5
Tm	ppm	0.40	0.35	0.33	0.33	0.34	0.52	0.35
U	ppm	2.30	3.10	3.01	5.24	4.18	1.82	2.07
V	ppm	180	182	187	94	139	190	162
W	ppm	2	2	3	3	14	<1	1
Y	ppm	27.3	25.9	22.4	22.6	23.4	35.9	23.5
Yb	ppm	2.55	2.12	2.19	2.16	2.24	3.28	2.18
Zr	ppm	206	202	248	251	231	182	189
As	ppm	12.5	NSS	2.2	2.6	3.5	7.5	27.8
Bi	ppm	0.06	NSS	0.09	0.08	0.73	0.03	0.07
Hg	ppm	0.018	NSS	0.024	0.068	0.033	0.011	<0.005
Sb	ppm	0.237	NSS	0.36	0.39	0.27	0.13	0.22
Se	ppm	0.433	NSS	0.60	0.50	1.80	0.40	0.30
Te	ppm	0.020	NSS	0.02	0.02	0.11	0.02	<0.01
Au	ppm	0.002	0.001	0.006	0.016	2.190	0.001	0.001
Ag	ppm	<0.5	<0.5				<0.5	<0.5
Cd	ppm	<0.5	<0.5				<0.5	<0.5
Co	ppm	26	33				30	22
Cu	ppm	16	62				19	13
Mo	ppm	2	1				<1	2
Ni	ppm	68	164				93	42
Pb	ppm	11	6				10	11
Zn	ppm	93	70				105	80
ΣREE	ppm	273	362				331	215
K/Al	molar	0.14	0.16	0.18	0.46	0.23	0.12	0.13
(2Ca+Na+K)/Al		1.35	1.48	1.32	1.51	1.05	1.50	1.25

* samples used to calculate average fresh values

u.g. underground hole

Major elements determined by ICP-AES following lithium metaborate fusion

Base metals determined by ICP-AES following 4 acid digestion

Trace elements determined by LA-ICP-MS following lithium metaborate fusion

Table B3. continued

Sample	Little Boulder Stock		Golden April			
	LBB76-1038	LBB102-3900	GA-34C-1280	GA-52C-1585	WB-04C-720	EX-29C-1783
Lithology	Granodiorite	Granodiorite	Lamprophyre	Lamprophyre	Lamprophyre	Rhyodacite por
East	555563	555003	550153	550481	550157	552027
North	4532983	4534762	4537827	4538654	4537501	4539222
Elev	1469	551	1226	1208	1382	1122
Depth	275	1189	385	455	219	543
SiO ₂	67.00	60.40	64.80	52.40	69.70	71.70
Al ₂ O ₃	14.25	13.90	14.60	14.50	14.25	15.80
Fe ₂ O ₃	3.35	5.93	3.07	6.40	3.20	1.88
CaO	2.63	5.58	3.55	5.87	1.94	0.41
MgO	1.88	3.48	1.45	3.16	1.07	0.43
Na ₂ O	2.71	2.10	1.62	2.19	0.03	0.05
K ₂ O	4.66	2.32	3.48	2.87	3.91	2.72
Cr ₂ O ₃	0.01	0.01	<0.01	<0.01	<0.01	<0.01
TiO ₂	0.61	0.82	0.49	1.06	0.49	0.45
MnO	0.02	0.10	0.08	0.10	0.06	0.01
P ₂ O ₅	0.14	0.25	0.15	0.31	0.16	0.21
SrO	0.05	0.08	0.05	0.15	0.02	<0.01
BaO	0.13	0.08	0.11	0.10	0.04	0.18
C	0.43	0.40	1.35	2.31	0.81	0.04
S	0.37	0.53	0.30	0.40	1.57	0.07
LOI	3.76	6.33	8.14	10.65	6.18	5.20
Total	101.00	101.50	101.50	99.80	101.00	99.00
Ba	1145	1145	1050	888	397	1585
Ce	124	105	117	177	122	98
Cr	50	50	<10	10	<10	<10
Cs	6.01	8.32	6.54	8.17	5.01	9.11
Dy	3.97	4.45	3.44	5.30	3.49	3.51
Er	2.03	2.34	1.81	2.50	1.93	1.84
Eu	1.32	1.74	1.43	2.81	1.43	1.39
Ga	16.2	16.6	16.0	18.2	15.7	18.6
Gd	4.36	5.13	3.81	7.06	3.66	3.85
Hf	7.9	5.4	6.0	6.0	6.6	6.2
Ho	0.76	0.86	0.68	1.00	0.71	0.70
La	66.5	56.1	66.8	93.3	68.7	52.8
Lu	0.32	0.34	0.33	0.36	0.34	0.31
Nb	23.1	16.3	26.4	19.4	27.1	19.2
Nd	41.6	40.8	37.6	69.3	39.1	36.6
Pr	13.10	11.85	12.10	19.95	12.50	10.95
Rb	199.0	83.3	107.0	90.0	143.0	101.0
Sm	6.96	7.51	6.07	11.95	6.17	6.68
Sn	2	2	1	2	2	2
Sr	414	639	409	1190	183	23
Ta	1.8	1.0	1.7	1.2	1.9	1.3
Tb	0.71	0.78	0.59	1.01	0.62	0.64
Th	30.70	12.75	16.65	18.80	17.30	12.55
Tl	<0.5	0.6	0.5	<0.5	3.9	1.6
Tm	0.32	0.36	0.29	0.38	0.30	0.29
U	8.91	3.84	4.79	4.07	4.87	4.72
V	70	169	42	158	41	38
W	1	11	1	1	5	5
Y	21.6	22.9	19.0	26.3	20.0	20.1
Yb	2.04	2.24	1.95	2.43	2.07	1.89
Zr	294	198	243	225	259	236
As	11.2	>250	29.1	9.5	>250	4.5
Bi	0.18	0.09	0.07	0.03	0.04	0.06
Hg	<0.005	0.187	0.020	0.012	2.240	0.229
Sb	1.21	3.50	0.22	0.26	2.86	0.47
Se	0.70	0.90	0.20	0.60	0.20	0.20
Te	0.01	0.02	<0.01	<0.01	<0.01	<0.01
Au	0.160	0.001	<0.001	<0.001	0.001	<0.001
Ag	<0.5	<0.5	<0.5	<0.5	<0.5	<0.5
Cd	<0.5	<0.5	<0.5	<0.5	<0.5	<0.5
Co	8	14	4	15	180	5
Cu	37	25	2	6	7	4
Mo	3	4	1	1	2	2
Ni	19	18	3	5	4	5
Pb	11	39	18	37	14	8
Zn	32	86	51	78	52	53
ΣREE	291	260	275	417	284	243
K/Al	0.35	0.18	0.26	0.21	0.30	0.19
(2Ca+Na+K)/Al	1.00	1.16	0.88	1.20	0.55	0.24

* samples used to calculate average fresh values

Major elements determined by ICP-AES following lithium metaborate fusion

Trace elements determined by LA-ICP-MS following lithium metaborate fusion

Table B3. continued

Sample	Banshee		Post fault			
	U16-H07-34-536	U16-H07-68-247	U10-P05-06-319	GBC5-751	GBC5-928	GBC5-1444
Lithology	Lamprophyre	Rhyodacite por	Lamprophyre	Lamprophyre	Lamprophyre	Lamprophyre
East	551714	551772	552601	552789	552789	552789
North	4539813	4539736	4537263	4537599	4537599	4537599
Elev	1259	1063	1255	1635	1355	1198
Depth	401	597	445	229	283	440
SiO ₂	48.20	71.10	62.90	80.00	84.20	46.00
Al ₂ O ₃	13.00	14.80	14.40	8.89	8.52	13.70
Fe ₂ O ₃	8.18	1.78	4.72	3.25	1.33	6.00
CaO	7.53	1.48	2.58	0.20	0.15	7.60
MgO	8.83	0.81	0.95	1.04	0.82	4.35
Na ₂ O	2.09	0.03	0.04	0.04	0.03	0.03
K ₂ O	1.92	4.09	2.33	2.94	2.37	3.71
Cr ₂ O ₃	0.08	<0.01	0.03	0.01	0.01	0.04
TiO ₂	1.18	0.28	1.08	0.41	0.37	1.02
MnO	0.11	0.03	0.02	0.01	0.01	0.11
P ₂ O ₅	0.34	0.09	0.47	0.13	0.09	0.25
SrO	0.12	0.01	0.01	0.01	<0.01	0.03
BaO	0.28	0.03	0.32	0.11	0.08	0.08
C	1.08	0.56	0.56	0.04	0.03	3.15
S	0.11	0.47	3.27	0.02	<0.01	2.51
LOI	6.99	5.10	8.77	3.80	2.83	14.80
Total	98.90	99.60	98.60	101.00	101.00	97.70
Ba	2510	316	2910	1055	766	723
Ce	150	53	145	51	47	68
Cr	540	10	200	50	50	300
Cs	3.90	8.05	6.52	11.50	6.54	6.77
Dy	5.40	1.89	4.43	2.98	2.51	3.97
Er	2.39	0.95	2.22	1.61	1.49	2.10
Eu	2.78	0.72	2.27	0.82	0.62	1.49
Ga	15.5	16.1	16.1	12.1	11.3	15.2
Gd	7.32	2.10	5.90	3.08	2.44	4.53
Hf	5.3	4.1	6.0	5.2	6.0	4.7
Ho	0.97	0.37	0.87	0.60	0.53	0.79
La	76.7	32.3	78.6	28.7	27.1	33.8
Lu	0.32	0.15	0.33	0.29	0.27	0.30
Nb	19.2	14.1	22.8	10.7	9.2	14.4
Nd	63.8	16.6	54.3	20.4	17.9	28.9
Pr	17.60	5.36	16.00	6.05	5.47	7.95
Rb	55.5	178.5	123.5	112.5	86.7	106.0
Sm	11.95	3.05	9.40	3.86	3.39	5.75
Sn	2	2	1	1	1	1
Sr	964	58	75	55	40	221
Ta	1.1	1.3	1.3	0.6	0.6	0.9
Tb	1.01	0.34	0.82	0.51	0.40	0.69
Th	12.55	13.30	13.85	8.71	8.58	6.77
Tl	0.6	4.2	14.0	0.8	0.5	1.4
Tm	0.35	0.14	0.34	0.25	0.24	0.30
U	3.10	4.84	6.11	2.77	2.48	2.58
V	182	22	184	112	109	173
W	2	11	16	2	2	11
Y	25.9	10.4	24.3	17.0	14.9	21.8
Yb	2.12	0.92	2.13	1.67	1.67	1.90
Zr	202	152	235	206	230	187
As	NSS	>250	>250	72.9	81.4	>250
Bi	NSS	0.05	0.22	0.12	0.10	0.06
Hg	NSS	1.245	13.650	0.183	0.069	0.554
Sb	NSS	1.08	70.00	0.90	1.07	13.10
Se	NSS	0.20	0.80	2.30	2.40	2.00
Te	NSS	0.01	0.04	0.03	0.03	0.10
Au	0.001	0.673	0.237	0.004	0.009	0.555
Ag	<0.5	<0.5	<0.5	<0.5	<0.5	<0.5
Cd	<0.5	<0.5	<0.5	0.5	<0.5	<0.5
Co	33	4	31	8	3	26
Cu	62	4	88	88	46	22
Mo	1	1	5	1	<1	1
Ni	164	3	60	34	15	140
Pb	6	13	10	6	6	11
Zn	70	37	78	130	15	37
ΣREE	362	138	344	138	127	179
K/Al	0.16	0.30	0.18	0.36	0.30	0.29
(2Ca+Na+K)/Al	1.48	0.48	0.51	0.41	0.34	1.31

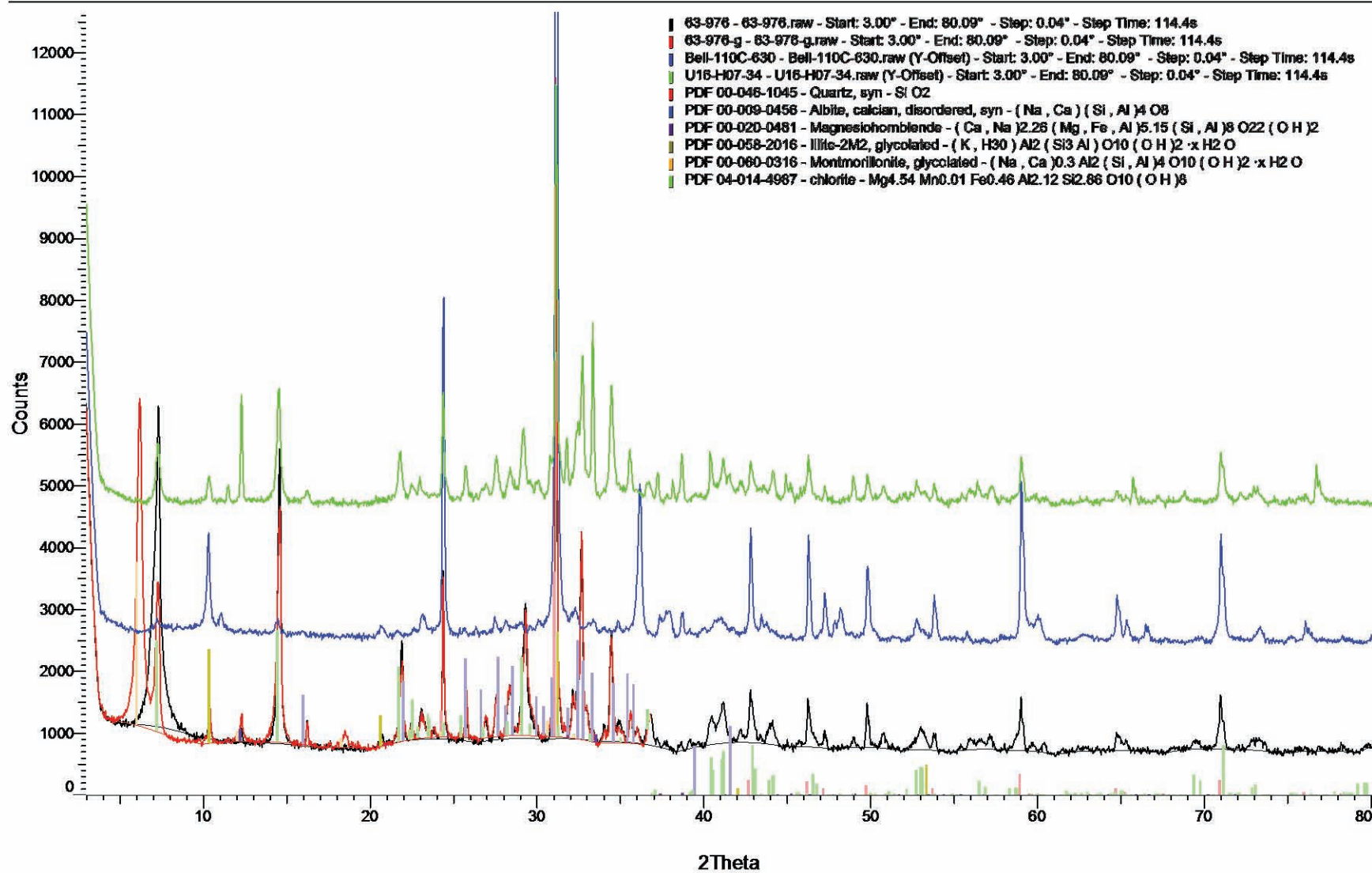
* samples used to calculate average fresh values

Major elements determined by ICP-AES following lithium metaborate fusion

Trace elements determined by LA-ICP-MS following lithium metaborate fusion

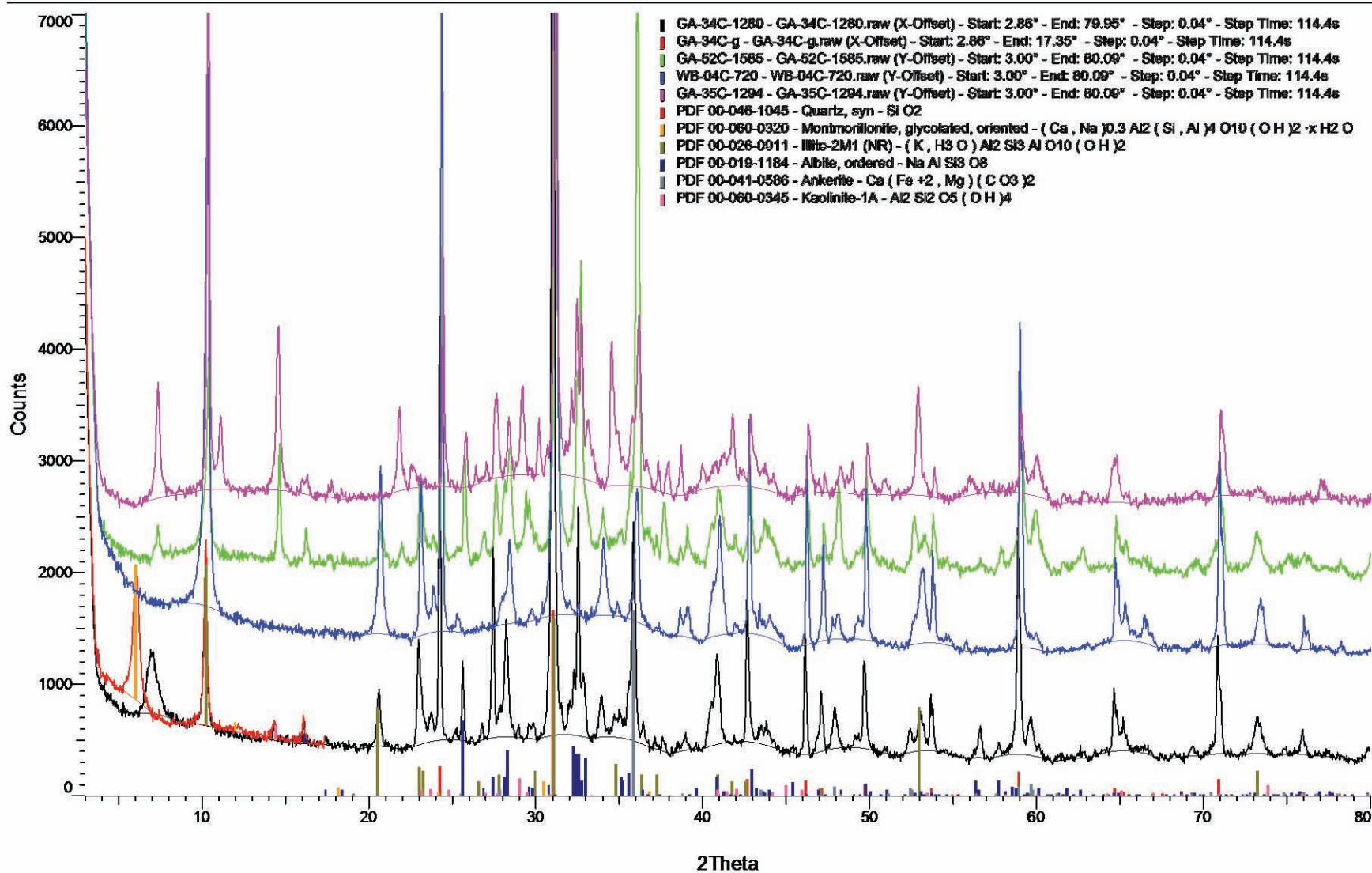
63-976

Banshee lamprophyre samples



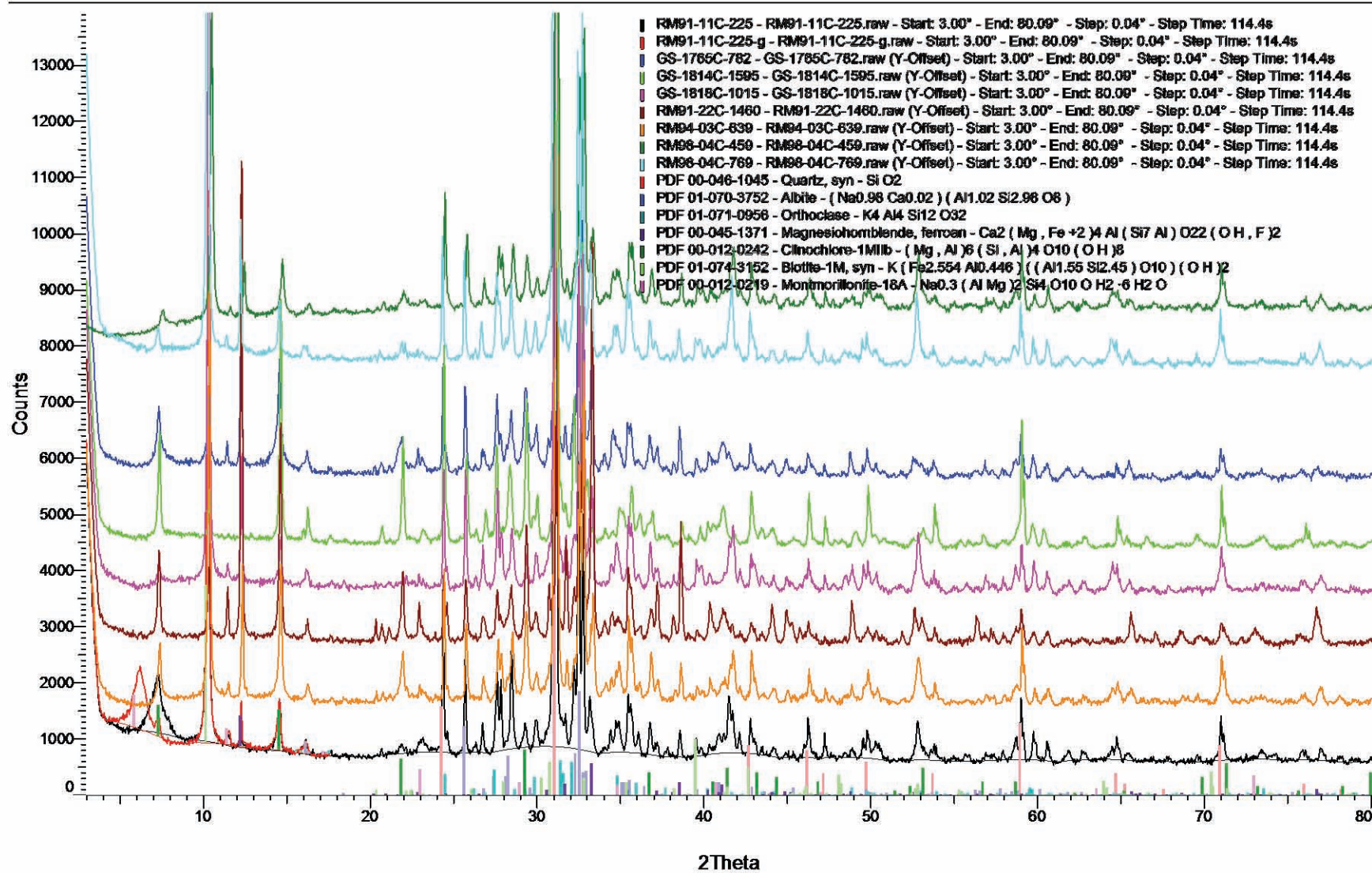
GA-34C-g

Golden April lamprophyre samples



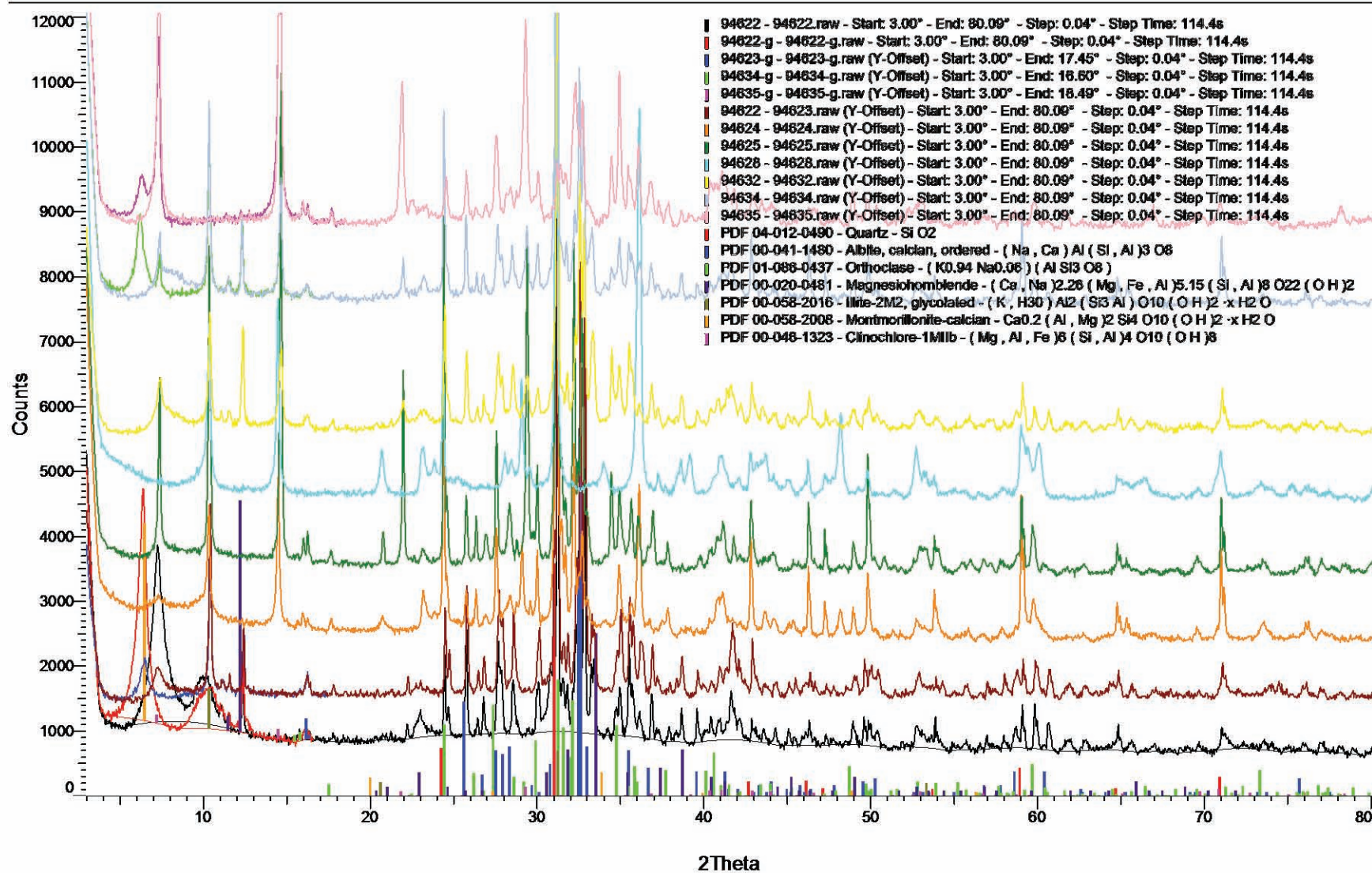
RM91-11C-225

Goldstrike Stock samples



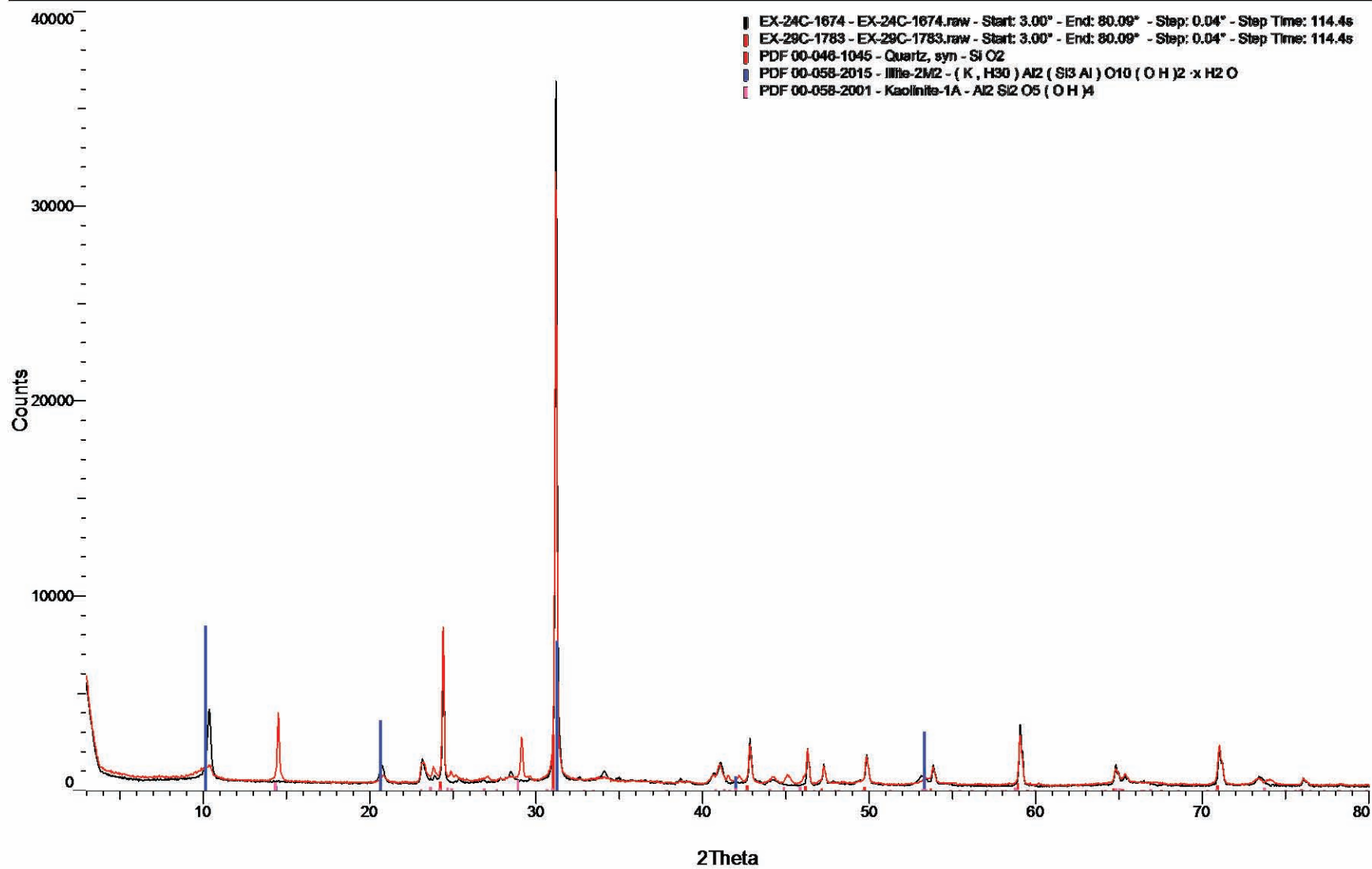
94635

Little Boulder Stock samples



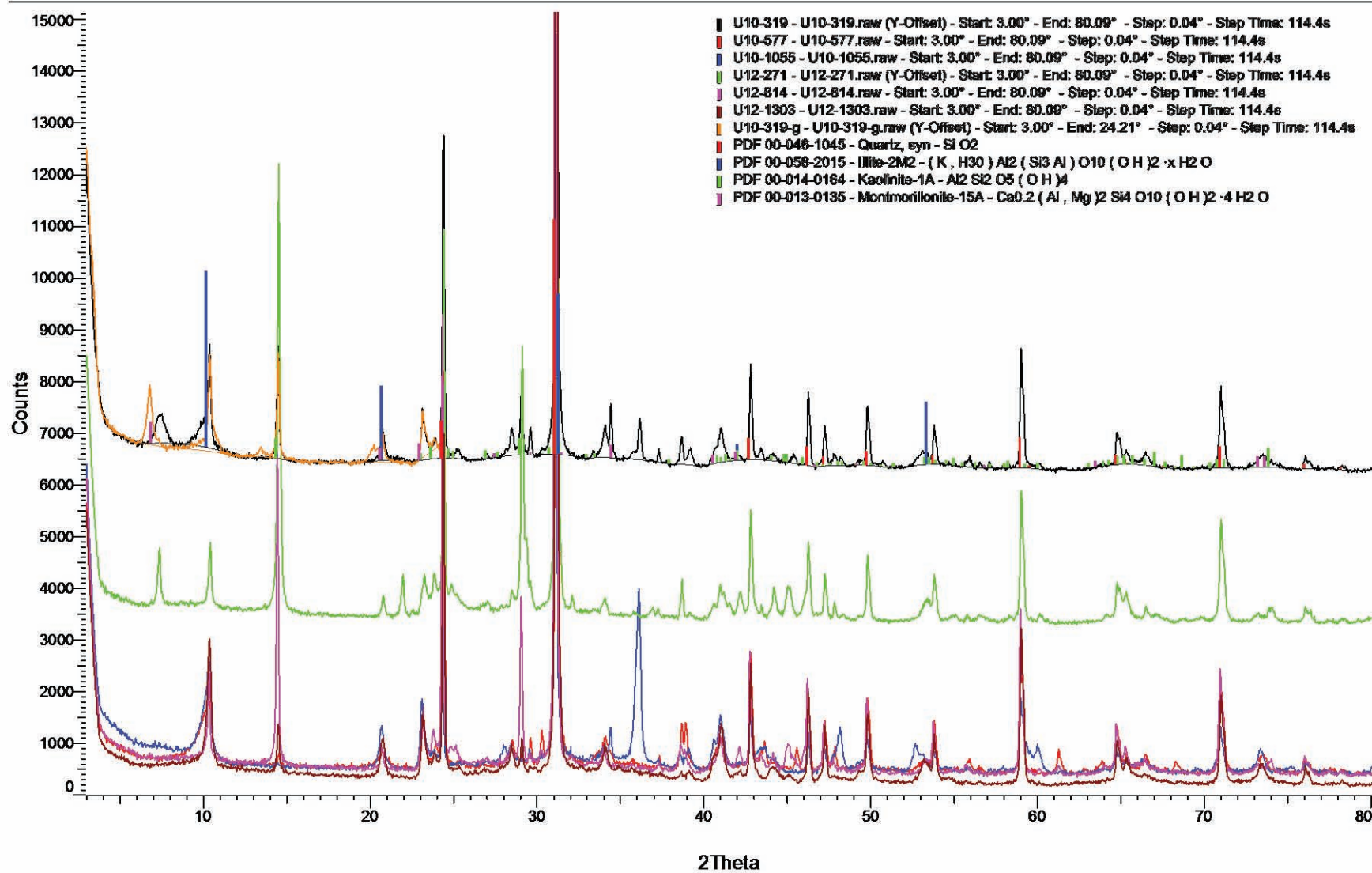
EX-29C-1783

Meikle samples



U10-319

Post Fault samples



Appendix C **Thermochronology data**

Table C1 contains all AFT single grain ages obtained using LA-ICP-MS

Table C2 contains all AFT single grain ages obtained using EDM

Table C3 contains all measured fission track lengths

Table C1 Apatite fission track single grain ages for all samples used in this thesis generated using the ICP-MS method

UBC	AZ	Grain number	FT age (Ma)	1 σ (Ma)	Dpar (μ m)	Etch Figs	Natural tracks	Area (cm ²)	²³⁸ U/ ⁴³ Ca (dmnls)	1 σ (dmnls)	⁴³ Ca back:sig	²³⁸ U back:sig	²³² Th back:sig	¹⁴⁷ Sm back:sig	U (ppm)	Th (ppm)	Sm (ppm)
5027	70608	1	34.47	11.62	1.98	4	9	1.92E-05	0.0942	0.00432	0.0227	4.94E-04			30.68	1.16	
5027	70608	2	98.53	24.58	1.88	4	17	1.92E-05	0.0619	0.00334	0.0254	6.98E-04			20.17	1.14	
5027	70608	3	35.76	9.16	2.04	4	16	4.48E-05	0.0692	0.00352	0.0246	0.00E+00			22.53	1.26	
5027	70608	4	61.53	23.55	2.12	4	7	1.92E-05	0.0410	0.00227	0.0275	7.13E-04			13.34	1.47	
5027	70608	5	49.48	15.88	1.93	4	10	1.92E-05	0.0728	0.00361	0.0279	8.22E-04			23.72	1.60	
5027	70608	6	59.82	12.89	1.75	4	23	5.12E-05	0.0519	0.00256	0.0317	7.59E-04			16.91	1.20	
5027	70608	7	30.58	9.36	2.06	4	11	2.69E-05	0.0927	0.00450	0.0259	6.54E-04			30.19	1.56	
5027	70608	8	55.99	14.32	2.09	4	16	1.92E-05	0.1030	0.00511	0.0295	2.44E-04			33.51	1.30	
5027	70608	9	64.13	21.67	1.94	4	9	1.28E-05	0.0758	0.00382	0.0273	2.64E-03			24.67	1.54	
5027	70608	10	36.48	21.16	2.09	4	3	2.56E-05	0.0223	0.00115	0.0283	8.49E-03			7.24	1.63	
5027	70608	11	32.37	10.68	2.09	4	10	1.92E-05	0.1110	0.01020	0.0268	1.07E-03			36.30	1.10	
5027	70608	12	43.14	12.71	1.98	4	12	2.30E-05	0.0836	0.00451	0.0236	9.09E-04			27.21	1.11	
5027	70608	13	68.00	24.36	1.70	4	8	2.88E-05	0.0282	0.00150	0.0259	3.50E-03			9.19	1.77	
5027	70608	14	23.73	7.30	1.75	4	11	4.10E-05	0.0785	0.00445	0.0272	2.41E-03			25.55	1.36	
5027	70608	15	12.89	7.48	1.96	4	3	2.56E-05	0.0631	0.00335	0.0238	1.22E-03			20.55	1.15	
5027	70608	16	41.43	15.84	2.15	4	7	2.56E-05	0.0457	0.00241	0.0273	2.44E-03			14.88	0.30	
5027	70608	17	23.84	9.82	1.93	4	6	2.69E-05	0.0649	0.00330	0.0279	0.00E+00			21.14	1.33	
5027	70608	18	56.41	14.86	1.91	4	15	3.20E-05	0.0575	0.00274	0.0298	2.78E-03			18.71	1.48	
5027	70608	19	30.59	8.65	2.21	4	13	3.84E-05	0.0767	0.00384	0.0310	8.95E-04			24.97	1.07	
5027	70608	20	59.12	22.57	1.96	4	7	2.56E-05	0.0320	0.00156	0.0320	0.00E+00			10.41	1.40	
5027	70608	21	55.59	17.04	1.89	4	11	1.92E-05	0.0713	0.00356	0.0337	1.19E-03			23.21	1.53	
5027	70608	22	35.52	11.41	1.90	4	10	2.56E-05	0.0762	0.00395	0.0301	0.00E+00			24.80	1.12	
5027	70608	23	45.40	15.37	1.88	4	9	2.05E-05	0.0670	0.00371	0.0255	1.10E-03			21.81	1.89	
5027	70608	24	55.36	17.76	1.99	3	10	2.05E-05	0.0610	0.00302	0.0294	1.41E-03			19.86	0.92	
5027	70608	25	81.68	29.38	2.04	4	8	2.30E-05	0.0293	0.00184	0.0311	4.09E-03			9.55	1.42	
5029	70610	1	63.24	12.06	2.89	4	30	3.20E-05	0.1010	0.00512	0.0228	1.07E-03			33.00	1.14	
5029	70610	2	286.25	102.56	2.63	4	12	1.28E-05	0.0220	0.00464	0.0196	9.42E-04			7.16	0.91	
5029	70610	3	89.07	22.99	2.90	4	16	1.60E-05	0.0766	0.00462	0.0234	9.01E-04			24.94	1.00	
5029	70610	4	82.80	21.89	2.84	4	15	1.02E-05	0.1210	0.00631	0.0252	6.62E-04			39.31	1.09	
5029	70610	5	53.16	11.51	2.48	4	24	3.84E-05	0.0804	0.00554	0.0260	2.31E-04			26.19	1.21	
5029	70610	6	61.50	20.76	2.67	4	9	1.28E-05	0.0782	0.00377	0.0289	2.41E-03			25.45	1.24	
5029	70610	7	34.23	9.11	2.47	4	16	2.56E-05	0.1250	0.01110	0.0238	6.79E-04			40.73	1.16	
5029	70610	8	30.28	10.26	2.16	4	9	1.92E-05	0.1060	0.00601	0.0221	1.77E-03			34.55	1.21	
5029	70610	9	36.63	10.83	2.90	4	12	1.54E-05	0.1460	0.00867	0.0247	6.90E-04			47.56	1.07	
5029	70610	10	35.99	14.84	2.29	4	6	1.02E-05	0.1120	0.00585	0.0330	0.00E+00			36.31	1.40	
5029	70610	11	57.33	21.92	2.66	4	7	9.60E-06	0.0870	0.00466	0.0313	3.18E-04			28.32	1.31	
5029	70610	12	54.85	18.53	2.39	4	9	2.30E-05	0.0487	0.00242	0.0284	2.74E-03			15.86	2.40	
5029	70610	13	40.56	14.52	2.56	4	8	1.60E-05	0.0844	0.00439	0.0266	3.18E-03			27.48	1.71	

Table C1 Apatite fission track single grain ages for all samples used in this thesis generated using the ICP-MS method

UBC	AZ	Grain number	FT age (Ma)	1 σ (Ma)	Dpar (μ m)	Etch Figs	Natural tracks	Area (cm ²)	²³⁸ U/ ⁴³ Ca (dmnls)	1 σ (dmnls)	⁴³ Ca back:sig	²³⁸ U back:sig	²³² Th back:sig	¹⁴⁷ Sm back:sig	U (ppm)	Th (ppm)	Sm (ppm)
5029	70610	14	37.68	13.49	2.47	4	8	1.79E-05	0.0811	0.00412	0.0246	2.80E-03			26.42	1.16	
5029	70610	15	39.50	13.37	3.17	4	9	1.60E-05	0.0975	0.00522	0.0281	1.61E-03			31.75	1.84	
5029	70610	16	32.41	10.96	2.84	4	9	1.92E-05	0.0991	0.00511	0.0297	1.39E-03			32.26	1.01	
5029	70610	17	64.14	22.94	2.48	4	8	7.68E-06	0.1110	0.00551	0.0289	4.68E-04			36.14	1.08	
5029	70610	18	38.62	13.85	2.67	4	8	1.28E-05	0.1110	0.00617	0.0290	1.92E-04			36.09	1.02	
5029	70610	19	27.14	12.23	2.65	4	5	1.02E-05	0.1230	0.00634	0.0298	5.74E-04			40.15	0.98	
5029	70610	20	42.26	13.58	2.80	4	10	1.15E-05	0.1410	0.00737	0.0267	1.21E-03			45.79	0.92	
5029	70610	21	15.63	7.05	2.42	4	5	1.15E-05	0.1910	0.01030	0.0243	5.74E-05			62.04	1.41	
5029	70610	22	43.75	16.71	2.72	2	7	1.92E-05	0.0570	0.00286	0.0290	1.36E-03			18.57	1.08	
5029	70610	23	50.35	14.79	2.99	4	12	2.30E-05	0.0708	0.00347	0.0283	1.06E-03			23.05	1.22	
5029	70610	24	45.39	18.69	2.33	4	6	1.02E-05	0.0884	0.00429	0.0346	1.07E-03			28.77	1.50	
5029	70610	25	52.18	17.62	2.21	4	9	1.54E-05	0.0768	0.00375	0.0310	2.19E-03			25.01	1.30	
5029	70610	26	14.08	8.17	2.66	3	3	1.28E-05	0.1140	0.00547	0.0315	1.49E-03			37.18	1.28	
5029	70610	27	8.37	8.38	2.33	1	1	7.68E-06	0.1070	0.00567	0.0347	1.62E-03			34.77	1.39	
5029	70610	28	24.43	12.29	2.49	4	4	1.28E-05	0.0877	0.00450	0.0288	2.16E-03			28.55	0.87	
5029	70610	29	10.87	7.71	2.82	3	2	1.28E-05	0.0987	0.00522	0.0294	2.54E-03			32.12	1.08	
5029	70610	30	31.14	14.04	2.50	3	5	1.28E-05	0.0859	0.00460	0.0295	1.06E-03			27.99	1.43	
5029	70610	31	34.47	12.38	2.13	4	8	2.56E-05	0.0621	0.00363	0.0301	2.35E-03			20.22	1.46	
5029	70610	32	35.47	14.60	2.37	4	6	1.79E-05	0.0647	0.00304	0.0306	4.10E-03			21.06	1.22	
5029	70610	33	47.70	24.03	2.40	4	4	7.68E-06	0.0747	0.00426	0.0300	0.00E+00			24.33	1.29	
5029	70610	34	16.98	12.04	2.22	4	2	9.60E-06	0.0842	0.00442	0.0323	1.98E-03			27.41	1.28	
5029	70610	35	36.37	18.30	2.37	4	4	1.02E-05	0.0736	0.00376	0.0290	1.26E-03			23.95	1.39	
5029	70610	36	26.90	12.12	2.65	4	5	1.02E-05	0.1240	0.00599	0.0344	3.07E-04			40.51	1.05	
5029	70610	37	45.38	15.31	2.26	4	9	1.02E-05	0.1330	0.00617	0.0397	1.22E-03			43.16	0.82	
5029	70610	38	29.58	14.88	2.50	4	4	1.92E-05	0.0483	0.00243	0.0298	2.39E-03			15.71	1.12	
5029	70610	39	37.60	12.70	2.45	4	9	1.73E-05	0.0949	0.00479	0.0335	2.01E-03			30.89	1.45	
5029	70610	40	26.05	9.95	2.52	4	7	2.30E-05	0.0800	0.00409	0.0313	1.53E-03			26.04	1.23	
6000A	86102	1	296.96	67.17	2.01	4	20	8.96E-06	0.0576	0.00092	0.0261	9.83E-03	3.13E-03	5.44E-04	22.36	119.89	857.99
6000A	86102	2	381.78	88.64	2.04	4	19	1.15E-05	0.0329	0.00063	0.0273	3.29E-04	1.56E-03	9.54E-04	12.76	35.72	396.66
6000A	86102	3	293.26	93.30	2.08	4	10	9.60E-06	0.0272	0.00047	0.0239	2.95E-04	1.83E-03	1.15E-03	10.57	17.38	272.15
6000A	86102	4	85.15	28.53	2.16	4	9	1.54E-05	0.0536	0.00087	0.0266	4.88E-02	4.58E-02	1.24E-03	20.81	52.46	569.97
6000A	86102	5	606.84	163.68	2.29	4	14	7.68E-06	0.0225	0.00046	0.0262	2.13E-01	6.87E-02	6.30E-04	8.72	38.70	667.17
6000A	86102	6	214.75	71.97	2.19	4	9	7.68E-06	0.0421	0.00071	0.0239	1.63E-02	1.71E-03	2.03E-03	16.33	61.38	362.74
6000A	86102	7	61.75	25.30	2.03	4	6	9.60E-06	0.0790	0.00130	0.0253	3.19E-02	6.33E-03	1.07E-03	30.66	41.89	634.12
6000A	86102	8	170.93	54.39	2.20	4	10	1.28E-05	0.0354	0.00066	0.0266	1.36E-02	1.56E-02	3.12E-02	13.73	47.36	426.70
6000A	86102	9	248.50	56.20	2.27	4	20	2.30E-05	0.0269	0.00041	0.0257	7.01E-04	2.67E-03	8.23E-04	10.43	42.65	642.27
6000A	86102	10	111.51	37.36	2.12	4	9	1.92E-05	0.0327	0.00050	0.0289	4.50E-03	3.63E-03	1.41E-03	12.68	66.05	668.15
6000A	86102	11	78.63	27.93	2.19	4	8	1.02E-05	0.0774	0.00125	0.0472	1.32E-03	3.83E-03	1.45E-03	30.06	110.36	882.36

Table C1 Apatite fission track single grain ages for all samples used in this thesis generated using the ICP-MS method

UBC	AZ	Grain number	FT age (Ma)	1 σ (Ma)	Dpar (μ m)	Etch Figs	Natural tracks	Area (cm ²)	238U/43Ca (dmnls)	1 σ (dmnls)	43Ca back:sig	238U back:sig	232Th back:sig	147Sm back:sig	U (ppm)	Th (ppm)	Sm (ppm)
6000A	86102	12	155.37	45.15	2.01	4	12	2.30E-05	0.0260	0.00039	0.0297	2.57E-03	6.21E-04	1.21E-03	10.08	48.44	684.43
6000A	86102	13	66.15	23.49	2.08	4	8	1.28E-05	0.0737	0.00108	0.0309	8.25E-02	1.01E-01	1.76E-03	28.61	68.54	698.47
6000A	86102	14	368.64	151.05	2.14	4	6	9.60E-06	0.0129	0.00023	0.0246	6.33E-01	4.54E-01	2.51E-03	5.01	34.38	564.40
6000A	86102	15	217.95	66.13	2.26	4	11	1.02E-05	0.0380	0.00059	0.0261	5.92E-03	4.98E-03	1.77E-03	14.75	46.20	424.87
6000A	86102	16	123.25	30.17	2.44	4	17	9.60E-06	0.1120	0.00159	0.0323	6.16E-04	2.64E-03	2.69E-03	43.32	64.06	509.41
6000A	86102	17	147.25	49.32	2.36	4	9	1.92E-05	0.0247	0.00032	0.0379	2.13E-03	1.13E-03	2.25E-03	9.58	59.94	619.29
6000A	86102	18	117.27	31.58	2.28	4	14	8.96E-06	0.1040	0.00143	0.0347	7.26E-04	2.45E-03	2.03E-03	40.19	55.35	435.81
6000A	86102	19	173.23	38.24	2.20	4	21	7.68E-06	0.1220	0.00170	0.0308	7.46E-04	2.44E-03	1.48E-03	47.40	59.24	591.86
6000A	86102	20	159.20	40.16	2.33	4	16	1.02E-05	0.0760	0.00114	0.0310	2.30E-04	1.66E-03	1.80E-03	29.51	51.09	603.41
6000A	86102	21	92.13	27.95	2.11	4	11	1.60E-05	0.0581	0.00091	0.0270	1.56E-03	1.91E-03	1.99E-03	22.55	61.08	498.64
6000A	86102	22	122.19	38.86	2.12	4	10	1.54E-05	0.0414	0.00065	0.0300	2.84E-03	4.11E-03	1.39E-03	16.07	60.11	690.74
6000A	86102	23	130.94	46.50	2.29	4	8	1.28E-05	0.0370	0.00051	0.0321	1.44E-03	1.28E-03	1.89E-03	14.38	58.16	684.82
6000A	86102	24	131.54	34.25	2.17	4	15	1.28E-05	0.0691	0.00104	0.0293	2.21E-04	1.83E-03	1.88E-03	26.84	44.27	219.54
6000A	86102	25	117.77	37.47	2.10	4	10	2.30E-05	0.0286	0.00049	0.0268	6.34E-03	2.26E-03	1.38E-03	11.12	57.05	648.54
6000B	1070-06	1	190.65	48.95	2.29	4	18	7.68E-06	0.1040	0.01040	0.0086	1.02E-03	3.48E-03	2.21E-04	38.29	46.14	627.27
6000B	1070-06	2	87.44	32.17	2.23	4	8	1.54E-05	0.0506	0.00506	0.0119	1.98E-03	2.38E-03	1.32E-03	18.70	37.01	459.69
6000B	1070-06	3	166.14	46.11	2.42	4	15	1.92E-05	0.0397	0.00397	0.0124	1.25E-03	1.61E-03	7.20E-04	14.67	40.64	620.84
6000B	1070-06	4	140.18	64.30	2.26	4	5	7.68E-06	0.0393	0.00393	0.0149	1.71E-03	2.12E-03	1.75E-03	14.52	57.04	667.14
6000B	1070-06	5	94.04	32.78	2.27	4	9	1.92E-05	0.0423	0.00423	0.0172	1.46E-03	4.23E-03	1.61E-03	15.64	48.91	687.80
6000B	1070-06	6	116.90	43.01	2.23	4	8	1.60E-05	0.0362	0.00362	0.0195	1.60E-03	6.30E-03	6.36E-04	13.40	42.21	659.26
6000B	1070-06	8	141.27	55.30	2.31	4	7	1.92E-05	0.0218	0.00218	0.0145	2.34E-03	4.71E-03	2.71E-04	8.07	35.44	682.79
6000B	1070-06	9	245.96	75.29	2.07	4	12	1.54E-05	0.0266	0.00266	0.0148	2.92E-03	8.39E-03	5.27E-03	9.85	40.63	479.47
6000B	1070-06	10	128.34	54.00	2.18	4	6	9.60E-06	0.0412	0.00412	0.0217	3.85E-03	6.57E-03	3.03E-03	15.24	41.79	667.69
6000B	1070-06	11	132.79	46.28	2.19	4	9	2.05E-05	0.0280	0.00280	0.0163	7.26E-03	3.02E-03	1.59E-03	10.35	40.71	619.92
6000B	1070-06	12	88.84	34.78	2.03	4	7	1.79E-05	0.0373	0.00373	0.0188	9.56E-04	7.51E-03	1.63E-03	13.81	41.72	494.74
6000B	1070-06	13	153.57	53.53	2.21	4	9	1.02E-05	0.0483	0.00483	0.0172	2.02E-03	7.62E-03	2.86E-03	17.88	40.55	561.98
6000B	1070-06	14	58.98	24.82	2.38	4	6	1.92E-05	0.0451	0.00451	0.0159	1.61E-03	3.55E-03	1.24E-03	16.67	39.32	559.94
6000B	1070-06	15	128.35	58.87	2.12	4	5	1.28E-05	0.0258	0.00258	0.0182	7.91E-03	8.64E-03	4.58E-03	9.53	34.20	419.93
6000B	1070-06	16	138.50	46.01	2.16	4	10	1.28E-05	0.0477	0.00477	0.0168	3.51E-03	2.77E-03	1.57E-03	17.64	46.45	662.77
6000B	1070-06	17	137.56	63.09	2.53	4	5	1.15E-05	0.0267	0.00267	0.0210	3.77E-03	7.33E-03	4.47E-03	9.87	43.01	691.70
6000B	1070-06	18	191.77	50.45	2.30	4	17	3.07E-05	0.0243	0.00243	0.0169	2.66E-03	8.28E-03	3.13E-03	8.99	41.62	569.31
6000B	1070-06	19	214.94	84.14	2.34	4	7	1.15E-05	0.0238	0.00238	0.0180	1.65E-03	4.31E-03	1.85E-03	8.79	38.05	399.53
6000B	1070-06	20	108.03	27.74	2.32	4	18	2.56E-05	0.0552	0.00552	0.0221	1.25E-03	1.01E-02	1.06E-03	20.40	37.80	638.58
6000B	1070-06	21	145.90	48.47	2.38	4	10	1.28E-05	0.0452	0.00452	0.0234	1.70E-03	8.93E-03	1.71E-03	16.74	36.14	499.19
6000B	1070-06	22	152.52	48.54	2.25	4	11	2.30E-05	0.0264	0.00264	0.0222	8.39E-03	4.90E-03	1.25E-03	9.78	39.04	656.23
6000B	1070-06	23	105.95	44.58	2.37	4	6	1.02E-05	0.0469	0.00469	0.0179	2.99E-03	3.91E-03	1.86E-03	17.34	38.49	600.86
6000B	1070-06	24	129.38	54.44	2.31	4	6	1.28E-05	0.0307	0.00307	0.0226	2.04E-03	5.74E-03	4.54E-03	11.34	45.30	444.21
6000B	1070-06	25	124.35	63.45	2.03	4	4	1.28E-05	0.0213	0.00213	0.0175	4.66E-03	3.25E-03	1.63E-03	7.87	35.43	486.83

Table C1 Apatite fission track single grain ages for all samples used in this thesis generated using the ICP-MS method

UBC	AZ	Grain number	FT age (Ma)	1 σ (Ma)	Dpar (μ m)	Etch Figs	Natural tracks	Area (cm ²)	238U/43Ca (dmnls)	1 σ (dmnls)	43Ca back:sig	238U back:sig	232Th back:sig	147Sm back:sig	U (ppm)	Th (ppm)	Sm (ppm)
6000B	1070-06	26	145.42	53.50	2.23	4	8	1.28E-05	0.0363	0.00363	0.0162	1.45E-03	3.68E-03	1.60E-03	13.43	53.85	686.45
6000B	1070-06	27	207.24	63.44	2.20	4	12	1.92E-05	0.0254	0.00254	0.0216	5.35E-03	7.12E-03	3.93E-03	9.38	45.73	633.32
6000B	1070-06	28	86.63	36.45	2.30	4	6	1.92E-05	0.0306	0.00306	0.0208	5.40E-03	4.67E-03	1.57E-03	11.33	44.98	508.67
6000B	1070-06	29	122.83	35.13	2.19	4	14	1.79E-05	0.0538	0.00538	0.0200	7.58E-04	4.23E-03	2.16E-03	19.92	38.33	570.95
6000B	1070-06	30	137.57	47.95	2.26	4	9	1.60E-05	0.0346	0.00346	0.0170	3.89E-03	5.97E-03	1.96E-03	12.79	40.32	620.35
6000B	1070-06	31	182.67	67.21	2.11	4	8	1.79E-05	0.0206	0.00206	0.0181	4.58E-03	4.03E-03	1.09E-03	7.62	35.35	550.54
6000B	1070-06	32	57.44	18.28	2.26	4	11	1.28E-05	0.1270	0.01270	0.0232	9.66E-04	4.25E-03	8.14E-04	47.09	59.68	632.18
6000B	1070-06	33	84.29	43.01	2.22	4	4	1.28E-05	0.0315	0.00315	0.0263	3.93E-03	6.78E-03	1.44E-03	11.64	38.56	567.24
6000B	1070-06	34	117.47	43.22	2.07	4	8	1.60E-05	0.0360	0.00360	0.0267	2.79E-03	7.35E-03	2.22E-03	13.33	37.61	577.48
6000B	1070-06	35	67.32	34.35	2.13	4	4	2.24E-05	0.0225	0.00225	0.0216	2.65E-03	6.97E-03	7.72E-04	8.34	35.72	606.71
6000B	1070-06	36	208.15	59.53	2.23	4	14	2.56E-05	0.0221	0.00221	0.0233	3.53E-03	8.13E-03	2.29E-03	8.17	37.67	604.05
6000B	1070-06	38	98.03	44.96	2.36	4	5	1.28E-05	0.0338	0.00338	0.0236	4.38E-03	5.93E-03	2.88E-03	12.50	40.08	451.85
6000B	1070-06	39	70.20	41.15	2.05	4	3	1.54E-05	0.0236	0.00236	0.0191	2.97E-03	6.09E-03	1.24E-03	8.75	37.66	538.55
6000B	1070-06	40	76.18	34.94	2.01	4	5	1.92E-05	0.0290	0.00290	0.0173	7.52E-03	5.89E-03	1.69E-03	10.74	38.80	593.87
EX-29C-1783	1178-03	1	52.66	12.10	2.58	4	5	5.76E-05	0.0227	0.00216					5.00	15.00	250.00
EX-29C-1783	1178-03	2	36.07	10.60	2.57	3	3	5.12E-05	0.0224	0.00216					7.00	16.00	192.00
EX-29C-1783	1178-03	3	21.08	4.80	2.31	4	5	6.40E-05	0.0511	0.00485					12.00	21.00	196.00
EX-29C-1783	1178-03	4	63.96	16.40	2.30	4	4	2.30E-05	0.0373	0.00358					9.00	18.00	258.00
EX-29C-1783	1178-03	5	34.56	8.80	2.43	4	4	3.84E-05	0.0415	0.00397					9.00	20.00	228.00
EX-29C-1783	1178-03	6	50.88	10.70	2.72	4	6	2.88E-05	0.0563	0.00535					15.00	109.00	437.00
EX-29C-1783	1178-03	7	29.95	15.10	3.06	4	1	3.20E-05	0.0144	0.00138					3.00	11.00	128.00
EX-29C-1783	1178-03	8	22.96	5.90	2.85	4	4	5.12E-05	0.0469	0.00452					10.00	24.00	301.00
EX-29C-1783	1178-03	9	57.20	12.10	2.67	4	6	6.40E-05	0.0225	0.00215					6.00	17.00	197.00
EX-29C-1783	1178-03	10	18.43	9.20	3.10	2	1	2.05E-05	0.0365	0.00348					10.00	29.00	239.00
EX-29C-1783	1178-03	11	21.13	10.70	2.90	4	1	2.30E-05	0.0283	0.00272					8.00	17.00	263.00
EX-29C-1783	1178-03	12	35.79	9.10	2.59	4	4	5.12E-05	0.0300	0.00291					8.00	18.00	230.00
EX-29C-1783	1178-03	13	50.57	12.90	3.21	4	4	4.10E-05	0.0265	0.00253					6.00	13.00	191.00
EX-29C-1783	1178-03	14	39.16	7.70	2.80	4	7	6.40E-05	0.0384	0.00367					9.00	19.00	237.00
EX-29C-1783	1178-03	15	19.64	5.70	2.68	4	3	6.40E-05	0.0329	0.00317					10.00	21.00	252.00
EX-29C-1783	1178-03	16	41.17	9.40	2.69	4	5	3.84E-05	0.0435	0.00415					10.00	20.00	205.00
EX-29C-1783	1178-03	17	63.25	16.20	3.24	4	4	3.84E-05	0.0226	0.00219					6.00	15.00	222.00
EX-29C-1783	1178-03	18	46.95	10.80	2.63	4	5	3.84E-05	0.0381	0.00364					9.00	32.00	235.00
EX-29C-1783	1178-03	19	39.50	9.10	2.63	4	5	3.84E-05	0.0454	0.00433					11.00	10.00	208.00
EX-29C-1783	1178-03	20	31.41	8.00	2.55	4	4	3.84E-05	0.0457	0.00434					10.00	18.00	240.00
EX-29C-1783	1178-03	21	83.04	24.40	2.55	2	3	2.56E-05	0.0193	0.00186					5.00	12.00	205.00
EX-29C-1783	1178-03	22	32.32	11.60	2.72	2	2	3.20E-05	0.0266	0.00256					7.00	16.00	196.00
EX-29C-1783	1178-03	23	24.91	6.40	2.52	4	4	6.40E-05	0.0345	0.00328					8.00	17.00	240.00
EX-29C-1783	1178-03	24	43.90	8.60	2.71	4	7	5.12E-05	0.0428	0.00411					9.00	19.00	247.00

Table C1 Apatite fission track single grain ages for all samples used in this thesis generated using the ICP-MS method

UBC	AZ	Grain number	FT age (Ma)	1 σ (Ma)	Dpar (μ m)	Etch Figs	Natural tracks	Area (cm ²)	238U/43Ca (dmnls)	1 σ (dmnls)	43Ca back:sig	238U back:sig	232Th back:sig	147Sm back:sig	U (ppm)	Th (ppm)	Sm (ppm)
EX-29C-1783	1178-03	25	82.11	16.10	2.71	4	7	3.20E-05	0.0365	0.00348					10.00	22.00	236.00
EX-29C-1783	1178-03	26	28.24	7.20	2.51	3	4	4.48E-05	0.0435	0.00412					11.00	24.00	241.00
EX-29C-1783	1178-03	27	130.17	30.00	2.51	4	5	1.92E-05	0.0273	0.00259					8.00	18.00	236.00
EX-29C-1783	1178-03	28	35.43	10.40	2.90	4	3	3.84E-05	0.0303	0.00288					9.00	19.00	220.00
EX-29C-1783	1178-03	29	51.51	13.20	2.86	4	4	2.56E-05	0.0417	0.00399					10.00	27.00	271.00
EX-29C-1783	1178-03	30	30.27	10.90	2.57	4	2	3.20E-05	0.0284	0.00270					8.00	19.00	288.00
EX-29C-1783	1178-03	31	24.94	5.70	2.77	4	5	6.40E-05	0.0431	0.00414					12.00	26.00	196.00
EX-29C-1783	1178-03	32	22.60	6.60	2.54	3	3	4.48E-05	0.0408	0.00387					10.00	21.00	238.00
EX-29C-1783	1178-03	33	22.76	8.10	2.70	3	2	3.84E-05	0.0315	0.00299					8.00	19.00	238.00
EX-29C-1783	1178-03	34	24.72	7.30	2.82	4	3	4.48E-05	0.0373	0.00355					9.00	20.00	214.00
EX-29C-1783	1178-03	35	0.00	0.00	2.88	4	2	3.20E-05	0.0000	0.00000					0.00	0.00	0.00
EX-29C-1783	1178-03	36	13.13	3.90	2.62	4	3	6.40E-05	0.0492	0.00469					13.00	28.00	243.00
EX-29C-1783	1178-03	37	53.07	12.20	2.84	4	5	3.84E-05	0.0337	0.00321					11.00	21.00	244.00
EX-29C-1783	1178-03	38	28.06	7.10	2.53	4	4	5.12E-05	0.0383	0.00363					10.00	19.00	224.00
EX-29C-1783	1178-03	39	0.00	0.00	2.53	2	2	3.84E-05	0.0000	0.00000					0.00	0.00	0.00
EX-29C-1783	1178-03	40	29.34	10.50	2.68	2	2	2.56E-05	0.0367	0.00350					10.00	19.00	171.00
GA-34C-1280	1070-04	1	0.00	42.43	1.79	4	0	1.60E-05	0.0188	0.00188	0.0104	4.41E-03	5.23E-03	1.80E-03	6.94	23.89	301.80
GA-34C-1280	1070-04	2	28.93	16.96	2.55	4	3	2.56E-05	0.0346	0.00346	0.0118	3.10E-04	2.12E-03	1.46E-04	12.78	42.85	370.47
GA-34C-1280	1070-04	3	45.77	32.70	2.25	4	2	1.60E-05	0.0233	0.00233	0.0153	5.09E-04	5.00E-03	4.65E-03	8.60	28.79	342.00
GA-34C-1280	1070-04	4	76.12	38.84	2.76	4	4	9.60E-06	0.0465	0.00465	0.0188	4.39E-04	3.53E-03	1.19E-03	17.20	74.86	426.11
GA-34C-1280	1070-04	5	52.06	37.19	2.49	3	2	1.28E-05	0.0256	0.00256	0.0152	1.95E-03	6.47E-03	1.10E-03	9.45	33.34	359.93
GA-34C-1280	1070-04	6	42.50	42.72	2.09	4	1	1.28E-05	0.0157	0.00157	0.0150	3.79E-03	1.08E-02	2.73E-03	5.79	15.99	286.64
GA-34C-1280	1070-04	7	33.98	24.28	2.00	4	2	1.28E-05	0.0392	0.00392	0.0143	1.54E-03	2.53E-03	9.53E-04	14.50	51.98	368.67
GA-34C-1280	1070-04	8	26.76	26.90	2.32	4	1	1.28E-05	0.0249	0.00249	0.0149	6.40E-03	1.24E-02	2.61E-03	9.21	17.09	293.56
GA-34C-1280	1070-04	9	19.98	20.09	2.44	2	1	1.92E-05	0.0223	0.00223	0.0169	2.38E-03	2.66E-03	1.42E-03	8.23	29.57	342.37
GA-34C-1280	1070-04	10	58.76	41.98	2.42	4	2	1.15E-05	0.0252	0.00252	0.0254	4.76E-03	5.67E-03	4.77E-03	9.30	28.77	336.27
GA-34C-1280	1070-04	11	29.41	17.24	2.24	1	3	3.07E-05	0.0283	0.00283	0.0204	5.96E-03	4.98E-03	3.36E-03	10.47	32.99	351.25
GA-34C-1280	1070-04	12	88.56	51.92	2.37	2	3	1.60E-05	0.0180	0.00180	0.0237	4.09E-03	1.28E-02	5.99E-03	6.65	17.57	242.40
GA-34C-1280	1070-04	13	26.12	26.25	2.32	3	1	1.28E-05	0.0255	0.00255	0.0261	7.67E-03	1.60E-02	5.22E-03	9.44	25.93	299.08
GA-34C-1280	1070-04	14	99.74	45.74	2.50	2	5	1.28E-05	0.0332	0.00332	0.0282	2.92E-03	3.71E-03	2.26E-03	12.29	43.41	366.81
GA-34C-1280	1070-04	15	0.00	35.23	2.38	1	0	1.28E-05	0.0283	0.00283	0.0157	4.63E-03	3.58E-03	2.31E-03	10.46	27.84	306.41
GA-34C-1280	1070-04	16	32.83	33.00	2.03	3	1	9.60E-06	0.0271	0.00271	0.0171	1.98E-03	9.08E-03	1.74E-03	10.01	27.88	331.04
GA-34C-1280	1070-04	17	25.43	25.56	2.34	1	1	2.24E-05	0.0150	0.00150	0.0156	2.20E-03	4.31E-03	6.63E-04	5.54	19.69	280.37
GA-34C-1280	1070-04	18	0.00	41.79	2.03	1	0	1.60E-05	0.0191	0.00191	0.0155	3.80E-03	7.98E-03	4.21E-03	7.05	21.67	123.56
GA-34C-1280	1070-04	19	17.24	17.33	2.17	1	1	1.15E-05	0.0430	0.00430	0.0155	1.74E-03	3.37E-03	1.36E-03	15.89	50.68	558.19
GA-34C-1280	1070-04	20	112.33	57.32	1.91	2	4	9.60E-06	0.0315	0.00315	0.0163	7.28E-03	6.47E-03	2.31E-03	11.62	37.68	353.18
GA-34C-1280	1070-04	21	83.26	48.81	2.31	4	3	1.15E-05	0.0266	0.00266	0.0168	1.84E-03	5.32E-03	1.69E-03	9.82	27.73	310.14
GA-34C-1280	1070-04	22	142.38	72.65	2.15	4	4	3.20E-05	0.0074	0.00074	0.0204	1.16E-02	2.94E-02	4.71E-03	2.74	7.05	190.17

Table C1 Apatite fission track single grain ages for all samples used in this thesis generated using the ICP-MS method

UBC	AZ	Grain number	FT age (Ma)	1 σ (Ma)	Dpar (μ m)	Etch Figs	Natural tracks	Area (cm ²)	238U/43Ca (dmnls)	1 σ (dmnls)	43Ca back:sig	238U back:sig	232Th back:sig	147Sm back:sig	U (ppm)	Th (ppm)	Sm (ppm)
GA-34C-1280	1070-04	23	32.72	32.89	1.99	2	1	2.05E-05	0.0127	0.00127	0.0245	1.55E-02	1.85E-02	5.11E-03	4.71	10.89	211.57
GA-34C-1280	1070-04	24	27.33	27.47	2.62	1	1	1.28E-05	0.0244	0.00244	0.0216	2.65E-03	1.37E-02	8.59E-04	9.02	27.92	311.68
GA-34C-1280	1070-04	25	0.00	19.42	2.31	1	0	1.92E-05	0.0343	0.00343	0.0255	2.01E-03	3.25E-03	4.77E-03	12.68	72.15	352.98
GA-34C-1280	1070-04	26	38.50	27.50	2.39	4	2	1.54E-05	0.0288	0.00288	0.0282	6.32E-03	7.55E-03	6.00E-03	10.66	32.05	348.44
GA-34C-1280	1070-04	27	25.46	25.60	2.33	3	1	2.05E-05	0.0164	0.00164	0.0334	1.33E-02	1.89E-02	9.90E-03	6.05	16.83	244.74
GA-34C-1280	1070-04	28	86.23	44.00	2.31	4	4	1.60E-05	0.0246	0.00246	0.0303	5.37E-03	1.57E-02	3.24E-03	9.10	26.25	300.59
GA-34C-1280	1070-04	29	56.26	40.19	2.52	4	2	1.15E-05	0.0263	0.00263	0.0259	4.19E-03	1.40E-02	2.19E-03	9.71	26.22	311.05
GA-34C-1280	1070-04	30	0.00	28.91	2.27	1	0	3.07E-05	0.0144	0.00144	0.0215	6.83E-03	4.23E-03	2.32E-03	5.31	17.09	269.62
GA-34C-1280	1070-04	31	0.00	41.74	2.16	4	0	1.60E-05	0.0191	0.00191	0.0242	9.45E-03	7.43E-03	5.13E-03	7.05	21.22	261.45
GA-34C-1280	1070-04	32	42.19	30.14	2.36	2	2	1.54E-05	0.0263	0.00263	0.0178	6.79E-04	3.57E-03	3.62E-03	9.72	41.24	326.31
GA-34C-1280	1070-04	33	25.16	17.97	2.61	4	2	2.05E-05	0.0331	0.00331	0.0168	3.09E-03	4.83E-03	1.98E-03	12.25	34.69	348.13
GA-34C-1280	1070-04	34	90.09	52.82	2.35	3	3	1.34E-05	0.0210	0.00210	0.0224	8.44E-03	1.42E-02	3.97E-03	7.78	21.34	292.67
GA-34C-1280	1070-04	35	44.94	26.34	2.29	2	3	1.34E-05	0.0423	0.00423	0.0251	3.98E-03	1.95E-03	3.04E-03	15.65	104.00	384.81
GA-34C-1280	1070-04	36	65.93	38.65	2.56	3	3	1.28E-05	0.0303	0.00303	0.0231	0.00E+00	9.68E-03	5.02E-03	11.18	30.17	326.85
GA-34C-1280	1070-04	37	57.37	33.63	2.23	4	3	1.73E-05	0.0258	0.00258	0.0328	7.73E-03	1.35E-02	3.98E-03	9.52	29.60	397.17
GA-34C-1280	1070-04	38	11.40	11.46	2.52	4	1	1.92E-05	0.0390	0.00390	0.0257	3.65E-03	3.32E-03	3.22E-03	14.43	43.12	354.48
GA-34C-1280	1070-04	39	46.43	33.17	2.29	4	2	1.02E-05	0.0359	0.00359	0.0189	1.50E-03	5.89E-03	1.07E-03	13.25	39.62	372.64
GA-34C-1280	1070-04	40	65.57	30.07	2.56	4	5	2.56E-05	0.0253	0.00253	0.0219	1.26E-02	6.37E-03	4.76E-03	9.37	40.85	300.99
GA-52C-1585	1110-05	1	57.84	41.32	2.50	4	2	1.92E-05	0.0128	0.00128	0.0176	6.52E-03	1.16E-02	1.90E-03	5.43	23.34	284.48
GA-52C-1585	1110-05	2	61.57	43.98	2.45	4	2	1.54E-05	0.0151	0.00151	0.0176	9.33E-04	9.76E-03	2.24E-03	6.38	25.04	235.98
GA-52C-1585	1110-05	3	27.49	14.03	2.27	4	4	2.30E-05	0.0451	0.00451	0.0186	1.50E-03	4.09E-03	1.27E-03	19.09	79.40	424.30
GA-52C-1585	1110-05	4	90.97	41.72	2.60	4	5	3.84E-05	0.0102	0.00102	0.0191	4.03E-03	1.72E-02	2.93E-03	4.31	17.62	197.96
GA-52C-1585	1110-05	5	47.85	48.10	2.30	4	1	1.54E-05	0.0097	0.00097	0.0189	2.34E-03	1.70E-02	3.28E-03	4.11	16.72	228.81
GA-52C-1585	1110-05	6	21.95	22.06	2.24	4	1	3.20E-05	0.0102	0.00102	0.0186	5.03E-03	1.96E-02	6.73E-03	4.31	16.33	202.22
GA-52C-1585	1110-05	7	47.89	48.13	2.25	2	1	1.60E-05	0.0093	0.00093	0.0239	4.70E-03	2.34E-02	4.21E-03	3.94	16.20	196.45
GA-52C-1585	1110-05	8	30.58	30.74	2.44	3	1	2.24E-05	0.0104	0.00104	0.0209	0.00E+00	1.62E-02	7.93E-03	4.41	19.90	189.19
GA-52C-1585	1110-05	10	30.10	15.36	2.56	4	4	3.20E-05	0.0297	0.00297	0.0214	0.00E+00	8.60E-03	2.42E-03	12.55	43.22	358.88
GA-52C-1585	1110-05	11	34.64	34.82	2.45	4	1	2.56E-05	0.0081	0.00081	0.0552	2.65E-02	4.59E-02	7.97E-03	3.41	24.30	276.51
GA-52C-1585	1110-05	12	36.24	36.42	2.39	4	1	1.60E-05	0.0123	0.00123	0.0189	4.52E-03	1.98E-02	3.64E-03	5.21	22.96	236.72
GA-52C-1585	1110-05	13	13.48	7.90	2.47	4	3	1.63E-04	0.0098	0.00098	0.0228	1.31E-02	3.11E-02	7.00E-03	4.14	18.32	243.47
GA-52C-1585	1110-05	14	183.10	93.43	2.52	4	4	1.28E-05	0.0120	0.00120	0.0235	6.42E-03	1.44E-02	4.03E-03	5.10	18.77	216.57
GA-52C-1585	1110-05	15	47.79	48.03	2.43	4	1	1.54E-05	0.0097	0.00097	0.0198	4.41E-03	9.52E-03	3.70E-03	4.11	28.62	264.10
GA-52C-1585	1110-05	16	45.55	45.78	2.37	4	1	1.60E-05	0.0098	0.00098	0.0210	0.00E+00	2.74E-02	6.43E-03	4.14	15.02	175.73
GA-52C-1585	1110-05	17	0.00	83.49	2.36	3	0	1.28E-05	0.0099	0.00099	0.0231	0.00E+00	2.68E-02	4.51E-03	4.20	17.64	213.69
GA-52C-1585	1110-05	18	0.00	19.82	2.36	4	0	1.92E-05	0.0281	0.00281	0.0189	4.32E-04	5.87E-03	3.74E-03	11.90	51.42	353.28
GA-52C-1585	1110-05	19	56.84	40.60	2.35	4	2	2.30E-05	0.0109	0.00109	0.0236	6.39E-03	1.67E-02	7.71E-03	4.61	19.13	215.51
GA-52C-1585	1110-05	20	109.61	50.27	2.29	4	5	2.88E-05	0.0112	0.00112	0.0221	7.16E-03	2.38E-02	4.93E-03	4.76	17.36	220.76
GA-52C-1585	1110-05	21	32.25	23.04	2.57	2	2	3.20E-05	0.0138	0.00138	0.0188	0.00E+00	1.30E-02	4.24E-03	5.86	22.60	202.00

Table C1 Apatite fission track single grain ages for all samples used in this thesis generated using the ICP-MS method

UBC	AZ	Grain number	FT age (Ma)	1 σ (Ma)	Dpar (μ m)	Etch Figs	Natural tracks	Area (cm ²)	238U/43Ca (dmnls)	1 σ (dmnls)	43Ca back:sig	238U back:sig	232Th back:sig	147Sm back:sig	U (ppm)	Th (ppm)	Sm (ppm)
GA-52C-1585	1110-05	22	68.96	35.19	2.36	4	4	3.84E-05	0.0108	0.00108	0.0254	8.64E-03	2.07E-02	1.02E-02	4.55	18.34	200.01
GA-52C-1585	1110-05	23	28.82	28.97	2.19	4	1	1.92E-05	0.0129	0.00129	0.0262	2.89E-03	1.26E-02	4.06E-03	5.46	22.11	248.05
GA-52C-1585	1110-05	24	68.34	40.07	2.15	4	3	1.60E-05	0.0195	0.00195	0.0257	4.00E-03	2.03E-02	5.35E-03	8.27	25.07	255.16
GA-52C-1585	1110-05	25	49.96	35.69	2.61	4	2	1.92E-05	0.0149	0.00149	0.0269	4.08E-03	1.18E-02	6.08E-03	6.29	20.05	212.69
GA-52C-1585	1110-05	26	76.94	54.97	2.40	4	2	1.54E-05	0.0120	0.00120	0.0251	2.33E-03	2.17E-02	3.88E-03	5.10	20.21	284.03
GA-52C-1585	1110-05	27	66.59	33.98	2.40	4	4	4.10E-05	0.0104	0.00104	0.0274	1.94E-03	1.90E-02	4.11E-03	4.42	18.75	205.90
GA-52C-1585	1110-05	29	56.33	40.24	2.56	4	2	2.56E-05	0.0099	0.00099	0.0259	7.48E-03	1.61E-02	2.18E-03	4.18	21.08	244.72
GA-52C-1585	1110-05	30	75.97	76.36	2.24	3	1	9.60E-06	0.0098	0.00098	0.0231	1.49E-02	1.98E-02	7.26E-03	4.13	16.19	170.52
GA-52C-1585	1110-05	31	42.65	42.87	2.83	3	1	2.05E-05	0.0082	0.00082	0.0258	8.08E-03	2.52E-02	6.20E-03	3.46	16.54	221.87
GA-52C-1585	1110-05	32	98.74	70.54	2.31	4	2	1.28E-05	0.0112	0.00112	0.0277	2.77E-03	2.17E-02	7.13E-03	4.76	19.14	214.61
GA-52C-1585	1110-05	33	0.00	25.97	2.16	4	0	4.10E-05	0.0101	0.00101	0.0198	7.45E-03	2.33E-02	5.42E-03	4.25	15.48	189.01
GA-52C-1585	1110-05	34	53.70	53.98	2.29	4	1	1.28E-05	0.0104	0.00104	0.0252	1.21E-03	1.78E-02	4.22E-03	4.39	20.05	234.67
GA-52C-1585	1110-05	35	0.00	73.99	2.41	3	0	1.54E-05	0.0093	0.00093	0.0226	1.25E-02	1.54E-02	5.36E-03	3.95	15.88	210.06
GA-52C-1585	1110-05	36	30.41	30.57	2.92	2	1	1.92E-05	0.0122	0.00122	0.0191	5.53E-03	1.48E-02	3.91E-03	5.18	17.66	209.96
GA-52C-1585	1110-05	37	25.59	25.72	2.43	3	1	2.56E-05	0.0109	0.00109	0.0209	2.14E-03	1.22E-02	4.07E-03	4.62	20.21	220.63
GA-52C-1585	1110-05	38	45.47	26.66	2.36	4	3	1.92E-05	0.0245	0.00245	0.0236	1.74E-03	1.06E-02	3.63E-03	10.37	27.24	305.19
GA-52C-1585	1110-05	39	38.29	22.45	2.50	4	3	2.56E-05	0.0218	0.00218	0.0176	3.43E-03	7.65E-03	3.50E-03	9.24	30.28	283.25
GA-52C-1585	1110-05	40	28.36	16.63	2.46	4	3	3.20E-05	0.0236	0.00236	0.0176	1.30E-03	5.73E-03	1.62E-03	9.99	38.43	343.29
GBC5-928	1103-09	1	0.00	84.78	1.96	1	0	1.28E-05	0.0098	0.00098	0.0107	0.00E+00	4.54E-02	9.78E-03	4.15	3.93	47.60
GBC5-928	1103-09	2	52.55	37.54	1.76	3	2	1.28E-05	0.0212	0.00212	0.0174	2.68E-03	1.74E-03	6.83E-04	9.01	72.76	1117.90
GBC5-928	1103-09	4	0.00	975.00	2.32	1	0	1.60E-05	0.0006	0.00006	0.0184	2.18E-02	4.82E-03	3.57E-03	0.25	37.42	221.06
GBC5-928	1103-09	5	0.00	46.15	1.97	1	0	1.02E-05	0.0225	0.00225	0.0193	2.11E-03	3.04E-02	9.81E-03	9.59	9.41	60.74
GBC5-928	1103-09	6	0.00	3896.56	1.85	1	0	1.60E-05	0.0001	0.00001	0.0164	1.91E-01	4.16E-01	2.51E-03	0.04	0.65	194.53
GBC5-928	1103-09	7	0.00	1377.73	1.91	1	0	2.56E-05	0.0002	0.00002	0.0166	1.41E-01	7.39E-02	2.52E-03	0.10	2.74	236.83
GBC5-928	1103-09	8	0.00	16.57	2.03	3	0	7.68E-06	0.0840	0.00840	0.0247	5.86E-04	8.96E-02	5.91E-03	35.77	3.03	151.00
GBC5-928	1103-09	9	0.00	113.92	1.64	2	0	1.60E-05	0.0058	0.00058	0.0186	9.00E-03	4.66E-02	2.05E-03	2.46	2.18	217.79
GBC5-928	1103-09	10	0.00	153.57	1.22	1	0	1.60E-05	0.0043	0.00043	0.0174	1.70E-02	4.32E-02	4.09E-03	1.81	4.83	125.46
GBC5-928	1103-09	12	0.00	234.51	1.93	1	0	1.60E-05	0.0028	0.00028	0.0230	2.94E-02	1.74E-02	6.86E-03	1.17	15.63	166.05
GBC5-928	1103-09	13	0.00	167.62	2.04	1	0	2.56E-05	0.0024	0.00024	0.0229	2.28E-02	4.65E-01	2.86E-02	1.04	0.51	30.90
GBC5-928	1103-09	14	0.00	68.96	1.83	2	0	1.54E-05	0.0100	0.00100	0.0169	1.78E-03	6.08E-03	2.26E-03	4.26	36.49	273.00
GBC5-928	1103-09	15	0.00	39.92	2.82	2	0	1.92E-05	0.0139	0.00139	0.0174	2.32E-03	1.03E-02	6.35E-03	5.92	21.38	138.31
GBC5-928	1103-09	16	0.00	2694.49	2.04	1	0	1.15E-05	0.0002	0.00002	0.0163	8.44E-02	5.47E-01	2.58E-03	0.09	0.18	112.40
GBC5-928	1103-09	17	0.00	717.40	1.86	1	0	2.05E-05	0.0007	0.00007	0.0190	1.77E-02	1.83E-01	5.04E-02	0.28	0.14	21.99
GBC5-928	1103-09	18	0.00	51.07	2.96	4	0	9.60E-06	0.0217	0.00217	0.0235	1.22E-03	2.07E-02	8.53E-03	9.24	16.64	156.23
GBC5-928	1103-09	19	0.00	747.11	1.73	1	0	2.30E-05	0.0006	0.00006	0.0188	3.58E-02	4.04E-01	1.81E-02	0.24	0.42	56.88
GBC5-928	1103-09	20	0.00	459.15	1.47	1	0	1.28E-05	0.0017	0.00017	0.0158	0.00E+00	5.92E-03	3.20E-03	0.72	24.61	119.10
GBC5-928	1103-09	23	29.66	29.81	1.39	1	1	1.92E-05	0.0125	0.00125	0.0157	6.12E-03	1.46E-02	7.09E-03	5.33	9.85	67.07
GBC5-928	1103-09	24	390.16	392.17	1.34	1	1	2.05E-05	0.0009	0.00009	0.0163	8.98E-02	9.20E-01	1.29E-02	0.37	0.04	45.01

Table C1 Apatite fission track single grain ages for all samples used in this thesis generated using the ICP-MS method

UBC	AZ	Grain number	FT age (Ma)	1 σ (Ma)	Dpar (μ m)	Etch Figs	Natural tracks	Area (cm ²)	238U/43Ca (dmnls)	1 σ (dmnls)	43Ca back:sig	238U back:sig	232Th back:sig	147Sm back:sig	U (ppm)	Th (ppm)	Sm (ppm)
GBC5-928	1103-09	26	2117.94	2128.86	1.37	1	1	3.84E-05	0.0001	0.00001	0.0196	2.25E-01	5.73E+00	5.17E-02	0.03	0.00	14.58
GBC5-928	1103-09	27	788.67	792.74	1.58	3	1	1.15E-05	0.0007	0.00007	0.0146	3.21E-02	2.37E-01	6.35E-02	0.31	0.25	2.69
GBC5-928	1103-09	28	0.00	359.54	1.75	1	0	7.68E-06	0.0037	0.00037	0.0184	0.00E+00	1.38E-02	1.01E-02	1.56	5.63	38.70
GBC5-928	1103-09	29	17.63	17.72	2.71	1	1	7.68E-06	0.0527	0.00527	0.0212	0.00E+00	7.11E-02	1.59E-02	22.45	2.99	96.87
GBC5-928	1103-09	30	0.00	5318.12	1.74	1	0	1.60E-05	0.0000	0.00000	0.0153	2.49E-01	2.28E+00	3.65E-01	0.02	0.07	2.00
GBC5-928	1103-09	31	48.17	48.42	2.30	4	1	7.68E-06	0.0192	0.00192	0.0184	2.91E-03	9.62E-03	1.30E-03	8.19	21.39	444.53
GBC5-928	1103-09	32	136.59	69.69	2.15	4	4	1.02E-05	0.0202	0.00202	0.0157	2.69E-03	3.30E-03	1.13E-03	8.61	39.58	630.20
GBC5-928	1103-09	33	0.00	930.55	2.28	1	0	1.28E-05	0.0008	0.00008	0.0149	7.77E-03	2.60E-01	3.39E-02	0.33	0.37	12.10
GBC5-928	1103-09	34	0.00	684.73	1.79	1	0	2.05E-05	0.0007	0.00007	0.0170	3.48E-02	1.70E-01	6.30E-03	0.29	0.67	44.82
GBC5-928	1103-09	35	0.00	2716.53	1.73	1	0	1.92E-05	0.0001	0.00001	0.0156	6.00E-01	8.46E-01	2.73E-03	0.06	0.04	220.30
GBC5-928	1103-09	36	0.00	2956.84	1.88	1	0	1.54E-05	0.0001	0.00001	0.0146	1.67E-01	3.14E-01	3.74E-03	0.06	0.19	128.60
GS-1765C-782	1070-07	2	14.88	10.63	1.86	4	2	1.28E-05	0.0895	0.00895	0.0138	3.06E-04	2.18E-03	1.59E-03	33.15	58.13	338.42
GS-1765C-782	1070-07	3	22.25	15.90	1.92	4	2	1.02E-05	0.0748	0.00748	0.0173	8.37E-04	3.04E-03	2.03E-03	27.70	48.88	464.33
GS-1765C-782	1070-07	4	48.62	13.91	2.17	4	14	1.54E-05	0.1590	0.01590	0.0187	6.73E-04	1.70E-03	1.00E-03	59.04	127.79	550.90
GS-1765C-782	1070-07	5	6.22	4.45	2.09	4	2	1.92E-05	0.1430	0.01430	0.0178	7.61E-04	3.09E-03	2.10E-03	52.87	108.60	492.42
GS-1765C-782	1070-07	6	8.36	8.40	1.81	4	1	1.34E-05	0.0759	0.00759	0.0189	1.02E-03	4.36E-03	2.52E-03	28.12	52.69	387.12
GS-1765C-782	1070-07	7	29.70	17.41	2.42	4	3	6.40E-06	0.1340	0.01340	0.0165	5.16E-04	2.14E-03	1.84E-03	49.78	102.59	638.74
GS-1765C-782	1070-07	8	46.30	23.62	1.92	4	4	9.60E-06	0.0766	0.00766	0.0182	1.74E-04	4.88E-03	3.06E-03	28.35	43.28	441.50
GS-1765C-782	1070-07	9	44.29	22.60	1.63	4	4	7.68E-06	0.1000	0.01000	0.0199	3.91E-03	3.55E-03	2.46E-03	37.05	59.00	381.87
GS-1765C-782	1070-07	10	10.77	10.83	2.00	4	1	1.54E-05	0.0516	0.00516	0.0237	1.99E-03	2.84E-03	5.27E-03	19.09	36.42	288.89
GS-1765C-782	1070-07	11	39.15	22.95	2.33	4	3	9.60E-06	0.0680	0.00680	0.0192	2.92E-04	3.50E-03	1.84E-03	25.16	52.93	478.58
GS-1765C-782	1070-07	12	38.61	13.46	1.86	4	9	2.56E-05	0.0775	0.00775	0.0186	7.50E-04	3.76E-03	5.96E-04	28.70	61.50	401.10
GS-1765C-782	1070-07	13	33.98	24.27	1.73	4	2	9.60E-06	0.0522	0.00522	0.0184	6.85E-04	8.07E-03	2.73E-03	19.33	34.05	315.15
GS-1765C-782	1070-07	14	34.32	15.74	1.80	4	5	2.05E-05	0.0606	0.00606	0.0166	1.82E-03	3.99E-03	2.36E-03	22.43	40.63	373.85
GS-1765C-782	1070-07	15	40.21	23.57	1.75	4	3	1.34E-05	0.0473	0.00473	0.0187	1.71E-03	4.84E-03	2.49E-03	17.50	34.79	351.61
GS-1765C-782	1070-07	16	39.13	16.46	1.82	4	6	1.79E-05	0.0728	0.00728	0.0198	2.89E-03	5.27E-03	2.69E-03	26.97	51.79	370.14
GS-1765C-782	1070-07	17	46.33	18.14	1.95	4	7	7.68E-06	0.1670	0.01670	0.0287	1.37E-03	2.61E-03	2.41E-03	61.96	124.97	681.56
GS-1765C-782	1070-07	18	57.73	20.12	2.01	4	9	9.60E-06	0.1380	0.01380	0.0202	8.95E-04	9.46E-04	1.17E-03	51.11	105.67	504.79
GS-1765C-782	1070-07	19	92.42	32.21	1.91	4	9	7.68E-06	0.1080	0.01080	0.0168	1.24E-03	4.34E-03	1.95E-03	39.79	48.47	418.56
GS-1765C-782	1070-07	20	55.08	25.26	1.92	4	5	1.73E-05	0.0447	0.00447	0.0184	1.39E-03	7.68E-03	4.63E-03	16.54	20.67	254.43
GS-1765C-782	1070-07	21	12.45	7.30	1.87	4	3	2.56E-05	0.0803	0.00803	0.0227	0.00E+00	4.21E-03	5.32E-03	29.74	56.50	423.15
GS-1765C-782	1070-07	22	41.07	18.84	1.85	4	5	1.28E-05	0.0809	0.00809	0.0220	2.58E-03	3.24E-03	1.71E-03	29.97	57.68	412.39
GS-1765C-782	1070-07	23	100.83	42.43	2.13	4	6	5.76E-06	0.0875	0.00875	0.0236	2.74E-03	2.96E-03	2.36E-03	32.40	55.78	384.20
GS-1765C-782	1070-07	24	23.11	13.55	2.05	4	3	7.68E-06	0.1440	0.01440	0.0246	1.99E-03	3.38E-03	4.09E-03	53.34	78.24	399.27
GS-1765C-782	1070-07	25	29.17	12.27	1.97	4	6	1.02E-05	0.1710	0.01710	0.0240	3.78E-03	5.33E-03	4.74E-03	63.35	74.43	407.25
GS-1765C-782	1070-07	26	63.62	18.80	2.29	4	13	3.84E-06	0.4520	0.04520	0.0241	5.81E-04	1.62E-03	1.07E-03	167.38	146.19	557.56
GS-1765C-782	1070-07	27	18.24	9.31	2.04	4	4	1.92E-05	0.0974	0.00974	0.0190	4.30E-03	1.39E-03	3.37E-03	36.06	68.75	389.32
GS-1765C-782	1070-07	28	60.63	25.51	1.84	4	6	1.92E-05	0.0438	0.00438	0.0282	8.64E-03	1.04E-02	5.61E-03	16.22	28.94	331.61

Table C1 Apatite fission track single grain ages for all samples used in this thesis generated using the ICP-MS method

UBC	AZ	Grain number	FT age (Ma)	1 σ (Ma)	Dpar (μ m)	Etch Figs	Natural tracks	Area (cm ²)	238U/43Ca (dmnls)	1 σ (dmnls)	43Ca back:sig	238U back:sig	232Th back:sig	147Sm back:sig	U (ppm)	Th (ppm)	Sm (ppm)
GS-1765C-782	1070-07	29	36.93	12.87	2.19	4	9	3.20E-05	0.0648	0.00648	0.0263	2.36E-03	8.00E-03	6.62E-03	24.01	42.58	337.30
GS-1765C-782	1070-07	30	52.01	30.49	1.90	2	3	7.68E-06	0.0639	0.00639	0.0184	1.39E-03	2.79E-03	4.93E-03	23.65	38.23	361.92
GS-1765C-782	1070-07	31	11.70	11.76	1.54	4	1	1.60E-05	0.0456	0.00456	0.0146	4.19E-03	2.77E-03	1.80E-03	16.87	42.91	430.29
GS-1765C-782	1070-07	32	64.07	25.08	1.93	4	7	8.96E-06	0.1040	0.01040	0.0165	5.98E-04	2.30E-03	2.36E-03	38.35	95.55	542.97
GS-1765C-782	1070-07	33	0.00	18.49	1.81	4	0	1.02E-05	0.0675	0.00675	0.0168	2.08E-03	4.30E-03	1.53E-03	24.97	46.32	374.74
GS-1765C-782	1070-07	34	0.00	11.29	1.82	4	0	1.28E-05	0.0885	0.00885	0.0217	3.05E-03	4.91E-03	1.35E-03	32.75	54.33	351.25
GS-1765C-782	1070-07	35	27.64	12.68	1.94	4	5	9.60E-06	0.1610	0.01610	0.0182	8.63E-04	1.46E-03	1.92E-03	59.44	138.87	567.48
GS-1765C-782	1070-07	36	115.28	32.00	2.07	4	15	1.02E-05	0.1080	0.01080	0.0199	9.07E-04	2.77E-03	2.36E-03	39.81	61.10	432.19
GS-1765C-782	1070-07	37	43.98	12.21	2.14	4	15	1.92E-05	0.1510	0.01510	0.0215	1.15E-03	1.64E-03	2.68E-03	55.97	125.73	647.59
GS-1765C-782	1070-07	38	75.29	26.24	2.19	4	9	7.68E-06	0.1320	0.01320	0.0239	3.36E-03	5.77E-03	7.85E-03	48.92	126.88	475.05
GS-1765C-782	1070-07	39	34.90	20.46	1.86	4	3	7.68E-06	0.0953	0.00953	0.0242	4.43E-03	5.83E-03	5.14E-03	35.28	91.96	456.67
GS-1765C-782	1070-07	40	48.21	22.11	1.98	4	5	9.60E-06	0.0919	0.00919	0.0220	1.24E-03	1.98E-03	1.75E-03	34.02	63.73	426.64
GS-1814C-1595	1178-06	1	58.68	13.40	2.17	4	5	2.30E-05	0.0508	0.00480					13.00	38.00	273.00
GS-1814C-1595	1178-06	2	22.56	5.20	2.00	4	5	7.68E-06	0.3975	0.03761					105.00	258.00	156.00
GS-1814C-1595	1178-06	3	0.00	0.00	2.01	4	8	1.92E-05	0.0000	0.00000					0.00	0.00	0.00
GS-1814C-1595	1178-06	4	6.41	3.20	1.95	4	1	1.28E-05	0.1680	0.01585					43.00	74.00	309.00
GS-1814C-1595	1178-06	5	44.10	10.10	2.05	4	5	1.02E-05	0.1523	0.01454					40.00	53.00	228.00
GS-1814C-1595	1178-06	6	77.75	15.20	1.97	4	7	1.28E-05	0.0965	0.00911					22.00	66.00	383.00
GS-1814C-1595	1178-06	7	108.14	19.90	2.04	4	8	1.28E-05	0.0791	0.00749					17.00	73.00	459.00
GS-1814C-1595	1178-06	8	15.79	3.10	1.95	4	7	2.05E-05	0.2984	0.02823					51.00	91.00	204.00
GS-1814C-1595	1178-06	9	52.47	9.10	1.84	4	9	1.02E-05	0.2302	0.02175					50.00	70.00	213.00
GS-1814C-1595	1178-06	10	116.38	22.80	1.99	4	7	7.68E-06	0.1071	0.01012					21.00	70.00	271.00
GS-1814C-1595	1178-06	11	57.24	13.10	1.86	4	5	1.60E-05	0.0750	0.00710					17.00	34.00	252.00
GS-1814C-1595	1178-06	12	41.65	12.20	2.01	4	3	1.28E-05	0.0774	0.00731					18.00	36.00	140.00
GS-1814C-1595	1178-06	13	19.05	4.30	1.83	4	5	2.05E-05	0.1766	0.01668					46.00	107.00	380.00
GS-1814C-1595	1178-06	14	57.21	13.10	1.83	4	5	1.28E-05	0.0938	0.00887					28.00	54.00	334.00
GS-1814C-1595	1178-06	15	20.13	5.90	1.98	4	3	1.60E-05	0.1283	0.01213					30.00	108.00	327.00
GS-1814C-1595	1178-06	16	33.75	12.10	2.30	4	2	2.30E-05	0.0354	0.00335					7.00	32.00	246.00
GS-1814C-1595	1178-06	17	0.00	0.00	2.32	4	3	9.60E-06	0.0000	0.00000					0.00	0.00	0.00
GS-1814C-1595	1178-06	18	36.00	10.50	2.13	4	3	1.02E-05	0.1120	0.01058					32.00	64.00	185.00
GS-1814C-1595	1178-06	19	23.49	8.40	1.60	4	2	3.20E-05	0.0366	0.00346					10.00	37.00	439.00
GS-1814C-1595	1178-06	20	44.41	22.30	1.95	4	1	1.02E-05	0.0302	0.00286					9.00	28.00	245.00
GS-1814C-1595	1178-06	21	28.97	10.30	2.19	2	2	1.54E-05	0.0619	0.00585					12.00	30.00	247.00
GS-1814C-1595	1178-06	22	50.57	11.60	2.20	4	5	6.40E-06	0.2123	0.02006					49.00	78.00	322.00
GS-1814C-1595	1178-06	23	112.01	25.70	2.04	4	5	9.60E-06	0.0636	0.00601					18.00	41.00	307.00
GS-1814C-1595	1178-06	24	61.08	12.80	1.95	4	6	1.92E-05	0.0703	0.00670					20.00	44.00	263.00
GS-1814C-1595	1178-06	25	14.73	5.30	1.88	4	2	1.92E-05	0.0975	0.00920					20.00	55.00	224.00
GS-1814C-1595	1178-06	26	44.19	11.30	2.01	4	4	1.15E-05	0.1081	0.01022					28.00	64.00	135.00

Table C1 Apatite fission track single grain ages for all samples used in this thesis generated using the ICP-MS method

UBC	AZ	Grain number	FT age (Ma)	1 σ (Ma)	Dpar (μ m)	Etch Figs	Natural tracks	Area (cm ²)	238U/43Ca (dmnls)	1 σ (dmnls)	43Ca back:sig	238U back:sig	232Th back:sig	147Sm back:sig	U (ppm)	Th (ppm)	Sm (ppm)
GS-1814C-1595	1178-06	27	22.82	5.80	2.17	4	4	9.60E-06	0.2515	0.02376					68.00	107.00	258.00
GS-1814C-1595	1178-06	28	14.45	5.10	2.05	4	2	1.54E-05	0.1242	0.01173					25.00	56.00	164.00
GS-1814C-1595	1178-06	29	18.52	6.60	2.09	4	2	4.10E-05	0.0363	0.00343					8.00	20.00	169.00
GS-1814C-1595	1178-06	30	68.66	10.50	2.03	4	12	5.76E-06	0.4164	0.03928					89.00	160.00	393.00
GS-1814C-1595	1178-06	31	109.87	20.20	2.11	4	8	2.05E-05	0.0486	0.00467					22.00	52.00	167.00
GS-1814C-1595	1178-06	32	57.38	14.70	1.73	4	4	2.56E-05	0.0374	0.00354					11.00	32.00	224.00
GS-1814C-1595	1178-06	33	0.29	0.10	1.78	4	1	1.62E-04	0.2890	0.02730					57.00	88.00	111.00
GS-1814C-1595	1178-06	34	46.89	10.70	1.84	4	5	1.28E-05	0.1145	0.01081					25.00	38.00	151.00
GS-1814C-1595	1178-06	35	44.24	7.30	1.94	4	10	1.92E-05	0.1619	0.01532					62.00	154.00	261.00
GS-1814C-1595	1178-06	36	116.52	16.60	1.94	4	14	1.28E-05	0.1284	0.01213					34.00	90.00	252.00
GS-1814C-1595	1178-06	37	27.78	8.10	1.68	4	3	1.28E-05	0.1162	0.01099					27.00	57.00	255.00
GS-1814C-1595	1178-06	38	54.89	14.00	2.14	4	4	1.60E-05	0.0626	0.00591					15.00	31.00	197.00
GS-1814C-1595	1178-06	39	41.92	15.00	1.94	4	2	2.30E-05	0.0285	0.00269					7.00	18.00	148.00
GS-1814C-1595	1178-06	40	51.49	15.10	2.11	4	3	2.30E-05	0.0348	0.00329					8.00	23.00	180.00
GS-1818C-1000	1110-01	1	52.86	14.27	2.05	4	16	1.15E-05	0.1910	0.01910	0.0122	3.91E-04	2.70E-03	2.83E-03	79.53	55.78	415.64
GS-1818C-1000	1110-01	2	102.61	34.08	2.15	4	10	5.12E-06	0.1380	0.01380	0.0126	5.83E-04	3.35E-03	3.73E-03	57.39	67.29	442.32
GS-1818C-1000	1110-01	3	20.95	12.28	2.36	4	3	6.40E-06	0.1630	0.01630	0.0134	2.82E-04	2.68E-03	2.79E-03	67.90	81.09	535.25
GS-1818C-1000	1110-01	4	81.83	24.17	2.06	4	13	5.76E-06	0.2000	0.02000	0.0126	5.83E-05	4.82E-03	3.08E-03	83.30	39.19	364.76
GS-1818C-1000	1110-01	5	35.34	16.21	2.29	4	5	7.68E-06	0.1340	0.01340	0.0132	5.28E-04	1.23E-03	2.04E-03	55.83	91.67	626.53
GS-1818C-1000	1110-01	6	34.80	10.65	2.09	4	12	7.68E-06	0.3270	0.03270	0.0160	1.27E-04	2.97E-03	2.99E-03	136.08	78.65	519.89
GS-1818C-1000	1110-01	7	42.47	17.87	2.05	4	6	9.60E-06	0.1070	0.01070	0.0182	1.00E-04	5.40E-03	2.60E-03	44.58	34.99	412.00
GS-1818C-1000	1110-01	8	53.07	17.63	2.24	4	10	7.68E-06	0.1790	0.01790	0.0159	7.96E-05	2.43E-03	1.66E-03	74.27	59.33	506.99
GS-1818C-1000	1110-01	9	57.58	20.06	2.07	4	9	1.02E-05	0.1110	0.01110	0.0166	2.01E-04	4.64E-03	3.08E-03	46.19	55.30	477.63
GS-1818C-1000	1110-01	10	41.29	13.14	2.05	4	11	8.96E-06	0.2170	0.02170	0.0163	3.81E-04	6.61E-04	2.21E-03	90.08	108.73	685.53
GS-1818C-1000	1110-01	11	20.41	8.59	2.31	4	6	1.15E-05	0.1860	0.01860	0.0140	9.93E-05	2.23E-03	2.13E-03	77.42	88.33	564.41
GS-1818C-1000	1110-01	12	105.77	23.36	2.23	4	26	5.12E-06	0.3480	0.03480	0.0156	0.00E+00	2.26E-03	4.38E-03	144.73	94.46	394.22
GS-1818C-1000	1110-01	13	16.25	9.53	2.08	4	3	7.68E-06	0.1760	0.01760	0.0147	6.45E-04	6.87E-04	1.53E-03	72.95	122.30	653.92
GS-1818C-1000	1110-01	14	52.18	15.97	2.11	4	12	7.68E-06	0.2180	0.02180	0.0150	3.33E-04	2.36E-03	2.82E-03	90.64	76.87	537.93
GS-1818C-1000	1110-01	15	63.35	18.11	2.12	4	14	7.68E-06	0.2090	0.02090	0.0164	6.16E-04	1.93E-03	2.47E-03	87.02	64.79	527.08
GS-1818C-1000	1110-01	16	38.85	15.21	2.22	4	7	1.02E-05	0.1280	0.01280	0.0162	4.20E-04	3.00E-03	3.25E-03	53.31	57.85	375.90
GS-1818C-1000	1110-01	17	59.82	22.01	2.08	4	8	6.40E-06	0.1520	0.01520	0.0228	0.00E+00	2.81E-03	4.26E-03	63.22	61.42	429.19
GS-1818C-1000	1110-01	18	52.00	15.36	2.12	4	13	1.34E-05	0.1350	0.01350	0.0226	6.91E-04	3.07E-03	3.01E-03	56.31	65.84	488.47
GS-1818C-1000	1110-01	19	62.48	19.88	2.27	4	11	5.12E-06	0.2500	0.02500	0.0197	0.00E+00	3.63E-03	2.76E-03	104.00	61.39	346.39
GS-1818C-1000	1110-01	20	74.34	20.63	2.35	4	15	6.40E-06	0.2290	0.02290	0.0164	2.33E-04	4.58E-03	3.45E-03	95.27	49.25	326.67
GS-1818C-1000	1110-01	22	19.38	8.89	2.26	4	5	7.68E-06	0.2450	0.02450	0.0162	1.48E-04	1.35E-03	2.51E-03	101.93	65.62	434.82
GS-1818C-1000	1110-01	23	46.68	18.27	2.12	4	7	6.40E-06	0.1710	0.01710	0.0159	1.43E-04	2.05E-03	1.45E-03	70.95	112.32	733.71
GS-1818C-1000	1110-01	24	87.53	23.02	2.21	4	17	5.12E-06	0.2750	0.02750	0.0226	4.11E-04	1.49E-03	3.31E-03	114.51	133.85	513.62
GS-1818C-1000	1110-01	25	37.33	15.70	2.22	4	6	5.12E-06	0.2290	0.02290	0.0226	0.00E+00	1.87E-03	2.21E-03	95.14	122.54	623.14

Table C1 Apatite fission track single grain ages for all samples used in this thesis generated using the ICP-MS method

UBC	AZ	Grain number	FT age (Ma)	1 σ (Ma)	Dpar (μ m)	Etch Figs	Natural tracks	Area (cm ²)	238U/43Ca (dmnls)	1 σ (dmnls)	43Ca back:sig	238U back:sig	232Th back:sig	147Sm back:sig	U (ppm)	Th (ppm)	Sm (ppm)
GS-1818C-1000	1110-01	26	40.92	18.77	1.92	4	5	6.40E-06	0.1390	0.01390	0.0191	4.36E-04	2.02E-03	2.30E-03	57.85	79.24	370.86
GS-1818C-1000	1110-01	28	78.69	30.80	2.03	4	7	5.12E-06	0.1260	0.01260	0.0140	1.37E-04	1.70E-03	1.72E-03	52.48	108.57	612.94
GS-1818C-1000	1110-01	29	33.72	24.09	2.07	4	2	5.12E-06	0.0845	0.00845	0.0202	8.49E-04	1.61E-03	5.96E-03	35.11	107.98	223.59
GS-1818C-1000	1110-01	30	39.65	12.61	1.96	4	11	6.40E-06	0.3160	0.03160	0.0201	9.52E-05	1.78E-03	2.19E-03	131.35	123.63	579.66
GS-1818C-1000	1110-01	31	68.49	22.75	2.18	4	10	5.76E-06	0.1840	0.01840	0.0211	1.99E-04	1.85E-03	2.74E-03	76.64	66.81	500.78
GS-1818C-1000	1110-01	32	111.61	35.51	2.00	4	11	1.02E-05	0.0698	0.00698	0.0206	1.63E-04	6.37E-03	3.40E-03	29.00	28.34	351.06
GS-1818C-1000	1110-01	33	31.85	10.13	1.93	4	11	1.34E-05	0.1870	0.01870	0.0180	2.26E-04	2.39E-03	1.30E-03	77.92	94.95	560.43
GS-1818C-1000	1110-01	34	57.61	13.61	2.40	4	22	5.76E-06	0.4830	0.04830	0.0213	2.54E-05	4.61E-04	1.34E-03	200.62	416.30	1065.30
GS-1818C-1000	1110-01	35	79.83	26.51	1.98	4	10	5.12E-06	0.1780	0.01780	0.0234	1.07E-03	5.99E-03	4.02E-03	73.91	50.26	393.74
GS-1818C-1000	1110-01	36	59.83	15.73	2.13	4	17	1.15E-05	0.1800	0.01800	0.0198	5.11E-04	4.28E-03	3.86E-03	74.61	47.86	394.16
GS-1818C-1000	1110-01	37	53.54	16.38	2.28	4	12	9.60E-06	0.1700	0.01700	0.0190	4.35E-04	2.39E-03	1.48E-03	70.67	103.97	534.79
GS-1818C-1000	1110-01	38	39.91	11.41	2.18	4	14	9.60E-06	0.2660	0.02660	0.0219	2.68E-04	2.34E-03	2.13E-03	110.72	105.36	590.19
GS-1818C-1000	1110-01	39	58.76	21.61	2.21	4	8	7.68E-06	0.1290	0.01290	0.0211	6.44E-04	1.81E-03	2.21E-03	53.64	69.96	575.33
GS-1818C-1000	1110-01	40	78.12	25.95	2.16	4	10	7.68E-06	0.1210	0.01210	0.0212	7.26E-04	3.13E-03	3.75E-03	50.35	52.46	456.50
GS1845C 1	75602	1	70.72	14.91	2.05	4	24	7.68E-06	0.2040	0.00942	0.0268	6.57E-05			66.31	0.13	
GS1845C 1	75602	2	102.93	34.85	2.00	4	9	9.60E-06	0.0419	0.00226	0.0273	1.31E-02			13.63	0.80	
GS1845C 1	75602	3	69.39	23.44	1.95	4	9	1.92E-05	0.0311	0.00152	0.0288	2.25E-02			10.14	1.53	
GS1845C 1	75602	4	58.41	14.92	2.13	4	16	1.15E-05	0.1100	0.00498	0.0292	7.35E-04			35.72	0.33	
GS1845C 1	75602	5	60.91	12.20	1.71	4	27	1.28E-05	0.1600	0.00783	0.0274	3.42E-04			52.00	0.23	
GS1845C 1	75602	6	83.13	21.96	1.91	4	15	1.02E-05	0.0811	0.00402	0.0257	8.33E-04			26.42	0.53	
GS1845C 1	75602	7	65.23	16.27	1.87	4	17	1.02E-05	0.1170	0.00617	0.0239	1.26E-03			38.20	0.46	
GS1845C 1	75602	8	40.39	23.42	1.73	4	3	9.60E-06	0.0357	0.00174	0.0247	2.17E-03			11.64	1.59	
GS1845C 1	75602	9	57.18	11.65	2.01	4	26	1.54E-05	0.1370	0.00670	0.0258	8.77E-04			44.46	0.32	
GS1845C 1	75602	10	75.17	16.92	1.94	4	21	1.15E-05	0.1120	0.00550	0.0263	3.50E-03			36.38	0.42	
GS1845C 1	75602	11	33.66	11.38	1.84	4	9	1.28E-05	0.0965	0.00483	0.0289	2.29E-03			31.44	0.53	
GS1845C 1	75602	12	38.95	8.70	2.03	4	21	7.68E-06	0.3240	0.01300	0.0398	1.65E-04			105.59	0.83	
GS1845C 1	75602	13	37.57	8.65	1.88	4	20	1.60E-05	0.1540	0.00750	0.0307	4.98E-03			50.06	0.57	
GS1845C 1	75602	15	77.78	20.22	2.03	4	16	9.60E-06	0.0987	0.00655	0.0235	4.51E-04			32.13	0.47	
GS1845C 1	75602	16	85.29	25.05	2.08	4	12	7.68E-06	0.0843	0.00404	0.0269	1.72E-03			27.46	0.53	
GS1845C 1	75602	18	62.45	17.02	1.91	4	14	7.68E-06	0.1350	0.00630	0.0269	1.97E-04			43.83	0.32	
GS1845C 1	75602	19	74.02	20.90	1.81	4	13	7.68E-06	0.1050	0.00485	0.0250	9.43E-04			34.30	0.39	
GS1845C 1	75602	21	68.21	15.68	2.13	4	20	7.68E-06	0.1760	0.00825	0.0262	4.57E-04			57.29	0.19	
GS1845C 1	75602	24	75.57	11.33	1.97	4	51	2.30E-05	0.1350	0.00638	0.0292	8.21E-05			43.94	0.30	
GS1845C 1	75602	25	100.30	19.43	1.95	4	29	1.60E-05	0.0831	0.00406	0.0253	6.45E-04			27.05	0.49	
GS1845CW1 2	75603	1	44.14	19.89	1.81	4	5	7.68E-06	0.0683	0.00333	0.0218	5.69E-04			22.24	1.14	
GS1845CW1 2	75603	2	76.28	16.43	2.03	4	23	9.60E-06	0.1450	0.00694	0.0224	9.62E-04			47.24	0.60	
GS1845CW1 2	75603	3	54.27	12.23	2.22	4	21	1.34E-05	0.1330	0.00664	0.0220	2.74E-03			43.38	0.71	
GS1845CW1 2	75603	4	64.76	14.29	2.13	4	22	1.15E-05	0.1360	0.00699	0.0207	1.03E-03			44.40	0.80	

Table C1 Apatite fission track single grain ages for all samples used in this thesis generated using the ICP-MS method

UBC	AZ	Grain number	FT age (Ma)	1 σ (Ma)	Dpar (μ m)	Etch Figs	Natural tracks	Area (cm ²)	238U/43Ca (dmnls)	1 σ (dmnls)	43Ca back:sig	238U back:sig	232Th back:sig	147Sm back:sig	U (ppm)	Th (ppm)	Sm (ppm)
GS1845CW1 2	75603	5	43.62	12.83	2.15	4	12	1.92E-05	0.0664	0.00331	0.0265	8.85E-03			21.61	1.14	
GS1845CW1 2	75603	6	63.08	13.89	2.12	4	22	1.79E-05	0.0900	0.00443	0.0261	1.54E-03			29.31	1.28	
GS1845CW1 2	75603	7	47.05	18.02	2.23	4	7	1.28E-05	0.0538	0.00304	0.0211	4.53E-03			17.52	1.92	
GS1845CW1 2	75603	8	90.58	26.58	1.86	4	12	5.76E-06	0.1060	0.00491	0.0272	6.77E-04			34.56	0.67	
GS1845CW1 2	75603	9	112.95	29.79	1.93	4	15	1.02E-05	0.0597	0.00285	0.0274	4.47E-03			19.45	0.92	
GS1845CW1 2	75603	10	56.13	14.87	1.99	4	15	1.15E-05	0.1070	0.00580	0.0228	1.12E-03			34.95	1.28	
GS1845CW1 2	75603	11	68.13	16.93	1.94	4	17	7.68E-06	0.1500	0.00718	0.0234	2.15E-04			48.90	0.94	
GS1845CW1 2	75603	12	78.88	20.88	1.81	4	15	1.15E-05	0.0762	0.00399	0.0256	1.28E-03			24.82	1.15	
GS1845CW1 2	75603	13	52.46	12.39	2.25	4	19	1.15E-05	0.1460	0.00734	0.0262	2.29E-04			47.38	0.92	
GS1845CW1 2	75603	14	59.63	14.80	2.05	4	17	1.28E-05	0.1030	0.00477	0.0309	6.57E-04			33.55	0.98	
GS1845CW1 2	75603	16	83.79	18.46	2.06	4	22	1.28E-05	0.0947	0.00468	0.0233	0.00E+00			30.84	1.30	
GS1845CW1 2	75603	17	70.31	18.58	1.93	4	15	9.60E-06	0.1030	0.00515	0.0249	1.08E-03			33.44	1.30	
GS1845CW1 2	75603	18	49.54	14.06	2.22	4	13	1.28E-05	0.0949	0.00515	0.0254	2.37E-03			30.90	0.68	
GS1845CW1 2	75603	19	44.30	13.02	2.44	4	12	1.15E-05	0.1090	0.00529	0.0283	1.94E-03			35.46	1.40	
GS1845CW1 2	75603	21	53.45	13.31	2.47	4	17	1.02E-05	0.1440	0.00727	0.0249	1.70E-04			46.80	0.85	
GS1845CW1 2	75603	22	59.74	15.32	1.98	4	16	1.02E-05	0.1210	0.00621	0.0496	1.65E-04			39.39	0.80	
GS1845CW1 2	75603	23	33.87	8.20	1.99	4	18	1.54E-05	0.1600	0.00799	0.0237	4.72E-04			52.22	1.32	
GS1845CW1 2	75603	24	76.10	23.36	1.90	4	11	1.02E-05	0.0652	0.00339	0.0250	1.61E-03			21.23	1.11	
GS1845CW1 2	75603	25	61.83	17.56	2.00	4	13	1.15E-05	0.0844	0.00472	0.0274	1.12E-03			27.48	0.75	
GS1845CW1 3	75604	1	99.19	25.38	1.82	4	16	1.73E-05	0.0432	0.00209	0.0256	0.00E+00			14.06	1.65	
GS1845CW1 3	75604	2	95.72	24.56	2.30	4	16	1.28E-05	0.0604	0.00315	0.0235	1.81E-04			19.67	1.98	
GS1845CW1 3	75604	3	41.30	15.80	1.87	4	7	1.15E-05	0.0683	0.00369	0.0230	1.49E-03			22.25	1.29	
GS1845CW1 3	75604	4	27.03	19.17	2.30	4	2	1.60E-05	0.0215	0.00110	0.0224	3.38E-03			7.00	1.08	
GS1845CW1 3	75604	5	65.35	15.43	2.31	4	19	2.30E-05	0.0585	0.00293	0.0248	3.01E-03			19.05	1.39	
GS1845CW1 3	75604	6	102.40	36.61	2.08	4	8	1.60E-05	0.0226	0.00105	0.0268	5.69E-04			7.35	1.63	
GS1845CW1 3	75604	7	77.38	29.55	1.72	4	7	1.73E-05	0.0243	0.00117	0.2900	5.40E-01			7.90	1.88	
GS1845CW1 3	75604	8	59.91	9.62	2.13	4	44	9.60E-06	0.3550	0.01750	0.0246	1.72E-04			115.55	0.46	
GS1845CW1 3	75604	9	33.33	13.74	2.25	4	6	1.28E-05	0.0654	0.00343	0.0215	2.12E-03			21.29	1.03	
GS1845CW1 3	75604	10	57.87	29.12	1.94	4	4	1.60E-05	0.0200	0.00101	0.0257	3.38E-03			6.53	2.06	
GS1845CW1 3	75604	11	37.81	17.08	2.07	4	5	1.92E-05	0.0320	0.00188	0.0307	4.42E-03			10.42	1.25	
GS1845CW1 3	75604	12	29.32	14.75	2.02	4	4	1.54E-05	0.0413	0.00202	0.0271	1.34E-03			13.45	1.31	
GS1845CW1 3	75604	13	46.70	15.77	1.92	4	9	1.28E-05	0.0699	0.00336	0.0264	9.21E-04			22.77	1.01	
GS1845CW1 3	75604	15	118.58	45.35	2.28	4	7	2.56E-05	0.0106	0.00056	0.0239	8.60E-04			3.47	1.21	
GS1845CW1 3	75604	16	75.53	25.52	1.98	4	9	1.54E-05	0.0359	0.00178	0.0274	8.53E-04			11.70	1.63	
GS1845CW1 3	75604	17	73.35	22.49	1.94	4	11	1.92E-05	0.0362	0.00181	0.0273	5.40E-03			11.79	1.42	
GS1845CW1 3	75604	18	64.29	14.51	2.00	4	21	1.92E-05	0.0789	0.00406	0.0242	1.00E-03			25.69	1.09	
GS1845CW1 3	75604	19	91.31	25.87	2.33	4	13	1.34E-05	0.0490	0.00254	0.0251	2.17E-03			15.96	1.50	
GS1845CW1 3	75604	20	93.93	28.79	2.04	4	11	1.54E-05	0.0353	0.00172	0.0252	1.46E-03			11.49	1.48	

Table C1 Apatite fission track single grain ages for all samples used in this thesis generated using the ICP-MS method

UBC	AZ	Grain number	FT age (Ma)	1 σ (Ma)	Dpar (μ m)	Etch Figs	Natural tracks	Area (cm ²)	238U/43Ca (dmnls)	1 σ (dmnls)	43Ca back:sig	238U back:sig	232Th back:sig	147Sm back:sig	U (ppm)	Th (ppm)	Sm (ppm)
GS1845CW1 3	75604	21	75.96	20.72	2.03	4	14	2.30E-05	0.0371	0.00179	0.0266	1.88E-03			12.07	1.36	
GS1845CW1 3	75604	22	71.56	13.46	2.12	4	31	1.15E-05	0.1740	0.00873	0.0244	2.73E-04			56.75	2.15	
GS1845CW1 3	75604	23	24.06	9.93	2.55	4	6	1.54E-05	0.0755	0.00423	0.0262	2.60E-03			24.59	1.80	
GS1845CW1 3	75604	24	41.43	12.18	2.24	4	12	1.15E-05	0.1170	0.00583	0.0277	2.80E-03			38.03	1.45	
GS1845CW1 3	75604	25	39.31	10.75	2.03	4	14	1.54E-05	0.1080	0.00561	0.0229	8.82E-04			35.08	0.87	
GS1845CW1 4	75605	1	68.96	18.30	2.22	4	15	1.28E-05	0.0790	0.00440	0.0201	2.24E-04			25.72	1.55	
GS1845CW1 4	75605	2	45.88	12.54	2.17	4	14	2.30E-05	0.0617	0.00320	0.0185	1.07E-03			20.09	2.01	
GS1845CW1 4	75605	3	37.63	8.31	2.14	4	22	5.12E-05	0.0532	0.00276	0.0198	1.96E-03			17.33	1.49	
GS1845CW1 4	75605	4	46.61	11.98	2.18	4	16	2.88E-05	0.0555	0.00300	0.0210	1.36E-03			18.08	1.49	
GS1845CW1 4	75605	5	92.15	22.98	2.43	4	18	1.28E-05	0.0708	0.00550	0.0199	3.81E-03			23.06	2.69	
GS1845CW1 4	75605	6	51.73	14.30	2.19	4	14	9.60E-06	0.1310	0.00864	0.0216	3.79E-04			42.73	1.37	
GS1845CW1 4	75605	7	69.20	18.60	1.93	4	15	1.60E-05	0.0630	0.00442	0.0239	3.04E-03			20.51	1.57	
GS1845CW1 4	75605	8	129.86	28.80	2.08	4	22	1.54E-05	0.0510	0.00285	0.0230	2.97E-03			16.62	1.98	
GS1845CW1 4	75605	9	78.75	19.54	2.12	4	17	2.05E-05	0.0490	0.00226	0.0304	3.40E-03			15.94	1.72	
GS1845CW1 4	75605	10	79.11	21.59	2.12	4	14	1.34E-05	0.0612	0.00302	0.0224	6.45E-04			19.92	2.69	
GS1845CW1 4	75605	11	52.62	14.47	2.27	4	14	1.79E-05	0.0691	0.00410	0.0240	1.36E-03			22.50	2.08	
GS1845CW1 4	75605	12	86.79	19.16	2.27	4	22	2.05E-05	0.0575	0.00295	0.0282	5.14E-03			18.71	1.72	
GS1845CW1 4	75605	13	58.77	16.05	2.28	4	14	2.56E-05	0.0433	0.00217	0.0268	3.70E-03			14.10	2.00	
GS1845CW1 4	75605	14	84.91	22.44	2.18	4	15	1.60E-05	0.0513	0.00259	0.0238	1.93E-03			16.69	2.32	
GS1845CW1 4	75605	15	49.61	10.93	2.13	4	22	2.24E-05	0.0922	0.00461	0.0260	8.28E-04			30.02	1.45	
GS1845CW1 4	75605	16	52.45	26.37	2.20	4	4	1.28E-05	0.0277	0.00131	0.0245	3.65E-03			9.03	0.96	
GS1845CW1 4	75605	17	33.67	12.88	2.19	4	7	1.28E-05	0.0757	0.00402	0.0286	1.65E-03			24.65	1.45	
GS1845CW1 4	75605	18	76.06	25.73	1.93	4	9	1.28E-05	0.0430	0.00224	0.0387	1.54E-02			13.99	1.80	
GS1845CW1 4	75605	19	56.20	21.43	1.68	4	7	1.92E-05	0.0302	0.00131	0.0332	4.79E-03			9.83	1.33	
GS1845CW1 4	75605	20	83.62	15.18	1.96	4	33	1.54E-05	0.1190	0.00536	0.0395	2.10E-03			38.85	1.57	
GS1845CW1 4	75605	21	33.99	12.98	2.18	4	7	1.60E-05	0.0600	0.00288	0.0303	5.88E-04			19.54	2.70	
GS1845CW1 4	75605	22	55.11	16.89	2.42	4	11	1.54E-05	0.0605	0.00297	0.0317	6.42E-04			19.69	1.69	
GS1845CW1 4	75605	23	53.15	15.01	2.25	4	13	1.28E-05	0.0889	0.00421	0.0304	1.76E-03			28.96	1.51	
GS1845CW1 4	75605	24	74.98	20.45	2.00	4	14	1.92E-05	0.0452	0.00217	0.0283	3.52E-03			14.71	2.36	
GS1845CW1 4	75605	25	40.53	11.06	2.19	4	14	1.92E-05	0.0838	0.00413	0.0264	5.23E-04			27.29	1.08	
GS1845CW1 5	75606	1	37.39	18.81	1.85	4	4	1.54E-05	0.0326	0.00162	0.0256	1.38E-03			10.60	1.69	
GS1845CW1 5	75606	4	21.27	15.09	1.77	4	2	1.15E-05	0.0382	0.00198	0.0244	1.03E-03			12.44	1.96	
GS1845CW1 5	75606	5	50.53	22.78	1.73	4	5	1.60E-05	0.0289	0.00149	0.0297	3.45E-03			9.40	1.95	
GS1845CW1 5	75606	6	136.21	38.63	1.61	4	13	1.34E-05	0.0329	0.00177	0.0403	8.21E-03			10.72	2.00	
GS1845CW1 5	75606	7	45.65	22.95	2.08	4	4	2.05E-05	0.0200	0.00091	0.0331	7.41E-03			6.51	2.18	
GS1845CW1 5	75606	9	82.79	23.40	1.92	4	13	2.56E-05	0.0286	0.00138	0.0266	1.36E-03			9.30	1.83	
GS1845CW1 5	75606	10	85.83	29.02	1.75	4	9	1.73E-05	0.0283	0.00143	0.0270	2.13E-03			9.20	1.60	
GS1845CW1 5	75606	11	65.86	16.47	1.83	4	17	2.30E-05	0.0522	0.00289	0.0251	1.31E-03			17.01	1.63	

Table C1 Apatite fission track single grain ages for all samples used in this thesis generated using the ICP-MS method

UBC	AZ	Grain number	FT age (Ma)	1 σ (Ma)	Dpar (μ m)	Etch Figs	Natural tracks	Area (cm ²)	238U/43Ca (dmnls)	1 σ (dmnls)	43Ca back:sig	238U back:sig	232Th back:sig	147Sm back:sig	U (ppm)	Th (ppm)	Sm (ppm)
GS1845CW1 5	75606	12	41.44	14.83	1.73	4	8	3.84E-05	0.0235	0.00117	0.0256	1.86E-03			7.65	1.90	
GS1845CW1 5	75606	13	60.06	30.27	1.57	4	4	9.60E-06	0.0324	0.00187	0.0265	1.69E-03			10.54	1.81	
GS1845CW1 5	75606	14	70.29	26.86	2.02	4	7	1.15E-05	0.0403	0.00205	0.0272	1.00E-03			13.12	1.88	
GS1845CW1 5	75606	15	67.01	24.03	2.20	4	8	2.56E-05	0.0217	0.00117	0.0248	5.03E-03			7.08	1.66	
GS1845CW1 5	75606	16	81.65	31.14	1.81	4	7	1.92E-05	0.0208	0.00093	0.0368	3.52E-03			6.77	2.37	
GS1845CW1 5	75606	17	74.74	20.39	1.95	4	14	2.30E-05	0.0379	0.00185	0.0306	1.76E-03			12.34	1.43	
GS1845CW1 5	75606	18	59.96	27.02	1.99	4	5	2.05E-05	0.0190	0.00094	0.0277	3.85E-03			6.19	1.90	
GS1845CW1 5	75606	19	51.87	19.80	2.09	4	7	2.30E-05	0.0273	0.00130	0.0297	3.00E-03			8.90	2.12	
GS1845CW1 5	75606	20	41.46	18.70	1.93	4	5	2.24E-05	0.0252	0.00132	0.0266	3.34E-03			8.19	1.93	
GS1845CW1 5	75606	22	36.19	20.99	1.74	4	3	1.28E-05	0.0303	0.00146	0.0252	0.00E+00			9.86	1.65	
GS1845CW1 5	75606	23	59.80	17.61	2.24	4	12	3.20E-05	0.0293	0.00154	0.0263	0.00E+00			9.53	2.66	
GS1845CW1 5	75606	24	61.53	22.10	2.10	4	8	1.60E-05	0.0379	0.00220	0.0263	2.63E-03			12.34	2.19	
GS1845CW1 5	75606	25	42.56	13.68	2.12	4	10	2.24E-05	0.0490	0.00254	0.0272	5.17E-04			15.96	1.57	
LBB100-4679	946-29	1	54.85	24.69	1.95	4	5	5.12E-06	0.1670	0.00752	0.0316	7.34E-04	3.54E-03	1.65E-03	56.24	33.41	558.71
LBB100-4679	946-29	2	95.03	42.69	1.88	4	5	2.56E-06	0.1920	0.00656	0.0345	1.70E-03	7.09E-03	2.28E-03	64.71	31.27	534.30
LBB100-4679	946-29	3	41.91	41.96	1.78	4	1	3.84E-06	0.0583	0.00268	0.0304	0.00E+00	3.69E-03	8.27E-04	19.65	33.41	650.34
LBB100-4679	946-29	4	69.22	69.27	2.78	4	1	5.76E-06	0.0235	0.00077	0.0355	4.77E-03	3.65E-03	1.07E-02	7.91	43.70	174.94
LBB100-4679	946-29	5	64.18	45.50	1.72	4	2	5.76E-06	0.0506	0.00227	0.0308	2.51E-03	3.95E-03	2.67E-03	17.08	46.38	396.40
LBB100-4679	946-29	6	41.16	15.68	1.84	4	7	3.84E-05	0.0415	0.00171	0.0314	3.06E-03	7.05E-03	3.30E-03	14.00	26.70	552.67
LBB100-4679	946-29	7	136.97	97.22	4.02	4	2	5.76E-06	0.0236	0.00133	0.0256	6.93E-03	4.10E-03	1.48E-02	7.96	46.12	124.80
LBB100-4679	946-29	8	71.19	41.37	1.98	4	3	7.68E-06	0.0513	0.00316	0.0239	1.22E-03	4.50E-03	9.97E-04	17.31	25.63	660.60
LBB100-4679	946-29	9	159.42	92.30	4.36	4	3	3.84E-06	0.0455	0.00164	0.0287	6.19E-04	1.47E-03	4.37E-03	15.35	138.58	159.42
LBB100-4679	946-29	10	151.68	54.68	2.96	4	8	9.60E-06	0.0511	0.00337	0.0297	6.73E-04	1.84E-03	4.51E-03	17.22	126.69	283.42
LBB100-4679	946-29	11	69.34	34.82	1.87	4	4	2.56E-06	0.2110	0.00832	0.0270	5.85E-04	5.43E-03	2.19E-03	71.10	35.47	630.35
LBB100-4679	946-29	12	0.00	53.22	1.86	4	0	6.40E-06	0.0411	0.00247	0.0224	1.60E-03	5.08E-03	1.28E-03	13.85	28.35	606.62
LBB100-4679	946-29	13	108.18	49.11	2.06	4	5	8.96E-06	0.0481	0.00357	0.0251	4.45E-04	3.61E-03	3.22E-03	16.23	46.68	495.24
LBB100-4679	946-29	14	117.91	33.16	2.02	4	13	3.84E-06	0.2680	0.01060	0.0249	6.28E-04	1.44E-03	1.82E-03	90.24	42.93	559.00
LBB100-4679	946-29	15	81.97	58.12	2.95	4	2	5.12E-06	0.0445	0.00211	0.0342	1.03E-02	4.64E-03	8.66E-03	15.02	97.14	231.05
LBB102-1035	946-31	1	122.20	50.29	2.07	4	6	5.76E-06	0.0794	0.00368	0.0356	2.38E-04	3.68E-03	1.39E-03	26.78	57.26	789.87
LBB102-1035	946-31	2	91.18	45.75	2.20	4	4	5.76E-06	0.0711	0.00237	0.0326	2.93E-03	1.04E-02	3.73E-03	23.99	24.81	537.94
LBB102-1035	946-31	3	77.48	29.51	2.09	4	7	1.28E-05	0.0659	0.00268	0.0318	7.51E-03	6.36E-03	3.78E-03	22.26	27.61	692.12
LBB102-1035	946-31	4	141.52	32.15	2.04	4	20	1.28E-05	0.1030	0.00331	0.0323	7.93E-04	7.83E-03	4.98E-03	34.64	35.78	629.61
LBB102-1035	946-31	5	72.68	42.13	2.06	4	3	7.68E-06	0.0502	0.00225	0.0313	1.10E-02	1.06E-02	4.01E-03	16.95	20.87	480.14
LBB102-1035	946-31	6	100.13	50.32	1.68	4	4	7.68E-06	0.0485	0.00217	0.0313	4.16E-03	4.71E-03	3.21E-03	16.37	33.23	572.92
LBB102-1035	946-31	7	177.62	63.33	1.99	4	8	1.54E-05	0.0272	0.00106	0.0303	0.00E+00	8.17E-03	3.16E-03	9.17	12.38	387.50
LBB102-1035	946-31	8	80.76	23.59	2.10	4	12	9.60E-06	0.1450	0.00540	0.0320	5.32E-04	3.52E-03	2.46E-03	48.79	43.49	676.54
LBB102-1035	946-31	9	55.15	24.77	2.05	4	5	1.54E-05	0.0552	0.00191	0.0324	2.13E-03	6.16E-03	2.23E-03	18.64	38.54	560.67
LBB102-1035	946-31	10	82.32	27.75	2.21	4	9	9.60E-06	0.1060	0.00465	0.0321	9.17E-04	1.26E-02	4.41E-03	35.89	36.42	676.63

Table C1 Apatite fission track single grain ages for all samples used in this thesis generated using the ICP-MS method

UBC	AZ	Grain number	FT age (Ma)	1 σ (Ma)	Dpar (μ m)	Etch Figs	Natural tracks	Area (cm ²)	238U/43Ca (dmnls)	1 σ (dmnls)	43Ca back:sig	238U back:sig	232Th back:sig	147Sm back:sig	U (ppm)	Th (ppm)	Sm (ppm)
LBB102-1035	946-31	11	149.28	39.25	1.91	4	15	5.76E-06	0.1620	0.00701	0.0339	2.85E-03	5.89E-03	5.67E-03	54.70	36.78	422.46
LBB102-1035	946-31	12	44.75	31.69	1.88	4	2	1.28E-05	0.0327	0.00102	0.0348	1.37E-02	1.43E-02	4.65E-03	11.04	19.66	418.81
LBB102-1035	946-31	13	80.40	33.09	1.99	4	6	5.76E-06	0.1210	0.00559	0.0291	9.85E-04	5.47E-03	2.44E-03	40.84	27.27	427.37
LBB102-1035	946-31	14	79.93	40.15	1.76	4	4	7.68E-06	0.0609	0.00251	0.0294	3.57E-03	6.93E-03	1.72E-03	20.54	35.94	754.18
LBB102-1035	946-31	15	37.21	21.57	2.02	4	3	1.79E-05	0.0422	0.00187	0.0278	8.69E-03	1.43E-02	4.51E-03	14.23	27.51	625.94
LBB102-1035	946-31	16	86.03	49.80	1.73	4	3	7.68E-06	0.0424	0.00140	0.0258	3.06E-03	5.17E-03	2.32E-03	14.31	22.55	528.74
LBB102-1035	946-31	17	73.07	42.32	1.90	4	3	7.68E-06	0.0500	0.00191	0.0275	8.13E-04	6.21E-03	1.92E-03	16.86	20.53	530.33
LBB102-1035	946-31	18	135.63	39.59	2.16	4	12	7.68E-06	0.1070	0.00387	0.0308	1.87E-03	2.62E-03	4.40E-03	36.16	69.34	678.19
LBB102-1035	946-31	19	94.99	31.89	1.90	4	9	6.40E-06	0.1380	0.00432	0.0331	1.57E-03	1.19E-02	4.77E-03	46.61	27.99	475.82
LBB102-1035	946-31	20	162.80	83.98	2.20	4	4	5.12E-06	0.0445	0.00554	0.0561	1.11E-03	1.47E-02	2.87E-03	15.03	11.78	291.00
LBB102-1035	946-31	21	153.00	58.45	1.95	4	7	5.12E-06	0.0830	0.00416	0.0248	2.61E-04	4.95E-03	1.42E-03	28.01	27.03	382.22
LBB102-1035	946-31	22	35.96	20.86	2.23	4	3	3.84E-06	0.2040	0.01060	0.0284	6.48E-04	6.97E-03	2.17E-03	68.72	36.25	598.30
LBB102-1035	946-31	23	62.29	31.28	1.87	4	4	7.68E-06	0.0782	0.00313	0.0324	4.77E-03	3.19E-03	2.99E-03	26.39	44.65	639.35
LBB102-1035	946-31	26	134.35	29.90	2.07	4	21	1.60E-05	0.0909	0.00332	0.0295	6.27E-04	5.35E-03	1.66E-03	30.67	25.48	546.25
LBB102-1035	946-31	28	180.73	43.23	2.01	4	18	7.68E-06	0.1200	0.00396	0.0291	5.80E-04	5.10E-03	1.75E-03	40.56	26.87	455.13
LBB102-1035	946-31	29	110.25	49.49	2.22	4	5	6.40E-06	0.0660	0.00201	0.0299	6.47E-04	2.94E-03	2.48E-03	22.29	29.41	478.08
LBB102-1035	946-31	30	55.35	22.71	1.61	4	6	1.15E-05	0.0881	0.00290	0.0269	2.63E-04	3.21E-03	2.58E-03	29.72	39.20	589.18
LBB102-1035	946-31	31	162.54	44.23	2.28	4	14	2.05E-05	0.0390	0.00176	0.0293	5.05E-02	4.17E-02	4.00E-03	13.17	20.94	517.24
LBB102-1035	946-31	32	63.02	21.27	2.17	4	9	1.28E-05	0.1040	0.00491	0.0279	8.21E-04	5.56E-03	2.05E-03	35.22	30.32	579.30
LBB102-1035	946-31	33	65.69	38.08	1.94	4	3	7.68E-06	0.0556	0.00259	0.0216	2.38E-04	2.38E-03	1.50E-03	18.77	32.90	637.65
LBB102-1035	946-31	34	88.36	44.45	1.79	4	4	9.60E-06	0.0440	0.00221	0.0227	3.05E-03	6.16E-03	2.28E-03	14.86	29.13	547.38
LBB102-1035	946-31	35	53.44	31.13	1.84	4	3	1.28E-05	0.0411	0.00302	0.0262	4.71E-03	7.51E-03	4.20E-03	13.86	36.52	684.00
LBB102-1035	946-31	36	67.82	19.09	2.13	4	13	7.68E-06	0.2330	0.00973	0.0247	9.32E-04	1.38E-03	6.85E-04	78.75	83.28	872.83
LBB102-1035	946-31	37	40.53	16.70	2.44	4	6	7.68E-06	0.1810	0.00909	0.0258	2.14E-03	1.17E-02	4.33E-03	60.94	30.60	562.04
LBB102-1035	946-31	38	112.36	35.91	1.88	4	10	5.12E-06	0.1620	0.00643	0.0289	1.71E-04	8.84E-03	3.45E-03	54.66	31.35	550.90
LBB102-1035	946-31	39	140.31	32.69	2.22	4	19	7.68E-06	0.1640	0.00536	0.0280	6.85E-04	5.41E-03	2.82E-03	55.32	32.44	559.03
LBB102-1035	946-31	40	70.99	35.71	1.91	4	4	1.54E-05	0.0343	0.00169	0.0263	1.12E-02	9.14E-03	4.48E-03	11.57	21.34	479.67
LBB102-1940	946-32	1	43.03	12.65	1.94	4	12	7.68E-06	0.3400	0.01720	0.0209	2.77E-04	1.68E-03	6.25E-03	114.80	13.40	162.08
LBB102-1940	946-32	2	21.97	22.01	2.04	4	1	1.28E-05	0.0333	0.00164	0.0266	1.31E-02	4.21E-03	1.92E-03	11.26	40.93	477.27
LBB102-1940	946-32	3	33.83	19.65	2.03	4	3	1.54E-05	0.0541	0.00314	0.0285	1.38E-03	5.49E-03	3.52E-03	18.27	60.38	804.34
LBB102-1940	946-32	4	95.06	42.98	2.04	4	5	1.28E-05	0.0383	0.00239	0.0346	4.70E-03	7.46E-03	9.11E-03	12.94	42.23	411.29
LBB102-1940	946-32	6	76.87	44.52	1.88	4	3	8.96E-06	0.0407	0.00158	0.0347	1.08E-03	7.21E-03	1.11E-03	13.73	46.74	568.22
LBB102-1940	946-32	7	112.83	56.58	2.17	4	4	1.02E-05	0.0322	0.00097	0.0320	4.23E-03	6.83E-03	3.17E-03	10.89	37.73	448.94
LBB102-1940	946-32	8	73.83	33.15	1.84	4	5	3.84E-06	0.1650	0.00525	0.0313	1.67E-03	2.77E-02	1.05E-01	55.63	13.25	25.75
LBB102-1940	946-32	9	7.78	7.79	2.09	4	1	5.76E-06	0.2100	0.00958	0.0315	2.45E-03	3.23E-03	1.56E-03	70.76	51.32	516.49
LBB102-1940	946-32	10	28.00	19.85	1.71	4	2	6.40E-06	0.1050	0.00473	0.0290	3.81E-03	7.42E-03	5.44E-03	35.33	39.86	559.04
LBB102-1940	946-32	11	166.03	74.78	1.87	4	5	1.28E-05	0.0218	0.00104	0.0286	1.07E-02	1.73E-02	8.59E-03	7.37	29.51	606.88
LBB102-1940	946-32	13	66.56	47.15	1.93	4	2	1.15E-05	0.0244	0.00085	0.0334	1.97E-03	1.44E-02	2.96E-03	8.23	18.34	435.32

Table C1 Apatite fission track single grain ages for all samples used in this thesis generated using the ICP-MS method

UBC	AZ	Grain number	FT age (Ma)	1 σ (Ma)	Dpar (μ m)	Etch Figs	Natural tracks	Area (cm ²)	238U/43Ca (dmnls)	1 σ (dmnls)	43Ca back:sig	238U back:sig	232Th back:sig	147Sm back:sig	U (ppm)	Th (ppm)	Sm (ppm)
LBB102-1940	946-32	14	61.82	13.84	2.09	4	21	5.12E-06	0.6200	0.02700	0.0315	2.47E-04	1.16E-02	6.60E-02	209.43	16.55	56.23
LBB102-1940	946-32	15	80.32	57.04	1.94	4	2	5.76E-06	0.0403	0.00248	0.0374	1.00E-01	4.74E-03	3.42E-03	13.63	51.27	473.58
LBB102-1940	946-32	16	22.24	22.26	1.93	4	1	1.28E-05	0.0329	0.00133	0.0322	2.29E-03	4.24E-03	5.73E-03	11.12	40.27	438.09
LBB102-1940	946-32	18	31.46	31.49	2.25	4	1	1.34E-05	0.0222	0.00091	0.0266	4.47E-03	5.44E-03	1.34E-03	7.48	22.98	557.71
LBB102-1940	946-32	19	34.86	14.38	1.77	4	6	6.40E-06	0.2520	0.01330	0.0301	8.47E-04	1.28E-02	5.68E-02	85.06	32.06	54.16
LBB102-1940	946-32	20	76.29	11.91	1.88	4	45	1.02E-05	0.5380	0.02140	0.0285	5.76E-04	4.72E-02	2.63E-02	181.63	3.20	29.54
LBB102-1940	946-32	22	55.81	55.86	1.49	4	1	5.76E-06	0.0291	0.00108	0.0293	1.45E-02	4.15E-03	2.22E-03	9.83	32.87	361.64
LBB102-1940	946-32	23	93.93	25.39	1.84	4	14	6.40E-06	0.2170	0.00706	0.0272	1.04E-04	1.48E-02	1.33E-02	73.33	16.27	50.76
LBB102-1940	946-32	26	39.32	39.35	2.28	4	1	9.60E-06	0.0248	0.00075	0.0345	0.00E+00	3.68E-03	2.99E-03	8.38	26.17	507.00
LBB102-1940	946-32	27	73.40	20.64	2.18	4	14	1.28E-05	0.1390	0.01170	0.0269	3.74E-04	1.52E-02	1.79E-02	47.00	18.15	46.64
LBB102-1940	946-32	29	44.30	14.89	1.86	4	9	1.15E-05	0.1650	0.00600	0.0263	8.27E-04	8.13E-03	2.18E-03	55.75	10.84	209.77
LBB102-1940	946-32	30	44.89	31.80	1.82	4	2	7.68E-06	0.0543	0.00201	0.0306	9.30E-03	4.16E-03	4.51E-03	18.34	42.89	458.26
LBB102-1940	946-32	31	159.43	71.69	1.80	4	5	9.60E-06	0.0303	0.00122	0.0347	6.35E-03	1.96E-02	1.06E-02	10.23	21.95	422.00
LBB102-1940	946-32	32	122.32	55.08	2.28	4	5	1.15E-05	0.0330	0.00153	0.0336	6.06E-03	5.67E-03	4.57E-03	11.15	38.07	442.36
LBB102-1940	946-32	33	82.46	41.45	2.01	4	4	7.68E-06	0.0589	0.00269	0.0333	5.94E-03	3.80E-03	2.60E-03	19.91	48.97	407.09
LBB102-1940	946-32	35	133.20	59.84	1.97	4	5	9.60E-06	0.0363	0.00126	0.0328	1.16E-03	5.06E-03	2.79E-03	12.28	43.04	478.57
LBB102-1940	946-32	36	112.93	50.80	1.91	4	5	1.02E-05	0.0403	0.00169	0.0285	4.75E-04	6.85E-03	3.53E-03	13.60	45.05	471.64
LBB102-1940	946-32	37	38.41	38.46	2.29	4	1	5.76E-06	0.0423	0.00190	0.0316	4.67E-03	8.94E-03	6.63E-03	14.30	40.40	504.31
LBB102-1940	946-32	38	46.96	14.46	1.84	4	11	8.96E-06	0.2450	0.01400	0.0285	3.89E-04	3.80E-02	1.78E-02	82.62	10.60	110.72
LBB102-1940	946-32	39	64.08	37.12	2.11	4	3	1.92E-05	0.0228	0.00089	0.0310	2.90E-02	6.68E-03	1.74E-03	7.70	22.15	447.88
LBB102-1940	946-32	40	111.38	64.60	2.12	4	3	7.68E-06	0.0327	0.00164	0.0324	6.83E-03	5.60E-03	6.51E-03	11.03	38.21	439.96
LBB102-3050	946-33	2	131.18	65.81	1.96	4	4	1.54E-05	0.0184	0.00061	0.0327	2.09E-03	7.39E-03	3.64E-03	6.23	23.88	488.46
LBB102-3050	946-33	3	37.50	26.57	2.09	4	2	9.60E-06	0.0520	0.00189	0.0309	3.02E-04	3.78E-03	2.51E-03	17.57	25.69	433.91
LBB102-3050	946-33	4	119.80	60.13	2.51	4	4	1.28E-05	0.0243	0.00090	0.0384	2.38E-03	1.03E-02	4.25E-03	8.20	22.77	491.78
LBB102-3050	946-33	5	86.66	38.93	1.62	4	5	1.92E-05	0.0280	0.00099	0.0403	2.14E-03	1.03E-02	1.42E-02	9.47	26.85	537.02
LBB102-3050	946-33	6	70.45	49.90	2.05	4	2	1.02E-05	0.0259	0.00084	0.0346	5.49E-03	7.18E-03	4.36E-03	8.75	25.14	561.25
LBB102-3050	946-33	8	120.52	49.68	2.15	4	6	1.28E-05	0.0362	0.00187	0.0289	9.23E-04	4.84E-03	2.69E-03	12.22	28.22	553.59
LBB102-3050	946-33	9	44.38	7.52	2.35	4	37	7.68E-06	1.0200	0.03360	0.0363	2.17E-04	2.49E-02	1.99E-02	343.13	18.41	168.12
LBB102-3050	946-33	10	80.52	40.43	2.14	4	4	8.96E-06	0.0517	0.00204	0.0374	2.71E-02	4.49E-03	1.16E-03	17.48	30.59	616.98
LBB102-3050	946-33	12	96.16	55.74	2.05	4	3	9.60E-06	0.0303	0.00137	0.0301	1.34E-03	7.63E-03	2.57E-03	10.23	34.83	551.07
LBB102-3050	946-33	13	98.89	49.61	2.04	4	4	1.15E-05	0.0327	0.00107	0.0362	2.21E-03	8.16E-03	8.05E-03	11.05	23.28	421.34
LBB102-3050	946-33	14	102.31	32.61	1.97	4	10	2.69E-05	0.0339	0.00107	0.0368	0.00E+00	2.64E-03	3.01E-03	11.44	32.36	494.93
LBB102-3050	946-33	15	182.41	75.09	2.03	4	6	1.02E-05	0.0297	0.00140	0.0358	2.62E-03	1.42E-02	3.88E-03	10.05	31.46	696.81
LBB102-3050	946-33	16	125.45	56.53	2.00	4	5	1.92E-05	0.0193	0.00096	0.0321	9.63E-03	1.42E-02	7.08E-03	6.52	17.92	488.74
LBB102-3050	946-33	17	269.52	95.87	1.78	4	8	1.28E-05	0.0213	0.00066	0.0383	1.25E-03	1.33E-02	5.54E-03	7.20	27.02	491.71
LBB102-3050	946-33	19	54.65	54.70	2.00	4	1	7.68E-06	0.0223	0.00073	0.0351	1.97E-03	6.72E-03	3.23E-03	7.53	29.54	508.85
LBB102-3050	946-33	20	81.21	40.75	2.29	4	4	1.28E-05	0.0359	0.00121	0.0354	8.50E-04	9.21E-03	3.01E-03	12.13	23.67	557.31
LBB102-3050	946-33	21	113.09	40.35	2.30	4	8	2.56E-05	0.0257	0.00107	0.0356	5.75E-03	7.92E-03	5.31E-03	8.69	21.61	410.88

Table C1 Apatite fission track single grain ages for all samples used in this thesis generated using the ICP-MS method

UBC	AZ	Grain number	FT age (Ma)	1 σ (Ma)	Dpar (μ m)	Etch Figs	Natural tracks	Area (cm ²)	238U/43Ca (dmnls)	1 σ (dmnls)	43Ca back:sig	238U back:sig	232Th back:sig	147Sm back:sig	U (ppm)	Th (ppm)	Sm (ppm)
LBB102-3050	946-33	22	31.23	31.26	2.25	4	1	1.34E-05	0.0223	0.00085	0.0431	7.30E-03	1.18E-02	5.20E-03	7.54	31.94	656.80
LBB102-3050	946-33	23	49.70	35.24	2.10	4	2	7.68E-06	0.0490	0.00223	0.0361	5.02E-04	1.82E-03	4.53E-03	16.56	84.45	882.66
LBB102-3050	946-33	24	127.36	63.92	2.38	4	4	6.40E-06	0.0456	0.00165	0.0317	2.40E-03	7.59E-03	6.68E-03	15.41	29.73	509.10
LBB102-3050	946-33	25	27.64	19.60	1.99	4	2	9.60E-06	0.0706	0.00357	0.0523	5.77E-03	7.87E-03	1.18E-02	23.86	28.27	560.91
LBB102-3050	946-33	26	38.30	27.13	2.03	4	2	1.28E-05	0.0382	0.00135	0.0337	1.50E-03	1.30E-02	1.70E-03	12.90	25.04	585.30
LBB102-3050	946-33	27	137.98	52.43	1.92	4	7	1.28E-05	0.0368	0.00114	0.0441	2.15E-03	8.19E-03	9.36E-03	12.44	26.50	475.60
LBB102-3050	946-33	28	165.72	62.97	2.05	4	7	1.28E-05	0.0306	0.00095	0.0389	1.12E-02	8.44E-03	3.66E-03	10.33	24.85	547.99
LBB102-3050	946-33	29	81.16	13.93	1.98	4	36	7.68E-06	0.5390	0.01790	0.0360	1.71E-04	3.72E-02	3.29E-02	182.05	10.13	104.14
LBB102-3050	946-33	30	127.61	42.82	1.90	4	9	9.60E-06	0.0683	0.00209	0.0463	4.05E-02	5.48E-03	3.38E-03	23.07	54.47	717.16
LBB102-3050	946-33	31	179.62	68.28	2.24	4	7	1.54E-05	0.0235	0.00077	0.0425	3.92E-03	1.72E-02	9.32E-03	7.94	29.00	559.33
LBB102-3050	946-33	32	77.69	29.52	2.24	4	7	7.68E-06	0.1090	0.00333	0.0380	0.00E+00	3.71E-03	2.38E-03	36.99	74.52	774.03
LBB102-3050	946-33	33	80.23	46.42	1.84	4	3	1.15E-05	0.0303	0.00087	0.0442	1.72E-02	1.43E-02	6.12E-03	10.23	25.44	445.41
LBB102-3050	946-33	34	83.96	24.51	2.19	4	12	1.92E-05	0.0694	0.00250	0.0377	9.65E-04	8.02E-03	7.59E-03	23.46	31.30	538.36
LBB102-3050	946-33	35	62.63	17.71	1.99	4	13	1.02E-05	0.1890	0.00944	0.0325	4.36E-04	5.23E-03	6.05E-03	63.98	54.49	459.55
LBB102-3050	946-33	36	84.92	13.28	1.78	4	45	7.68E-06	0.6430	0.02620	0.0305	1.90E-03	1.89E-02	3.11E-02	217.41	17.48	130.69
LBB102-3050	946-33	37	46.58	9.01	2.26	4	29	3.84E-06	1.5200	0.07400	0.0275	6.64E-04	1.04E-02	7.22E-03	512.44	39.58	177.12
LBB102-3050	946-33	38	109.52	63.44	2.30	4	3	6.40E-06	0.0398	0.00165	0.0353	4.35E-02	3.26E-03	2.70E-03	13.46	37.85	616.95
LBB102-3050	946-33	39	253.45	77.27	2.14	4	11	1.79E-05	0.0223	0.00086	0.0408	2.38E-02	8.82E-03	7.26E-03	7.53	32.75	560.22
LBB102-3050	946-33	40	92.33	46.32	2.08	4	4	1.34E-05	0.0300	0.00102	0.0286	2.26E-03	5.13E-03	3.41E-03	10.15	40.95	638.36
LBB102-3900	946-34	1	42.96	6.59	2.28	4	47	5.12E-06	2.0000	0.08230	0.0250	2.89E-05	6.29E-03	1.22E-02	675.44	33.29	73.97
LBB102-3900	946-34	2	116.03	33.94	1.98	4	12	1.60E-05	0.0601	0.00247	0.0287	1.22E-02	4.35E-03	9.55E-03	20.32	43.24	142.69
LBB102-3900	946-34	3	100.91	45.36	1.97	4	5	2.30E-05	0.0200	0.00077	0.0346	1.82E-02	1.58E-02	4.06E-03	6.77	19.80	388.89
LBB102-3900	946-34	4	75.95	28.89	2.09	4	7	3.07E-05	0.0280	0.00100	0.0334	3.18E-03	9.91E-03	6.88E-03	9.46	25.20	284.29
LBB102-3900	946-34	5	137.40	40.32	2.41	4	12	3.84E-05	0.0211	0.00099	0.0290	6.36E-03	7.72E-03	6.98E-03	7.14	18.36	230.10
LBB102-3900	946-34	6	129.65	49.34	1.68	4	7	1.54E-05	0.0326	0.00122	0.0365	0.00E+00	6.97E-03	7.72E-03	11.04	28.95	424.82
LBB102-3900	946-34	7	63.34	44.88	2.17	4	2	1.28E-05	0.0230	0.00087	0.0294	7.58E-03	4.81E-03	3.04E-03	7.79	25.60	491.53
LBB102-3900	946-34	9	42.04	21.10	1.84	4	4	4.48E-05	0.0199	0.00069	0.0315	1.87E-03	5.46E-03	3.05E-03	6.71	24.81	488.03
LBB102-3900	946-34	10	62.58	10.20	2.18	4	40	7.68E-06	0.7770	0.02470	0.0330	3.65E-05	1.88E-02	8.66E-03	262.72	8.55	88.61
LBB102-3900	946-34	11	155.09	38.57	1.80	4	17	1.28E-05	0.0794	0.00393	0.0364	4.36E-02	9.93E-03	4.41E-03	26.84	28.70	378.64
LBB102-3900	946-34	12	123.61	27.76	2.55	4	21	5.12E-05	0.0308	0.00146	0.0299	2.60E-03	1.13E-02	5.94E-03	10.42	26.44	275.20
LBB102-3900	946-34	13	54.56	22.68	2.07	4	6	2.56E-05	0.0401	0.00300	0.0234	3.85E-03	5.32E-03	1.91E-03	13.57	31.89	561.66
LBB102-3900	946-34	14	74.62	33.54	1.85	4	5	9.60E-06	0.0651	0.00254	0.0276	0.00E+00	4.66E-03	4.19E-03	22.01	78.07	487.98
LBB102-3900	946-34	15	54.20	16.46	4.15	4	11	7.68E-06	0.2470	0.00676	0.0334	2.39E-04	9.11E-02	1.26E-01	83.47	1.19	11.69
LBB102-3900	946-34	16	109.83	45.14	2.29	4	6	2.56E-05	0.0198	0.00081	0.0317	4.65E-02	1.21E-02	2.78E-03	6.71	17.67	301.27
LBB102-3900	946-34	17	85.38	35.03	2.42	4	6	2.05E-05	0.0320	0.00106	0.0365	3.67E-03	8.02E-03	6.35E-03	10.81	38.70	445.41
LBB102-3900	946-34	21	92.49	31.06	2.31	4	9	3.20E-05	0.0283	0.00093	0.0341	4.15E-03	7.75E-03	5.00E-03	9.58	22.70	257.69
LBB102-3900	946-34	22	28.59	8.02	2.38	4	13	6.40E-05	0.0665	0.00242	0.0302	1.08E-03	3.77E-03	3.06E-03	22.49	55.83	332.80
LBB102-3900	946-34	23	163.03	81.85	1.90	4	4	1.28E-05	0.0178	0.00069	0.0358	8.75E-03	2.83E-02	3.43E-03	6.00	17.22	381.19

Table C1 Apatite fission track single grain ages for all samples used in this thesis generated using the ICP-MS method

UBC	AZ	Grain number	FT age (Ma)	1 σ (Ma)	Dpar (μ m)	Etch Figs	Natural tracks	Area (cm ²)	238U/43Ca (dmnls)	1 σ (dmnls)	43Ca back:sig	238U back:sig	232Th back:sig	147Sm back:sig	U (ppm)	Th (ppm)	Sm (ppm)
LBB102-3900	946-34	24	38.76	27.45	2.17	4	2	2.05E-05	0.0236	0.00068	0.0341	1.24E-03	6.25E-03	2.36E-03	7.97	20.98	413.15
LBB102-3900	946-34	25	111.53	42.37	1.88	4	7	2.56E-05	0.0228	0.00069	0.0355	4.39E-03	1.20E-02	3.24E-03	7.71	21.62	337.70
LBB102-3900	946-34	26	127.33	45.53	2.18	4	8	1.60E-05	0.0365	0.00174	0.0326	1.44E-03	7.11E-03	4.21E-03	12.33	27.92	292.66
LBB102-3900	946-34	28	67.84	24.23	2.00	4	8	4.48E-05	0.0246	0.00111	0.0295	0.00E+00	6.44E-03	1.18E-03	8.31	22.61	489.54
LBB102-3900	946-34	29	120.50	49.46	2.17	4	6	2.30E-05	0.0201	0.00071	0.0335	2.40E-03	8.98E-03	2.83E-03	6.79	18.13	421.39
LBB102-3900	946-34	30	91.64	30.85	1.94	4	9	4.10E-05	0.0223	0.00090	0.0336	4.16E-03	4.68E-03	3.29E-03	7.55	18.85	400.63
LBB102-3900	946-34	31	111.48	45.75	2.31	4	6	2.24E-05	0.0223	0.00076	0.0339	0.00E+00	2.18E-02	1.44E-02	7.56	19.88	226.47
LBB102-3900	946-34	32	76.98	34.54	1.95	4	5	2.56E-05	0.0237	0.00064	0.0449	1.08E-02	8.32E-03	1.44E-02	8.00	24.15	191.61
LBB102-3900	946-34	33	58.19	9.68	2.18	4	40	7.68E-06	0.8360	0.03840	0.0301	0.00E+00	9.46E-04	1.35E-03	282.63	210.91	858.13
LBB102-3900	946-34	35	67.67	19.77	2.47	4	12	2.30E-05	0.0718	0.00273	0.0359	1.91E-03	2.80E-03	3.48E-03	24.29	78.93	405.61
LBB102-3900	946-34	36	92.70	31.17	2.24	4	9	4.10E-05	0.0221	0.00081	0.0410	4.59E-03	1.74E-02	1.00E-02	7.46	18.35	201.37
LBB102-3900	946-34	37	64.56	11.46	1.93	4	34	6.40E-06	0.7680	0.03020	0.0371	7.71E-04	1.80E-02	3.09E-02	259.70	12.01	72.71
LBB102-3900	946-34	38	78.44	32.27	1.90	4	6	1.54E-05	0.0464	0.00212	0.0279	1.90E-02	4.20E-03	5.40E-04	15.70	36.51	693.20
LBB102-3900	946-34	39	89.40	44.86	2.15	4	4	1.28E-05	0.0326	0.00116	0.0319	4.25E-03	8.22E-03	7.29E-03	11.01	29.26	313.97
LBB102-3900	946-34	40	62.83	8.36	2.12	4	64	7.68E-06	1.2400	0.04800	0.0285	7.52E-05	1.03E-02	2.74E-02	418.67	17.00	44.74
LBB76-1038	946-25	1	97.29	31.14	1.82	4	10	1.54E-05	0.0626	0.00270	0.0326	2.14E-03	1.19E-03	3.36E-03	21.07	59.39	369.81
LBB76-1038	946-25	2	89.59	22.90	2.09	4	16	2.56E-05	0.0653	0.00310	0.0291	1.61E-03	3.27E-03	2.24E-03	21.98	56.78	430.62
LBB76-1038	946-25	3	144.97	39.23	1.92	4	14	2.05E-05	0.0439	0.00152	0.0329	9.11E-03	6.61E-03	6.48E-03	14.79	58.55	382.16
LBB76-1038	946-25	4	66.92	22.52	1.83	4	9	3.20E-05	0.0394	0.00153	0.0467	1.96E-02	1.98E-02	1.30E-02	13.26	45.25	503.50
LBB76-1038	946-25	5	47.40	23.91	2.12	4	4	2.30E-05	0.0344	0.00214	0.0305	6.93E-03	9.04E-03	5.21E-03	11.57	31.32	360.23
LBB76-1038	946-25	6	51.83	15.78	1.75	4	11	6.40E-05	0.0311	0.00110	0.0319	1.18E-02	1.38E-02	2.64E-03	10.48	33.33	492.55
LBB76-1038	946-25	7	33.18	13.65	1.80	4	6	3.58E-05	0.0474	0.00215	0.0284	2.06E-03	2.60E-03	2.20E-03	15.96	44.95	420.30
LBB76-1038	946-25	8	90.32	32.28	1.62	4	8	1.54E-05	0.0539	0.00251	0.0332	4.85E-03	4.30E-03	2.94E-03	18.16	55.30	381.05
LBB76-1038	946-25	9	48.78	8.97	1.99	4	32	9.60E-06	0.6410	0.02830	0.0319	5.23E-04	1.38E-03	1.70E-03	215.93	130.52	916.04
LBB76-1038	946-25	10	46.78	21.10	1.81	4	5	1.54E-05	0.0653	0.00343	0.0259	1.08E-02	2.42E-03	3.95E-03	21.99	69.48	355.14
LBB76-1038	946-25	11	100.93	45.53	1.63	4	5	1.60E-05	0.0289	0.00156	0.0282	6.78E-04	4.90E-03	2.27E-03	9.74	36.12	312.13
LBB76-1038	946-25	12	46.42	20.87	1.72	4	5	9.60E-06	0.1050	0.00421	0.0333	1.32E-03	3.84E-03	2.26E-03	35.46	83.98	401.80
LBB76-1038	946-25	13	45.93	23.12	1.98	4	4	1.34E-05	0.0608	0.00325	0.0302	1.65E-03	4.14E-03	3.66E-03	20.48	49.27	285.50
LBB76-1038	946-25	14	228.29	51.81	2.03	4	20	1.28E-05	0.0633	0.00191	0.0336	1.12E-03	4.19E-03	6.15E-03	21.33	69.06	379.02
LBB76-1038	946-25	15	11.58	5.82	1.71	4	4	1.15E-05	0.2820	0.01370	0.0300	1.23E-03	4.07E-03	4.46E-03	95.01	143.82	598.15
LBB76-1038	946-25	16	68.05	20.81	1.87	4	11	1.28E-05	0.1180	0.00529	0.0273	5.99E-04	2.76E-03	2.11E-03	39.85	107.68	492.23
LBB76-1038	946-25	17	54.83	22.57	1.57	4	6	2.05E-05	0.0501	0.00236	0.0275	1.98E-03	4.48E-03	9.12E-03	16.88	233.01	130.44
LBB76-1038	946-25	18	93.82	23.77	2.29	4	16	5.12E-05	0.0311	0.00102	0.0328	8.12E-03	4.20E-03	4.32E-03	10.49	35.81	262.60
LBB76-1038	946-25	19	96.93	25.43	2.15	4	15	4.10E-05	0.0353	0.00139	0.0381	8.82E-03	5.66E-03	4.94E-03	11.89	36.94	381.78
LBB76-1038	946-25	20	108.44	44.45	1.79	4	6	1.28E-05	0.0404	0.00112	0.0357	3.04E-03	4.34E-03	7.08E-03	13.60	48.31	399.73
LBB76-1038	946-25	21	56.01	21.44	2.14	4	7	1.02E-05	0.1140	0.00633	0.0266	1.17E-03	1.87E-03	1.25E-03	38.54	85.45	545.03
LBB76-1038	946-25	22	89.76	30.20	1.99	4	9	1.92E-05	0.0488	0.00190	0.0304	6.25E-03	1.07E-02	6.43E-03	16.45	55.06	340.52
LBB76-1038	946-25	23	6.91	4.00	2.08	4	3	9.60E-06	0.4260	0.01820	0.0426	1.17E-03	1.53E-03	2.27E-03	143.38	153.21	830.90

Table C1 Apatite fission track single grain ages for all samples used in this thesis generated using the ICP-MS method

UBC	AZ	Grain number	FT age (Ma)	1 σ (Ma)	Dpar (μ m)	Etch Figs	Natural tracks	Area (cm ²)	238U/43Ca (dmnls)	1 σ (dmnls)	43Ca back:sig	238U back:sig	232Th back:sig	147Sm back:sig	U (ppm)	Th (ppm)	Sm (ppm)
LBB76-1038	946-25	24	92.57	25.09	1.61	4	14	2.30E-05	0.0614	0.00233	0.0379	8.87E-02	2.62E-02	2.59E-02	20.67	88.40	551.74
LBB76-1038	946-25	25	52.47	21.55	1.86	4	6	1.54E-05	0.0698	0.00266	0.0282	2.44E-03	2.12E-03	1.82E-03	23.52	65.87	514.37
LBB76-1038	946-25	26	33.42	16.80	1.75	4	4	2.56E-05	0.0439	0.00208	0.0292	2.80E-03	6.42E-03	3.88E-03	14.79	29.75	353.62
LBB76-1038	946-25	27	108.18	38.97	1.93	4	8	9.60E-06	0.0720	0.00463	0.0247	5.57E-04	2.53E-03	2.89E-03	24.23	71.24	427.67
LBB76-1038	946-25	29	91.71	32.77	2.28	4	8	1.92E-05	0.0425	0.00196	0.0275	2.32E-03	3.76E-03	1.85E-03	14.31	59.74	428.68
LBB76-1038	946-25	30	80.83	19.48	1.68	4	18	2.56E-05	0.0814	0.00359	0.0274	2.44E-04	2.37E-03	2.88E-03	27.42	66.75	423.06
LBB76-1038	946-25	31	73.95	28.14	1.84	4	7	1.92E-05	0.0462	0.00172	0.0346	8.42E-03	1.04E-02	9.30E-03	15.55	46.97	364.54
LBB76-1038	946-25	32	108.54	30.37	1.87	4	13	2.30E-05	0.0486	0.00135	0.0388	3.03E-03	3.29E-03	4.44E-03	16.35	53.71	375.26
LBB76-1038	946-25	33	60.09	26.99	1.92	4	5	1.73E-05	0.0451	0.00155	0.0350	3.79E-03	4.10E-03	2.77E-03	15.20	51.48	464.13
LBB76-1038	946-25	34	91.69	27.92	1.69	4	11	2.56E-05	0.0438	0.00153	0.0419	7.01E-03	8.46E-03	9.53E-03	14.76	45.25	331.25
LBB76-1038	946-25	35	168.52	47.19	2.13	4	13	1.92E-05	0.0374	0.00112	0.0384	2.78E-03	9.11E-03	4.94E-03	12.58	46.95	453.89
LBB76-1038	946-25	36	121.46	43.27	2.23	4	8	1.02E-05	0.0600	0.00219	0.0319	4.52E-04	4.63E-03	2.04E-03	20.21	55.90	396.15
LBB76-1038	946-25	37	90.80	30.67	1.87	4	9	2.56E-05	0.0362	0.00178	0.0279	4.97E-03	6.79E-03	3.57E-03	12.20	27.95	374.51
LBB76-1038	946-25	38	114.98	38.64	1.42	4	9	1.92E-05	0.0381	0.00132	0.0247	1.42E-03	4.40E-03	1.99E-03	12.82	29.39	426.53
LBB76-1038	946-25	39	75.95	10.64	1.83	4	63	1.92E-05	0.4050	0.02270	0.0244	0.00E+00	9.93E-04	1.77E-03	136.22	86.38	503.74
LBB76-1038	946-25	40	53.93	27.07	2.04	4	4	1.60E-05	0.0435	0.00157	0.0303	0.00E+00	4.13E-03	2.09E-03	14.64	46.90	454.15
LBB76-1228	946-26	1	84.58	21.64	2.29	4	16	2.56E-05	0.0691	0.00336	0.0161	2.90E-04	1.81E-03	1.03E-03	23.29	73.94	617.32
LBB76-1228	946-26	2	75.94	27.09	2.12	4	8	1.92E-05	0.0513	0.00209	0.0238	2.33E-03	3.83E-03	2.73E-03	17.30	43.73	339.38
LBB76-1228	946-26	3	80.56	16.88	1.63	4	24	5.12E-05	0.0544	0.00222	0.0296	3.28E-03	2.85E-03	1.97E-03	18.34	69.21	536.53
LBB76-1228	946-26	4	123.78	44.23	1.61	4	8	9.60E-06	0.0628	0.00285	0.0293	2.11E-03	2.91E-03	2.31E-03	21.15	78.52	460.00
LBB76-1228	946-26	5	81.98	26.34	2.25	4	10	2.24E-05	0.0509	0.00261	0.0284	1.90E-03	6.16E-03	5.06E-03	17.16	28.81	224.49
LBB76-1228	946-26	6	63.25	26.06	2.08	4	6	1.34E-05	0.0661	0.00331	0.0309	3.03E-03	2.98E-03	2.85E-03	22.28	66.73	293.56
LBB76-1228	946-26	7	44.78	22.46	1.71	4	4	1.73E-05	0.0485	0.00147	0.0507	5.43E-03	6.43E-03	6.20E-03	16.34	67.98	494.51
LBB76-1228	946-26	8	98.20	24.91	1.99	4	16	4.10E-05	0.0372	0.00132	0.0226	1.43E-03	1.74E-03	1.28E-03	12.52	42.98	409.61
LBB76-1228	946-26	9	106.56	34.00	1.98	4	10	2.30E-05	0.0380	0.00133	0.0243	4.59E-03	3.91E-03	2.40E-03	12.81	46.89	331.54
LBB76-1228	946-26	10	104.63	22.80	1.75	4	22	2.30E-05	0.0852	0.00325	0.0279	1.62E-03	3.41E-03	2.87E-03	28.71	72.33	480.15
LBB76-1228	946-26	11	77.62	14.63	1.93	4	30	3.07E-05	0.1180	0.00468	0.0234	1.58E-03	4.00E-03	3.79E-03	39.67	43.42	397.81
LBB76-1228	946-26	12	116.34	44.27	1.74	4	7	1.79E-05	0.0313	0.00116	0.0284	4.45E-03	4.09E-03	3.78E-03	10.55	39.77	297.37
LBB76-1228	946-26	13	186.90	46.03	2.28	4	17	2.24E-05	0.0377	0.00132	0.0258	3.65E-03	2.85E-03	2.06E-03	12.69	46.52	470.51
LBB76-1228	946-26	14	83.54	28.11	2.10	4	9	3.20E-05	0.0315	0.00121	0.0299	4.50E-03	8.76E-03	5.74E-03	10.61	33.02	354.24
LBB76-1228	946-26	15	116.38	27.56	2.39	4	19	3.84E-05	0.0397	0.00213	0.0325	2.09E-03	5.35E-03	4.00E-03	13.36	53.93	385.27
LBB76-1228	946-26	16	130.87	39.89	1.62	4	11	1.60E-05	0.0489	0.00182	0.0332	2.70E-03	3.89E-03	2.36E-03	16.49	67.05	480.57
LBB76-1228	946-26	17	126.74	48.16	1.63	4	7	1.60E-05	0.0322	0.00098	0.0414	3.75E-03	6.21E-03	3.07E-03	10.84	33.99	445.66
LBB76-1228	946-26	18	44.28	25.68	1.41	4	3	1.60E-05	0.0397	0.00188	0.0392	3.14E-03	1.17E-02	5.29E-03	13.38	29.64	479.78
LBB76-1228	946-26	19	153.94	43.15	1.67	4	13	1.92E-05	0.0409	0.00132	0.0411	7.08E-03	4.49E-03	7.26E-03	13.79	53.29	371.55
LBB76-1228	946-26	20	155.95	43.78	1.93	4	13	2.30E-05	0.0336	0.00121	0.0353	2.93E-03	6.37E-03	6.84E-03	11.34	37.41	401.25
LBB76-1228	946-26	21	47.01	21.15	1.75	4	5	1.60E-05	0.0623	0.00266	0.0286	1.64E-03	4.44E-03	3.06E-03	21.01	55.18	516.07
LBB76-1228	946-26	22	155.85	37.75	2.18	4	18	1.28E-05	0.0839	0.00422	0.0279	1.18E-03	2.53E-03	4.68E-03	28.28	76.84	475.81

Table C1 Apatite fission track single grain ages for all samples used in this thesis generated using the ICP-MS method

UBC	AZ	Grain number	FT age (Ma)	1 σ (Ma)	Dpar (μ m)	Etch Figs	Natural tracks	Area (cm ²)	238U/43Ca (dmnls)	1 σ (dmnls)	43Ca back:sig	238U back:sig	232Th back:sig	147Sm back:sig	U (ppm)	Th (ppm)	Sm (ppm)
LBB76-1228	946-26	23	55.05	15.63	1.96	4	13	3.20E-05	0.0692	0.00386	0.0321	6.19E-03	7.31E-03	6.30E-03	23.31	48.59	338.83
LBB76-1228	946-26	24	53.68	19.11	1.91	4	8	2.56E-05	0.0546	0.00189	0.0310	3.36E-03	2.07E-02	6.13E-03	18.39	17.88	237.61
LBB76-1228	946-26	25	131.35	30.80	2.14	4	19	3.20E-05	0.0421	0.00177	0.0272	8.54E-04	8.34E-03	1.93E-03	14.19	35.68	394.52
LBB76-1228	946-26	26	144.83	33.05	2.15	4	20	2.56E-05	0.0502	0.00194	0.0327	3.89E-03	9.70E-03	9.44E-03	16.92	44.79	326.15
LBB76-1228	946-26	27	124.41	39.66	2.25	4	10	1.60E-05	0.0468	0.00150	0.0314	2.22E-03	3.99E-03	4.36E-03	15.78	41.22	343.39
LBB76-1228	946-26	28	16.10	16.14	1.58	4	1	1.54E-05	0.0380	0.00240	0.0313	7.25E-03	1.10E-02	4.77E-03	12.81	40.29	373.36
LBB76-1228	946-26	29	94.63	31.95	2.37	4	9	1.60E-05	0.0555	0.00269	0.0319	8.10E-04	5.15E-03	5.21E-03	18.72	48.59	365.85
LBB76-1228	946-26	30	73.46	30.17	1.91	4	6	1.54E-05	0.0498	0.00188	0.0312	1.10E-03	5.26E-03	5.53E-03	16.77	43.43	266.54
LBB76-1228	946-26	31	129.90	27.93	1.90	4	23	3.84E-05	0.0430	0.00199	0.0334	3.79E-03	3.04E-03	4.05E-03	14.48	45.08	316.61
LBB76-1228	946-26	32	57.37	16.87	1.47	4	12	3.20E-05	0.0613	0.00309	0.0422	5.58E-03	1.01E-02	1.02E-02	20.64	47.19	248.21
LBB76-1228	946-26	33	62.57	22.31	2.47	4	8	1.02E-05	0.1170	0.00452	0.0406	2.60E-03	1.57E-03	7.37E-03	39.41	148.72	488.74
LBB76-1228	946-26	34	46.18	17.57	1.75	4	7	2.56E-05	0.0555	0.00196	0.0323	4.20E-03	7.16E-03	5.26E-03	18.71	59.27	457.44
LBB76-1228	946-26	35	88.44	21.32	1.84	4	18	1.54E-05	0.1240	0.00552	0.0327	1.05E-03	2.59E-03	7.02E-03	41.74	86.74	262.73
LBB76-1228	946-26	36	90.60	37.23	1.72	4	6	1.28E-05	0.0484	0.00192	0.0305	6.86E-03	7.26E-03	6.07E-03	16.30	43.46	317.05
LBB76-1228	946-26	37	76.91	31.56	1.75	4	6	1.54E-05	0.0475	0.00161	0.0288	1.60E-03	4.50E-03	1.90E-03	16.02	56.67	423.89
LBB76-1228	946-26	38	55.46	17.72	1.96	4	10	4.48E-05	0.0377	0.00147	0.0322	6.17E-03	1.10E-02	8.40E-03	12.71	37.81	396.03
LBB76-1228	946-26	39	68.94	26.40	2.79	4	7	1.34E-05	0.0707	0.00399	0.0322	8.65E-04	3.18E-03	2.70E-03	23.83	94.63	646.45
LBB76-1228	946-26	40	61.86	18.14	1.79	4	12	2.69E-05	0.0676	0.00309	0.0322	6.06E-03	1.20E-02	8.16E-03	22.78	44.71	418.46
LBB76-343	946-22	1	107.63	38.45	2.35	4	8	1.54E-05	0.0464	0.00197	0.0167	2.20E-03	2.14E-03	8.45E-04	15.23	50.49	561.90
LBB76-343	946-22	2	199.54	38.85	2.19	4	28	2.30E-05	0.0580	0.00214	0.0259	2.25E-03	9.50E-03	3.59E-03	19.04	51.28	490.77
LBB76-343	946-22	3	102.55	36.53	2.53	4	8	2.30E-05	0.0325	0.00103	0.0305	7.37E-03	7.35E-03	7.95E-03	10.66	31.61	366.00
LBB76-343	946-22	4	151.35	33.71	2.54	4	21	3.20E-05	0.0414	0.00141	0.0274	5.41E-03	5.04E-03	4.68E-03	13.60	41.08	533.25
LBB76-343	946-22	5	206.80	54.29	2.28	4	15	2.56E-05	0.0269	0.00101	0.0309	6.92E-03	1.08E-02	8.23E-03	8.85	28.81	509.70
LBB76-343	946-22	7	107.02	28.91	2.13	4	14	3.20E-05	0.0392	0.00103	0.0290	2.14E-03	5.31E-03	1.60E-03	12.87	41.41	549.69
LBB76-343	946-22	8	127.59	34.49	2.31	4	14	2.56E-05	0.0410	0.00118	0.0332	4.58E-03	7.85E-03	5.49E-03	13.47	46.22	639.97
LBB76-343	946-22	9	57.67	19.36	2.34	4	9	2.56E-05	0.0587	0.00161	0.0567	7.02E-04	3.53E-03	1.28E-03	19.27	77.71	670.58
LBB76-343	946-22	11	139.22	37.62	2.28	4	14	2.30E-05	0.0417	0.00114	0.0284	1.76E-03	2.47E-03	1.95E-03	13.71	45.59	544.49
LBB76-343	946-22	12	158.07	46.03	2.56	4	12	1.92E-05	0.0377	0.00095	0.0280	3.99E-03	3.48E-03	3.65E-03	12.40	46.73	586.51
LBB76-343	946-22	13	107.84	31.42	2.38	4	12	2.56E-05	0.0417	0.00110	0.0300	1.36E-03	2.99E-03	3.49E-03	13.68	44.48	543.80
LBB76-343	946-22	14	76.86	29.20	2.22	4	7	1.92E-05	0.0456	0.00115	0.0340	1.79E-03	6.01E-03	3.77E-03	14.97	48.51	567.09
LBB76-343	946-22	15	167.71	46.98	2.51	4	13	2.05E-05	0.0361	0.00097	0.0317	4.57E-03	5.59E-03	4.92E-03	11.86	42.01	511.03
LBB76-343	946-22	16	72.59	32.59	2.46	4	5	1.92E-05	0.0345	0.00089	0.0310	4.95E-03	9.66E-03	5.36E-03	11.32	35.20	402.63
LBB76-343	946-22	17	52.26	16.65	2.30	4	10	1.92E-05	0.0959	0.00251	0.0449	2.02E-03	2.67E-03	5.29E-03	31.51	112.05	545.16
LBB76-343	946-22	18	92.75	33.04	2.45	4	8	1.92E-05	0.0431	0.00142	0.0267	2.72E-03	4.43E-03	1.52E-03	14.16	41.66	607.12
LBB76-343	946-22	19	87.78	20.43	2.54	4	19	5.12E-05	0.0406	0.00108	0.0293	6.92E-04	4.41E-03	5.92E-03	13.33	64.58	541.96
LBB76-343	946-22	20	101.94	27.54	2.10	4	14	3.20E-05	0.0411	0.00109	0.0270	1.06E-03	4.04E-03	2.61E-03	13.52	47.88	509.19
LBB76-343	946-22	21	89.99	30.23	2.40	4	9	2.30E-05	0.0417	0.00125	0.0216	2.23E-03	4.56E-03	4.12E-03	13.68	46.19	407.87
LBB76-343	946-22	22	175.78	51.26	2.53	4	12	1.92E-05	0.0339	0.00100	0.0248	1.97E-03	3.14E-03	1.99E-03	11.13	41.58	534.98

Table C1 Apatite fission track single grain ages for all samples used in this thesis generated using the ICP-MS method

UBC	AZ	Grain number	FT age (Ma)	1 σ (Ma)	Dpar (μ m)	Etch Figs	Natural tracks	Area (cm ²)	238U/43Ca (dmnls)	1 σ (dmnls)	43Ca back:sig	238U back:sig	232Th back:sig	147Sm back:sig	U (ppm)	Th (ppm)	Sm (ppm)
LBB76-343	946-22	23	64.07	17.37	2.38	4	14	2.30E-05	0.0912	0.00319	0.0338	1.13E-03	5.02E-03	3.88E-03	29.96	83.67	642.22
LBB76-343	946-22	24	260.97	47.35	2.57	4	32	3.20E-05	0.0363	0.00105	0.0251	8.87E-04	4.57E-03	1.81E-03	11.92	44.88	611.33
LBB76-343	946-22	25	113.84	34.64	2.30	4	11	1.92E-05	0.0482	0.00139	0.0257	1.35E-03	2.83E-03	2.08E-03	15.83	49.46	640.70
LBB76-343	946-22	26	155.44	40.70	2.17	4	15	2.30E-05	0.0400	0.00131	0.0253	1.63E-03	6.83E-03	5.53E-03	13.14	44.69	604.21
LBB76-343	946-22	27	123.27	35.96	2.53	4	12	2.24E-05	0.0416	0.00125	0.0270	1.44E-03	4.02E-03	2.05E-03	13.66	48.70	555.19
LBB76-343	946-22	28	94.93	30.32	2.37	4	10	2.56E-05	0.0395	0.00136	0.0293	1.79E-03	3.08E-03	1.96E-03	12.97	46.51	647.56
LBB76-343	946-22	29	124.85	25.01	2.47	4	26	3.84E-05	0.0519	0.00149	0.0288	7.01E-04	4.41E-03	2.60E-03	17.05	52.51	476.63
LBB76-343	946-22	30	167.90	33.56	2.15	4	26	3.84E-05	0.0385	0.00099	0.0342	2.76E-03	6.21E-03	3.79E-03	12.64	38.87	518.17
LBB76-343	946-22	31	168.05	43.87	2.40	4	15	2.56E-05	0.0333	0.00086	0.0333	3.71E-03	9.79E-03	6.32E-03	10.92	40.73	458.28
LBB76-343	946-22	32	202.00	51.12	2.28	4	16	2.05E-05	0.0368	0.00098	0.0351	1.95E-03	9.93E-03	3.90E-03	12.09	39.86	545.67
LBB76-343	946-22	33	129.46	28.80	2.50	4	21	3.84E-05	0.0404	0.00130	0.0399	6.12E-03	1.04E-02	6.18E-03	13.28	41.12	546.39
LBB76-343	946-22	34	103.21	28.93	2.37	4	13	3.20E-05	0.0377	0.00107	0.0380	3.81E-03	2.11E-02	7.26E-03	12.40	36.86	497.60
LBB76-343	946-22	35	176.23	41.03	2.35	4	19	3.20E-05	0.0321	0.00087	0.0408	5.93E-03	7.20E-03	9.07E-03	10.55	37.90	415.05
LBB76-343	946-22	36	178.54	52.16	2.41	4	12	1.60E-05	0.0400	0.00137	0.0387	7.71E-03	9.57E-03	4.40E-03	13.15	46.12	583.38
LBB76-343	946-22	37	120.39	38.42	2.47	4	10	1.92E-05	0.0414	0.00130	0.0404	9.81E-03	1.53E-02	1.11E-02	13.60	36.84	525.87
LBB76-343	946-22	38	186.34	54.39	2.26	4	12	1.60E-05	0.0383	0.00122	0.0404	1.48E-02	1.35E-02	1.83E-02	12.59	34.73	373.35
LBB76-343	946-22	39	158.21	48.24	2.22	4	11	2.30E-05	0.0288	0.00102	0.0373	6.38E-03	1.01E-02	4.87E-03	9.46	32.72	472.38
LBB76-343	946-22	40	97.67	31.17	2.36	4	10	2.56E-05	0.0384	0.00120	0.0434	1.66E-02	1.31E-02	1.30E-02	12.60	38.37	527.37
LBB76-576	946-23	1	135.48	37.98	2.24	4	13	1.92E-05	0.0476	0.00141	0.0306	0.00E+00	2.15E-03	3.16E-03	15.69	47.50	302.33
LBB76-576	946-23	2	85.97	25.04	2.30	4	12	2.05E-05	0.0651	0.00169	0.0311	2.73E-04	5.22E-03	2.11E-03	21.48	41.20	493.05
LBB76-576	946-23	3	162.48	42.40	2.41	4	15	2.24E-05	0.0392	0.00099	0.0365	1.33E-03	5.73E-03	6.79E-03	12.92	42.57	564.01
LBB76-576	946-23	4	180.59	35.40	2.38	4	27	4.10E-05	0.0346	0.00085	0.0314	2.31E-03	8.77E-03	3.32E-03	11.42	39.06	575.13
LBB76-576	946-23	5	179.93	34.13	2.37	4	29	4.10E-05	0.0373	0.00100	0.0356	3.22E-03	1.16E-02	8.77E-03	12.31	35.18	501.00
LBB76-576	946-23	6	77.89	26.26	2.42	4	9	1.92E-05	0.0576	0.00239	0.0343	1.15E-03	3.20E-03	3.22E-03	18.98	58.19	524.51
LBB76-576	946-23	7	124.18	26.95	2.23	4	22	4.10E-05	0.0412	0.00120	0.0378	8.85E-03	1.24E-02	4.68E-03	13.59	41.63	461.69
LBB76-576	946-23	8	134.53	40.91	2.46	4	11	2.30E-05	0.0338	0.00095	0.0324	2.12E-03	4.53E-03	4.71E-03	11.15	40.50	543.80
LBB76-576	946-23	9	163.48	42.71	2.12	4	15	1.92E-05	0.0454	0.00128	0.0330	4.05E-03	7.72E-03	8.68E-03	14.97	40.61	512.08
LBB76-576	946-23	10	191.64	39.10	2.06	4	25	3.20E-05	0.0386	0.00111	0.0424	6.11E-03	7.31E-03	9.23E-03	12.75	37.60	461.65
LBB76-576	946-23	12	186.83	43.42	2.18	4	19	2.56E-05	0.0377	0.00091	0.0384	1.11E-03	1.53E-03	4.40E-03	12.43	47.36	375.88
LBB76-576	946-23	13	7.59	1.93	1.97	4	16	3.84E-05	0.5280	0.01680	0.0530	1.27E-03	2.58E-03	4.59E-03	174.07	351.44	953.41
LBB76-576	946-23	14	96.49	28.09	2.34	4	12	3.20E-05	0.0371	0.00094	0.0302	1.36E-02	1.06E-02	3.01E-03	12.24	44.00	566.10
LBB76-576	946-23	15	120.31	36.57	2.53	4	11	2.30E-05	0.0378	0.00099	0.0332	3.16E-03	4.45E-03	2.03E-03	12.48	41.95	553.02
LBB76-576	946-23	16	121.71	20.54	2.50	4	37	6.40E-05	0.0453	0.00115	0.0348	4.19E-03	7.33E-03	3.12E-03	14.93	44.92	550.02
LBB76-576	946-23	17	165.89	48.30	2.25	4	12	2.05E-05	0.0336	0.00086	0.0349	7.66E-03	7.22E-03	6.04E-03	11.07	35.20	442.79
LBB76-576	946-23	18	138.70	40.39	2.15	4	12	2.05E-05	0.0402	0.00106	0.0341	0.00E+00	9.61E-03	5.90E-03	13.26	40.87	475.30
LBB76-576	946-23	19	155.50	29.12	2.32	4	30	5.12E-05	0.0358	0.00110	0.0321	0.00E+00	4.37E-03	3.76E-03	11.82	39.79	540.27
LBB76-576	946-23	21	120.17	45.69	2.32	4	7	1.28E-05	0.0434	0.00129	0.0296	1.74E-03	4.29E-03	2.28E-03	14.31	46.56	330.15
LBB76-576	946-23	22	141.30	30.68	2.23	4	22	3.20E-05	0.0463	0.00138	0.0384	2.60E-03	7.71E-03	4.49E-03	15.27	45.74	609.20

Table C1 Apatite fission track single grain ages for all samples used in this thesis generated using the ICP-MS method

UBC	AZ	Grain number	FT age (Ma)	1 σ (Ma)	Dpar (μ m)	Etch Figs	Natural tracks	Area (cm ²)	238U/43Ca (dmnls)	1 σ (dmnls)	43Ca back:sig	238U back:sig	232Th back:sig	147Sm back:sig	U (ppm)	Th (ppm)	Sm (ppm)
LBB76-576	946-23	23	180.29	47.19	2.12	4	15	2.30E-05	0.0343	0.00111	0.0371	9.80E-03	8.54E-03	4.44E-03	11.30	36.59	510.11
LBB76-576	946-23	24	158.85	36.94	2.44	4	19	2.69E-05	0.0423	0.00109	0.0354	6.61E-04	6.67E-03	1.91E-03	13.95	41.22	574.69
LBB76-576	946-23	25	150.60	48.05	2.18	4	10	1.60E-05	0.0395	0.00124	0.0385	7.56E-03	1.30E-02	6.56E-03	13.02	38.10	510.02
LBB76-576	946-23	26	140.31	33.57	2.24	4	18	2.56E-05	0.0477	0.00144	0.0337	2.24E-03	5.91E-03	4.50E-03	15.73	44.52	519.37
LBB76-576	946-23	27	145.12	35.66	2.47	4	17	3.20E-05	0.0348	0.00096	0.0308	7.06E-04	4.56E-03	2.60E-03	11.49	38.77	473.84
LBB76-576	946-23	28	113.47	29.64	2.42	4	15	3.84E-05	0.0328	0.00091	0.0326	2.35E-03	1.00E-02	4.46E-03	10.83	36.04	535.70
LBB76-576	946-23	29	87.35	25.45	2.24	4	12	3.07E-05	0.0427	0.00117	0.0340	3.53E-03	1.35E-02	5.35E-03	14.10	41.83	572.97
LBB76-576	946-23	30	107.36	27.18	2.25	4	16	3.20E-05	0.0444	0.00125	0.0347	7.98E-03	8.96E-03	7.90E-03	14.66	44.96	560.20
LBB76-576	946-23	31	136.93	43.65	2.53	4	10	2.30E-05	0.0302	0.00086	0.0288	2.03E-03	8.47E-03	2.63E-03	9.95	38.74	590.29
LBB76-576	946-23	32	83.47	28.05	2.43	4	9	2.56E-05	0.0403	0.00128	0.0276	2.91E-03	3.39E-03	2.19E-03	13.28	40.74	568.28
LBB76-576	946-23	33	108.85	34.66	2.46	4	10	2.24E-05	0.0391	0.00097	0.0249	1.38E-03	3.90E-03	2.51E-03	12.91	37.27	485.74
LBB76-576	946-23	34	130.51	34.23	2.45	4	15	3.20E-05	0.0342	0.00125	0.0266	9.25E-04	1.99E-03	1.55E-03	11.28	40.61	547.15
LBB76-576	946-23	35	143.45	31.87	2.08	4	21	3.84E-05	0.0363	0.00112	0.0271	8.33E-03	8.10E-03	4.87E-03	11.96	36.78	480.85
LBB76-576	946-23	36	107.73	38.33	2.26	4	8	1.92E-05	0.0369	0.00105	0.0274	1.44E-03	5.23E-03	3.02E-03	12.17	36.49	346.01
LBB76-576	946-23	37	138.36	30.66	2.31	4	21	3.84E-05	0.0376	0.00098	0.0292	5.03E-03	7.33E-03	4.00E-03	12.41	37.86	483.55
LBB76-576	946-23	38	113.79	33.19	2.10	4	12	3.07E-05	0.0327	0.00099	0.0280	2.34E-03	5.91E-03	1.35E-03	10.80	31.99	398.60
LBB76-576	946-23	39	167.89	40.17	2.58	4	18	2.56E-05	0.0398	0.00120	0.0258	3.38E-03	5.39E-03	2.25E-03	13.12	38.45	542.09
LBB76-576	946-23	40	161.87	35.08	2.31	4	22	3.07E-05	0.0420	0.00112	0.0263	2.51E-03	5.55E-03	4.45E-03	13.87	41.02	557.54
LBB76-762	946-24	1	153.87	54.86	1.77	4	8	1.28E-05	0.0385	0.00143	0.0230	3.26E-03	8.79E-04	6.29E-04	12.73	42.07	330.99
LBB76-762	946-24	2	151.16	75.88	1.77	4	4	6.40E-06	0.0392	0.00138	0.0274	4.88E-03	4.32E-03	2.80E-03	12.97	53.28	650.48
LBB76-762	946-24	3	77.63	29.51	1.86	4	7	1.60E-05	0.0537	0.00164	0.0304	8.04E-03	7.52E-03	1.24E-02	17.77	50.60	294.28
LBB76-762	946-24	4	38.75	9.52	1.86	4	17	7.68E-06	0.5460	0.01570	0.0289	5.79E-04	2.66E-03	3.07E-03	180.69	123.50	587.21
LBB76-762	946-24	5	176.09	72.19	1.85	4	6	9.60E-06	0.0335	0.00085	0.0335	1.01E-01	2.42E-02	5.76E-03	11.11	48.58	545.12
LBB76-762	946-24	6	117.41	35.69	1.81	4	11	3.84E-05	0.0232	0.00064	0.0289	7.42E-03	7.12E-03	4.77E-03	7.67	28.31	326.37
LBB76-762	946-24	7	105.52	25.89	1.96	4	17	3.84E-05	0.0399	0.00100	0.0322	2.02E-03	7.06E-03	4.62E-03	13.20	46.61	393.62
LBB76-762	946-24	9	38.42	14.60	1.77	4	7	1.28E-05	0.1360	0.00383	0.0310	4.66E-04	9.71E-04	1.96E-03	45.03	179.32	686.45
LBB76-762	946-24	10	119.13	48.86	1.87	4	6	1.28E-05	0.0374	0.00104	0.0290	9.09E-03	9.45E-04	1.30E-03	12.37	51.01	420.86
LBB76-762	946-24	11	83.69	31.78	1.74	4	7	1.92E-05	0.0415	0.00103	0.0323	2.89E-03	1.64E-02	5.90E-03	13.73	50.93	425.21
LBB76-762	946-24	13	100.01	41.03	1.76	4	6	1.60E-05	0.0357	0.00105	0.0246	1.11E-03	3.42E-03	1.88E-03	11.80	45.68	381.63
LBB76-762	946-24	14	56.13	19.97	1.80	4	8	3.20E-05	0.0425	0.00121	0.0255	3.03E-03	2.72E-03	3.18E-03	14.07	55.50	408.96
LBB76-762	946-24	15	63.74	26.14	1.97	4	6	2.05E-05	0.0438	0.00122	0.0271	2.87E-03	7.57E-03	2.50E-03	14.51	53.24	534.76
LBB76-762	946-24	17	91.24	40.95	1.71	4	5	1.92E-05	0.0272	0.00067	0.0389	6.92E-02	7.09E-02	4.74E-03	8.99	37.51	349.42
LBB76-762	946-24	18	79.60	20.77	1.83	4	15	3.20E-05	0.0561	0.00144	0.0387	4.87E-03	6.22E-03	5.56E-03	18.57	60.88	562.08
LBB76-762	946-24	19	130.43	39.66	1.79	4	11	2.30E-05	0.0347	0.00098	0.0327	2.32E-03	7.88E-03	1.99E-03	11.50	37.30	455.16
LBB76-762	946-24	20	41.64	18.69	1.77	4	5	3.84E-05	0.0299	0.00078	0.0402	8.41E-03	1.55E-02	1.08E-02	9.89	40.05	427.14
LBB76-762	946-24	21	45.96	23.07	1.60	4	4	2.30E-05	0.0361	0.00125	0.0306	4.45E-03	8.14E-03	4.54E-03	11.94	39.70	463.47
LBB76-762	946-24	22	98.45	37.46	1.92	4	7	1.60E-05	0.0423	0.00147	0.0315	4.83E-03	1.33E-02	1.22E-02	13.99	43.19	373.28
LBB76-762	946-24	23	71.01	41.10	1.86	4	3	9.60E-06	0.0419	0.00130	0.0338	3.15E-03	9.47E-03	6.16E-03	13.89	45.69	425.19

Table C1 Apatite fission track single grain ages for all samples used in this thesis generated using the ICP-MS method

UBC	AZ	Grain number	FT age (Ma)	1 σ (Ma)	Dpar (μ m)	Etch Figs	Natural tracks	Area (cm ²)	238U/43Ca (dmnls)	1 σ (dmnls)	43Ca back:sig	238U back:sig	232Th back:sig	147Sm back:sig	U (ppm)	Th (ppm)	Sm (ppm)
LBB76-762	946-24	24	90.33	45.30	2.12	4	4	1.34E-05	0.0314	0.00089	0.0361	1.11E-02	1.34E-02	1.30E-02	10.38	33.94	334.11
LBB76-762	946-24	25	109.60	49.18	1.92	4	5	1.28E-05	0.0339	0.00082	0.0405	9.93E-03	9.06E-03	9.27E-03	11.21	42.52	345.66
LBB76-762	946-24	26	102.93	28.83	2.17	4	13	2.56E-05	0.0469	0.00128	0.0407	7.60E-03	1.40E-02	7.95E-03	15.53	68.63	514.50
LBB76-762	946-24	28	105.66	33.63	1.84	4	10	1.54E-05	0.0586	0.00138	0.0329	6.62E-03	4.64E-03	1.75E-03	19.39	83.81	574.94
LBB76-762	946-24	29	40.35	18.11	1.76	4	5	2.56E-05	0.0462	0.00122	0.0401	3.92E-03	6.01E-03	8.38E-03	15.31	49.14	300.15
LBB76-762	946-24	30	122.94	39.15	1.69	4	10	1.34E-05	0.0574	0.00146	0.0284	6.38E-04	2.99E-03	1.64E-03	19.02	62.05	358.31
LBB76-762	946-24	31	49.21	16.51	2.00	4	9	1.34E-05	0.1300	0.00355	0.0352	0.00E+00	7.72E-04	1.89E-03	43.01	160.64	647.70
LBB76-762	946-24	32	140.48	47.24	1.77	4	9	1.60E-05	0.0380	0.00132	0.0315	1.93E-03	5.27E-03	2.15E-03	12.57	45.03	434.81
LBB76-762	946-24	34	124.96	42.00	1.90	4	9	1.54E-05	0.0445	0.00147	0.0315	4.91E-03	3.55E-03	2.53E-03	14.73	55.12	518.93
LBB76-762	946-24	35	108.73	48.81	1.93	4	5	1.15E-05	0.0379	0.00106	0.0358	4.96E-03	1.31E-02	9.86E-03	12.56	42.94	406.38
LBB76-762	946-24	36	158.13	44.25	1.99	4	13	2.30E-05	0.0338	0.00084	0.0351	3.82E-03	9.56E-03	4.15E-03	11.18	39.63	475.78
LBB76-762	946-24	37	93.73	42.08	2.00	4	5	1.54E-05	0.0330	0.00092	0.0441	1.61E-02	1.59E-02	1.96E-02	10.94	40.16	371.12
LBB76-762	946-24	38	35.45	20.52	1.92	4	3	1.60E-05	0.0505	0.00150	0.0366	1.37E-03	5.09E-03	5.02E-03	16.73	60.22	460.50
LBB76-762	946-24	39	110.35	39.23	1.84	4	8	1.92E-05	0.0359	0.00088	0.0398	5.90E-03	9.76E-03	9.42E-03	11.88	47.59	391.86
LBB76-762	946-24	40	109.38	33.28	1.72	4	11	2.30E-05	0.0415	0.00125	0.0262	3.26E-03	3.95E-03	4.03E-03	13.73	43.72	479.38
RM91-11C-225	1070-08	1	13.50	9.65	1.77	4	2	1.60E-05	0.0789	0.00789	0.0124	1.08E-03	3.73E-04	2.64E-03	29.24	69.41	233.93
RM91-11C-225	1070-08	3	59.82	30.53	1.91	4	4	9.60E-06	0.0592	0.00592	0.0140	1.03E-03	6.11E-03	8.88E-04	21.92	18.09	501.30
RM91-11C-225	1070-08	4	270.88	82.93	1.99	4	12	5.76E-06	0.0643	0.00643	0.0134	8.69E-04	5.33E-03	7.24E-04	23.81	28.23	547.85
RM91-11C-225	1070-08	5	107.75	49.42	1.87	4	5	7.68E-06	0.0511	0.00511	0.0131	2.14E-04	5.02E-03	1.21E-03	18.94	24.33	457.59
RM91-11C-225	1070-08	6	96.42	27.58	1.87	4	14	2.05E-05	0.0600	0.00600	0.0146	0.00E+00	3.06E-03	8.33E-04	22.24	64.31	902.13
RM91-11C-225	1070-08	7	35.97	16.50	2.09	4	5	1.73E-05	0.0684	0.00684	0.0141	1.56E-03	2.85E-03	2.19E-03	25.36	39.96	617.80
RM91-11C-225	1070-08	8	53.21	27.15	1.98	4	4	5.76E-06	0.1110	0.01110	0.0161	3.76E-04	1.89E-03	6.03E-04	41.08	62.07	653.46
RM91-11C-225	1070-08	9	144.42	53.14	1.70	4	8	8.96E-06	0.0522	0.00522	0.0177	2.67E-03	1.37E-02	9.68E-04	19.33	22.83	557.16
RM91-11C-225	1070-08	10	72.04	36.76	1.99	4	4	6.40E-06	0.0736	0.00736	0.0229	5.64E-04	5.70E-03	1.82E-03	27.27	54.49	622.41
RM91-11C-225	1070-08	11	89.39	28.45	1.86	4	11	5.12E-06	0.2040	0.02040	0.0151	2.52E-04	7.17E-04	8.56E-04	75.45	93.91	939.13
RM91-11C-225	1070-08	12	161.87	59.56	1.88	4	8	5.12E-06	0.0813	0.00813	0.0175	9.73E-04	4.04E-02	3.55E-03	30.13	6.56	397.70
RM91-11C-225	1070-08	13	33.31	33.48	1.72	4	1	1.60E-05	0.0160	0.00160	0.0239	1.28E-02	3.09E-03	8.60E-04	5.92	26.32	614.85
RM91-11C-225	1070-08	14	11.17	5.12	1.88	4	5	1.01E-04	0.0377	0.00377	0.0285	0.00E+00	1.06E-02	1.23E-03	13.98	30.17	623.62
RM91-11C-225	1070-08	15	6.28	6.31	1.87	4	1	9.60E-06	0.1410	0.01410	0.0244	5.34E-04	5.04E-03	2.36E-03	52.40	34.26	506.54
RM91-11C-225	1070-08	16	46.47	13.29	2.15	4	14	1.02E-05	0.2500	0.02500	0.0265	5.85E-04	1.16E-02	1.08E-03	92.66	21.22	602.08
RM91-11C-225	1070-08	17	96.35	33.58	2.21	4	9	2.24E-05	0.0353	0.00353	0.0267	2.41E-02	5.41E-03	1.79E-03	13.08	29.86	537.81
RM91-11C-225	1070-08	18	88.05	37.05	1.77	4	6	7.68E-06	0.0752	0.00752	0.0183	9.47E-04	8.40E-03	1.37E-03	27.86	30.42	635.22
RM91-11C-225	1070-08	19	67.89	18.85	2.27	4	15	2.56E-06	0.7330	0.07330	0.0189	0.00E+00	3.39E-04	4.59E-04	271.39	525.57	1669.40
RM91-11C-225	1070-08	20	198.43	55.08	1.80	4	15	7.68E-06	0.0827	0.00827	0.0190	6.53E-03	9.04E-03	3.18E-03	30.64	57.25	654.87
RM91-11C-225	1070-08	21	58.70	34.41	1.69	4	3	7.68E-06	0.0565	0.00565	0.0252	4.70E-03	6.06E-03	1.37E-03	20.94	27.19	535.95
RM91-11C-225	1070-08	22	41.04	20.94	1.77	4	4	7.68E-06	0.1080	0.01080	0.0253	2.78E-03	5.64E-03	2.77E-03	39.99	45.59	501.82
RM91-11C-225	1070-08	23	98.93	29.23	1.88	4	13	7.68E-06	0.1450	0.01450	0.0161	1.03E-03	2.26E-03	1.35E-03	53.68	51.03	657.91
RM91-11C-225	1070-08	24	29.39	21.00	2.01	4	2	1.28E-05	0.0453	0.00453	0.0217	9.90E-03	1.38E-02	3.71E-03	16.77	33.84	618.66

Table C1 Apatite fission track single grain ages for all samples used in this thesis generated using the ICP-MS method

UBC	AZ	Grain number	FT age (Ma)	1 σ (Ma)	Dpar (μ m)	Etch Figs	Natural tracks	Area (cm ²)	238U/43Ca (dmnls)	1 σ (dmnls)	43Ca back:sig	238U back:sig	232Th back:sig	147Sm back:sig	U (ppm)	Th (ppm)	Sm (ppm)
RM91-11C-225	1070-08	25	24.27	24.40	1.78	3	1	6.40E-06	0.0548	0.00548	0.0215	2.21E-03	5.13E-03	2.46E-03	20.31	34.61	523.55
RM91-11C-225	1070-08	27	70.93	29.85	1.93	4	6	1.28E-05	0.0561	0.00561	0.0189	2.14E-03	3.51E-03	2.07E-03	20.78	39.07	580.11
RM91-11C-225	1070-08	28	67.93	31.16	1.67	4	5	1.54E-05	0.0407	0.00407	0.0226	6.18E-03	5.99E-03	1.63E-03	15.07	27.81	531.21
RM91-11C-225	1070-08	29	48.09	28.19	1.96	4	3	1.15E-05	0.0460	0.00460	0.0246	2.80E-03	1.02E-02	2.58E-03	17.06	32.25	606.34
RM91-11C-225	1070-08	30	44.07	25.84	1.91	4	3	7.68E-06	0.0754	0.00754	0.0234	5.30E-04	4.59E-03	4.07E-03	27.92	47.69	454.66
RM91-11C-225	1070-08	31	26.93	15.79	2.08	4	3	7.68E-06	0.1230	0.01230	0.0211	4.39E-04	4.07E-03	3.45E-03	45.75	36.78	406.44
RM91-11C-225	1070-08	32	20.97	14.98	1.94	4	2	7.68E-06	0.1060	0.01060	0.0235	8.44E-04	7.00E-03	4.31E-03	39.19	43.54	455.09
RM91-11C-225	1070-08	33	61.13	25.72	1.86	4	6	6.40E-06	0.1300	0.01300	0.0202	1.58E-04	5.62E-03	3.34E-03	48.25	35.60	274.11
RM91-11C-225	1070-08	34	98.21	38.45	1.77	4	7	6.40E-06	0.0943	0.00943	0.0238	9.72E-04	2.80E-03	1.42E-03	34.94	34.14	563.97
RM91-11C-225	1070-08	35	98.05	41.26	1.98	4	6	6.40E-06	0.0810	0.00810	0.0245	8.60E-04	3.87E-03	1.43E-03	30.00	43.22	529.94
RM91-11C-225	1070-08	36	31.63	31.79	1.56	4	1	5.76E-06	0.0467	0.00467	0.0227	1.79E-03	5.05E-03	4.25E-03	17.31	28.20	397.70
RM91-11C-225	1070-08	37	67.16	28.26	2.05	4	6	1.60E-05	0.0474	0.00474	0.0232	2.48E-03	1.13E-02	8.44E-04	17.56	25.30	620.21
RM91-11C-225	1070-08	38	48.96	24.99	1.58	4	4	9.60E-06	0.0723	0.00723	0.0203	1.01E-03	6.12E-03	2.75E-03	26.80	37.29	624.19
RM91-11C-225	1070-08	39	96.77	35.61	1.83	4	8	9.60E-06	0.0729	0.00729	0.0197	5.50E-04	3.17E-03	1.68E-03	27.02	34.22	545.16
RM91-11C-225	1070-08	40	53.26	20.85	2.07	4	7	9.60E-06	0.1160	0.01160	0.0239	1.78E-04	3.66E-03	1.10E-03	43.10	52.52	686.88
RM91-22C-1460	1110-02	1	15.91	15.99	2.05	2	1	1.28E-05	0.0364	0.00364	0.0191	1.60E-03	4.25E-03	5.27E-03	14.89	46.10	191.79
RM91-22C-1460	1110-02	4	40.25	40.46	1.98	3	1	5.76E-06	0.0319	0.00319	0.0195	4.84E-04	3.28E-03	3.68E-03	13.05	57.35	319.86
RM91-22C-1460	1110-02	5	23.25	23.37	1.92	2	1	9.60E-06	0.0332	0.00332	0.0223	1.58E-03	2.01E-03	3.96E-03	13.57	55.19	187.81
RM91-22C-1460	1110-02	6	0.00	40.03	1.92	4	0	7.68E-06	0.0360	0.00360	0.0192	1.27E-03	3.00E-03	5.44E-03	14.72	48.72	206.80
RM91-22C-1460	1110-02	7	43.23	30.88	1.76	4	2	1.15E-05	0.0297	0.00297	0.0244	1.85E-03	1.05E-02	5.74E-03	12.15	32.89	145.13
RM91-22C-1460	1110-02	8	0.00	80.54	1.85	3	0	3.84E-06	0.0355	0.00355	0.0200	1.01E-03	1.25E-03	6.07E-03	14.54	49.70	194.26
RM91-22C-1460	1110-02	9	0.00	83.35	1.76	1	0	3.84E-06	0.0343	0.00343	0.0190	0.00E+00	4.59E-03	5.50E-03	14.04	44.56	199.22
RM91-22C-1460	1110-02	10	25.73	25.86	2.03	4	1	5.12E-06	0.0562	0.00562	0.0203	1.41E-03	2.00E-03	4.01E-03	23.00	65.74	220.57
RM91-22C-1460	1110-02	11	0.00	2080.76	1.69	4	0	5.12E-06	0.0007	0.00007	0.0370	2.50E-02	9.04E-03	1.48E+00	0.30	0.02	0.31
RM91-22C-1460	1110-02	12	48.73	34.81	1.92	4	2	5.12E-06	0.0592	0.00592	0.0194	7.84E-04	1.26E-03	2.47E-03	24.24	120.89	290.34
RM91-22C-1460	1110-02	13	31.13	22.24	2.09	2	2	7.68E-06	0.0619	0.00619	0.0153	0.00E+00	2.07E-03	3.34E-03	25.33	83.76	264.00
RM91-22C-1460	1110-02	16	0.00	25.04	2.31	4	0	9.60E-06	0.0461	0.00461	0.0224	1.74E-03	5.11E-03	1.00E-02	18.86	61.09	205.60
RM91-22C-1460	1110-02	17	0.00	42.83	1.94	3	0	5.12E-06	0.0504	0.00504	0.0166	4.03E-04	3.25E-03	4.41E-03	20.63	62.03	206.60
RM91-22C-1460	1110-02	18	12.10	12.16	2.24	1	1	1.60E-05	0.0383	0.00383	0.0184	8.45E-04	5.91E-03	3.38E-03	15.66	47.25	215.44
RM91-22C-1460	1110-02	19	39.71	28.37	1.99	3	2	6.40E-06	0.0582	0.00582	0.0174	1.18E-03	1.61E-03	6.40E-03	23.81	65.09	164.37
RM94-03C-639	1110-03	1	20.92	12.27	2.31	4	3	1.92E-05	0.0561	0.00561	0.0386	0.00E+00	4.40E-03	2.36E-03	22.59	70.08	591.79
RM94-03C-639	1110-03	2	167.31	70.39	2.23	4	6	1.54E-05	0.0173	0.00173	0.0166	1.24E-03	5.41E-03	3.15E-03	6.98	24.44	318.37
RM94-03C-639	1110-03	4	10.90	10.95	2.29	4	1	1.28E-05	0.0539	0.00539	0.0138	0.00E+00	4.12E-03	1.51E-03	21.70	57.37	537.02
RM94-03C-639	1110-03	7	31.70	16.18	2.07	4	4	1.15E-05	0.0822	0.00822	0.0193	2.03E-04	5.21E-03	2.41E-03	33.10	31.36	353.70
RM94-03C-639	1110-03	8	0.00	23.13	2.20	4	0	1.15E-05	0.0422	0.00422	0.0266	3.85E-04	4.04E-03	1.83E-03	17.00	49.35	580.88
RM94-03C-639	1110-03	9	44.86	26.30	2.24	4	3	1.15E-05	0.0435	0.00435	0.0184	2.23E-03	3.37E-03	2.18E-03	17.53	57.14	638.62
RM94-03C-639	1110-03	10	83.91	35.30	2.32	4	6	1.02E-05	0.0522	0.00522	0.0211	1.31E-03	3.90E-03	1.38E-03	21.02	45.94	626.57
RM94-03C-639	1110-03	11	112.53	47.34	2.00	4	6	7.68E-06	0.0518	0.00518	0.0170	5.75E-04	3.79E-03	2.22E-03	20.85	36.85	426.45

Table C1 Apatite fission track single grain ages for all samples used in this thesis generated using the ICP-MS method

UBC	AZ	Grain number	FT age (Ma)	1 σ (Ma)	Dpar (μ m)	Etch Figs	Natural tracks	Area (cm ²)	238U/43Ca (dmnls)	1 σ (dmnls)	43Ca back:sig	238U back:sig	232Th back:sig	147Sm back:sig	U (ppm)	Th (ppm)	Sm (ppm)
RM94-03C-639	1110-03	12	41.72	41.93	2.14	4	1	1.02E-05	0.0176	0.00176	0.0175	6.68E-04	7.73E-03	1.87E-03	7.07	28.64	403.53
RM94-03C-639	1110-03	13	108.95	45.83	2.39	4	6	9.60E-06	0.0428	0.00428	0.0194	1.53E-03	6.32E-03	1.34E-03	17.24	32.66	479.54
RM94-03C-639	1110-03	14	106.89	44.97	2.28	4	6	1.60E-05	0.0262	0.00262	0.0183	1.82E-03	6.99E-03	3.92E-03	10.54	20.29	223.64
RM94-03C-639	1110-03	15	158.83	72.84	2.33	4	5	1.54E-05	0.0152	0.00152	0.0335	7.88E-03	1.59E-02	5.01E-03	6.13	25.20	468.93
RM94-03C-639	1110-03	16	0.00	97.94	2.20	4	0	5.12E-06	0.0222	0.00222	0.0268	5.36E-03	6.43E-03	7.19E-03	8.93	28.00	245.04
RM94-03C-639	1110-03	17	126.43	64.51	2.01	4	4	1.54E-05	0.0153	0.00153	0.0218	2.53E-03	7.13E-03	9.45E-04	6.18	25.36	427.61
RM94-03C-639	1110-03	18	36.85	16.90	2.31	4	5	1.54E-05	0.0663	0.00663	0.0217	1.04E-03	3.47E-03	3.20E-03	26.69	39.54	242.21
RM94-03C-639	1110-03	19	114.04	47.98	2.37	4	6	2.56E-05	0.0153	0.00153	0.0254	1.23E-02	1.34E-02	4.96E-03	6.17	24.71	273.30
RM94-03C-639	1110-03	22	57.33	33.61	2.28	4	3	1.28E-05	0.0306	0.00306	0.0203	4.14E-04	6.98E-03	1.32E-03	12.33	28.57	516.34
RM94-03C-639	1110-03	23	63.93	37.47	2.21	4	3	1.92E-05	0.0183	0.00183	0.0214	0.00E+00	5.12E-03	3.25E-03	7.37	25.52	407.32
RM94-03C-639	1110-03	24	70.93	27.76	2.32	4	7	5.76E-06	0.1280	0.01280	0.0190	1.21E-04	4.34E-03	1.71E-03	51.62	35.26	523.17
RM94-03C-639	1110-03	25	24.30	24.42	2.00	4	1	7.68E-06	0.0402	0.00402	0.0183	1.44E-03	4.38E-03	1.38E-03	16.21	42.13	577.03
RM94-03C-639	1110-03	26	37.66	19.21	2.34	4	4	1.34E-05	0.0593	0.00593	0.0219	1.93E-03	5.12E-03	1.84E-03	23.88	36.02	440.39
RM94-03C-639	1110-03	28	62.25	31.76	2.03	4	4	7.68E-06	0.0627	0.00627	0.0199	9.90E-04	4.03E-03	1.96E-03	25.23	31.36	488.63
RM94-03C-639	1110-03	30	38.22	19.50	2.49	4	4	1.28E-05	0.0613	0.00613	0.0209	2.22E-04	3.25E-03	2.21E-03	24.70	43.18	539.73
RM94-03C-639	1110-03	31	49.38	18.17	2.48	4	8	1.92E-05	0.0633	0.00633	0.0250	1.62E-03	4.41E-03	1.99E-03	25.47	44.20	476.73
RM94-03C-639	1110-03	32	60.29	30.76	2.35	4	4	7.68E-06	0.0647	0.00647	0.0213	6.27E-04	4.07E-03	5.91E-03	26.05	44.63	208.57
RM94-03C-639	1110-03	33	188.69	55.74	2.08	4	13	1.92E-05	0.0266	0.00266	0.0235	1.27E-03	8.65E-03	2.76E-03	10.71	30.76	396.84
RM94-03C-639	1110-03	34	0.00	48.48	1.91	4	0	1.28E-05	0.0181	0.00181	0.0238	2.86E-03	8.14E-03	2.94E-03	7.27	28.38	374.36
RM94-03C-639	1110-03	35	86.52	28.74	2.56	4	10	5.12E-06	0.1690	0.01690	0.0224	3.60E-04	5.35E-03	2.09E-03	67.94	52.05	475.25
RM94-03C-639	1110-03	36	70.45	41.30	2.05	4	3	1.34E-05	0.0237	0.00237	0.0228	2.16E-03	6.13E-03	9.42E-04	9.55	34.65	533.18
RM94-03C-639	1110-03	37	85.39	50.06	2.25	4	3	5.76E-06	0.0456	0.00456	0.0265	2.08E-03	6.05E-03	7.83E-03	18.36	26.68	200.73
RM94-03C-639	1110-03	39	43.29	30.92	2.29	4	2	2.56E-05	0.0135	0.00135	0.0305	0.00E+00	1.81E-02	3.12E-03	5.45	19.84	316.70
RM94-03C-639	1110-03	40	66.32	25.96	2.27	4	7	1.54E-05	0.0514	0.00514	0.0296	6.44E-04	9.20E-03	2.51E-03	20.71	37.72	373.53
RM98-04C-459	1110-04	1	34.74	20.36	2.25	4	3	2.24E-05	0.0273	0.00273	0.0131	1.95E-03	3.64E-03	5.43E-04	11.66	40.77	502.58
RM98-04C-459	1110-04	2	16.24	16.33	2.10	4	1	2.05E-05	0.0213	0.00213	0.0118	4.12E-04	5.73E-03	8.13E-04	9.11	41.13	598.85
RM98-04C-459	1110-04	3	38.54	27.53	2.18	4	2	1.02E-05	0.0359	0.00359	0.0214	9.26E-04	1.29E-02	2.81E-03	15.33	28.58	459.70
RM98-04C-459	1110-04	5	41.72	29.80	2.24	4	2	5.76E-06	0.0589	0.00589	0.0156	1.43E-03	7.97E-03	1.90E-03	25.16	35.99	462.43
RM98-04C-459	1110-04	7	183.39	107.51	2.34	4	3	9.60E-06	0.0119	0.00119	0.0172	0.00E+00	1.61E-02	3.34E-03	5.09	19.74	229.37
RM98-04C-459	1110-04	8	26.11	15.31	2.16	4	3	1.60E-05	0.0509	0.00509	0.0203	9.28E-04	1.30E-02	3.47E-03	21.74	32.13	353.63
RM98-04C-459	1110-04	9	35.12	25.09	2.19	4	2	1.28E-05	0.0315	0.00315	0.0200	8.07E-04	8.08E-03	1.69E-03	13.46	33.61	355.12
RM98-04C-459	1110-04	10	44.16	31.55	2.39	4	2	1.02E-05	0.0313	0.00313	0.0239	6.33E-04	5.38E-03	1.88E-03	13.37	55.64	537.10
RM98-04C-459	1110-04	11	46.77	27.42	2.30	4	3	1.54E-05	0.0296	0.00296	0.0234	3.88E-03	5.44E-03	2.61E-03	12.62	53.98	548.84
RM98-04C-459	1110-04	12	33.22	23.73	2.19	4	2	7.68E-06	0.0555	0.00555	0.0194	1.48E-03	3.89E-02	2.78E-03	23.71	11.07	272.66
RM98-04C-459	1110-04	13	21.26	21.37	2.16	4	1	1.28E-05	0.0261	0.00261	0.0190	4.64E-04	1.05E-02	1.72E-03	11.13	33.79	446.29
RM98-04C-459	1110-04	14	29.07	29.22	2.14	4	1	9.60E-06	0.0254	0.00254	0.0189	9.35E-04	5.82E-03	1.17E-03	10.84	44.95	518.47
RM98-04C-459	1110-04	15	17.27	17.36	2.25	4	1	9.60E-06	0.0428	0.00428	0.0191	1.08E-03	1.12E-02	2.59E-03	18.27	40.97	427.15
RM98-04C-459	1110-04	16	24.89	14.59	2.14	4	3	7.68E-06	0.1110	0.01110	0.0165	5.26E-04	4.40E-03	1.71E-03	47.51	72.36	528.88

Table C1 Apatite fission track single grain ages for all samples used in this thesis generated using the ICP-MS method

UBC	AZ	Grain number	FT age (Ma)	1 σ (Ma)	Dpar (μ m)	Etch Figs	Natural tracks	Area (cm ²)	238U/43Ca (dmnls)	1 σ (dmnls)	43Ca back:sig	238U back:sig	232Th back:sig	147Sm back:sig	U (ppm)	Th (ppm)	Sm (ppm)
RM98-04C-459	1110-04	18	65.71	30.14	2.08	4	5	1.92E-05	0.0280	0.00280	0.0197	4.59E-04	1.23E-02	1.65E-03	11.96	35.96	547.99
RM98-04C-459	1110-04	19	112.40	51.55	2.13	4	5	1.28E-05	0.0245	0.00245	0.0183	2.87E-03	5.68E-03	1.03E-03	10.45	43.00	627.69
RM98-04C-459	1110-04	20	61.50	43.94	2.20	4	2	1.28E-05	0.0180	0.00180	0.0218	3.92E-03	1.60E-02	3.11E-03	7.67	30.31	442.64
RM98-04C-459	1110-04	21	20.32	14.51	2.08	3	2	1.28E-05	0.0546	0.00546	0.0206	1.93E-03	9.35E-03	2.88E-03	23.29	31.35	410.91
RM98-04C-459	1110-04	22	77.05	35.34	1.79	4	5	1.15E-05	0.0398	0.00398	0.0211	1.17E-03	1.91E-02	3.89E-03	16.98	23.05	355.99
RM98-04C-459	1110-04	23	23.89	10.96	2.40	4	5	1.15E-05	0.1290	0.01290	0.0200	2.68E-04	4.47E-03	2.65E-03	54.99	101.36	489.22
RM98-04C-459	1110-04	24	30.28	30.44	1.98	4	1	1.28E-05	0.0183	0.00183	0.0217	6.54E-04	1.12E-02	2.03E-03	7.81	31.77	581.65
RM98-04C-459	1110-04	25	64.94	33.13	2.52	4	4	1.28E-05	0.0340	0.00340	0.0199	1.35E-03	5.16E-03	2.80E-03	14.52	52.19	358.99
RM98-04C-459	1110-04	26	20.02	14.30	2.00	4	2	4.10E-05	0.0173	0.00173	0.0200	6.23E-04	1.18E-02	1.83E-03	7.39	28.66	455.97
RM98-04C-459	1110-04	27	39.72	14.62	2.07	4	8	7.68E-06	0.1860	0.01860	0.0232	9.66E-05	3.81E-03	2.25E-03	79.28	65.46	244.92
RM98-04C-459	1110-04	28	88.37	45.09	2.02	4	4	7.68E-06	0.0416	0.00416	0.0201	2.34E-03	1.27E-02	2.30E-03	17.75	23.84	308.67
RM98-04C-459	1110-04	29	55.23	28.18	2.04	4	4	1.60E-05	0.0320	0.00320	0.0203	1.40E-03	7.43E-03	5.77E-04	13.67	43.45	354.08
RM98-04C-459	1110-04	30	33.35	33.52	2.02	4	1	5.76E-06	0.0369	0.00369	0.0184	2.04E-03	1.20E-02	1.82E-03	15.75	23.48	377.56
RM98-04C-459	1110-04	31	49.00	20.61	2.28	4	6	1.34E-05	0.0645	0.00645	0.0216	8.18E-04	4.12E-03	1.77E-03	27.53	67.10	529.09
RM98-04C-459	1110-04	32	57.83	26.53	2.42	4	5	1.28E-05	0.0478	0.00478	0.0220	8.44E-04	8.53E-03	2.60E-03	20.39	47.83	338.30
RM98-04C-459	1110-04	33	28.10	20.08	2.26	4	2	9.60E-06	0.0525	0.00525	0.0253	1.22E-03	3.39E-03	3.41E-03	22.43	92.42	477.79
RM98-04C-459	1110-04	34	28.97	16.99	1.94	4	3	2.69E-05	0.0273	0.00273	0.0216	3.62E-03	9.98E-03	2.52E-03	11.66	31.03	297.73
RM98-04C-459	1110-04	35	29.62	21.16	2.25	4	2	1.28E-05	0.0374	0.00374	0.0187	3.93E-04	7.02E-03	2.33E-03	15.96	43.35	465.70
RM98-04C-459	1110-04	36	18.08	18.17	2.02	4	1	1.15E-05	0.0341	0.00341	0.0192	1.91E-03	1.25E-02	2.39E-03	14.54	33.56	476.42
RM98-04C-459	1110-04	38	43.57	31.13	2.25	4	2	1.28E-05	0.0254	0.00254	0.0216	1.33E-03	8.96E-03	3.05E-03	10.84	34.68	453.25
RM98-04C-459	1110-04	40	36.46	36.65	2.13	4	1	1.28E-05	0.0152	0.00152	0.0204	5.27E-03	9.69E-03	2.20E-03	6.48	26.81	492.73
U10-P05-06-1055	1103-07	1	0.00	14361.57	2.57	1	0	5.12E-06	0.0000	0.00000	0.0143	1.20E+00	6.18E-01	9.97E-04	0.00	0.11	593.72
U10-P05-06-1055	1103-07	2	7.37	4.32	1.72	4	3	1.02E-05	0.2780	0.02780	0.0303	3.25E-04	5.99E-04	1.60E-03	120.93	562.49	964.50
U10-P05-06-1055	1103-07	3	291.81	293.31	1.85	4	1	1.02E-05	0.0023	0.00023	0.0119	1.80E-02	1.80E+00	3.71E-03	1.00	0.06	103.98
U10-P05-06-1055	1103-07	5	0.00	151.28	1.76	4	0	7.68E-06	0.0088	0.00088	0.0178	3.79E-03	4.90E-01	5.68E-03	3.84	0.11	132.34
U10-P05-06-1055	1103-07	6	7.98	8.02	1.48	2	1	9.60E-06	0.0915	0.00915	0.0138	4.16E-04	8.19E-03	1.91E-04	39.71	19.04	1263.60
U10-P05-06-1055	1103-07	7	14.55	14.62	1.63	1	1	1.60E-05	0.0301	0.00301	0.0207	3.50E-03	1.08E-02	1.85E-04	13.06	22.94	1778.10
U10-P05-06-1055	1103-07	8	0.00	85.88	1.81	1	0	7.68E-06	0.0157	0.00157	0.0142	8.05E-03	6.75E-05	4.45E-04	6.83	1466.60	918.17
U10-P05-06-319	1103-04	1	36.61	26.15	2.35	4	2	1.02E-05	0.0361	0.00361	0.0134	2.43E-03	4.44E-03	1.42E-03	16.17	45.99	325.30
U10-P05-06-319	1103-04	2	0.00	126.44	3.16	1	0	7.68E-06	0.0103	0.00103	0.0115	4.61E-03	8.49E-03	6.48E-03	4.60	17.00	119.84
U10-P05-06-319	1103-04	3	0.00	16.67	3.24	2	0	6.40E-05	0.0095	0.00095	0.0140	1.66E-02	1.01E-02	5.07E-03	4.26	13.93	111.37
U10-P05-06-319	1103-04	4	26.47	26.60	2.40	1	1	1.92E-05	0.0133	0.00133	0.0133	2.49E-03	1.07E-02	8.15E-03	5.97	15.63	115.93
U10-P05-06-319	1103-04	5	0.00	29.14	2.68	4	0	2.56E-05	0.0136	0.00136	0.0134	4.49E-03	1.05E-02	2.75E-03	6.08	18.88	124.23
U10-P05-06-319	1103-04	6	134.08	68.41	2.60	4	4	1.60E-05	0.0125	0.00125	0.0161	2.95E-03	1.25E-02	7.01E-03	5.61	19.64	141.68
U10-P05-06-319	1103-04	7	0.00	28.74	3.16	1	0	3.20E-05	0.0110	0.00110	0.0170	3.17E-03	1.05E-02	6.58E-03	4.93	16.78	116.93
U10-P05-06-319	1103-04	8	29.31	29.46	3.01	1	1	1.28E-05	0.0180	0.00180	0.0166	2.53E-03	1.04E-02	5.40E-03	8.08	21.51	141.41
U10-P05-06-319	1103-04	9	21.69	21.80	2.08	1	1	2.56E-05	0.0122	0.00122	0.0180	7.13E-03	2.14E-02	9.11E-03	5.46	17.71	116.78
U10-P05-06-319	1103-04	10	47.86	48.11	3.24	1	1	1.28E-05	0.0110	0.00110	0.0173	3.49E-03	1.40E-02	7.27E-03	4.94	15.24	117.04

Table C1 Apatite fission track single grain ages for all samples used in this thesis generated using the ICP-MS method

UBC	AZ	Grain number	FT age (Ma)	1 σ (Ma)	Dpar (μ m)	Etch Figs	Natural tracks	Area (cm ²)	238U/43Ca (dmnls)	1 σ (dmnls)	43Ca back:sig	238U back:sig	232Th back:sig	147Sm back:sig	U (ppm)	Th (ppm)	Sm (ppm)
U10-P05-06-319	1103-04	11	40.12	40.33	3.16	1	1	1.54E-05	0.0110	0.00110	0.0230	1.18E-02	1.60E-02	1.59E-02	4.92	17.49	110.53
U10-P05-06-319	1103-04	12	0.00	80.60	2.71	1	0	1.54E-05	0.0081	0.00081	0.0190	3.09E-03	1.57E-02	6.95E-03	3.64	11.55	104.11
U10-P05-06-319	1103-04	13	0.00	38.19	2.58	1	0	1.92E-05	0.0138	0.00138	0.0174	5.18E-03	1.42E-02	6.31E-03	6.18	18.98	121.39
U10-P05-06-319	1103-04	14	87.69	62.65	3.09	1	2	1.28E-05	0.0120	0.00120	0.0145	9.57E-03	6.30E-03	6.89E-03	5.38	19.91	114.44
U10-P05-06-319	1103-04	16	46.18	32.99	2.62	1	2	2.30E-05	0.0127	0.00127	0.0247	1.28E-02	8.56E-03	6.60E-03	5.69	21.08	115.68
U10-P05-06-319	1103-04	18	31.37	31.53	2.21	1	1	1.92E-05	0.0112	0.00112	0.0199	1.93E-03	1.03E-02	6.35E-03	5.03	18.04	110.91
U10-P05-06-319	1103-04	20	21.85	21.96	2.98	4	1	1.92E-05	0.0161	0.00161	0.0186	2.57E-03	1.07E-02	1.82E-03	7.23	20.96	142.75
U10-P05-06-319	1103-04	21	22.59	22.71	2.01	2	1	1.60E-05	0.0187	0.00187	0.0193	2.90E-03	4.98E-03	2.76E-03	8.39	54.71	408.82
U10-P05-06-319	1103-04	22	51.21	21.54	2.35	4	6	4.48E-05	0.0177	0.00177	0.0154	2.68E-03	1.15E-02	2.23E-03	7.92	25.70	162.14
U10-P05-06-319	1103-04	23	27.00	27.14	2.26	1	1	1.92E-05	0.0130	0.00130	0.0162	4.92E-03	1.65E-02	6.37E-03	5.85	19.06	127.48
U10-P05-06-319	1103-04	24	31.34	31.50	2.47	1	1	2.30E-05	0.0094	0.00094	0.0154	7.77E-03	1.86E-02	5.55E-03	4.20	14.70	98.53
U10-P05-06-319	1103-04	25	34.57	34.75	2.24	1	1	1.60E-05	0.0122	0.00122	0.0209	3.98E-03	1.75E-02	1.45E-02	5.48	17.76	124.30
U10-P05-06-319	1103-04	26	0.00	57.15	3.13	1	0	1.28E-05	0.0138	0.00138	0.0147	7.16E-03	1.58E-02	4.16E-03	6.18	19.08	139.68
U10-P05-06-319	1103-04	27	27.25	27.39	2.54	4	1	1.92E-05	0.0129	0.00129	0.0142	3.35E-03	5.10E-03	4.66E-03	5.80	19.25	144.18
U10-P05-06-319	1103-04	28	68.92	40.40	2.77	4	3	2.56E-05	0.0115	0.00115	0.0129	4.13E-03	7.61E-03	5.26E-03	5.14	17.80	123.32
U10-P05-06-319	1103-04	29	0.00	34.17	1.82	1	0	1.92E-05	0.0154	0.00154	0.0178	7.29E-03	1.03E-02	5.86E-03	6.91	27.46	116.63
U10-P05-06-319	1103-04	30	101.18	72.28	2.52	1	2	1.54E-05	0.0087	0.00087	0.0182	5.02E-03	2.15E-02	7.06E-03	3.88	13.45	109.25
U10-P05-06-319	1103-04	31	29.91	30.06	2.82	2	1	1.54E-05	0.0147	0.00147	0.0131	3.49E-03	8.64E-03	3.34E-03	6.60	23.04	123.98
U10-P05-06-319	1103-04	32	59.69	42.64	2.60	2	2	1.92E-05	0.0118	0.00118	0.0140	3.46E-03	1.04E-02	7.96E-03	5.28	17.40	103.72
U10-P05-06-319	1103-04	33	25.09	25.22	2.88	1	1	2.05E-05	0.0132	0.00132	0.0132	0.00E+00	8.91E-03	4.45E-03	5.90	19.58	113.17
U10-P05-06-319	1103-04	34	28.99	29.14	2.78	1	1	1.28E-05	0.0182	0.00182	0.0148	5.48E-03	1.04E-02	5.40E-03	8.17	13.52	135.03
U10-P05-06-319	1103-04	35	25.83	25.96	3.03	1	1	2.30E-05	0.0114	0.00114	0.0220	8.50E-03	1.73E-02	5.48E-03	5.10	21.32	114.63
U10-P05-06-319	1103-04	36	21.88	21.99	2.89	3	1	2.05E-05	0.0151	0.00151	0.0173	4.53E-03	8.76E-03	4.96E-03	6.77	19.84	131.20
U10-P05-06-319	1103-04	37	0.00	64.44	2.09	4	0	1.28E-05	0.0122	0.00122	0.0158	3.77E-03	8.83E-03	2.99E-03	5.47	17.06	122.55
U10-P05-06-319	1103-04	38	51.08	51.34	2.73	2	1	1.28E-05	0.0103	0.00103	0.0161	1.10E-03	8.87E-03	4.76E-03	4.63	15.25	115.71
U10-P05-06-319	1103-04	39	0.00	47.32	2.58	1	0	1.60E-05	0.0133	0.00133	0.0146	4.86E-03	3.11E-03	4.62E-03	5.98	20.97	130.85
U10-P05-06-319	1103-04	40	29.57	29.72	2.81	2	1	2.30E-05	0.0099	0.00099	0.0179	1.29E-03	1.80E-02	3.80E-03	4.45	15.61	115.71
U10-P05-06-577	1103-06	1	0.00	46.82	1.82	4	0	7.68E-06	0.0287	0.00287	0.0112	0.00E+00	1.22E-02	1.97E-03	12.60	13.20	165.24
U10-P05-06-577	1103-06	3	35.16	17.94	2.21	4	4	1.28E-05	0.0614	0.00614	0.0113	1.39E-04	2.66E-03	2.07E-03	26.97	42.63	216.58
U10-P05-06-577	1103-06	4	15.14	6.94	2.14	4	5	4.10E-05	0.0557	0.00557	0.0096	3.69E-04	3.80E-03	2.56E-03	24.50	37.06	199.59
U10-P05-06-577	1103-06	5	26.18	13.36	1.91	4	4	1.60E-05	0.0660	0.00660	0.0133	8.16E-04	2.78E-03	2.63E-03	28.99	43.80	235.20
U10-P05-06-577	1103-06	6	19.02	7.00	2.16	4	8	4.10E-05	0.0710	0.00710	0.0168	1.41E-03	5.75E-03	3.50E-03	31.19	49.35	204.15
U10-P05-06-577	1103-06	7	35.52	16.29	2.21	4	5	1.92E-05	0.0506	0.00506	0.0200	1.09E-03	1.69E-03	2.02E-03	22.25	68.19	300.27
U10-P05-06-577	1103-06	8	21.91	11.18	2.12	4	4	1.54E-05	0.0821	0.00821	0.0139	1.13E-03	2.26E-03	1.91E-03	36.11	78.22	256.85
U10-P05-06-577	1103-06	9	68.75	49.11	2.49	4	2	7.68E-06	0.0261	0.00261	0.0136	2.14E-03	5.65E-03	3.15E-03	11.46	33.44	239.94
U10-P05-06-577	1103-06	10	53.27	20.85	2.24	4	7	1.02E-05	0.0885	0.00885	0.0193	1.05E-03	2.04E-03	2.50E-03	38.88	95.69	349.48
U10-P05-06-577	1103-06	12	18.93	8.68	2.08	4	5	2.56E-05	0.0713	0.00713	0.0134	0.00E+00	3.41E-03	2.38E-03	31.35	54.33	217.26
U10-P05-06-577	1103-06	14	18.43	9.40	2.24	4	4	2.30E-05	0.0651	0.00651	0.0177	2.11E-04	4.95E-03	2.55E-03	28.62	41.47	201.90

Table C1 Apatite fission track single grain ages for all samples used in this thesis generated using the ICP-MS method

UBC	AZ	Grain number	FT age (Ma)	1 σ (Ma)	Dpar (μ m)	Etch Figs	Natural tracks	Area (cm ²)	238U/43Ca (dmnls)	1 σ (dmnls)	43Ca back:sig	238U back:sig	232Th back:sig	147Sm back:sig	U (ppm)	Th (ppm)	Sm (ppm)
U10-P05-06-577	1103-06	15	23.76	9.30	2.05	4	7	2.56E-05	0.0795	0.00795	0.0418	2.59E-03	1.43E-02	8.13E-03	34.95	56.16	205.58
U10-P05-06-577	1103-06	16	11.97	12.03	2.14	4	1	9.60E-06	0.0602	0.00602	0.0149	0.00E+00	5.78E-03	3.43E-03	26.46	43.32	205.52
U10-P05-06-577	1103-06	17	33.37	17.02	2.19	4	4	1.28E-05	0.0647	0.00647	0.0152	1.23E-03	2.56E-03	2.24E-03	28.42	46.89	252.73
U10-P05-06-577	1103-06	18	18.99	11.13	2.26	4	3	1.60E-05	0.0682	0.00682	0.0165	3.04E-04	3.22E-03	2.61E-03	29.99	49.34	210.58
U10-P05-06-577	1103-06	19	34.05	15.62	2.11	4	5	1.15E-05	0.0880	0.00880	0.0194	1.44E-03	4.08E-03	3.33E-03	38.68	77.52	256.74
U10-P05-06-577	1103-06	20	26.21	9.64	2.31	4	8	1.28E-05	0.1650	0.01650	0.0198	6.05E-04	2.54E-03	6.03E-03	72.41	99.09	156.82
U10-P05-06-577	1103-06	21	36.99	26.42	1.93	4	2	1.28E-05	0.0292	0.00292	0.0214	3.13E-03	3.18E-02	5.85E-03	12.82	7.40	147.15
U10-P05-06-577	1103-06	22	59.57	21.92	2.15	4	8	1.15E-05	0.0803	0.00803	0.0181	7.23E-04	1.51E-03	1.13E-03	35.30	78.67	309.95
U10-P05-06-577	1103-06	23	42.94	14.97	2.02	4	9	2.24E-05	0.0645	0.00645	0.0220	3.87E-04	5.72E-03	4.80E-03	28.37	46.86	229.14
U10-P05-06-577	1103-06	25	32.40	23.15	2.37	4	2	7.68E-06	0.0555	0.00555	0.0167	1.06E-03	2.34E-03	2.28E-03	24.39	71.04	233.81
U10-P05-06-577	1103-06	26	17.93	9.15	2.28	4	4	2.24E-05	0.0688	0.00688	0.0203	1.81E-03	5.16E-03	6.16E-03	30.25	57.71	193.46
U10-P05-06-577	1103-06	27	14.37	10.26	2.15	4	2	1.92E-05	0.0501	0.00501	0.0197	1.10E-03	5.21E-03	1.77E-03	22.03	47.09	224.36
U10-P05-06-577	1103-06	28	29.10	17.06	1.97	4	3	9.60E-06	0.0742	0.00742	0.0225	4.47E-04	9.48E-03	3.59E-03	32.60	48.29	245.86
U10-P05-06-577	1103-06	29	32.59	19.11	2.21	4	3	9.60E-06	0.0662	0.00662	0.0198	6.56E-04	7.34E-03	4.12E-03	29.10	45.93	202.38
U10-P05-06-577	1103-06	30	28.13	16.49	2.22	4	3	1.60E-05	0.0460	0.00460	0.0191	1.30E-03	3.78E-03	4.95E-03	20.24	45.56	170.40
U10-P05-06-577	1103-06	31	67.55	28.42	2.01	4	6	7.68E-06	0.0796	0.00796	0.0192	0.00E+00	2.79E-03	2.11E-03	35.00	71.30	292.03
U10-P05-06-577	1103-06	33	39.31	15.39	1.93	4	7	1.92E-05	0.0640	0.00640	0.0158	1.15E-03	6.51E-03	3.85E-03	28.13	42.87	226.23
U10-P05-06-577	1103-06	34	26.78	15.70	1.83	4	3	5.76E-06	0.1340	0.01340	0.0194	0.00E+00	2.00E-03	3.63E-03	59.05	91.84	290.34
U10-P05-06-577	1103-06	35	14.02	14.09	2.19	2	1	7.68E-06	0.0642	0.00642	0.0196	2.32E-04	3.35E-03	3.33E-03	28.23	44.55	237.92
U10-P05-06-577	1103-06	36	52.80	30.96	2.43	4	3	1.28E-05	0.0306	0.00306	0.0184	5.16E-03	9.43E-03	2.82E-03	13.45	31.52	282.18
U10-P05-06-577	1103-06	37	51.08	19.99	2.01	4	7	7.68E-06	0.1230	0.01230	0.0148	7.12E-04	1.67E-03	1.66E-03	54.08	85.60	411.36
U10-P05-06-577	1103-06	38	88.46	29.38	2.01	4	10	1.54E-05	0.0506	0.00506	0.0161	1.70E-04	5.38E-03	3.18E-03	22.24	33.09	189.00
U10-P05-06-577	1103-06	39	11.34	8.10	2.12	4	2	1.92E-05	0.0635	0.00635	0.0186	6.15E-04	4.25E-03	2.90E-03	27.92	41.20	191.76
U10-P05-06-577	1103-06	40	26.73	9.83	2.18	4	8	2.56E-05	0.0808	0.00808	0.0184	3.54E-04	1.65E-03	1.29E-03	35.50	60.57	255.33
U12-P05-16-1303	1103-03	1	8.35	5.96	2.72	1	2	1.28E-05	0.1240	0.01240	0.0107	4.51E-04	3.34E-02	7.69E-04	56.70	4.43	329.05
U12-P05-16-1303	1103-03	2	0.00	32.39	2.43	1	0	1.02E-05	0.0298	0.00298	0.0119	5.19E-03	1.44E-02	2.58E-03	13.64	14.32	354.19
U12-P05-16-1303	1103-03	3	13.05	13.12	2.01	1	1	7.68E-06	0.0659	0.00659	0.0160	9.35E-04	2.01E-03	3.28E-03	30.23	137.05	405.34
U12-P05-16-1303	1103-03	4	9.83	5.77	2.35	4	3	9.60E-06	0.2100	0.02100	0.0129	3.92E-04	2.22E-02	3.51E-03	96.26	13.45	352.08
U12-P05-16-1303	1103-03	5	0.00	8.20	2.64	2	0	5.76E-06	0.2100	0.02100	0.0131	2.70E-04	1.57E-02	1.74E-03	96.16	11.92	375.69
U12-P05-16-1303	1103-03	6	33.76	14.21	2.24	4	6	5.76E-06	0.2040	0.02040	0.0142	2.77E-03	2.92E-02	2.29E-03	93.29	11.12	332.40
U12-P05-16-1303	1103-03	7	17.34	12.39	2.09	4	2	5.76E-06	0.1320	0.01320	0.0163	1.54E-03	2.28E-02	2.55E-03	60.62	6.65	354.01
U12-P05-16-1303	1103-03	8	13.27	6.77	2.36	3	4	7.68E-06	0.2590	0.02590	0.0130	4.05E-04	4.63E-02	3.10E-03	118.91	5.39	329.46
U12-P05-16-1303	1103-03	9	19.12	13.66	2.47	3	2	5.76E-06	0.1200	0.01200	0.0117	1.16E-03	4.77E-03	6.47E-04	54.99	29.08	410.19
U12-P05-16-1303	1103-03	10	22.58	16.13	2.34	2	2	5.76E-06	0.1020	0.01020	0.0168	1.54E-03	5.79E-02	2.56E-03	46.54	5.13	278.55
U12-P05-16-1303	1103-03	11	12.21	3.49	2.66	4	14	1.02E-05	0.7400	0.07400	0.0155	8.15E-05	5.57E-03	1.84E-03	339.02	23.54	435.47
U12-P05-16-1303	1103-03	12	34.67	11.52	2.56	4	10	1.02E-05	0.1860	0.01860	0.0185	1.16E-03	6.65E-02	2.70E-03	85.16	3.40	348.10
U12-P05-16-1303	1103-03	13	29.40	6.82	2.47	4	23	1.60E-05	0.3230	0.03230	0.0117	2.10E-04	5.34E-03	1.57E-03	147.89	27.83	399.29
U12-P05-16-1303	1103-03	14	12.55	7.35	2.32	4	3	5.12E-06	0.3090	0.03090	0.0176	6.20E-04	2.04E-03	1.92E-03	141.46	127.79	306.69

Table C1 Apatite fission track single grain ages for all samples used in this thesis generated using the ICP-MS method

UBC	AZ	Grain number	FT age (Ma)	1 σ (Ma)	Dpar (μ m)	Etch Figs	Natural tracks	Area (cm ²)	238U/43Ca (dmnls)	1 σ (dmnls)	43Ca back:sig	238U back:sig	232Th back:sig	147Sm back:sig	U (ppm)	Th (ppm)	Sm (ppm)
U12-P05-16-1303	1103-03	15	13.25	6.76	2.23	4	4	7.68E-06	0.2600	0.02600	0.0140	1.61E-04	6.42E-03	9.35E-04	119.02	31.11	512.79
U12-P05-16-1303	1103-03	16	13.89	9.92	2.44	4	2	5.76E-06	0.1650	0.01650	0.0139	9.08E-04	3.07E-02	2.42E-03	75.72	7.86	417.38
U12-P05-16-1303	1103-03	17	29.30	13.44	2.76	4	5	1.02E-05	0.1100	0.01100	0.0138	1.49E-03	5.70E-02	1.69E-03	50.41	2.08	306.62
U12-P05-16-1303	1103-03	18	61.72	36.18	2.43	4	3	1.28E-05	0.0250	0.00250	0.0211	2.42E-03	8.98E-02	1.92E-03	11.46	2.46	370.90
U12-P05-16-1303	1103-03	19	38.49	16.19	2.23	4	6	7.68E-06	0.1340	0.01340	0.0181	1.60E-03	2.49E-02	4.82E-03	61.35	9.54	318.62
U12-P05-16-1303	1103-03	20	21.57	9.08	2.00	4	6	1.02E-05	0.1790	0.01790	0.0186	1.24E-03	5.09E-03	3.40E-03	82.22	33.05	352.86
U12-P05-16-1303	1103-03	21	13.63	5.33	2.65	4	7	1.54E-05	0.2210	0.02210	0.0189	9.90E-04	1.79E-02	2.81E-03	101.29	14.49	449.41
U12-P05-16-1303	1103-03	22	23.45	9.18	2.36	4	7	5.12E-06	0.3850	0.03850	0.0133	1.74E-04	4.62E-02	2.06E-03	176.43	6.00	348.86
U12-P05-16-1303	1103-03	23	13.13	9.38	2.25	4	2	3.84E-06	0.2620	0.02620	0.0139	2.29E-03	1.02E-02	1.85E-03	120.11	19.47	438.89
U12-P05-16-1303	1103-03	24	22.10	11.27	2.18	4	4	7.68E-06	0.1560	0.01560	0.0154	3.15E-04	7.81E-03	1.95E-03	71.34	26.49	432.91
U12-P05-16-1303	1103-03	25	28.72	13.17	2.45	4	5	7.68E-06	0.1500	0.01500	0.0152	1.36E-03	3.85E-02	1.36E-03	68.58	6.92	351.57
U12-P05-16-1303	1103-03	26	33.16	12.20	2.38	4	8	9.60E-06	0.1660	0.01660	0.0155	3.14E-04	3.37E-02	3.42E-03	75.99	6.42	332.53
U12-P05-16-1303	1103-03	27	22.43	6.86	2.42	4	12	1.02E-05	0.3450	0.03450	0.0103	2.57E-05	8.16E-03	1.70E-04	158.31	12.74	368.49
U12-P05-16-1303	1103-03	28	10.15	7.25	2.78	3	2	5.76E-06	0.2260	0.02260	0.0135	1.87E-04	6.86E-02	2.18E-03	103.70	4.57	280.72
U12-P05-16-1303	1103-03	29	9.39	4.79	2.20	3	4	7.68E-06	0.3670	0.03670	0.0117	3.33E-04	4.79E-03	1.53E-03	168.18	55.92	356.70
U12-P05-16-1303	1103-03	30	0.00	39.86	2.56	3	0	5.76E-06	0.0430	0.00430	0.0195	7.87E-03	1.50E-02	7.56E-03	19.71	26.22	217.32
U12-P05-16-1303	1103-03	31	54.69	17.40	2.39	4	11	7.68E-06	0.1720	0.01720	0.0125	1.90E-04	1.55E-02	1.13E-03	79.14	8.23	339.40
U12-P05-16-1303	1103-03	32	12.15	8.68	2.46	4	2	9.60E-06	0.1130	0.01130	0.0152	9.66E-04	3.97E-03	1.45E-03	51.99	50.76	543.91
U12-P05-16-1303	1103-03	33	338.98	198.73	2.15	4	3	1.60E-05	0.0036	0.00036	0.0153	6.90E-02	6.07E-02	9.64E-02	1.64	5.20	16.17
U12-P05-16-1303	1103-03	34	25.17	7.70	2.58	4	12	2.56E-06	1.2300	0.12300	0.0145	6.49E-05	1.53E-02	1.59E-03	564.22	12.53	469.25
U12-P05-16-1303	1103-03	35	27.18	9.47	2.42	4	9	5.76E-06	0.3800	0.03800	0.0157	1.98E-03	1.31E-02	2.76E-03	174.14	17.30	393.38
U12-P05-16-1303	1103-03	36	30.00	17.59	2.32	4	3	3.84E-06	0.1720	0.01720	0.0145	1.77E-04	6.18E-03	1.83E-03	78.87	35.86	452.29
U12-P05-16-1303	1103-03	37	21.65	9.11	2.42	4	6	6.40E-06	0.2860	0.02860	0.0153	6.78E-05	5.75E-03	9.75E-04	131.23	45.54	563.25
U12-P05-16-1303	1103-03	38	18.88	6.95	2.11	4	8	1.15E-05	0.2430	0.02430	0.0146	4.89E-04	5.78E-03	2.15E-03	111.47	35.50	457.32
U12-P05-16-271	1103-01	1	0.00	6539.52	1.83	4	0	9.60E-06	0.0000	0.00000	0.0138	3.15E-01	2.20E-01	4.11E-03	0.02	0.91	173.01
U12-P05-16-271	1103-01	2	73.20	23.29	2.24	4	11	7.68E-06	0.1270	0.01270	0.0212	2.25E-04	4.30E-03	1.01E-02	58.89	80.40	195.14
U12-P05-16-271	1103-01	3	0.00	123.71	1.99	4	0	7.68E-06	0.0101	0.00101	0.0187	2.65E-02	2.49E-02	2.23E-02	4.69	18.53	55.78
U12-P05-16-271	1103-01	4	33.13	33.30	2.79	4	1	6.40E-06	0.0307	0.00307	0.0120	1.14E-03	3.78E-03	7.63E-03	14.24	60.48	99.45
U12-P05-16-271	1103-01	5	12.37	12.43	2.07	3	1	1.54E-05	0.0343	0.00343	0.0269	5.58E-03	1.32E-02	1.84E-02	15.92	29.60	85.28
U12-P05-16-271	1103-01	6	0.00	31.64	2.61	2	0	9.60E-06	0.0321	0.00321	0.0241	4.01E-03	1.39E-02	3.01E-02	14.88	25.07	57.50
U12-P05-16-271	1103-01	7	0.00	59.18	2.10	1	0	7.68E-06	0.0214	0.00214	0.0134	4.54E-03	7.04E-03	1.76E-02	9.90	22.10	45.75
U12-P05-16-271	1103-01	8	64.19	64.52	2.82	2	1	3.84E-06	0.0264	0.00264	0.0104	3.57E-03	1.70E-03	2.74E-03	12.22	92.39	201.68
U12-P05-16-271	1103-01	9	17.68	17.77	2.66	2	1	1.02E-05	0.0360	0.00360	0.0118	2.13E-03	4.07E-03	5.42E-03	16.69	62.34	104.64
U12-P05-16-271	1103-01	10	136.56	69.68	3.15	4	4	1.02E-05	0.0185	0.00185	0.0195	7.09E-03	2.67E-02	5.21E-03	8.57	18.08	122.50
U12-P05-16-271	1103-01	11	22.01	22.12	3.00	4	1	7.68E-06	0.0386	0.00386	0.0161	2.39E-03	5.78E-03	5.83E-03	17.87	51.24	76.95
U12-P05-16-271	1103-01	12	100.89	59.14	1.92	3	3	1.02E-05	0.0188	0.00188	0.0170	7.25E-03	8.56E-03	2.67E-03	8.72	23.04	379.20
U12-P05-16-271	1103-01	13	47.87	48.12	2.90	1	1	3.84E-06	0.0354	0.00354	0.0150	1.19E-03	1.25E-02	9.68E-03	16.41	24.39	53.15

Table C1 Apatite fission track single grain ages for all samples used in this thesis generated using the ICP-MS method

UBC	AZ	Grain number	FT age (Ma)	1 σ (Ma)	Dpar (μ m)	Etch Figs	Natural tracks	Area (cm ²)	238U/43Ca (dmnls)	1 σ (dmnls)	43Ca back:sig	238U back:sig	232Th back:sig	147Sm back:sig	U (ppm)	Th (ppm)	Sm (ppm)
U16-H07-34-537	1070-09	1	67.45	48.19	2.06	2	2	1.02E-05	0.0246	0.00246	0.0153	2.95E-03	5.36E-03	1.52E-03	9.11	38.07	147.37
U16-H07-34-537	1070-09	2	15.29	15.37	2.24	4	1	1.92E-05	0.0290	0.00290	0.0198	1.85E-03	5.09E-03	1.63E-03	10.76	47.02	128.28
U16-H07-34-537	1070-09	3	124.04	34.43	1.77	4	15	7.68E-06	0.1330	0.01330	0.0185	2.77E-04	1.03E-02	1.03E-02	49.30	36.00	122.13
U16-H07-34-537	1070-09	4	0.00	41.47	2.98	4	0	9.60E-06	0.0319	0.00319	0.0210	6.10E-03	7.03E-03	1.23E-02	11.83	49.77	123.67
U16-H07-34-537	1070-09	5	64.24	37.66	2.65	2	3	1.15E-05	0.0344	0.00344	0.0220	1.93E-03	5.18E-03	6.00E-03	12.75	43.93	124.46
U16-H07-34-537	1070-09	6	67.17	34.28	3.06	4	4	9.60E-06	0.0526	0.00526	0.0179	1.46E-03	2.13E-03	6.52E-03	19.51	76.25	143.14
U16-H07-34-537	1070-09	7	101.49	51.79	1.68	4	4	1.02E-05	0.0326	0.00326	0.0196	1.20E-03	1.77E-02	9.23E-03	12.07	15.17	70.04
U16-H07-34-537	1070-09	8	74.54	43.70	2.81	4	3	7.68E-06	0.0444	0.00444	0.0258	4.38E-03	2.91E-03	6.57E-03	16.47	64.59	138.69
U16-H07-34-537	1070-09	9	90.78	30.16	1.66	4	10	5.12E-06	0.1820	0.01820	0.0283	1.17E-03	1.79E-02	1.96E-02	67.54	20.40	48.86
U16-H07-34-537	1070-09	10	55.92	15.10	1.72	4	16	5.12E-06	0.4740	0.04740	0.0211	3.52E-04	6.23E-04	1.94E-03	175.88	210.30	299.35
U16-H07-34-537	1070-09	11	34.75	24.83	2.73	3	2	1.34E-05	0.0364	0.00364	0.0311	6.85E-02	3.47E-02	1.76E-02	13.50	53.02	155.06
U16-H07-34-537	1070-09	12	0.00	23.51	2.48	1	0	7.68E-06	0.0706	0.00706	0.0257	1.97E-03	3.67E-03	6.00E-03	26.17	118.88	284.91
U16-H07-34-537	1070-09	13	151.76	44.85	1.92	4	13	1.28E-05	0.0564	0.00564	0.0198	2.24E-03	4.71E-03	6.76E-03	20.91	27.09	154.45
U16-H07-34-537	1070-09	14	50.04	29.34	3.14	4	3	1.02E-05	0.0497	0.00497	0.0268	1.28E-03	6.03E-03	9.57E-03	18.44	74.14	138.44
U16-H07-34-537	1070-09	15	66.76	47.69	2.33	3	2	9.60E-06	0.0265	0.00265	0.0339	9.42E-03	7.25E-03	1.19E-02	9.81	39.72	117.73
U16-H07-34-537	1070-09	16	54.89	55.18	3.01	2	1	7.68E-06	0.0201	0.00201	0.0163	5.61E-04	1.62E-03	4.46E-03	7.47	26.03	208.43
U16-H07-34-537	1070-09	17	43.76	43.99	2.56	1	1	7.68E-06	0.0253	0.00253	0.0208	3.01E-03	1.02E-02	6.13E-03	9.37	34.45	98.65
U16-H07-34-537	1070-09	18	34.52	34.70	2.82	3	1	6.40E-06	0.0385	0.00385	0.0220	2.55E-03	5.37E-03	6.14E-03	14.27	58.56	125.51
U16-H07-34-537	1070-09	19	28.39	28.54	2.22	1	1	7.68E-06	0.0390	0.00390	0.0266	2.77E-03	3.10E-03	6.73E-03	14.46	64.67	128.07
U16-H07-34-537	1070-09	20	51.99	37.14	3.10	4	2	7.68E-06	0.0425	0.00425	0.0136	1.37E-03	1.66E-03	9.48E-03	15.77	69.16	130.02
U16-H07-34-537	1070-09	22	46.31	13.68	1.84	4	13	1.60E-05	0.1490	0.01490	0.0197	4.27E-04	1.67E-02	7.46E-03	55.27	13.92	151.03
U16-H07-34-537	1070-09	23	3301.39	2358.59	1.48	4	2	7.68E-06	0.0005	0.00005	0.0192	2.52E-01	1.93E-01	2.35E-02	0.19	0.61	31.09
U16-H07-34-537	1070-09	24	50.96	51.23	2.05	1	1	5.76E-06	0.0289	0.00289	0.0170	5.71E-03	3.91E-03	8.01E-03	10.73	39.74	79.81
U16-H07-34-537	1070-09	25	20.41	20.51	2.78	3	1	9.60E-06	0.0435	0.00435	0.0162	2.56E-03	4.33E-03	4.17E-03	16.11	59.12	143.06
U16-H07-34-537	1070-09	26	37.10	37.29	1.94	1	1	7.68E-06	0.0298	0.00298	0.0194	0.00E+00	4.08E-03	1.30E-02	11.06	49.38	158.11
U16-H07-34-537	1070-09	27	140.74	64.56	3.20	4	5	7.68E-06	0.0390	0.00390	0.0171	1.52E-03	2.87E-03	4.22E-03	14.46	54.63	116.17

Table C2 Apatite fission track single grain ages for central Tuscarora samples used in this thesis generated using the EDM

UBC	AZ	Grain number	FT age (Ma)	1 σ (Ma)	Dpar (μ m)	Etch Figs	Natural tracks, Ns	Induced tracks, Ni	Quads (dmnls)	U (ppm)
S7	304-07	1	122.62	26.54	1.63	4	31	73	40	26
S7	304-07	2	96.45	78.8	2.21	4	2	6	10	8
S7	304-07	3	377.42	288.48	2.13	2	4	3	18	2
S7	304-07	4	0	176.58	1.67	2	0	2	40	1
S7	304-07	5	132.24	48.31	2.23	4	11	24	6	56
S7	304-07	6	131.16	70.85	2.71	4	5	11	36	4
S7	304-07	7	75.6	34.73	2.19	4	6	23	10	32
S7	304-07	8	207.96	51.1	2.04	4	29	40	9	63
S7	304-07	9	285.11	232.95	2.27	4	3	3	25	2
S7	304-07	10	144.13	102.01	2.52	4	3	6	12	7
S7	304-07	11	346.8	156.22	1.98	4	11	9	8	16
S7	304-07	12	377.42	288.48	2.24	4	4	3	15	3
S7	304-07	13	79.02	29.81	1.43	4	9	33	24	19
S7	304-07	14	204.93	120.15	2.2	4	5	7	30	3
S7	304-07	15	185.92	72.16	2.2	4	11	17	24	10
S7	304-07	16	208.6	97.13	2.37	4	8	11	48	3
S7	304-07	17	423.08	386.42	2.53	2	3	2	32	1
S7	304-07	18	58.04	63.6	2.16	2	1	5	25	3
S7	304-07	19	377.42	288.48	2.14	4	4	3	30	1
S7	304-07	20	100.61	29.35	1.78	4	16	46	12	54
S7	304-07	21	191.47	174.88	2.01	1	2	3	24	2
S7	304-07	22	215.01	164.34	2.23	3	3	4	24	2
S7	304-07	23	153.63	47.78	3.64	4	16	30	12	35
S7	304-07	24	191.47	174.88	2.46	2	2	3	18	2
S7	304-07	25	121.59	51.37	2	3	8	19	27	10
S7	304-07	26	58.04	63.6	2.49	1	1	5	25	3
S12	304-10	1	146.14	38.55	2.03	4	24	37	8	83
S12	304-10	2	82.73	22.31	2.04	4	19	52	21	45
S12	304-10	3	82.91	19.17	2.01	4	26	71	12	107
S12	304-10	4	79.93	38.03	1.98	4	6	17	20	15
S12	304-10	5	90.51	37.96	1.97	4	8	20	15	24
S12	304-10	6	93.16	29.71	1.85	4	14	34	5	123
S12	304-10	7	84.89	33.28	1.75	4	9	24	15	29
S12	304-10	8	22.02	13.33	1.86	3	3	31	36	16
S12	304-10	9	38.79	15.91	2.13	4	7	41	8	92
S12	304-10	10	130.34	32.34	2.09	4	26	45	20	41
S12	304-10	11	71.15	15.84	2.46	4	27	86	6	258
S12	304-10	12	84.89	28.85	2	4	12	32	4	144
S12	304-10	13	160.75	66.73	2.23	4	10	14	9	28
S12	304-10	14	62.99	31.9	1.54	4	5	18	24	14
S12	304-10	15	96.93	18.11	2.04	4	42	98	10	177
S12	304-10	16	223.94	158.49	1.99	2	4	4	28	3
S12	304-10	17	56.72	31.75	2.19	4	4	16	20	14
S12	304-10	18	168.68	128.93	1.64	2	3	4	18	4
S12	304-10	19	154.79	60.8	2.53	4	11	16	20	14
S12	304-10	20	38.67	14.84	2.1	4	8	47	24	35
S12	304-10	21	61.06	15.12	2.22	3	21	78	30	47
S12	304-10	22	0	87.23	1.84	1	0	3	12	5
S12	304-10	23	76.26	15.29	2.14	4	34	101	8	228
S12	304-10	24	102.76	55.51	1.86	4	5	11	12	17
S12	304-10	25	98.32	37.36	2.19	4	10	23	8	52
S12	304-10	26	80.88	42.2	2.45	3	5	14	16	16

Table C2 Apatite fission track single grain ages for central Tuscarora samples used in this thesis generated using the EDM

UBC	AZ	Grain number	FT age (Ma)	1 σ (Ma)	Dpar (μ m)	Etch Figs	Natural tracks, Ns	Induced tracks, Ni	Quads (dmnls)	U (ppm)
S12	304-10	27	52.37	33.58	1.53	3	3	13	30	8
S12	304-10	28	137.78	52.89	1.72	4	11	18	16	20
S12	304-10	29	172.95	51.7	2.32	4	20	26	8	59
S12	304-10	30	179.77	120.71	2.31	1	4	5	9	10
S12	304-10	31	98.93	31.84	1.75	4	14	32	9	64
S12	304-10	32	131.58	62.7	1.91	2	7	12	24	9
S12	304-10	33	176.61	71.35	3.25	4	11	14	10	25
S13	304-11	1	204.53	119.91	1.98	4	5	7	6	16
S13	304-11	2	94.3	27.3	1.75	4	16	49	20	35
S13	304-11	3	96.25	111.18	2.48	2	1	3	9	5
S13	304-11	4	87.94	38.05	1.74	4	7	23	15	22
S13	304-11	5	127.81	19.15	2.02	4	67	151	18	118
S13	304-11	6	151.89	35.78	1.93	4	28	53	30	25
S13	304-11	7	26.39	27.58	1.77	2	1	11	20	8
S13	304-11	8	52.68	40.53	1.59	3	2	11	16	10
S13	304-11	9	110.94	58.47	2.33	1	5	13	80	2
S13	304-11	10	201.54	43.1	2.25	4	38	54	32	24
S13	304-11	11	0	111.18	1.49	1	0	3	12	4
S13	304-11	12	72.32	80.89	2.16	1	1	4	9	6
S13	304-11	13	82.59	33.2	2.15	4	8	28	3	132
S13	304-11	14	86.83	12.94	2.2	4	61	203	40	72
S13	304-11	15	48.31	21.35	1.93	4	6	36	6	85
S13	304-11	16	92.43	37.65	1.97	4	8	25	9	39
S13	304-11	17	172.24	125.89	2.1	3	3	5	8	9
S13	304-11	18	93.05	15.69	2.01	4	48	149	36	58
S13	304-11	19	48.31	52.2	1.71	2	1	6	18	5
S13	304-11	20	111.44	32	1.93	4	17	44	12	52
S13	304-11	21	131.98	48.22	1.84	4	11	24	32	11
S13	304-11	22	191.09	78.22	1.68	4	10	15	8	26
S13	304-11	23	128.02	34.62	1.79	4	20	45	50	13
S13	304-11	24	72.32	40.49	1.79	4	4	16	12	19
S13	304-11	25	121.92	44	1.71	4	11	26	6	61
S13	304-11	26	127.09	39.58	1.76	4	15	34	18	27
S13	304-11	27	179.31	72.48	1.75	4	10	16	21	11
S13	304-11	28	162.79	49.66	1.87	4	17	30	40	11
S13	304-11	29	58.99	19.59	1.94	4	11	54	10	76
S15	304-13	1	57.87	63.41	1.87	1	1	5	24	3
S15	304-13	2	119.39	34.63	1.81	4	17	41	27	21
S15	304-13	3	467.06	341.37	1.61	4	5	3	25	2
S15	304-13	4	173.24	41.07	2.02	4	29	48	10	68
S15	304-13	5	274.68	73.24	1.8	4	28	29	24	17
S15	304-13	6	165.2	47.83	1.91	4	19	33	6	78
S15	304-13	7	126.63	45.97	1.79	4	11	25	12	29
S15	304-13	8	149.17	25.41	2.15	4	54	104	15	98
S15	304-13	9	139.52	29.89	2.18	4	33	68	18	53
S15	304-13	10	177.45	31.76	1.98	4	52	84	12	99
S15	304-13	11	67.24	23.69	1.85	4	10	43	9	68
S15	304-13	12	108.08	73.24	2.08	4	3	8	8	14
S15	304-13	13	125.14	47.55	2.24	4	10	23	8	41
S15	304-13	14	147.01	27.6	1.94	4	44	86	12	101
S15	304-13	15	122.62	30.75	2.33	3	23	54	6	127
S15	304-13	16	97.63	24.26	1.73	4	22	65	9	102

Table C2 Apatite fission track single grain ages for central Tuscarora samples used in this thesis generated using the EDM

UBC	AZ	Grain number	FT age (Ma)	1 σ (Ma)	Dpar (μ m)	Etch Figs	Natural tracks, Ns	Induced tracks, Ni	Quads (dmnls)	U (ppm)
S15	304-13	17	64.26	50.27	1.57	3	2	9	24	5
S15	304-13	18	116.03	15.3	1.83	4	85	211	32	93
S15	304-13	19	244.42	136.18	1.82	4	6	7	18	5
S15	304-13	20	72.25	57.16	1.87	2	2	8	12	9
S15	304-13	21	42.6	20.44	1.7	4	5	34	28	17
S15	304-13	22	144.84	22.79	2.08	4	63	125	40	44
S15	304-13	23	244.42	61.25	2.15	4	30	35	6	82
S15	304-13	24	166.4	39.16	1.93	4	29	50	20	35
S15	304-13	25	96.16	29.81	1.89	4	14	42	8	74
S15	304-13	26	132.76	65.64	1.74	3	6	13	15	12
S15	304-13	27	52.63	40.49	1.96	4	2	11	12	13
S15	304-13	28	140.06	18.02	2.06	4	95	195	32	86
S15	304-13	29	92.34	26.67	1.66	4	16	50	25	28
S15	304-13	30	284.27	201.19	1.56	3	4	4	9	6
S15	304-13	31	0	176.05	1.6	1	0	2	30	1
S15	304-13	32	195.85	50.19	2.06	4	26	38	12	45
S15	304-13	33	222.18	112.16	1.48	3	7	9	10	13
S15	304-13	34	139.12	25.6	1.83	4	45	93	30	44
S15	304-13	35	134.22	35.7	1.84	4	21	45	16	40
S15	304-13	36	441.26	213.75	1.78	4	11	7	24	4
S15	304-13	37	112.05	29.01	2.16	4	21	54	24	32
S15	304-13	38	176.42	39.99	2.27	4	32	52	12	61
S15	304-13	39	201.34	60.59	1.65	4	19	27	40	10
S16	304-14	1	100.83	44.38	1.88	2	7	20	6	47
S16	304-14	2	214.16	163.69	1.53	2	3	4	16	4
S16	304-14	3	98.03	19.97	2.21	4	33	97	21	65
S16	304-14	4	76.5	18.49	1.91	4	22	83	36	33
S16	304-14	5	171.89	125.64	1.93	3	3	5	10	7
S16	304-14	6	72.18	40.41	1.65	2	4	16	15	15
S16	304-14	7	98.19	14.85	1.88	4	61	179	24	106
S16	304-14	8	151.91	62.78	1.64	4	9	17	30	8
S16	304-14	9	100.07	20.44	1.76	4	33	95	45	30
S16	304-14	10	49.12	17.77	1.88	4	9	53	12	63
S16	304-14	11	41.34	44.22	1.68	2	1	7	20	5
S16	304-14	12	83.85	19.22	1.97	4	25	86	25	49
S16	304-14	13	46.66	22.53	1.72	3	5	31	15	29
S16	304-14	14	123.25	49.24	1.78	4	9	21	12	25
S16	304-14	15	41.34	44.22	1.3	1	1	7	9	11
S16	304-14	16	76.96	25.11	1.97	4	12	45	8	80
S16	304-14	17	163.81	59.48	1.91	3	12	21	9	33
S16	304-14	18	160.85	42.18	2.16	4	23	41	16	36
S16	304-14	19	159.32	88.99	1.67	4	5	9	15	8
S16	304-14	20	73.64	16.65	2.22	4	25	98	16	87
S16	304-14	21	0	44.22	1.57	2	0	7	24	4
S17	304-15	1	89.56	17.84	1.91	4	36	91	25	66
S17	304-15	2	70.85	36.36	2.01	4	5	16	8	36
S17	304-15	3	62.59	25.06	1.56	4	8	29	20	26
S17	304-15	4	29.24	10.39	1.66	3	9	70	50	25
S17	304-15	5	17.51	18.18	1.56	2	1	13	25	9
S17	304-15	6	88.05	39.31	2.21	4	7	18	25	13
S17	304-15	7	0	40.94	1.54	1	0	6	12	9
S17	304-15	8	67.2	13.67	2.15	4	32	108	40	49

Table C2 Apatite fission track single grain ages for central Tuscarora samples used in this thesis generated using the EDM

UBC	AZ	Grain number	FT age (Ma)	1 σ (Ma)	Dpar (μ m)	Etch Figs	Natural tracks, Ns	Induced tracks, Ni	Quads (dmnls)	U (ppm)
S17	304-15	9	41.32	18.38	1.86	4	6	33	12	50
S17	304-15	10	88.95	31.76	1.68	4	11	28	12	42
S17	304-15	11	124.57	38.97	2.21	4	16	29	6	87
S17	304-15	12	143.47	49.24	2.03	3	14	22	30	13
S17	304-15	13	63.98	21.93	1.69	4	11	39	12	59
S17	304-15	14	63.02	22.6	2.14	4	10	36	12	54
S17	304-15	15	75.55	43.68	1.85	4	4	12	10	22
S17	304-15	16	103.65	37.87	1.81	4	11	24	10	43
S17	304-15	17	81.55	22.55	2.02	4	18	50	28	32
S17	304-15	18	87.55	11.36	2.09	4	87	225	18	225
S17	304-15	19	196.46	101.84	1.7	4	7	8	15	10
S17	304-15	20	98.04	32.69	1.99	4	13	30	15	36
S17	304-15	21	56.74	25.96	1.88	4	6	24	18	24
S17	304-15	22	95.28	40.26	1.76	2	8	19	40	9
S17	304-15	23	75.55	43.68	1.85	4	4	12	10	22
S17	304-15	24	98.62	20.48	1.91	4	34	78	12	117
S17	304-15	25	148.1	40	1.62	4	23	35	16	39
S17	304-15	26	93.94	23.99	2.2	4	22	53	4	239
S17	304-15	27	132.73	53.04	1.73	4	10	17	8	38
S17	304-15	28	31.59	15.1	1.69	2	5	36	15	43
S17	304-15	29	80.91	29.9	2.04	4	10	28	12	42
S17	304-15	30	64.81	23.32	2.07	4	10	35	5	126
S17	304-15	31	53.42	29.73	1.78	2	4	17	18	17
S17	304-15	32	98.04	32.69	1.89	4	13	30	9	60
S17	304-15	33	109.6	33.55	1.71	4	16	33	25	24
S17	304-15	34	90.55	53.64	1.69	4	4	10	15	12
S17	304-15	35	7.86	7.99	1.64	3	1	29	12	44
S17	304-15	36	67.2	27.12	1.94	4	8	27	7	70
S18	304-16	1	88.63	50.75	1.81	4	4	13	16	12
S18	304-16	2	72.11	32.98	2.17	4	6	24	6	57
S18	304-16	3	72.11	57.05	1.84	1	2	8	12	9
S18	304-16	4	135.07	33.68	2.33	4	24	51	12	60
S18	304-16	5	111.63	23.14	1.86	4	33	85	30	40
S18	304-16	6	149.32	37.1	2.15	4	25	48	16	42
S18	304-16	7	121.89	39.05	1.74	4	14	33	6	78
S18	304-16	8	82.34	66.07	2.04	3	2	7	15	7
S18	304-16	9	41.3	44.17	1.47	1	1	7	9	11
S18	304-16	10	82.34	46.75	1.63	3	4	14	16	12
S18	304-16	11	124.48	41.5	1.91	4	13	30	12	35
S18	304-16	12	143.42	87.93	1.88	4	4	8	6	19
S18	304-16	13	51.36	19.77	1.74	4	8	45	18	35
S18	304-16	14	114.99	48.23	2.04	4	8	20	24	12
S18	304-16	15	0	23.12	1.73	2	0	13	15	12
S18	304-16	16	190.52	123.11	1.79	4	4	6	8	11
S18	304-16	17	555.46	481.33	2.05	3	4	2	20	1
S18	304-16	18	87.68	37.94	2.37	2	7	23	16	20
S18	304-16	19	61.86	39.4	2.21	4	3	14	6	33
S18	304-16	20	99.7	9.9	1.99	4	150	433	60	102
S18	304-16	21	61.86	39.4	1.74	4	3	14	15	13
S18	304-16	22	157.58	59.34	1.79	4	11	20	12	24
S18	304-16	23	87.68	26.89	1.85	4	14	46	12	54
S18	304-16	24	57.75	28.34	1.5	4	5	25	16	22

Table C2 Apatite fission track single grain ages for central Tuscarora samples used in this thesis generated using the EDM

UBC	AZ	Grain number	FT age (Ma)	1 σ (Ma)	Dpar (μ m)	Etch Figs	Natural tracks, Ns	Induced tracks, Ni	Quads (dmnls)	U (ppm)
S18	304-16	25	131.91	38.85	2.12	4	17	37	24	22
S18	304-16	26	117.79	28.19	1.76	4	25	61	25	35
S18	304-16	27	131.59	27.94	1.61	4	33	72	10	102
S18	304-16	28	124.89	47.45	1.77	4	10	23	40	8
S18	304-16	29	157.87	38.13	2.05	4	27	49	9	77
S18	304-16	30	157.13	47.65	2.43	4	17	31	15	29
S18	304-16	31	118.34	53.26	1.97	4	7	17	8	30
S18	304-16	32	92.3	21.39	1.7	4	25	78	40	28
S18	304-16	33	103.58	28.64	1.74	4	18	50	20	35
S18	304-16	34	57.75	63.29	2.11	1	1	5	24	3
S18	304-16	35	90.95	42.68	1.97	4	6	19	18	15
S18	304-16	36	150.88	41.92	2.21	4	20	38	20	27
S18	304-16	37	70.51	23.81	1.94	4	11	45	6	106
S19	304-17	1	204.47	31.33	2.19	4	76	106	36	42
S19	304-17	2	125.97	35.82	1.84	4	18	41	36	16
S19	304-17	3	101.11	13.25	2.01	4	83	236	25	134
S19	304-17	4	95.87	41.94	2.07	4	7	21	15	20
S19	304-17	5	64.07	35.47	2.39	4	4	18	8	32
S19	304-17	6	124.77	47.41	1.56	4	10	23	15	22
S19	304-17	7	109.45	45.59	2.54	4	8	21	8	37
S19	304-17	8	76.81	30.65	1.7	4	8	30	30	14
S19	304-17	9	114.87	55.59	1.78	4	6	15	6	35
S19	304-17	10	171.55	88.74	1.75	4	6	10	14	10
S19	304-17	11	107.75	24.53	2.2	4	27	72	12	85
S19	304-17	12	243.7	135.78	1.65	2	6	7	12	8
S19	304-17	13	151.6	44.42	2	4	18	34	10	48
S19	304-17	14	114.09	25.27	1.93	4	29	73	30	35
S19	304-17	15	143.27	58.65	1.81	4	9	18	12	21
S19	304-17	16	178.6	72.19	2.07	4	10	16	24	9
S19	304-17	17	99.33	18.92	1.9	4	38	110	20	78
S19	304-17	18	65.52	32.52	1.7	4	5	22	30	10
S19	304-17	19	134.41	42.25	1.91	4	15	32	6	76
S19	304-17	20	41.26	44.13	2.02	1	1	7	20	5
S19	304-17	21	56.1	23.23	2.13	4	7	36	15	34
S19	304-17	22	213.73	163.37	1.79	4	3	4	16	4
S19	304-17	23	86.35	40.27	1.96	4	6	20	16	18
S19	304-17	24	183.63	78.65	1.86	4	9	14	10	20
S19	304-17	25	64.07	50.12	1.8	4	2	9	10	13
S19	304-17	26	121.89	18.83	2.08	4	62	146	14	148
S19	304-17	27	171.55	62.85	1.66	4	12	20	16	18
S19	304-17	28	68.62	34.21	1.82	4	5	21	18	17
S19	304-17	29	55.48	27.14	1.88	4	5	26	20	18
S19	304-17	30	28.91	30.33	1.54	1	1	10	36	4
S20	304-18	1	68.55	34.17	1.71	2	5	21	14	21
S20	304-18	2	20.64	21.38	1.71	1	1	14	5	40
S20	304-18	3	203.51	119.32	1.88	4	5	7	6	17
S20	304-18	4	28.88	30.3	1.75	3	1	10	9	16
S20	304-18	5	152.56	47.45	1.68	4	16	30	10	43
S20	304-18	6	84.58	43.1	1.83	2	5	17	9	27
S20	304-18	7	33.96	25.41	1.45	1	2	17	10	24
S20	304-18	8	45.54	28.33	1.81	4	3	19	15	18
S20	304-18	9	198.28	64.82	2.21	4	16	23	9	36

Table C2 Apatite fission track single grain ages for central Tuscarora samples used in this thesis generated using the EDM

UBC	AZ	Grain number	FT age (Ma)	1 σ (Ma)	Dpar (μ m)	Etch Figs	Natural tracks, Ns	Induced tracks, Ni	Quads (dmnls)	U (ppm)
S20	304-18	10	54.9	30	1.97	4	4	21	5	60
S20	304-18	11	33.96	17.98	1.64	4	4	34	12	40
S20	304-18	12	44.38	33.73	1.91	2	2	13	8	23
S20	304-18	13	82.18	46.65	1.67	3	4	14	8	25
S20	304-18	14	88.46	50.65	1.77	4	4	13	4	46
S20	304-18	15	120.74	51.02	1.74	4	8	19	5	54
S20	304-18	16	78.46	36.21	1.8	4	6	22	6	52
S20	304-18	17	13.77	14.1	1.6	3	1	21	10	30
S20	304-18	18	65.45	32.49	1.81	3	5	22	16	20
S20	304-18	19	61.11	25.5	2.02	4	7	33	10	47
S20	304-18	20	47.54	13.32	2.07	4	15	91	40	32
S20	304-18	21	80.9	30.62	1.87	4	9	32	20	23
S20	304-18	22	54.9	30	1.88	4	4	21	9	33
S20	304-18	23	55.78	24.94	1.95	3	6	31	18	24
S21	304-19	1	45.45	13.38	1.83	2	14	70	30	42
S21	304-19	2	159.02	34.94	2.36	4	36	51	20	46
S21	304-19	3	55.24	20.6	2.19	4	9	37	4	167
S21	304-19	4	75.58	35.7	1.83	3	6	18	6	54
S21	304-19	5	58.38	15.53	1.69	4	18	70	50	25
S21	304-19	6	77.08	21.76	2.19	4	17	50	30	30
S21	304-19	7	64.01	15.57	1.91	4	22	78	18	78
S21	304-19	8	87.69	29.93	2.21	4	12	31	4	140
S21	304-19	9	113.04	33.75	1.8	4	17	34	36	17
S21	304-19	10	107.44	30.11	1.81	4	19	40	20	36
S21	304-19	11	48.34	16.9	1.76	4	10	47	20	42
S21	304-19	12	115.77	31.26	1.82	4	21	41	25	30
S21	304-19	13	100.1	25.24	2.13	4	23	52	12	78
S21	304-19	14	64.84	36.81	1.65	4	4	14	12	21
S21	304-19	15	31.6	15.11	2.03	4	5	36	16	41
S21	304-19	16	113.04	37.16	1.78	4	14	28	8	63
S21	304-19	17	107.44	30.11	2.23	4	19	40	24	30
S21	304-19	18	113.04	25.93	2.03	4	29	58	20	52
S21	304-19	19	54.31	18.3	1.89	4	11	46	25	33
S21	304-19	20	88.09	27.87	2.14	4	14	36	14	46
S21	304-19	21	85.59	17.42	2.21	4	34	90	12	135
S21	304-19	22	43.11	14.24	1.92	3	11	58	30	35
S21	304-19	23	20.7	21.63	1.69	2	1	11	12	17
S22	304-20	1	8.14	5.87	1.77	1	2	56	40	25
S22	304-20	2	347.01	111.58	1.74	4	25	16	25	12
S22	304-20	3	75.11	12.46	2.75	4	50	151	30	91
S22	304-20	4	83.78	23.91	2.02	4	17	46	10	83
S22	304-20	5	64.86	36.83	2.35	1	4	14	50	5
S22	304-20	6	113.09	62.03	2	2	5	10	16	11
S22	304-20	7	87.17	32.54	2.1	4	10	26	9	52
S22	304-20	8	109.31	20.56	2.43	4	43	89	30	53
S22	304-20	9	153.32	48.42	1.98	4	17	25	10	45
S22	304-20	10	61.93	40.38	1.99	3	3	11	12	17
S22	304-20	11	145.04	62.12	1.84	4	9	14	9	28
S22	304-20	12	109.22	35.69	2.06	4	14	29	6	87
S22	304-20	13	154.26	55.71	2.78	4	13	19	4	86
S22	304-20	14	71.65	23.82	1.83	4	12	38	6	114
S22	304-20	15	58.89	25.04	1.94	4	7	27	14	35

Table C2 Apatite fission track single grain ages for central Tuscarora samples used in this thesis generated using the EDM

UBC	AZ	Grain number	FT age (Ma)	1 σ (Ma)	Dpar (μ m)	Etch Figs	Natural tracks, Ns	Induced tracks, Ni	Quads (dmnls)	U (ppm)
S22	304-20	16	113.09	98	1.72	2	2	4	16	5
S22	304-20	17	165.19	65.76	2.09	4	11	15	6	45
S22	304-20	18	131.75	28.3	2.13	4	35	60	12	90
S22	304-20	19	187.39	57.01	2.29	4	20	24	12	36
S22	304-20	20	129.08	81	1.96	4	4	7	4	32
S22	304-20	21	90.63	75.87	1.58	2	2	5	28	3
S23	304-21	1	103.65	15.83	2.04	4	65	142	30	85
S23	304-21	2	167.38	43.62	1.74	4	26	35	25	25
S23	304-21	3	251.82	122.59	1.88	4	9	8	6	24
S23	304-21	4	149.08	31.9	1.71	4	37	56	30	34
S23	304-21	5	224.32	142.03	1.85	4	5	5	8	11
S23	304-21	6	106.27	27.05	2.18	4	23	49	30	29
S23	304-21	7	122.22	34.12	1.92	4	20	37	30	22
S23	304-21	8	113.14	56.67	1.84	4	6	12	8	27
S23	304-21	9	132.9	53.11	1.99	4	10	17	8	38
S23	304-21	10	75.64	87.38	1.55	4	1	3	15	4
S23	304-21	11	138.97	62.58	1.83	4	8	13	4	58
S23	304-21	12	28.47	21.37	1.65	4	2	16	12	24
S23	304-21	13	107.99	18.48	2.11	4	52	109	25	78
S23	304-21	14	22.79	16.91	1.47	4	2	20	8	45
S23	304-21	15	66.79	15.33	1.93	4	25	85	40	38
S23	304-21	16	102.93	39.38	1.76	4	10	22	12	33
S23	304-21	17	127.14	53.11	1.69	4	9	16	9	32
S23	304-21	18	113.14	56.67	1.86	4	6	12	9	24
S23	304-21	19	146.04	56.68	1.68	4	11	17	10	31
S23	304-21	20	107.53	30.13	1.83	4	19	40	4	180
S23	304-21	21	95.86	34.6	2.06	4	11	26	4	117
S23	304-21	22	132.9	53.11	1.84	4	10	17	6	51
S23	304-21	23	135.53	99.06	2.35	4	3	5	6	15
S25	304-23	1	71.82	40.2	2.02	4	4	16	4	57
S25	304-23	2	65.86	15.69	1.57	4	22	96	36	38
S25	304-23	3	116.3	38.41	2.12	4	13	32	4	114
S25	304-23	4	80.64	18.41	2.31	4	25	89	21	60
S25	304-23	5	104.2	60.92	1.99	4	4	11	4	39
S25	304-23	6	77.31	23.39	1.91	4	14	52	6	123
S25	304-23	7	106.26	14.35	1.78	4	79	213	25	121
S25	304-23	8	0	43.99	1.53	1	0	7	16	6
S25	304-23	9	82.01	26.96	2.15	4	12	42	2	299
S25	304-23	10	107.43	72.8	1.94	4	3	8	12	9
S25	304-23	11	0	80.32	1.77	1	0	4	25	2
S25	304-23	12	71.82	46.41	1.8	3	3	12	25	7
S25	304-23	13	79.2	31.72	1.85	4	8	29	10	41
S25	304-23	14	73.12	22	1.52	4	14	55	40	20
S25	304-23	15	84	27.68	1.85	4	12	41	12	49
S25	304-23	16	175.36	78.97	2.19	4	8	13	12	15
S25	304-23	17	69.35	29.28	1.66	4	7	29	10	41
S25	304-23	18	90.58	42.51	1.88	4	6	19	12	23
S25	304-23	19	135.78	38.05	1.94	4	19	40	24	24
S25	304-23	20	303.82	117.37	1.9	4	14	13	30	6
S25	304-23	21	48.39	12.09	1.74	4	19	113	18	89
S25	304-23	22	145.02	31.3	1.94	4	33	65	30	31
S25	304-23	23	106.11	27.96	1.74	4	20	54	15	51

Table C2 Apatite fission track single grain ages for central Tuscarora samples used in this thesis generated using the EDM

UBC	AZ	Grain number	FT age (Ma)	1 σ (Ma)	Dpar (μ m)	Etch Figs	Natural tracks, Ns	Induced tracks, Ni	Quads (dmnls)	U (ppm)
S25	304-23	24	122.63	48.99	1.94	4	9	21	24	12
S25	304-23	25	120.68	24.59	2.04	4	35	83	8	148
S25	304-23	26	119.26	63.58	1.7	4	5	12	40	4
S32	304-28	1	186.51	38.35	2.06	4	40	61	30	29
S32	304-28	2	157.28	28.67	1.87	4	48	87	30	41
S32	304-28	3	100.22	44.11	1.75	4	7	20	12	24
S32	304-28	4	140.46	31.1	2.34	4	31	63	4	224
S32	304-28	5	92.57	13.7	2.22	4	63	195	9	308
S32	304-28	6	47.92	51.78	1.44	1	1	6	12	7
S32	304-28	7	131.83	65.19	1.55	3	6	13	16	12
S32	304-28	8	139.56	36.55	2.01	4	22	45	12	53
S32	304-28	9	71.75	28.44	1.51	4	8	32	30	15
S32	304-28	10	142.7	123.66	1.72	1	2	4	12	5
S32	304-28	11	131.83	26.85	1.69	4	36	78	40	28
S32	304-28	12	95.48	26.14	1.66	4	18	54	6	128
S32	304-28	13	47.92	16.43	1.84	4	10	60	24	36
S32	304-28	14	120.71	33.22	1.8	4	19	45	15	43
S32	304-28	15	128.85	32.59	1.65	4	23	51	10	73
S32	304-28	16	153.55	51.11	1.72	4	14	26	16	23
S32	304-28	17	122.51	16.39	1.78	4	84	196	25	112
S32	304-28	18	189.57	173.15	1.6	1	2	3	12	4
S32	304-28	19	106.01	27.93	1.86	4	20	54	9	85
S32	304-28	20	149.64	32.97	2.06	4	32	61	6	145
S32	304-28	21	145.09	32.82	2.12	4	30	59	8	105
S32	304-28	22	95.48	23.68	1.98	4	22	66	15	63
S32	304-28	23	53.88	33.94	1.72	4	3	16	12	19
S32	304-28	24	104.09	60.86	1.68	2	4	11	21	7
S32	304-28	25	26.18	27.36	1.87	4	1	11	16	10
S32	304-28	26	62.43	30.86	1.77	4	5	23	10	33
S32	304-28	27	71.75	46.36	1.83	2	3	12	36	5
S32	304-28	28	81.93	46.51	1.75	4	4	14	6	33
S32	304-28	29	270.79	79.43	1.69	4	23	24	40	9
S33	304-29	1	170.69	29.82	2	4	54	90	50	26
S33	304-29	2	168.61	53.43	1.65	4	16	27	24	16
S33	304-29	3	111.22	14.52	2.02	4	86	221	40	79
S33	304-29	4	0	33.69	1.72	2	0	9	8	16
S33	304-29	5	95.39	110.18	1.77	1	1	3	12	4
S33	304-29	6	117.99	32.37	1.73	4	19	46	32	20
S33	304-29	7	62.76	26.25	1.67	4	7	32	12	38
S33	304-29	8	76.42	24.93	1.8	4	12	45	4	160
S33	304-29	9	113.46	18.56	2.04	4	54	136	30	65
S33	304-29	10	99.95	21.77	1.8	4	29	83	7	169
S33	304-29	11	78.15	50.95	1.69	2	3	11	15	10
S33	304-29	12	124.06	19.08	1.9	4	63	145	40	52
S33	304-29	13	35.06	16.64	1.84	4	5	41	12	49
S33	304-29	14	52.2	40.16	1.85	4	2	11	12	13
S33	304-29	15	57.4	36.34	1.42	2	3	15	36	6
S33	304-29	16	118.67	15.63	1.68	4	86	207	36	82
S33	304-29	17	180.9	87.63	1.9	4	7	11	12	13
S33	304-29	18	205.55	32.62	2.11	4	71	98	20	70
S33	304-29	19	95.39	30.68	1.84	4	13	39	10	56
S34	304-30	1	101.39	35.71	1.65	2	11	31	50	9

Table C2 Apatite fission track single grain ages for central Tuscarora samples used in this thesis generated using the EDM

UBC	AZ	Grain number	FT age (Ma)	1 σ (Ma)	Dpar (μ m)	Etch Figs	Natural tracks, Ns	Induced tracks, Ni	Quads (dmnls)	U (ppm)
S34	304-30	2	71.6	32.75	1.52	1	6	24	25	14
S34	304-30	3	57.34	28.14	1.93	2	5	25	25	14
S34	304-30	4	0	80.08	1.67	2	0	4	12	5
S34	304-30	5	189.19	172.8	1.91	3	2	3	8	5
S34	304-30	6	33.15	20.23	1.74	3	3	26	24	15
S34	304-30	7	133.02	43.24	1.62	4	14	30	36	12
S34	304-30	8	63.68	49.82	1.67	1	2	9	30	4
S34	304-30	9	95.29	63.59	1.69	2	3	9	20	6
S34	304-30	10	130.15	34.5	1.98	4	21	46	4	164
S34	304-30	11	28.04	14.71	1.71	4	4	41	8	73
S34	304-30	12	107.1	72.58	1.56	2	3	8	60	2
S34	304-30	13	84.77	24.26	2.14	4	16	54	8	96
S34	304-30	14	61.42	39.12	1.56	1	3	14	8	25
S34	304-30	15	152.65	25.05	2.14	3	59	110	36	44
S34	304-30	16	122.26	84.45	1.58	2	3	7	9	11
S34	304-30	17	13.7	9.92	1.82	2	2	42	12	50
S34	304-30	18	88.76	19.73	1.81	4	27	87	36	34
S34	304-30	19	85.83	28.36	1.68	4	12	40	5	114
S34	304-30	20	114.18	95.59	1.8	1	2	5	40	2
S34	304-30	21	124.98	24.29	1.96	4	39	89	21	60
S34	304-30	22	81.76	65.6	1.73	2	2	7	9	11
S34	304-30	23	142.41	35.86	1.85	4	24	48	21	33
S34	304-30	24	31.23	14.73	2.15	3	5	46	36	18

Table C3 Apatite fission track lengths for all samples analysed in this thesis

UBC	A2Z	Track	Angle				Dpar (μm)	UBC	A2Z	Track	Angle				Dpar (μm)
			Length (μm)	to c- axis	Lo calc (μm)	Lc calc (μm)					Length (μm)	to c- axis	Lo calc (μm)	Lc calc (μm)	
5027	70608	1	16.44	39.10	16.40	16.60	2.72	LBB102-3900	94634	183	14.08	76.96	16.22	15.26	2.09
5027	70608	2	14.63	88.78	16.40	15.63	2.72	LBB102-3900	94634	184	12.79	78.25	16.15	14.47	1.85
5027	70608	3	12.22	63.87	16.30	13.95	2.36	LBB102-3900	94634	185	13.49	26.06	16.16	13.97	1.88
5027	70608	4	11.12	80.64	16.20	13.45	2.01	LBB102-3900	94634	186	15.39	63.44	16.16	16.01	1.88
5027	70608	5	15.62	58.33	16.20	16.13	2.01	LBB102-3900	94634	187	15.56	38.71	16.16	15.90	1.88
5027	70608	6	12.70	46.44	16.20	13.92	2.01	LBB102-3900	94634	188	12.87	53.50	16.16	14.19	1.88
5027	70608	7	14.21	16.10	16.20	14.38	2.01	LBB102-3900	94634	189	16.80	66.60	16.17	16.94	1.92
5027	70608	8	14.87	33.44	16.27	15.28	2.26	LBB102-3900	94634	190	11.11	37.46	16.17	12.51	1.92
5027	70608	9	14.37	68.50	16.27	15.39	2.26	LBB102-3900	94634	191	15.20	53.45	16.17	15.80	1.92
5027	70608	10	16.30	43.15	16.15	16.51	1.85	LBB102-3900	94634	192	12.96	52.59	16.20	14.24	2.02
5027	70608	11	14.29	35.20	16.00	14.84	1.32	LBB102-3900	94634	193	14.91	16.44	16.20	15.04	2.02
5027	70608	12	15.70	17.45	16.00	15.79	1.32	LBB102-3900	94634	194	14.01	78.03	16.13	15.22	1.75
5027	70608	13	15.06	42.82	16.00	15.57	1.32	LBB102-3900	94634	195	13.68	40.41	16.16	14.49	1.88
5027	70608	14	17.42	38.57	16.00	17.38	1.32	LBB102-3900	94634	196	15.02	41.09	16.16	15.51	1.88
5027	70608	15	15.44	62.89	16.00	16.04	1.32	LBB102-3900	94634	197	15.05	42.22	16.27	15.55	2.26
5027	70608	16	12.99	56.09	16.00	14.32	1.32	LBB102-3900	94634	198	11.13	58.37	16.25	13.15	2.20
5027	70608	17	14.32	46.51	16.00	15.08	1.32	LBB102-3900	94634	199	15.19	26.75	16.19	15.44	1.97
5027	70608	18	14.45	73.74	16.17	15.47	1.90	LBB102-3900	94634	200	13.98	5.01	16.08	14.00	1.60
5027	70608	19	15.13	4.28	16.27	15.14	2.25	LBB76-1038	94625	1	13.41	60.31	16.13	14.67	1.78
5027	70608	20	14.08	51.69	16.27	14.99	2.25	LBB76-1038	94625	2	9.66	65.57	16.13	12.36	1.78
5027	70608	21	14.76	69.52	16.27	15.64	2.25	LBB76-1038	94625	3	9.84	55.43	16.13	12.24	1.78
5027	70608	22	13.08	63.29	16.41	14.50	2.76	LBB76-1038	94625	4	15.49	50.28	16.13	15.97	1.78
5027	70608	23	15.62	49.13	16.24	16.05	2.15	LBB76-1038	94625	5	13.41	48.37	16.17	14.46	1.92
5027	70608	24	13.90	77.46	16.24	15.15	2.15	LBB76-1038	94625	6	15.36	41.23	16.15	15.77	1.84
5027	70608	25	14.70	78.78	16.27	15.65	2.26	LBB76-1038	94625	7	16.77	6.99	16.16	16.77	1.89
5027	70608	26	13.45	33.45	16.21	14.14	2.05	LBB76-1038	94625	8	14.31	40.66	16.16	14.97	1.89
5027	70608	27	14.10	13.65	16.24	14.23	2.14	LBB76-1038	94625	9	15.46	42.57	16.16	15.87	1.89
5027	70608	28	11.96	67.69	16.24	13.84	2.14	LBB76-1038	94625	10	13.66	48.97	16.16	14.65	1.89
5027	70608	29	15.93	74.99	16.18	16.41	1.96	LBB76-1038	94625	11	14.78	72.56	16.16	15.67	1.89
5027	70608	30	13.27	69.13	16.26	14.69	2.23	LBB76-1038	94625	12	12.51	63.31	16.16	14.13	1.89
5027	70608	31	15.53	82.19	16.26	16.17	2.23	LBB76-1038	94625	13	12.81	59.59	16.16	14.27	1.89
5027	70608	32	15.48	35.72	16.19	15.80	1.98	LBB76-1038	94625	14	15.85	7.32	16.19	15.86	1.97
5027	70608	33	14.16	25.23	16.19	14.52	1.98	LBB76-1038	94625	15	14.92	28.88	16.20	15.24	2.00
5027	70608	34	11.87	56.68	16.15	13.59	1.82	LBB76-1038	94625	16	13.82	67.98	16.09	15.03	1.62
5027	70608	35	10.89	48.82	16.19	12.74	1.99	LBB76-1038	94625	17	13.68	46.45	16.09	14.62	1.62
5027	70608	36	14.86	48.28	16.19	15.49	1.99	LBB76-1038	94625	18	13.55	78.49	16.09	14.94	1.62
5027	70608	37	15.82	57.94	16.20	16.26	2.01	LBB76-1038	94625	19	12.13	44.89	16.09	13.48	1.62
5027	70608	38	13.13	60.85	16.25	14.50	2.18	LBB76-1038	94625	20	5.23	54.09	16.18	11.16	1.95
5027	70608	39	15.70	16.72	16.30	15.78	2.37	LBB76-1038	94625	21	14.60	9.08	16.18	14.65	1.95
5027	70608	40	18.34	13.24	16.20	18.31	2.02	LBB76-1038	94625	22	16.29	59.86	16.18	16.59	1.95
5027	70608	41	13.80	49.08	16.16	14.75	1.87	LBB76-1038	94625	23	16.83	25.72	16.18	16.87	1.95
5027	70608	42	12.64	52.87	16.08	14.03	1.60	LBB76-1038	94625	24	15.88	53.53	16.18	16.27	1.95
5027	70608	43	10.57	59.45	16.20	12.81	2.01	LBB76-1038	94625	25	14.63	44.15	16.13	15.27	1.78
5027	70608	44	9.73	56.81	16.16	12.21	1.87	LBB76-1038	94625	26	16.34	73.63	16.13	16.66	1.78
5027	70608	45	8.78	78.11	16.31	12.57	2.39	LBB76-1038	94625	27	13.89	68.41	16.16	15.08	1.88
5027	70608	46	11.72	50.82	16.22	13.36	2.08	LBB76-1038	94625	28	14.02	71.76	16.16	15.19	1.88
5027	70608	47	14.85	51.24	16.34	15.53	2.52	LBB76-1038	94625	29	14.74	58.34	16.21	15.53	2.05
5027	70608	48	13.26	79.64	16.31	14.77	2.40	LBB76-1038	94625	30	13.15	64.91	16.21	14.56	2.05
5027	70608	49	15.00	45.52	16.29	15.56	2.34	LBB76-1038	94625	31	14.72	85.66	16.24	15.68	2.15
5027	70608	50	15.30	55.81	16.23	15.89	2.11	LBB76-1038	94625	32	14.67	37.78	16.24	15.19	2.15
5027	70608	51	13.94	50.32	16.09	14.87	1.62	LBB76-1038	94625	33	13.13	78.03	16.24	14.68	2.15
5027	70608	52	13.50	52.87	16.35	14.61	2.56	LBB76-1038	94625	34	14.07	53.73	16.24	15.02	2.15
5027	70608	53	13.99	87.62	16.35	15.24	2.56	LBB76-1038	94625	35	14.66	68.57	16.24	15.57	2.15
5027	70608	54	15.62	38.90	16.35	15.95	2.56	LBB76-1038	94625	36	12.99	34.28	16.19	13.80	1.99
5027	70608	55	14.97	73.60	16.35	15.80	2.56	LBB76-1038	94625	37	13.98	49.29	16.19	14.88	1.99
5027	70608	56	16.32	51.79	16.35	16.57	2.56	LBB76-1038	94625	38	12.69	68.73	16.19	14.32	1.99
5027	70608	57	14.23	66.72	16.35	15.28	2.56	LBB76-1038	94625	39	12.68	60.21	16.15	14.19	1.83
5027	70608	58	13.50	71.13	16.35	14.85	2.56	LBB76-1038	94625	40	13.85	62.80	16.15	14.99	1.83
5027	70608	59	15.70	62.73	16.32	16.21	2.44	LBB76-1038	94625	41	13.11	37.73	16.15	13.99	1.83
5027	70608	60	13.89	75.02	16.32	15.13	2.44	LBB76-1038	94625	42	14.55	64.63	16.15	15.47	1.85
5027	70608	61	14.74	47.57	16.32	15.40	2.44	LBB76-1038	94625	43	11.52	79.32	16.15	13.69	1.85

Table C3 Apatite fission track lengths for all samples analysed in this thesis

UBC	A2Z	Track	Angle				Dpar (µm)	UBC	A2Z	Track	Angle				Dpar (µm)
			Length (µm)	to c- axis	Lo calc (µm)	Lc calc (µm)					Length (µm)	to c- axis	Lo calc (µm)	Lc calc (µm)	
5027	70608	62	17.55	60.17	16.18	17.44	1.95	LBB76-1038	94625	44	14.07	23.32	16.15	14.40	1.84
5027	70608	63	14.98	70.67	16.12	15.79	1.73	LBB76-1038	94625	45	12.75	63.50	16.15	14.29	1.84
5027	70608	64	14.19	71.31	16.12	15.29	1.73	LBB76-1038	94625	46	11.84	46.94	16.15	13.33	1.84
5027	70608	65	15.84	76.24	16.12	16.35	1.73	LBB76-1038	94625	47	14.47	54.99	16.15	15.31	1.84
5027	70608	66	14.98	34.62	16.12	15.38	1.73	LBB76-1038	94625	48	15.38	53.14	16.15	15.92	1.84
5027	70608	67	16.28	29.99	16.11	16.41	1.71	LBB76-1038	94625	49	14.38	68.51	16.16	15.39	1.87
5027	70608	68	13.83	82.59	16.11	15.13	1.68	LBB76-1038	94625	50	16.47	53.75	16.13	16.69	1.77
5027	70608	69	11.21	37.71	16.11	12.59	1.68	LBB76-1038	94625	51	13.25	60.42	16.22	14.57	2.07
5027	70608	70	15.88	77.70	16.11	16.38	1.68	LBB76-1038	94625	52	13.17	72.80	16.22	14.66	2.07
5027	70608	71	14.40	67.50	16.11	15.40	1.68	LBB76-1038	94625	53	14.02	58.95	16.22	15.06	2.07
5027	70608	72	16.09	42.60	16.21	16.35	2.06	LBB76-1038	94625	54	13.88	65.68	16.17	15.04	1.90
5027	70608	73	10.58	65.48	16.24	12.94	2.15	LBB76-1038	94625	55	15.12	49.20	16.17	15.69	1.90
5027	70608	74	11.08	67.73	16.36	13.29	2.57	LBB76-1038	94625	56	15.82	82.66	16.17	16.35	1.90
5027	70608	75	14.20	84.07	16.18	15.36	1.96	LBB76-1038	94625	57	14.66	59.99	16.17	15.50	1.90
5027	70608	76	12.53	78.74	16.18	14.31	1.96	LBB76-1038	94625	58	14.36	33.36	16.17	14.86	1.90
5027	70608	77	13.86	56.92	16.18	14.92	1.96	LBB76-1038	94625	59	14.97	62.33	16.18	15.72	1.95
5027	70608	78	14.79	2.00	16.15	14.79	1.84	LBB76-1038	94625	60	14.41	58.66	16.18	15.31	1.95
5027	70608	79	14.57	85.01	16.15	15.59	1.84	LBB76-1038	94625	61	13.47	68.51	16.17	14.81	1.90
5027	70608	80	12.84	79.30	16.37	14.50	2.62	LBB76-1038	94625	62	12.79	48.69	16.17	14.04	1.90
5027	70608	81	15.74	56.32	16.12	16.19	1.73	LBB76-1038	94625	63	16.66	51.34	16.17	16.81	1.90
5027	70608	82	16.14	73.93	16.42	16.54	2.80	LBB76-1038	94625	64	14.02	67.39	16.17	15.15	1.90
5027	70608	83	15.06	27.28	16.26	15.33	2.24	LBB76-1038	94625	65	15.93	19.59	16.17	16.02	1.90
5027	70608	84	14.20	73.33	16.18	15.31	1.93	LBB76-1038	94625	66	14.88	20.05	16.17	15.06	1.90
5027	70608	85	15.42	79.37	16.21	16.10	2.04	LBB76-1038	94625	67	14.64	62.30	16.17	15.51	1.90
5027	70608	86	15.11	69.22	16.41	15.86	2.75	LBB76-1038	94625	68	14.63	83.65	16.15	15.62	1.85
5027	70608	87	13.28	56.40	16.17	14.52	1.91	LBB76-1038	94625	69	14.60	32.70	16.15	15.04	1.85
5027	70608	88	13.10	75.25	16.16	14.64	1.89	LBB76-1038	94625	70	15.43	56.75	16.15	15.98	1.85
5027	70608	89	14.30	68.55	16.31	15.34	2.41	LBB76-1038	94625	71	14.37	76.75	16.15	15.44	1.85
5027	70608	90	17.57	80.95	16.30	17.43	2.37	LBB76-1038	94625	72	16.99	20.58	16.15	17.01	1.85
5027	70608	91	14.44	19.15	16.45	14.64	2.91	LBB76-1038	94625	73	12.42	72.97	16.15	14.19	1.85
5027	70608	92	13.50	67.23	16.06	14.82	1.53	LBB76-1038	94625	74	15.57	14.27	16.15	15.64	1.85
5027	70608	93	12.38	76.48	16.13	14.20	1.76	LBB76-1038	94625	75	13.73	46.53	16.18	14.65	1.93
5027	70608	94	12.40	37.78	16.13	13.46	1.76	LBB76-1038	94625	76	14.17	48.12	16.15	15.00	1.85
5027	70608	95	15.12	75.97	16.13	15.90	1.76	LBB76-1038	94625	77	14.49	51.67	16.15	15.28	1.85
5027	70608	96	14.83	58.35	16.10	15.59	1.67	LBB76-1038	94625	78	12.97	29.16	16.22	13.63	2.08
5027	70608	97	16.29	22.26	16.37	16.37	2.60	LBB76-1038	94625	79	14.17	64.59	16.22	15.22	2.08
5027	70608	98	14.92	51.09	16.27	15.57	2.27	LBB76-1038	94625	80	15.37	78.93	16.22	16.07	2.08
5027	70608	99	12.62	68.93	16.23	14.28	2.12	LBB76-1038	94625	81	14.45	62.74	16.22	15.39	2.08
5027	70608	100	14.76	78.44	16.32	15.69	2.44	LBB76-1038	94625	82	12.64	72.48	16.22	14.33	2.08
5027	70608	101	13.79	29.91	16.45	14.32	2.91	LBB76-1038	94625	83	15.77	42.78	16.13	16.11	1.76
5027	70608	102	14.99	67.23	16.45	15.77	2.91	LBB76-1038	94625	84	16.48	67.55	16.13	16.74	1.76
5027	70608	103	15.25	71.82	16.45	15.97	2.91	LBB76-1038	94625	85	14.37	70.49	16.24	15.40	2.14
5027	70608	104	13.61	46.21	16.20	14.56	2.03	LBB76-1038	94625	86	16.36	50.80	16.24	16.60	2.14
5027	70608	105	16.27	60.09	16.43	16.58	2.83	LBB76-1038	94625	87	9.23	39.00	16.24	11.28	2.14
5027	70608	106	14.28	84.13	16.26	15.41	2.24	LBB76-1038	94625	88	17.45	15.86	16.24	17.44	2.14
5027	70608	107	12.93	89.38	16.08	14.59	1.58	LBB76-1038	94625	89	13.43	54.98	16.12	14.60	1.74
5027	70608	108	14.34	29.89	16.45	14.77	2.89	LBB76-1038	94625	90	14.66	63.62	16.12	15.53	1.74
5027	70608	109	13.87	79.37	16.16	15.14	1.87	LBB76-1038	94625	91	15.51	43.63	16.22	15.92	2.09
5027	70608	110	15.01	62.06	16.39	15.75	2.70	LBB76-1038	94625	92	14.75	60.44	16.21	15.56	2.04
5027	70608	111	14.90	76.45	16.22	15.77	2.07	LBB76-1038	94625	93	14.19	71.53	16.07	15.29	1.57
5027	70608	112	13.97	60.12	16.37	15.04	2.60	LBB76-1038	94625	94	16.34	21.98	16.17	16.41	1.92
5027	70608	113	13.79	81.04	16.09	15.10	1.63	LBB76-1038	94625	95	13.72	78.65	16.17	15.04	1.92
5027	70608	114	16.55	48.99	16.09	16.73	1.63	LBB76-1038	94625	96	15.54	34.08	16.17	15.83	1.91
5027	70608	115	16.25	68.85	16.26	16.59	2.24	LBB76-1038	94625	97	15.04	47.41	16.12	15.61	1.74
5027	70608	116	15.01	45.51	16.43	15.57	2.82	LBB76-1038	94625	98	14.25	62.80	16.12	15.25	1.74
5027	70608	117	14.06	71.55	16.42	15.21	2.80	LBB76-1038	94625	99	16.27	36.54	16.18	16.45	1.95
5027	70608	118	15.65	89.57	16.28	16.26	2.29	LBB76-1038	94625	100	13.63	81.03	16.18	15.00	1.95
5027	70608	119	10.08	36.37	16.28	11.74	2.29	LBB76-1038	94625	101	14.36	49.76	16.21	15.16	2.06
5027	70608	120	14.38	46.91	16.28	15.13	2.29	LBB76-1038	94625	102	14.06	46.62	16.21	14.89	2.06
5027	70608	121	14.09	59.23	16.10	15.11	1.65	LBB76-1038	94625	103	14.81	54.06	16.21	15.53	2.06
5027	70608	122	15.21	80.84	16.18	15.97	1.96	LBB76-1038	94625	104	14.09	44.02	16.12	14.87	1.74

Table C3 Apatite fission track lengths for all samples analysed in this thesis

UBC	A2Z	Track	Angle				Dpar	UBC	A2Z	Track	Angle				Dpar
			Length (μm)	to c- axis	Lo calc (μm)	Lc calc (μm)					Length (μm)	to c- axis	Lo calc (μm)	Lc calc (μm)	
5027	70608	123	15.14	76.51	16.40	15.92	2.72	LBB76-1038	94625	105	13.84	40.41	16.13	14.61	1.75
5027	70608	124	16.50	42.87	16.40	16.66	2.72	LBB76-1038	94625	106	15.66	64.85	16.15	16.19	1.83
5027	70608	125	15.60	47.46	16.26	16.02	2.22	LBB76-1038	94625	107	17.01	10.73	16.15	17.01	1.83
5027	70608	126	15.62	67.28	16.30	16.18	2.36	LBB76-1038	94625	108	15.36	78.36	16.15	16.06	1.83
5027	70608	127	15.58	73.29	16.27	16.18	2.27	LBB76-1038	94625	109	15.73	75.37	16.15	16.28	1.83
5027	70608	128	12.91	27.52	16.49	13.53	3.04	LBB76-1038	94625	110	14.74	44.93	16.22	15.36	2.07
5027	70608	129	14.69	89.88	16.34	15.67	2.52	LBB76-1038	94625	111	14.82	51.10	16.22	15.50	2.07
5027	70608	130	14.88	70.57	16.34	15.72	2.52	LBB76-1038	94625	112	13.42	82.59	16.22	14.88	2.07
5027	70608	131	14.62	29.40	16.26	15.00	2.22	LBB76-1038	94625	113	15.15	45.47	16.22	15.67	2.07
5027	70608	132	15.17	24.44	16.39	15.39	2.70	LBB76-1038	94625	114	13.39	88.81	16.22	14.87	2.07
5027	70608	133	16.31	62.40	16.16	16.61	1.86	LBB76-1038	94625	115	15.18	40.18	16.18	15.62	1.95
5027	70608	134	10.77	68.02	16.16	13.10	1.86	LBB76-1038	94625	116	14.84	83.50	16.18	15.75	1.95
5027	70608	135	14.76	61.70	16.28	15.58	2.29	LBB76-1038	94625	117	11.09	53.76	16.18	13.01	1.95
5027	70608	136	14.61	54.09	16.29	15.39	2.34	LBB76-1038	94625	118	14.49	26.85	16.16	14.84	1.87
5027	70608	137	13.79	47.00	16.30	14.71	2.35	LBB76-1038	94625	119	15.65	43.93	16.16	16.03	1.87
5027	70608	138	11.57	73.38	16.25	13.67	2.20	LBB76-1038	94625	120	12.75	72.81	16.16	14.40	1.87
5027	70608	139	15.59	66.89	16.10	16.16	1.65	LBB76-1038	94625	121	13.83	53.55	16.09	14.85	1.62
5027	70608	140	16.09	82.89	16.22	16.52	2.07	LBB76-1038	94625	122	15.15	19.94	16.09	15.31	1.62
5027	70608	141	14.08	73.44	16.38	15.24	2.66	LBB76-1038	94625	123	13.76	44.45	16.12	14.63	1.73
5027	70608	142	11.85	48.50	16.30	13.38	2.38	LBB76-1038	94625	124	15.16	80.56	16.15	15.94	1.82
5027	70608	143	16.02	37.12	16.31	16.25	2.42	LBB76-1038	94625	125	12.99	87.51	16.15	14.62	1.82
5027	70608	144	13.73	63.35	16.32	14.92	2.43	LBB76-1038	94625	126	15.05	49.41	16.15	15.65	1.82
5027	70608	145	11.07	45.13	16.02	12.75	1.38	LBB76-1038	94625	127	12.84	62.53	16.15	14.33	1.82
5027	70608	146	14.46	74.07	16.27	15.48	2.26	LBB76-1038	94625	128	13.86	72.87	16.15	15.10	1.82
5027	70608	147	14.61	49.11	16.27	15.33	2.26	LBB76-1038	94625	129	12.27	81.11	16.15	14.16	1.82
5027	70608	148	14.12	26.05	16.20	14.50	2.01	LBB76-1038	94625	130	15.22	68.72	16.15	15.93	1.82
5027	70608	149	14.60	35.40	16.20	15.09	2.01	LBB76-1038	94625	131	15.37	33.53	16.15	15.68	1.82
5027	70608	150	14.25	59.24	16.29	15.21	2.34	LBB76-1038	94625	132	15.57	8.87	16.15	15.60	1.82
5027	70608	151	14.53	69.74	16.29	15.50	2.34	LBB76-1038	94625	133	14.48	61.71	16.15	15.39	1.82
5027	70608	152	14.57	68.96	16.38	15.52	2.66	LBB76-1038	94625	134	12.76	65.59	16.12	14.32	1.72
5027	70608	153	15.36	43.87	16.38	15.81	2.66	LBB76-1038	94625	135	10.78	56.42	16.12	12.88	1.72
5027	70608	154	14.77	63.33	16.43	15.60	2.83	LBB76-1038	94625	136	13.55	74.63	16.12	14.91	1.72
5027	70608	155	15.63	74.17	16.43	16.22	2.83	LBB76-1038	94625	137	14.56	79.51	16.12	15.57	1.72
5027	70608	156	14.15	49.74	16.18	15.01	1.94	LBB76-1038	94625	138	13.49	47.95	16.12	14.51	1.72
5027	70608	157	13.33	38.00	16.18	14.16	1.94	LBB76-1038	94625	139	12.14	67.77	16.12	13.96	1.72
5027	70608	158	14.80	60.12	16.03	15.59	1.40	LBB76-1038	94625	140	13.97	55.21	16.12	14.97	1.72
5027	70608	159	13.80	69.84	16.03	15.03	1.40	LBB76-1038	94625	141	13.46	73.78	16.12	14.85	1.72
5027	70608	160	13.20	88.42	16.55	14.75	3.24	LBB76-1038	94625	142	14.69	41.35	16.10	15.27	1.65
5027	70608	161	16.98	41.43	16.07	17.03	1.55	LBB76-1038	94625	143	15.69	38.12	16.10	16.00	1.65
5027	70608	162	16.28	83.85	16.07	16.64	1.55	LBB76-1038	94625	144	11.74	30.98	16.12	12.72	1.72
5027	70608	163	16.27	48.89	16.31	16.52	2.42	LBB76-1038	94625	145	15.26	10.23	16.12	15.30	1.72
5029	70610	1	14.23	83.01	16.47	15.38	2.96	LBB76-1038	94625	146	15.88	31.75	16.15	16.09	1.83
5029	70610	2	13.72	62.56	16.35	14.90	2.54	LBB76-1038	94625	147	15.42	48.87	16.15	15.91	1.83
5029	70610	3	17.35	52.70	16.35	17.31	2.54	LBB76-1038	94625	148	12.01	55.81	16.15	13.67	1.83
5029	70610	4	14.80	29.66	16.35	15.15	2.54	LBB76-1038	94625	149	12.04	31.61	16.15	12.98	1.83
5029	70610	5	12.42	67.93	16.35	14.14	2.54	LBB76-1038	94625	150	14.38	75.74	16.15	15.44	1.83
5029	70610	6	17.33	77.98	16.35	17.29	2.54	LBB76-1038	94625	151	14.46	79.86	16.15	15.51	1.83
5029	70610	7	14.50	40.68	16.35	15.11	2.54	LBB76-1038	94625	152	14.78	52.39	16.18	15.49	1.94
5029	70610	8	14.38	57.52	16.35	15.28	2.54	LBB76-1038	94625	153	16.07	49.83	16.18	16.38	1.94
5029	70610	9	12.01	40.25	16.39	13.25	2.69	LBB76-1038	94625	154	12.60	72.61	16.21	14.30	2.05
5029	70610	10	13.95	36.06	16.34	14.59	2.51	LBB76-1038	94625	155	13.59	72.12	16.21	14.92	2.05
5029	70610	11	17.23	22.90	16.25	17.23	2.20	LBB76-1038	94625	156	15.20	58.13	16.21	15.84	2.05
5029	70610	12	16.96	54.94	16.25	17.04	2.20	LBB76-1038	94625	157	15.97	29.62	16.19	16.14	1.97
5029	70610	13	15.09	58.10	16.25	15.77	2.20	LBB76-1038	94625	158	15.08	38.21	16.19	15.52	1.97
5029	70610	14	15.58	53.95	16.25	16.07	2.20	LBB76-1038	94625	159	13.29	30.23	16.19	13.92	1.97
5029	70610	15	16.48	71.98	16.35	16.75	2.55	LBB76-1038	94625	160	15.12	47.15	16.11	15.67	1.70
5029	70610	16	14.19	41.28	16.55	14.89	3.25	LBB76-1038	94625	161	10.91	86.05	16.11	13.35	1.70
5029	70610	17	12.70	47.46	16.75	13.94	3.97	LBB76-1038	94625	162	13.89	68.38	16.11	15.08	1.70
5029	70610	18	14.64	74.84	16.24	15.60	2.17	LBB76-1038	94625	163	15.45	72.87	16.11	16.10	1.70
5029	70610	19	16.52	39.15	16.37	16.66	2.62	LBB76-1038	94625	164	15.99	44.23	16.11	16.28	1.70
5029	70610	20	15.50	47.32	16.37	15.95	2.62	LBB76-1038	94625	165	11.94	81.58	16.11	13.96	1.70

Table C3 Apatite fission track lengths for all samples analysed in this thesis

UBC	A2Z	Track	Angle				Dpar	UBC	A2Z	Track	Angle				Dpar
			Length (μm)	to c- axis	Lo calc (μm)	Lc calc (μm)					Length (μm)	to c- axis	Lo calc (μm)	Lc calc (μm)	
5029	70610	21	16.32	48.43	16.37	16.56	2.62	LBB76-1038	94625	166	11.71	66.55	16.11	13.67	1.70
5029	70610	22	16.66	35.04	16.37	16.76	2.62	LBB76-1038	94625	167	14.87	5.31	16.11	14.88	1.70
5029	70610	23	12.56	69.81	16.43	14.25	2.82	LBB76-1038	94625	168	14.02	69.88	16.13	15.17	1.75
5029	70610	24	16.19	35.81	16.57	16.38	3.33	LBB76-1038	94625	169	13.90	60.42	16.13	15.00	1.75
5029	70610	25	15.69	56.76	16.60	16.16	3.44	LBB76-1038	94625	170	13.85	48.67	16.16	14.78	1.89
5029	70610	26	14.02	78.00	16.46	15.23	2.94	LBB76-1038	94625	171	13.37	65.62	16.16	14.72	1.89
5029	70610	27	14.19	75.58	16.46	15.32	2.94	LBB76-1038	94625	172	13.95	79.42	16.16	15.19	1.89
5029	70610	28	15.09	71.99	16.30	15.87	2.36	LBB76-1038	94625	173	14.55	40.82	16.16	15.15	1.89
5029	70610	29	13.71	40.17	16.30	14.50	2.36	LBB76-1038	94625	174	14.73	57.83	16.16	15.52	1.89
5029	70610	30	14.78	9.58	16.30	14.83	2.36	LBB76-1038	94625	175	14.47	42.80	16.20	15.12	2.03
5029	70610	31	15.66	59.71	16.26	16.16	2.24	LBB76-1038	94625	176	13.25	66.61	16.20	14.65	2.03
5029	70610	32	13.70	83.14	16.26	15.05	2.24	LBB76-1038	94625	177	14.58	81.21	16.20	15.59	2.03
5029	70610	33	13.02	44.40	16.26	14.10	2.24	LBB76-1038	94625	178	12.82	73.80	16.10	14.45	1.66
5029	70610	34	16.32	26.37	16.40	16.42	2.71	LBB76-1038	94625	179	14.62	69.99	16.10	15.56	1.66
5029	70610	35	15.09	76.72	16.19	15.89	1.97	LBB76-1038	94625	180	13.68	36.15	16.10	14.39	1.66
5029	70610	36	15.77	80.59	16.19	16.32	1.97	LBB76-1038	94625	181	14.53	28.32	16.10	14.90	1.66
5029	70610	37	15.81	77.64	16.25	16.34	2.18	LBB76-1038	94625	182	15.21	62.12	16.10	15.88	1.66
5029	70610	38	15.54	82.35	16.25	16.18	2.18	LBB76-1038	94625	183	13.60	51.58	16.10	14.66	1.66
5029	70610	39	13.52	44.20	16.58	14.45	3.35	LBB76-1038	94625	184	14.98	5.83	16.10	15.00	1.66
5029	70610	40	16.27	44.90	16.58	16.50	3.35	LBB76-1038	94625	185	14.49	45.78	16.15	15.19	1.85
5029	70610	41	13.82	60.19	16.32	14.94	2.45	LBB76-1038	94625	186	14.25	51.61	16.15	15.11	1.85
5029	70610	42	15.85	41.35	16.35	16.15	2.56	LBB76-1038	94625	187	13.50	61.80	16.15	14.75	1.85
5029	70610	43	16.14	13.66	16.27	16.18	2.27	LBB76-1038	94625	188	15.73	28.85	16.15	15.93	1.85
5029	70610	44	14.79	26.91	16.22	15.10	2.09	LBB76-1038	94625	189	14.90	47.33	16.11	15.51	1.68
5029	70610	45	14.81	76.35	16.22	15.71	2.09	LBB76-1038	94625	190	14.34	69.97	16.11	15.38	1.68
5029	70610	46	14.25	52.12	16.09	15.12	1.64	LBB76-1038	94625	191	14.32	80.79	16.11	15.42	1.68
5029	70610	47	15.84	68.86	16.33	16.33	2.46	LBB76-1038	94625	192	14.04	74.58	16.11	15.22	1.68
5029	70610	48	13.99	57.79	16.43	15.02	2.82	LBB76-1038	94625	193	14.34	61.02	16.16	15.29	1.89
5029	70610	49	14.73	51.08	16.43	15.44	2.82	LBB76-1038	94625	194	14.53	45.72	16.11	15.22	1.71
5029	70610	50	15.52	37.76	16.33	15.86	2.48	LBB76-1038	94625	195	14.78	64.71	16.18	15.62	1.93
5029	70610	51	13.78	47.08	16.33	14.70	2.48	LBB76-1038	94625	196	15.20	30.87	16.18	15.51	1.93
5029	70610	52	7.86	40.21	16.33	11.04	2.48	LBB76-1038	94625	197	14.49	63.52	16.18	15.42	1.93
5029	70610	53	14.69	69.98	16.38	15.60	2.66	LBB76-1038	94625	198	14.94	75.43	16.18	15.79	1.93
5029	70610	54	15.19	77.28	16.24	15.95	2.17	LBB76-1038	94625	199	12.03	80.69	16.18	14.01	1.93
5029	70610	55	16.15	69.91	16.35	16.53	2.54	LBB76-1038	94625	200	13.92	69.44	16.18	15.11	1.93
5029	70610	56	14.17	77.63	16.35	15.32	2.54	LBB76-1038	94625	201	14.63	50.65	16.18	15.36	1.93
5029	70610	57	14.46	89.47	16.34	15.53	2.51	LBB76-1228	94626	1	14.10	81.27	16.21	15.29	2.05
5029	70610	58	13.95	21.66	16.27	14.25	2.25	LBB76-1228	94626	2	13.54	83.92	16.21	14.95	2.05
5029	70610	59	13.73	60.30	16.27	14.88	2.25	LBB76-1228	94626	3	14.00	22.01	16.10	14.31	1.66
5029	70610	60	15.54	62.01	16.27	16.10	2.25	LBB76-1228	94626	4	10.84	64.14	16.10	13.08	1.66
5029	70610	61	16.09	70.09	16.46	16.49	2.92	LBB76-1228	94626	5	13.67	53.67	16.13	14.74	1.77
5029	70610	62	15.69	61.84	16.40	16.20	2.72	LBB76-1228	94626	6	14.77	37.43	16.16	15.26	1.87
5029	70610	63	15.78	60.11	16.37	16.25	2.60	LBB76-1228	94626	7	13.65	85.86	16.16	15.03	1.87
5029	70610	64	15.17	82.92	16.00	15.95	1.32	LBB76-1228	94626	8	15.02	34.03	16.16	15.41	1.87
5029	70610	65	14.13	50.30	16.48	15.00	3.01	LBB76-1228	94626	9	15.38	67.93	16.14	16.03	1.79
5029	70610	66	17.11	53.22	16.38	17.14	2.65	LBB76-1228	94626	10	12.43	69.11	16.14	14.16	1.79
5029	70610	67	13.19	63.28	16.38	14.57	2.65	LBB76-1228	94626	11	14.17	52.02	16.14	15.06	1.79
5029	70610	68	14.29	86.92	16.39	15.42	2.68	LBB76-1228	94626	12	14.81	52.42	16.14	15.51	1.79
5029	70610	69	17.46	28.26	16.39	17.43	2.68	LBB76-1228	94626	13	13.94	50.83	16.14	14.88	1.81
5029	70610	70	13.20	61.01	16.10	14.54	1.65	LBB76-1228	94626	14	14.52	66.32	16.13	15.46	1.76
5029	70610	71	16.99	78.74	16.27	17.07	2.27	LBB76-1228	94626	15	13.75	24.24	16.13	14.14	1.78
5029	70610	72	16.71	43.02	16.71	16.83	3.81	LBB76-1228	94626	16	14.57	40.24	16.13	15.16	1.78
5029	70610	73	14.71	81.92	16.71	15.67	3.81	LBB76-1228	94626	17	14.12	77.41	16.13	15.29	1.78
5029	70610	74	15.08	75.67	16.32	15.88	2.45	LBB76-1228	94626	18	13.17	71.40	16.13	14.65	1.78
5029	70610	75	15.62	61.06	16.30	16.14	2.37	LBB76-1228	94626	19	14.50	64.33	16.13	15.43	1.78
5029	70610	76	16.34	59.44	16.30	16.62	2.37	LBB76-1228	94626	20	14.40	82.28	16.13	15.48	1.78
5029	70610	77	13.95	70.49	16.40	15.13	2.73	LBB76-1228	94626	21	14.18	82.58	16.13	15.34	1.78
5029	70610	78	14.84	8.18	16.37	14.87	2.61	LBB76-1228	94626	22	13.61	64.55	16.17	14.86	1.91
5029	70610	79	15.57	67.70	16.47	16.15	2.98	LBB76-1228	94626	23	14.25	65.16	16.17	15.28	1.91
5029	70610	80	14.09	57.82	16.47	15.09	2.98	LBB76-1228	94626	24	15.77	43.78	16.16	16.11	1.88
5029	70610	81	15.19	83.75	16.29	15.97	2.34	LBB76-1228	94626	25	14.25	28.64	16.16	14.67	1.88

Table C3 Apatite fission track lengths for all samples analysed in this thesis

UBC	A2Z	Track	Angle				Dpar	UBC	A2Z	Track	Angle				Dpar
			Length (μm)	to c- axis	Lo calc (μm)	Lc calc (μm)					Length (μm)	to c- axis	Lo calc (μm)	Lc calc (μm)	
5029	70610	82	14.20	60.35	16.33	15.19	2.46	LBB76-1228	94626	26	13.81	67.37	16.16	15.02	1.88
5029	70610	83	19.38	45.10	16.33	18.87	2.46	LBB76-1228	94626	27	14.56	16.99	16.16	14.72	1.88
5029	70610	84	15.77	13.56	16.36	15.82	2.59	LBB76-1228	94626	28	13.46	59.81	16.16	14.70	1.88
5029	70610	85	12.99	79.04	16.38	14.59	2.64	LBB76-1228	94626	29	13.33	73.06	16.16	14.76	1.88
5029	70610	86	15.57	2.89	16.38	15.57	2.64	LBB76-1228	94626	30	13.30	57.18	16.11	14.55	1.69
5029	70610	87	15.10	67.37	16.38	15.85	2.64	LBB76-1228	94626	31	12.77	59.27	16.14	14.23	1.79
5029	70610	88	15.96	70.20	16.38	16.41	2.64	LBB76-1228	94626	32	13.20	76.17	16.14	14.71	1.79
5029	70610	89	17.51	83.77	16.22	17.40	2.10	LBB76-1228	94626	33	12.67	80.96	16.14	14.41	1.79
5029	70610	90	13.68	63.00	16.41	14.88	2.77	LBB76-1228	94626	34	10.27	36.27	16.14	11.86	1.79
5029	70610	91	15.87	70.13	16.41	16.35	2.77	LBB76-1228	94626	35	13.27	64.57	16.14	14.64	1.79
5029	70610	92	14.66	66.79	16.41	15.56	2.77	LBB76-1228	94626	36	14.23	45.77	16.15	15.00	1.83
5029	70610	93	12.59	70.33	16.49	14.27	3.04	LBB76-1228	94626	37	14.50	5.14	16.20	14.52	2.01
5029	70610	94	15.75	44.63	16.52	16.11	3.15	LBB76-1228	94626	38	14.33	58.69	16.13	15.26	1.77
5029	70610	95	13.65	62.53	16.70	14.86	3.77	LBB76-1228	94626	39	12.35	66.89	16.13	14.08	1.75
5029	70610	96	15.81	34.81	16.37	16.06	2.60	LBB76-1228	94626	40	15.27	58.78	16.13	15.89	1.75
5029	70610	97	11.41	70.84	16.21	13.54	2.06	LBB76-1228	94626	41	9.94	41.02	16.13	11.83	1.75
5029	70610	98	15.47	30.39	16.18	15.73	1.96	LBB76-1228	94626	42	15.57	21.93	16.10	15.71	1.67
5029	70610	99	16.51	50.18	16.36	16.70	2.58	LBB76-1228	94626	43	12.72	28.13	16.15	13.39	1.85
5029	70610	100	17.43	49.60	16.36	17.37	2.58	LBB76-1228	94626	44	14.57	79.93	16.15	15.58	1.85
5029	70610	101	13.98	77.20	16.50	15.20	3.06	LBB76-1228	94626	45	14.46	27.94	16.16	14.83	1.86
5029	70610	102	15.50	81.44	16.50	16.15	3.06	LBB76-1228	94626	46	11.99	81.14	16.16	13.99	1.86
5029	70610	103	14.47	12.45	16.50	14.56	3.06	LBB76-1228	94626	47	12.99	33.01	16.16	13.76	1.86
5029	70610	104	14.83	48.14	16.50	15.47	3.06	LBB76-1228	94626	48	14.89	35.45	16.14	15.32	1.80
5029	70610	105	15.75	29.44	16.50	15.95	3.06	LBB76-1228	94626	49	13.77	86.08	16.14	15.10	1.80
5029	70610	106	13.92	58.42	16.50	14.98	3.06	LBB76-1228	94626	50	11.33	74.06	16.14	13.53	1.80
5029	70610	107	13.56	68.22	16.50	14.87	3.06	LBB76-1228	94626	51	15.52	14.95	16.12	15.59	1.74
5029	70610	108	14.99	44.27	16.50	15.53	3.06	LBB76-1228	94626	52	15.05	77.27	16.12	15.86	1.74
5029	70610	109	14.48	70.48	16.52	15.47	3.14	LBB76-1228	94626	53	14.35	52.49	16.11	15.19	1.69
5029	70610	110	14.71	45.55	16.39	15.35	2.69	LBB76-1228	94626	54	11.15	71.40	16.11	13.38	1.69
5029	70610	111	13.67	81.83	16.38	15.03	2.64	LBB76-1228	94626	55	12.48	56.12	16.11	13.98	1.69
5029	70610	112	13.32	77.02	16.37	14.79	2.60	LBB76-1228	94626	56	15.76	49.96	16.10	16.16	1.67
5029	70610	113	16.26	35.90	16.27	16.43	2.25	LBB76-1228	94626	57	13.66	70.16	16.10	14.95	1.67
5029	70610	114	14.38	32.07	16.34	14.85	2.52	LBB76-1228	94626	58	14.21	73.83	16.10	15.32	1.67
5029	70610	115	14.83	35.39	16.52	15.28	3.15	LBB76-1228	94626	59	9.15	87.78	16.12	12.65	1.74
5029	70610	116	15.02	42.63	16.43	15.53	2.83	LBB76-1228	94626	60	15.01	45.66	16.12	15.57	1.74
5029	70610	117	13.47	84.10	16.43	14.91	2.83	LBB76-1228	94626	61	15.10	20.80	16.12	15.27	1.74
5029	70610	118	15.60	17.47	16.43	15.69	2.83	LBB76-1228	94626	62	14.25	77.35	16.12	15.37	1.74
5029	70610	119	14.83	15.08	16.43	14.94	2.83	LBB76-1228	94626	63	13.54	34.01	16.11	14.22	1.68
5029	70610	120	14.04	43.62	16.49	14.82	3.03	LBB76-1228	94626	64	14.27	67.19	16.11	15.31	1.68
5029	70610	121	16.52	57.47	16.70	16.74	3.79	LBB76-1228	94626	65	13.18	82.42	16.09	14.73	1.63
5029	70610	122	14.82	64.78	16.70	15.65	3.79	LBB76-1228	94626	66	15.98	36.57	16.22	16.21	2.08
5029	70610	123	13.91	43.35	16.59	14.72	3.39	LBB76-1228	94626	67	14.68	48.58	16.22	15.37	2.08
5029	70610	124	14.56	86.94	16.55	15.59	3.25	LBB76-1228	94626	68	15.04	53.60	16.22	15.69	2.08
5029	70610	125	17.01	62.00	16.25	17.08	2.20	LBB76-1228	94626	69	15.75	34.65	16.05	16.01	1.50
5029	70610	126	14.06	53.65	16.58	15.01	3.37	LBB76-1228	94626	70	13.25	56.24	16.14	14.50	1.80
5029	70610	127	14.73	50.69	16.58	15.43	3.37	LBB76-1228	94626	71	15.09	75.37	16.14	15.88	1.80
5029	70610	128	13.98	78.32	16.24	15.20	2.16	LBB76-1228	94626	72	16.56	69.33	16.22	16.79	2.07
5029	70610	129	14.35	33.50	16.25	14.86	2.18	LBB76-1228	94626	73	14.95	80.79	16.22	15.81	2.07
5029	70610	130	14.82	41.77	16.31	15.37	2.42	LBB76-1228	94626	74	15.01	45.45	16.14	15.57	1.79
5029	70610	131	18.02	39.19	16.29	17.86	2.34	LBB76-1228	94626	75	14.91	65.56	16.12	15.71	1.72
5029	70610	132	14.31	86.21	16.29	15.43	2.34	LBB76-1228	94626	76	12.79	58.09	16.13	14.23	1.78
5029	70610	133	14.89	87.61	16.53	15.79	3.19	LBB76-1228	94626	77	15.14	40.71	16.11	15.60	1.70
5029	70610	134	14.39	77.82	16.53	15.46	3.19	LBB76-1228	94626	78	13.34	75.64	16.11	14.79	1.70
5029	70610	135	15.44	73.79	16.13	16.09	1.76	LBB76-1228	94626	79	15.48	47.01	16.17	15.93	1.91
5029	70610	136	18.47	54.66	16.13	18.10	1.76	LBB76-1228	94626	80	13.82	66.90	16.13	15.02	1.78
5029	70610	137	16.01	53.84	16.30	16.37	2.35	LBB76-1228	94626	81	15.49	28.36	16.13	15.72	1.78
5029	70610	138	16.56	57.20	16.48	16.76	3.00	LBB76-1228	94626	82	15.66	18.91	16.13	15.76	1.77
5029	70610	139	10.78	72.96	16.48	13.17	3.00	LBB76-1228	94626	83	12.70	58.71	16.13	14.18	1.77
5029	70610	140	17.34	21.17	16.48	17.33	3.00	LBB76-1228	94626	84	14.13	33.47	16.16	14.68	1.89
5029	70610	141	14.71	72.30	16.50	15.63	3.08	LBB76-1228	94626	85	9.63	39.40	16.16	11.56	1.89
5029	70610	142	13.53	70.99	16.37	14.87	2.60	LBB76-1228	94626	86	14.16	37.91	16.07	14.80	1.54

Table C3 Apatite fission track lengths for all samples analysed in this thesis

UBC	A2Z	Track	Angle				Dpar (μm)	UBC	A2Z	Track	Angle				Dpar (μm)
			Length (μm)	to c- axis	Lo calc (μm)	Lc calc (μm)					Length (μm)	to c- axis	Lo calc (μm)	Lc calc (μm)	
5029	70610	143	16.57	52.22	16.16	16.75	1.88	LBB76-1228	94626	87	13.01	77.06	16.09	14.59	1.62
5029	70610	144	15.52	37.89	16.24	15.86	2.14	LBB76-1228	94626	88	12.96	63.33	16.09	14.42	1.62
5029	70610	145	15.03	70.68	16.24	15.82	2.14	LBB76-1228	94626	89	14.19	88.33	16.10	15.36	1.65
5029	70610	146	14.10	82.19	16.24	15.29	2.14	LBB76-1228	94626	90	12.81	41.48	16.15	13.87	1.85
5029	70610	147	15.47	65.23	16.31	16.07	2.41	LBB76-1228	94626	91	14.53	55.43	16.15	15.36	1.85
5029	70610	148	15.12	35.94	16.28	15.52	2.28	LBB76-1228	94626	92	15.26	31.48	16.14	15.57	1.79
5029	70610	149	14.94	17.52	16.50	15.08	3.06	LBB76-1228	94626	93	15.03	17.43	16.14	15.16	1.79
5029	70610	150	15.93	80.35	16.50	16.42	3.06	LBB76-1228	94626	94	15.20	58.78	16.14	15.85	1.79
5029	70610	151	12.80	87.25	16.50	14.51	3.06	LBB76-1228	94626	95	15.08	43.69	16.11	15.59	1.68
5029	70610	152	14.85	13.27	16.18	14.94	1.95	LBB76-1228	94626	96	11.91	64.88	16.11	13.77	1.68
5029	70610	153	13.43	72.40	16.18	14.82	1.95	LBB76-1228	94626	97	12.71	75.24	16.11	14.39	1.68
5029	70610	154	15.98	38.96	16.40	16.23	2.71	LBB76-1228	94626	98	15.10	23.39	16.18	15.31	1.94
5029	70610	155	13.57	16.55	16.18	13.79	1.95	LBB76-1228	94626	99	16.65	65.47	16.18	16.84	1.94
5029	70610	156	14.76	54.30	16.18	15.50	1.95	LBB76-1228	94626	100	15.88	32.34	16.19	16.09	1.98
5029	70610	157	15.26	71.39	16.18	15.97	1.95	LBB76-1228	94626	101	14.11	75.61	16.19	15.27	1.98
5029	70610	158	13.81	30.75	16.32	14.36	2.44	LBB76-1228	94626	102	15.57	79.16	16.22	16.19	2.07
5029	70610	159	13.18	81.46	16.32	14.72	2.44	LBB76-1228	94626	103	15.36	57.87	16.22	15.95	2.07
5029	70610	160	16.68	56.81	16.32	16.84	2.44	LBB76-1228	94626	104	14.06	75.82	16.11	15.24	1.71
5029	70610	161	16.50	8.70	16.44	16.51	2.87	LBB76-1228	94626	105	12.97	63.67	16.11	14.43	1.71
5029	70610	162	11.12	62.67	16.31	13.23	2.39	LBB76-1228	94626	106	15.06	78.95	16.17	15.88	1.91
5029	70610	163	14.78	81.73	16.35	15.71	2.56	LBB76-1228	94626	107	12.63	45.55	16.17	13.85	1.91
5029	70610	164	14.61	22.71	16.35	14.86	2.56	LBB76-1228	94626	108	14.08	45.20	16.17	14.88	1.91
5029	70610	165	12.43	53.61	16.36	13.90	2.59	LBB76-1228	94626	109	12.77	48.72	16.14	14.02	1.81
5029	70610	166	14.29	39.70	16.36	14.93	2.59	LBB76-1228	94626	110	15.45	14.89	16.14	15.53	1.81
5029	70610	167	15.63	23.20	16.36	15.78	2.59	LBB76-1228	94626	111	13.32	74.65	16.15	14.77	1.83
5029	70610	168	17.52	50.11	16.36	17.44	2.59	LBB76-1228	94626	112	13.51	50.11	16.14	14.57	1.80
5029	70610	169	14.24	14.67	16.36	14.38	2.59	LBB76-1228	94626	113	15.78	35.11	16.13	16.04	1.77
5029	70610	170	16.14	61.25	16.40	16.49	2.71	LBB76-1228	94626	114	16.11	14.13	16.13	16.15	1.77
5029	70610	171	13.97	38.15	16.40	14.66	2.71	LBB76-1228	94626	115	15.30	60.64	16.11	15.93	1.71
5029	70610	172	15.73	84.31	16.50	16.30	3.08	LBB76-1228	94626	116	15.42	82.54	16.11	16.11	1.71
5029	70610	173	15.48	23.14	16.50	15.65	3.08	LBB76-1228	94626	117	13.77	44.52	16.11	14.64	1.71
5029	70610	174	15.17	37.95	16.50	15.58	3.08	LBB76-1228	94626	118	13.53	74.77	16.11	14.90	1.71
5029	70610	175	13.83	62.25	16.50	14.97	3.08	LBB76-1228	94626	119	15.15	37.71	16.11	15.57	1.71
5029	70610	176	14.98	89.92	16.28	15.85	2.28	LBB76-1228	94626	120	15.30	42.67	16.11	15.75	1.71
5029	70610	177	14.78	51.90	16.35	15.48	2.53	LBB76-1228	94626	121	14.13	82.30	16.11	15.31	1.71
5029	70610	178	14.64	73.88	16.35	15.59	2.53	LBB76-1228	94626	122	15.83	63.98	16.11	16.30	1.71
5029	70610	179	16.53	88.71	16.35	16.79	2.53	LBB76-1228	94626	123	14.41	23.86	16.14	14.71	1.79
5029	70610	180	15.13	57.92	16.42	15.79	2.79	LBB76-1228	94626	124	13.85	46.46	16.14	14.74	1.79
5029	70610	181	13.90	64.73	16.47	15.05	2.98	LBB76-1228	94626	125	16.37	48.67	16.14	16.59	1.79
5029	70610	182	15.96	43.30	16.47	16.25	2.98	LBB76-1228	94626	126	15.27	66.52	16.13	15.95	1.78
5029	70610	183	15.38	36.47	16.56	15.73	3.27	LBB76-1228	94626	127	14.63	59.30	16.13	15.47	1.78
5029	70610	184	12.19	55.20	16.56	13.77	3.27	LBB76-1228	94626	128	13.88	53.17	16.13	14.88	1.75
5029	70610	185	14.87	57.10	16.56	15.61	3.27	LBB76-1228	94626	129	14.48	41.32	16.13	15.11	1.75
5029	70610	186	14.20	79.75	16.56	15.35	3.27	LBB76-1228	94626	130	13.14	84.31	16.13	14.71	1.75
5029	70610	187	15.83	80.95	16.56	16.36	3.27	LBB76-1228	94626	131	13.40	69.46	16.19	14.78	1.98
5029	70610	188	16.27	51.72	16.40	16.54	2.73	LBB76-1228	94626	132	12.94	72.52	16.19	14.52	1.98
5029	70610	189	13.49	88.45	16.35	14.93	2.56	LBB76-1228	94626	133	15.30	28.01	16.19	15.55	1.98
5029	70610	190	13.67	59.73	16.35	14.83	2.56	LBB76-1228	94626	134	11.18	40.21	16.15	12.66	1.85
5029	70610	191	16.81	30.36	16.11	16.87	1.68	LBB76-1228	94626	135	14.13	39.24	16.15	14.80	1.85
5029	70610	192	14.50	62.50	16.25	15.42	2.19	LBB76-1228	94626	136	15.84	20.84	16.15	15.95	1.85
6000A	86102	1	8.09	74.50	16.28	12.23	2.29	LBB76-1228	94626	137	11.20	61.63	16.15	13.26	1.83
6000A	86102	2	12.32	54.71	16.28	13.85	2.29	LBB76-1228	94626	138	12.27	69.62	16.15	14.06	1.83
6000A	86102	3	14.48	70.21	16.26	15.47	2.24	LBB76-1228	94626	139	15.22	47.98	16.15	15.75	1.83
6000A	86102	4	12.39	42.66	16.26	13.60	2.24	LBB76-1228	94626	140	12.96	77.53	16.13	14.57	1.77
6000A	86102	5	15.07	21.19	16.21	15.25	2.05	LBB76-1228	94626	141	14.88	35.81	16.13	15.32	1.77
6000A	86102	6	16.84	26.88	16.16	16.88	1.87	LBB76-1228	94626	142	15.18	24.46	16.11	15.40	1.69
6000A	86102	7	16.32	59.10	16.22	16.61	2.09	LBB76-1228	94626	143	14.66	52.00	16.11	15.40	1.69
6000A	86102	8	15.72	46.12	16.24	16.10	2.15	LBB76-1228	94626	144	13.82	50.69	16.11	14.79	1.69
6000A	86102	9	16.06	40.98	16.24	16.31	2.15	LBB76-1228	94626	145	14.92	49.29	16.09	15.55	1.64
6000A	86102	10	11.21	29.54	16.24	12.26	2.15	LBB76-1228	94626	146	15.04	67.68	16.09	15.81	1.64
6000A	86102	11	15.51	41.52	16.17	15.89	1.92	LBB76-1228	94626	147	14.60	23.20	16.09	14.86	1.64

Table C3 Apatite fission track lengths for all samples analysed in this thesis

UBC	A2Z	Track	Angle				Dpar		UBC	A2Z	Track	Angle				Dpar
			Length (μm)	to c- axis	Lo calc (μm)	Lc calc (μm)						Length (μm)	to c- axis	Lo calc (μm)	Lc calc (μm)	
6000A	86102	12	15.92	81.97	16.17	16.41	1.92		LBB76-1228	94626	148	14.48	50.27	16.09	15.25	1.64
6000A	86102	13	15.01	45.33	16.17	15.56	1.92		LBB76-1228	94626	149	15.45	48.64	16.13	15.92	1.78
6000A	86102	14	14.97	35.61	16.17	15.39	1.92		LBB76-1228	94626	150	12.03	66.85	16.12	13.88	1.72
6000A	86102	15	13.91	31.95	16.18	14.47	1.94		LBB76-1228	94626	151	15.02	69.79	16.15	15.81	1.83
6000A	86102	16	14.57	85.71	16.25	15.59	2.18		LBB76-1228	94626	152	14.41	46.36	16.15	15.14	1.83
6000A	86102	17	15.45	71.51	16.25	16.09	2.18		LBB76-1228	94626	153	14.58	58.91	16.14	15.43	1.79
6000A	86102	18	14.93	75.40	16.25	15.78	2.18		LBB76-1228	94626	154	14.76	85.85	16.14	15.71	1.79
6000A	86102	19	9.05	73.07	16.21	12.40	2.06		LBB76-1228	94626	155	15.53	57.98	16.14	16.06	1.79
6000A	86102	20	14.77	40.39	16.21	15.31	2.06		LBB76-1228	94626	156	13.95	70.52	16.15	15.13	1.82
6000A	86102	21	15.58	27.18	16.21	15.78	2.06		LBB76-1228	94626	157	11.58	82.21	16.17	13.74	1.91
6000A	86102	22	8.92	73.17	16.27	12.38	2.25		LBB76-1228	94626	158	13.69	48.84	16.17	14.67	1.91
6000A	86102	23	15.55	37.63	16.27	15.88	2.25		LBB76-1228	94626	159	14.91	24.84	16.17	15.16	1.91
6000A	86102	24	14.92	81.88	16.22	15.80	2.07		LBB76-1228	94626	160	14.24	45.81	16.15	15.01	1.83
6000A	86102	25	13.72	72.85	16.22	15.01	2.07		LBB76-1228	94626	161	14.60	83.39	16.15	15.60	1.83
6000A	86102	26	14.35	85.12	16.22	15.45	2.07		LBB76-1228	94626	162	13.78	78.31	16.15	15.08	1.83
6000A	86102	27	14.35	79.72	16.29	15.44	2.32		LBB76-1228	94626	163	11.78	53.40	16.15	13.46	1.83
6000A	86102	28	14.29	70.95	16.30	15.35	2.35		LBB76-1228	94626	164	14.10	57.98	16.15	15.10	1.83
6000A	86102	29	12.01	41.49	16.30	13.29	2.35		LBB76-1228	94626	165	14.71	23.12	16.18	14.96	1.93
6000A	86102	30	14.34	77.54	16.30	15.42	2.35		LBB76-1228	94626	166	14.83	61.62	16.18	15.62	1.93
6000A	86102	31	9.89	31.36	16.30	11.37	2.35		LBB76-1228	94626	167	14.97	76.17	16.11	15.81	1.71
6000A	86102	32	13.88	40.90	16.30	14.65	2.35		LBB76-1228	94626	168	15.24	20.69	16.11	15.40	1.71
6000A	86102	33	15.76	76.26	16.30	16.30	2.35		LBB76-1228	94626	169	12.38	55.45	16.11	13.90	1.71
6000A	86102	34	14.30	13.75	16.30	14.42	2.35		LBB76-1228	94626	170	13.97	55.58	16.11	14.98	1.71
6000A	86102	35	10.41	58.56	16.18	12.69	1.93		LBB76-1228	94626	171	14.05	83.16	16.11	15.27	1.71
6000A	86102	36	9.29	49.29	16.25	11.71	2.19		LBB76-1228	94626	172	16.84	6.98	16.11	16.84	1.71
6000A	86102	37	14.55	55.35	16.24	15.37	2.17		LBB76-1228	94626	173	15.57	58.41	16.11	16.09	1.71
6000A	86102	38	14.81	71.11	16.24	15.68	2.17		LBB76-1228	94626	174	13.89	73.91	16.16	15.12	1.89
6000A	86102	39	12.89	66.34	16.28	14.42	2.31		LBB76-1228	94626	175	14.81	69.73	16.16	15.68	1.89
6000A	86102	40	14.20	60.93	16.31	15.20	2.39		LBB76-1228	94626	176	12.49	76.88	16.16	14.27	1.89
6000A	86102	41	12.42	73.46	16.31	14.20	2.39		LBB76-1228	94626	177	11.73	67.17	16.16	13.69	1.89
6000A	86102	42	14.72	40.65	16.28	15.28	2.28		LBB76-1228	94626	178	14.95	84.58	16.12	15.82	1.74
6000A	86102	43	9.96	55.67	16.22	12.33	2.07		LBB76-1228	94626	179	15.35	43.83	16.12	15.80	1.74
6000A	86102	44	14.77	57.43	16.22	15.54	2.07		LBB76-1228	94626	180	12.62	44.94	16.12	13.82	1.74
6000A	86102	45	15.29	63.07	16.22	15.94	2.07		LBB76-1228	94626	181	14.12	58.96	16.12	15.12	1.74
6000A	86102	46	15.76	75.58	16.22	16.30	2.07		LBB76-1228	94626	182	14.16	59.55	16.12	15.16	1.74
6000A	86102	47	14.98	65.95	16.25	15.76	2.18		LBB76-1228	94626	183	11.67	52.41	16.12	13.36	1.74
6000A	86102	48	14.94	58.78	16.26	15.67	2.23		LBB76-1228	94626	184	11.80	56.35	16.17	13.54	1.91
6000A	86102	49	10.02	56.54	16.26	12.39	2.23		LBB76-1228	94626	185	13.70	83.21	16.17	15.05	1.91
6000A	86102	50	9.62	73.35	16.35	12.54	2.53		LBB76-1228	94626	186	14.91	52.47	16.17	15.58	1.91
6000A	86102	51	14.16	56.95	16.30	15.12	2.36		LBB76-1228	94626	187	16.45	24.07	16.15	16.52	1.83
6000A	86102	52	14.47	50.93	16.30	15.25	2.36		LBB76-1228	94626	188	14.76	66.97	16.15	15.62	1.83
6000A	86102	53	12.03	89.72	16.30	14.04	2.36		LBB76-1228	94626	189	14.63	13.70	16.15	14.73	1.83
6000A	86102	54	14.58	19.03	16.27	14.77	2.27		LBB76-1228	94626	190	14.09	84.70	16.15	15.29	1.83
6000A	86102	55	13.83	81.74	16.27	15.13	2.27		LBB76-1228	94626	191	14.16	88.71	16.15	15.34	1.83
6000A	86102	56	12.25	41.26	16.27	13.46	2.27		LBB76-1228	94626	192	14.22	83.67	16.19	15.37	1.99
6000A	86102	57	9.84	55.30	16.18	12.24	1.93		LBB76-1228	94626	193	15.33	72.50	16.19	16.02	1.99
6000A	86102	58	15.16	47.61	16.20	15.70	2.00		LBB76-1228	94626	194	12.34	86.28	16.19	14.22	1.99
6000A	86102	59	10.19	37.12	16.20	11.84	2.00		LBB76-1228	94626	195	14.74	74.08	16.19	15.66	1.99
6000A	86102	60	11.46	46.77	16.20	13.07	2.00		LBB76-1228	94626	196	14.87	27.79	16.15	15.18	1.82
6000A	86102	61	13.37	26.67	16.24	13.88	2.16		LBB76-1228	94626	197	14.58	62.74	16.15	15.47	1.82
6000A	86102	62	9.55	60.97	16.28	12.20	2.28		LBB76-1228	94626	198	14.19	81.51	16.15	15.35	1.82
6000A	86102	63	14.79	41.35	16.24	15.34	2.16		LBB76-1228	94626	199	14.99	8.20	16.15	15.02	1.82
6000A	86102	64	16.31	89.95	16.26	16.66	2.24		LBB76-1228	94626	200	14.16	47.58	16.15	14.98	1.82
6000A	86102	65	11.04	62.43	16.27	13.17	2.27		LBB76-343	94622	1	16.29	80.34	16.26	16.64	2.21
6000A	86102	66	15.28	61.68	16.27	15.92	2.27		LBB76-343	94622	2	9.85	55.87	16.26	12.26	2.21
6000A	86102	67	14.28	60.69	16.27	15.25	2.27		LBB76-343	94622	3	14.23	61.25	16.27	15.22	2.27
6000A	86102	68	15.94	77.52	16.28	16.42	2.29		LBB76-343	94622	4	15.54	38.88	16.27	15.89	2.27
6000A	86102	69	11.75	23.97	16.28	12.45	2.29		LBB76-343	94622	5	12.74	59.63	16.27	14.22	2.27
6000A	86102	70	12.54	72.00	16.22	14.26	2.10		LBB76-343	94622	6	14.21	66.70	16.28	15.27	2.31
6000A	86102	71	9.04	61.15	16.22	12.08	2.10		LBB76-343	94622	7	8.51	64.59	16.28	12.09	2.31
6000A	86102	72	14.43	41.42	16.22	15.07	2.10		LBB76-343	94622	8	10.76	56.97	16.28	12.88	2.28

Table C3 Apatite fission track lengths for all samples analysed in this thesis

UBC	A2Z	Track	Angle				Dpar		UBC	A2Z	Track	Angle				Dpar
			Length (μm)	to c- axis	Lo calc (μm)	Lc calc (μm)						Length (μm)	to c- axis	Lo calc (μm)	Lc calc (μm)	
6000A	86102	73	13.49	49.32	16.22	14.54	2.10		LBB76-343	94622	9	13.45	75.61	16.28	14.86	2.28
6000A	86102	74	9.00	72.68	16.22	12.39	2.10		LBB76-343	94622	10	8.90	32.45	16.28	10.75	2.28
6000A	86102	75	16.20	25.58	16.30	16.31	2.37		LBB76-343	94622	11	13.37	47.09	16.23	14.41	2.13
6000A	86102	76	11.49	36.62	16.30	12.75	2.37		LBB76-343	94622	12	15.20	59.69	16.26	15.85	2.21
6000A	86102	77	15.60	35.33	16.29	15.89	2.32		LBB76-343	94622	13	16.39	32.86	16.26	16.52	2.21
6000A	86102	78	14.81	85.36	16.26	15.74	2.23		LBB76-343	94622	14	10.46	56.68	16.26	12.67	2.21
6000A	86102	79	11.06	70.81	16.18	13.32	1.96		LBB76-343	94622	15	18.07	55.69	16.20	17.81	2.02
6000A	86102	80	13.39	74.63	16.27	14.81	2.25		LBB76-343	94622	16	13.51	71.09	16.20	14.86	2.02
6000A	86102	81	10.14	36.54	16.27	11.79	2.25		LBB76-343	94622	17	12.47	28.35	16.30	13.20	2.37
6000A	86102	82	10.58	54.00	16.25	12.68	2.20		LBB76-343	94622	18	16.89	25.60	16.30	16.92	2.37
6000A	86102	83	15.42	51.78	16.25	15.93	2.20		LBB76-343	94622	19	11.49	84.87	16.30	13.70	2.37
6000A	86102	84	9.98	52.09	16.25	12.24	2.20		LBB76-343	94622	20	9.97	66.68	16.28	12.57	2.28
6000A	86102	85	14.09	66.53	16.27	15.19	2.26		LBB76-343	94622	21	14.63	59.06	16.28	15.47	2.28
6000A	86102	86	14.85	55.00	16.28	15.57	2.28		LBB76-343	94622	22	15.86	60.02	16.28	16.30	2.28
6000A	86102	87	13.85	52.47	16.28	14.85	2.28		LBB76-343	94622	23	10.46	65.12	16.28	12.85	2.28
6000A	86102	88	14.78	52.00	16.24	15.49	2.16		LBB76-343	94622	24	15.63	82.11	16.28	16.24	2.28
6000A	86102	89	15.76	24.21	16.24	15.91	2.16		LBB76-343	94622	25	15.71	45.30	16.28	16.08	2.28
6000A	86102	90	13.87	74.29	16.24	15.11	2.16		LBB76-343	94622	26	16.14	86.62	16.31	16.55	2.39
6000A	86102	91	13.73	85.10	16.31	15.07	2.40		LBB76-343	94622	27	11.67	67.30	16.31	13.65	2.39
6000A	86102	92	14.32	54.14	16.31	15.19	2.40		LBB76-343	94622	28	15.54	57.00	16.31	16.06	2.39
6000A	86102	93	15.17	63.24	16.31	15.86	2.40		LBB76-343	94622	29	11.35	35.03	16.31	12.59	2.39
6000A	86102	94	11.59	38.44	16.31	12.89	2.40		LBB76-343	94622	30	10.44	41.65	16.29	12.20	2.33
6000A	86102	95	9.56	45.09	16.17	11.74	1.90		LBB76-343	94622	31	10.22	52.92	16.29	12.42	2.33
6000A	86102	96	14.62	85.48	16.17	15.62	1.90		LBB76-343	94622	32	12.20	28.10	16.29	12.97	2.33
6000A	86102	97	15.22	58.52	16.17	15.86	1.90		LBB76-343	94622	33	14.10	57.88	16.29	15.10	2.33
6000A	86102	98	15.66	64.26	16.25	16.19	2.19		LBB76-343	94622	34	15.25	48.19	16.29	15.77	2.33
6000A	86102	99	14.32	68.46	16.25	15.35	2.19		LBB76-343	94622	35	11.00	17.05	16.29	11.52	2.33
6000A	86102	100	14.10	75.80	16.19	15.27	1.99		LBB76-343	94622	36	13.78	63.38	16.29	14.95	2.33
6000A	86102	101	14.94	42.12	16.19	15.47	1.99		LBB76-343	94622	37	12.97	57.81	16.29	14.34	2.34
6000A	86102	102	15.32	29.21	16.19	15.59	1.99		LBB76-343	94622	38	16.11	31.74	16.29	16.28	2.34
6000A	86102	103	15.42	50.30	16.19	15.92	1.99		LBB76-343	94622	39	9.73	76.38	16.29	12.64	2.34
6000A	86102	104	14.81	59.03	16.30	15.59	2.35		LBB76-343	94622	40	10.57	40.10	16.25	12.23	2.20
6000A	86102	105	15.74	8.17	16.30	15.76	2.36		LBB76-343	94622	41	10.56	55.96	16.25	12.72	2.20
6000A	86102	106	14.36	83.91	16.30	15.46	2.36		LBB76-343	94622	42	11.84	77.34	16.25	13.87	2.20
6000A	86102	107	14.68	34.77	16.12	15.14	1.74		LBB76-343	94622	43	15.54	59.42	16.25	16.08	2.20
6000A	86102	108	15.12	67.20	16.12	15.86	1.74		LBB76-343	94622	44	13.27	47.24	16.30	14.34	2.37
6000A	86102	109	15.11	47.01	16.31	15.66	2.42		LBB76-343	94622	45	14.35	39.50	16.30	14.97	2.37
6000A	86102	110	14.89	71.16	16.31	15.73	2.42		LBB76-343	94622	46	14.95	75.50	16.30	15.79	2.37
6000A	86102	111	9.34	67.10	16.20	12.32	2.01		LBB76-343	94622	47	16.83	73.15	16.30	16.97	2.35
6000A	86102	112	15.00	61.55	16.20	15.74	2.01		LBB76-343	94622	48	15.32	14.58	16.30	15.40	2.35
6000A	86102	113	14.59	51.82	16.15	15.35	1.82		LBB76-343	94622	49	14.24	75.36	16.35	15.35	2.56
6000A	86102	114	15.02	42.71	16.15	15.54	1.82		LBB76-343	94622	50	12.29	77.41	16.35	14.15	2.56
6000A	86102	115	10.43	36.09	16.18	11.97	1.94		LBB76-343	94622	51	11.40	68.53	16.35	13.50	2.56
6000A	86102	116	16.22	84.15	16.26	16.60	2.22		LBB76-343	94622	52	16.27	43.62	16.35	16.49	2.56
6000A	86102	117	15.50	65.83	16.26	16.09	2.22		LBB76-343	94622	53	15.68	49.67	16.28	16.10	2.31
6000A	86102	118	10.74	55.69	16.26	12.83	2.22		LBB76-343	94622	54	14.54	86.47	16.29	15.57	2.34
6000A	86102	119	12.92	67.88	16.23	14.45	2.12		LBB76-343	94622	55	13.92	53.12	16.29	14.90	2.34
6000A	86102	120	16.52	12.22	16.23	16.54	2.12		LBB76-343	94622	56	8.06	55.36	16.29	11.72	2.34
6000A	86102	121	14.64	60.71	16.23	15.49	2.12		LBB76-343	94622	57	4.79	79.10	16.29	11.57	2.34
6000A	86102	122	14.93	83.19	16.23	15.81	2.12		LBB76-343	94622	58	11.40	78.36	16.29	13.61	2.34
6000A	86102	123	12.27	85.19	16.20	14.18	2.00		LBB76-343	94622	59	10.85	66.09	16.29	13.12	2.34
6000A	86102	124	14.54	77.94	16.20	15.55	2.00		LBB76-343	94622	60	10.96	66.94	16.29	13.20	2.34
6000A	86102	125	9.14	52.11	16.24	11.77	2.16		LBB76-343	94622	61	13.92	30.20	16.37	14.43	2.60
6000A	86102	126	13.65	56.62	16.22	14.78	2.10		LBB76-343	94622	62	15.40	64.27	16.26	16.02	2.21
6000A	86102	127	15.31	50.10	16.22	15.84	2.10		LBB76-343	94622	63	8.40	88.96	16.26	12.49	2.21
6000A	86102	128	15.18	66.87	16.22	15.89	2.10		LBB76-343	94622	64	16.45	68.22	16.26	16.72	2.23
6000A	86102	129	14.42	67.93	16.32	15.41	2.43		LBB76-343	94622	65	14.57	48.59	16.26	15.29	2.23
6000A	86102	130	14.59	36.21	16.23	15.10	2.11		LBB76-343	94622	66	13.83	80.42	16.22	15.12	2.08
6000B	107006	1	11.61	45.90	16.34	13.14	2.52		LBB76-343	94622	67	13.62	80.03	16.22	14.99	2.08
6000B	107006	2	15.07	63.30	16.28	15.80	2.28		LBB76-343	94622	68	8.63	63.99	16.32	12.09	2.43
6000B	107006	3	10.69	38.68	16.28	12.26	2.28		LBB76-343	94622	69	15.57	33.73	16.31	15.85	2.39

Table C3 Apatite fission track lengths for all samples analysed in this thesis

UBC	A2Z	Track	Angle				Dpar	UBC	A2Z	Track	Angle				Dpar
			Length (μm)	to c- axis	Lo calc (μm)	Lc calc (μm)					Length (μm)	to c- axis	Lo calc (μm)	Lc calc (μm)	
6000B	107006	4	16.58	23.71	16.43	16.64	2.82	LBB76-343	94622	70	13.84	82.22	16.25	15.13	2.18
6000B	107006	5	10.99	62.38	16.43	13.14	2.82	LBB76-343	94622	71	15.22	85.07	16.19	15.99	1.98
6000B	107006	6	11.06	29.18	16.34	12.13	2.51	LBB76-343	94622	72	14.62	59.89	16.19	15.47	1.98
6000B	107006	7	12.76	68.46	16.32	14.36	2.43	LBB76-343	94622	73	15.49	43.45	16.19	15.90	1.98
6000B	107006	8	15.76	60.90	16.32	16.24	2.43	LBB76-343	94622	74	14.64	75.62	16.30	15.60	2.36
6000B	107006	9	16.15	52.83	16.26	16.46	2.24	LBB76-343	94622	75	16.12	79.63	16.30	16.54	2.36
6000B	107006	10	16.85	37.30	16.19	16.88	1.98	LBB76-343	94622	76	16.84	49.00	16.26	16.94	2.24
6000B	107006	11	15.21	62.53	16.27	15.88	2.27	LBB76-343	94622	77	12.82	20.18	16.26	13.22	2.24
6000B	107006	12	15.27	63.92	16.37	15.93	2.62	LBB76-343	94622	78	10.57	75.05	16.26	13.06	2.24
6000B	107006	13	13.34	58.06	16.30	14.59	2.36	LBB76-343	94622	79	11.69	71.60	16.26	13.72	2.24
6000B	107006	14	15.37	15.87	16.30	15.46	2.36	LBB76-343	94622	80	14.78	69.67	16.25	15.66	2.19
6000B	107006	15	15.22	18.31	16.33	15.35	2.47	LBB76-343	94622	81	14.77	61.82	16.25	15.59	2.19
6000B	107006	16	16.57	37.30	16.33	16.69	2.47	LBB76-343	94622	82	14.71	84.42	16.25	15.67	2.19
6000B	107006	17	9.03	41.44	16.33	11.25	2.47	LBB76-343	94622	83	14.36	70.61	16.33	15.40	2.48
6000B	107006	18	10.48	53.81	16.37	12.61	2.63	LBB76-343	94622	84	15.40	68.56	16.25	16.05	2.18
6000B	107006	19	11.73	30.32	16.37	12.69	2.63	LBB76-343	94622	85	10.74	66.94	16.25	13.06	2.18
6000B	107006	20	14.96	79.68	16.30	15.82	2.38	LBB76-343	94622	86	11.64	66.74	16.25	13.63	2.18
6000B	107006	21	14.89	62.89	16.33	15.68	2.47	LBB76-343	94622	87	13.01	70.05	16.21	14.54	2.05
6000B	107006	22	14.83	24.00	16.33	15.08	2.47	LBB76-343	94622	88	13.00	49.71	16.21	14.20	2.05
6000B	107006	23	14.93	44.85	16.33	15.50	2.47	LBB76-343	94622	89	7.39	64.24	16.21	11.86	2.05
6000B	107006	24	11.03	69.28	16.31	13.28	2.39	LBB76-343	94622	90	10.02	74.23	16.21	12.71	2.05
6000B	107006	25	9.99	73.73	16.31	12.69	2.39	LBB76-343	94622	91	13.47	76.38	16.21	14.88	2.05
6000B	107006	26	7.80	77.30	16.35	12.22	2.55	LBB76-343	94622	92	9.16	82.97	16.24	12.60	2.16
6000B	107006	27	13.84	56.27	16.25	14.90	2.20	LBB76-343	94622	93	14.00	56.09	16.31	15.00	2.39
6000B	107006	28	10.65	51.95	16.30	12.67	2.36	LBB76-343	94622	94	9.29	89.45	16.30	12.69	2.35
6000B	107006	29	14.33	82.48	16.31	15.44	2.39	LBB76-343	94622	95	12.58	51.37	16.31	13.95	2.40
6000B	107006	30	11.27	63.77	16.31	13.34	2.39	LBB76-343	94622	96	8.86	87.01	16.31	12.57	2.40
6000B	107006	31	11.70	23.89	16.32	12.40	2.44	LBB76-343	94622	97	11.05	74.97	16.30	13.36	2.38
6000B	107006	32	13.43	32.78	16.32	14.10	2.44	LBB76-343	94622	98	14.48	50.87	16.30	15.26	2.38
6000B	107006	33	16.38	58.62	16.28	16.64	2.31	LBB76-343	94622	99	15.71	88.82	16.21	16.29	2.04
6000B	107006	34	10.77	79.01	16.24	13.22	2.17	LBB76-343	94622	100	12.73	14.09	16.21	12.95	2.04
6000B	107006	35	13.64	50.29	16.33	14.66	2.47	LBB76-343	94622	101	11.01	31.74	16.21	12.20	2.04
6000B	107006	36	14.82	77.68	16.30	15.72	2.36	LBB76-343	94622	102	10.10	51.50	16.33	12.30	2.49
6000B	107006	37	10.68	60.30	16.30	12.90	2.36	LBB76-343	94622	103	14.23	21.17	16.33	14.49	2.49
6000B	107006	38	10.45	74.25	16.30	12.98	2.36	LBB76-343	94622	104	16.74	86.84	16.34	16.92	2.52
6000B	107006	39	14.80	83.89	16.30	15.73	2.36	LBB76-343	94622	105	16.12	33.77	16.26	16.30	2.21
6000B	107006	40	15.72	38.39	16.32	16.02	2.45	LBB76-343	94622	106	15.56	79.52	16.26	16.19	2.21
6000B	107006	41	15.76	45.92	16.31	16.13	2.40	LBB76-343	94622	107	14.08	24.74	16.26	14.44	2.21
6000B	107006	42	11.63	52.55	16.27	13.34	2.25	LBB76-343	94622	108	14.58	55.50	16.26	15.39	2.21
6000B	107006	43	15.39	72.48	16.27	16.06	2.26	LBB76-343	94622	109	15.24	83.47	16.26	16.00	2.21
6000B	107006	44	15.14	88.59	16.23	15.94	2.11	LBB76-343	94622	110	14.89	67.93	16.26	15.71	2.21
6000B	107006	45	13.67	51.92	16.23	14.71	2.11	LBB76-343	94622	111	13.41	65.00	16.20	14.73	2.02
6000B	107006	46	8.91	59.62	16.29	12.01	2.32	LBB76-343	94622	112	14.27	51.14	16.14	15.12	1.81
6000B	107006	47	15.22	63.22	16.29	15.89	2.32	LBB76-343	94622	113	14.72	83.09	16.31	15.68	2.39
6000B	107006	48	10.52	28.61	16.38	11.70	2.65	LBB76-343	94622	114	15.05	28.58	16.31	15.35	2.39
6000B	107006	49	13.93	51.79	16.38	14.89	2.65	LBB76-343	94622	115	9.23	56.92	16.21	11.97	2.05
6000B	107006	50	16.16	36.64	16.31	16.36	2.41	LBB76-343	94622	116	10.60	65.92	16.21	12.96	2.05
6000B	107006	51	9.95	34.91	16.29	11.58	2.34	LBB76-343	94622	117	9.52	57.17	16.21	12.09	2.05
6000B	107006	52	8.91	58.00	16.29	11.96	2.34	LBB76-343	94622	118	13.96	21.40	16.21	14.26	2.05
6000B	107006	53	15.59	64.26	16.31	16.14	2.40	LBB76-343	94622	119	10.63	46.83	16.21	12.51	2.05
6000B	107006	54	15.88	34.90	16.25	16.12	2.19	LBB76-343	94622	120	11.17	35.95	16.24	12.49	2.15
6000B	107006	55	15.82	77.07	16.30	16.34	2.38	LBB76-343	94622	121	16.39	38.28	16.24	16.55	2.15
6000B	107006	56	14.31	22.90	16.26	14.60	2.24	LBB76-343	94622	122	15.19	78.17	16.24	15.95	2.16
6000B	107006	57	15.34	72.89	16.30	16.03	2.36	LBB76-343	94622	123	10.38	52.12	16.25	12.50	2.20
6000B	107006	58	15.95	8.64	16.29	15.97	2.32	LBB76-343	94622	124	13.70	89.14	16.25	15.06	2.20
6000B	107006	59	15.72	73.67	16.29	16.27	2.32	LBB76-343	94622	125	12.74	60.25	16.25	14.23	2.20
6000B	107006	60	11.40	65.51	16.29	13.46	2.32	LBB76-343	94622	126	14.78	68.52	16.25	15.65	2.20
6000B	107006	61	14.61	44.19	16.30	15.25	2.37	LBB76-343	94622	127	15.06	86.84	16.20	15.89	2.03
6000B	107006	62	15.33	43.78	16.38	15.78	2.65	LBB76-343	94622	128	16.11	62.69	16.20	16.48	2.03
6000B	107006	63	13.68	24.07	16.29	14.08	2.33	LBB76-343	94622	129	13.59	62.63	16.20	14.82	2.03
6000B	107006	64	15.77	73.82	16.28	16.30	2.29	LBB76-343	94622	130	15.26	73.51	16.23	15.98	2.11

Table C3 Apatite fission track lengths for all samples analysed in this thesis

Angle								Angle							
UBC	A2Z	Track	Length (μm)	to c- axis	Lo calc (μm)	Lc calc (μm)	Dpar (μm)	UBC	A2Z	Track	Length (μm)	to c- axis	Lo calc (μm)	Lc calc (μm)	Dpar (μm)
6000B	107006	65	15.61	44.14	16.28	16.00	2.30	LBB76-343	94622	131	15.67	27.28	16.23	15.86	2.11
6000B	107006	66	14.46	50.61	16.28	15.24	2.30	LBB76-343	94622	132	14.08	42.49	16.23	14.83	2.11
6000B	107006	67	15.04	66.23	16.28	15.80	2.30	LBB76-343	94622	133	14.08	38.40	16.23	14.74	2.11
6000B	107006	68	15.35	67.45	16.28	16.01	2.30	LBB76-343	94622	134	10.90	42.31	16.34	12.54	2.50
6000B	107006	69	8.98	71.01	16.30	12.34	2.37	LBB76-343	94622	135	12.09	36.69	16.34	13.19	2.50
6000B	107006	70	9.74	70.96	16.35	12.52	2.55	LBB76-343	94622	136	12.01	20.25	16.34	12.52	2.50
6000B	107006	71	15.42	49.32	16.33	15.91	2.48	LBB76-343	94622	137	10.25	84.64	16.34	12.94	2.50
6000B	107006	72	16.38	22.74	16.33	16.45	2.48	LBB76-343	94622	138	14.65	59.16	16.34	15.48	2.50
6000B	107006	73	8.87	59.39	16.31	12.00	2.40	LBB76-343	94622	139	15.74	46.40	16.34	16.12	2.50
6000B	107006	74	10.18	27.63	16.31	11.40	2.40	LBB76-343	94622	140	14.00	89.96	16.20	15.24	2.03
6000B	107006	75	14.35	53.77	16.31	15.21	2.40	LBB76-343	94622	141	15.60	68.24	16.20	16.17	2.03
6000B	107006	76	14.79	54.11	16.31	15.52	2.40	LBB76-343	94622	142	16.14	35.29	16.23	16.33	2.13
6000B	107006	77	15.69	41.76	16.31	16.03	2.41	LBB76-343	94622	143	11.14	66.67	16.20	13.31	2.00
6000B	107006	78	13.88	76.33	16.30	15.13	2.37	LBB76-343	94622	144	16.37	30.82	16.26	16.49	2.21
6000B	107006	79	15.16	69.92	16.30	15.90	2.37	LBB76-343	94622	145	14.53	47.57	16.26	15.25	2.21
6000B	107006	80	10.52	53.43	16.30	12.63	2.37	LBB76-343	94622	146	13.53	83.53	16.26	14.95	2.21
6000B	107006	81	11.70	22.69	16.30	12.35	2.37	LBB76-343	94622	147	16.00	57.84	16.18	16.38	1.95
6000B	107006	82	14.66	70.25	16.31	15.58	2.40	LBB76-343	94622	148	15.70	59.31	16.31	16.19	2.41
6000B	107006	83	14.63	37.92	16.31	15.16	2.40	LBB76-343	94622	149	15.66	55.16	16.30	16.13	2.37
6000B	107006	84	9.42	76.34	16.25	12.56	2.20	LBB76-343	94622	150	17.28	5.89	16.30	17.28	2.37
6000B	107006	85	15.70	40.30	16.37	16.03	2.61	LBB76-343	94622	151	15.92	75.27	16.22	16.40	2.08
6000B	107006	86	12.95	72.79	16.37	14.52	2.61	LBB76-343	94622	152	12.57	60.18	16.30	14.12	2.37
6000B	107006	87	10.90	21.63	16.27	11.65	2.27	LBB76-343	94622	153	14.46	52.49	16.30	15.27	2.37
6000B	107006	88	15.98	79.42	16.27	16.45	2.27	LBB76-343	94622	154	15.10	28.18	16.30	15.38	2.37
6000B	107006	89	10.18	41.14	16.27	12.00	2.27	LBB76-343	94622	155	11.65	79.34	16.30	13.77	2.37
6000B	107006	90	16.30	81.75	16.36	16.65	2.57	LBB76-343	94622	156	16.22	62.49	16.23	16.55	2.13
6000B	107006	91	14.58	54.60	16.37	15.38	2.62	LBB76-343	94622	157	15.06	83.60	16.23	15.89	2.13
6000B	107006	92	6.92	70.72	16.37	11.91	2.62	LBB76-343	94622	158	15.12	45.46	16.25	15.65	2.20
6000B	107006	93	12.99	67.94	16.37	14.50	2.60	LBB76-343	94622	159	10.62	27.53	16.23	11.72	2.11
6000B	107006	94	17.25	26.91	16.37	17.25	2.60	LBB76-343	94622	160	15.23	26.27	16.23	15.47	2.11
6000B	107006	95	14.98	70.79	16.37	15.79	2.60	LBB76-343	94622	161	11.37	50.80	16.25	13.12	2.19
6000B	107006	96	14.15	80.77	16.35	15.32	2.53	LBB76-343	94622	162	10.59	55.99	16.25	12.74	2.19
6000B	107006	97	16.17	75.47	16.37	16.56	2.60	LBB76-343	94622	163	14.35	25.16	16.24	14.68	2.17
6000B	107006	98	13.82	50.18	16.28	14.79	2.30	LBB76-343	94622	164	16.18	32.69	16.24	16.35	2.17
6000B	107006	99	11.58	22.91	16.30	12.26	2.37	LBB76-343	94622	165	10.52	85.45	16.24	13.11	2.17
6000B	107006	100	10.65	23.66	16.28	11.55	2.29	LBB76-343	94622	166	11.51	45.15	16.24	13.05	2.17
6000B	107006	101	15.28	46.46	16.28	15.78	2.29	LBB76-343	94622	167	11.67	34.22	16.25	12.79	2.20
6000B	107006	102	11.24	33.18	16.28	12.43	2.29	LBB76-343	94622	168	15.82	49.38	16.25	16.20	2.20
6000B	107006	103	15.90	33.06	16.28	16.12	2.29	LBB76-343	94622	169	14.93	75.99	16.27	15.78	2.27
6000B	107006	104	15.89	64.55	16.30	16.34	2.37	LBB76-343	94622	170	16.50	83.08	16.22	16.77	2.10
6000B	107006	105	10.47	60.53	16.31	12.77	2.42	LBB76-343	94622	171	12.44	17.98	16.22	12.81	2.10
6000B	107006	106	13.98	33.77	16.31	14.56	2.42	LBB76-343	94622	172	14.14	52.53	16.22	15.05	2.10
6000B	107006	107	15.10	72.39	16.35	15.87	2.53	LBB76-343	94622	173	13.53	59.71	16.23	14.74	2.13
6000B	107006	108	11.69	57.43	16.35	13.49	2.53	LBB76-343	94622	174	10.33	47.93	16.23	12.34	2.13
6000B	107006	109	15.19	64.04	16.28	15.88	2.30	LBB76-343	94622	175	14.87	44.16	16.28	15.44	2.30
6000B	107006	110	13.78	86.12	16.40	15.11	2.73	LBB76-343	94622	176	9.41	77.29	16.26	12.57	2.23
6000B	107006	111	16.43	53.73	16.40	16.66	2.73	LBB76-343	94622	177	14.31	39.12	16.26	14.94	2.23
6000B	107006	112	14.84	49.06	16.40	15.49	2.73	LBB76-343	94622	178	13.39	67.49	16.26	14.75	2.23
6000B	107006	113	13.02	38.79	16.27	13.95	2.25	LBB76-343	94622	179	15.09	36.55	16.23	15.50	2.11
6000B	107006	114	12.20	22.06	16.29	12.75	2.32	LBB76-343	94622	180	10.13	64.31	16.23	12.63	2.11
6000B	107006	115	12.74	63.00	16.33	14.27	2.48	LBB76-343	94622	181	11.42	61.89	16.30	13.40	2.37
6000B	107006	116	16.29	29.05	16.34	16.41	2.51	LBB76-343	94622	182	13.59	64.09	16.30	14.84	2.37
6000B	107006	117	9.97	46.29	16.34	12.05	2.51	LBB76-343	94622	183	15.04	72.92	16.30	15.84	2.37
6000B	107006	118	15.27	52.21	16.38	15.83	2.66	LBB76-343	94622	184	13.65	76.86	16.30	14.99	2.37
6000B	107006	119	15.62	55.90	16.25	16.11	2.18	LBB76-343	94622	185	14.37	53.61	16.29	15.22	2.34
6000B	107006	120	16.56	43.73	16.37	16.71	2.60	LBB76-343	94622	186	12.23	14.73	16.29	12.51	2.34
6000B	107006	121	11.71	33.40	16.33	12.79	2.49	LBB76-343	94622	187	14.71	77.03	16.32	15.65	2.43
6000B	107006	122	11.28	54.66	16.31	13.16	2.40	LBB76-343	94622	188	13.67	70.45	16.22	14.96	2.09
6000B	107006	123	15.14	36.49	16.33	15.54	2.49	LBB76-343	94622	189	9.68	81.06	16.28	12.71	2.31
6000B	107006	124	16.00	81.71	16.34	16.46	2.50	LBB76-343	94622	190	13.93	42.48	16.28	14.72	2.31
6000B	107006	125	10.05	64.53	16.27	12.59	2.26	LBB76-343	94622	191	15.58	81.92	16.25	16.21	2.20

Table C3 Apatite fission track lengths for all samples analysed in this thesis

UBC	A2Z	Track	Angle				Dpar	UBC	A2Z	Track	Angle				Dpar
			Length (μm)	to c- axis	Lo calc (μm)	Lc calc (μm)					Length (μm)	to c- axis	Lo calc (μm)	Lc calc (μm)	
6000B	107006	126	16.05	40.27	16.40	16.30	2.73	LBB76-343	94622	192	14.10	85.31	16.25	15.30	2.20
6000B	107006	127	15.32	68.49	16.40	15.99	2.73	LBB76-343	94622	193	16.47	20.28	16.26	16.52	2.24
6000B	107006	128	9.05	63.86	16.34	12.17	2.50	LBB76-343	94622	194	14.54	73.08	16.26	15.53	2.24
6000B	107006	129	14.47	77.03	16.41	15.50	2.75	LBB76-343	94622	195	16.82	37.66	16.31	16.90	2.41
6000B	107006	130	15.12	78.30	16.31	15.91	2.39	LBB76-343	94622	196	10.64	43.00	16.31	12.38	2.41
6000B	107006	131	16.13	60.04	16.31	16.48	2.41	LBB76-343	94622	197	15.81	30.73	16.26	16.02	2.24
6000B	107006	132	15.04	66.70	16.33	15.80	2.49	LBB76-343	94622	198	14.30	60.58	16.29	15.26	2.34
6000B	107006	133	17.07	30.02	16.27	17.09	2.26	LBB76-343	94622	199	14.86	49.95	16.17	15.52	1.90
6000B	107006	134	9.56	49.73	16.30	11.90	2.38	LBB76-343	94622	200	16.53	18.65	16.17	16.57	1.90
6000B	107006	135	14.73	60.70	16.30	15.55	2.38	LBB76-343	94622	201	13.95	76.08	16.17	15.17	1.90
6000B	107006	136	16.48	40.08	16.30	16.63	2.38	LBB76-576	94623	1	13.18	38.12	16.20	14.05	2.00
6000B	107006	137	14.65	54.57	16.31	15.43	2.41	LBB76-576	94623	2	16.57	55.36	16.20	16.76	2.00
6000B	107006	138	15.01	34.54	16.36	15.41	2.57	LBB76-576	94623	3	15.15	87.20	16.26	15.95	2.24
6000B	107006	139	10.97	48.40	16.36	12.78	2.57	LBB76-576	94623	4	15.49	35.29	16.26	15.80	2.24
6000B	107006	140	13.09	11.67	16.30	13.23	2.36	LBB76-576	94623	5	14.49	70.66	16.26	15.48	2.24
6000B	107006	141	12.76	58.54	16.30	14.21	2.38	LBB76-576	94623	6	10.93	25.51	16.26	11.86	2.24
6000B	107006	142	14.97	8.41	16.27	15.00	2.26	LBB76-576	94623	7	10.36	27.33	16.25	11.52	2.20
6000B	107006	143	14.83	30.69	16.27	15.20	2.26	LBB76-576	94623	8	14.75	44.51	16.25	15.36	2.20
6000B	107006	144	13.23	73.91	16.31	14.71	2.40	LBB76-576	94623	9	10.52	33.79	16.24	11.93	2.14
6000B	107006	145	15.12	64.42	16.26	15.84	2.24	LBB76-576	94623	10	15.63	61.06	16.24	16.15	2.14
6000B	107006	146	15.11	58.30	16.29	15.78	2.33	LBB76-576	94623	11	10.64	71.83	16.26	13.07	2.21
6000B	107006	147	15.79	30.76	16.29	16.00	2.33	LBB76-576	94623	12	14.32	59.14	16.29	15.26	2.33
6000B	107006	148	15.63	33.13	16.34	15.89	2.52	LBB76-576	94623	13	11.77	25.32	16.29	12.52	2.33
6000B	107006	149	7.94	75.39	16.34	12.21	2.52	LBB76-576	94623	14	16.12	3.21	16.29	16.12	2.33
6000B	107006	150	11.59	51.14	16.34	13.28	2.52	LBB76-576	94623	15	13.44	42.72	16.29	14.36	2.33
6000B	107006	151	16.54	3.58	16.33	16.54	2.47	LBB76-576	94623	16	12.78	88.56	16.29	14.50	2.33
6000B	107006	152	9.57	63.05	16.33	12.25	2.49	LBB76-576	94623	17	14.59	57.69	16.29	15.42	2.33
6000B	107006	153	14.05	17.08	16.30	14.25	2.36	LBB76-576	94623	18	14.63	73.41	16.29	15.58	2.33
6000B	107006	154	14.34	70.35	16.29	15.38	2.34	LBB76-576	94623	19	9.85	84.28	16.29	12.80	2.33
6000B	107006	155	15.56	21.25	16.29	15.70	2.34	LBB76-576	94623	20	14.21	44.13	16.29	14.96	2.33
6000B	107006	156	14.79	32.31	16.29	15.19	2.34	LBB76-576	94623	21	15.12	71.92	16.29	15.88	2.33
6000B	107006	157	14.28	70.91	16.30	15.35	2.35	LBB76-576	94623	22	12.34	13.72	16.29	12.58	2.33
6000B	107006	158	13.81	69.21	16.30	15.03	2.35	LBB76-576	94623	23	9.98	65.21	16.29	12.55	2.33
6000B	107006	159	10.35	42.04	16.37	12.15	2.61	LBB76-576	94623	24	15.78	69.23	16.22	16.29	2.09
6000B	107006	160	14.76	73.71	16.37	15.67	2.61	LBB76-576	94623	25	10.05	61.39	16.22	12.52	2.09
6000B	107006	161	10.35	77.61	16.29	12.95	2.34	LBB76-576	94623	26	11.91	19.06	16.22	12.38	2.09
6000B	107006	162	15.33	49.34	16.32	15.85	2.43	LBB76-576	94623	27	15.17	28.13	16.18	15.44	1.93
6000B	107006	163	11.09	37.58	16.30	12.50	2.36	LBB76-576	94623	28	16.77	63.30	16.18	16.92	1.93
6000B	107006	164	14.82	28.85	16.30	15.16	2.36	LBB76-576	94623	29	14.63	38.14	16.24	15.17	2.16
6000B	107006	165	15.42	63.66	16.28	16.03	2.28	LBB76-576	94623	30	15.93	66.56	16.24	16.38	2.16
6000B	107006	166	14.72	56.12	16.25	15.49	2.18	LBB76-576	94623	31	6.42	75.59	16.24	11.90	2.16
6000B	107006	167	14.46	79.94	16.25	15.51	2.18	LBB76-576	94623	32	9.52	54.89	16.24	12.03	2.16
6000B	107006	168	15.67	20.11	16.25	15.79	2.18	LBB76-576	94623	33	9.44	76.49	16.24	12.57	2.16
6000B	107006	169	15.52	61.30	16.25	16.08	2.18	LBB76-576	94623	34	15.49	61.10	16.24	16.06	2.16
6000B	107006	170	10.70	61.74	16.25	12.94	2.18	LBB76-576	94623	35	10.24	32.10	16.28	11.66	2.31
6000B	107006	171	16.14	48.74	16.29	16.43	2.34	LBB76-576	94623	36	16.28	49.43	16.28	16.53	2.31
6000B	107006	172	15.19	29.09	16.29	15.47	2.34	LBB76-576	94623	37	12.26	16.24	16.23	12.59	2.13
6000B	107006	173	11.25	53.70	16.35	13.12	2.54	LBB76-576	94623	38	11.33	68.66	16.23	13.46	2.13
EX-24C-1674	117802	1	12.59	14.69	16.28	12.84	2.31	LBB76-576	94623	39	16.53	51.99	16.23	16.72	2.13
EX-24C-1674	117802	2	11.98	53.16	16.28	13.59	2.31	LBB76-576	94623	40	14.97	57.83	16.23	15.68	2.13
EX-24C-1674	117802	3	14.13	80.81	16.28	15.31	2.31	LBB76-576	94623	41	10.22	54.06	16.28	12.45	2.29
EX-24C-1674	117802	4	12.80	57.69	16.28	14.23	2.31	LBB76-576	94623	42	8.85	17.46	16.28	9.84	2.29
EX-24C-1674	117802	5	13.06	34.21	16.28	13.85	2.31	LBB76-576	94623	43	14.44	61.14	16.33	15.36	2.46
EX-29C-1783	117803	1	15.05	71.93	16.52	15.84	3.15	LBB76-576	94623	44	14.93	52.04	16.33	15.59	2.46
EX-29C-1783	117803	2	13.06	58.41	16.52	14.41	3.15	LBB76-576	94623	45	10.09	73.65	16.28	12.75	2.28
EX-29C-1783	117803	3	16.05	67.79	16.52	16.46	3.15	LBB76-576	94623	46	14.85	64.61	16.28	15.66	2.28
EX-29C-1783	117803	4	12.65	69.35	16.54	14.30	3.21	LBB76-576	94623	47	16.54	78.38	16.28	16.79	2.28
EX-29C-1783	117803	5	13.90	82.17	16.54	15.17	3.21	LBB76-576	94623	48	14.85	25.18	16.28	15.12	2.28
EX-29C-1783	117803	6	15.99	82.02	16.55	16.46	3.25	LBB76-576	94623	49	15.21	79.39	16.32	15.97	2.44
EX-29C-1783	117803	7	13.17	61.18	16.55	14.53	3.25	LBB76-576	94623	50	10.45	61.72	16.32	12.78	2.44
EX-29C-1783	117803	8	13.15	35.98	16.43	13.97	2.84	LBB76-576	94623	51	16.19	53.54	16.32	16.49	2.44

Table C3 Apatite fission track lengths for all samples analysed in this thesis

UBC	A2Z	Track	Angle				Dpar	UBC	A2Z	Track	Angle				Dpar
			Length (μm)	to c- axis	Lo calc (μm)	Lc calc (μm)					Length (μm)	to c- axis	Lo calc (μm)	Lc calc (μm)	
EX-29C-1783	117803	9	16.25	54.65	16.43	16.54	2.84	LBB76-576	94623	52	14.14	85.85	16.25	15.33	2.19
EX-29C-1783	117803	10	16.26	63.79	16.43	16.58	2.84	LBB76-576	94623	53	12.59	50.41	16.29	13.94	2.32
EX-29C-1783	117803	11	13.69	70.97	16.46	14.97	2.93	LBB76-576	94623	54	15.34	66.96	16.29	16.00	2.32
EX-29C-1783	117803	12	12.04	72.33	16.41	13.95	2.75	LBB76-576	94623	55	15.90	50.97	16.29	16.27	2.32
EX-29C-1783	117803	13	15.22	69.62	16.46	15.94	2.94	LBB76-576	94623	56	8.12	60.75	16.29	11.90	2.32
EX-29C-1783	117803	14	14.29	42.79	16.46	14.99	2.94	LBB76-576	94623	57	14.95	64.48	16.29	15.73	2.32
EX-29C-1783	117803	15	11.86	83.77	16.48	13.92	3.02	LBB76-576	94623	58	15.33	41.03	16.27	15.75	2.27
EX-29C-1783	117803	16	14.52	49.39	16.48	15.27	3.02	LBB76-576	94623	59	10.81	57.32	16.27	12.92	2.27
EX-29C-1783	117803	17	15.67	41.91	16.48	16.02	3.02	LBB76-576	94623	60	15.66	71.32	16.27	16.22	2.27
EX-29C-1783	117803	18	16.22	33.20	16.51	16.38	3.10	LBB76-576	94623	61	11.80	60.44	16.27	13.62	2.27
EX-29C-1783	117803	19	15.33	38.58	16.51	15.72	3.10	LBB76-576	94623	62	15.46	74.82	16.20	16.11	2.03
EX-29C-1783	117803	20	15.80	46.31	16.43	16.16	2.81	LBB76-576	94623	63	14.61	61.84	16.20	15.48	2.03
EX-29C-1783	117803	21	11.28	64.11	16.43	13.36	2.81	LBB76-576	94623	64	14.04	56.77	16.26	15.04	2.23
EX-29C-1783	117803	22	15.92	33.93	16.41	16.14	2.76	LBB76-576	94623	65	11.60	7.40	16.26	11.70	2.23
EX-29C-1783	117803	23	14.55	60.39	16.35	15.43	2.53	LBB76-576	94623	66	7.94	74.30	16.26	12.19	2.23
EX-29C-1783	117803	24	13.75	56.90	16.38	14.85	2.65	LBB76-576	94623	67	9.40	80.10	16.26	12.62	2.23
EX-29C-1783	117803	25	13.76	56.36	16.50	14.85	3.07	LBB76-576	94623	68	15.83	36.19	16.26	16.09	2.23
EX-29C-1783	117803	26	16.01	72.32	16.43	16.45	2.83	LBB76-576	94623	69	13.19	84.66	16.26	14.74	2.23
EX-29C-1783	117803	27	11.89	29.96	16.43	12.80	2.83	LBB76-576	94623	70	7.08	79.14	16.20	12.09	2.00
EX-29C-1783	117803	28	15.39	87.22	16.50	16.10	3.09	LBB76-576	94623	71	13.48	37.52	16.20	14.27	2.00
EX-29C-1783	117803	29	13.74	48.71	16.54	14.70	3.22	LBB76-576	94623	72	14.17	61.76	16.18	15.19	1.94
EX-29C-1783	117803	30	14.80	86.78	16.47	15.73	2.98	LBB76-576	94623	73	9.73	24.25	16.18	10.89	1.94
EX-29C-1783	117803	31	14.59	89.44	16.47	15.61	2.96	LBB76-576	94623	74	13.62	21.55	16.24	13.96	2.15
EX-29C-1783	117803	32	12.83	46.23	16.47	14.01	2.96	LBB76-576	94623	75	14.56	66.67	16.24	15.49	2.15
EX-29C-1783	117803	33	14.35	51.47	16.42	15.18	2.79	LBB76-576	94623	76	14.96	28.89	16.24	15.27	2.15
EX-29C-1783	117803	34	14.67	79.31	16.42	15.64	2.79	LBB76-576	94623	77	16.32	88.97	16.28	16.67	2.30
EX-29C-1783	117803	35	10.09	69.21	16.47	12.69	2.96	LBB76-576	94623	78	16.20	56.14	16.28	16.51	2.30
EX-29C-1783	117803	36	14.40	81.24	16.47	15.48	2.96	LBB76-576	94623	79	12.07	40.01	16.28	13.29	2.30
EX-29C-1783	117803	37	13.78	57.40	16.47	14.87	2.96	LBB76-576	94623	80	8.88	38.81	16.28	11.09	2.31
EX-29C-1783	117803	38	12.12	67.61	16.45	13.94	2.91	LBB76-576	94623	81	9.20	55.88	16.28	11.93	2.31
EX-29C-1783	117803	39	10.82	51.58	16.45	12.77	2.91	LBB76-576	94623	82	9.80	42.80	16.28	11.81	2.31
EX-29C-1783	117803	40	16.38	54.05	16.54	16.63	3.22	LBB76-576	94623	83	16.25	21.83	16.28	16.33	2.31
EX-29C-1783	117803	41	14.32	45.21	16.54	15.06	3.22	LBB76-576	94623	84	10.51	86.98	16.28	13.10	2.31
EX-29C-1783	117803	42	12.80	85.32	16.26	14.50	2.21	LBB76-576	94623	85	15.84	64.31	16.20	16.31	2.00
EX-29C-1783	117803	43	15.13	62.47	16.26	15.83	2.21	LBB76-576	94623	86	10.42	80.63	16.20	13.02	2.00
EX-29C-1783	117803	44	14.42	60.86	16.26	15.35	2.21	LBB76-576	94623	87	10.52	59.84	16.32	12.79	2.45
EX-29C-1783	117803	45	14.17	72.91	16.26	15.29	2.21	LBB76-576	94623	88	12.22	43.43	16.32	13.50	2.45
EX-29C-1783	117803	46	14.86	84.15	16.26	15.77	2.21	LBB76-576	94623	89	10.10	60.74	16.32	12.54	2.45
EX-29C-1783	117803	47	16.89	26.05	16.26	16.93	2.21	LBB76-576	94623	90	11.90	54.45	16.21	13.56	2.06
EX-29C-1783	117803	48	16.16	37.79	16.26	16.37	2.21	LBB76-576	94623	91	12.45	56.67	16.21	13.98	2.06
EX-29C-1783	117803	49	14.91	87.83	16.26	15.80	2.21	LBB76-576	94623	92	14.92	82.15	16.21	15.80	2.06
EX-29C-1783	117803	50	13.77	84.10	16.40	15.10	2.72	LBB76-576	94623	93	10.92	60.65	16.19	13.06	1.97
EX-29C-1783	117803	51	15.25	68.32	16.40	15.95	2.72	LBB76-576	94623	94	16.81	41.23	16.19	16.90	1.97
EX-29C-1783	117803	52	15.23	78.50	16.32	15.98	2.44	LBB76-576	94623	95	15.71	45.27	16.31	16.08	2.42
EX-29C-1783	117803	53	14.87	80.23	16.50	15.76	3.09	LBB76-576	94623	96	8.57	70.38	16.31	12.24	2.42
EX-29C-1783	117803	54	14.06	50.75	16.50	14.96	3.09	LBB76-576	94623	97	15.30	51.26	16.31	15.84	2.42
EX-29C-1783	117803	55	13.35	76.88	16.31	14.81	2.42	LBB76-576	94623	98	12.43	23.25	16.31	12.98	2.42
EX-29C-1783	117803	56	13.37	34.72	16.37	14.11	2.61	LBB76-576	94623	99	15.04	71.27	16.31	15.83	2.42
EX-29C-1783	117803	57	14.81	22.90	16.37	15.04	2.61	LBB76-576	94623	100	11.03	46.26	16.34	12.76	2.51
EX-29C-1783	117803	58	14.53	24.39	16.51	14.82	3.10	LBB76-576	94623	101	11.11	16.71	16.34	11.59	2.51
EX-29C-1783	117803	59	15.89	18.78	16.43	15.98	2.82	LBB76-576	94623	102	15.31	68.07	16.27	15.98	2.27
EX-29C-1783	117803	60	14.78	16.82	16.43	14.92	2.82	LBB76-576	94623	103	7.50	75.09	16.27	12.12	2.27
EX-29C-1783	117803	61	13.39	52.30	16.48	14.53	3.00	LBB76-576	94623	104	14.05	23.71	16.27	14.39	2.27
EX-29C-1783	117803	62	14.76	65.88	16.48	15.62	3.00	LBB76-576	94623	105	16.34	26.04	16.27	16.44	2.27
EX-29C-1783	117803	63	14.86	67.10	16.37	15.69	2.60	LBB76-576	94623	106	8.37	68.63	16.27	12.16	2.27
EX-29C-1783	117803	64	16.47	82.22	16.49	16.75	3.05	LBB76-576	94623	107	10.63	29.09	16.25	11.80	2.18
EX-29C-1783	117803	65	13.73	50.63	16.42	14.73	2.79	LBB76-576	94623	108	14.59	70.74	16.22	15.54	2.09
EX-29C-1783	117803	66	15.64	72.26	16.46	16.22	2.92	LBB76-576	94623	109	14.51	32.17	16.22	14.96	2.09
EX-29C-1783	117803	67	16.53	29.85	16.55	16.62	3.25	LBB76-576	94623	110	14.22	75.48	16.28	15.34	2.31
EX-29C-1783	117803	68	17.15	49.84	16.45	17.17	2.88	LBB76-576	94623	111	10.97	17.98	16.28	11.53	2.31
EX-29C-1783	117803	69	13.92	86.68	16.45	15.19	2.88	LBB76-576	94623	112	14.87	19.36	16.25	15.04	2.19

Table C3 Apatite fission track lengths for all samples analysed in this thesis

UBC	A2Z	Track	Angle				Dpar		UBC	A2Z	Track	Angle				Dpar
			Length (μm)	to c- axis	Lo calc (μm)	Lc calc (μm)						Length (μm)	to c- axis	Lo calc (μm)	Lc calc (μm)	
EX-29C-1783	117803	70	12.75	40.22	16.45	13.79	2.88		LBB76-576	94623	113	14.82	49.82	16.25	15.49	2.19
EX-29C-1783	117803	71	14.56	49.53	16.45	15.30	2.88		LBB76-576	94623	114	7.80	46.17	16.25	11.32	2.19
EX-29C-1783	117803	72	14.77	77.88	16.33	15.69	2.48		LBB76-576	94623	115	9.88	48.35	16.25	12.06	2.19
EX-29C-1783	117803	73	12.36	64.74	16.33	14.06	2.48		LBB76-576	94623	116	14.54	63.24	16.25	15.45	2.19
EX-29C-1783	117803	74	14.77	67.99	16.50	15.64	3.07		LBB76-576	94623	117	8.91	59.55	16.22	12.01	2.07
EX-29C-1783	117803	75	16.34	83.40	16.50	16.68	3.07		LBB76-576	94623	118	13.12	18.01	16.22	13.42	2.07
EX-29C-1783	117803	76	15.93	41.18	16.36	16.21	2.58		LBB76-576	94623	119	15.64	41.47	16.22	15.99	2.07
EX-29C-1783	117803	77	14.17	51.07	16.36	15.05	2.58		LBB76-576	94623	120	9.02	75.29	16.22	12.44	2.07
EX-29C-1783	117803	78	14.51	47.30	16.50	15.23	3.09		LBB76-576	94623	121	13.86	17.02	16.22	14.07	2.07
EX-29C-1783	117803	79	14.86	64.50	16.50	15.67	3.09		LBB76-576	94623	122	15.26	48.20	16.22	15.78	2.07
EX-29C-1783	117803	80	13.80	76.69	16.35	15.08	2.56		LBB76-576	94623	123	13.95	52.89	16.22	14.92	2.07
EX-29C-1783	117803	81	13.02	80.93	16.35	14.62	2.56		LBB76-576	94623	124	15.24	74.90	16.28	15.97	2.28
EX-29C-1783	117803	82	15.98	40.22	16.35	16.24	2.56		LBB76-576	94623	125	16.00	62.25	16.26	16.40	2.23
EX-29C-1783	117803	83	15.88	67.69	16.35	16.35	2.56		LBB76-576	94623	126	10.39	85.53	16.27	13.03	2.26
EX-29C-1783	117803	84	15.07	68.40	16.37	15.83	2.61		LBB76-576	94623	127	8.97	70.83	16.27	12.34	2.26
EX-29C-1783	117803	85	13.88	67.21	16.37	15.06	2.61		LBB76-576	94623	128	11.93	27.05	16.27	12.72	2.26
EX-29C-1783	117803	86	16.68	25.77	16.37	16.74	2.61		LBB76-576	94623	129	10.75	23.04	16.20	11.60	2.01
EX-29C-1783	117803	87	14.87	36.87	16.37	15.33	2.61		LBB76-576	94623	130	15.01	76.38	16.20	15.84	2.01
EX-29C-1783	117803	88	10.87	44.76	16.37	12.60	2.61		LBB76-576	94623	131	14.36	53.49	16.20	15.21	2.01
EX-29C-1783	117803	89	14.18	43.07	16.44	14.91	2.85		LBB76-576	94623	132	13.49	50.49	16.20	14.56	2.01
EX-29C-1783	117803	90	14.37	70.96	16.44	15.40	2.85		LBB76-576	94623	133	15.39	70.64	16.20	16.05	2.01
EX-29C-1783	117803	91	13.27	85.33	16.48	14.79	3.00		LBB76-576	94623	134	9.94	89.78	16.20	12.87	2.01
EX-29C-1783	117803	92	14.96	32.86	16.47	15.34	2.98		LBB76-576	94623	135	15.71	81.53	16.34	16.28	2.50
EX-29C-1783	117803	93	14.80	33.97	16.47	15.23	2.98		LBB76-576	94623	136	13.81	21.60	16.34	14.13	2.50
EX-29C-1783	117803	94	13.49	77.40	16.39	14.90	2.68		LBB76-576	94623	137	11.98	56.03	16.34	13.65	2.50
EX-29C-1783	117803	95	13.61	64.50	16.39	14.86	2.68		LBB76-576	94623	138	12.55	15.53	16.35	12.83	2.55
EX-29C-1783	117803	96	13.64	62.68	16.47	14.85	2.97		LBB76-576	94623	139	11.62	52.90	16.25	13.34	2.20
EX-29C-1783	117803	97	14.60	47.58	16.47	15.30	2.97		LBB76-576	94623	140	15.35	63.63	16.25	15.98	2.20
EX-29C-1783	117803	98	14.20	55.15	16.39	15.13	2.69		LBB76-576	94623	141	10.38	75.85	16.23	12.95	2.13
EX-29C-1783	117803	99	13.91	77.76	16.51	15.16	3.11		LBB76-576	94623	142	15.23	45.47	16.23	15.73	2.13
EX-29C-1783	117803	100	13.97	86.92	16.51	15.22	3.11		LBB76-576	94623	143	12.98	44.81	16.23	14.08	2.13
EX-29C-1783	117803	101	11.54	66.12	16.46	13.55	2.95		LBB76-576	94623	144	13.31	78.59	16.23	14.79	2.13
EX-29C-1783	117803	102	14.34	82.87	16.46	15.44	2.95		LBB76-576	94623	145	13.35	80.73	16.23	14.83	2.13
EX-29C-1783	117803	103	13.41	82.64	16.42	14.87	2.79		LBB76-576	94623	146	17.46	30.72	16.35	17.43	2.56
EX-29C-1783	117803	104	15.97	15.19	16.39	16.03	2.69		LBB76-576	94623	147	14.76	50.93	16.35	15.46	2.56
EX-29C-1783	117803	105	13.36	63.95	16.52	14.69	3.13		LBB76-576	94623	148	8.69	49.98	16.35	11.61	2.56
EX-29C-1783	117803	106	13.31	89.89	16.52	14.82	3.13		LBB76-576	94623	149	11.11	59.19	16.24	13.15	2.15
EX-29C-1783	117803	107	13.96	63.70	16.43	15.07	2.83		LBB76-576	94623	150	13.98	82.74	16.24	15.22	2.15
EX-29C-1783	117803	108	12.24	86.22	16.43	14.16	2.83		LBB76-576	94623	151	12.86	24.60	16.24	13.39	2.15
EX-29C-1783	117803	109	15.87	48.48	16.43	16.23	2.83		LBB76-576	94623	152	16.13	89.10	16.24	16.55	2.15
EX-29C-1783	117803	110	13.70	51.23	16.46	14.72	2.94		LBB76-576	94623	153	14.22	59.28	16.25	15.19	2.20
EX-29C-1783	117803	111	11.20	28.24	16.46	12.19	2.94		LBB76-576	94623	154	10.00	85.77	16.25	12.86	2.20
EX-29C-1783	117803	112	13.62	55.16	16.46	14.73	2.94		LBB76-576	94623	155	11.62	32.73	16.33	12.70	2.47
EX-29C-1783	117803	113	16.01	50.09	16.47	16.34	2.98		LBB76-576	94623	156	11.02	65.25	16.30	13.21	2.37
EX-29C-1783	117803	114	13.23	63.19	16.47	14.59	2.98		LBB76-576	94623	157	15.02	60.21	16.30	15.74	2.37
EX-29C-1783	117803	115	14.03	80.21	16.43	15.24	2.84		LBB76-576	94623	158	15.91	47.81	16.30	16.25	2.37
EX-29C-1783	117803	116	12.92	74.08	16.43	14.52	2.84		LBB76-576	94623	159	14.17	57.61	16.30	15.14	2.37
EX-29C-1783	117803	117	15.62	27.90	16.43	15.83	2.84		LBB76-576	94623	160	15.64	65.87	16.30	16.19	2.37
EX-29C-1783	117803	118	13.90	56.29	16.43	14.94	2.84		LBB76-576	94623	161	12.36	33.18	16.30	13.28	2.37
EX-29C-1783	117803	119	16.35	88.37	16.43	16.68	2.84		LBB76-576	94623	162	15.17	46.41	16.26	15.70	2.22
EX-29C-1783	117803	120	12.75	51.19	16.34	14.06	2.52		LBB76-576	94623	163	14.52	60.91	16.25	15.41	2.18
EX-29C-1783	117803	121	14.33	54.93	16.34	15.21	2.52		LBB76-576	94623	164	15.14	58.48	16.30	15.80	2.36
EX-29C-1783	117803	122	14.10	21.02	16.34	14.37	2.52		LBB76-576	94623	165	14.05	43.62	16.31	14.83	2.41
EX-29C-1783	117803	123	12.85	30.05	16.44	13.56	2.87		LBB76-576	94623	166	9.93	66.53	16.21	12.55	2.06
EX-29C-1783	117803	124	12.49	49.20	16.31	13.84	2.40		LBB76-576	94623	167	13.88	37.64	16.21	14.58	2.06
EX-29C-1783	117803	125	15.39	39.20	16.31	15.77	2.40		LBB76-576	94623	168	11.17	80.44	16.32	13.48	2.44
EX-29C-1783	117803	126	12.62	81.59	16.50	14.38	3.07		LBB76-576	94623	169	16.64	67.70	16.32	16.84	2.44
EX-29C-1783	117803	127	14.16	68.48	16.43	15.25	2.83		LBB76-576	94623	170	12.28	16.68	16.20	12.62	2.01
EX-29C-1783	117803	128	14.80	48.43	16.33	15.45	2.47		LBB76-576	94623	171	12.04	80.41	16.20	14.02	2.01
EX-29C-1783	117803	129	15.38	33.79	16.33	15.70	2.47		LBB76-576	94623	172	14.56	77.75	16.20	15.56	2.01
EX-29C-1783	117803	130	14.06	46.67	16.37	14.89	2.60		LBB76-576	94623	173	15.89	12.19	16.20	15.93	2.01

Table C3 Apatite fission track lengths for all samples analysed in this thesis

UBC	A2Z	Track	Angle				Dpar (μm)	UBC	A2Z	Track	Angle				Dpar (μm)
			Length (μm)	to c- axis	Lo calc (μm)	Lc calc (μm)					Length (μm)	to c- axis	Lo calc (μm)	Lc calc (μm)	
EX-29C-1783	117803	131	10.26	52.62	16.37	12.44	2.60	LBB76-576	94623	174	14.96	56.28	16.20	15.66	2.03
EX-29C-1783	117803	132	15.16	75.41	16.42	15.93	2.79	LBB76-576	94623	175	12.68	36.57	16.26	13.63	2.21
EX-29C-1783	117803	133	12.98	71.48	16.39	14.53	2.67	LBB76-576	94623	176	13.61	45.51	16.26	14.55	2.21
EX-29C-1783	117803	134	16.46	73.20	16.42	16.74	2.80	LBB76-576	94623	177	15.31	44.34	16.26	15.77	2.21
EX-29C-1783	117803	135	14.68	18.85	16.42	14.86	2.80	LBB76-576	94623	178	14.74	79.32	16.34	15.68	2.50
EX-29C-1783	117803	136	15.03	75.16	16.34	15.84	2.51	LBB76-576	94623	179	9.23	60.36	16.34	12.09	2.50
EX-29C-1783	117803	137	14.83	64.84	16.34	15.65	2.51	LBB76-576	94623	180	15.21	27.36	16.32	15.46	2.43
EX-29C-1783	117803	138	12.44	26.80	16.49	13.12	3.03	LBB76-576	94623	181	12.12	59.42	16.32	13.81	2.43
EX-29C-1783	117803	139	16.50	34.63	16.49	16.62	3.03	LBB76-576	94623	182	13.54	48.27	16.23	14.55	2.11
EX-29C-1783	117803	140	13.40	49.51	16.38	14.48	2.66	LBB76-576	94623	183	14.51	87.60	16.31	15.56	2.40
EX-29C-1783	117803	141	12.94	83.93	16.48	14.59	3.02	LBB76-576	94623	184	12.23	72.97	16.31	14.08	2.40
EX-29C-1783	117803	142	14.89	41.34	16.41	15.42	2.74	LBB76-576	94623	185	14.80	60.53	16.31	15.59	2.40
EX-29C-1783	117803	143	15.14	73.43	16.41	15.90	2.74	LBB76-576	94623	186	9.77	76.20	16.31	12.64	2.40
EX-29C-1783	117803	144	14.95	74.21	16.50	15.79	3.06	LBB76-576	94623	187	11.68	73.55	16.31	13.74	2.40
EX-29C-1783	117803	145	13.58	75.63	16.48	14.94	3.00	LBB76-576	94623	188	13.82	78.36	16.31	15.11	2.40
EX-29C-1783	117803	146	12.85	47.84	16.48	14.06	3.00	LBB76-576	94623	189	12.18	69.30	16.31	14.00	2.40
EX-29C-1783	117803	147	15.57	34.91	16.48	15.86	3.00	LBB76-576	94623	190	14.14	66.81	16.31	15.22	2.40
EX-29C-1783	117803	148	15.80	11.56	16.48	15.84	3.00	LBB76-576	94623	191	8.67	49.03	16.25	11.57	2.18
EX-29C-1783	117803	149	14.75	68.61	16.38	15.63	2.65	LBB76-576	94623	192	15.61	37.08	16.25	15.92	2.18
EX-29C-1783	117803	150	14.98	37.42	16.49	15.43	3.04	LBB76-576	94623	193	15.57	4.17	16.25	15.58	2.18
EX-29C-1783	117803	151	14.14	54.98	16.49	15.08	3.04	LBB76-576	94623	194	16.41	61.77	16.25	16.68	2.18
EX-29C-1783	117803	152	14.78	49.21	16.47	15.45	2.96	LBB76-576	94623	195	13.31	34.35	16.20	14.05	2.03
EX-29C-1783	117803	153	16.58	22.80	16.47	16.64	2.96	LBB76-576	94623	196	14.54	36.28	16.20	15.06	2.03
EX-29C-1783	117803	154	14.12	48.08	16.64	14.96	3.58	LBB76-576	94623	197	11.81	62.79	16.20	13.67	2.03
EX-29C-1783	117803	155	12.33	52.06	16.58	13.80	3.34	LBB76-576	94623	198	9.86	68.32	16.20	12.53	2.03
EX-29C-1783	117803	156	15.88	9.17	16.35	15.90	2.55	LBB76-576	94623	199	16.66	48.00	16.20	16.80	2.03
EX-29C-1783	117803	157	13.83	80.22	16.44	15.12	2.87	LBB76-576	94623	200	14.30	70.64	16.25	15.36	2.20
EX-29C-1783	117803	158	15.72	78.23	16.44	16.28	2.87	LBB76-576	94623	201	13.89	81.76	16.25	15.16	2.20
EX-29C-1783	117803	159	14.14	78.25	16.47	15.30	2.96	LBB76-576	94623	202	14.36	73.17	16.25	15.41	2.20
EX-29C-1783	117803	160	14.85	82.73	16.47	15.76	2.96	LBB76-576	94623	203	12.79	35.73	16.25	13.69	2.20
EX-29C-1783	117803	161	14.91	16.92	16.47	15.04	2.96	LBB76-762	94624	1	14.17	60.47	16.21	15.18	2.06
EX-29C-1783	117803	162	15.44	23.76	16.42	15.62	2.80	LBB76-762	94624	2	15.12	41.87	16.21	15.60	2.06
EX-29C-1783	117803	163	15.43	84.72	16.42	16.12	2.80	LBB76-762	94624	3	13.01	66.76	16.21	14.50	2.06
EX-29C-1783	117803	164	13.38	51.68	16.36	14.51	2.59	LBB76-762	94624	4	15.94	38.16	16.21	16.20	2.06
EX-29C-1783	117803	165	14.79	41.35	16.36	15.34	2.59	LBB76-762	94624	5	11.50	34.76	16.07	12.69	1.56
EX-29C-1783	117803	166	13.18	45.47	16.44	14.24	2.87	LBB76-762	94624	6	14.77	64.86	16.13	15.61	1.77
EX-29C-1783	117803	167	12.72	87.09	16.44	14.46	2.87	LBB76-762	94624	7	14.88	75.18	16.13	15.75	1.77
EX-29C-1783	117803	168	12.86	72.82	16.44	14.47	2.87	LBB76-762	94624	8	12.01	39.42	16.13	13.22	1.77
EX-29C-1783	117803	169	12.84	65.70	16.44	14.38	2.87	LBB76-762	94624	9	14.88	38.44	16.13	15.36	1.77
EX-29C-1783	117803	170	13.74	44.03	16.44	14.61	2.87	LBB76-762	94624	10	12.05	82.96	16.15	14.03	1.82
EX-29C-1783	117803	171	15.31	72.61	16.44	16.01	2.87	LBB76-762	94624	11	12.84	84.62	16.16	14.53	1.89
EX-29C-1783	117803	172	12.67	26.75	16.35	13.31	2.54	LBB76-762	94624	12	12.69	57.67	16.16	14.15	1.89
EX-29C-1783	117803	173	11.46	71.49	16.44	13.58	2.87	LBB76-762	94624	13	15.32	48.37	16.15	15.83	1.84
EX-29C-1783	117803	174	13.06	68.85	16.39	14.55	2.69	LBB76-762	94624	14	12.90	38.41	16.15	13.85	1.84
EX-29C-1783	117803	175	13.62	55.62	16.46	14.74	2.92	LBB76-762	94624	15	13.61	88.69	16.18	15.01	1.93
EX-29C-1783	117803	176	14.56	31.96	16.33	15.00	2.47	LBB76-762	94624	16	14.23	23.82	16.18	14.55	1.93
EX-29C-1783	117803	177	16.14	78.01	16.42	16.55	2.79	LBB76-762	94624	17	15.03	58.48	16.18	15.73	1.93
EX-29C-1783	117803	178	15.59	51.56	16.42	16.05	2.79	LBB76-762	94624	18	16.82	51.23	16.14	16.93	1.79
EX-29C-1783	117803	179	14.37	36.28	16.48	14.93	3.00	LBB76-762	94624	19	12.42	64.07	16.15	14.08	1.85
EX-29C-1783	117803	180	14.42	87.43	16.46	15.50	2.92	LBB76-762	94624	20	14.93	47.44	16.13	15.53	1.75
EX-29C-1783	117803	181	14.12	81.53	16.41	15.30	2.77	LBB76-762	94624	21	13.72	30.95	16.13	14.29	1.75
EX-29C-1783	117803	182	15.97	66.49	16.45	16.40	2.90	LBB76-762	94624	22	13.27	57.97	16.13	14.54	1.75
EX-29C-1783	117803	183	15.56	66.67	16.46	16.14	2.94	LBB76-762	94624	23	13.86	54.26	16.08	14.88	1.60
EX-29C-1783	117803	184	15.68	24.96	16.41	15.85	2.74	LBB76-762	94624	24	14.43	30.99	16.19	14.87	1.98
EX-29C-1783	117803	185	14.72	24.46	16.47	14.99	2.98	LBB76-762	94624	25	14.65	41.17	16.20	15.23	2.00
EX-29C-1783	117803	186	15.60	67.70	16.47	16.17	2.98	LBB76-762	94624	26	13.18	79.84	16.08	14.72	1.60
EX-29C-1783	117803	187	15.23	59.89	16.51	15.88	3.10	LBB76-762	94624	27	12.56	55.33	16.08	14.02	1.60
EX-29C-1783	117803	188	14.82	32.40	16.51	15.22	3.10	LBB76-762	94624	28	17.04	43.65	16.10	17.08	1.67
EX-29C-1783	117803	189	14.22	57.61	16.51	15.17	3.10	LBB76-762	94624	29	15.88	53.04	16.10	16.27	1.67
EX-29C-1783	117803	190	14.60	57.13	16.50	15.42	3.07	LBB76-762	94624	30	11.02	67.57	16.10	13.25	1.67
EX-29C-1783	117803	191	12.38	80.57	16.50	14.23	3.07	LBB76-762	94624	31	15.90	16.14	16.09	15.97	1.63

Table C3 Apatite fission track lengths for all samples analysed in this thesis

UBC	A2Z	Track	Angle				Dpar (μm)	UBC	A2Z	Track	Angle				Dpar (μm)
			Length (μm)	to c- axis	Lo calc (μm)	Lc calc (μm)					Length (μm)	to c- axis	Lo calc (μm)	Lc calc (μm)	
EX-29C-1783	117803	192	13.62	59.56	16.50	14.80	3.07	LBB76-762	94624	32	15.09	29.89	16.09	15.40	1.63
EX-29C-1783	117803	193	14.51	36.03	16.44	15.03	2.87	LBB76-762	94624	33	14.80	20.29	16.11	14.99	1.70
EX-29C-1783	117803	194	14.50	70.92	16.44	15.49	2.87	LBB76-762	94624	34	11.91	82.35	16.11	13.95	1.70
EX-29C-1783	117803	195	14.04	50.03	16.53	14.94	3.19	LBB76-762	94624	35	12.75	75.67	16.11	14.42	1.70
EX-29C-1783	117803	196	14.10	21.43	16.53	14.38	3.19	LBB76-762	94624	36	12.78	79.95	16.14	14.47	1.79
EX-29C-1783	117803	197	13.09	45.57	16.41	14.17	2.75	LBB76-762	94624	37	13.65	84.96	16.07	15.02	1.55
EX-29C-1783	117803	198	15.65	60.39	16.41	16.16	2.75	LBB76-762	94624	38	16.35	45.24	16.03	16.56	1.41
EX-29C-1783	117803	199	14.56	55.38	16.47	15.38	2.96	LBB76-762	94624	39	16.18	26.15	16.13	16.30	1.78
EX-29C-1783	117803	200	13.63	41.27	16.45	14.47	2.90	LBB76-762	94624	40	12.85	83.96	16.13	14.53	1.76
EX-29C-1783	117803	201	15.12	64.00	16.45	15.83	2.90	LBB76-762	94624	41	14.54	42.69	16.13	15.17	1.76
EX-29C-1783	117803	202	14.35	72.94	16.45	15.40	2.90	LBB76-762	94624	42	11.59	61.50	16.06	13.51	1.52
EX-29C-1783	117803	203	15.03	71.27	16.50	15.82	3.06	LBB76-762	94624	43	11.49	54.69	16.06	13.30	1.52
GA-34C-1280	107004	1	11.69	35.87	16.24	12.87	2.14	LBB76-762	94624	44	13.61	48.79	16.12	14.61	1.72
GA-34C-1280	107004	2	14.15	29.06	16.30	14.60	2.37	LBB76-762	94624	45	14.84	37.18	16.15	15.31	1.82
GA-34C-1280	107004	3	14.56	24.29	16.39	14.85	2.67	LBB76-762	94624	46	14.18	78.06	16.15	15.33	1.82
GA-34C-1280	107004	4	16.36	38.38	16.34	16.53	2.51	LBB76-762	94624	47	16.45	25.81	16.10	16.53	1.65
GA-34C-1280	107004	5	14.61	45.66	16.27	15.28	2.26	LBB76-762	94624	48	16.36	30.75	16.10	16.48	1.65
GA-34C-1280	107004	6	16.08	40.04	16.36	16.32	2.58	LBB76-762	94624	49	8.36	30.67	16.10	10.51	1.65
GA-34C-1280	107004	7	14.23	48.74	16.26	15.05	2.23	LBB76-762	94624	50	14.58	76.65	16.13	15.57	1.75
GA-34C-1280	107004	8	14.90	89.24	16.31	15.80	2.41	LBB76-762	94624	51	13.17	80.13	16.12	14.71	1.73
GA-34C-1280	107004	9	14.38	71.37	16.20	15.41	2.03	LBB76-762	94624	52	13.23	46.27	16.12	14.29	1.73
GA-34C-1280	107004	10	15.72	86.39	16.29	16.30	2.33	LBB76-762	94624	53	14.88	66.99	16.12	15.70	1.73
GA-34C-1280	107004	11	14.25	29.64	16.29	14.69	2.33	LBB76-762	94624	54	12.87	74.82	16.12	14.49	1.73
GA-34C-1280	107004	12	15.16	54.39	16.39	15.78	2.67	LBB76-762	94624	55	13.01	78.62	16.14	14.61	1.79
GA-34C-1280	107004	13	14.95	79.75	16.39	15.81	2.67	LBB76-762	94624	56	12.66	62.19	16.09	14.21	1.61
GA-34C-1280	107004	14	11.31	76.32	16.39	13.54	2.67	LBB76-762	94624	57	15.69	50.60	16.09	16.12	1.61
GA-34C-1280	107004	15	11.76	88.61	16.37	13.87	2.61	LBB76-762	94624	58	15.18	31.96	16.16	15.51	1.86
GA-34C-1280	107004	16	14.84	70.64	16.39	15.70	2.68	LBB76-762	94624	59	14.46	40.58	16.16	15.08	1.86
GA-34C-1280	107004	17	16.36	47.83	16.39	16.58	2.68	LBB76-762	94624	60	14.38	69.54	16.16	15.40	1.86
GA-34C-1280	107004	18	16.33	54.40	16.33	16.59	2.48	LBB76-762	94624	61	15.78	9.18	16.17	15.80	1.91
GA-34C-1280	107004	19	14.81	32.95	16.28	15.22	2.28	LBB76-762	94624	62	11.11	65.16	16.17	13.27	1.91
GA-34C-1280	107004	20	15.77	58.66	16.26	16.23	2.24	LBB76-762	94624	63	11.42	54.76	16.17	13.25	1.91
GA-34C-1280	107004	21	14.44	6.33	16.45	14.47	2.89	LBB76-762	94624	64	14.92	70.11	16.15	15.75	1.84
GA-34C-1280	107004	22	15.04	59.70	16.26	15.75	2.22	LBB76-762	94624	65	15.84	60.77	16.11	16.29	1.68
GA-34C-1280	107004	23	13.17	76.92	16.28	14.69	2.31	LBB76-762	94624	66	15.64	71.40	16.18	16.21	1.96
GA-34C-1280	107004	24	15.32	82.70	16.45	16.05	2.89	LBB76-762	94624	67	10.60	45.01	16.13	12.42	1.77
GA-34C-1280	107004	25	12.54	61.76	16.38	14.13	2.66	LBB76-762	94624	68	15.38	51.64	16.13	15.90	1.77
GA-34C-1280	107004	26	14.00	39.66	16.32	14.71	2.43	LBB76-762	94624	69	14.73	45.40	16.15	15.36	1.83
GA-34C-1280	107004	27	15.38	69.03	16.21	16.03	2.05	LBB76-762	94624	70	16.64	11.03	16.20	16.65	2.01
GA-34C-1280	107004	28	16.98	14.09	16.33	16.99	2.48	LBB76-762	94624	71	11.68	32.41	16.20	12.73	2.01
GA-34C-1280	107004	29	15.33	23.15	16.27	15.51	2.27	LBB76-762	94624	72	6.20	68.53	16.20	11.72	2.01
GA-34C-1280	107004	30	13.73	43.30	16.31	14.59	2.41	LBB76-762	94624	73	13.88	84.93	16.16	15.17	1.88
GA-34C-1280	107004	31	15.18	50.68	16.30	15.75	2.38	LBB76-762	94624	74	13.94	43.18	16.09	14.74	1.62
GA-34C-1280	107004	32	13.13	82.28	16.30	14.70	2.36	LBB76-762	94624	75	15.85	70.60	16.11	16.34	1.69
GA-34C-1280	107004	33	11.94	71.06	16.28	13.87	2.30	LBB76-762	94624	76	14.63	52.51	16.11	15.39	1.69
GA-34C-1280	107004	34	16.54	27.19	16.33	16.62	2.49	LBB76-762	94624	77	13.52	37.51	16.16	14.30	1.87
GA-34C-1280	107004	35	14.14	84.70	16.28	15.33	2.31	LBB76-762	94624	78	13.63	56.56	16.17	14.76	1.90
GA-34C-1280	107004	36	15.55	37.45	16.27	15.88	2.26	LBB76-762	94624	79	10.70	56.65	16.17	12.83	1.90
GA-34C-1280	107004	37	14.09	64.95	16.29	15.17	2.33	LBB76-762	94624	80	13.40	67.13	16.15	14.75	1.82
GA-34C-1280	107004	38	14.18	77.19	16.45	15.32	2.88	LBB76-762	94624	81	14.79	36.41	16.09	15.26	1.64
GA-34C-1280	107004	39	14.52	35.76	16.27	15.04	2.27	LBB76-762	94624	82	12.89	38.49	16.09	13.84	1.64
GA-34C-1280	107004	40	16.05	37.87	16.26	16.28	2.23	LBB76-762	94624	83	12.67	50.32	16.09	13.99	1.64
GA-34C-1280	107004	41	13.05	66.62	16.29	14.52	2.34	LBB76-762	94624	84	14.54	31.38	16.15	14.97	1.84
GA-34C-1280	107004	42	13.91	73.99	16.40	15.14	2.73	LBB76-762	94624	85	14.15	79.02	16.15	15.31	1.85
GA-34C-1280	107004	43	15.60	43.65	16.44	15.98	2.85	LBB76-762	94624	86	14.17	74.63	16.15	15.30	1.85
GA-34C-1280	107004	44	13.80	50.62	16.32	14.78	2.45	LBB76-762	94624	87	13.20	61.37	16.12	14.55	1.73
GA-34C-1280	107004	45	15.93	70.96	16.40	16.39	2.72	LBB76-762	94624	88	14.59	30.20	16.12	14.99	1.73
GA-34C-1280	107004	46	15.71	0.00	16.23	15.71	2.11	LBB76-762	94624	89	14.26	75.61	16.13	15.36	1.78
GA-34C-1280	107004	47	14.79	53.60	16.43	15.51	2.81	LBB76-762	94624	90	15.43	28.73	16.15	15.67	1.85
GA-34C-1280	107004	48	13.60	32.25	16.29	14.22	2.34	LBB76-762	94624	91	13.82	66.68	16.15	15.02	1.85
GA-34C-1280	107004	49	11.56	87.38	16.35	13.75	2.53	LBB76-762	94624	92	14.50	41.22	16.15	15.12	1.85

Table C3 Apatite fission track lengths for all samples analysed in this thesis

UBC	A2Z	Track	Angle				Dpar		UBC	A2Z	Track	Angle				Dpar
			Length (μm)	to c- axis	Lo calc (μm)	Lc calc (μm)						Length (μm)	to c- axis	Lo calc (μm)	Lc calc (μm)	
GA-34C-1280	107004	50	14.12	28.86	16.37	14.57	2.62		LBB76-762	94624	93	14.06	52.73	16.17	14.99	1.92
GA-34C-1280	107004	51	11.35	56.41	16.19	13.25	1.99		LBB76-762	94624	94	12.56	69.79	16.09	14.25	1.64
GA-34C-1280	107004	52	13.03	65.27	16.39	14.49	2.69		LBB76-762	94624	95	13.86	20.14	16.09	14.14	1.64
GA-34C-1280	107004	53	17.21	55.93	16.43	17.21	2.84		LBB76-762	94624	96	14.87	41.43	16.09	15.40	1.64
GA-34C-1280	107004	54	13.96	59.67	16.41	15.03	2.75		LBB76-762	94624	97	13.88	54.94	16.13	14.91	1.77
GA-34C-1280	107004	55	14.48	55.23	16.39	15.32	2.67		LBB76-762	94624	98	14.48	50.54	16.13	15.25	1.77
GA-34C-1280	107004	56	13.99	56.96	16.31	15.01	2.41		LBB76-762	94624	99	15.09	36.98	16.16	15.51	1.87
GA-34C-1280	107004	57	13.13	88.72	16.25	14.71	2.19		LBB76-762	94624	100	14.42	63.56	16.17	15.37	1.92
GA-34C-1280	107004	58	15.01	66.36	16.32	15.78	2.43		LBB76-762	94624	101	14.85	72.79	16.25	15.72	2.18
GA-34C-1280	107004	59	13.52	80.95	16.32	14.93	2.43		LBB76-762	94624	102	12.66	74.69	16.25	14.36	2.18
GA-34C-1280	107004	60	15.35	27.52	16.31	15.59	2.42		LBB76-762	94624	103	14.07	47.89	16.25	14.92	2.18
GA-34C-1280	107004	61	14.30	84.42	16.17	15.42	1.91		LBB76-762	94624	104	16.86	52.41	16.25	16.96	2.18
GA-34C-1280	107004	62	13.67	69.88	16.37	14.95	2.61		LBB76-762	94624	105	14.31	57.11	16.25	15.23	2.18
GA-34C-1280	107004	63	15.60	58.13	16.32	16.11	2.44		LBB76-762	94624	106	14.56	22.52	16.18	14.82	1.94
GA-34C-1280	107004	64	15.09	34.95	16.39	15.48	2.69		LBB76-762	94624	107	14.49	78.80	16.18	15.52	1.94
GA-34C-1280	107004	65	12.27	53.45	16.37	13.79	2.63		LBB76-762	94624	108	14.92	41.81	16.18	15.45	1.94
GA-34C-1280	107004	66	15.16	10.88	16.37	15.21	2.63		LBB76-762	94624	109	14.42	77.75	16.18	15.47	1.94
GA-34C-1280	107004	67	13.78	31.35	16.37	14.35	2.63		LBB76-762	94624	110	14.40	60.48	16.10	15.33	1.67
GA-34C-1280	107004	68	14.57	53.87	16.35	15.36	2.53		LBB76-762	94624	111	12.85	60.35	16.10	14.30	1.67
GA-34C-1280	107004	69	13.92	73.97	16.41	15.14	2.75		LBB76-762	94624	112	16.24	48.87	16.12	16.50	1.73
GA-34C-1280	107004	70	14.27	64.74	16.38	15.29	2.66		LBB76-762	94624	113	13.55	74.82	16.18	14.92	1.94
GA-34C-1280	107004	71	15.20	87.28	16.33	15.98	2.47		LBB76-762	94624	114	12.51	75.78	16.18	14.27	1.94
GA-34C-1280	107004	72	14.62	61.55	16.32	15.48	2.45		LBB76-762	94624	115	14.49	72.04	16.18	15.49	1.94
GA-34C-1280	107004	73	14.35	62.44	16.38	15.32	2.65		LBB76-762	94624	116	10.86	62.25	16.13	13.05	1.78
GA-34C-1280	107004	74	16.16	45.27	16.34	16.42	2.51		LBB76-762	94624	117	13.11	71.90	16.13	14.62	1.78
GA-34C-1280	107004	75	14.39	9.16	16.37	14.44	2.60		LBB76-762	94624	118	14.19	70.72	16.13	15.29	1.78
GA-34C-1280	107004	76	14.55	78.69	16.30	15.56	2.35		LBB76-762	94624	119	15.62	44.60	16.19	16.01	1.98
GA-34C-1280	107004	77	14.47	66.56	16.30	15.43	2.35		LBB76-762	94624	120	13.32	28.60	16.13	13.90	1.76
GA-34C-1280	107004	78	9.65	76.01	16.38	12.61	2.66		LBB76-762	94624	121	11.37	60.88	16.13	13.35	1.76
GA-34C-1280	107004	79	14.60	85.05	16.36	15.61	2.57		LBB76-762	94624	122	14.04	45.67	16.13	14.86	1.76
GA-34C-1280	107004	80	16.68	81.50	16.32	16.88	2.43		LBB76-762	94624	123	13.35	45.82	16.09	14.37	1.62
GA-34C-1280	107004	81	16.21	21.58	16.26	16.29	2.24		LBB76-762	94624	124	13.79	88.51	16.09	15.12	1.62
GA-34C-1280	107004	82	14.00	72.86	16.41	15.18	2.76		LBB76-762	94624	125	15.66	21.96	16.09	15.80	1.62
GA-34C-1280	107004	83	15.70	70.01	16.33	16.24	2.49		LBB76-762	94624	126	14.44	1.54	16.21	14.44	2.06
GA-34C-1280	107004	84	14.17	77.06	16.28	15.32	2.31		LBB76-762	94624	127	15.10	45.66	16.21	15.63	2.06
GA-34C-1280	107004	85	13.75	47.99	16.43	14.70	2.82		LBB76-762	94624	128	14.25	83.86	16.21	15.39	2.06
GA-34C-1280	107004	86	15.31	67.52	16.24	15.98	2.15		LBB76-762	94624	129	14.62	43.66	16.11	15.25	1.69
GA-34C-1280	107004	87	14.53	35.48	16.50	15.04	3.06		LBB76-762	94624	130	11.41	73.56	16.20	13.57	2.00
GA-34C-1280	107004	88	15.74	86.76	16.45	16.31	2.88		LBB76-762	94624	131	16.84	42.39	16.11	16.92	1.70
GA-34C-1280	107004	89	14.07	67.26	16.37	15.18	2.63		LBB76-762	94624	132	15.10	47.65	16.14	15.66	1.79
GA-34C-1280	107004	90	15.62	7.76	16.37	15.64	2.63		LBB76-762	94624	133	13.97	76.31	16.14	15.19	1.79
GA-34C-1280	107004	91	15.29	17.54	16.36	15.41	2.58		LBB76-762	94624	134	16.78	13.90	16.16	16.80	1.87
GA-34C-1280	107004	92	14.84	63.13	16.37	15.64	2.62		LBB76-762	94624	135	15.20	72.60	16.16	15.94	1.87
GA-34C-1280	107004	93	15.32	81.48	16.35	16.04	2.53		LBB76-762	94624	136	16.01	39.79	16.16	16.26	1.87
GA-34C-1280	107004	94	14.00	72.69	16.31	15.18	2.40		LBB76-762	94624	137	14.22	71.76	16.16	15.31	1.87
GA-34C-1280	107004	95	15.35	29.12	16.36	15.61	2.59		LBB76-762	94624	138	13.56	85.85	16.16	14.97	1.87
GA-34C-1280	107004	96	15.05	56.21	16.30	15.72	2.37		LBB76-762	94624	139	15.15	74.90	16.16	15.92	1.87
GA-34C-1280	107004	97	16.09	43.46	16.35	16.35	2.56		LBB76-762	94624	140	13.36	81.95	16.16	14.84	1.87
GA-34C-1280	107004	98	13.88	76.07	16.29	15.13	2.32		LBB76-762	94624	141	14.36	24.26	16.24	14.67	2.15
GA-34C-1280	107004	99	14.24	55.88	16.28	15.16	2.31		LBB76-762	94624	142	16.00	74.21	16.07	16.45	1.57
GA-34C-1280	107004	100	14.71	54.65	16.26	15.47	2.24		LBB76-762	94624	143	18.34	36.15	16.07	18.14	1.57
GA-34C-1280	107004	101	14.86	79.42	16.34	15.75	2.50		LBB76-762	94624	144	13.89	75.07	16.18	15.13	1.96
GA-34C-1280	107004	102	14.23	87.83	16.30	15.38	2.36		LBB76-762	94624	145	15.88	81.97	16.18	16.39	1.96
GA-34C-1280	107004	103	15.56	55.11	16.42	16.06	2.79		LBB76-762	94624	146	14.81	59.32	16.15	15.59	1.82
GA-34C-1280	107004	104	14.69	70.21	16.30	15.60	2.35		LBB76-762	94624	147	13.73	64.24	16.15	14.93	1.82
GA-34C-1280	107004	105	16.55	52.26	16.27	16.74	2.26		LBB76-762	94624	148	14.33	86.00	16.15	15.44	1.83
GA-34C-1280	107004	106	15.59	59.43	16.31	16.11	2.40		LBB76-762	94624	149	13.12	50.85	16.16	14.31	1.88
GA-34C-1280	107004	107	12.26	86.04	16.37	14.17	2.61		LBB76-762	94624	150	12.92	62.11	16.14	14.38	1.80
GA-34C-1280	107004	108	14.09	55.99	16.32	15.06	2.43		LBB76-762	94624	151	14.60	38.40	16.13	15.15	1.78
GA-34C-1280	107004	109	15.39	30.55	16.39	15.66	2.68		LBB76-762	94624	152	15.27	50.44	16.07	15.81	1.57
GA-34C-1280	107004	110	15.34	12.89	16.35	15.40	2.55		LBB76-762	94624	153	13.37	69.78	16.09	14.76	1.63

Table C3 Apatite fission track lengths for all samples analysed in this thesis

UBC	A2Z	Track	Angle				Dpar		UBC	A2Z	Track	Angle				Dpar
			Length (μm)	to c- axis	Lo calc (μm)	Lc calc (μm)						Length (μm)	to c- axis	Lo calc (μm)	Lc calc (μm)	
GA-34C-1280	107004	111	15.09	40.44	16.35	15.56	2.55		LBB76-762	94624	154	16.71	33.26	16.15	16.79	1.83
GA-34C-1280	107004	112	15.08	53.39	16.34	15.71	2.52		LBB76-762	94624	155	11.46	46.77	16.12	13.07	1.72
GA-34C-1280	107004	113	15.66	73.99	16.34	16.23	2.52		LBB76-762	94624	156	14.36	72.12	16.10	15.41	1.65
GA-34C-1280	107004	114	13.91	59.87	16.36	15.00	2.57		LBB76-762	94624	157	14.70	40.70	16.13	15.26	1.75
GA-34C-1280	107004	115	16.50	82.58	16.25	16.77	2.20		LBB76-762	94624	158	15.47	41.16	16.13	15.86	1.75
GA-34C-1280	107004	116	16.10	29.14	16.31	16.25	2.39		LBB76-762	94624	159	13.64	53.95	16.16	14.73	1.89
GA-35C-1265	104909	1	13.05	70.95	16.20	14.57	2.02		LBB76-762	94624	160	14.92	69.86	16.11	15.75	1.69
GA-35C-1265	104909	2	10.24	49.33	16.22	12.33	2.10		LBB76-762	94624	161	15.29	78.71	16.07	16.02	1.54
GA-35C-1265	104909	3	13.15	84.88	16.14	14.72	1.79		LBB76-762	94624	162	12.90	78.27	16.07	14.53	1.54
GA-35C-1265	104909	4	15.27	51.97	16.21	15.83	2.05		LBB76-762	94624	163	14.94	56.09	16.15	15.64	1.83
GA-35C-1265	104909	5	10.59	58.01	16.21	12.79	2.05		LBB76-762	94624	164	14.47	68.88	16.16	15.45	1.86
GA-35C-1265	104909	6	13.78	42.86	16.16	14.61	1.89		LBB76-762	94624	165	15.41	56.90	16.09	15.97	1.61
GA-35C-1265	104909	7	12.59	35.16	16.20	13.52	2.00		LBB76-762	94624	166	14.90	67.37	16.08	15.72	1.59
GA-35C-1265	104909	8	12.35	77.15	16.14	14.19	1.80		LBB76-762	94624	167	14.29	82.45	16.08	15.41	1.59
GA-35C-1265	104909	9	13.52	81.58	16.14	14.93	1.80		LBB76-762	94624	168	14.83	59.69	16.08	15.61	1.59
GA-35C-1265	104909	10	14.54	84.35	16.14	15.57	1.79		LBB76-762	94624	169	16.30	47.83	16.16	16.54	1.86
GA-35C-1265	104909	11	14.87	46.47	16.21	15.48	2.04		LBB76-762	94624	170	14.52	66.21	16.13	15.46	1.76
GA-35C-1265	104909	12	14.59	40.63	16.21	15.18	2.04		LBB76-762	94624	171	15.59	45.59	16.18	16.00	1.93
GA-35C-1265	104909	13	15.67	86.79	16.24	16.27	2.17		LBB76-762	94624	172	14.71	65.12	16.18	15.58	1.93
GA-35C-1265	104909	14	12.62	76.77	16.23	14.35	2.12		LBB76-762	94624	173	11.61	16.49	16.17	12.02	1.91
GA-35C-1265	104909	15	12.17	76.53	16.13	14.07	1.76		LBB76-762	94624	174	14.61	55.87	16.17	15.42	1.91
GA-35C-1265	104909	16	16.32	37.95	16.24	16.50	2.17		LBB76-762	94624	175	15.04	49.25	16.17	15.64	1.90
GA-35C-1265	104909	17	14.46	20.36	16.14	14.68	1.80		LBB76-762	94624	176	14.08	52.50	16.17	15.01	1.90
GA-35C-1265	104909	18	12.62	81.96	16.24	14.38	2.15		LBB76-762	94624	177	12.14	69.02	16.17	13.97	1.90
GA-35C-1265	104909	19	15.26	23.82	16.24	15.46	2.15		LBB76-762	94624	178	14.96	40.02	16.10	15.45	1.67
GA-35C-1265	104909	20	13.64	65.35	16.24	14.89	2.15		LBB76-762	94624	179	14.19	59.00	16.10	15.17	1.67
GA-35C-1265	104909	21	13.12	65.80	16.24	14.56	2.15		LBB76-762	94624	180	14.48	31.28	16.12	14.92	1.74
GA-35C-1265	104909	22	12.83	59.64	16.21	14.28	2.04		LBB76-762	94624	181	12.95	44.40	16.12	14.05	1.74
GA-35C-1265	104909	23	15.87	20.65	16.21	15.97	2.04		LBB76-762	94624	182	14.40	30.42	16.12	14.83	1.74
GA-35C-1265	104909	24	14.70	38.45	16.21	15.22	2.04		LBB76-762	94624	183	14.87	36.38	16.12	15.32	1.74
GA-35C-1265	104909	25	14.81	67.86	16.19	15.66	1.97		LBB76-762	94624	184	10.28	31.65	16.09	11.67	1.61
GA-35C-1265	104909	26	15.23	27.54	16.22	15.48	2.08		LBB76-762	94624	185	13.93	33.61	16.09	14.52	1.61
GA-35C-1265	104909	27	13.66	89.43	16.22	15.04	2.08		LBB76-762	94624	186	14.36	67.53	16.16	15.37	1.87
GA-35C-1265	104909	28	13.95	48.88	16.26	14.85	2.24		LBB76-762	94624	187	14.73	35.62	16.15	15.20	1.82
GA-35C-1265	104909	29	16.10	55.69	16.26	16.44	2.24		LBB76-762	94624	188	15.32	76.81	16.14	16.03	1.81
GA-35C-1265	104909	30	12.44	64.88	16.26	14.11	2.24		LBB76-762	94624	189	14.53	45.62	16.14	15.22	1.81
GA-35C-1265	104909	31	13.28	67.90	16.24	14.68	2.16		LBB76-762	94624	190	14.94	54.27	16.08	15.62	1.60
GA-35C-1265	104909	32	14.78	55.45	16.26	15.53	2.21		LBB76-762	94624	191	14.63	68.72	16.08	15.55	1.60
GA-35C-1265	104909	33	15.04	55.08	16.22	15.70	2.09		LBB76-762	94624	192	14.99	61.60	16.08	15.73	1.60
GA-35C-1265	104909	34	14.45	22.77	16.23	14.72	2.11		LBB76-762	94624	193	9.82	74.18	16.11	12.61	1.69
GA-35C-1265	104909	35	14.21	12.11	16.23	14.31	2.11		LBB76-762	94624	194	17.57	63.67	16.11	17.45	1.69
GA-35C-1265	104909	36	13.89	59.88	16.18	14.98	1.94		LBB76-762	94624	195	15.35	67.98	16.12	16.01	1.73
GA-35C-1265	104909	37	13.50	57.90	16.16	14.70	1.88		LBB76-762	94624	196	14.41	35.86	16.13	14.95	1.78
GA-35C-1265	104909	38	14.33	78.17	16.26	15.42	2.23		LBB76-762	94624	197	13.91	31.01	16.13	14.44	1.78
GA-35C-1265	104909	39	14.45	48.54	16.26	15.20	2.23		LBB76-762	94624	198	14.92	53.63	16.10	15.60	1.67
GA-35C-1265	104909	40	14.53	47.43	16.26	15.24	2.23		LBB76-762	94624	199	13.51	74.49	16.10	14.89	1.67
GA-35C-1265	104909	41	14.47	80.15	16.18	15.51	1.94		LBB76-762	94624	200	12.45	53.10	16.12	13.90	1.73
GA-35C-1265	104909	42	11.37	41.30	16.16	12.83	1.88		LBB76-762	94624	201	15.80	57.27	16.12	16.24	1.73
GA-35C-1265	104909	43	11.89	74.51	16.19	13.88	1.97		LBB76-762	94624	202	14.09	58.84	16.12	15.10	1.73
GA-35C-1265	104909	44	12.90	82.16	16.19	14.55	1.97		LBB76-762	94624	203	14.24	38.73	16.12	14.87	1.73
GA-35C-1265	104909	45	13.74	88.48	16.19	15.08	1.97		RM91-11C-225	107008	1	12.68	66.64	16.34	14.29	2.50
GA-35C-1265	104909	46	13.13	62.02	16.19	14.51	1.97		RM91-11C-225	107008	2	15.58	57.66	16.28	16.09	2.30
GA-35C-1265	104909	47	12.76	62.37	16.23	14.28	2.13		RM91-11C-225	107008	3	10.09	50.34	16.25	12.26	2.19
GA-35C-1265	104909	48	14.49	54.85	16.18	15.32	1.94		RM91-11C-225	107008	4	15.33	57.71	16.25	15.92	2.19
GA-35C-1265	104909	49	13.42	69.45	16.18	14.79	1.94		RM91-11C-225	107008	5	8.97	45.57	16.18	11.46	1.96
GA-35C-1265	104909	50	13.60	72.47	16.18	14.93	1.95		RM91-11C-225	107008	6	15.91	46.00	16.15	16.24	1.84
GA-35C-1265	104909	51	14.24	56.96	16.14	15.18	1.79		RM91-11C-225	107008	7	14.07	39.02	16.22	14.75	2.08
GA-35C-1265	104909	52	13.78	52.82	16.21	14.80	2.05		RM91-11C-225	107008	8	12.02	45.88	16.18	13.43	1.93
GA-35C-1265	104909	53	13.52	36.59	16.21	14.27	2.05		RM91-11C-225	107008	9	13.67	71.14	16.18	14.96	1.93
GA-35C-1265	104909	54	12.91	52.47	16.13	14.20	1.76		RM91-11C-225	107008	10	9.58	35.52	16.23	11.36	2.13
GA-35C-1265	104909	55	14.42	55.67	16.13	15.28	1.76		RM91-11C-225	107008	11	10.43	13.71	16.20	10.86	2.00

Table C3 Apatite fission track lengths for all samples analysed in this thesis

UBC	A2Z	Track	Angle				Dpar	UBC	A2Z	Track	Angle				Dpar
			Length (μm)	to c- axis	Lo calc (μm)	Lc calc (μm)					Length (μm)	to c- axis	Lo calc (μm)	Lc calc (μm)	
GA-35C-1265	104909	56	14.01	71.20	16.21	15.18	2.05	RM91-11C-225	107008	12	16.67	40.28	16.14	16.78	1.80
GA-35C-1265	104909	57	13.36	83.66	16.24	14.84	2.17	RM91-11C-225	107008	13	15.87	31.51	16.19	16.08	1.98
GA-35C-1265	104909	58	14.65	38.27	16.24	15.18	2.17	RM91-11C-225	107008	14	14.94	83.46	16.19	15.81	1.98
GA-35C-1265	104909	59	14.81	76.27	16.14	15.71	1.81	RM91-11C-225	107008	15	12.85	59.34	16.22	14.29	2.07
GA-35C-1265	104909	60	15.47	10.12	16.14	15.51	1.81	RM91-11C-225	107008	16	17.07	78.01	16.29	17.12	2.34
GA-35C-1265	104909	61	14.28	67.25	16.20	15.32	2.01	RM91-11C-225	107008	17	12.20	24.61	16.29	12.84	2.34
GA-35C-1265	104909	62	14.51	61.91	16.15	15.42	1.83	RM91-11C-225	107008	18	15.22	79.28	16.19	15.98	1.99
GA-35C-1265	104909	63	13.88	83.36	16.14	15.16	1.79	RM91-11C-225	107008	19	14.41	53.23	16.13	15.24	1.77
GA-35C-1265	104909	64	10.43	39.30	16.14	12.10	1.79	RM91-11C-225	107008	20	14.95	56.24	16.33	15.65	2.46
GA-35C-1265	104909	65	14.17	62.20	16.18	15.20	1.93	RM91-11C-225	107008	21	9.25	23.00	16.19	10.47	1.98
GA-35C-1265	104909	66	14.42	71.08	16.22	15.44	2.10	RM91-11C-225	107008	22	15.82	67.28	16.23	16.31	2.13
GA-35C-1265	104909	67	14.40	73.33	16.21	15.44	2.06	RM91-11C-225	107008	23	15.01	43.32	16.15	15.54	1.84
GA-35C-1265	104909	68	14.47	33.69	16.21	14.96	2.06	RM91-11C-225	107008	24	14.76	47.47	16.19	15.41	1.98
GA-35C-1265	104909	69	14.51	74.63	16.21	15.52	2.06	RM91-11C-225	107008	25	14.90	42.49	16.17	15.44	1.91
GA-35C-1265	104909	70	16.34	18.59	16.21	16.40	2.06	RM91-11C-225	107008	26	14.83	42.86	16.16	15.40	1.86
GA-35C-1265	104909	71	14.86	31.08	16.21	15.23	2.06	RM91-11C-225	107008	27	13.20	41.96	16.21	14.17	2.05
GA-35C-1265	104909	72	14.60	64.18	16.21	15.50	2.06	RM91-11C-225	107008	28	8.35	70.63	16.26	12.20	2.23
GA-35C-1265	104909	73	13.70	49.11	16.21	14.68	2.06	RM91-11C-225	107008	29	11.41	54.37	16.26	13.24	2.23
GA-35C-1265	104909	74	13.12	63.48	16.21	14.53	2.06	RM91-11C-225	107008	30	10.21	44.43	16.28	12.14	2.30
GA-35C-1265	104909	75	15.13	70.39	16.21	15.88	2.06	RM91-11C-225	107008	31	14.14	76.79	16.20	15.30	2.03
GA-35C-1265	104909	76	12.38	69.75	16.22	14.13	2.09	RM91-11C-225	107008	32	15.40	69.88	16.20	16.05	2.03
GA-35C-1265	104909	77	13.96	75.75	16.15	15.18	1.84	RM91-11C-225	107008	33	15.94	51.17	16.16	16.30	1.87
GA-35C-1265	104909	78	10.68	61.16	16.26	12.92	2.21	RM91-11C-225	107008	34	15.50	57.00	16.24	16.03	2.15
GA-35C-1265	104909	79	13.63	67.73	16.14	14.91	1.80	RM91-11C-225	107008	35	12.46	21.35	16.24	12.94	2.15
GA-35C-1265	104909	80	13.80	30.46	16.21	14.34	2.05	RM91-11C-225	107008	36	5.10	53.53	16.28	11.12	2.30
GA-35C-1265	104909	81	9.48	79.39	16.21	12.63	2.05	RM91-11C-225	107008	37	14.78	59.56	16.24	15.57	2.17
GA-35C-1265	104909	82	14.45	71.49	16.10	15.46	1.65	RM91-11C-225	107008	38	13.03	57.06	16.24	14.37	2.17
GA-35C-1265	104909	83	15.00	77.80	16.10	15.84	1.65	RM91-11C-225	107008	39	15.05	59.43	16.25	15.75	2.18
GA-35C-1265	104909	84	15.53	84.86	16.13	16.18	1.78	RM91-11C-225	107008	40	14.11	67.96	16.31	15.21	2.39
GA-35C-1265	104909	85	16.27	25.98	16.28	16.38	2.28	RM91-11C-225	107008	41	14.34	49.96	16.23	15.15	2.13
GA-35C-1265	104909	86	12.41	86.72	16.28	14.27	2.28	RM91-11C-225	107008	42	13.96	42.77	16.17	14.74	1.91
GA-35C-1265	104909	87	14.46	57.29	16.31	15.33	2.40	RM91-11C-225	107008	43	10.41	69.64	16.19	12.90	1.99
GA-35C-1265	104909	88	13.81	61.72	16.31	14.95	2.40	RM91-11C-225	107008	44	10.62	44.43	16.19	12.42	1.99
GA-35C-1265	104909	89	16.11	66.56	16.12	16.49	1.73	RM91-11C-225	107008	45	9.90	82.52	16.19	12.79	1.99
GA-35C-1265	104909	90	13.63	41.99	16.12	14.48	1.73	RM91-11C-225	107008	46	15.82	33.77	16.19	16.06	1.99
GA-35C-1265	104909	91	13.65	48.68	16.12	14.64	1.73	RM91-11C-225	107008	47	10.80	65.37	16.19	13.07	1.99
GA-35C-1265	104909	92	13.54	84.70	16.12	14.96	1.73	RM91-11C-225	107008	48	16.72	82.34	16.26	16.91	2.21
GA-35C-1265	104909	93	10.66	62.07	16.22	12.92	2.08	RM91-11C-225	107008	49	16.32	73.55	16.19	16.65	1.97
GA-35C-1265	104909	94	14.23	28.07	16.20	14.64	2.01	RM91-11C-225	107008	50	15.97	50.01	16.32	16.31	2.43
GA-35C-1265	104909	95	14.57	80.56	16.22	15.58	2.10	RM91-11C-225	107008	51	18.25	40.53	16.28	18.04	2.30
GA-35C-1265	104909	96	14.55	60.60	16.22	15.43	2.10	RM91-11C-225	107008	52	14.41	41.88	16.22	15.06	2.07
GA-35C-1265	104909	97	14.41	79.26	16.22	15.47	2.10	RM91-11C-225	107008	53	12.96	63.73	16.26	14.43	2.23
GA-35C-1265	104909	98	13.29	57.35	16.26	14.55	2.23	RM91-11C-225	107008	54	13.63	49.02	16.28	14.63	2.28
GA-35C-1265	104909	99	15.11	56.17	16.26	15.76	2.21	RM91-11C-225	107008	55	11.09	29.35	16.20	12.16	2.02
GA-35C-1265	104909	100	16.25	3.89	16.26	16.25	2.21	RM91-11C-225	107008	56	14.16	80.16	16.13	15.32	1.76
GA-35C-1265	104909	101	13.95	54.22	16.15	14.94	1.82	RM91-11C-225	107008	57	8.17	79.42	16.20	12.33	2.03
GA-35C-1265	104909	102	13.59	57.85	16.11	14.75	1.68	RM91-11C-225	107008	58	14.64	73.23	16.16	15.59	1.89
GA-35C-1265	104909	103	14.75	25.68	16.11	15.04	1.68	RM91-11C-225	107008	59	15.34	14.30	16.21	15.42	2.04
GA-35C-1265	104909	104	16.56	78.33	16.17	16.81	1.92	RM91-11C-225	107008	60	14.10	82.76	16.20	15.30	2.01
GA-35C-1265	104909	105	12.68	74.91	16.17	14.37	1.92	RM91-11C-225	107008	61	9.54	85.71	16.27	12.73	2.27
GA-35C-1265	104909	106	14.46	52.14	16.23	15.26	2.13	RM91-11C-225	107008	62	13.55	46.21	16.23	14.52	2.12
GA-35C-1265	104909	107	11.27	82.30	16.23	13.55	2.13	RM91-11C-225	107008	63	14.60	30.38	16.22	15.00	2.08
GA-35C-1265	104909	108	14.63	12.63	16.20	14.72	2.03	RM91-11C-225	107008	64	14.74	58.66	16.32	15.54	2.43
GA-35C-1265	104909	109	11.82	72.19	16.20	13.81	2.03	RM91-11C-225	107008	65	15.72	20.96	16.25	15.84	2.20
GA-35C-1265	104909	110	13.07	86.18	16.20	14.67	2.01	RM91-11C-225	107008	66	15.37	42.57	16.26	15.80	2.23
GA-35C-1265	104909	111	14.31	45.81	16.18	15.06	1.96	RM91-11C-225	107008	67	15.10	15.08	16.17	15.20	1.92
GA-35C-1265	104909	112	13.30	46.71	16.18	14.35	1.96	RM91-11C-225	107008	68	11.07	39.99	16.17	12.57	1.92
GA-35C-1265	104909	113	14.97	84.14	16.25	15.83	2.20	RM91-11C-225	107008	69	14.45	47.76	16.23	15.19	2.13
GA-35C-1265	104909	114	13.58	65.02	16.25	14.84	2.20	RM91-11C-225	107008	70	14.63	62.21	16.23	15.50	2.13
GA-35C-1265	104909	115	15.33	59.67	16.28	15.94	2.30	RM91-11C-225	107008	71	15.08	46.99	16.34	15.64	2.51
GA-35C-1265	104909	116	14.49	51.35	16.21	15.27	2.06	RM91-11C-225	107008	72	14.36	36.42	16.28	14.92	2.28

Table C3 Apatite fission track lengths for all samples analysed in this thesis

UBC	A2Z	Track	Angle					UBC	A2Z	Track	Angle				
			Length (μm)	to c- axis	Lo calc (μm)	Lc calc (μm)	Dpar (μm)				Length (μm)	to c- axis	Lo calc (μm)	Lc calc (μm)	Dpar (μm)
GA-35C-1265	104909	117	13.34	59.57	16.23	14.61	2.12	RM91-11C-225	107008	73	14.94	49.00	16.30	15.56	2.35
GA-35C-1265	104909	118	12.17	47.04	16.23	13.56	2.12	RM91-11C-225	107008	74	15.35	36.23	16.24	15.70	2.15
GA-35C-1265	104909	119	15.33	81.75	16.23	16.05	2.12	RM91-11C-225	107008	75	11.23	17.63	16.24	11.74	2.15
GA-35C-1265	104909	120	14.34	72.99	16.22	15.40	2.07	RM91-11C-225	107008	76	8.06	55.09	16.23	11.71	2.13
GA-35C-1265	104909	121	14.73	85.57	16.32	15.69	2.43	RM91-11C-225	107008	77	10.54	27.89	16.30	11.68	2.38
GA-35C-1265	104909	122	13.90	85.78	16.32	15.18	2.43	RM91-11C-225	107008	78	13.85	61.54	16.20	14.98	2.00
GA-35C-1265	104909	123	15.46	27.27	16.32	15.68	2.43	RM91-11C-225	107008	79	15.03	80.12	16.14	15.86	1.80
GA-35C-1265	104909	124	14.10	79.57	16.24	15.28	2.17	RM91-11C-225	107008	80	16.57	61.51	16.22	16.78	2.09
GA-35C-1265	104909	125	14.35	87.49	16.24	15.46	2.17	RM91-11C-225	107008	81	16.32	52.55	16.22	16.58	2.09
GA-35C-1265	104909	126	14.39	57.85	16.24	15.29	2.17	RM91-11C-225	107008	82	14.68	42.99	16.22	15.28	2.09
GA-35C-1265	104909	127	13.70	61.88	16.24	14.88	2.17	RM91-11C-225	107008	83	12.10	37.81	16.23	13.24	2.11
GA-35C-1265	104909	128	14.48	35.52	16.15	15.00	1.84	RM91-11C-225	107008	84	13.06	17.16	16.23	13.34	2.11
GA-35C-1265	104909	129	14.30	79.21	16.15	15.41	1.84	RM91-11C-225	107008	85	13.26	87.79	16.17	14.79	1.92
GA-35C-1265	104909	130	14.07	85.87	16.15	15.28	1.84	RM91-11C-225	107008	86	12.36	79.31	16.20	14.21	2.02
GA-35C-1265	104909	131	14.60	52.59	16.19	15.37	1.99	RM91-11C-225	107008	87	12.03	8.50	16.30	12.14	2.35
GA-35C-1265	104909	132	14.15	73.11	16.19	15.28	1.99	RM91-11C-225	107008	88	15.81	50.93	16.30	16.20	2.35
GA-35C-1265	104909	133	15.31	9.27	16.17	15.34	1.90	RM91-11C-225	107008	89	14.25	57.58	16.30	15.19	2.35
GA-35C-1265	104909	134	15.60	25.26	16.25	15.78	2.18	RM91-11C-225	107008	90	9.87	44.23	16.20	11.91	2.00
GA-35C-1265	104909	135	11.29	40.28	16.25	12.74	2.18	RM91-11C-225	107008	91	16.38	61.94	16.20	16.66	2.00
GA-35C-1265	104909	136	15.65	23.83	16.22	15.81	2.07	RM91-11C-225	107008	92	8.96	31.92	16.08	10.77	1.58
GA-35C-1265	104909	137	13.62	65.11	16.22	14.87	2.07	RM91-11C-225	107008	93	15.83	45.73	16.13	16.18	1.76
GA-35C-1265	104909	138	15.61	13.04	16.22	15.66	2.07	RM91-11C-225	107008	94	8.07	70.21	16.13	12.14	1.76
GA-35C-1265	104909	139	13.60	54.30	16.23	14.70	2.11	RM91-11C-225	107008	95	14.60	18.86	16.20	14.79	2.03
GA-35C-1265	104909	140	12.08	60.81	16.23	13.81	2.11	RM91-11C-225	107008	96	12.42	11.02	16.30	12.58	2.35
GA-35C-1265	104909	141	13.64	30.63	16.23	14.21	2.13	RM91-11C-225	107008	97	15.52	55.60	16.16	16.04	1.89
GA-35C-1265	104909	142	13.33	83.87	16.22	14.82	2.09	RM91-11C-225	107008	98	13.36	48.11	16.18	14.42	1.96
GA-35C-1265	104909	143	15.71	26.30	16.20	15.89	2.00	RM91-11C-225	107008	99	14.46	31.11	16.18	14.90	1.96
GA-35C-1265	104909	144	12.92	72.88	16.20	14.51	2.00	RM91-11C-225	107008	100	11.55	30.22	16.18	12.55	1.96
GA-35C-1265	104909	145	13.51	55.15	16.20	14.66	2.00	RM91-11C-225	107008	101	14.72	43.64	16.25	15.33	2.20
GA-35C-1265	104909	146	13.91	38.34	16.35	14.61	2.56	RM91-11C-225	107008	102	14.18	58.45	16.24	15.16	2.17
GA-35C-1265	104909	147	14.65	34.27	16.19	15.11	1.98	RM91-11C-225	107008	103	14.44	48.26	16.23	15.19	2.12
GA-35C-1265	104909	148	12.87	43.18	16.14	13.96	1.79	RM91-11C-225	107008	104	15.49	53.01	16.20	15.99	2.00
GA-35C-1265	104909	149	13.90	67.29	16.14	15.07	1.79	RM91-11C-225	107008	105	14.30	70.08	16.24	15.35	2.17
GA-35C-1265	104909	150	12.63	63.92	16.20	14.22	2.00	RM91-11C-225	107008	106	10.96	32.46	16.21	12.20	2.04
GA-35C-1265	104909	151	14.26	83.33	16.20	15.40	2.00	RM91-11C-225	107008	107	16.53	75.19	16.25	16.78	2.19
GA-35C-1265	104909	152	15.40	53.80	16.20	15.94	2.00	RM91-11C-225	107008	108	14.94	14.71	16.25	15.04	2.19
GA-35C-1265	104909	153	13.06	66.98	16.28	14.53	2.31	RM91-11C-225	107008	109	15.45	54.07	16.25	15.98	2.19
GA-35C-1265	104909	154	12.21	53.49	16.28	13.75	2.31	RM91-11C-225	107008	110	9.14	65.49	16.25	12.24	2.19
GA-35C-1265	104909	155	13.33	89.59	16.24	14.83	2.14	RM91-11C-225	107008	111	15.33	68.18	16.26	16.00	2.24
GA-35C-1265	104909	156	14.52	27.49	16.21	14.88	2.05	RM91-11C-225	107008	112	13.64	62.97	16.26	14.86	2.24
GA-35C-1265	104909	157	11.28	30.84	16.21	12.37	2.05	RM91-11C-225	107008	113	9.48	73.41	16.26	12.51	2.24
GA-35C-1265	104909	158	12.91	46.04	16.21	14.06	2.05	RM91-11C-225	107008	114	14.02	51.52	16.29	14.95	2.33
GA-35C-1265	104909	159	15.64	17.86	16.21	15.74	2.05	RM91-11C-225	107008	115	16.27	57.12	16.23	16.56	2.13
GA-35C-1265	104909	160	13.69	71.91	16.22	14.98	2.09	RM91-11C-225	107008	116	13.23	68.85	16.28	14.66	2.28
GA-35C-1265	104909	161	13.14	31.27	16.24	13.83	2.15	RM91-11C-225	107008	117	15.12	33.07	16.28	15.47	2.28
GA-35C-1265	104909	162	9.44	76.76	16.24	12.57	2.14	RM91-11C-225	107008	118	9.18	48.53	16.28	11.62	2.28
GA-35C-1265	104909	163	10.86	50.89	16.15	12.78	1.84	RM91-11C-225	107008	119	10.71	44.06	16.19	12.47	1.97
GA-35C-1265	104909	164	11.77	65.84	16.15	13.70	1.84	RM91-11C-225	107008	120	15.28	23.32	16.21	15.47	2.05
GA-35C-1265	104909	165	14.29	49.75	16.15	15.11	1.84	RM91-11C-225	107008	121	13.61	69.56	16.21	14.91	2.05
GA-35C-1265	104909	166	14.11	50.15	16.15	14.99	1.84	RM91-11C-225	107008	122	13.78	68.13	16.14	15.01	1.80
GA-35C-1265	104909	167	13.37	55.02	16.26	14.56	2.21	RM91-11C-225	107008	123	12.00	27.55	16.14	12.79	1.80
GA-35C-1265	104909	168	15.00	88.18	16.19	15.86	1.99	RM91-11C-225	107008	124	14.01	85.75	16.20	15.25	2.02
GA-35C-1265	104909	169	13.38	47.43	16.19	14.42	1.99	RM91-11C-225	107008	125	16.16	10.26	16.22	16.18	2.07
GA-35C-1265	104909	170	14.08	54.53	16.21	15.04	2.04	RM91-11C-225	107008	126	12.43	46.54	16.25	13.73	2.18
GA-35C-1265	104909	171	15.16	23.92	16.18	15.37	1.93	RM91-11C-225	107008	127	15.21	23.92	16.25	15.42	2.18
GA-35C-1265	104909	172	14.01	74.16	16.18	15.20	1.93	RM91-11C-225	107008	128	15.98	38.04	16.26	16.23	2.22
GA-35C-1265	104909	173	13.62	54.38	16.17	14.72	1.91	RM91-11C-225	107008	129	6.95	69.19	16.30	11.89	2.38
GA-35C-1265	104909	174	9.46	66.66	16.12	12.34	1.74	RM91-11C-225	107008	130	15.99	42.86	16.23	16.27	2.12
GA-35C-1265	104909	175	14.90	13.37	16.12	14.99	1.74	RM91-11C-225	107008	131	16.09	55.10	16.22	16.43	2.09
GA-35C-1265	104909	176	14.98	34.05	16.21	15.37	2.05	RM91-11C-225	107008	132	14.50	50.00	16.28	15.26	2.30
GA-35C-1265	104909	177	15.21	51.87	16.23	15.79	2.11	RM91-11C-225	107008	133	16.02	57.14	16.25	16.39	2.18

Table C3 Apatite fission track lengths for all samples analysed in this thesis

UBC	A2Z	Track	Angle				Dpar	UBC	A2Z	Track	Angle				Dpar
			Length (μm)	to c- axis	Lo calc (μm)	Lc calc (μm)					Length (μm)	to c- axis	Lo calc (μm)	Lc calc (μm)	
GA-35C-1265	104909	178	13.52	73.07	16.23	14.88	2.11	RM91-11C-225	107008	134	16.36	45.20	16.22	16.57	2.10
GA-35C-1265	104909	179	15.04	67.95	16.15	15.81	1.82	RM91-11C-225	107008	135	17.17	61.01	16.19	17.18	1.97
GA-35C-1265	104909	180	11.97	50.87	16.15	13.52	1.82	RM91-11C-225	107008	136	16.06	12.26	16.28	16.09	2.29
GA-35C-1265	104909	181	13.50	61.90	16.21	14.75	2.05	RM91-11C-225	107008	137	15.26	59.38	16.19	15.89	1.98
GA-35C-1265	104909	182	12.36	26.18	16.21	13.03	2.05	RM91-11C-225	107008	138	10.14	63.53	16.22	12.62	2.07
GA-35C-1265	104909	183	13.91	59.39	16.11	14.99	1.68	RM91-11C-225	107008	139	14.88	21.11	16.31	15.08	2.41
GA-35C-1265	104909	184	14.49	41.43	16.11	15.12	1.68	RM91-11C-225	107008	140	10.71	24.04	16.31	11.62	2.41
GA-35C-1265	104909	185	13.83	79.33	16.21	15.12	2.06	RM91-11C-225	107008	141	13.66	63.18	16.29	14.87	2.34
GA-35C-1265	104909	186	15.16	13.43	16.21	15.24	2.06	RM91-11C-225	107008	142	15.39	59.54	16.29	15.98	2.34
GA-35C-1265	104909	187	14.40	54.63	16.21	15.26	2.06	RM91-11C-225	107008	143	11.31	49.05	16.28	13.03	2.28
GA-35C-1265	104909	188	14.61	81.96	16.21	15.61	2.06	RM91-11C-225	107008	144	14.88	78.62	16.19	15.76	1.99
GA-35C-1265	104909	189	14.95	76.08	16.21	15.80	2.06	RM91-11C-225	107008	145	9.68	69.94	16.19	12.47	1.97
GA-35C-1265	104909	190	9.01	65.09	16.21	12.20	2.04	RM91-11C-225	107008	146	15.73	73.55	16.19	16.28	1.97
GA-35C-1265	104909	191	14.49	33.13	16.18	14.96	1.93	RM91-11C-225	107008	147	6.42	36.83	16.19	10.68	1.97
GA-35C-1265	104909	192	14.93	56.62	16.18	15.64	1.93	RM91-11C-225	107008	148	15.61	74.45	16.20	16.20	2.00
GA-35C-1265	104909	193	14.17	77.85	16.18	15.32	1.93	RM91-22C-1460	111002	1	16.37	34.53	16.21	16.52	2.04
GA-35C-1265	104909	194	16.81	9.50	16.18	16.82	1.93	RM91-22C-1460	111002	2	14.12	69.43	16.30	15.23	2.36
GA-35C-1265	104909	195	13.95	54.30	16.25	14.94	2.19	RM91-22C-1460	111002	3	13.90	28.51	16.24	14.38	2.15
GA-52C-1585	111005	1	13.09	61.06	16.11	14.47	1.70	RM91-22C-1460	111002	4	13.81	52.24	16.17	14.81	1.91
GA-52C-1585	111005	2	12.12	84.11	16.23	14.08	2.11	RM91-22C-1460	111002	5	14.72	58.94	16.17	15.53	1.91
GA-52C-1585	111005	3	12.04	85.64	16.35	14.04	2.55	RM91-22C-1460	111002	6	14.96	39.92	16.17	15.45	1.91
GA-52C-1585	111005	4	13.41	57.20	16.38	14.62	2.65	RM91-22C-1460	111002	7	6.12	39.13	16.15	10.75	1.84
GA-52C-1585	111005	5	14.52	50.41	16.38	15.28	2.65	RM91-22C-1460	111002	8	14.17	30.12	16.06	14.64	1.51
GA-52C-1585	111005	6	15.42	24.13	16.40	15.60	2.73	RM91-22C-1460	111002	9	7.37	57.78	16.24	11.68	2.14
GA-52C-1585	111005	7	12.67	76.67	16.41	14.38	2.74	RM91-22C-1460	111002	10	15.28	68.87	16.23	15.97	2.12
GA-52C-1585	111005	8	13.79	86.76	16.29	15.11	2.33	RM91-22C-1460	111002	11	13.35	84.72	16.16	14.84	1.87
GA-52C-1585	111005	9	15.33	60.27	16.30	15.95	2.38	RM91-22C-1460	111002	12	17.45	79.59	16.32	17.36	2.45
GA-52C-1585	111005	10	13.94	83.58	16.20	15.20	2.03	RM91-22C-1460	111002	13	15.61	53.45	16.24	16.08	2.17
GA-52C-1585	111005	11	14.63	70.14	16.34	15.56	2.50	RM91-22C-1460	111002	14	14.07	46.97	16.30	14.91	2.36
GA-52C-1585	111005	12	14.50	41.33	16.37	15.12	2.62	RM91-22C-1460	111002	15	14.07	75.94	16.20	15.25	2.03
GA-52C-1585	111005	13	14.36	59.87	16.36	15.29	2.57	RM91-22C-1460	111002	16	12.66	50.99	16.20	14.00	2.03
GA-52C-1585	111005	14	15.04	84.62	16.21	15.88	2.04	RM91-22C-1460	111002	17	14.06	84.76	16.27	15.28	2.27
GA-52C-1585	111005	15	13.90	35.10	16.36	14.53	2.58	RM91-22C-1460	111002	18	11.98	72.64	16.19	13.92	1.99
GA-52C-1585	111005	16	14.71	1.25	16.26	14.71	2.23	RM91-22C-1460	111002	19	13.25	87.54	16.16	14.78	1.87
GA-52C-1585	111005	17	10.59	33.03	16.25	11.95	2.19	RM91-22C-1460	111002	20	14.11	31.42	16.07	14.62	1.54
GA-52C-1585	111005	18	13.57	73.56	16.28	14.92	2.31	RM91-22C-1460	111002	21	14.55	44.63	16.24	15.21	2.16
GA-52C-1585	111005	19	13.14	70.86	16.27	14.63	2.27	RM91-22C-1460	111002	22	13.42	84.63	16.26	14.88	2.23
GA-52C-1585	111005	20	12.35	76.86	16.33	14.18	2.49	RM91-22C-1460	111002	23	12.11	60.92	16.26	13.83	2.23
GA-52C-1585	111005	21	13.42	74.85	16.18	14.84	1.93	RM91-22C-1460	111002	24	13.48	43.86	16.31	14.42	2.41
GA-52C-1585	111005	22	13.84	50.21	16.33	14.80	2.46	RM91-22C-1460	111002	25	11.86	41.26	16.21	13.18	2.05
GA-52C-1585	111005	23	14.07	85.00	16.37	15.28	2.63	RM91-22C-1460	111002	26	13.19	33.94	16.17	13.95	1.92
GA-52C-1585	111005	24	9.50	73.17	16.37	12.51	2.63	RM91-22C-1460	111002	27	13.59	59.50	16.27	14.78	2.27
GA-52C-1585	111005	25	13.90	89.59	16.41	15.18	2.75	RM91-22C-1460	111002	28	14.43	23.80	16.27	14.72	2.27
GA-52C-1585	111005	26	12.66	53.92	16.39	14.06	2.68	RM91-22C-1460	111002	29	14.10	80.95	16.27	15.29	2.27
GA-52C-1585	111005	27	14.53	78.39	16.36	15.55	2.59	RM91-22C-1460	111002	30	14.01	43.21	16.23	14.79	2.13
GA-52C-1585	111005	28	13.02	85.13	16.28	14.64	2.30	RM91-22C-1460	111002	31	4.70	66.10	16.32	11.34	2.44
GA-52C-1585	111005	29	15.65	27.55	16.32	15.85	2.43	RM91-22C-1460	111002	32	15.67	89.82	16.23	16.27	2.11
GA-52C-1585	111005	30	12.92	69.66	16.23	14.47	2.12	RM91-22C-1460	111002	33	14.90	56.47	16.25	15.62	2.18
GA-52C-1585	111005	31	14.03	77.19	16.39	15.23	2.69	RM91-22C-1460	111002	34	9.33	20.78	16.19	10.40	1.98
GA-52C-1585	111005	32	15.16	34.20	16.33	15.52	2.49	RM91-22C-1460	111002	35	13.21	81.57	16.20	14.74	2.01
GA-52C-1585	111005	33	16.07	4.82	16.41	16.08	2.74	RM91-22C-1460	111002	36	14.02	39.21	16.23	14.72	2.12
GA-52C-1585	111005	34	14.59	68.46	16.25	15.53	2.19	RM91-22C-1460	111002	37	13.89	16.16	16.28	14.08	2.30
GA-52C-1585	111005	35	13.76	47.01	16.28	14.68	2.30	RM91-22C-1460	111002	38	5.65	57.36	16.28	11.34	2.31
GA-52C-1585	111005	36	14.75	59.27	16.39	15.55	2.69	RM91-22C-1460	111002	39	15.74	43.18	16.29	16.09	2.34
GA-52C-1585	111005	37	12.68	87.86	16.33	14.43	2.46	RM91-22C-1460	111002	40	15.27	25.05	16.21	15.48	2.05
GA-52C-1585	111005	38	12.44	73.11	16.34	14.21	2.52	RM91-22C-1460	111002	41	8.15	86.11	16.24	12.41	2.17
GA-52C-1585	111005	39	14.11	48.04	16.43	14.95	2.81	RM91-22C-1460	111002	42	11.25	39.76	16.24	12.69	2.17
GA-52C-1585	111005	40	15.12	74.60	16.37	15.90	2.61	RM91-22C-1460	111002	43	14.43	54.02	16.14	15.27	1.80
GA-52C-1585	111005	41	14.70	34.48	16.42	15.16	2.79	RM91-22C-1460	111002	44	15.44	51.39	16.31	15.94	2.40
GA-52C-1585	111005	42	12.45	84.74	16.37	14.29	2.60	RM91-22C-1460	111002	45	11.51	66.97	16.31	13.55	2.40
GA-52C-1585	111005	43	16.24	53.11	16.35	16.52	2.54	RM91-22C-1460	111002	46	15.34	34.10	16.33	15.67	2.48

Table C3 Apatite fission track lengths for all samples analysed in this thesis

UBC	A2Z	Track	Angle				Dpar	UBC	A2Z	Track	Angle				Dpar
			Length (μm)	to c- axis	Lo calc (μm)	Lc calc (μm)					Length (μm)	to c- axis	Lo calc (μm)	Lc calc (μm)	
GA-52C-1585	111005	44	15.91	54.27	16.27	16.30	2.26	RM91-22C-1460	111002	47	13.58	78.14	16.32	14.96	2.43
GA-52C-1585	111005	45	14.05	72.48	16.26	15.21	2.22	RM91-22C-1460	111002	48	15.00	31.17	16.16	15.34	1.87
GA-52C-1585	111005	46	13.96	80.08	16.34	15.20	2.51	RM94-03C-639	111003	1	10.28	60.01	16.21	12.64	2.04
GA-52C-1585	111005	47	14.14	72.42	16.37	15.27	2.63	RM94-03C-639	111003	2	12.44	45.56	16.31	13.71	2.41
GA-52C-1585	111005	48	14.87	83.54	16.16	15.77	1.86	RM94-03C-639	111003	3	8.82	85.75	16.16	12.55	1.87
GA-52C-1585	111005	49	15.86	40.64	16.23	16.15	2.13	RM94-03C-639	111003	4	8.28	79.34	16.18	12.35	1.94
GA-52C-1585	111005	50	15.41	68.38	16.24	16.05	2.15	RM94-03C-639	111003	5	15.07	30.48	16.21	15.39	2.04
GA-52C-1585	111005	51	16.11	73.18	16.37	16.52	2.60	RM94-03C-639	111003	6	12.07	59.72	16.22	13.78	2.09
GA-52C-1585	111005	52	14.44	67.06	16.38	15.42	2.65	RM94-03C-639	111003	7	14.33	31.65	16.22	14.80	2.09
GA-52C-1585	111005	53	14.80	8.26	16.35	14.84	2.56	RM94-03C-639	111003	8	8.69	46.29	16.22	11.45	2.09
GA-52C-1585	111005	54	15.18	65.77	16.38	15.89	2.66	RM94-03C-639	111003	9	14.36	37.01	16.21	14.93	2.05
GA-52C-1585	111005	55	14.80	55.68	16.31	15.54	2.39	RM94-03C-639	111003	10	15.06	67.94	16.20	15.82	2.02
GA-52C-1585	111005	56	14.34	50.24	16.28	15.15	2.30	RM94-03C-639	111003	11	14.61	63.84	16.31	15.50	2.39
GA-52C-1585	111005	57	14.03	60.90	16.24	15.09	2.16	RM94-03C-639	111003	12	14.48	43.68	16.36	15.15	2.58
GA-52C-1585	111005	58	15.05	9.47	16.30	15.09	2.36	RM94-03C-639	111003	13	10.42	65.96	16.23	12.84	2.12
GA-52C-1585	111005	59	14.71	89.44	16.35	15.68	2.55	RM94-03C-639	111003	14	13.19	61.09	16.23	14.54	2.12
GA-52C-1585	111005	60	15.05	67.71	16.39	15.82	2.68	RM94-03C-639	111003	15	16.21	79.79	16.13	16.59	1.76
GA-52C-1585	111005	61	13.75	88.72	16.25	15.09	2.20	RM94-03C-639	111003	16	14.15	62.06	16.13	15.18	1.76
GA-52C-1585	111005	62	13.49	24.75	16.29	13.93	2.33	RM94-03C-639	111003	17	16.77	42.74	16.29	16.87	2.32
GA-52C-1585	111005	63	13.40	42.93	16.40	14.34	2.72	RM94-03C-639	111003	18	9.06	32.75	16.25	10.87	2.20
GA-52C-1585	111005	64	14.65	69.37	16.37	15.57	2.61	RM94-03C-639	111003	19	14.87	60.91	16.34	15.64	2.52
GA-52C-1585	111005	65	14.98	68.25	16.42	15.77	2.78	RM94-03C-639	111003	20	14.59	57.84	16.26	15.43	2.21
GA-52C-1585	111005	66	13.49	37.07	16.30	14.26	2.37	RM94-03C-639	111003	21	12.71	31.82	16.25	13.51	2.19
GA-52C-1585	111005	67	14.92	84.49	16.31	15.80	2.42	RM94-03C-639	111003	22	17.21	77.90	16.29	17.21	2.34
GA-52C-1585	111005	68	13.46	22.13	16.26	13.84	2.22	RM94-03C-639	111003	23	11.76	39.52	16.33	13.05	2.46
GA-52C-1585	111005	69	14.18	78.40	16.22	15.33	2.09	RM94-03C-639	111003	24	13.38	51.08	16.35	14.50	2.55
GA-52C-1585	111005	70	15.49	23.29	16.25	15.66	2.19	RM94-03C-639	111003	25	15.26	22.64	16.34	15.44	2.52
GA-52C-1585	111005	71	14.86	48.87	16.26	15.50	2.22	RM94-03C-639	111003	26	15.97	75.65	16.17	16.43	1.90
GA-52C-1585	111005	72	14.63	42.51	16.35	15.24	2.53	RM94-03C-639	111003	27	13.64	77.14	16.25	14.99	2.19
GA-52C-1585	111005	73	13.62	67.51	16.18	14.90	1.93	RM94-03C-639	111003	28	9.36	56.24	16.23	11.97	2.11
GA-52C-1585	111005	74	15.12	65.41	16.31	15.85	2.40	RM94-03C-639	111003	29	16.80	54.83	16.23	16.92	2.11
GA-52C-1585	111005	75	14.30	57.53	16.29	15.23	2.32	RM94-03C-639	111003	30	13.74	39.83	16.28	14.52	2.30
GA-52C-1585	111005	76	14.19	70.55	16.25	15.29	2.18	RM94-03C-639	111003	31	14.88	29.08	16.26	15.21	2.24
GA-52C-1585	111005	77	14.79	26.88	16.28	15.10	2.29	RM94-03C-639	111003	32	15.18	40.61	16.26	15.63	2.24
GA-52C-1585	111005	78	13.36	68.93	16.31	14.75	2.42	RM94-03C-639	111003	33	13.87	33.45	16.28	14.47	2.28
GA-52C-1585	111005	79	15.02	32.11	16.31	15.38	2.42	RM94-03C-639	111003	34	15.79	75.63	16.21	16.32	2.05
GA-52C-1585	111005	80	13.47	68.46	16.40	14.81	2.73	RM94-03C-639	111003	35	15.85	20.53	16.21	15.95	2.05
GA-52C-1585	111005	81	13.75	41.79	16.45	14.57	2.89	RM94-03C-639	111003	36	13.69	56.22	16.21	14.80	2.05
GA-52C-1585	111005	82	13.63	67.88	16.29	14.91	2.34	RM94-03C-639	111003	37	15.34	81.48	16.24	16.06	2.17
GA-52C-1585	111005	83	14.01	64.09	16.28	15.11	2.29	RM94-03C-639	111003	38	15.29	49.25	16.20	15.82	2.02
GA-52C-1585	111005	84	13.20	44.56	16.28	14.23	2.29	RM94-03C-639	111003	39	13.32	41.73	16.16	14.25	1.89
GA-52C-1585	111005	85	14.55	79.98	16.16	15.56	1.86	RM94-03C-639	111003	40	10.68	61.42	16.27	12.92	2.25
GA-52C-1585	111005	86	13.98	81.36	16.21	15.22	2.06	RM94-03C-639	111003	41	14.12	28.51	16.19	14.56	1.99
GA-52C-1585	111005	87	14.41	74.50	16.37	15.45	2.60	RM94-03C-639	111003	42	16.18	58.75	16.33	16.51	2.48
GA-52C-1585	111005	88	15.89	8.41	16.38	15.91	2.64	RM94-03C-639	111003	43	10.29	42.14	16.33	12.11	2.48
GA-52C-1585	111005	89	13.97	77.94	16.31	15.20	2.42	RM94-03C-639	111003	44	14.62	79.90	16.26	15.61	2.22
GA-52C-1585	111005	90	14.24	79.41	16.31	15.37	2.42	RM94-03C-639	111003	45	17.20	65.72	16.23	17.20	2.13
GA-52C-1585	111005	91	13.15	21.97	16.35	13.56	2.54	RM94-03C-639	111003	46	14.51	58.36	16.23	15.38	2.13
GA-52C-1585	111005	92	13.62	82.78	16.37	15.00	2.60	RM94-03C-639	111003	47	15.72	73.13	16.30	16.27	2.37
GA-52C-1585	111005	93	16.39	80.39	16.17	16.70	1.90	RM94-03C-639	111003	48	15.81	63.10	16.20	16.28	2.01
GA-52C-1585	111005	94	15.12	28.66	16.28	15.41	2.29	RM94-03C-639	111003	49	15.07	40.35	16.33	15.54	2.49
GA-52C-1585	111005	95	15.32	60.64	16.39	15.94	2.68	RM94-03C-639	111003	50	13.98	76.38	16.30	15.19	2.37
GA-52C-1585	111005	96	13.83	39.25	16.26	14.57	2.22	RM94-03C-639	111003	51	15.03	54.02	16.30	15.68	2.37
GA-52C-1585	111005	97	13.13	68.36	16.29	14.59	2.32	RM94-03C-639	111003	52	13.77	73.11	16.30	15.04	2.37
GA-52C-1585	111005	98	15.00	66.38	16.35	15.77	2.55	RM94-03C-639	111003	53	14.29	70.43	16.19	15.35	1.99
GA-52C-1585	111005	99	16.17	86.75	16.26	16.57	2.23	RM94-03C-639	111003	54	14.41	33.63	16.19	14.91	1.99
GA-52C-1585	111005	100	14.19	44.51	16.26	14.95	2.23	RM94-03C-639	111003	55	16.87	25.38	16.32	16.91	2.44
GA-52C-1585	111005	101	14.90	85.34	16.32	15.79	2.43	RM94-03C-639	111003	56	12.99	68.70	16.31	14.51	2.42
GA-52C-1585	111005	102	13.92	54.75	16.40	14.93	2.71	RM94-03C-639	111003	57	15.45	80.96	16.31	16.12	2.42
GA-52C-1585	111005	103	15.57	41.19	16.33	15.94	2.48	RM94-03C-639	111003	58	8.51	64.15	16.31	12.07	2.42
GA-52C-1585	111005	104	12.53	72.85	16.28	14.26	2.29	RM94-03C-639	111003	59	15.53	64.93	16.31	16.11	2.42

Table C3 Apatite fission track lengths for all samples analysed in this thesis

UBC	A2Z	Track	Angle				Dpar	UBC	A2Z	Track	Angle				Dpar
			Length (μm)	to c- axis	Lo calc (μm)	Lc calc (μm)					Length (μm)	to c- axis	Lo calc (μm)	Lc calc (μm)	
GA-52C-1585	111005	105	13.62	60.72	16.44	14.82	2.85	RM94-03C-639	111003	60	14.42	62.34	16.27	15.36	2.26
GA-52C-1585	111005	106	14.50	29.96	16.33	14.91	2.46	RM94-03C-639	111003	61	15.14	55.86	16.19	15.78	1.99
GA-52C-1585	111005	107	16.25	9.62	16.27	16.27	2.26	RM94-03C-639	111003	62	9.42	71.37	16.20	12.45	2.02
GA-52C-1585	111005	108	14.63	80.77	16.37	15.62	2.60	RM94-03C-639	111003	63	14.24	66.87	16.20	15.29	2.02
GA-52C-1585	111005	109	14.34	28.83	16.33	14.75	2.46	RM94-03C-639	111003	64	16.02	67.92	16.27	16.44	2.25
GA-52C-1585	111005	110	14.22	52.74	16.29	15.11	2.33	RM94-03C-639	111003	65	9.11	82.83	16.27	12.59	2.25
GA-52C-1585	111005	111	14.40	18.67	16.39	14.60	2.70	RM94-03C-639	111003	66	13.61	84.76	16.18	15.00	1.96
GA-52C-1585	111005	112	11.99	47.62	16.29	13.45	2.32	RM94-03C-639	111003	67	14.25	56.86	16.28	15.18	2.31
GA-52C-1585	111005	113	14.43	60.51	16.22	15.35	2.07	RM94-03C-639	111003	68	15.61	63.10	16.29	16.15	2.33
GA-52C-1585	111005	114	14.09	77.35	16.29	15.27	2.34	RM94-03C-639	111003	69	16.04	40.08	16.29	16.29	2.33
GA-52C-1585	111005	115	14.64	53.25	16.40	15.40	2.71	RM94-03C-639	111003	70	10.34	37.23	16.33	11.95	2.47
GBC5-928	110309	1	12.82	56.84	16.33	14.22	2.49	RM94-03C-639	111003	71	11.16	47.85	16.27	12.89	2.26
GBC5-928	110309	2	13.07	51.27	16.33	14.29	2.49	RM94-03C-639	111003	72	13.01	88.92	16.27	14.64	2.26
GBC5-928	110309	3	14.22	87.56	16.19	15.38	1.99	RM94-03C-639	111003	73	14.98	78.77	16.38	15.83	2.64
GBC5-928	110309	4	13.82	85.80	15.99	15.13	1.26	RM94-03C-639	111003	74	14.54	89.61	16.35	15.58	2.56
GBC5-928	110309	5	11.87	80.20	16.13	13.91	1.77	RM94-03C-639	111003	75	14.83	36.11	16.35	15.29	2.56
GBC5-928	110309	6	11.98	74.77	16.10	13.94	1.66	RM94-03C-639	111003	76	15.17	88.60	16.24	15.96	2.14
GBC5-928	110309	7	14.75	54.25	16.05	15.49	1.49	RM94-03C-639	111003	77	11.74	54.73	16.24	13.46	2.17
GBC5-928	110309	8	14.92	71.04	16.05	15.75	1.49	RM94-03C-639	111003	78	16.90	43.65	16.24	16.97	2.16
GBC5-928	110309	9	12.50	66.76	16.20	14.17	2.03	RM94-03C-639	111003	79	14.96	76.60	16.25	15.81	2.20
GBC5-928	110309	10	12.82	60.12	16.11	14.28	1.71	RM94-03C-639	111003	80	15.50	29.67	16.10	15.74	1.65
GBC5-928	110309	11	11.28	56.99	16.11	13.21	1.71	RM94-03C-639	111003	81	13.51	47.05	16.10	14.51	1.65
GBC5-928	110309	12	14.27	32.06	16.34	14.76	2.51	RM94-03C-639	111003	82	16.47	66.11	16.32	16.73	2.44
GBC5-928	110309	13	13.48	54.45	16.18	14.63	1.94	RM94-03C-639	111003	83	14.03	71.31	16.35	15.19	2.54
GBC5-928	110309	14	15.03	21.41	16.19	15.22	1.97	RM94-03C-639	111003	84	14.66	73.04	16.35	15.60	2.54
GBC5-928	110309	15	12.18	29.25	16.25	13.00	2.19	RM94-03C-639	111003	85	15.48	45.21	16.22	15.91	2.09
GBC5-928	110309	16	16.94	22.55	16.22	16.96	2.10	RM94-03C-639	111003	86	14.62	35.85	16.22	15.12	2.09
GS-1765C-782	107007	1	9.18	71.63	16.26	12.40	2.22	RM94-03C-639	111003	87	7.68	56.01	16.24	11.67	2.15
GS-1765C-782	107007	2	14.23	39.20	16.26	14.88	2.22	RM94-03C-639	111003	88	11.88	28.73	16.36	12.74	2.58
GS-1765C-782	107007	3	11.69	47.11	16.22	13.23	2.07	RM94-03C-639	111003	89	16.07	79.88	16.36	16.51	2.58
GS-1765C-782	107007	4	14.20	29.43	16.18	14.65	1.96	RM94-03C-639	111003	90	13.75	46.59	16.23	14.67	2.13
GS-1765C-782	107007	5	16.10	64.38	16.20	16.48	2.03	RM94-03C-639	111003	91	16.47	37.49	16.42	16.61	2.79
GS-1765C-782	107007	6	11.48	60.61	16.25	13.42	2.18	RM94-03C-639	111003	92	13.60	57.54	16.34	14.76	2.52
GS-1765C-782	107007	7	14.08	58.41	16.23	15.09	2.12	RM94-03C-639	111003	93	12.13	62.97	16.34	13.88	2.52
GS-1765C-782	107007	8	13.76	78.40	16.23	15.07	2.12	RM94-03C-639	111003	94	14.98	84.91	16.31	15.84	2.40
GS-1765C-782	107007	9	14.24	72.16	16.23	15.33	2.12	RM94-03C-639	111003	95	15.48	53.55	16.31	15.99	2.40
GS-1765C-782	107007	10	16.17	44.24	16.23	16.42	2.12	RM94-03C-639	111003	96	13.19	26.48	16.31	13.73	2.41
GS-1765C-782	107007	11	15.37	19.02	16.21	15.50	2.06	RM94-03C-639	111003	97	13.42	40.54	16.31	14.29	2.41
GS-1765C-782	107007	12	7.86	50.86	16.22	11.52	2.07	RM94-03C-639	111003	98	15.04	35.89	16.32	15.45	2.43
GS-1765C-782	107007	13	15.03	67.94	16.22	15.80	2.08	RM94-03C-639	111003	99	12.81	62.90	16.32	14.32	2.43
GS-1765C-782	107007	14	8.85	81.03	16.21	12.50	2.05	RM94-03C-639	111003	100	13.19	79.77	16.42	14.72	2.78
GS-1765C-782	107007	15	15.88	14.87	16.18	15.94	1.94	RM94-03C-639	111003	101	15.36	62.02	16.28	15.98	2.31
GS-1765C-782	107007	16	12.01	38.10	16.30	13.18	2.36	RM94-03C-639	111003	102	10.62	37.89	16.24	12.18	2.17
GS-1765C-782	107007	17	10.64	31.07	16.30	11.90	2.36	RM94-03C-639	111003	103	9.12	82.26	16.36	12.58	2.58
GS-1765C-782	107007	18	9.94	64.42	16.30	12.51	2.36	RM94-03C-639	111003	104	15.78	28.75	16.23	15.97	2.13
GS-1765C-782	107007	19	16.21	52.54	16.30	16.50	2.36	RM94-03C-639	111003	105	15.63	81.07	16.23	16.23	2.13
GS-1765C-782	107007	20	12.09	55.83	16.30	13.72	2.36	RM94-03C-639	111003	106	14.47	80.47	16.23	15.52	2.13
GS-1765C-782	107007	21	13.57	70.88	16.25	14.90	2.20	RM94-03C-639	111003	107	14.24	63.13	16.22	15.25	2.09
GS-1765C-782	107007	22	13.74	51.52	16.25	14.75	2.20	RM94-03C-639	111003	108	13.58	61.98	16.21	14.81	2.05
GS-1765C-782	107007	23	15.76	89.05	16.25	16.32	2.20	RM94-03C-639	111003	109	16.23	80.36	16.28	16.60	2.28
GS-1765C-782	107007	24	15.03	61.58	16.22	15.76	2.10	RM94-03C-639	111003	110	15.06	30.81	16.28	15.39	2.28
GS-1765C-782	107007	25	11.37	35.38	16.24	12.61	2.17	RM94-03C-639	111003	111	10.06	29.35	16.28	11.40	2.28
GS-1765C-782	107007	26	14.77	44.63	16.24	15.38	2.17	RM94-03C-639	111003	112	14.37	52.61	16.31	15.21	2.40
GS-1765C-782	107007	27	8.99	76.14	16.29	12.45	2.34	RM94-03C-639	111003	113	11.44	54.27	16.25	13.25	2.20
GS-1765C-782	107007	28	14.64	66.36	16.18	15.54	1.94	RM94-03C-639	111003	114	11.41	44.68	16.26	12.97	2.22
GS-1765C-782	107007	29	8.75	47.37	16.15	11.51	1.82	RM94-03C-639	111003	115	12.16	66.98	16.26	13.96	2.22
GS-1765C-782	107007	30	15.68	45.56	16.16	16.06	1.89	RM94-03C-639	111003	116	14.10	83.83	16.26	15.30	2.24
GS-1765C-782	107007	31	15.01	50.81	16.20	15.63	2.01	RM94-03C-639	111003	117	14.36	74.40	16.26	15.42	2.24
GS-1765C-782	107007	32	12.81	53.72	16.20	14.16	2.02	RM94-03C-639	111003	118	9.45	70.51	16.22	12.44	2.10
GS-1765C-782	107007	33	15.32	44.40	16.20	15.78	2.02	RM94-03C-639	111003	119	15.80	8.15	16.22	15.82	2.10
GS-1765C-782	107007	34	8.22	63.77	16.19	12.01	1.97	RM94-03C-639	111003	120	15.49	40.50	16.24	15.87	2.14

Table C3 Apatite fission track lengths for all samples analysed in this thesis

UBC	A2Z	Track	Angle				Dpar	UBC	A2Z	Track	Angle				Dpar
			Length (μm)	to c- axis	Lo calc (μm)	Lc calc (μm)					Length (μm)	to c- axis	Lo calc (μm)	Lc calc (μm)	
GS-1765C-782	107007	35	13.92	50.08	16.25	14.85	2.18	RM94-03C-639	111003	121	14.21	77.50	16.21	15.34	2.06
GS-1765C-782	107007	36	11.05	33.55	16.17	12.31	1.90	RM94-03C-639	111003	122	12.84	59.73	16.21	14.29	2.06
GS-1765C-782	107007	37	15.38	55.08	16.20	15.94	2.01	RM94-03C-639	111003	123	15.33	48.33	16.21	15.83	2.06
GS-1765C-782	107007	38	8.75	38.99	16.16	11.08	1.89	RM94-03C-639	111003	124	13.80	32.94	16.26	14.40	2.23
GS-1765C-782	107007	39	11.11	70.26	16.20	13.34	2.01	RM94-03C-639	111003	125	15.12	67.64	16.21	15.86	2.05
GS-1765C-782	107007	40	14.92	45.81	16.20	15.50	2.01	RM94-03C-639	111003	126	13.92	61.69	16.25	15.03	2.20
GS-1765C-782	107007	41	10.03	3.75	16.20	10.08	2.01	RM94-03C-639	111003	127	10.49	55.01	16.24	12.65	2.15
GS-1765C-782	107007	42	10.52	47.13	16.30	12.44	2.35	RM94-03C-639	111003	128	16.48	15.10	16.24	16.51	2.15
GS-1765C-782	107007	43	8.91	48.18	16.17	11.57	1.90	RM94-03C-639	111003	129	7.39	63.39	16.24	11.84	2.15
GS-1765C-782	107007	44	12.02	42.72	16.17	13.33	1.90	RM94-03C-639	111003	130	15.35	76.28	16.24	16.05	2.15
GS-1765C-782	107007	45	14.46	67.42	16.25	15.43	2.20	RM94-03C-639	111003	131	15.20	88.48	16.24	15.98	2.15
GS-1765C-782	107007	46	14.90	88.62	16.24	15.80	2.14	RM94-03C-639	111003	132	18.01	43.30	16.24	17.83	2.15
GS-1765C-782	107007	47	14.49	79.66	16.21	15.53	2.05	RM94-03C-639	111003	133	15.59	39.64	16.30	15.93	2.36
GS-1765C-782	107007	48	15.45	57.29	16.21	16.00	2.05	RM94-03C-639	111003	134	14.66	77.55	16.31	15.62	2.40
GS-1765C-782	107007	49	14.86	79.84	16.28	15.76	2.30	RM94-03C-639	111003	135	15.87	74.32	16.28	16.37	2.31
GS-1765C-782	107007	50	15.61	23.35	16.31	15.77	2.41	RM94-03C-639	111003	136	14.34	68.00	16.28	15.36	2.31
GS-1765C-782	107007	51	6.96	56.14	16.31	11.55	2.41	RM94-03C-639	111003	137	14.11	56.11	16.25	15.08	2.20
GS-1765C-782	107007	52	14.97	62.47	16.22	15.72	2.07	RM94-03C-639	111003	138	12.45	31.92	16.30	13.31	2.36
GS-1765C-782	107007	53	15.83	73.36	16.22	16.34	2.07	RM94-03C-639	111003	139	16.19	21.60	16.24	16.27	2.15
GS-1765C-782	107007	54	14.97	68.59	16.20	15.77	2.01	RM94-03C-639	111003	140	14.71	64.37	16.28	15.57	2.29
GS-1765C-782	107007	55	9.54	82.23	16.25	12.69	2.19	RM94-03C-639	111003	141	13.25	68.93	16.28	14.68	2.29
GS-1765C-782	107007	56	10.82	32.71	16.25	12.10	2.19	RM94-03C-639	111003	142	15.52	66.48	16.16	16.11	1.89
GS-1765C-782	107007	57	13.98	82.38	16.25	15.22	2.19	RM94-03C-639	111003	143	14.06	30.14	16.28	14.55	2.30
GS-1765C-782	107007	58	13.87	85.59	16.29	15.16	2.33	RM94-03C-639	111003	144	13.94	68.39	16.28	15.11	2.30
GS-1765C-782	107007	59	15.95	75.17	16.26	16.42	2.24	RM94-03C-639	111003	145	16.05	82.54	16.28	16.50	2.31
GS-1765C-782	107007	60	14.10	69.99	16.26	15.23	2.24	RM94-03C-639	111003	146	16.17	66.81	16.24	16.54	2.14
GS-1765C-782	107007	61	13.04	73.08	16.21	14.58	2.05	RM94-03C-639	111003	147	16.13	32.21	16.27	16.30	2.25
GS-1765C-782	107007	62	15.41	62.15	16.17	16.01	1.91	RM94-03C-639	111003	148	15.39	73.94	16.21	16.06	2.04
GS-1765C-782	107007	63	12.99	57.97	16.17	14.36	1.91	RM94-03C-639	111003	149	15.45	52.03	16.28	15.96	2.29
GS-1765C-782	107007	64	15.01	79.42	16.30	15.85	2.35	RM94-03C-639	111003	150	15.69	27.12	16.25	15.88	2.20
GS-1765C-782	107007	65	12.77	17.80	16.21	13.10	2.06	RM94-03C-639	111003	151	15.65	74.85	16.25	16.23	2.20
GS-1765C-782	107007	66	9.21	50.63	16.19	11.72	1.97	RM94-03C-639	111003	152	15.17	68.00	16.35	15.89	2.55
GS-1765C-782	107007	67	3.70	65.72	16.19	11.07	1.97	RM94-03C-639	111003	153	16.18	76.07	16.35	16.57	2.55
GS-1765C-782	107007	68	10.53	70.47	16.19	12.98	1.97	RM94-03C-639	111003	154	14.05	35.29	16.30	14.65	2.37
GS-1765C-782	107007	69	13.72	46.35	16.20	14.64	2.00	RM94-03C-639	111003	155	13.23	65.90	16.30	14.63	2.37
GS-1765C-782	107007	70	15.15	7.90	16.20	15.18	2.00	RM94-03C-639	111003	156	15.81	46.95	16.30	16.17	2.37
GS-1765C-782	107007	71	14.85	40.06	16.20	15.37	2.00	RM94-03C-639	111003	157	15.85	66.21	16.29	16.32	2.33
GS-1765C-782	107007	72	16.05	81.98	16.31	16.50	2.39	RM94-03C-639	111003	158	16.71	35.67	16.21	16.80	2.04
GS-1765C-782	107007	73	10.53	41.68	16.25	12.26	2.19	RM94-03C-639	111003	159	8.49	58.46	16.35	11.90	2.53
GS-1765C-782	107007	74	15.13	86.94	16.26	15.94	2.24	RM98-04C-459	111004	1	14.24	43.24	16.17	14.96	1.90
GS-1765C-782	107007	75	14.08	52.57	16.26	15.01	2.24	RM98-04C-459	111004	2	16.71	74.83	16.26	16.90	2.21
GS-1765C-782	107007	76	13.13	68.48	16.26	14.59	2.24	RM98-04C-459	111004	3	10.96	54.85	16.26	12.95	2.21
GS-1765C-782	107007	77	9.88	56.24	16.25	12.29	2.18	RM98-04C-459	111004	4	15.82	26.25	16.26	15.98	2.21
GS-1765C-782	107007	78	14.47	36.97	16.25	15.02	2.18	RM98-04C-459	111004	5	11.27	59.14	16.22	13.25	2.10
GS-1765C-782	107007	79	15.11	75.34	16.30	15.89	2.35	RM98-04C-459	111004	6	15.45	22.94	16.30	15.62	2.38
GS-1765C-782	107007	80	15.72	83.06	16.19	16.29	1.99	RM98-04C-459	111004	7	11.96	79.94	16.21	13.96	2.05
GS-1765C-782	107007	81	11.20	29.64	16.30	12.25	2.35	RM98-04C-459	111004	8	15.18	72.64	16.15	15.93	1.83
GS-1765C-782	107007	82	10.59	71.16	16.30	13.03	2.35	RM98-04C-459	111004	9	12.94	81.87	16.22	14.58	2.08
GS-1765C-782	107007	83	15.32	40.57	16.15	15.74	1.84	RM98-04C-459	111004	10	14.96	57.18	16.22	15.67	2.08
GS-1765C-782	107007	84	13.20	61.23	16.24	14.55	2.16	RM98-04C-459	111004	11	15.47	27.08	16.22	15.69	2.08
GS-1765C-782	107007	85	9.68	51.16	16.18	12.02	1.93	RM98-04C-459	111004	12	14.37	61.85	16.22	15.32	2.08
GS-1765C-782	107007	86	14.20	68.51	16.27	15.28	2.27	RM98-04C-459	111004	13	12.39	70.24	16.19	14.15	1.98
GS-1765C-782	107007	87	12.31	67.24	16.33	14.06	2.46	RM98-04C-459	111004	14	16.36	86.79	16.31	16.69	2.41
GS-1765C-782	107007	88	16.19	53.05	16.33	16.49	2.46	RM98-04C-459	111004	15	14.37	72.38	16.31	15.41	2.41
GS-1765C-782	107007	89	9.27	52.08	16.25	11.79	2.20	RM98-04C-459	111004	16	14.37	50.50	16.12	15.18	1.72
GS-1765C-782	107007	90	7.86	54.33	16.19	11.65	1.97	RM98-04C-459	111004	17	14.70	86.87	16.16	15.67	1.89
GS-1765C-782	107007	91	13.59	48.43	16.29	14.59	2.33	RM98-04C-459	111004	18	14.75	48.73	16.16	15.42	1.89
GS-1765C-782	107007	92	8.32	48.58	16.29	11.50	2.33	RM98-04C-459	111004	19	12.56	79.15	16.22	14.33	2.08
GS-1765C-782	107007	93	10.92	31.69	16.29	12.13	2.33	RM98-04C-459	111004	20	14.77	50.96	16.15	15.47	1.85
GS-1765C-782	107007	94	14.39	83.36	16.25	15.48	2.18	RM98-04C-459	111004	21	14.07	82.83	16.15	15.28	1.85
GS-1765C-782	107007	95	14.15	22.14	16.27	14.44	2.27	RM98-04C-459	111004	22	15.62	73.94	16.24	16.21	2.16

Table C3 Apatite fission track lengths for all samples analysed in this thesis

UBC	A2Z	Track	Angle				Dpar	UBC	A2Z	Track	Angle				Dpar
			Length (μm)	to c- axis	Lo calc (μm)	Lc calc (μm)					Length (μm)	to c- axis	Lo calc (μm)	Lc calc (μm)	
GS-1765C-782	107007	96	8.73	78.81	16.27	12.44	2.27	RM98-04C-459	111004	23	14.75	64.65	16.13	15.60	1.77
GS-1765C-782	107007	97	6.50	55.75	16.20	11.46	2.03	RM98-04C-459	111004	24	13.61	57.95	16.14	14.77	1.81
GS-1765C-782	107007	98	12.33	59.21	16.27	13.94	2.25	RM98-04C-459	111004	25	8.71	48.26	16.35	11.54	2.53
GS-1765C-782	107007	99	13.51	80.91	16.26	14.93	2.23	RM98-04C-459	111004	26	15.18	63.09	16.20	15.87	2.01
GS-1765C-782	107007	100	14.04	63.58	16.26	15.13	2.23	RM98-04C-459	111004	27	13.87	74.99	16.20	15.12	2.00
GS-1765C-782	107007	101	5.89	59.59	16.09	11.45	1.63	RM98-04C-459	111004	28	14.95	69.10	16.18	15.76	1.96
GS-1765C-782	107007	102	5.35	41.65	16.24	10.74	2.14	RM98-04C-459	111004	29	13.30	32.36	16.18	13.99	1.96
GS-1765C-782	107007	103	10.19	24.16	16.19	11.23	1.97	RM98-04C-459	111004	30	10.86	45.15	16.18	12.61	1.96
GS-1765C-782	107007	104	16.77	43.20	16.31	16.87	2.39	RM98-04C-459	111004	31	14.51	54.53	16.18	15.33	1.96
GS-1765C-782	107007	105	10.86	59.76	16.26	13.00	2.23	RM98-04C-459	111004	32	15.05	61.99	16.25	15.77	2.19
GS-1765C-782	107007	106	14.71	45.13	16.27	15.34	2.25	RM98-04C-459	111004	33	13.58	68.63	16.25	14.88	2.19
GS-1765C-782	107007	107	13.07	67.05	16.25	14.54	2.19	RM98-04C-459	111004	34	12.95	19.52	16.17	13.31	1.91
GS-1765C-782	107007	108	11.24	64.85	16.33	13.34	2.46	RM98-04C-459	111004	35	15.10	74.88	16.29	15.89	2.32
GS-1765C-782	107007	109	13.15	18.27	16.33	13.45	2.46	RM98-04C-459	111004	36	14.46	27.56	16.09	14.83	1.64
GS-1765C-782	107007	110	16.26	82.97	16.21	16.63	2.06	RM98-04C-459	111004	37	12.68	89.66	16.22	14.44	2.10
GS-1765C-782	107007	111	15.32	10.91	16.21	15.37	2.06	RM98-04C-459	111004	38	13.73	81.77	16.22	15.06	2.10
GS-1765C-782	107007	112	8.11	49.07	16.28	11.49	2.30	RM98-04C-459	111004	39	13.96	42.68	16.25	14.74	2.20
GS-1765C-782	107007	113	14.89	67.50	16.17	15.71	1.91	RM98-04C-459	111004	40	13.50	42.56	16.25	14.40	2.20
GS-1765C-782	107007	114	9.58	61.00	16.24	12.22	2.17	RM98-04C-459	111004	41	15.56	82.97	16.25	16.19	2.20
GS-1765C-782	107007	115	13.07	47.88	16.24	14.21	2.17	RM98-04C-459	111004	42	15.50	84.83	16.25	16.16	2.20
GS-1765C-782	107007	116	7.38	42.45	16.29	11.09	2.32	RM98-04C-459	111004	43	14.78	64.11	16.30	15.61	2.37
GS-1765C-782	107007	117	13.60	59.58	16.31	14.79	2.41	RM98-04C-459	111004	44	12.07	54.55	16.30	13.68	2.37
GS-1765C-782	107007	118	10.89	86.58	16.31	13.34	2.41	RM98-04C-459	111004	45	15.73	38.58	16.20	16.03	2.01
GS-1765C-782	107007	119	9.49	63.01	16.31	12.23	2.41	RM98-04C-459	111004	46	16.31	81.87	16.20	16.66	2.01
GS-1765C-782	107007	120	10.25	58.73	16.26	12.59	2.24	RM98-04C-459	111004	47	14.06	77.49	16.20	15.25	2.03
GS-1765C-782	107007	121	15.91	72.15	16.22	16.39	2.08	RM98-04C-459	111004	48	14.68	49.47	16.20	15.38	2.00
GS-1765C-782	107007	122	14.90	47.36	16.17	15.51	1.91	RM98-04C-459	111004	49	14.06	83.95	16.24	15.27	2.17
GS-1765C-782	107007	123	14.73	63.21	16.29	15.57	2.33	RM98-04C-459	111004	50	12.78	89.38	16.35	14.50	2.55
GS-1765C-782	107007	124	14.06	42.76	16.22	14.82	2.10	RM98-04C-459	111004	51	12.47	36.60	16.23	13.47	2.11
GS-1765C-782	107007	125	14.77	43.06	16.24	15.35	2.17	RM98-04C-459	111004	52	15.70	55.54	16.28	16.16	2.29
GS-1765C-782	107007	126	12.37	44.76	16.24	13.64	2.17	RM98-04C-459	111004	53	15.80	23.53	16.28	15.94	2.29
GS-1765C-782	107007	127	15.40	34.90	16.12	15.73	1.72	RM98-04C-459	111004	54	13.30	89.74	16.29	14.82	2.32
GS-1765C-782	107007	128	14.92	75.98	16.18	15.78	1.95	RM98-04C-459	111004	55	13.42	80.79	16.26	14.87	2.21
GS-1765C-782	107007	129	13.90	83.43	16.18	15.17	1.93	RM98-04C-459	111004	56	16.03	7.49	16.26	16.04	2.21
GS-1765C-782	107007	130	12.79	69.08	16.18	14.39	1.93	RM98-04C-459	111004	57	14.04	89.32	16.27	15.27	2.27
GS-1765C-782	107007	131	16.12	77.15	16.38	16.53	2.65	RM98-04C-459	111004	58	10.70	46.58	16.22	12.54	2.10
GS-1765C-782	107007	132	15.43	50.99	16.38	15.93	2.65	RM98-04C-459	111004	59	16.84	84.13	16.22	16.98	2.10
GS-1765C-782	107007	133	15.09	21.28	16.38	15.27	2.65	RM98-04C-459	111004	60	16.89	63.86	16.23	17.00	2.11
GS-1765C-782	107007	134	15.61	39.18	16.18	15.94	1.93	RM98-04C-459	111004	61	14.44	75.47	16.24	15.48	2.16
GS-1765C-782	107007	135	13.80	62.38	16.27	14.96	2.26	RM98-04C-459	111004	62	11.54	77.55	16.29	13.69	2.32
GS-1765C-782	107007	136	10.93	72.41	16.27	13.26	2.26	RM98-04C-459	111004	63	14.79	25.76	16.27	15.08	2.27
GS-1765C-782	107007	137	8.96	44.52	16.20	11.40	2.03	RM98-04C-459	111004	64	11.96	88.88	16.27	13.99	2.27
GS-1765C-782	107007	138	15.62	32.40	16.15	15.88	1.84	RM98-04C-459	111004	65	14.82	67.43	16.18	15.67	1.95
GS-1765C-782	107007	139	8.85	56.94	16.22	11.91	2.07	RM98-04C-459	111004	66	14.81	59.97	16.16	15.60	1.87
GS-1765C-782	107007	140	11.40	30.93	16.25	12.46	2.20	RM98-04C-459	111004	67	12.88	42.05	16.16	13.93	1.87
GS-1765C-782	107007	141	12.54	54.66	16.22	13.99	2.08	RM98-04C-459	111004	68	14.58	83.96	16.27	15.59	2.27
GS-1765C-782	107007	142	9.76	44.15	16.18	11.83	1.95	RM98-04C-459	111004	69	15.74	34.73	16.22	16.00	2.07
GS-1765C-782	107007	143	14.30	27.32	16.26	14.68	2.22	RM98-04C-459	111004	70	14.48	38.56	16.18	15.06	1.96
GS-1765C-782	107007	144	9.86	61.00	16.26	12.39	2.22	RM98-04C-459	111004	71	15.03	66.09	16.27	15.79	2.25
GS-1765C-782	107007	145	10.42	13.26	16.26	10.83	2.22	RM98-04C-459	111004	72	14.72	60.62	16.24	15.54	2.16
GS-1765C-782	107007	146	15.13	61.80	16.16	15.82	1.87	RM98-04C-459	111004	73	14.02	54.70	16.27	15.00	2.26
GS-1765C-782	107007	147	14.72	62.75	16.28	15.56	2.28	RM98-04C-459	111004	74	15.53	73.74	16.27	16.15	2.26
GS-1765C-782	107007	148	10.62	51.28	16.16	12.63	1.88	RM98-04C-459	111004	75	13.17	27.08	16.27	13.73	2.26
GS-1765C-782	107007	149	11.45	51.93	16.35	13.20	2.53	RM98-04C-459	111004	76	14.33	81.28	16.15	15.43	1.85
GS-1765C-782	107007	150	14.38	41.82	16.35	15.04	2.53	RM98-04C-459	111004	77	15.83	42.62	16.15	16.15	1.85
GS-1765C-782	107007	151	5.89	67.42	16.23	11.63	2.11	RM98-04C-459	111004	78	13.77	53.31	16.16	14.80	1.86
GS-1765C-782	107007	152	9.42	47.63	16.27	11.74	2.26	RM98-04C-459	111004	79	15.98	38.99	16.30	16.23	2.36
GS-1765C-782	107007	153	9.92	69.79	16.27	12.59	2.26	RM98-04C-459	111004	80	14.58	46.36	16.21	15.26	2.05
GS-1765C-782	107007	154	8.15	65.13	16.18	12.03	1.95	RM98-04C-459	111004	81	16.19	87.04	16.21	16.59	2.05
GS-1765C-782	107007	155	15.65	73.44	16.23	16.23	2.11	RM98-04C-459	111004	82	15.76	76.30	16.14	16.30	1.81
GS-1765C-782	107007	156	11.39	74.96	16.22	13.57	2.08	RM98-04C-459	111004	83	17.02	64.60	16.14	17.09	1.81

Table C3 Apatite fission track lengths for all samples analysed in this thesis

UBC	A2Z	Track	Angle				Dpar	UBC	A2Z	Track	Angle				Dpar
			Length (μm)	to c- axis	Lo calc (μm)	Lc calc (μm)					Length (μm)	to c- axis	Lo calc (μm)	Lc calc (μm)	
GS-1765C-782	107007	157	12.61	28.59	16.21	13.32	2.06	RM98-04C-459	111004	84	15.62	67.83	16.23	16.18	2.11
GS-1765C-782	107007	158	8.49	67.36	16.23	12.15	2.12	RM98-04C-459	111004	85	14.94	66.26	16.22	15.73	2.10
GS-1765C-782	107007	159	8.68	53.95	16.23	11.77	2.12	RM98-04C-459	111004	86	12.06	57.03	16.31	13.72	2.42
GS-1765C-782	107007	160	15.72	66.80	16.21	16.24	2.04	RM98-04C-459	111004	87	13.38	70.07	16.23	14.77	2.11
GS-1814C-1595	117806	1	13.47	73.96	16.27	14.86	2.25	RM98-04C-459	111004	88	13.09	25.62	16.23	13.62	2.11
GS-1814C-1595	117806	2	13.59	41.58	16.27	14.44	2.25	RM98-04C-459	111004	89	14.22	50.19	16.28	15.07	2.28
GS-1814C-1595	117806	3	13.34	53.73	16.14	14.52	1.80	RM98-04C-459	111004	90	13.64	66.36	16.25	14.90	2.20
GS-1814C-1595	117806	4	11.32	73.47	16.14	13.51	1.80	RM98-04C-459	111004	91	14.84	73.64	16.20	15.72	2.02
GS-1814C-1595	117806	5	14.20	75.80	16.16	15.33	1.86	RM98-04C-459	111004	92	14.33	74.72	16.24	15.40	2.17
GS-1814C-1595	117806	6	13.99	54.21	16.16	14.97	1.86	RM98-04C-459	111004	93	18.35	80.38	16.27	17.92	2.26
GS-1814C-1595	117806	7	12.86	28.94	16.20	13.53	2.00	RM98-04C-459	111004	94	14.70	60.19	16.20	15.52	2.03
GS-1814C-1595	117806	8	9.45	64.40	16.21	12.27	2.05	RM98-04C-459	111004	95	11.46	70.41	16.20	13.56	2.03
GS-1814C-1595	117806	9	15.96	69.35	16.21	16.41	2.05	RM98-04C-459	111004	96	14.37	79.89	16.29	15.45	2.32
GS-1814C-1595	117806	10	9.66	54.79	16.30	12.11	2.38	RM98-04C-459	111004	97	14.36	59.27	16.20	15.29	2.01
GS-1814C-1595	117806	11	9.59	19.62	16.30	10.52	2.38	RM98-04C-459	111004	98	7.39	36.17	16.22	10.76	2.10
GS-1814C-1595	117806	12	13.70	43.00	16.21	14.56	2.05	RM98-04C-459	111004	99	14.32	65.67	16.22	15.33	2.09
GS-1814C-1595	117806	13	16.03	57.62	16.18	16.40	1.95	RM98-04C-459	111004	100	16.47	5.06	16.29	16.47	2.32
GS-1814C-1595	117806	14	15.11	37.67	16.23	15.53	2.13	RM98-04C-459	111004	101	14.45	67.32	16.20	15.43	2.02
GS-1814C-1595	117806	15	14.30	56.53	16.22	15.21	2.08	RM98-04C-459	111004	102	15.45	62.61	16.28	16.04	2.30
GS-1814C-1595	117806	16	14.63	12.77	16.24	14.72	2.16	RM98-04C-459	111004	103	14.67	29.69	16.20	15.04	2.01
GS-1814C-1595	117806	17	14.75	62.72	16.11	15.58	1.68	RM98-04C-459	111004	104	15.69	76.84	16.19	16.26	1.98
GS-1814C-1595	117806	18	13.82	36.45	16.11	14.50	1.68	RM98-04C-459	111004	105	14.96	62.31	16.29	15.72	2.33
GS-1814C-1595	117806	19	13.42	49.60	16.21	14.49	2.05	RM98-04C-459	111004	106	15.74	36.51	16.18	16.02	1.96
GS-1814C-1595	117806	20	14.90	45.21	16.34	15.48	2.50	RM98-04C-459	111004	107	14.57	56.20	16.12	15.39	1.73
GS-1814C-1595	117806	21	12.27	85.63	16.24	14.18	2.14	RM98-04C-459	111004	108	15.07	84.62	16.16	15.90	1.87
GS-1814C-1595	117806	22	14.04	78.83	16.24	15.24	2.14	RM98-04C-459	111004	109	16.42	38.79	16.20	16.58	2.00
GS-1814C-1595	117806	23	4.20	72.55	16.24	11.33	2.14	RM98-04C-459	111004	110	13.13	51.43	16.25	14.33	2.18
GS-1814C-1595	117806	24	11.31	68.93	16.24	13.45	2.14	RM98-04C-459	111004	111	15.47	13.88	16.12	15.54	1.73
GS-1814C-1595	117806	25	14.41	72.59	16.24	15.44	2.14	RM98-04C-459	111004	112	17.41	32.17	16.25	17.38	2.18
GS-1814C-1595	117806	26	12.93	42.78	16.24	13.99	2.14	RM98-04C-459	111004	113	16.13	34.88	16.26	16.32	2.21
GS-1814C-1595	117806	27	13.62	82.00	16.24	15.00	2.14	RM98-04C-459	111004	114	15.38	83.31	16.30	16.08	2.36
GS-1814C-1595	117806	28	14.09	76.69	16.23	15.26	2.12	RM98-04C-459	111004	115	14.61	54.92	16.23	15.40	2.11
GS-1814C-1595	117806	29	11.21	64.07	16.23	13.31	2.12	RM98-04C-459	111004	116	11.12	45.82	16.18	12.80	1.93
GS-1814C-1595	117806	30	13.92	67.16	16.23	15.09	2.12	RM98-04C-459	111004	117	14.12	40.43	16.23	14.82	2.11
GS-1814C-1595	117806	31	15.65	62.54	16.24	16.17	2.15	RM98-04C-459	111004	118	15.41	46.04	16.18	15.87	1.93
GS-1814C-1595	117806	32	16.04	63.23	16.26	16.44	2.23	RM98-04C-459	111004	119	15.09	78.44	16.29	15.89	2.32
GS-1814C-1595	117806	33	14.90	51.78	16.21	15.57	2.04	RM98-04C-459	111004	120	16.78	21.14	16.22	16.81	2.07
GS-1814C-1595	117806	34	14.90	70.18	16.27	15.74	2.26	RM98-04C-459	111004	121	12.22	35.16	16.22	13.24	2.07
GS-1814C-1595	117806	35	14.76	60.37	16.27	15.57	2.26	RM98-04C-459	111004	122	14.37	67.87	16.20	15.38	2.02
GS-1814C-1595	117806	36	8.30	66.58	16.27	12.10	2.26	RM98-04C-459	111004	123	15.31	48.55	16.22	15.82	2.09
GS-1814C-1595	117806	37	14.93	48.91	16.34	15.55	2.52	RM98-04C-459	111004	124	12.69	58.69	16.12	14.17	1.72
GS-1814C-1595	117806	38	14.63	79.08	16.34	15.61	2.52	RM98-04C-459	111004	125	14.78	32.31	16.26	15.18	2.23
GS-1814C-1595	117806	39	16.50	26.96	16.34	16.58	2.52	RM98-04C-459	111004	126	12.47	49.19	16.34	13.83	2.52
GS-1814C-1595	117806	40	10.22	33.76	16.34	11.72	2.52	RM98-04C-459	111004	127	13.70	77.16	16.37	15.02	2.60
GS-1814C-1595	117806	41	15.43	34.52	16.34	15.75	2.52	RM98-04C-459	111004	128	15.43	47.62	16.30	15.90	2.35
GS-1814C-1595	117806	42	14.42	50.66	16.34	15.21	2.52	RM98-04C-459	111004	129	10.05	60.69	16.24	12.51	2.16
GS-1814C-1595	117806	43	8.33	68.14	16.34	12.14	2.52	RM98-04C-459	111004	130	14.85	62.78	16.22	15.65	2.10
GS-1814C-1595	117806	44	13.01	65.66	16.34	14.48	2.52	RM98-04C-459	111004	131	14.53	44.61	16.21	15.20	2.04
GS-1814C-1595	117806	45	14.81	55.68	16.27	15.55	2.25	RM98-04C-459	111004	132	13.26	60.59	16.26	14.58	2.24
GS-1814C-1595	117806	46	12.31	63.92	16.16	14.01	1.86	RM98-04C-459	111004	133	13.21	66.85	16.29	14.63	2.32
GS-1814C-1595	117806	47	14.80	54.41	16.15	15.53	1.84	RM98-04C-459	111004	134	13.14	77.20	16.28	14.68	2.29
GS-1814C-1595	117806	48	11.24	83.61	16.20	13.54	2.02	RM98-04C-459	111004	135	14.98	64.62	16.17	15.75	1.92
GS-1814C-1595	117806	49	14.25	24.08	16.20	14.57	2.02	RM98-04C-459	111004	136	14.45	7.04	16.28	14.48	2.29
GS-1814C-1595	117806	50	13.45	68.94	16.26	14.80	2.24	RM98-04C-459	111004	137	14.84	37.23	16.22	15.31	2.09
GS-1814C-1595	117806	51	13.48	52.11	16.19	14.58	1.99	RM98-04C-459	111004	138	14.29	75.48	16.21	15.38	2.06
GS-1814C-1595	117806	52	16.02	18.31	16.19	16.09	1.99	RM98-04C-459	111004	139	14.55	89.26	16.27	15.58	2.26
GS-1814C-1595	117806	53	14.98	45.74	16.13	15.55	1.78	RM98-04C-459	111004	140	13.04	56.49	16.27	14.36	2.26
GS-1814C-1595	117806	54	14.65	85.48	16.13	15.64	1.78	RM98-04C-459	111004	141	14.70	58.92	16.24	15.51	2.14
GS-1814C-1595	117806	55	13.67	65.44	16.19	14.91	1.97	S12	30410	1	14.52	16.88	16.20	14.68	2.03
GS-1814C-1595	117806	56	14.33	0.58	16.19	14.33	1.97	S12	30410	2	13.79	76.74	16.20	15.08	2.03
GS-1814C-1595	117806	57	12.50	59.46	16.22	14.06	2.08	S12	30410	3	14.87	23.29	16.20	15.10	2.03

Table C3 Apatite fission track lengths for all samples analysed in this thesis

Angle								Angle							
UBC	A2Z	Track	Length (μm)	to c- axis	Lo calc (μm)	Lc calc (μm)	Dpar (μm)	UBC	A2Z	Track	Length (μm)	to c- axis	Lo calc (μm)	Lc calc (μm)	Dpar (μm)
GS-1814C-1595	117806	58	12.70	52.01	16.22	14.05	2.07	S12	30410	4	15.32	27.49	16.20	15.56	2.03
GS-1814C-1595	117806	59	8.35	78.73	16.22	12.36	2.07	S12	30410	5	14.44	43.04	16.20	15.11	2.03
GS-1814C-1595	117806	60	13.07	71.44	16.22	14.59	2.07	S12	30410	6	14.01	72.88	16.20	15.19	2.03
GS-1814C-1595	117806	61	11.78	86.97	16.22	13.88	2.07	S12	30410	7	12.98	44.19	16.16	14.06	1.88
GS-1814C-1595	117806	62	14.65	82.54	16.22	15.63	2.07	S12	30410	8	12.54	79.48	16.16	14.32	1.88
GS-1814C-1595	117806	63	10.65	39.00	16.22	12.24	2.07	S12	30410	9	13.33	47.03	16.16	14.38	1.87
GS-1814C-1595	117806	64	16.95	22.93	16.20	16.97	2.02	S12	30410	10	13.28	84.88	16.09	14.80	1.64
GS-1814C-1595	117806	65	13.72	74.30	16.16	15.02	1.89	S12	30410	11	14.13	83.25	16.18	15.32	1.95
GS-1814C-1595	117806	66	13.99	42.10	16.23	14.75	2.13	S12	30410	12	12.94	62.39	16.18	14.39	1.95
GS-1814C-1595	117806	67	13.07	63.36	16.23	14.49	2.13	S12	30410	13	14.99	36.75	16.11	15.43	1.68
GS-1814C-1595	117806	68	14.60	31.64	16.20	15.02	2.01	S12	30410	14	10.50	42.09	16.15	12.25	1.85
GS-1814C-1595	117806	69	16.00	68.27	16.24	16.43	2.15	S12	30410	15	12.73	62.10	16.18	14.25	1.96
GS-1814C-1595	117806	70	12.82	30.17	16.17	13.54	1.92	S12	30410	16	13.93	28.73	16.17	14.41	1.90
GS-1814C-1595	117806	71	9.13	64.36	16.24	12.20	2.14	S12	30410	17	11.35	66.22	16.19	13.44	1.97
GS-1814C-1595	117806	72	14.71	60.22	16.18	15.53	1.94	S12	30410	18	13.96	56.31	16.19	14.98	1.97
GS-1814C-1595	117806	73	9.42	29.68	16.18	10.96	1.94	S12	30410	19	15.01	34.04	16.19	15.40	1.97
GS-1814C-1595	117806	74	13.43	39.04	16.29	14.26	2.34	S12	30410	20	12.73	73.23	16.19	14.39	1.97
GS-1814C-1595	117806	75	9.86	35.92	16.23	11.57	2.11	S12	30410	21	13.21	41.63	16.24	14.17	2.15
GS-1814C-1595	117806	76	12.07	57.39	16.23	13.74	2.11	S12	30410	22	12.96	67.61	16.18	14.48	1.95
GS-1814C-1595	117806	77	15.10	38.94	16.14	15.54	1.80	S12	30410	23	9.92	86.43	16.30	12.85	2.35
GS-1814C-1595	117806	78	15.50	50.19	16.20	15.98	2.00	S12	30410	24	12.30	60.62	16.30	13.95	2.35
GS-1814C-1595	117806	79	13.45	22.83	16.29	13.85	2.33	S12	30410	25	9.62	87.85	16.10	12.89	1.66
GS-1814C-1595	117806	80	14.80	61.47	16.23	15.60	2.13	S12	30410	26	14.09	66.39	16.10	15.19	1.66
GS-1814C-1595	117806	81	14.28	48.07	16.23	15.07	2.13	S12	30410	27	8.05	70.72	16.17	12.28	1.92
GS-1814C-1595	117806	82	13.64	62.74	16.20	14.85	2.00	S12	30410	28	13.37	83.19	16.23	14.85	2.12
GS-1814C-1595	117806	83	14.25	65.69	16.27	15.28	2.25	S12	30410	29	12.72	53.43	16.23	14.09	2.12
GS-1814C-1595	117806	84	12.00	78.15	16.13	13.98	1.75	S12	30410	30	12.67	71.65	16.23	14.34	2.12
GS-1814C-1595	117806	85	11.58	65.24	16.28	13.57	2.30	S12	30410	31	12.98	45.18	16.23	14.09	2.12
GS-1814C-1595	117806	86	11.09	35.18	16.28	12.40	2.30	S12	30410	32	14.63	64.43	16.23	15.52	2.12
GS-1814C-1595	117806	87	13.92	23.00	16.21	14.26	2.06	S12	30410	33	12.13	86.75	16.23	14.10	2.12
GS-1814C-1595	117806	88	8.71	69.12	16.17	12.24	1.92	S12	30410	34	11.40	59.02	16.14	13.34	1.81
GS-1814C-1595	117806	89	13.18	42.70	16.17	14.17	1.92	S12	30410	35	13.13	87.35	16.25	14.71	2.20
GS-1814C-1595	117806	90	15.20	87.26	16.17	15.98	1.92	S12	30410	36	12.28	38.87	16.16	13.40	1.87
GS-1814C-1595	117806	91	14.33	72.45	16.16	15.39	1.86	S12	30410	37	10.76	49.31	16.10	12.67	1.65
GS-1814C-1595	117806	92	13.84	77.96	16.16	15.12	1.86	S12	30410	38	13.10	50.21	16.11	14.28	1.68
GS-1814C-1595	117806	93	12.82	32.41	16.16	13.61	1.86	S12	30410	39	14.58	47.53	16.11	15.28	1.68
GS-1814C-1595	117806	94	15.92	34.46	16.23	16.15	2.11	S12	30410	40	10.72	63.06	16.11	12.98	1.68
GS-1814C-1595	117806	95	14.64	62.72	16.23	15.51	2.11	S12	30410	41	13.64	58.75	16.21	14.80	2.05
GS-1814C-1595	117806	96	12.41	63.29	16.13	14.07	1.76	S12	30410	42	13.08	49.57	16.26	14.26	2.23
GS-1814C-1595	117806	97	11.23	59.46	16.13	13.23	1.76	S12	30410	43	13.60	44.68	16.26	14.52	2.23
GS-1814C-1595	117806	98	14.43	38.58	16.20	15.02	2.00	S12	30410	44	13.25	66.02	16.09	14.64	1.63
GS-1814C-1595	117806	99	15.66	30.61	16.18	15.89	1.94	S12	30410	45	14.06	42.26	16.09	14.81	1.63
GS-1814C-1595	117806	100	14.98	71.57	16.18	15.79	1.94	S12	30410	46	13.74	52.50	16.09	14.77	1.63
GS-1814C-1595	117806	101	14.26	82.32	16.19	15.39	1.98	S12	30410	47	13.91	67.44	16.20	15.08	2.00
GS-1814C-1595	117806	102	15.01	37.70	16.19	15.46	1.98	S12	30410	48	13.54	48.49	16.20	14.56	2.00
GS-1814C-1595	117806	103	15.67	30.11	16.18	15.89	1.96	S12	30410	49	12.42	54.40	16.20	13.91	2.00
GS-1814C-1595	117806	104	12.62	49.98	16.18	13.95	1.96	S12	30410	50	11.23	14.23	16.20	11.59	2.00
GS-1814C-1595	117806	105	14.65	78.17	16.29	15.62	2.32	S12	30410	51	12.72	48.56	16.17	13.98	1.92
GS-1814C-1595	117806	106	10.51	81.09	16.20	13.08	2.00	S12	30410	52	13.09	48.43	16.17	14.24	1.92
GS-1814C-1595	117806	107	11.38	75.58	16.20	13.57	2.00	S12	30410	53	13.52	42.78	16.17	14.42	1.92
GS-1814C-1595	117806	108	13.65	35.04	16.35	14.33	2.53	S12	30410	54	13.69	75.20	16.21	15.01	2.06
GS-1814C-1595	117806	109	15.10	56.74	16.26	15.76	2.22	S12	30410	55	13.21	84.01	16.32	14.75	2.44
GS-1814C-1595	117806	110	13.45	35.70	16.20	14.20	2.03	S12	30410	56	10.17	50.76	16.10	12.32	1.67
GS-1814C-1595	117806	111	9.80	64.11	16.20	12.42	2.03	S12	30410	57	16.70	43.07	16.17	16.82	1.92
GS-1814C-1595	117806	112	14.51	63.89	16.20	15.44	2.03	S12	30410	58	11.76	70.22	16.13	13.75	1.75
GS-1814C-1595	117806	113	10.71	24.78	16.20	11.65	2.03	S12	30410	59	15.47	89.88	16.23	16.14	2.12
GS-1814C-1595	117806	114	13.94	54.87	16.20	14.95	2.03	S12	30410	60	15.71	71.07	16.23	16.25	2.12
GS-1814C-1595	117806	115	10.05	71.94	16.20	12.71	2.03	S12	30410	61	14.85	88.26	16.23	15.76	2.12
GS-1814C-1595	117806	116	14.72	42.53	16.22	15.31	2.07	S12	30410	62	14.56	20.14	16.23	14.77	2.12
GS-1814C-1595	117806	117	10.20	70.32	16.26	12.78	2.23	S12	30410	63	14.69	64.84	16.23	15.56	2.12
GS-1814C-1595	117806	118	13.80	70.48	16.26	15.04	2.23	S12	30410	64	10.92	10.86	16.23	11.17	2.12

Table C3 Apatite fission track lengths for all samples analysed in this thesis

UBC	A2Z	Track	Angle				Dpar	UBC	A2Z	Track	Angle				Dpar
			Length (μm)	to c- axis	Lo calc (μm)	Lc calc (μm)					Length (μm)	to c- axis	Lo calc (μm)	Lc calc (μm)	
GS-1814C-1595	117806	119	13.66	32.73	16.26	14.28	2.23	S12	30410	65	15.41	81.97	16.23	16.10	2.12
GS-1814C-1595	117806	120	11.98	6.90	16.22	12.06	2.10	S12	30410	66	12.62	72.82	16.23	14.32	2.12
GS-1814C-1595	117806	121	14.41	42.72	16.22	15.08	2.10	S12	30410	67	14.53	65.55	16.10	15.46	1.67
GS-1814C-1595	117806	122	15.43	66.60	16.25	16.05	2.19	S12	30410	68	14.37	49.78	16.13	15.17	1.78
GS-1814C-1595	117806	123	13.74	76.62	16.25	15.05	2.19	S12	30410	69	15.55	66.87	16.14	16.13	1.81
GS-1814C-1595	117806	124	14.91	53.39	16.15	15.59	1.83	S12	30410	70	16.58	37.74	16.33	16.70	2.48
GS-1814C-1595	117806	125	13.85	81.86	16.15	15.14	1.83	S12	30410	71	14.02	20.81	16.33	14.30	2.48
GS-1814C-1595	117806	126	13.50	40.27	16.23	14.35	2.12	S12	30410	72	14.53	21.33	16.33	14.77	2.48
GS-1814C-1595	117806	127	12.11	52.80	16.23	13.67	2.12	S12	30410	73	14.03	68.23	16.25	15.17	2.19
GS-1814C-1595	117806	128	13.56	36.60	16.20	14.30	2.01	S12	30410	74	13.14	87.66	16.25	14.72	2.19
GS-1814C-1595	117806	129	14.53	63.25	16.21	15.44	2.05	S12	30410	75	15.31	18.39	16.16	15.43	1.88
GS-1814C-1595	117806	130	14.06	39.56	16.21	14.75	2.05	S12	30410	76	14.58	43.43	16.31	15.22	2.41
GS-1814C-1595	117806	131	14.49	76.19	16.24	15.51	2.17	S12	30410	77	13.29	55.78	16.31	14.52	2.41
GS-1814C-1595	117806	132	11.21	62.43	16.24	13.28	2.17	S12	30410	78	13.78	81.72	16.13	15.09	1.78
GS-1814C-1595	117806	133	11.28	83.48	16.30	13.56	2.37	S12	30410	79	13.28	82.77	16.13	14.79	1.78
GS-1814C-1595	117806	134	9.50	41.72	16.30	11.57	2.37	S12	30410	80	12.73	71.90	16.13	14.38	1.78
GS-1814C-1595	117806	135	14.54	50.71	16.30	15.30	2.37	S12	30410	81	13.75	45.89	16.13	14.65	1.78
GS-1814C-1595	117806	136	14.54	70.59	16.23	15.51	2.11	S12	30410	82	14.52	23.35	16.13	14.79	1.78
GS-1814C-1595	117806	137	15.34	43.44	16.18	15.79	1.93	S12	30410	83	12.02	63.18	16.13	13.81	1.78
GS-1814C-1595	117806	138	9.90	57.19	16.19	12.33	1.98	S12	30410	84	11.61	80.77	16.13	13.75	1.78
GS-1814C-1595	117806	139	11.42	35.43	16.19	12.65	1.98	S12	30410	85	14.02	69.19	16.61	15.17	3.47
GS-1814C-1595	117806	140	15.86	63.46	16.19	16.32	1.98	S12	30410	86	12.76	87.60	16.61	14.48	3.47
GS-1814C-1595	117806	141	14.87	64.97	16.28	15.68	2.31	S12	30410	87	14.70	49.08	16.61	15.39	3.47
GS-1814C-1595	117806	142	12.64	62.36	16.28	14.20	2.31	S12	30410	88	15.13	26.79	16.11	15.39	1.71
GS-1814C-1595	117806	143	13.35	71.53	16.18	14.76	1.93	S13	30411	1	12.96	81.73	16.10	14.59	1.66
GS-1814C-1595	117806	144	13.74	57.30	16.18	14.85	1.93	S13	30411	2	15.40	88.87	16.10	16.10	1.66
GS-1814C-1595	117806	145	9.23	50.17	16.18	11.70	1.93	S13	30411	3	9.67	83.81	16.10	12.78	1.66
GS-1814C-1595	117806	146	11.24	46.16	16.21	12.90	2.05	S13	30411	4	12.02	66.23	16.13	13.86	1.76
GS-1814C-1595	117806	147	10.09	63.44	16.31	12.59	2.39	S13	30411	5	13.30	59.86	16.13	14.59	1.76
GS-1814C-1595	117806	148	13.44	61.60	16.14	14.71	1.79	S13	30411	6	13.02	65.23	16.13	14.49	1.76
GS-1814C-1595	117806	149	14.37	48.65	16.28	15.15	2.30	S13	30411	7	13.80	24.32	16.14	14.19	1.79
GS-1814C-1595	117806	150	16.57	34.43	16.26	16.68	2.22	S13	30411	8	6.71	81.57	16.14	12.47	1.79
GS-1814C-1595	117806	151	14.07	51.69	16.28	14.99	2.29	S13	30411	9	13.68	43.17	16.14	14.55	1.79
GS-1814C-1595	117806	152	12.12	49.09	16.24	13.58	2.14	S13	30411	10	9.89	51.93	16.14	12.18	1.79
GS-1814C-1595	117806	153	9.46	86.65	16.25	12.71	2.18	S13	30411	11	14.09	37.61	16.14	14.74	1.79
GS-1814C-1595	117806	154	12.99	72.02	16.25	14.54	2.18	S13	30411	12	13.28	22.70	16.19	13.69	1.97
GS-1814C-1595	117806	155	14.74	84.11	16.13	15.69	1.76	S13	30411	13	11.46	62.55	16.19	13.44	1.97
GS-1814C-1595	117806	156	7.38	73.11	16.24	12.05	2.15	S13	30411	14	13.12	32.06	16.19	13.84	1.97
GS-1814C-1595	117806	157	15.32	39.78	16.26	15.73	2.24	S13	30411	15	8.93	69.14	16.19	12.31	1.97
GS-1814C-1595	117806	158	12.07	45.41	16.26	13.45	2.24	S13	30411	16	13.82	31.08	16.19	14.37	1.97
GS-1814C-1595	117806	159	15.40	19.32	16.25	15.53	2.19	S13	30411	17	14.50	44.81	16.19	15.18	1.97
GS-1814C-1595	117806	160	15.61	81.68	16.19	16.22	1.97	S13	30411	18	14.29	50.09	16.19	15.11	1.97
GS-1814C-1595	117806	161	14.67	32.93	16.19	15.10	1.97	S13	30411	19	14.44	44.52	16.19	15.13	1.97
GS-1814C-1595	117806	162	10.31	52.74	16.19	12.47	1.99	S13	30411	20	15.40	6.56	16.19	15.42	1.97
GS-1814C-1595	117806	163	13.16	66.91	16.19	14.60	1.99	S13	30411	21	14.63	64.49	16.27	15.52	2.25
GS-1814C-1595	117806	164	9.07	55.26	16.19	11.89	1.99	S13	30411	22	13.42	72.86	16.15	14.82	1.83
GS-1814C-1595	117806	165	14.29	68.85	16.30	15.34	2.37	S13	30411	23	14.00	73.82	16.15	15.19	1.83
GS-1814C-1595	117806	166	15.66	81.88	16.30	16.25	2.37	S13	30411	24	12.59	79.51	16.19	14.35	1.98
GS-1814C-1595	117806	167	14.70	28.46	16.30	15.05	2.37	S13	30411	25	14.03	85.67	16.19	15.26	1.98
GS-1814C-1595	117806	168	14.02	70.84	16.13	15.18	1.75	S13	30411	26	13.00	76.22	16.19	14.58	1.98
GS-1814C-1595	117806	169	12.21	81.33	16.13	14.13	1.75	S13	30411	27	12.77	81.32	16.19	14.47	1.98
GS-1814C-1595	117806	170	12.85	57.45	16.20	14.26	2.00	S13	30411	28	15.19	20.81	16.19	15.35	1.98
GS-1814C-1595	117806	171	12.62	46.63	16.20	13.87	2.00	S13	30411	29	13.85	66.80	16.19	15.04	1.98
GS-1814C-1595	117806	172	14.95	53.27	16.24	15.62	2.14	S13	30411	30	15.13	46.02	16.19	15.66	1.98
GS-1814C-1595	117806	173	12.90	22.48	16.21	13.36	2.06	S13	30411	31	11.23	9.48	16.19	11.41	1.98
GS-1814C-1595	117806	174	5.43	60.49	16.21	11.38	2.06	S13	30411	32	13.02	76.88	16.19	14.60	1.98
GS-1814C-1595	117806	175	15.28	77.64	16.21	16.01	2.06	S13	30411	33	11.75	56.08	16.12	13.50	1.74
GS-1814C-1595	117806	176	13.56	61.16	16.25	14.78	2.19	S13	30411	34	13.05	50.89	16.12	14.26	1.74
GS-1814C-1595	117806	177	12.89	83.10	16.27	14.55	2.25	S13	30411	35	14.46	48.76	16.10	15.21	1.67
GS-1814C-1595	117806	178	13.11	23.70	16.27	13.58	2.25	S13	30411	36	13.36	65.94	16.10	14.71	1.67
GS-1814C-1595	117806	179	12.71	76.04	16.16	14.40	1.88	S13	30411	37	14.49	20.45	16.10	14.71	1.67

Table C3 Apatite fission track lengths for all samples analysed in this thesis

Angle								Angle							
UBC	A2Z	Track	Length (μm)	to c- axis	Lo calc (μm)	Lc calc (μm)	Dpar (μm)	UBC	A2Z	Track	Length (μm)	to c- axis	Lo calc (μm)	Lc calc (μm)	Dpar (μm)
GS-1814C-1595	117806	180	12.43	83.08	16.16	14.27	1.88	S13	30411	38	14.71	50.22	16.11	15.41	1.68
GS-1814C-1595	117806	181	15.48	42.53	16.16	15.88	1.88	S13	30411	39	16.00	46.13	16.11	16.31	1.68
GS-1814C-1595	117806	182	13.90	83.31	16.16	15.17	1.88	S13	30411	40	13.11	62.46	16.08	14.51	1.58
GS-1814C-1595	117806	183	8.20	72.91	16.25	12.22	2.18	S13	30411	41	14.29	67.99	16.16	15.33	1.88
GS-1818C-1000	111001	1	16.60	10.68	16.10	16.61	1.65	S13	30411	42	12.27	64.54	16.16	13.99	1.88
GS-1818C-1000	111001	2	14.76	89.34	16.10	15.71	1.65	S13	30411	43	14.37	73.94	16.16	15.42	1.88
GS-1818C-1000	111001	3	14.71	59.82	16.24	15.53	2.17	S13	30411	44	13.87	44.82	16.16	14.72	1.88
GS-1818C-1000	111001	4	16.08	25.40	16.24	16.20	2.17	S13	30411	45	11.65	77.06	16.16	13.75	1.88
GS-1818C-1000	111001	5	14.60	88.30	16.16	15.61	1.87	S13	30411	46	14.54	59.45	16.16	15.41	1.88
GS-1818C-1000	111001	6	15.71	41.32	16.16	16.05	1.87	S13	30411	47	13.17	81.63	16.18	14.72	1.94
GS-1818C-1000	111001	7	14.43	47.49	16.23	15.17	2.11	S13	30411	48	13.16	52.12	16.18	14.36	1.94
GS-1818C-1000	111001	8	15.38	64.67	16.23	16.01	2.11	S13	30411	49	12.33	35.27	16.16	13.32	1.87
GS-1818C-1000	111001	9	10.88	77.68	16.23	13.28	2.11	S13	30411	50	14.21	58.85	16.09	15.18	1.61
GS-1818C-1000	111001	10	12.06	84.86	16.23	14.05	2.11	S13	30411	51	14.54	55.68	16.09	15.37	1.61
GS-1818C-1000	111001	11	15.16	47.11	16.23	15.70	2.11	S13	30411	52	11.23	74.10	16.18	13.46	1.95
GS-1818C-1000	111001	12	14.72	54.52	16.23	15.48	2.11	S13	30411	53	14.36	26.69	16.18	14.72	1.95
GS-1818C-1000	111001	13	15.46	56.87	16.20	16.01	2.02	S13	30411	54	12.43	40.39	16.17	13.56	1.90
GS-1818C-1000	111001	14	13.72	56.65	16.20	14.82	2.02	S13	30411	55	13.73	37.57	16.16	14.46	1.89
GS-1818C-1000	111001	15	11.19	50.84	16.28	13.00	2.28	S13	30411	56	14.15	48.33	16.33	14.99	2.47
GS-1818C-1000	111001	16	8.96	59.47	16.28	12.02	2.28	S13	30411	57	14.67	54.01	16.33	15.43	2.47
GS-1818C-1000	111001	17	9.77	36.14	16.28	11.51	2.28	S13	30411	58	15.15	47.16	16.13	15.69	1.78
GS-1818C-1000	111001	18	13.72	71.58	16.28	15.00	2.28	S13	30411	59	16.05	38.95	16.13	16.29	1.76
GS-1818C-1000	111001	19	15.27	78.89	16.28	16.01	2.28	S13	30411	60	13.48	48.89	16.13	14.52	1.76
GS-1818C-1000	111001	20	12.67	50.55	16.32	13.99	2.45	S13	30411	61	13.23	72.63	16.13	14.70	1.76
GS-1818C-1000	111001	21	15.35	61.93	16.19	15.97	1.99	S13	30411	62	12.95	39.49	16.18	13.92	1.95
GS-1818C-1000	111001	22	8.90	41.78	16.19	11.25	1.98	S13	30411	63	14.06	34.52	16.12	14.65	1.74
GS-1818C-1000	111001	23	8.72	74.61	16.19	12.36	1.98	S13	30411	64	14.12	50.31	16.11	15.00	1.70
GS-1818C-1000	111001	24	14.60	79.67	16.19	15.59	1.98	S13	30411	65	13.22	70.37	16.09	14.67	1.62
GS-1818C-1000	111001	25	13.73	65.62	16.11	14.95	1.71	S15	30413	1	14.02	64.16	16.14	15.12	1.79
GS-1818C-1000	111001	26	12.44	66.36	16.21	14.13	2.06	S15	30413	2	10.87	72.61	16.14	13.22	1.79
GS-1818C-1000	111001	27	13.73	69.76	16.21	14.99	2.06	S15	30413	3	13.97	31.68	16.19	14.51	1.97
GS-1818C-1000	111001	28	14.66	50.63	16.21	15.38	2.06	S15	30413	4	15.16	47.97	16.19	15.71	1.97
GS-1818C-1000	111001	29	14.60	60.30	16.21	15.46	2.06	S15	30413	5	12.21	68.29	16.19	14.01	1.97
GS-1818C-1000	111001	30	13.96	39.21	16.22	14.67	2.09	S15	30413	6	16.18	61.65	16.19	16.52	1.97
GS-1818C-1000	111001	31	16.07	45.87	16.22	16.36	2.09	S15	30413	7	11.91	32.70	16.11	12.92	1.69
GS-1818C-1000	111001	32	8.49	35.08	16.22	10.82	2.09	S15	30413	8	9.65	87.95	16.11	12.89	1.69
GS-1818C-1000	111001	33	11.18	74.01	16.31	13.43	2.39	S15	30413	9	12.39	80.21	16.11	14.23	1.69
GS-1818C-1000	111001	34	15.36	46.67	16.22	15.84	2.09	S15	30413	10	13.84	53.52	16.11	14.86	1.69
GS-1818C-1000	111001	35	16.47	42.12	16.22	16.64	2.09	S15	30413	11	11.37	17.88	16.13	11.87	1.75
GS-1818C-1000	111001	36	12.72	77.64	16.20	14.42	2.00	S15	30413	12	15.81	44.62	16.13	16.15	1.75
GS-1818C-1000	111001	37	15.33	62.33	16.27	15.96	2.26	S15	30413	13	14.20	63.93	16.13	15.23	1.75
GS-1818C-1000	111001	38	11.51	35.99	16.22	12.74	2.10	S15	30413	14	14.62	89.09	16.09	15.62	1.62
GS-1818C-1000	111001	39	13.69	74.64	16.22	15.00	2.10	S15	30413	15	11.84	62.51	16.09	13.69	1.62
GS-1818C-1000	111001	40	14.33	49.45	16.22	15.13	2.10	S15	30413	16	12.89	38.52	16.09	13.85	1.62
GS-1818C-1000	111001	41	13.75	87.49	16.22	15.09	2.10	S15	30413	17	14.05	87.47	16.09	15.27	1.62
GS-1818C-1000	111001	42	15.98	63.98	16.07	16.40	1.57	S15	30413	18	13.24	78.72	16.09	14.75	1.62
GS-1818C-1000	111001	43	14.70	45.56	16.21	15.34	2.05	S15	30413	19	13.75	82.48	16.11	15.08	1.71
GS-1818C-1000	111001	44	13.38	77.03	16.21	14.82	2.05	S15	30413	20	13.94	52.68	16.11	14.91	1.71
GS-1818C-1000	111001	45	13.17	76.71	16.21	14.69	2.05	S15	30413	21	14.34	65.29	16.11	15.34	1.71
GS-1818C-1000	111001	46	8.22	70.79	16.21	12.18	2.05	S15	30413	22	14.19	66.43	16.11	15.25	1.71
GS-1818C-1000	111001	47	14.17	41.65	16.21	14.88	2.05	S15	30413	23	8.98	88.91	16.22	12.91	2.10
GS-1818C-1000	111001	48	15.40	46.05	16.20	15.86	2.03	S15	30413	24	13.58	54.44	16.22	14.69	2.10
GS-1818C-1000	111001	49	13.80	59.63	16.28	14.92	2.28	S15	30413	25	14.53	80.69	16.15	15.55	1.83
GS-1818C-1000	111001	50	7.31	39.45	16.22	10.93	2.09	S15	30413	26	13.36	50.72	16.15	14.47	1.83
GS-1818C-1000	111001	51	11.75	73.41	16.26	13.78	2.24	S15	30413	27	9.47	45.57	16.14	11.70	1.80
GS-1818C-1000	111001	52	10.97	79.68	16.16	13.35	1.88	S15	30413	28	13.13	60.01	16.14	14.48	1.80
GS-1818C-1000	111001	53	14.57	43.28	16.16	15.21	1.88	S15	30413	29	10.65	49.98	16.14	12.62	1.80
GS-1818C-1000	111001	54	14.91	57.84	16.16	15.64	1.88	S15	30413	30	13.79	50.86	16.14	14.78	1.79
GS-1818C-1000	111001	55	9.95	65.48	16.31	12.54	2.41	S15	30413	31	13.85	83.03	16.14	15.14	1.79
GS-1818C-1000	111001	56	10.07	43.70	16.31	12.02	2.41	S15	30413	32	13.69	66.92	16.14	14.94	1.79
GS-1818C-1000	111001	57	7.53	56.91	16.31	11.68	2.41	S15	30413	33	13.55	66.35	16.14	14.84	1.79

Table C3 Apatite fission track lengths for all samples analysed in this thesis

UBC	A2Z	Track	Angle				Dpar	UBC	A2Z	Track	Angle				Dpar
			Length (μm)	to c- axis	Lo calc (μm)	Lc calc (μm)					Length (μm)	to c- axis	Lo calc (μm)	Lc calc (μm)	
GS-1818C-1000	111001	58	13.95	73.99	16.31	15.16	2.41	S15	30413	34	11.52	50.77	16.20	13.22	2.02
GS-1818C-1000	111001	59	16.59	66.42	16.26	16.81	2.24	S15	30413	35	13.92	69.77	16.20	15.11	2.02
GS-1818C-1000	111001	60	12.57	22.01	16.26	13.06	2.22	S15	30413	36	14.49	83.91	16.14	15.54	1.79
GS-1818C-1000	111001	61	11.19	69.71	16.28	13.39	2.28	S15	30413	37	16.89	43.37	16.12	16.96	1.73
GS-1818C-1000	111001	62	15.64	44.95	16.28	16.03	2.28	S15	30413	38	13.78	88.28	16.22	15.11	2.09
GS-1818C-1000	111001	63	15.95	59.69	16.28	16.36	2.28	S15	30413	39	14.39	65.99	16.22	15.38	2.09
GS-1818C-1000	111001	64	12.91	13.36	16.28	13.10	2.28	S15	30413	40	15.12	62.86	16.22	15.83	2.09
GS-1818C-1000	111001	65	14.11	88.59	16.15	15.31	1.84	S15	30413	41	14.28	79.89	16.12	15.40	1.74
GS-1818C-1000	111001	66	12.29	76.41	16.21	14.14	2.06	S15	30413	42	13.56	89.60	16.12	14.97	1.74
GS-1818C-1000	111001	67	14.88	63.76	16.27	15.68	2.27	S15	30413	43	14.01	36.11	16.12	14.64	1.74
GS-1818C-1000	111001	68	13.34	42.25	16.14	14.28	1.81	S15	30413	44	14.26	62.69	16.12	15.26	1.74
GS-1818C-1000	111001	69	14.77	63.83	16.18	15.60	1.94	S15	30413	45	11.98	57.52	16.12	13.68	1.74
GS-1818C-1000	111001	70	12.18	52.94	16.18	13.72	1.94	S15	30413	46	14.17	60.74	16.12	15.18	1.74
GS-1818C-1000	111001	71	9.08	81.16	16.15	12.56	1.85	S15	30413	47	14.98	70.88	16.12	15.79	1.74
GS-1818C-1000	111001	72	8.98	70.09	16.17	12.32	1.92	S15	30413	48	12.81	82.52	16.14	14.50	1.81
GS-1818C-1000	111001	73	10.49	51.90	16.28	12.57	2.30	S15	30413	49	12.79	89.97	16.14	14.50	1.81
GS-1818C-1000	111001	74	12.64	76.60	16.28	14.36	2.30	S15	30413	50	13.92	57.21	16.14	14.97	1.81
GS-1818C-1000	111001	75	13.51	64.18	16.28	14.79	2.30	S15	30413	51	11.40	63.13	16.14	13.42	1.81
GS-1818C-1000	111001	76	10.07	34.13	16.28	11.63	2.30	S15	30413	52	10.55	73.04	16.14	13.03	1.81
GS-1818C-1000	111001	77	11.08	76.59	16.28	13.40	2.30	S15	30413	53	9.86	62.72	16.14	12.43	1.81
GS-1818C-1000	111001	78	14.88	37.35	16.10	15.35	1.66	S15	30413	54	15.17	69.29	16.14	15.90	1.81
GS-1818C-1000	111001	79	13.69	63.40	16.16	14.90	1.87	S15	30413	55	10.38	83.58	16.36	13.01	2.58
GS-1818C-1000	111001	80	12.43	36.84	16.14	13.45	1.79	S15	30413	56	14.23	77.89	16.36	15.36	2.58
GS-1818C-1000	111001	81	15.25	40.26	16.23	15.68	2.12	S15	30413	57	13.33	79.45	16.36	14.81	2.58
GS-1818C-1000	111001	82	13.21	66.50	16.31	14.62	2.39	S15	30413	58	9.61	50.58	16.13	11.96	1.78
GS-1818C-1000	111001	83	16.25	46.36	16.10	16.49	1.67	S15	30413	59	14.82	13.23	16.13	14.91	1.78
GS-1818C-1000	111001	84	11.57	64.50	16.20	13.55	2.01	S15	30413	60	16.23	3.43	16.13	16.23	1.78
GS-1818C-1000	111001	85	12.56	21.59	16.20	13.04	2.01	S15	30413	61	12.81	62.86	16.15	14.32	1.85
GS-1818C-1000	111001	86	14.92	67.21	16.17	15.73	1.90	S15	30413	62	12.94	41.95	16.18	13.98	1.93
GS-1818C-1000	111001	87	11.66	46.99	16.12	13.21	1.72	S15	30413	63	14.52	81.81	16.18	15.55	1.93
GS-1818C-1000	111001	88	12.94	72.11	16.12	14.51	1.72	S15	30413	64	10.66	61.79	16.18	12.92	1.93
GS-1818C-1000	111001	89	15.88	46.97	16.23	16.22	2.13	S15	30413	65	13.87	56.24	16.16	14.92	1.88
GS-1818C-1000	111001	90	11.09	41.44	16.23	12.64	2.13	S15	30413	66	14.94	58.73	16.13	15.67	1.75
GS-1818C-1000	111001	91	14.71	79.62	16.30	15.66	2.35	S15	30413	67	14.57	60.87	16.13	15.44	1.78
GS-1818C-1000	111001	92	9.63	65.85	16.19	12.35	1.98	S15	30413	68	12.63	75.18	16.13	14.34	1.78
GS-1818C-1000	111001	93	13.49	76.64	16.24	14.89	2.14	S15	30413	69	14.07	51.77	16.13	14.99	1.78
GS-1818C-1000	111001	94	15.60	55.14	16.24	16.09	2.14	S15	30413	70	13.43	55.70	16.13	14.61	1.78
GS-1818C-1000	111001	95	16.75	15.11	16.19	16.77	1.97	S15	30413	71	14.61	85.94	16.13	15.62	1.78
GS-1818C-1000	111001	96	15.78	20.29	16.25	15.89	2.18	S15	30413	72	14.20	68.06	16.07	15.27	1.56
GS-1818C-1000	111001	97	14.41	71.54	16.22	15.43	2.10	S15	30413	73	16.73	61.37	16.07	16.89	1.56
GS-1818C-1000	111001	98	16.09	48.12	16.13	16.39	1.77	S15	30413	74	10.14	69.00	16.07	12.72	1.56
GS-1818C-1000	111001	99	14.74	39.84	16.13	15.28	1.77	S15	30413	75	8.51	75.67	16.20	12.47	2.00
GS-1818C-1000	111001	100	11.66	41.54	16.24	13.04	2.17	S15	30413	76	11.01	52.67	16.20	12.93	2.00
GS-1818C-1000	111001	101	8.55	88.50	16.17	12.52	1.90	S15	30413	77	15.38	36.79	16.20	15.74	2.00
GS-1818C-1000	111001	102	14.26	87.03	16.17	15.40	1.90	S15	30413	78	15.53	37.01	16.20	15.86	2.00
GS-1818C-1000	111001	103	14.85	36.78	16.20	15.31	2.00	S15	30413	79	16.19	81.64	16.20	16.58	2.00
GS-1818C-1000	111001	104	12.07	86.08	16.20	14.06	2.00	S15	30413	80	12.87	44.27	16.20	13.98	2.00
GS-1818C-1000	111001	105	7.32	46.35	16.17	11.25	1.92	S15	30413	81	15.14	34.26	16.20	15.51	2.00
GS-1818C-1000	111001	106	14.72	57.88	16.17	15.51	1.92	S15	30413	82	8.43	53.22	16.20	11.69	2.00
GS-1818C-1000	111001	107	8.40	50.43	16.17	11.59	1.92	S15	30413	83	7.23	55.66	16.17	11.67	1.92
GS-1818C-1000	111001	108	14.35	73.61	16.14	15.41	1.81	S15	30413	84	14.99	78.68	16.19	15.83	1.98
GS-1818C-1000	111001	109	14.38	79.46	16.14	15.46	1.81	S15	30413	85	15.24	62.80	16.12	15.91	1.72
GS-1818C-1000	111001	110	15.17	87.48	16.14	15.96	1.81	S15	30413	86	16.34	32.80	16.18	16.48	1.94
GS-1818C-1000	111001	111	15.35	12.21	16.14	15.41	1.81	S15	30413	87	10.82	48.51	16.19	12.69	1.98
GS-1818C-1000	111001	112	14.48	64.93	16.14	15.43	1.81	S15	30413	88	14.47	47.53	16.28	15.20	2.31
GS-1818C-1000	111001	113	11.37	81.86	16.28	13.61	2.28	S15	30413	89	13.47	65.18	16.13	14.77	1.76
GS-1818C-1000	111001	114	15.12	60.51	16.28	15.81	2.28	S15	30413	90	16.54	29.63	16.10	16.63	1.67
GS-1818C-1000	111001	115	14.92	68.37	16.22	15.74	2.09	S15	30413	91	11.49	48.33	16.10	13.13	1.67
GS-1818C-1000	111001	116	9.58	81.10	16.20	12.68	2.02	S15	30413	92	14.63	27.56	16.10	14.97	1.67
GS-1818C-1000	111001	117	7.55	52.40	16.20	11.53	2.02	S15	30413	93	9.55	75.22	16.10	12.53	1.67
GS-1818C-1000	111001	118	12.77	56.52	16.20	14.19	2.02	S15	30413	94	13.61	46.20	16.15	14.56	1.85

Table C3 Apatite fission track lengths for all samples analysed in this thesis

UBC	A2Z	Track	Angle				Dpar	UBC	A2Z	Track	Angle				Dpar
			Length (μm)	to c- axis	Lo calc (μm)	Lc calc (μm)					Length (μm)	to c- axis	Lo calc (μm)	Lc calc (μm)	
GS-1818C-1000	111001	119	13.44	54.77	16.18	14.60	1.96	S15	30413	95	11.27	65.65	16.15	13.38	1.85
GS-1818C-1000	111001	120	13.77	66.03	16.13	14.98	1.76	S15	30413	96	12.56	65.27	16.15	14.19	1.85
GS-1818C-1000	111001	121	12.91	27.79	16.13	13.54	1.76	S15	30413	97	11.80	47.56	16.15	13.32	1.85
GS-1818C-1000	111001	122	14.98	66.16	16.21	15.76	2.05	S15	30413	98	10.77	56.90	16.15	12.88	1.85
GS-1818C-1000	111001	123	6.21	61.37	16.21	11.56	2.05	S15	30413	99	13.42	67.71	16.15	14.77	1.85
GS-1818C-1000	111001	124	11.16	46.99	16.08	12.87	1.60	S15	30413	100	12.35	40.47	16.15	13.50	1.85
GS-1818C-1000	111001	125	14.63	55.14	16.08	15.42	1.60	S15	30413	101	10.84	25.01	16.15	11.77	1.85
GS-1818C-1000	111001	126	14.73	50.17	16.18	15.43	1.94	S15	30413	102	11.50	42.56	16.15	12.96	1.85
GS-1818C-1000	111001	127	9.51	88.98	16.18	12.75	1.94	S15	30413	103	14.04	35.73	16.15	14.66	1.85
GS-1818C-1000	111001	128	14.78	54.93	16.18	15.52	1.94	S15	30413	104	15.50	65.27	16.14	16.09	1.79
GS-1818C-1000	111001	129	15.15	73.37	16.18	15.91	1.94	S15	30413	105	10.19	42.59	16.14	12.06	1.79
GS-1818C-1000	111001	130	12.47	69.67	16.11	14.19	1.71	S15	30413	106	13.90	70.79	16.09	15.11	1.62
GS-1818C-1000	111001	131	14.81	75.17	16.11	15.71	1.71	S15	30413	107	14.50	44.90	16.09	15.18	1.62
GS-1818C-1000	111001	132	5.23	62.77	16.11	11.39	1.71	S15	30413	108	14.47	49.09	16.12	15.23	1.72
GS-1818C-1000	111001	133	15.89	30.02	16.23	16.08	2.13	S15	30413	109	14.17	83.11	16.16	15.34	1.89
GS-1818C-1000	111001	134	14.14	40.18	16.21	14.83	2.04	S15	30413	110	14.26	85.84	16.16	15.40	1.89
GS-1818C-1000	111001	135	16.95	24.86	16.21	16.98	2.04	S15	30413	111	14.33	63.86	16.16	15.32	1.89
GS-1818C-1000	111001	136	11.00	65.07	16.21	13.19	2.04	S15	30413	112	10.71	56.98	16.10	12.84	1.66
GS-1818C-1000	111001	137	7.05	39.73	16.14	10.91	1.81	S15	30413	113	10.76	27.57	16.11	11.83	1.68
GS-1818C-1000	111001	138	14.29	89.36	16.16	15.42	1.88	S15	30413	114	13.64	81.65	16.11	15.01	1.68
GS-1818C-1000	111001	139	11.12	89.13	16.16	13.48	1.88	S15	30413	115	14.37	52.85	16.11	15.21	1.68
GS-1818C-1000	111001	140	15.57	68.11	16.16	16.15	1.88	S15	30413	116	14.73	16.04	16.19	14.86	1.99
GS-1818C-1000	111001	141	10.66	50.60	16.16	12.64	1.88	S15	30413	117	13.30	81.09	16.19	14.80	1.99
GS-1818C-1000	111001	142	15.21	67.66	16.21	15.92	2.06	S15	30413	118	13.56	67.37	16.19	14.86	1.99
GS-1818C-1000	111001	143	15.72	43.60	16.21	16.07	2.06	S15	30413	119	10.44	68.07	16.19	12.89	1.99
GS-1818C-1000	111001	144	10.37	73.01	16.15	12.92	1.82	S15	30413	120	13.93	50.32	16.19	14.86	1.99
GS-1818C-1000	111001	145	6.78	72.93	16.15	11.93	1.82	S15	30413	121	14.90	52.45	16.19	15.58	1.99
GS-1818C-1000	111001	146	11.75	49.37	16.15	13.34	1.82	S15	30413	122	13.95	6.52	16.19	13.98	1.99
GS-1818C-1000	111001	147	9.57	82.07	16.15	12.69	1.82	S15	30413	123	12.94	34.51	16.19	13.77	1.99
GS-1818C-1000	111001	148	16.40	28.81	16.24	16.51	2.17	S15	30413	124	11.82	44.20	16.19	13.24	1.99
GS-1818C-1000	111001	149	11.82	67.69	16.24	13.75	2.17	S15	30413	125	13.47	88.34	16.06	14.92	1.52
GS-1818C-1000	111001	150	14.63	36.42	16.26	15.13	2.23	S15	30413	126	15.63	5.23	16.06	15.64	1.52
GS-1818C-1000	111001	151	15.92	65.01	16.26	16.36	2.23	S15	30413	127	14.52	66.82	16.16	15.47	1.87
GS-1818C-1000	111001	152	11.14	61.82	16.26	13.22	2.23	S15	30413	128	8.82	38.77	16.16	11.03	1.87
GS-1818C-1000	111001	153	13.01	64.19	16.12	14.47	1.74	S15	30413	129	14.06	61.33	16.09	15.11	1.62
GS-1818C-1000	111001	154	13.74	48.59	16.25	14.70	2.20	S15	30413	130	14.20	48.74	16.09	15.03	1.62
GS-1818C-1000	111001	155	15.66	87.55	16.25	16.26	2.20	S15	30413	131	15.02	77.70	16.15	15.85	1.82
GS-1818C-1000	111001	156	13.07	42.48	16.25	14.08	2.20	S15	30413	132	13.19	36.16	16.10	14.01	1.67
GS-1818C-1000	111001	157	9.48	74.33	16.20	12.53	2.01	S15	30413	133	10.34	55.13	16.09	12.56	1.62
GS-1818C-1000	111001	158	15.15	53.95	16.20	15.77	2.01	S15	30413	134	14.12	71.80	16.18	15.25	1.96
GS-1818C-1000	111001	159	13.52	22.30	16.18	13.89	1.95	S15	30413	135	16.33	41.44	16.20	16.53	2.03
GS-1818C-1000	111001	160	12.49	70.14	16.22	14.21	2.09	S15	30413	136	13.84	69.34	16.25	15.05	2.19
GS-1818C-1000	111001	161	11.27	64.07	16.22	13.35	2.09	S15	30413	137	15.74	13.88	16.25	15.80	2.19
GS-1818C-1000	111001	162	6.53	54.13	16.23	11.41	2.13	S15	30413	138	15.30	8.99	16.20	15.33	2.00
GS-1818C-1000	111001	163	6.32	78.32	16.23	11.92	2.13	S15	30413	139	15.13	37.30	16.20	15.54	2.00
GS-1818C-1000	111001	164	13.83	27.43	16.23	14.29	2.13	S15	30413	140	13.58	77.45	16.12	14.95	1.74
GS-1818C-1000	111001	165	15.35	75.79	16.23	16.05	2.13	S15	30413	141	13.46	22.78	16.06	13.85	1.52
GS-1818C-1000	111001	166	11.82	83.17	16.23	13.89	2.13	S15	30413	142	14.01	74.43	16.23	15.20	2.11
GS-1818C-1000	111001	167	11.18	88.00	16.23	13.52	2.13	S15	30413	143	13.77	16.07	16.16	13.97	1.87
GS-1818C-1000	111001	168	11.46	42.83	16.23	12.94	2.13	S15	30413	144	12.95	18.85	16.16	13.29	1.87
GS-1818C-1000	111001	169	9.80	88.07	16.23	12.82	2.13	S15	30413	145	13.96	89.11	16.16	15.22	1.87
GS-1818C-1000	111001	170	14.81	63.93	16.22	15.63	2.07	S15	30413	146	14.99	17.33	16.16	15.12	1.87
GS-1818C-1000	111001	171	15.36	52.15	16.27	15.89	2.26	S15	30413	147	10.69	86.22	16.16	13.21	1.87
GS-1818C-1000	111001	172	14.87	51.26	16.27	15.54	2.26	S15	30413	148	11.36	58.26	16.20	13.29	2.03
GS-1818C-1000	111001	173	15.82	33.06	16.28	16.05	2.29	S15	30413	149	12.67	56.70	16.20	14.12	2.03
GS-1818C-1000	111001	174	12.33	82.03	16.28	14.20	2.28	S15	30413	150	15.34	58.87	16.12	15.94	1.73
GS-1818C-1000	111001	175	9.85	50.52	16.20	12.11	2.01	S15	30413	151	9.20	66.02	16.18	12.23	1.93
GS-1818C-1000	111001	176	15.80	40.37	16.20	16.11	2.01	S15	30413	152	9.46	49.09	16.10	11.81	1.65
GS-1818C-1000	111001	177	12.44	48.05	16.20	13.78	2.01	S15	30413	153	10.41	70.43	16.10	12.91	1.65
GS-1818C-1000	111001	178	8.21	51.46	16.20	11.60	2.01	S15	30413	154	12.58	33.98	16.18	13.47	1.95
GS-1818C-1000	111001	179	15.01	50.92	16.17	15.63	1.90	S15	30413	155	13.04	1.30	16.18	13.04	1.95

Table C3 Apatite fission track lengths for all samples analysed in this thesis

Angle								Angle							
UBC	A2Z	Track	Length (μm)	to c- axis	Lo calc (μm)	Lc calc (μm)	Dpar (μm)	UBC	A2Z	Track	Length (μm)	to c- axis	Lo calc (μm)	Lc calc (μm)	Dpar (μm)
GS-1818C-1000	111001	180	9.31	31.95	16.17	11.00	1.90	S15	30413	156	10.76	80.15	16.18	13.23	1.95
GS-1818C-1000	111001	181	9.53	77.46	16.17	12.61	1.90	S15	30413	157	10.38	53.88	16.18	12.55	1.95
GS-1818C-1000	111001	182	12.30	43.18	16.17	13.55	1.90	S15	30413	158	3.57	85.43	16.12	11.79	1.74
GS-1818C-1000	111001	183	10.88	58.77	16.17	12.99	1.90	S15	30413	159	14.86	80.93	16.12	15.76	1.74
GS-1818C-1000	111001	184	15.58	62.55	16.17	16.13	1.90	S15	30413	160	11.56	61.36	16.12	13.48	1.74
GS-1818C-1000	111001	185	13.09	64.60	16.23	14.52	2.11	S15	30413	161	14.15	68.97	16.12	15.25	1.74
GS-1818C-1000	111001	186	16.67	47.28	16.28	16.81	2.28	S15	30413	162	12.52	77.55	16.14	14.29	1.80
GS-1818C-1000	111001	187	13.71	75.37	16.24	15.02	2.17	S15	30413	163	16.70	76.28	16.14	16.89	1.80
GS-1818C-1000	111001	188	14.86	67.81	16.17	15.69	1.92	S15	30413	164	14.75	31.04	16.14	15.14	1.80
GS-1818C-1000	111001	189	10.91	51.17	16.13	12.82	1.78	S15	30413	165	13.30	50.20	16.14	14.42	1.80
GS-1818C-1000	111001	190	15.62	82.29	16.13	16.23	1.78	S15	30413	166	16.95	19.33	16.14	16.97	1.80
GS-1818C-1000	111001	191	15.71	47.81	16.13	16.11	1.78	S15	30413	167	15.01	57.35	16.14	15.70	1.79
GS-1818C-1000	111001	192	15.34	48.27	16.13	15.84	1.78	S15	30413	168	15.38	77.84	16.14	16.07	1.79
GS-1818C-1000	111001	193	15.01	21.35	16.17	15.20	1.90	S15	30413	169	14.92	26.53	16.09	15.20	1.62
GS-1818C-1000	111001	194	15.02	66.21	16.24	15.79	2.14	S15	30413	170	14.60	38.70	16.09	15.15	1.62
GS-1818C-1000	111001	195	16.20	44.52	16.18	16.44	1.96	S15	30413	171	14.49	54.40	16.22	15.32	2.07
GS-1818C-1000	111001	196	10.86	42.23	16.12	12.51	1.72	S15	30413	172	13.86	41.09	16.22	14.64	2.07
GS-1818C-1000	111001	197	16.58	33.32	16.12	16.68	1.72	S15	30413	173	13.20	27.34	16.13	13.76	1.77
GS-1818C-1000	111001	198	12.74	46.60	16.16	13.95	1.86	S15	30413	174	12.10	47.32	16.15	13.52	1.85
GS-1818C-1000	111001	199	15.13	63.29	16.16	15.84	1.86	S15	30413	175	13.19	60.56	16.15	14.53	1.85
GS-1818C-1000	111001	200	16.41	19.47	16.18	16.46	1.95	S15	30413	176	14.08	73.69	16.15	15.24	1.85
GS-1818C-1000	111001	201	14.55	71.65	16.18	15.52	1.95	S15	30413	177	10.94	38.05	16.11	12.41	1.70
GS-1818C-1000	111001	202	13.69	73.27	16.18	14.99	1.95	S15	30413	178	13.12	54.08	16.14	14.37	1.80
GS-1818C-1000	111001	203	15.12	48.41	16.23	15.68	2.11	S15	30413	179	10.44	78.84	16.14	13.02	1.80
GS-1818C-1000	111001	204	11.10	50.60	16.29	12.93	2.33	S15	30413	180	14.51	78.34	16.06	15.53	1.53
GS-1818C-1000	111001	205	14.31	45.54	16.27	15.05	2.25	S15	30413	181	9.90	87.11	16.17	12.87	1.90
GS-1818C-1000	111001	206	10.72	56.81	16.27	12.85	2.25	S15	30413	182	14.51	37.34	16.17	15.06	1.90
GS-1818C-1000	111001	207	14.90	50.76	16.15	15.56	1.85	S15	30413	183	12.04	56.54	16.11	13.70	1.70
GS-1818C-1000	111001	208	10.92	53.58	16.19	12.89	1.98	S15	30413	184	15.86	50.22	16.20	16.23	2.00
GS-1818C-1000	111001	209	15.76	53.17	16.36	16.19	2.57	S15	30413	185	14.18	59.72	16.20	15.17	2.00
GS-1818C-1000	111001	210	11.74	41.79	16.36	13.11	2.57	S15	30413	186	14.11	58.16	16.20	15.11	2.00
GS1845C 1	75602	1	6.78	52.78	16.20	11.15	2.03	S16	30414	1	7.59	19.03	16.17	9.43	1.91
GS1845C 1	75602	2	13.93	36.81	16.16	14.59	1.87	S16	30414	2	12.92	89.65	16.17	14.58	1.91
GS1845C 1	75602	3	10.17	84.77	16.16	12.93	1.87	S16	30414	3	15.84	53.69	16.16	16.25	1.86
GS1845C 1	75602	4	12.72	16.49	16.24	13.01	2.14	S16	30414	4	11.51	51.11	16.16	13.22	1.86
GS1845C 1	75602	5	15.20	46.56	16.24	15.72	2.14	S16	30414	5	13.02	53.61	16.09	14.30	1.62
GS1845C 1	75602	6	12.93	31.75	16.24	13.68	2.14	S16	30414	6	11.04	33.36	16.15	12.29	1.82
GS1845C 1	75602	7	15.82	21.28	16.20	15.93	2.03	S16	30414	7	10.18	87.74	16.24	12.90	2.16
GS1845C 1	75602	8	15.59	60.06	16.20	16.12	2.03	S16	30414	8	13.39	80.72	16.24	14.85	2.16
GS1845C 1	75602	9	8.99	68.58	16.17	12.22	1.92	S16	30414	9	11.63	85.72	16.12	13.79	1.72
GS1845C 1	75602	10	11.53	45.14	16.15	13.07	1.84	S16	30414	10	14.77	34.47	16.15	15.21	1.85
GS1845C 1	75602	11	13.64	10.08	16.18	13.73	1.93	S16	30414	11	13.20	81.29	16.24	14.74	2.14
GS1845C 1	75602	12	11.81	61.10	16.20	13.64	2.01	S16	30414	12	12.07	47.33	16.24	13.50	2.14
GS1845C 1	75602	13	15.10	79.26	16.20	15.90	2.01	S16	30414	13	9.98	38.69	16.24	11.77	2.14
GS1845C 1	75602	14	14.11	61.18	16.20	15.14	2.01	S16	30414	14	13.42	51.75	16.25	14.54	2.19
GS1845C 1	75602	15	6.67	58.43	16.20	11.35	2.00	S16	30414	15	15.15	10.79	16.25	15.20	2.19
GS1845C 1	75602	16	13.81	82.76	16.13	15.12	1.78	S16	30414	16	11.92	71.00	16.15	13.86	1.84
GS1845C 1	75602	17	12.54	51.25	16.13	13.92	1.78	S16	30414	17	10.38	79.07	16.15	12.98	1.84
GS1845C 1	75602	18	11.23	28.42	16.23	12.22	2.12	S16	30414	18	12.78	60.98	16.10	14.27	1.65
GS1845C 1	75602	19	11.41	60.19	16.15	13.37	1.83	S16	30414	19	11.34	41.17	16.10	12.80	1.65
GS1845C 1	75602	20	15.78	57.16	16.13	16.23	1.76	S16	30414	20	15.67	58.77	16.18	16.16	1.96
GS1845C 1	75602	21	14.97	47.99	16.14	15.57	1.79	S16	30414	21	8.82	69.92	16.18	12.32	1.96
GS1845C 1	75602	22	14.96	17.31	16.26	15.09	2.23	S16	30414	22	15.56	43.12	16.25	15.95	2.18
GS1845C 1	75602	23	15.06	39.63	16.26	15.52	2.23	S16	30414	23	9.78	88.79	16.25	12.92	2.18
GS1845C 1	75602	24	13.61	58.48	16.18	14.78	1.94	S16	30414	24	15.20	65.82	16.10	15.90	1.67
GS1845C 1	75602	25	11.51	57.39	16.18	13.37	1.94	S16	30414	25	15.62	39.13	16.10	15.95	1.67
GS1845C 1	75602	26	15.40	42.30	16.25	15.82	2.18	S16	30414	26	16.13	65.42	16.08	16.50	1.60
GS1845C 1	75602	27	15.44	51.84	16.25	15.95	2.18	S16	30414	27	14.32	42.39	16.07	15.01	1.57
GS1845C 1	75602	28	13.78	81.27	16.24	15.09	2.16	S16	30414	28	13.92	67.65	16.15	15.09	1.84
GS1845C 1	75602	29	10.52	64.09	16.24	12.87	2.16	S16	30414	29	13.96	4.91	16.15	13.98	1.84
GS1845C 1	75602	30	11.09	13.00	16.24	11.41	2.16	S16	30414	30	13.24	52.51	16.15	14.43	1.84

Table C3 Apatite fission track lengths for all samples analysed in this thesis

UBC	A2Z	Track	Angle				Dpar	UBC	A2Z	Track	Angle				Dpar
			Length (μm)	to c- axis	Lo calc (μm)	Lc calc (μm)					Length (μm)	to c- axis	Lo calc (μm)	Lc calc (μm)	
GS1845C 1	75602	31	12.41	70.04	16.22	14.16	2.09	S16	30414	31	14.35	47.23	16.09	15.11	1.64
GS1845C 1	75602	32	11.26	62.39	16.21	13.31	2.04	S16	30414	32	14.13	56.30	16.09	15.10	1.64
GS1845C 1	75602	33	10.43	60.32	16.21	12.74	2.04	S16	30414	33	8.90	66.36	16.15	12.21	1.83
GS1845C 1	75602	34	14.29	68.49	16.18	15.33	1.96	S16	30414	34	10.41	58.11	16.25	12.68	2.20
GS1845C 1	75602	35	14.05	52.38	16.26	14.98	2.23	S16	30414	35	15.00	79.45	16.09	15.84	1.63
GS1845C 1	75602	36	12.70	12.72	16.26	12.89	2.23	S16	30414	36	14.77	34.71	16.15	15.22	1.82
GS1845C 1	75602	37	10.45	41.05	16.30	12.18	2.35	S16	30414	37	14.73	61.50	16.20	15.56	2.01
GS1845C 1	75602	38	11.04	70.23	16.16	13.30	1.88	S16	30414	38	13.11	53.78	16.20	14.36	2.01
GS1845C 1	75602	39	14.55	35.03	16.14	15.05	1.80	S16	30414	39	15.73	48.14	16.20	16.12	2.01
GS1845C 1	75602	40	15.18	69.23	16.26	15.91	2.22	S16	30414	40	9.88	86.10	16.20	12.85	2.01
GS1845C 1	75602	41	11.16	74.14	16.26	13.42	2.22	S16	30414	41	14.76	69.27	16.23	15.64	2.13
GS1845C 1	75602	42	9.96	68.68	16.26	12.60	2.22	S16	30414	42	16.21	78.38	16.23	16.59	2.13
GS1845C 1	75602	43	5.25	74.16	16.26	11.40	2.22	S16	30414	43	14.83	62.33	16.23	15.63	2.13
GS1845C 1	75602	44	15.64	82.18	16.19	16.24	1.97	S16	30414	44	13.11	85.79	16.23	14.69	2.13
GS1845C 1	75602	45	13.38	38.45	16.21	14.21	2.04	S16	30414	45	12.11	76.34	16.23	14.03	2.13
GS1845C 1	75602	46	12.54	81.50	16.21	14.33	2.04	S16	30414	46	15.12	59.13	16.23	15.80	2.13
GS1845C 1	75602	47	11.81	34.46	16.21	12.91	2.04	S16	30414	47	15.04	78.71	16.15	15.86	1.85
GS1845C 1	75602	48	12.58	51.20	16.15	13.95	1.82	S16	30414	48	14.09	66.64	16.15	15.19	1.85
GS1845C 1	75602	49	14.57	78.78	16.15	15.57	1.82	S16	30414	49	15.49	1.03	16.15	15.49	1.85
GS1845C 1	75602	50	13.93	70.26	16.21	15.12	2.06	S16	30414	50	15.68	38.12	16.15	15.99	1.85
GS1845C 1	75602	51	13.40	70.13	16.21	14.78	2.06	S16	30414	51	12.62	59.78	16.15	14.14	1.85
GS1845C 1	75602	52	14.25	55.42	16.21	15.16	2.05	S16	30414	52	13.50	50.44	16.22	14.57	2.09
GS1845C 1	75602	53	9.76	57.17	16.21	12.24	2.05	S16	30414	53	13.88	44.28	16.18	14.72	1.94
GS1845C 1	75602	54	11.45	19.98	16.22	12.03	2.08	S16	30414	54	12.55	63.59	16.18	14.16	1.94
GS1845C 1	75602	55	13.01	50.48	16.22	14.23	2.08	S16	30414	55	14.89	46.77	16.12	15.50	1.74
GS1845C 1	75602	56	14.23	58.47	16.22	15.19	2.08	S16	30414	56	14.44	23.74	16.12	14.73	1.74
GS1845C 1	75602	57	14.74	77.08	16.22	15.67	2.08	S16	30414	57	14.03	44.28	16.11	14.83	1.69
GS1845C 1	75602	58	11.18	55.15	16.22	13.10	2.08	S16	30414	58	12.56	69.58	16.15	14.25	1.83
GS1845C 1	75602	59	15.97	34.80	16.25	16.19	2.18	S16	30414	59	14.30	79.01	16.19	15.41	1.98
GS1845C 1	75602	60	14.21	47.80	16.25	15.02	2.18	S16	30414	60	13.72	55.40	16.19	14.80	1.98
GS1845C 1	75602	61	13.04	17.29	16.25	13.33	2.18	S16	30414	61	13.31	61.15	16.11	14.62	1.70
GS1845C 1	75602	62	15.06	46.96	16.24	15.62	2.15	S16	30414	62	15.03	81.19	16.15	15.86	1.84
GS1845C 1	75602	63	17.54	17.54	16.24	17.52	2.15	S16	30414	63	12.72	76.06	16.19	14.41	1.97
GS1845C 1	75602	64	13.81	19.92	16.19	14.09	1.98	S16	30414	64	14.36	82.12	16.18	15.45	1.93
GS1845C 1	75602	65	12.74	88.11	16.19	14.47	1.98	S16	30414	65	12.50	62.40	16.09	14.11	1.62
GS1845C 1	75602	66	17.19	61.61	16.19	17.20	1.98	S16	30414	66	12.53	73.59	16.14	14.27	1.79
GS1845C 1	75602	67	10.57	84.09	16.19	13.13	1.97	S16	30414	67	13.25	68.99	16.05	14.68	1.49
GS1845C 1	75602	68	12.05	41.19	16.19	13.31	1.97	S16	30414	68	16.58	65.46	16.05	16.80	1.49
GS1845C 1	75602	69	13.77	24.09	16.22	14.16	2.07	S16	30414	69	12.88	73.92	16.17	14.49	1.90
GS1845C 1	75602	70	11.61	88.86	16.11	13.78	1.70	S16	30414	70	12.31	38.65	16.20	13.42	2.00
GS1845C 1	75602	71	10.48	59.87	16.11	12.76	1.70	S16	30414	71	10.45	53.08	16.11	12.57	1.70
GS1845C 1	75602	72	12.13	75.93	16.19	14.04	1.99	S16	30414	72	11.08	87.58	16.11	13.45	1.70
GS1845C 1	75602	73	14.32	34.92	16.19	14.86	1.99	S16	30414	73	14.15	11.45	16.08	14.24	1.58
GS1845C 1	75602	74	10.06	83.53	16.19	12.87	1.99	S16	30414	74	15.08	63.00	16.13	15.80	1.78
GS1845C 1	75602	75	13.20	37.15	16.16	14.04	1.87	S16	30414	75	14.66	88.40	16.13	15.65	1.78
GS1845C 1	75602	76	15.15	64.22	16.26	15.86	2.23	S16	30414	76	11.92	41.46	16.13	13.22	1.78
GS1845C 1	75602	77	15.69	46.82	16.23	16.08	2.13	S16	30414	77	13.82	38.25	16.13	14.54	1.78
GS1845C 1	75602	78	14.93	60.57	16.23	15.68	2.13	S16	30414	78	9.22	74.14	16.15	12.48	1.85
GS1845C 1	75602	79	12.93	73.37	16.22	14.52	2.07	S16	30414	79	14.76	39.16	16.16	15.28	1.86
GS1845C 1	75602	80	15.32	78.82	16.20	16.04	2.02	S16	30414	80	13.84	74.81	16.16	15.10	1.86
GS1845C 1	75602	81	15.16	51.46	16.26	15.75	2.21	S16	30414	81	13.47	69.96	16.16	14.83	1.86
GS1845C 1	75602	82	12.31	88.09	16.26	14.21	2.24	S16	30414	82	12.28	62.44	16.16	13.97	1.86
GS1845C 1	75602	83	15.10	37.37	16.24	15.52	2.16	S16	30414	83	13.46	88.40	16.22	14.91	2.08
GS1845C 1	75602	84	11.47	82.83	16.24	13.68	2.16	S16	30414	84	14.47	63.05	16.38	15.40	2.65
GS1845C 1	75602	85	12.18	77.31	16.18	14.08	1.95	S16	30414	85	8.97	36.79	16.15	11.01	1.82
GS1845C 1	75602	86	15.16	63.37	16.20	15.86	2.02	S16	30414	86	12.03	17.28	16.15	12.42	1.82
GS1845C 1	75602	87	10.01	71.50	16.20	12.67	2.02	S16	30414	87	13.29	86.04	16.12	14.81	1.72
GS1845C 1	75602	88	14.19	36.68	16.20	14.79	2.02	S16	30414	88	15.34	9.88	16.13	15.38	1.75
GS1845C 1	75602	89	15.46	47.03	16.20	15.92	2.02	S16	30414	89	11.35	66.88	16.16	13.45	1.86
GS1845C 1	75602	90	14.68	34.12	16.18	15.13	1.94	S16	30414	90	15.10	59.86	16.16	15.79	1.86
GS1845C 1	75602	91	12.86	66.09	16.18	14.39	1.94	S16	30414	91	13.37	81.38	16.21	14.84	2.06

Table C3 Apatite fission track lengths for all samples analysed in this thesis

UBC	A2Z	Track	Angle				Dpar	UBC	A2Z	Track	Angle				Dpar
			Length (μm)	to c- axis	Lo calc (μm)	Lc calc (μm)					Length (μm)	to c- axis	Lo calc (μm)	Lc calc (μm)	
GS1845C 1	75602	92	15.14	88.03	16.27	15.94	2.25	S16	30414	92	14.22	45.34	16.21	14.98	2.06
GS1845C 1	75602	93	11.69	71.37	16.17	13.72	1.90	S16	30414	93	9.95	77.96	16.21	12.71	2.06
GS1845C 1	75602	94	15.64	35.52	16.23	15.93	2.11	S16	30414	94	14.85	45.89	16.19	15.45	1.97
GS1845C 1	75602	95	13.86	85.83	16.23	15.15	2.11	S16	30414	95	13.89	58.10	16.19	14.96	1.97
GS1845C 1	75602	96	11.38	55.05	16.22	13.23	2.10	S16	30414	96	11.35	81.94	16.19	13.60	1.97
GS1845C 1	75602	97	13.77	34.50	16.22	14.42	2.10	S16	30414	97	14.90	43.44	16.16	15.46	1.88
GS1845C 1	75602	98	14.53	60.04	16.11	15.41	1.68	S16	30414	98	15.18	17.89	16.07	15.31	1.57
GS1845C 1	75602	99	12.69	86.47	16.11	14.44	1.68	S17	30415	1	13.90	58.67	16.21	14.97	2.05
GS1845C 1	75602	100	8.73	45.94	16.18	11.23	1.94	S17	30415	2	12.88	68.38	16.18	14.43	1.94
GS1845C 1	75602	101	12.91	87.41	16.26	14.57	2.24	S17	30415	3	13.95	23.02	16.01	14.29	1.36
GS1845C 1	75602	102	14.44	73.52	16.26	15.46	2.24	S17	30415	4	14.89	18.95	16.15	15.05	1.83
GS1845C 1	75602	103	11.17	62.73	16.15	13.26	1.85	S17	30415	5	12.94	55.83	16.15	14.29	1.83
GS1845C 1	75602	104	15.14	48.93	16.19	15.70	1.97	S17	30415	6	13.76	71.50	16.20	15.02	2.03
GS1845C 1	75602	105	13.08	79.32	16.19	14.65	1.97	S17	30415	7	14.31	82.21	16.20	15.42	2.03
GS1845C 1	75602	106	14.92	57.39	16.17	15.64	1.92	S17	30415	8	14.47	50.76	16.26	15.25	2.23
GS1845C 1	75602	107	15.43	64.16	16.24	16.04	2.17	S17	30415	9	15.97	54.61	16.26	16.34	2.23
GS1845C 1	75602	108	14.92	61.88	16.24	15.69	2.17	S17	30415	10	14.97	13.33	16.26	15.05	2.23
GS1845C 1	75602	109	13.12	51.96	16.19	14.33	1.97	S17	30415	11	14.60	11.17	16.26	14.67	2.23
GS1845C 1	75602	110	16.02	52.85	16.17	16.37	1.90	S17	30415	12	12.79	50.47	16.14	14.08	1.81
GS1845C 1	75602	111	15.11	57.17	16.18	15.77	1.96	S17	30415	13	14.85	49.86	16.11	15.51	1.68
GS1845C 1	75602	112	14.72	29.57	16.21	15.08	2.06	S17	30415	14	14.18	46.35	16.28	14.97	2.31
GS1845C 1	75602	113	13.82	43.29	16.21	14.65	2.06	S17	30415	15	11.85	62.74	16.28	13.70	2.31
GS1845C 1	75602	114	15.64	37.51	16.21	15.95	2.06	S17	30415	16	15.54	25.22	16.28	15.72	2.31
GS1845C 1	75602	115	15.36	88.32	16.21	16.08	2.06	S17	30415	17	12.30	78.70	16.20	14.17	2.03
GS1845C 1	75602	116	14.70	54.18	16.21	15.46	2.06	S17	30415	18	15.83	15.92	16.15	15.90	1.84
GS1845C 1	75602	117	14.03	25.81	16.21	14.42	2.06	S17	30415	19	14.06	50.17	16.15	14.95	1.84
GS1845C 1	75602	118	16.35	24.06	16.23	16.43	2.13	S17	30415	20	14.35	37.28	16.28	14.93	2.28
GS1845C 1	75602	119	14.06	76.96	16.23	15.25	2.13	S17	30415	21	13.83	75.31	16.19	15.09	1.97
GS1845C 1	75602	120	14.46	63.33	16.23	15.40	2.13	S17	30415	22	14.15	89.95	16.20	15.34	2.01
GS1845C 1	75602	121	8.34	62.93	16.21	11.88	2.06	S17	30415	23	13.17	73.25	16.20	14.67	2.01
GS1845C 1	75602	122	10.50	73.08	16.22	13.00	2.08	S17	30415	24	12.83	62.30	16.20	14.32	2.01
GS1845C 1	75602	123	15.01	34.24	16.15	15.40	1.82	S17	30415	25	14.93	6.53	16.15	14.95	1.85
GS1845C 1	75602	124	15.03	39.90	16.15	15.50	1.82	S17	30415	26	14.93	19.85	16.15	15.10	1.85
GS1845C 1	75602	125	12.11	73.93	16.15	14.01	1.82	S17	30415	27	12.75	69.34	16.14	14.36	1.81
GS1845C 1	75602	126	11.55	87.00	16.15	13.74	1.82	S17	30415	28	15.28	26.41	16.07	15.51	1.57
GS1845C 1	75602	127	8.70	75.18	16.15	12.32	1.82	S17	30415	29	15.16	63.25	16.26	15.86	2.24
GS1845C 1	75602	128	14.79	41.16	16.17	15.34	1.92	S17	30415	30	13.72	19.61	16.11	14.00	1.69
GS1845C 1	75602	129	11.41	70.29	16.21	13.53	2.05	S17	30415	31	13.90	64.24	16.10	15.04	1.67
GS1845C 1	75602	130	12.91	59.71	16.21	14.33	2.06	S17	30415	32	15.12	29.96	16.10	15.43	1.67
GS1845C 1	75602	131	14.02	60.96	16.21	15.08	2.04	S17	30415	33	15.71	30.29	16.22	15.93	2.10
GS1845C 1	75602	132	8.52	35.28	16.21	10.65	2.04	S17	30415	34	12.12	12.66	16.12	12.34	1.72
GS1845CW1 2	75603	1	7.47	49.12	16.11	11.13	1.69	S17	30415	35	14.07	60.06	16.12	15.10	1.72
GS1845CW1 2	75603	2	9.91	83.55	16.11	12.82	1.69	S17	30415	36	17.37	46.72	16.13	17.33	1.77
GS1845CW1 2	75603	3	15.05	63.22	16.24	15.78	2.15	S17	30415	37	14.76	67.20	16.13	15.63	1.77
GS1845CW1 2	75603	4	17.53	43.89	16.24	17.46	2.15	S17	30415	38	15.25	71.23	16.13	15.96	1.77
GS1845CW1 2	75603	5	7.56	89.37	16.24	12.24	2.15	S17	30415	39	14.90	73.60	16.16	15.75	1.88
GS1845CW1 2	75603	6	10.75	63.56	16.14	13.01	1.81	S17	30415	40	14.94	82.67	16.16	15.81	1.88
GS1845CW1 2	75603	7	9.39	80.90	16.18	12.62	1.96	S17	30415	41	14.51	53.56	16.19	15.32	1.99
GS1845CW1 2	75603	8	12.50	22.62	16.21	13.02	2.05	S17	30415	42	14.42	22.92	16.22	14.70	2.07
GS1845CW1 2	75603	9	12.79	45.22	16.22	13.95	2.08	S17	30415	43	13.54	64.06	16.11	14.81	1.68
GS1845CW1 2	75603	10	14.91	35.92	16.18	15.35	1.93	S17	30415	44	12.65	79.13	16.39	14.39	2.69
GS1845CW1 2	75603	11	9.89	64.57	16.18	12.49	1.93	S17	30415	45	14.96	71.30	16.39	15.78	2.69
GS1845CW1 2	75603	12	14.34	65.55	16.17	15.34	1.90	S17	30415	46	13.13	50.79	16.19	14.32	1.98
GS1845CW1 2	75603	13	11.06	51.19	16.22	12.92	2.09	S17	30415	47	13.14	83.38	16.14	14.71	1.81
GS1845CW1 2	75603	14	8.29	68.23	16.22	12.04	2.09	S17	30415	48	13.27	78.44	16.14	14.77	1.81
GS1845CW1 2	75603	15	14.68	71.06	16.18	15.60	1.96	S17	30415	49	14.19	53.10	16.14	15.09	1.81
GS1845CW1 2	75603	16	10.05	45.57	16.18	12.08	1.96	S17	30415	50	13.77	57.12	16.17	14.86	1.91
GS1845CW1 2	75603	17	15.32	76.85	16.18	16.03	1.96	S17	30415	51	15.99	37.88	16.15	16.23	1.84
GS1845CW1 2	75603	18	14.57	44.09	16.18	15.22	1.96	S17	30415	52	14.43	31.48	16.15	14.88	1.84
GS1845CW1 2	75603	19	9.96	77.35	16.18	12.73	1.96	S17	30415	53	16.01	59.24	16.22	16.40	2.10
GS1845CW1 2	75603	20	15.57	67.54	16.13	16.15	1.76	S17	30415	54	14.88	58.37	16.22	15.63	2.10

Table C3 Apatite fission track lengths for all samples analysed in this thesis

UBC	A2Z	Track	Angle				Dpar	UBC	A2Z	Track	Angle				Dpar
			Length (μm)	to c- axis	Lo calc (μm)	Lc calc (μm)					Length (μm)	to c- axis	Lo calc (μm)	Lc calc (μm)	
GS1845CW1 2	75603	21	12.48	66.25	16.13	14.15	1.76	S17	30415	55	10.87	30.56	16.22	12.05	2.10
GS1845CW1 2	75603	22	9.61	58.23	16.17	12.17	1.90	S17	30415	56	15.48	84.25	16.22	16.15	2.10
GS1845CW1 2	75603	23	12.94	62.93	16.07	14.40	1.57	S17	30415	57	13.61	80.60	16.11	14.99	1.69
GS1845CW1 2	75603	24	11.78	28.06	16.07	12.64	1.57	S17	30415	58	14.63	38.74	16.14	15.18	1.81
GS1845CW1 2	75603	25	13.05	62.00	16.07	14.46	1.57	S17	30415	59	13.29	50.60	16.14	14.42	1.81
GS1845CW1 2	75603	26	5.79	47.31	16.07	10.70	1.57	S17	30415	60	15.88	80.65	16.14	16.39	1.81
GS1845CW1 2	75603	27	12.76	51.92	16.07	14.09	1.57	S17	30415	61	13.21	10.40	16.11	13.32	1.68
GS1845CW1 2	75603	28	16.19	81.92	16.11	16.58	1.68	S18	30416	1	13.97	49.87	16.20	14.88	2.00
GS1845CW1 2	75603	29	14.89	51.28	16.11	15.55	1.68	S18	30416	2	13.22	72.51	16.09	14.69	1.62
GS1845CW1 2	75603	30	14.30	55.84	16.30	15.20	2.37	S18	30416	3	14.81	30.79	16.23	15.18	2.13
GS1845CW1 2	75603	31	15.89	19.83	16.22	15.99	2.09	S18	30416	4	14.56	27.63	16.23	14.91	2.13
GS1845CW1 2	75603	32	15.33	86.03	16.25	16.06	2.18	S18	30416	5	13.96	89.98	16.23	15.22	2.13
GS1845CW1 2	75603	33	11.88	72.61	16.18	13.85	1.96	S18	30416	6	15.08	77.41	16.10	15.88	1.65
GS1845CW1 2	75603	34	10.78	62.82	16.12	13.01	1.73	S18	30416	7	12.69	86.92	16.14	14.44	1.80
GS1845CW1 2	75603	35	14.27	5.51	16.12	14.29	1.73	S18	30416	8	15.33	58.85	16.14	15.93	1.80
GS1845CW1 2	75603	36	14.05	40.12	16.12	14.76	1.73	S18	30416	9	13.44	65.31	16.14	14.76	1.80
GS1845CW1 2	75603	37	13.40	49.49	16.26	14.48	2.24	S18	30416	10	12.41	42.91	16.14	13.62	1.80
GS1845CW1 2	75603	38	9.88	33.76	16.19	11.48	1.98	S18	30416	11	15.07	69.79	16.14	15.84	1.80
GS1845CW1 2	75603	39	14.71	36.37	16.19	15.20	1.98	S18	30416	12	11.38	86.40	16.14	13.63	1.80
GS1845CW1 2	75603	40	16.08	70.87	16.39	16.49	2.68	S18	30416	13	16.72	26.13	16.22	16.77	2.09
GS1845CW1 2	75603	41	14.36	77.82	16.39	15.44	2.68	S18	30416	14	14.20	72.00	16.22	15.30	2.09
GS1845CW1 2	75603	42	15.54	72.52	16.39	16.15	2.68	S18	30416	15	14.41	47.43	16.25	15.16	2.20
GS1845CW1 2	75603	43	14.29	37.07	16.15	14.88	1.82	S18	30416	16	14.06	62.15	16.17	15.12	1.92
GS1845CW1 2	75603	44	12.18	54.31	16.24	13.75	2.14	S18	30416	17	13.93	67.67	16.17	15.10	1.92
GS1845CW1 2	75603	45	13.05	72.53	16.23	14.58	2.12	S18	30416	18	13.26	77.28	16.09	14.75	1.61
GS1845CW1 2	75603	46	13.59	70.87	16.15	14.91	1.84	S18	30416	19	11.77	48.89	16.18	13.34	1.95
GS1845CW1 2	75603	47	15.77	43.41	16.12	16.11	1.73	S18	30416	20	16.38	38.87	16.11	16.55	1.70
GS1845CW1 2	75603	48	14.07	58.46	16.12	15.08	1.73	S18	30416	21	14.44	83.54	16.17	15.51	1.90
GS1845CW1 2	75603	49	14.10	56.18	16.19	15.07	1.98	S18	30416	22	12.03	84.96	16.12	14.03	1.73
GS1845CW1 2	75603	50	14.32	68.73	16.19	15.36	1.98	S18	30416	23	15.59	81.32	16.37	16.21	2.62
GS1845CW1 2	75603	51	9.94	67.85	16.24	12.58	2.16	S18	30416	24	13.27	18.19	16.05	13.56	1.50
GS1845CW1 2	75603	52	13.30	52.83	16.24	14.47	2.16	S18	30416	25	14.14	67.74	16.07	15.23	1.55
GS1845CW1 2	75603	53	10.44	67.41	16.24	12.88	2.16	S18	30416	26	14.07	83.50	16.26	15.28	2.21
GS1845CW1 2	75603	54	10.58	76.66	16.24	13.09	2.16	S18	30416	27	11.45	45.70	16.11	13.03	1.69
GS1845CW1 2	75603	55	15.09	51.99	16.20	15.70	2.01	S18	30416	28	15.08	84.08	16.26	15.90	2.23
GS1845CW1 2	75603	56	16.09	84.58	16.20	16.52	2.01	S18	30416	29	14.14	25.78	16.26	14.51	2.23
GS1845CW1 2	75603	57	14.04	53.28	16.22	14.99	2.10	S18	30416	30	15.75	66.38	16.26	16.26	2.23
GS1845CW1 2	75603	58	11.66	27.96	16.22	12.54	2.10	S18	30416	31	9.16	76.91	16.26	12.56	2.23
GS1845CW1 2	75603	59	7.67	72.03	16.20	11.98	2.02	S18	30416	32	14.45	44.91	16.11	15.15	1.68
GS1845CW1 2	75603	60	11.42	75.02	16.37	13.59	2.61	S18	30416	33	13.03	73.10	16.20	14.58	2.03
GS1845CW1 2	75603	61	13.08	56.69	16.22	14.39	2.08	S18	30416	34	16.06	50.87	16.20	16.38	2.03
GS1845CW1 2	75603	62	9.25	51.11	16.22	11.74	2.08	S18	30416	35	12.20	74.36	16.20	14.07	2.03
GS1845CW1 2	75603	63	10.15	50.21	16.26	12.29	2.22	S18	30416	36	14.87	89.43	16.20	15.78	2.03
GS1845CW1 2	75603	64	10.39	56.15	16.26	12.62	2.22	S18	30416	37	14.52	73.20	16.20	15.51	2.03
GS1845CW1 2	75603	65	8.35	62.31	16.23	11.86	2.12	S18	30416	38	14.26	53.49	16.20	15.14	2.03
GS1845CW1 2	75603	66	12.26	23.40	16.23	12.85	2.12	S18	30416	39	14.42	38.15	16.20	15.00	2.03
GS1845CW1 2	75603	67	11.30	68.82	16.19	13.44	1.99	S18	30416	40	13.99	63.20	16.20	15.09	2.03
GS1845CW1 2	75603	68	10.27	49.05	16.19	12.34	1.99	S18	30416	41	14.74	68.42	16.20	15.62	2.03
GS1845CW1 2	75603	69	13.35	51.92	16.24	14.49	2.17	S18	30416	42	13.60	45.00	16.20	14.53	2.03
GS1845CW1 2	75603	70	15.44	56.33	16.20	15.99	2.01	S18	30416	43	13.50	64.16	16.20	14.78	2.03
GS1845CW1 2	75603	71	12.39	57.24	16.20	13.95	2.01	S18	30416	44	13.59	64.50	16.20	14.84	2.03
GS1845CW1 2	75603	72	15.55	88.34	16.34	16.19	2.50	S18	30416	45	15.84	47.85	16.20	16.20	2.03
GS1845CW1 2	75603	73	14.69	69.90	16.34	15.60	2.50	S18	30416	46	12.02	76.08	16.20	13.97	2.03
GS1845CW1 2	75603	74	13.66	54.33	16.16	14.75	1.88	S18	30416	47	13.40	50.92	16.20	14.51	2.03
GS1845CW1 2	75603	75	12.81	45.49	16.12	13.97	1.73	S18	30416	48	14.05	71.34	16.14	15.20	1.80
GS1845CW1 2	75603	76	13.73	60.08	16.26	14.88	2.23	S18	30416	49	14.92	49.65	16.14	15.55	1.80
GS1845CW1 2	75603	77	16.89	27.84	16.24	16.93	2.15	S18	30416	50	12.28	36.78	16.15	13.34	1.84
GS1845CW1 2	75603	78	13.03	71.57	16.24	14.56	2.15	S18	30416	51	14.37	37.89	16.13	14.96	1.78
GS1845CW1 2	75603	79	14.07	70.46	16.24	15.21	2.15	S18	30416	52	15.88	36.01	16.20	16.13	2.00
GS1845CW1 2	75603	80	14.06	57.75	16.24	15.07	2.15	S18	30416	53	13.05	65.07	16.11	14.50	1.68
GS1845CW1 2	75603	81	14.11	64.08	16.21	15.18	2.06	S18	30416	54	12.90	59.64	16.26	14.33	2.24

Table C3 Apatite fission track lengths for all samples analysed in this thesis

UBC	A2Z	Track	Angle				Dpar	UBC	A2Z	Track	Angle				Dpar
			Length (μm)	to c- axis	Lo calc (μm)	Lc calc (μm)					Length (μm)	to c- axis	Lo calc (μm)	Lc calc (μm)	
GS1845CW1 2	75603	82	13.32	81.68	16.21	14.81	2.06	S18	30416	55	16.44	25.55	16.26	16.52	2.24
GS1845CW1 2	75603	83	12.85	43.40	16.24	13.95	2.15	S18	30416	56	14.59	42.37	16.16	15.21	1.87
GS1845CW1 2	75603	84	13.57	33.90	16.24	14.24	2.14	S18	30416	57	14.45	84.69	16.12	15.51	1.72
GS1845CW1 2	75603	85	10.68	77.68	16.24	13.16	2.14	S18	30416	58	15.26	16.21	16.12	15.36	1.72
GS1845CW1 2	75603	86	16.45	43.19	16.10	16.63	1.67	S18	30416	59	13.45	87.12	16.07	14.91	1.56
GS1845CW1 2	75603	87	8.89	78.16	16.10	12.43	1.67	S18	30416	60	14.31	55.62	16.15	15.21	1.85
GS1845CW1 2	75603	88	9.15	71.39	16.27	12.34	2.26	S18	30416	61	15.34	50.54	16.15	15.87	1.85
GS1845CW1 2	75603	89	14.87	38.33	16.27	15.36	2.26	S18	30416	62	14.80	74.52	16.20	15.70	2.00
GS1845CW1 2	75603	90	9.20	51.58	16.27	11.72	2.26	S18	30416	63	14.61	32.26	16.20	15.04	2.00
GS1845CW1 2	75603	91	10.72	60.76	16.27	12.93	2.26	S18	30416	64	13.59	82.40	16.20	14.98	2.00
GS1845CW1 2	75603	92	15.81	68.85	16.25	16.31	2.20	S18	30416	65	16.23	35.87	16.20	16.41	2.00
GS1845CW1 2	75603	93	11.75	69.89	16.13	13.74	1.77	S18	30416	66	15.30	11.51	16.24	15.35	2.15
GS1845CW1 2	75603	94	13.31	71.25	16.03	14.74	1.42	S18	30416	67	12.54	79.20	16.10	14.32	1.67
GS1845CW1 2	75603	95	10.55	50.88	16.19	12.58	1.98	S18	30416	68	10.70	52.63	16.10	12.73	1.65
GS1845CW1 2	75603	96	14.10	82.64	16.19	15.29	1.98	S18	30416	69	13.58	80.34	16.19	14.97	1.97
GS1845CW1 2	75603	97	12.30	56.53	16.20	13.87	2.03	S18	30416	70	17.48	29.87	16.19	17.44	1.97
GS1845CW1 2	75603	98	12.51	74.77	16.20	14.27	2.03	S18	30416	71	14.74	33.96	16.19	15.18	1.97
GS1845CW1 2	75603	99	13.80	48.80	16.23	14.75	2.12	S18	30416	72	12.20	47.22	16.10	13.59	1.65
GS1845CW1 2	75603	100	13.03	58.81	16.12	14.40	1.73	S18	30416	73	11.46	80.96	16.10	13.66	1.65
GS1845CW1 2	75603	101	14.40	65.51	16.19	15.38	1.99	S18	30416	74	9.97	46.16	16.10	12.04	1.65
GS1845CW1 2	75603	102	8.50	79.32	16.19	12.35	1.99	S18	30416	75	14.58	48.51	16.18	15.30	1.94
GS1845CW1 2	75603	103	12.99	56.58	16.32	14.33	2.44	S18	30416	76	13.19	48.84	16.18	14.32	1.94
GS1845CW1 2	75603	104	10.12	57.54	16.11	12.48	1.71	S18	30416	77	15.89	19.24	16.18	15.98	1.94
GS1845CW1 2	75603	105	12.88	38.32	16.21	13.83	2.06	S18	30416	78	13.04	28.84	16.18	13.68	1.94
GS1845CW1 2	75603	106	13.60	49.05	16.21	14.61	2.06	S18	30416	79	15.03	60.94	16.25	15.75	2.20
GS1845CW1 2	75603	107	14.59	72.61	16.12	15.55	1.72	S18	30416	80	8.24	70.47	16.25	12.29	2.20
GS1845CW1 2	75603	108	12.98	71.99	16.12	14.54	1.72	S18	30416	81	15.39	44.74	16.13	15.84	1.76
GS1845CW1 2	75603	109	13.07	46.21	16.26	14.17	2.21	S18	30416	82	14.00	39.94	16.13	14.72	1.76
GS1845CW1 2	75603	110	13.63	25.34	16.26	14.07	2.21	S18	30416	83	14.55	47.64	16.13	15.26	1.76
GS1845CW1 2	75603	111	14.68	74.08	16.27	15.62	2.25	S18	30416	84	15.74	8.47	16.17	15.76	1.90
GS1845CW1 2	75603	112	14.24	54.71	16.27	15.15	2.25	S18	30416	85	12.96	22.87	16.18	13.42	1.93
GS1845CW1 2	75603	113	13.30	67.90	16.22	14.70	2.08	S18	30416	86	10.81	56.82	16.18	12.90	1.93
GS1845CW1 2	75603	114	14.76	70.57	16.22	15.65	2.08	S18	30416	87	13.62	52.63	16.18	14.69	1.93
GS1845CW1 2	75603	115	14.38	25.31	16.22	14.71	2.08	S18	30416	88	13.97	75.60	16.15	15.18	1.82
GS1845CW1 2	75603	116	14.46	37.90	16.12	15.03	1.72	S18	30416	89	14.86	9.84	16.21	14.91	2.04
GS1845CW1 2	75603	117	8.78	74.95	16.21	12.33	2.05	S18	30416	90	11.13	55.93	16.21	13.09	2.04
GS1845CW1 2	75603	118	11.79	60.72	16.21	13.62	2.05	S18	30416	91	16.24	34.27	16.13	16.41	1.76
GS1845CW1 2	75603	119	13.24	5.15	16.21	13.27	2.05	S19	30417	1	15.70	45.08	16.13	16.07	1.77
GS1845CW1 2	75603	120	11.44	58.21	16.20	13.34	2.00	S19	30417	2	14.43	29.80	16.13	14.85	1.77
GS1845CW1 2	75603	121	9.82	58.73	16.20	12.32	2.00	S19	30417	3	13.38	68.38	16.13	14.75	1.77
GS1845CW1 2	75603	122	11.06	75.16	16.20	13.37	2.00	S19	30417	4	15.25	86.54	16.13	16.01	1.77
GS1845CW1 2	75603	123	11.31	58.56	16.24	13.27	2.14	S19	30417	5	15.41	19.75	16.13	15.54	1.77
GS1845CW1 2	75603	124	11.53	70.93	16.24	13.61	2.14	S19	30417	6	14.31	67.85	16.13	15.34	1.77
GS1845CW1 2	75603	125	14.00	65.88	16.24	15.12	2.14	S19	30417	7	13.78	74.80	16.13	15.06	1.77
GS1845CW1 2	75603	126	15.18	81.23	16.24	15.96	2.14	S19	30417	8	12.45	33.31	16.13	13.35	1.77
GS1845CW1 2	75603	127	14.88	20.46	16.27	15.07	2.26	S19	30417	9	12.94	31.86	16.13	13.69	1.77
GS1845CW1 2	75603	128	14.94	69.02	16.27	15.75	2.26	S19	30417	10	14.59	38.12	16.13	15.13	1.77
GS1845CW1 2	75603	129	13.60	78.92	16.27	14.97	2.26	S19	30417	11	15.57	80.19	16.13	16.20	1.77
GS1845CW1 2	75603	130	10.30	63.17	16.16	12.72	1.86	S19	30417	12	14.94	37.59	16.13	15.40	1.77
GS1845CW1 2	75603	131	13.41	52.38	16.26	14.54	2.24	S19	30417	13	13.05	81.62	16.13	14.64	1.77
GS1845CW1 2	75603	132	14.82	41.83	16.15	15.37	1.85	S19	30417	14	14.90	69.34	16.13	15.73	1.77
GS1845CW1 2	75603	133	13.64	81.65	16.15	15.01	1.85	S19	30417	15	16.08	47.49	16.13	16.37	1.77
GS1845CW1 2	75603	134	11.51	33.85	16.15	12.66	1.85	S19	30417	16	12.26	71.09	16.27	14.07	2.26
GS1845CW1 2	75603	135	13.91	61.06	16.15	15.01	1.85	S19	30417	17	14.09	86.39	16.27	15.30	2.26
GS1845CW1 3	75604	1	13.57	46.24	16.13	14.53	1.76	S19	30417	18	16.07	67.58	16.27	16.47	2.26
GS1845CW1 3	75604	2	10.97	51.88	16.21	12.88	2.04	S19	30417	19	14.44	75.85	16.27	15.48	2.26
GS1845CW1 3	75604	3	13.38	20.57	16.28	13.72	2.28	S19	30417	20	13.87	42.41	16.27	14.67	2.26
GS1845CW1 3	75604	4	12.65	79.75	16.28	14.39	2.28	S19	30417	21	13.05	42.29	16.27	14.06	2.26
GS1845CW1 3	75604	5	13.72	71.43	16.22	15.00	2.10	S19	30417	22	12.42	42.23	16.27	13.61	2.26
GS1845CW1 3	75604	6	14.89	54.14	16.22	15.59	2.10	S19	30417	23	15.46	58.30	16.27	16.02	2.26
GS1845CW1 3	75604	7	10.56	58.04	16.33	12.77	2.49	S19	30417	24	15.30	1.71	16.27	15.30	2.26

Table C3 Apatite fission track lengths for all samples analysed in this thesis

UBC	A2Z	Track	Angle				Dpar	UBC	A2Z	Track	Angle				Dpar
			Length (μm)	to c- axis	Lo calc (μm)	Lc calc (μm)					Length (μm)	to c- axis	Lo calc (μm)	Lc calc (μm)	
GS1845CW1 3	75604	8	14.25	60.66	16.33	15.23	2.49	S19	30417	25	13.62	85.33	16.27	15.01	2.26
GS1845CW1 3	75604	9	14.97	16.79	16.33	15.10	2.49	S19	30417	26	13.18	48.14	16.27	14.30	2.26
GS1845CW1 3	75604	10	16.50	51.69	16.33	16.70	2.49	S19	30417	27	14.84	43.32	16.27	15.41	2.26
GS1845CW1 3	75604	11	9.87	53.08	16.33	12.20	2.49	S19	30417	28	16.36	46.97	16.15	16.58	1.82
GS1845CW1 3	75604	12	14.56	60.63	16.24	15.44	2.14	S19	30417	29	11.98	71.91	16.15	13.91	1.82
GS1845CW1 3	75604	13	16.17	25.51	16.24	16.28	2.14	S19	30417	30	12.75	76.03	16.15	14.43	1.82
GS1845CW1 3	75604	14	14.54	73.07	16.23	15.53	2.12	S19	30417	31	16.06	44.62	16.15	16.34	1.82
GS1845CW1 3	75604	15	12.84	65.17	16.23	14.37	2.12	S19	30417	32	13.74	70.67	16.15	15.00	1.82
GS1845CW1 3	75604	16	10.37	56.87	16.25	12.62	2.18	S19	30417	33	9.37	86.46	16.15	12.84	1.82
GS1845CW1 3	75604	17	10.62	63.49	16.24	12.93	2.16	S19	30417	34	9.26	64.10	16.15	12.17	1.82
GS1845CW1 3	75604	18	11.61	57.79	16.26	13.45	2.23	S19	30417	35	12.53	18.94	16.15	12.92	1.82
GS1845CW1 3	75604	19	11.25	53.74	16.26	13.12	2.23	S19	30417	36	11.64	46.24	16.15	13.17	1.82
GS1845CW1 3	75604	20	14.11	64.94	16.19	15.19	1.97	S19	30417	37	8.53	75.37	16.15	12.47	1.82
GS1845CW1 3	75604	21	7.98	83.20	16.20	12.27	2.02	S19	30417	38	11.30	53.36	16.20	13.14	2.03
GS1845CW1 3	75604	22	11.74	36.86	16.20	12.94	2.02	S19	30417	39	14.46	28.38	16.20	14.84	2.03
GS1845CW1 3	75604	23	12.70	38.77	16.20	13.71	2.02	S19	30417	40	13.86	56.12	16.21	14.91	2.04
GS1845CW1 3	75604	24	14.16	66.93	16.14	15.24	1.80	S19	30417	41	14.40	78.59	16.14	15.47	1.81
GS1845CW1 3	75604	25	11.59	59.51	16.14	13.47	1.80	S19	30417	42	14.03	52.34	16.14	14.97	1.81
GS1845CW1 3	75604	26	11.37	30.22	16.22	12.41	2.10	S19	30417	43	14.95	44.02	16.14	15.50	1.81
GS1845CW1 3	75604	27	14.26	55.26	16.22	15.17	2.10	S19	30417	44	14.05	49.73	16.14	14.94	1.81
GS1845CW1 3	75604	28	14.91	76.54	16.22	15.77	2.10	S19	30417	45	15.63	19.59	16.14	15.74	1.81
GS1845CW1 3	75604	29	10.54	72.54	16.22	13.02	2.10	S19	30417	46	14.31	42.22	16.14	14.99	1.81
GS1845CW1 3	75604	30	11.66	48.05	16.27	13.24	2.26	S19	30417	47	10.56	60.09	16.14	12.82	1.81
GS1845CW1 3	75604	31	14.67	51.96	16.11	15.41	1.70	S19	30417	48	16.25	22.43	16.19	16.33	1.98
GS1845CW1 3	75604	32	11.56	59.16	16.23	13.44	2.12	S19	30417	49	11.29	63.55	16.19	13.35	1.98
GS1845CW1 3	75604	33	15.41	85.34	16.23	16.11	2.12	S19	30417	50	14.84	65.87	16.19	15.67	1.98
GS1845CW1 3	75604	34	15.47	88.95	16.23	16.14	2.12	S19	30417	51	14.63	78.46	16.19	15.61	1.98
GS1845CW1 3	75604	35	9.79	62.24	16.23	12.38	2.12	S19	30417	52	14.79	46.04	16.19	15.41	1.98
GS1845CW1 3	75604	36	13.32	73.39	16.23	14.76	2.12	S19	30417	53	14.52	55.66	16.06	15.35	1.51
GS1845CW1 3	75604	37	13.76	38.56	16.27	14.50	2.25	S19	30417	54	15.34	59.33	16.06	15.95	1.51
GS1845CW1 3	75604	38	15.85	25.46	16.30	16.00	2.38	S19	30417	55	15.36	33.47	16.06	15.68	1.51
GS1845CW1 3	75604	39	15.06	71.65	16.30	15.85	2.38	S19	30417	56	13.39	52.15	16.22	14.52	2.07
GS1845CW1 3	75604	40	14.77	82.47	16.27	15.71	2.25	S19	30417	57	15.67	57.10	16.22	16.15	2.07
GS1845CW1 3	75604	41	14.29	60.32	16.27	15.25	2.25	S19	30417	58	12.19	39.97	16.19	13.37	1.99
GS1845CW1 3	75604	42	9.68	51.83	16.25	12.04	2.19	S19	30417	59	9.23	55.99	16.10	11.87	1.66
GS1845CW1 3	75604	43	13.88	88.34	16.22	15.17	2.08	S19	30417	60	15.76	74.27	16.10	16.30	1.66
GS1845CW1 3	75604	44	13.45	34.33	16.27	14.16	2.27	S19	30417	61	15.22	67.99	16.10	15.93	1.66
GS1845CW1 3	75604	45	14.90	50.74	16.22	15.55	2.09	S19	30417	62	14.09	75.67	16.10	15.26	1.66
GS1845CW1 3	75604	46	13.11	53.79	16.15	14.36	1.85	S19	30417	63	14.85	73.04	16.15	15.72	1.85
GS1845CW1 3	75604	47	10.47	47.74	16.22	12.43	2.10	S19	30417	64	14.69	70.91	16.15	15.61	1.85
GS1845CW1 3	75604	48	10.40	73.03	16.21	12.94	2.05	S19	30417	65	12.82	78.83	16.15	14.49	1.85
GS1845CW1 3	75604	49	14.56	78.78	16.25	15.57	2.20	S19	30417	66	14.48	2.90	16.15	14.49	1.85
GS1845CW1 3	75604	50	15.43	63.55	16.20	16.04	2.00	S19	30417	67	10.61	64.05	16.15	12.93	1.85
GS1845CW1 3	75604	51	10.15	87.15	16.20	12.95	2.00	S19	30417	68	13.96	45.08	16.15	14.79	1.85
GS1845CW1 3	75604	52	12.28	75.44	16.20	14.13	2.00	S19	30417	69	11.55	33.68	16.15	12.68	1.85
GS1845CW1 3	75604	53	13.30	88.36	16.20	14.82	2.00	S19	30417	70	10.28	80.88	16.15	12.94	1.85
GS1845CW1 3	75604	54	15.67	47.65	16.23	16.08	2.13	S19	30417	71	15.92	60.85	16.15	16.34	1.82
GS1845CW1 3	75604	55	13.63	62.78	16.26	14.85	2.22	S19	30417	72	14.35	64.39	16.15	15.34	1.82
GS1845CW1 3	75604	56	16.02	2.34	16.26	16.02	2.22	S19	30417	73	13.75	49.05	16.15	14.72	1.82
GS1845CW1 3	75604	57	11.37	89.09	16.20	13.63	2.01	S19	30417	74	12.76	24.93	16.15	13.32	1.82
GS1845CW1 3	75604	58	14.60	47.17	16.20	15.29	2.01	S19	30417	75	13.91	89.79	16.14	15.19	1.81
GS1845CW1 3	75604	59	14.72	46.04	16.24	15.36	2.16	S19	30417	76	9.49	82.07	16.14	12.72	1.81
GS1845CW1 3	75604	60	8.46	30.95	16.24	10.39	2.16	S19	30417	77	13.54	35.79	16.14	14.27	1.81
GS1845CW1 3	75604	61	12.12	33.89	16.24	13.12	2.17	S19	30417	78	15.39	30.32	16.14	15.66	1.81
GS1845CW1 3	75604	62	15.35	47.43	16.14	15.84	1.79	S19	30417	79	13.49	68.20	16.13	14.82	1.77
GS1845CW1 3	75604	63	15.05	33.60	16.17	15.42	1.91	S19	30417	80	13.66	70.64	16.13	14.95	1.77
GS1845CW1 3	75604	64	10.60	83.78	16.20	13.15	2.03	S19	30417	81	13.50	52.63	16.13	14.61	1.77
GS1845CW1 3	75604	65	11.56	46.03	16.20	13.11	2.03	S19	30417	82	13.57	88.05	16.08	14.98	1.60
GS1845CW1 3	75604	66	11.27	44.40	16.20	12.86	2.03	S19	30417	83	12.67	74.64	16.08	14.37	1.60
GS1845CW1 3	75604	67	11.40	42.08	16.20	12.88	2.01	S19	30417	84	13.85	77.75	16.19	15.12	1.97
GS1845CW1 3	75604	68	11.84	81.21	16.20	13.90	2.01	S19	30417	85	11.25	55.87	16.29	13.17	2.33

Table C3 Apatite fission track lengths for all samples analysed in this thesis

UBC	A2Z	Track	Angle				Dpar	UBC	A2Z	Track	Angle				Dpar
			Length (μm)	to c- axis	Lo calc (μm)	Lc calc (μm)					Length (μm)	to c- axis	Lo calc (μm)	Lc calc (μm)	
GS1845CW1 3	75604	69	11.41	37.00	16.20	12.70	2.01	S19	30417	86	15.71	44.06	16.09	16.07	1.61
GS1845CW1 3	75604	70	15.59	74.12	16.20	16.19	2.01	S19	30417	87	12.86	43.79	16.09	13.97	1.61
GS1845CW1 3	75604	71	15.32	69.87	16.17	16.00	1.92	S19	30417	88	14.89	35.99	16.10	15.33	1.67
GS1845CW1 3	75604	72	8.54	56.60	16.22	11.68	2.10	S19	30417	89	13.40	75.61	16.10	14.83	1.67
GS1845CW1 3	75604	73	11.87	66.76	16.22	13.77	2.10	S19	30417	90	10.15	72.05	16.11	12.77	1.70
GS1845CW1 3	75604	74	11.92	22.45	16.22	12.53	2.10	S19	30417	91	12.45	87.66	16.11	14.29	1.70
GS1845CW1 3	75604	75	13.05	48.90	16.21	14.22	2.05	S19	30417	92	13.38	41.38	16.11	14.28	1.70
GS1845CW1 3	75604	76	11.30	55.07	16.17	13.18	1.90	S20	30418	1	14.22	56.59	16.23	15.16	2.11
GS1845CW1 3	75604	77	14.33	40.99	16.25	14.99	2.18	S20	30418	2	14.69	52.78	16.23	15.43	2.11
GS1845CW1 3	75604	78	15.00	22.32	16.25	15.20	2.18	S20	30418	3	17.14	16.91	16.10	17.14	1.65
GS1845CW1 3	75604	79	14.44	65.35	16.25	15.40	2.18	S20	30418	4	13.95	55.45	16.21	14.96	2.04
GS1845CW1 3	75604	80	15.71	64.27	16.22	16.22	2.08	S20	30418	5	13.87	18.89	16.12	14.12	1.72
GS1845CW1 3	75604	81	14.93	89.12	16.22	15.81	2.08	S20	30418	6	15.49	53.84	16.13	16.00	1.75
GS1845CW1 3	75604	82	15.18	63.72	16.22	15.87	2.08	S20	30418	7	15.64	28.50	16.23	15.85	2.11
GS1845CW1 3	75604	83	13.00	61.58	16.22	14.42	2.08	S20	30418	8	15.29	31.65	16.15	15.59	1.82
GS1845CW1 3	75604	84	6.61	64.73	16.22	11.53	2.07	S20	30418	9	11.72	74.21	16.15	13.77	1.84
GS1845CW1 3	75604	85	15.01	78.14	16.22	15.84	2.07	S20	30418	10	14.03	45.32	16.13	14.85	1.77
GS1845CW1 3	75604	86	17.08	50.11	16.30	17.12	2.35	S20	30418	11	10.52	58.01	16.20	12.75	2.03
GS1845CW1 3	75604	87	11.55	84.32	16.31	13.73	2.42	S20	30418	12	13.94	61.71	16.20	15.04	2.03
GS1845CW1 3	75604	88	15.08	73.58	16.31	15.87	2.42	S20	30418	13	13.11	70.38	16.06	14.60	1.52
GS1845CW1 3	75604	89	15.26	39.16	16.22	15.67	2.10	S20	30418	14	14.63	65.97	16.11	15.53	1.71
GS1845CW1 3	75604	90	11.45	64.03	16.22	13.46	2.10	S20	30418	15	13.78	80.60	16.11	15.09	1.69
GS1845CW1 3	75604	91	14.12	31.69	16.31	14.63	2.41	S20	30418	16	14.57	57.46	16.07	15.41	1.57
GS1845CW1 3	75604	92	13.85	89.23	16.31	15.15	2.41	S20	30418	17	14.46	55.26	16.12	15.31	1.73
GS1845CW1 3	75604	93	11.35	60.54	16.31	13.33	2.41	S20	30418	18	14.16	66.06	16.15	15.23	1.84
GS1845CW1 3	75604	94	11.05	42.55	16.29	12.65	2.33	S20	30418	19	11.87	62.13	16.08	13.70	1.58
GS1845CW1 3	75604	95	15.54	53.83	16.29	16.04	2.33	S20	30418	20	15.47	78.12	16.11	16.13	1.68
GS1845CW1 3	75604	96	11.14	38.53	16.29	12.57	2.33	S20	30418	21	12.79	58.37	16.13	14.23	1.78
GS1845CW1 3	75604	97	12.55	47.93	16.29	13.85	2.33	S20	30418	22	13.60	10.45	16.13	13.69	1.78
GS1845CW1 3	75604	98	9.32	73.84	16.28	12.45	2.28	S20	30418	23	14.24	56.88	16.13	15.18	1.78
GS1845CW1 3	75604	99	12.73	73.11	16.28	14.39	2.28	S20	30418	24	6.76	82.07	16.13	12.49	1.78
GS1845CW1 3	75604	100	12.32	23.93	16.18	12.92	1.95	S20	30418	25	15.47	51.47	16.17	15.97	1.90
GS1845CW1 3	75604	101	14.83	66.16	16.18	15.66	1.95	S20	30418	26	13.93	45.13	16.17	14.77	1.90
GS1845CW1 3	75604	102	8.50	75.97	16.18	12.28	1.95	S20	30418	27	11.30	63.43	16.13	13.36	1.78
GS1845CW1 3	75604	103	14.77	28.10	16.18	15.10	1.95	S20	30418	28	14.20	50.58	16.12	15.06	1.73
GS1845CW1 3	75604	104	12.35	38.31	16.18	13.44	1.95	S20	30418	29	15.85	44.82	16.19	16.18	1.97
GS1845CW1 3	75604	105	10.93	56.73	16.22	12.98	2.08	S20	30418	30	13.26	81.94	16.14	14.78	1.80
GS1845CW1 3	75604	106	14.15	37.69	16.22	14.78	2.08	S20	30418	31	13.18	78.13	16.18	14.71	1.93
GS1845CW1 3	75604	107	15.07	44.70	16.23	15.60	2.13	S20	30418	32	14.37	71.06	16.18	15.40	1.93
GS1845CW1 3	75604	108	16.99	55.39	16.23	17.06	2.13	S20	30418	33	12.44	81.67	16.08	14.27	1.59
GS1845CW1 3	75604	109	14.41	69.75	16.16	15.42	1.86	S20	30418	34	14.09	48.78	16.15	14.95	1.84
GS1845CW1 3	75604	110	12.95	81.77	16.24	14.58	2.16	S21	30419	1	14.72	43.01	16.19	15.32	1.98
GS1845CW1 3	75604	111	16.89	42.78	16.26	16.96	2.24	S21	30419	2	13.65	66.55	16.19	14.91	1.98
GS1845CW1 3	75604	112	14.24	41.56	16.26	14.93	2.24	S21	30419	3	16.04	19.67	16.16	16.12	1.88
GS1845CW1 3	75604	113	10.77	77.38	16.20	13.21	2.03	S21	30419	4	14.30	76.43	16.16	15.39	1.88
GS1845CW1 3	75604	114	15.34	50.76	16.20	15.87	2.03	S21	30419	5	13.74	69.69	16.16	14.99	1.88
GS1845CW1 3	75604	115	14.80	63.72	16.20	15.62	2.03	S21	30419	6	13.44	59.55	16.16	14.68	1.88
GS1845CW1 3	75604	116	14.79	32.32	16.19	15.19	1.98	S21	30419	7	15.81	84.20	16.16	16.35	1.88
GS1845CW1 3	75604	117	11.72	18.42	16.15	12.19	1.85	S21	30419	8	12.37	50.90	16.16	13.80	1.88
GS1845CW1 3	75604	118	14.56	47.14	16.31	15.26	2.41	S21	30419	9	15.74	32.35	16.14	15.98	1.80
GS1845CW1 3	75604	119	15.04	78.64	16.31	15.86	2.39	S21	30419	10	15.80	66.89	16.10	16.29	1.65
GS1845CW1 3	75604	120	9.38	46.86	16.31	11.68	2.39	S21	30419	11	14.58	58.74	16.10	15.43	1.65
GS1845CW1 3	75604	121	14.80	85.87	16.31	15.73	2.39	S21	30419	12	10.45	88.37	16.10	13.07	1.65
GS1845CW1 3	75604	122	11.49	68.80	16.31	13.56	2.39	S21	30419	13	13.41	34.05	16.22	14.12	2.10
GS1845CW1 3	75604	123	8.86	34.86	16.27	10.85	2.26	S21	30419	14	14.26	51.46	16.22	15.11	2.10
GS1845CW1 3	75604	124	15.62	75.38	16.32	16.21	2.43	S21	30419	15	12.78	84.96	16.22	14.49	2.10
GS1845CW1 3	75604	125	8.58	81.55	16.11	12.41	1.68	S21	30419	16	14.04	34.18	16.22	14.62	2.10
GS1845CW1 3	75604	126	15.05	43.20	16.11	15.57	1.68	S21	30419	17	15.18	77.75	16.22	15.95	2.10
GS1845CW1 3	75604	127	16.63	13.94	16.22	16.65	2.10	S21	30419	18	11.67	80.01	16.15	13.79	1.83
GS1845CW1 3	75604	128	13.63	22.03	16.24	13.98	2.15	S21	30419	19	16.60	32.40	16.15	16.70	1.83
GS1845CW1 3	75604	129	14.07	22.41	16.24	14.38	2.15	S21	30419	20	15.19	56.52	16.17	15.82	1.91

Table C3 Apatite fission track lengths for all samples analysed in this thesis

UBC	A2Z	Track	Angle				Dpar	UBC	A2Z	Track	Angle				Dpar
			Length (μm)	to c- axis	Lo calc (μm)	Lc calc (μm)					Length (μm)	to c- axis	Lo calc (μm)	Lc calc (μm)	
GS1845CW1 3	75604	130	14.85	68.28	16.21	15.69	2.04	S21	30419	21	13.24	63.09	16.17	14.60	1.91
GS1845CW1 3	75604	131	15.63	55.93	16.21	16.12	2.04	S21	30419	22	13.63	55.55	16.17	14.75	1.91
GS1845CW1 3	75604	132	13.89	62.25	16.21	15.01	2.04	S21	30419	23	15.21	69.58	16.18	15.93	1.95
GS1845CW1 3	75604	133	9.02	57.59	16.18	11.83	1.96	S21	30419	24	13.44	60.81	16.18	14.70	1.95
GS1845CW1 4	75605	1	13.85	72.12	16.20	15.08	2.02	S21	30419	25	13.58	23.56	16.15	13.98	1.85
GS1845CW1 4	75605	2	10.02	68.09	16.39	12.63	2.67	S21	30419	26	15.08	21.05	16.15	15.26	1.85
GS1845CW1 4	75605	3	14.52	58.18	16.39	15.38	2.67	S21	30419	27	13.94	74.33	16.22	15.16	2.07
GS1845CW1 4	75605	4	14.81	75.88	16.39	15.71	2.67	S21	30419	28	12.67	88.04	16.22	14.43	2.07
GS1845CW1 4	75605	5	4.04	89.04	16.21	11.24	2.05	S21	30419	29	16.59	68.67	16.22	16.81	2.07
GS1845CW1 4	75605	6	13.91	61.45	16.21	15.02	2.05	S21	30419	30	12.49	64.44	16.32	14.13	2.44
GS1845CW1 4	75605	7	10.24	59.92	16.21	12.61	2.05	S21	30419	31	16.14	19.11	16.29	16.21	2.34
GS1845CW1 4	75605	8	13.64	36.53	16.21	14.36	2.05	S21	30419	32	14.66	61.63	16.18	15.51	1.94
GS1845CW1 4	75605	9	11.40	60.67	16.30	13.37	2.38	S21	30419	33	12.60	35.68	16.18	13.54	1.94
GS1845CW1 4	75605	10	8.97	63.73	16.22	12.06	2.09	S21	30419	34	14.47	76.94	16.18	15.50	1.94
GS1845CW1 4	75605	11	12.02	25.92	16.22	12.74	2.09	S21	30419	35	13.82	28.45	16.18	14.31	1.94
GS1845CW1 4	75605	12	14.14	53.11	16.26	15.06	2.23	S21	30419	36	12.53	7.47	16.12	12.60	1.74
GS1845CW1 4	75605	13	12.73	52.89	16.16	14.09	1.88	S21	30419	37	14.42	58.83	16.31	15.32	2.42
GS1845CW1 4	75605	14	11.39	75.49	16.16	13.58	1.88	S21	30419	38	13.14	42.04	16.31	14.12	2.42
GS1845CW1 4	75605	15	11.47	76.95	16.18	13.64	1.96	S21	30419	39	14.70	58.93	16.22	15.51	2.09
GS1845CW1 4	75605	16	10.79	27.34	16.18	11.84	1.96	S21	30419	40	14.73	50.74	16.22	15.43	2.09
GS1845CW1 4	75605	17	12.59	51.05	16.29	13.95	2.32	S21	30419	41	13.23	64.03	16.22	14.61	2.09
GS1845CW1 4	75605	18	14.84	62.58	16.29	15.64	2.32	S21	30419	42	14.56	83.34	16.18	15.58	1.93
GS1845CW1 4	75605	19	14.98	71.48	16.24	15.79	2.15	S21	30419	43	13.83	57.88	16.18	14.92	1.93
GS1845CW1 4	75605	20	15.94	47.30	16.24	16.27	2.15	S21	30419	44	15.08	64.11	16.35	15.81	2.54
GS1845CW1 4	75605	21	14.42	15.20	16.24	14.56	2.15	S21	30419	45	15.24	36.40	16.35	15.62	2.54
GS1845CW1 4	75605	22	16.93	26.16	16.24	16.96	2.15	S21	30419	46	12.52	62.07	16.20	14.12	2.00
GS1845CW1 4	75605	23	14.44	68.11	16.24	15.43	2.15	S21	30419	47	13.91	21.73	16.31	14.22	2.39
GS1845CW1 4	75605	24	13.12	59.21	16.22	14.46	2.09	S21	30419	48	15.28	65.57	16.20	15.95	2.03
GS1845CW1 4	75605	25	13.40	80.66	16.22	14.86	2.09	S22	30420	1	12.25	71.60	16.09	14.07	1.61
GS1845CW1 4	75605	26	10.93	54.68	16.28	12.93	2.30	S22	30420	2	14.41	85.53	16.25	15.49	2.19
GS1845CW1 4	75605	27	17.71	49.06	16.28	17.58	2.30	S22	30420	3	14.66	80.00	16.14	15.63	1.79
GS1845CW1 4	75605	28	7.60	76.49	16.32	12.06	2.45	S22	30420	4	10.16	57.42	16.09	12.50	1.64
GS1845CW1 4	75605	29	10.86	82.82	16.24	13.30	2.15	S22	30420	5	13.29	26.57	16.09	13.81	1.64
GS1845CW1 4	75605	30	10.73	51.34	16.31	12.71	2.42	S22	30420	6	11.63	78.89	16.10	13.75	1.65
GS1845CW1 4	75605	31	9.16	76.61	16.31	12.47	2.42	S22	30420	7	12.33	89.12	16.10	14.22	1.65
GS1845CW1 4	75605	32	12.75	57.60	16.25	14.19	2.19	S22	30420	8	14.08	46.86	16.10	14.91	1.65
GS1845CW1 4	75605	33	12.47	39.37	16.25	13.56	2.19	S22	30420	9	10.86	87.73	16.17	13.32	1.90
GS1845CW1 4	75605	34	14.44	53.44	16.25	15.27	2.19	S22	30420	10	14.67	76.23	16.11	15.62	1.69
GS1845CW1 4	75605	35	13.31	66.73	16.23	14.69	2.11	S22	30420	11	12.65	61.99	16.19	14.20	1.98
GS1845CW1 4	75605	36	14.36	87.29	16.23	15.46	2.11	S22	30420	12	13.24	71.74	16.53	14.70	3.18
GS1845CW1 4	75605	37	14.09	80.09	16.27	15.28	2.26	S22	30420	13	14.24	30.43	16.19	14.70	1.97
GS1845CW1 4	75605	38	10.22	35.02	16.27	11.78	2.26	S22	30420	14	9.45	82.36	16.19	12.73	1.97
GS1845CW1 4	75605	39	11.53	22.65	16.18	12.21	1.96	S22	30420	15	10.30	77.93	16.26	12.93	2.24
GS1845CW1 4	75605	40	12.05	82.14	16.26	14.03	2.21	S22	30420	16	13.89	47.17	16.12	14.78	1.73
GS1845CW1 4	75605	41	4.05	65.29	16.26	10.85	2.21	S22	30420	17	15.04	70.45	16.11	15.83	1.69
GS1845CW1 4	75605	42	10.91	66.06	16.26	13.15	2.21	S22	30420	18	14.82	5.10	16.16	14.83	1.86
GS1845CW1 4	75605	43	14.90	70.39	16.23	15.74	2.12	S22	30420	19	16.16	86.31	16.16	16.57	1.89
GS1845CW1 4	75605	44	10.94	44.71	16.17	12.65	1.90	S22	30420	20	15.69	41.13	16.16	16.03	1.88
GS1845CW1 4	75605	45	12.76	80.21	16.17	14.46	1.90	S22	30420	21	11.89	53.97	16.30	13.55	2.36
GS1845CW1 4	75605	46	12.31	61.88	16.24	13.98	2.16	S22	30420	22	11.77	72.34	16.30	13.78	2.36
GS1845CW1 4	75605	47	13.39	58.73	16.24	14.63	2.16	S22	30420	23	15.71	54.65	16.15	16.16	1.82
GS1845CW1 4	75605	48	14.60	56.27	16.24	15.41	2.16	S22	30420	24	14.40	71.01	16.15	15.42	1.82
GS1845CW1 4	75605	49	13.37	36.97	16.25	14.17	2.18	S22	30420	25	7.67	78.84	16.23	12.50	2.11
GS1845CW1 4	75605	50	11.75	84.71	16.25	13.86	2.18	S22	30420	26	12.81	71.06	16.23	14.42	2.11
GS1845CW1 4	75605	51	15.34	12.87	16.30	15.40	2.37	S22	30420	27	15.41	66.62	16.23	16.04	2.11
GS1845CW1 4	75605	52	10.47	85.13	16.30	13.07	2.37	S22	30420	28	16.06	89.09	16.12	16.51	1.74
GS1845CW1 4	75605	53	12.04	34.99	16.30	13.10	2.37	S22	30420	29	15.83	43.68	16.12	16.16	1.74
GS1845CW1 4	75605	54	14.81	77.51	16.23	15.72	2.12	S22	30420	30	9.95	71.24	16.12	12.63	1.74
GS1845CW1 4	75605	55	13.22	50.19	16.15	14.37	1.82	S22	30420	31	13.10	69.06	16.12	14.58	1.74
GS1845CW1 4	75605	56	3.08	68.61	16.23	10.58	2.11	S22	30420	32	15.43	78.84	16.12	16.11	1.74
GS1845CW1 4	75605	57	16.03	55.13	16.23	16.39	2.11	S22	30420	33	14.13	82.71	16.12	15.31	1.73

Table C3 Apatite fission track lengths for all samples analysed in this thesis

UBC	A2Z	Track	Angle				Dpar	UBC	A2Z	Track	Angle				Dpar
			Length (μm)	to c- axis	Lo calc (μm)	Lc calc (μm)					Length (μm)	to c- axis	Lo calc (μm)	Lc calc (μm)	
GS1845CW1 4	75605	58	12.42	65.67	16.25	14.11	2.19	S22	30420	34	13.76	50.97	16.12	14.76	1.73
GS1845CW1 4	75605	59	12.33	8.50	16.34	12.43	2.51	S22	30420	35	14.51	76.93	16.12	15.53	1.73
GS1845CW1 4	75605	60	15.00	74.81	16.34	15.82	2.51	S22	30420	36	11.73	70.54	16.29	13.74	2.32
GS1845CW1 4	75605	61	15.22	74.61	16.18	15.96	1.93	S22	30420	37	14.18	48.16	16.29	15.00	2.32
GS1845CW1 4	75605	62	11.12	71.22	16.25	13.36	2.18	S22	30420	38	14.57	89.60	16.29	15.59	2.32
GS1845CW1 4	75605	63	16.18	40.38	16.28	16.40	2.31	S22	30420	39	13.87	50.59	16.29	14.83	2.32
GS1845CW1 4	75605	64	9.94	84.30	16.28	12.84	2.31	S22	30420	40	14.15	46.64	16.29	14.96	2.32
GS1845CW1 4	75605	65	10.65	63.33	16.27	12.94	2.26	S22	30420	41	14.12	63.81	16.29	15.18	2.32
GS1845CW1 4	75605	66	14.86	73.51	16.16	15.73	1.87	S22	30420	42	13.18	59.27	16.18	14.50	1.93
GS1845CW1 4	75605	67	11.02	13.13	16.24	11.36	2.16	S22	30420	43	15.44	83.19	16.28	16.12	2.31
GS1845CW1 4	75605	68	14.49	19.03	16.24	14.69	2.16	S22	30420	44	15.30	69.28	16.28	15.99	2.31
GS1845CW1 4	75605	69	13.40	41.02	16.24	14.29	2.14	S22	30420	45	12.40	79.34	16.28	14.23	2.31
GS1845CW1 4	75605	70	13.58	71.97	16.24	14.91	2.14	S22	30420	46	15.16	46.39	16.28	15.69	2.31
GS1845CW1 4	75605	71	12.24	74.60	16.21	14.10	2.06	S23	30421	1	14.73	46.73	16.19	15.38	1.99
GS1845CW1 4	75605	72	9.89	71.23	16.21	12.60	2.06	S23	30421	2	15.58	34.54	16.15	15.87	1.82
GS1845CW1 4	75605	73	12.40	71.21	16.29	14.16	2.32	S23	30421	3	15.27	34.63	16.15	15.62	1.83
GS1845CW1 4	75605	74	15.12	56.60	16.20	15.77	2.02	S23	30421	4	14.27	68.59	16.11	15.32	1.69
GS1845CW1 4	75605	75	11.78	53.64	16.29	13.46	2.34	S23	30421	5	14.55	50.39	16.11	15.30	1.68
GS1845CW1 4	75605	76	13.49	86.92	16.36	14.93	2.57	S23	30421	6	14.11	58.91	16.15	15.12	1.84
GS1845CW1 4	75605	77	13.26	42.46	16.36	14.22	2.57	S23	30421	7	14.55	87.52	16.24	15.58	2.14
GS1845CW1 4	75605	78	8.70	55.64	16.36	11.67	2.57	S23	30421	8	14.95	81.56	16.24	15.82	2.14
GS1845CW1 4	75605	79	10.16	74.15	16.36	12.80	2.57	S23	30421	9	14.49	77.62	16.24	15.52	2.14
GS1845CW1 4	75605	80	9.86	41.09	16.36	11.78	2.57	S23	30421	10	15.08	46.95	16.20	15.64	2.00
GS1845CW1 4	75605	81	13.30	75.80	16.33	14.77	2.46	S23	30421	11	11.69	55.79	16.22	13.46	2.10
GS1845CW1 4	75605	82	12.09	16.36	16.30	12.44	2.35	S23	30421	12	15.33	66.19	16.14	15.99	1.81
GS1845CW1 4	75605	83	14.08	53.51	16.14	15.02	1.81	S23	30421	13	11.96	55.09	16.11	13.62	1.68
GS1845CW1 4	75605	84	10.25	40.13	16.14	12.01	1.81	S23	30421	14	13.68	80.99	16.30	15.03	2.38
GS1845CW1 4	75605	85	9.36	67.56	16.14	12.28	1.81	S23	30421	15	14.10	69.99	16.08	15.23	1.59
GS1845CW1 4	75605	86	11.62	40.11	16.19	12.97	1.97	S23	30421	16	14.90	71.46	16.14	15.74	1.81
GS1845CW1 4	75605	87	11.69	69.70	16.19	13.70	1.97	S23	30421	17	15.13	67.40	16.14	15.87	1.81
GS1845CW1 4	75605	88	9.55	57.58	16.20	12.12	2.01	S23	30421	18	14.28	16.17	16.14	14.44	1.81
GS1845CW1 4	75605	89	10.97	43.45	16.33	12.62	2.47	S23	30421	19	15.45	86.15	16.14	16.13	1.81
GS1845CW1 4	75605	90	10.07	71.89	16.26	12.72	2.21	S23	30421	20	15.89	44.90	16.13	16.21	1.78
GS1845CW1 4	75605	91	10.91	79.44	16.32	13.31	2.45	S23	30421	21	12.56	76.36	16.18	14.31	1.95
GS1845CW1 4	75605	92	14.56	15.48	16.32	14.69	2.45	S23	30421	22	14.98	20.08	16.35	15.15	2.53
GS1845CW1 4	75605	93	16.98	19.51	16.32	17.00	2.45	S23	30421	23	14.89	67.90	16.04	15.71	1.46
GS1845CW1 4	75605	94	10.61	75.68	16.18	13.10	1.95	S23	30421	24	14.22	35.50	16.23	14.79	2.12
GS1845CW1 4	75605	95	11.94	74.26	16.18	13.91	1.95	S23	30421	25	15.98	29.40	16.23	16.15	2.12
GS1845CW1 4	75605	96	14.21	59.15	16.24	15.19	2.17	S23	30421	26	6.31	89.40	16.18	12.71	1.95
GS1845CW1 4	75605	97	14.55	78.49	16.24	15.56	2.17	S23	30421	27	13.48	59.88	16.18	14.71	1.95
GS1845CW1 4	75605	98	10.00	65.50	16.24	12.57	2.17	S23	30421	28	15.41	46.44	16.18	15.87	1.94
GS1845CW1 4	75605	99	14.03	61.16	16.26	15.09	2.23	S23	30421	29	13.63	66.31	16.11	14.89	1.70
GS1845CW1 4	75605	100	16.01	61.83	16.24	16.41	2.16	S23	30421	30	16.21	18.55	16.11	16.27	1.70
GS1845CW1 4	75605	101	10.31	75.44	16.23	12.91	2.13	S23	30421	31	13.55	72.83	16.11	14.90	1.70
GS1845CW1 4	75605	102	15.10	67.44	16.23	15.85	2.13	S23	30421	32	14.67	62.96	16.11	15.53	1.70
GS1845CW1 4	75605	103	10.06	50.96	16.23	12.26	2.13	S23	30421	33	11.81	57.02	16.11	13.56	1.70
GS1845CW1 4	75605	104	14.73	34.00	16.23	15.17	2.13	S23	30421	34	11.66	73.19	16.14	13.72	1.81
GS1845CW1 4	75605	105	13.07	32.58	16.26	13.81	2.22	S23	30421	35	16.43	74.09	16.18	16.72	1.96
GS1845CW1 4	75605	106	11.43	34.12	16.26	12.61	2.22	S23	30421	36	14.16	27.47	16.18	14.57	1.95
GS1845CW1 4	75605	107	14.09	41.84	16.26	14.82	2.22	S23	30421	37	13.62	68.29	16.14	14.90	1.81
GS1845CW1 4	75605	108	14.18	32.30	16.33	14.69	2.49	S23	30421	38	16.00	79.63	16.11	16.46	1.68
GS1845CW1 4	75605	109	17.97	14.89	16.22	17.94	2.10	S23	30421	39	12.45	49.86	16.11	13.83	1.68
GS1845CW1 4	75605	110	15.04	17.74	16.22	15.18	2.10	S23	30421	40	8.98	68.36	16.11	12.29	1.68
GS1845CW1 4	75605	111	14.88	76.83	16.22	15.76	2.10	S23	30421	41	14.82	45.96	16.15	15.43	1.82
GS1845CW1 4	75605	112	7.54	38.18	16.33	10.51	2.49	S23	30421	42	9.94	55.08	16.17	12.30	1.90
GS1845CW1 4	75605	113	16.26	36.47	16.33	16.44	2.49	S23	30421	43	12.00	71.62	16.17	13.92	1.90
GS1845CW1 4	75605	114	14.93	62.23	16.24	15.70	2.16	S23	30421	44	14.15	22.82	16.15	14.46	1.82
GS1845CW1 4	75605	115	13.78	86.50	16.24	15.11	2.16	S23	30421	45	12.63	40.44	16.15	13.71	1.82
GS1845CW1 4	75605	116	6.59	50.63	16.24	11.02	2.16	S23	30421	46	10.94	88.96	16.14	13.37	1.80
GS1845CW1 4	75605	117	14.30	64.16	16.24	15.30	2.16	S23	30421	47	14.83	54.94	16.17	15.56	1.92
GS1845CW1 4	75605	118	11.49	79.10	16.31	13.67	2.41	S23	30421	48	13.16	70.53	16.17	14.64	1.92

Table C3 Apatite fission track lengths for all samples analysed in this thesis

UBC	A2Z	Track	Angle				Dpar	UBC	A2Z	Track	Angle				Dpar
			Length (μm)	to c- axis	Lo calc (μm)	Lc calc (μm)					Length (μm)	to c- axis	Lo calc (μm)	Lc calc (μm)	
GS1845CW1 4	75605	119	16.12	37.99	16.31	16.34	2.41	S23	30421	49	14.03	57.60	16.17	15.05	1.92
GS1845CW1 4	75605	120	14.47	49.18	16.22	15.23	2.07	S23	30421	50	13.89	57.33	16.37	14.95	2.60
GS1845CW1 4	75605	121	14.36	45.40	16.22	15.09	2.07	S23	30421	51	13.19	60.11	16.26	14.52	2.24
GS1845CW1 4	75605	122	12.22	46.78	16.22	13.59	2.07	S23	30421	52	14.14	75.61	16.17	15.29	1.92
GS1845CW1 4	75605	123	13.50	72.08	16.13	14.86	1.77	S23	30421	53	13.81	53.00	16.17	14.83	1.92
GS1845CW1 4	75605	124	13.42	41.57	16.13	14.32	1.77	S23	30421	54	13.29	61.69	16.13	14.61	1.76
GS1845CW1 4	75605	125	16.12	56.43	16.31	16.46	2.40	S23	30421	55	15.27	50.44	16.13	15.81	1.76
GS1845CW1 4	75605	126	14.78	72.04	16.31	15.67	2.40	S23	30421	56	12.46	68.75	16.21	14.17	2.04
GS1845CW1 4	75605	127	13.04	47.78	16.31	14.19	2.40	S23	30421	57	15.07	51.17	16.25	15.68	2.19
GS1845CW1 4	75605	128	8.55	53.21	16.29	11.53	2.33	S23	30421	58	9.78	58.20	16.25	12.28	2.19
GS1845CW1 4	75605	129	9.73	28.36	16.29	11.11	2.33	S23	30421	59	15.34	76.87	16.22	16.04	2.09
GS1845CW1 4	75605	130	14.58	75.69	16.22	15.56	2.09	S23	30421	60	13.74	73.38	16.22	15.02	2.09
GS1845CW1 4	75605	131	14.84	22.65	16.22	15.07	2.09	S23	30421	61	15.64	38.50	16.22	15.96	2.10
GS1845CW1 5	75606	1	14.16	44.89	16.19	14.93	1.98	S23	30421	62	13.35	65.51	16.22	14.70	2.10
GS1845CW1 5	75606	2	13.89	70.11	16.10	15.09	1.67	S23	30421	63	13.05	53.35	16.19	14.31	1.97
GS1845CW1 5	75606	3	15.23	46.89	16.20	15.75	2.01	S23	30421	64	14.37	41.47	16.19	15.03	1.97
GS1845CW1 5	75606	4	15.47	23.15	16.20	15.64	2.01	S23	30421	65	12.12	68.33	16.17	13.95	1.92
GS1845CW1 5	75606	5	16.21	36.50	16.37	16.40	2.60	S23	30421	66	11.41	54.43	16.17	13.24	1.92
GS1845CW1 5	75606	6	9.68	61.36	16.13	12.29	1.78	S23	30421	67	13.35	84.10	16.17	14.84	1.92
GS1845CW1 5	75606	7	14.43	42.48	16.09	15.09	1.61	S23	30421	68	15.43	56.34	16.11	15.98	1.68
GS1845CW1 5	75606	8	10.05	82.10	16.16	12.85	1.88	S23	30421	69	13.73	75.01	16.21	15.03	2.04
GS1845CW1 5	75606	9	10.46	66.60	16.13	12.88	1.77	S23	30421	70	14.74	57.59	16.14	15.52	1.81
GS1845CW1 5	75606	10	14.01	21.79	16.20	14.31	2.00	S23	30421	71	14.84	82.00	16.22	15.75	2.07
GS1845CW1 5	75606	11	15.47	52.34	16.20	15.97	2.00	S23	30421	72	15.25	78.76	16.12	15.99	1.72
GS1845CW1 5	75606	12	13.04	50.73	16.20	14.25	2.01	S23	30421	73	16.68	82.01	16.16	16.88	1.89
GS1845CW1 5	75606	13	13.94	56.24	16.20	14.97	2.01	S23	30421	74	11.92	73.49	16.22	13.89	2.10
GS1845CW1 5	75606	14	11.71	50.32	16.21	13.34	2.06	S23	30421	75	13.51	46.87	16.22	14.50	2.10
GS1845CW1 5	75606	15	14.44	23.05	16.21	14.72	2.06	S23	30421	76	13.91	62.90	16.23	15.03	2.13
GS1845CW1 5	75606	16	15.39	62.91	16.27	16.00	2.26	S23	30421	77	9.24	71.92	16.08	12.41	1.58
GS1845CW1 5	75606	17	14.63	56.51	16.10	15.44	1.66	S23	30421	78	14.66	55.36	16.08	15.44	1.58
GS1845CW1 5	75606	18	14.02	27.37	16.20	14.45	2.03	S23	30421	79	16.13	30.99	16.10	16.29	1.66
GS1845CW1 5	75606	19	12.64	37.12	16.18	13.62	1.93	S23	30421	80	13.58	50.83	16.14	14.63	1.79
GS1845CW1 5	75606	20	13.13	44.76	16.12	14.18	1.73	S23	30421	81	12.23	59.61	16.15	13.89	1.83
GS1845CW1 5	75606	21	14.76	39.34	16.13	15.29	1.77	S23	30421	82	7.41	56.79	16.17	11.73	1.91
GS1845CW1 5	75606	22	15.46	26.71	16.19	15.67	1.98	S23	30421	83	12.32	76.96	16.17	14.17	1.91
GS1845CW1 5	75606	23	13.31	55.73	16.26	14.53	2.22	S23	30421	84	11.24	74.56	16.15	13.48	1.82
GS1845CW1 5	75606	24	13.30	42.60	16.18	14.26	1.94	S23	30421	85	13.33	47.80	16.32	14.39	2.44
GS1845CW1 5	75606	25	8.39	52.92	16.04	11.49	1.44	S23	30421	86	11.11	48.23	16.21	12.87	2.06
GS1845CW1 5	75606	26	15.07	25.23	16.15	15.31	1.85	S23	30421	87	12.69	53.31	16.21	14.07	2.06
GS1845CW1 5	75606	27	11.81	57.29	16.19	13.57	1.97	S23	30421	88	11.05	84.06	16.16	13.43	1.89
GS1845CW1 5	75606	28	14.75	72.47	16.11	15.65	1.70	S23	30421	89	14.48	58.65	16.16	15.36	1.89
GS1845CW1 5	75606	29	10.93	55.01	16.11	12.94	1.70	S23	30421	90	12.50	65.36	16.51	14.15	3.11
GS1845CW1 5	75606	30	13.77	23.91	16.20	14.15	2.00	S23	30421	91	14.95	70.13	16.21	15.77	2.06
GS1845CW1 5	75606	31	13.38	59.13	16.15	14.63	1.83	S23	30421	92	8.28	46.88	16.21	11.41	2.06
GS1845CW1 5	75606	32	13.57	41.41	16.18	14.43	1.96	S23	30421	93	14.56	76.07	16.25	15.55	2.18
GS1845CW1 5	75606	33	10.01	67.21	16.16	12.61	1.87	S23	30421	94	16.11	28.08	16.25	16.25	2.18
GS1845CW1 5	75606	34	14.48	10.55	16.16	14.55	1.87	S23	30421	95	10.77	89.52	16.12	13.27	1.74
GS1845CW1 5	75606	35	17.23	38.61	16.16	17.23	1.87	S23	30421	96	15.53	85.63	16.12	16.18	1.74
GS1845CW1 5	75606	36	14.61	84.38	16.25	15.61	2.18	S23	30421	97	17.44	35.54	16.18	17.40	1.96
GS1845CW1 5	75606	37	14.44	73.46	16.20	15.46	2.03	S23	30421	98	13.96	72.17	16.27	15.15	2.27
GS1845CW1 5	75606	38	15.71	35.27	16.24	15.98	2.17	S23	30421	99	13.17	55.49	16.20	14.43	2.00
GS1845CW1 5	75606	39	13.87	64.48	16.13	15.03	1.75	S23	30421	100	15.13	49.32	16.13	15.70	1.75
GS1845CW1 5	75606	40	14.19	40.58	16.17	14.87	1.90	S23	30421	101	11.60	35.21	16.13	12.78	1.78
GS1845CW1 5	75606	41	12.57	55.90	16.20	14.04	2.00	S23	30421	102	11.60	54.18	16.39	13.36	2.67
GS1845CW1 5	75606	42	15.13	42.63	16.21	15.62	2.05	S23	30421	103	14.47	50.06	16.29	15.24	2.32
GS1845CW1 5	75606	43	14.32	50.44	16.16	15.14	1.89	S23	30421	104	13.37	83.89	16.29	14.85	2.32
GS1845CW1 5	75606	44	15.04	59.88	16.20	15.75	2.03	S23	30421	105	15.35	50.04	16.32	15.87	2.45
GS1845CW1 5	75606	45	15.58	45.44	16.19	15.99	1.98	S23	30421	106	10.46	78.97	16.22	13.03	2.10
GS1845CW1 5	75606	46	16.29	44.57	16.11	16.51	1.69	S23	30421	107	11.95	43.80	16.37	13.32	2.62
GS1845CW1 5	75606	47	13.78	81.52	16.14	15.09	1.79	S23	30421	108	15.71	74.75	16.37	16.27	2.62
GS1845CW1 5	75606	48	11.29	76.32	16.11	13.52	1.69	S23	30421	109	13.94	50.97	16.15	14.88	1.83

Table C3 Apatite fission track lengths for all samples analysed in this thesis

UBC	A2Z	Track	Angle				Dpar	UBC	A2Z	Track	Angle				Dpar
			Length (μm)	to c- axis	Lo calc (μm)	Lc calc (μm)					Length (μm)	to c- axis	Lo calc (μm)	Lc calc (μm)	
GS1845CW1 5	75606	49	13.58	58.28	16.17	14.75	1.90	S23	30421	110	11.77	66.27	16.20	13.70	2.01
GS1845CW1 5	75606	50	14.22	55.74	16.17	15.15	1.90	S23	30421	111	14.51	57.79	16.29	15.37	2.33
GS1845CW1 5	75606	51	13.88	57.94	16.19	14.95	1.98	S23	30421	112	13.66	66.55	16.29	14.91	2.33
GS1845CW1 5	75606	52	14.17	18.59	16.20	14.39	2.03	S23	30421	113	14.42	31.92	16.13	14.88	1.78
GS1845CW1 5	75606	53	15.46	73.81	16.24	16.11	2.16	S23	30421	114	15.40	58.28	16.15	15.98	1.84
GS1845CW1 5	75606	54	14.31	59.96	16.24	15.26	2.15	S23	30421	115	14.22	53.75	16.24	15.12	2.16
GS1845CW1 5	75606	55	10.81	73.03	16.13	13.19	1.76	S23	30421	116	14.04	82.13	16.18	15.26	1.96
GS1845CW1 5	75606	56	13.57	82.99	16.17	14.97	1.90	S23	30421	117	14.35	62.41	16.18	15.32	1.96
GS1845CW1 5	75606	57	14.05	27.57	16.17	14.48	1.90	S23	30421	118	12.89	57.49	16.11	14.28	1.69
GS1845CW1 5	75606	58	14.28	57.51	16.17	15.21	1.91	S23	30421	119	12.18	72.34	16.22	14.04	2.10
GS1845CW1 5	75606	59	14.61	51.63	16.17	15.36	1.91	S23	30421	120	16.99	48.82	16.22	17.05	2.10
GS1845CW1 5	75606	60	6.50	55.53	16.17	11.20	1.91	S23	30421	121	14.23	50.48	16.22	15.08	2.08
GS1845CW1 5	75606	61	11.62	56.73	16.27	13.43	2.26	S23	30421	122	14.46	61.19	16.21	15.38	2.04
GS1845CW1 5	75606	62	15.13	54.17	16.18	15.75	1.96	S23	30421	123	14.25	42.77	16.21	14.96	2.04
GS1845CW1 5	75606	63	9.48	32.99	16.18	11.17	1.96	S23	30421	124	12.51	72.58	16.21	14.25	2.04
GS1845CW1 5	75606	64	13.55	47.65	16.21	14.55	2.05	S23	30421	125	13.89	73.93	16.23	15.12	2.12
GS1845CW1 5	75606	65	13.04	39.55	16.20	13.99	2.00	S23	30421	126	13.63	42.63	16.22	14.50	2.08
GS1845CW1 5	75606	66	9.18	22.63	16.12	10.40	1.74	S23	30421	127	14.46	51.21	16.14	15.25	1.79
GS1845CW1 5	75606	67	14.14	49.09	16.12	14.99	1.74	S23	30421	128	15.54	72.28	16.20	16.15	2.00
GS1845CW1 5	75606	68	9.34	43.65	16.12	11.54	1.74	S25	30423	1	15.72	71.85	16.11	16.26	1.70
GS1845CW1 5	75606	69	11.48	74.17	16.24	13.62	2.15	S25	30423	2	14.13	42.50	16.11	14.87	1.70
GS1845CW1 5	75606	70	13.19	81.54	16.24	14.73	2.15	S25	30423	3	11.53	65.81	16.20	13.54	2.02
GS1845CW1 5	75606	71	10.05	33.75	16.15	11.60	1.83	S25	30423	4	15.31	71.52	16.20	16.00	2.02
GS1845CW1 5	75606	72	13.65	68.73	16.18	14.93	1.93	S25	30423	5	15.64	39.43	16.20	15.97	2.02
GS1845CW1 5	75606	73	14.96	74.66	16.18	15.80	1.93	S25	30423	6	11.58	72.74	16.11	13.67	1.68
GS1845CW1 5	75606	74	14.37	57.12	16.18	15.27	1.93	S25	30423	7	14.71	68.66	16.11	15.60	1.68
GS1845CW1 5	75606	75	14.55	40.94	16.20	15.15	2.01	S25	30423	8	12.12	61.79	16.15	13.85	1.84
GS1845CW1 5	75606	76	5.38	73.50	16.29	11.43	2.33	S25	30423	9	10.44	10.72	16.09	10.73	1.62
GS1845CW1 5	75606	77	12.32	65.62	16.29	14.04	2.33	S25	30423	10	14.28	60.07	16.10	15.24	1.65
GS1845CW1 5	75606	78	13.38	43.61	16.18	14.34	1.93	S25	30423	11	13.24	46.77	16.10	14.31	1.65
GS1845CW1 5	75606	79	13.28	70.68	16.18	14.71	1.93	S25	30423	12	13.29	70.12	16.11	14.71	1.70
GS1845CW1 5	75606	80	14.78	71.05	16.14	15.66	1.79	S25	30423	13	15.03	25.64	16.11	15.28	1.70
GS1845CW1 5	75606	81	14.36	58.57	16.23	15.28	2.11	S25	30423	14	13.82	86.04	16.11	15.13	1.70
GS1845CW1 5	75606	82	15.59	40.53	16.24	15.94	2.16	S25	30423	15	12.17	80.04	16.11	14.09	1.70
GS1845CW1 5	75606	83	11.82	60.09	16.26	13.63	2.22	S25	30423	16	10.84	46.60	16.11	12.64	1.70
GS1845CW1 5	75606	84	12.69	48.36	16.15	13.96	1.85	S25	30423	17	9.76	56.14	16.09	12.21	1.64
GS1845CW1 5	75606	85	12.25	31.59	16.28	13.14	2.28	S25	30423	18	11.82	48.18	16.13	13.35	1.75
GS1845CW1 5	75606	86	7.34	66.98	16.28	11.77	2.28	S25	30423	19	14.62	87.14	16.11	15.62	1.69
GS1845CW1 5	75606	87	15.51	39.93	16.18	15.88	1.96	S25	30423	20	14.10	56.84	16.09	15.08	1.62
GS1845CW1 5	75606	88	13.48	85.19	16.19	14.92	1.97	S25	30423	21	14.24	64.29	16.09	15.26	1.62
GS1845CW1 5	75606	89	12.34	72.06	16.15	14.13	1.84	S25	30423	22	11.71	67.42	16.32	13.68	2.43
GS1845CW1 5	75606	90	14.57	25.36	16.10	14.88	1.66	S25	30423	23	12.95	32.70	16.32	13.72	2.43
GS1845CW1 5	75606	91	14.18	55.15	16.13	15.11	1.77	S25	30423	24	14.85	78.47	16.32	15.74	2.43
GS1845CW1 5	75606	92	14.11	57.63	16.15	15.10	1.85	S25	30423	25	13.33	46.29	16.32	14.36	2.43
GS1845CW1 5	75606	93	13.33	72.53	16.18	14.76	1.94	S25	30423	26	13.17	76.61	16.11	14.69	1.68
GS1845CW1 5	75606	94	13.11	82.70	16.17	14.69	1.90	S25	30423	27	16.38	64.85	16.12	16.67	1.73
GS1845CW1 5	75606	95	12.67	22.44	16.22	13.16	2.09	S25	30423	28	12.17	81.17	16.12	14.10	1.73
GS1845CW1 5	75606	96	16.52	25.03	16.22	16.59	2.09	S25	30423	29	12.85	69.46	16.16	14.43	1.88
GS1845CW1 5	75606	97	14.42	55.52	16.21	15.28	2.05	S25	30423	30	14.26	56.05	16.16	15.18	1.88
GS1845CW1 5	75606	98	11.70	32.78	16.24	12.76	2.17	S25	30423	31	13.75	87.09	16.24	15.09	2.15
GS1845CW1 5	75606	99	14.26	72.57	16.12	15.35	1.72	S25	30423	32	16.23	71.29	16.23	16.59	2.11
GS1845CW1 5	75606	100	15.30	26.89	16.12	15.54	1.72	S25	30423	33	14.13	42.28	16.23	14.86	2.11
GS1845CW1 5	75606	101	12.41	63.51	16.23	14.07	2.11	S25	30423	34	8.66	46.68	16.23	11.43	2.11
GS1845CW1 5	75606	102	14.47	44.95	16.19	15.16	1.97	S25	30423	35	14.32	44.88	16.23	15.05	2.11
GS1845CW1 5	75606	103	14.45	35.15	16.16	14.97	1.86	S25	30423	36	12.39	61.90	16.23	14.03	2.11
GS1845CW1 5	75606	104	14.51	61.99	16.16	15.42	1.86	S25	30423	37	7.36	73.38	16.34	12.29	2.51
GS1845CW1 5	75606	105	13.87	58.29	16.18	14.95	1.95	S25	30423	38	9.09	62.79	16.17	12.11	1.92
GS1845CW1 5	75606	106	12.22	84.93	16.25	14.15	2.20	S25	30423	39	12.79	67.26	16.17	14.36	1.92
GS1845CW1 5	75606	107	12.84	53.26	16.28	14.17	2.29	S25	30423	40	13.74	50.58	16.17	14.74	1.92
GS1845CW1 5	75606	108	15.34	65.23	16.22	15.99	2.10	S25	30423	41	13.75	23.93	16.17	14.13	1.92
GS1845CW1 5	75606	109	11.37	85.14	16.22	13.63	2.10	S25	30423	42	12.79	14.90	16.17	13.03	1.92

Table C3 Apatite fission track lengths for all samples analysed in this thesis

UBC	A2Z	Track	Angle				Dpar	UBC	A2Z	Track	Angle				Dpar
			Length (μm)	to c- axis	Lo calc (μm)	Lc calc (μm)					Length (μm)	to c- axis	Lo calc (μm)	Lc calc (μm)	
GS1845CW1 5	75606	110	13.30	42.81	16.22	14.26	2.07	S25	30423	43	16.79	59.77	16.12	16.93	1.73
GS1845CW1 5	75606	111	11.21	79.68	16.20	13.50	2.02	S25	30423	44	15.73	24.69	16.12	15.89	1.73
GS1845CW1 5	75606	112	13.53	28.47	16.12	14.07	1.74	S25	30423	45	14.26	24.05	16.12	14.58	1.73
GS1845CW1 5	75606	113	13.65	56.88	16.21	14.78	2.06	S25	30423	46	13.18	84.92	16.12	14.74	1.73
GS1845CW1 5	75606	114	10.99	69.06	16.19	13.25	1.97	S25	30423	47	10.96	38.33	16.18	12.43	1.96
GS1845CW1 5	75606	115	11.58	74.91	16.18	13.69	1.93	S25	30423	48	11.85	55.88	16.18	13.56	1.96
GS1845CW1 5	75606	116	12.54	63.31	16.18	14.15	1.93	S25	30423	49	14.43	42.59	16.22	15.09	2.08
GS1845CW1 5	75606	117	11.96	79.84	16.13	13.96	1.78	S25	30423	50	13.05	1.77	16.13	13.05	1.77
GS1845CW1 5	75606	118	15.18	40.98	16.26	15.63	2.23	S32	30428	1	11.85	59.18	16.26	13.63	2.22
GS1845CW1 5	75606	119	14.64	74.69	16.22	15.60	2.09	S32	30428	2	14.36	60.13	16.26	15.30	2.22
GS1845CW1 5	75606	120	10.11	62.10	16.22	12.57	2.07	S32	30428	3	14.77	63.02	16.26	15.60	2.22
GS1845CW1 5	75606	121	15.86	46.92	16.22	16.21	2.08	S32	30428	4	11.24	72.91	16.26	13.46	2.22
GS1845CW1 5	75606	122	15.37	60.55	16.26	15.97	2.21	S32	30428	5	12.36	76.83	16.26	14.19	2.22
GS1845CW1 5	75606	123	15.00	17.72	16.14	15.14	1.81	S32	30428	6	12.80	65.62	16.26	14.35	2.22
GS1845CW1 5	75606	124	12.79	71.74	16.18	14.41	1.93	S32	30428	7	11.95	67.15	16.15	13.83	1.85
GS1845CW1 5	75606	125	14.25	49.31	16.17	15.07	1.92	S32	30428	8	11.53	55.34	16.11	13.34	1.70
GS1845CW1 5	75606	126	15.56	43.55	16.11	15.95	1.69	S32	30428	9	7.86	43.00	16.09	11.18	1.61
GS1845CW1 5	75606	127	14.25	42.81	16.16	14.96	1.87	S32	30428	10	14.35	77.15	16.09	15.43	1.61
GS1845CW1 5	75606	128	10.86	50.49	16.24	12.77	2.14	S32	30428	11	14.28	77.39	16.09	15.39	1.61
GS1845CW1 5	75606	129	14.76	52.12	16.16	15.47	1.88	S32	30428	12	14.30	67.93	16.09	15.34	1.61
GS1845CW1 5	75606	130	11.60	34.08	16.22	12.73	2.10	S32	30428	13	13.68	49.68	16.09	14.68	1.61
GS1845CW1 5	75606	131	12.99	58.43	16.18	14.37	1.95	S32	30428	14	13.40	74.14	16.12	14.82	1.72
GS1845CW1 5	75606	132	13.78	22.45	16.19	14.12	1.97	S32	30428	15	14.16	84.69	16.12	15.34	1.72
GS1845CW1 5	75606	133	12.24	71.86	16.17	14.07	1.90	S32	30428	16	13.62	62.99	16.12	14.84	1.72
GS1845CW1 5	75606	134	12.78	22.86	16.15	13.27	1.83	S32	30428	17	13.58	76.44	16.11	14.95	1.71
GS1845CW1 5	75606	135	13.35	41.70	16.15	14.27	1.83	S32	30428	18	13.89	0.32	16.12	13.89	1.72
LBB100-4679	94629	1	13.16	86.15	16.13	14.73	1.78	S32	30428	19	13.67	39.63	16.13	14.46	1.76
LBB100-4679	94629	2	6.03	65.13	16.10	11.61	1.66	S32	30428	20	14.84	47.74	16.13	15.47	1.76
LBB100-4679	94629	3	13.46	74.49	16.11	14.86	1.70	S32	30428	21	14.19	60.56	16.13	15.19	1.76
LBB100-4679	94629	4	9.71	72.30	16.13	12.54	1.75	S32	30428	22	8.94	70.29	16.09	12.34	1.64
LBB100-4679	94629	5	13.32	71.34	16.08	14.74	1.58	S32	30428	23	11.23	83.94	16.09	13.53	1.64
LBB100-4679	94629	6	15.11	35.25	16.41	15.50	2.74	S32	30428	24	13.83	43.13	16.10	14.66	1.66
LBB100-4679	94629	7	15.32	49.02	16.56	15.83	3.29	S32	30428	25	12.31	77.75	16.10	14.17	1.66
LBB100-4679	94629	8	13.23	61.03	16.33	14.56	2.49	S32	30428	26	15.37	21.73	16.10	15.53	1.66
LBB100-5400	94630	1	11.64	51.65	16.16	13.32	1.89	S32	30428	27	15.11	40.99	16.10	15.58	1.65
LBB100-5400	94630	2	15.26	43.38	16.16	15.73	1.89	S32	30428	28	12.82	81.66	16.10	14.50	1.65
LBB100-5400	94630	3	10.84	74.21	16.16	13.22	1.89	S32	30428	29	14.72	64.35	16.10	15.58	1.65
LBB100-5400	94630	4	13.57	75.55	16.11	14.93	1.71	S32	30428	30	14.34	46.98	16.10	15.10	1.65
LBB102-1035	94631	1	9.07	47.18	16.09	11.55	1.62	S32	30428	31	16.33	21.64	16.03	16.40	1.41
LBB102-1035	94631	2	14.08	40.38	16.11	14.79	1.71	S32	30428	32	13.45	33.47	16.12	14.14	1.74
LBB102-1035	94631	3	12.34	52.56	16.11	13.82	1.71	S32	30428	33	10.60	89.09	16.12	13.16	1.74
LBB102-1035	94631	4	14.99	31.29	16.14	15.34	1.81	S32	30428	34	11.67	63.77	16.12	13.60	1.74
LBB102-1035	94631	5	7.73	78.38	16.14	12.22	1.81	S32	30428	35	13.60	12.06	16.12	13.72	1.74
LBB102-1035	94631	6	13.38	68.93	16.17	14.76	1.92	S32	30428	36	14.97	33.55	16.12	15.36	1.74
LBB102-1035	94631	7	12.75	74.09	16.13	14.41	1.78	S32	30428	37	12.62	51.44	16.14	13.98	1.80
LBB102-1035	94631	8	13.97	35.54	16.19	14.60	1.98	S32	30428	38	14.25	86.09	16.09	15.40	1.63
LBB102-1035	94631	9	13.58	85.92	16.19	14.98	1.98	S32	30428	39	14.55	64.83	16.09	15.47	1.63
LBB102-1035	94631	10	15.01	76.64	16.19	15.84	1.98	S32	30428	40	14.40	75.67	16.09	15.45	1.61
LBB102-1035	94631	11	13.05	79.61	16.19	14.64	1.98	S32	30428	41	13.85	69.97	16.10	15.07	1.67
LBB102-1035	94631	12	13.33	48.07	16.16	14.40	1.88	S32	30428	42	12.93	70.59	16.15	14.49	1.82
LBB102-1035	94631	13	12.02	35.66	16.07	13.11	1.55	S32	30428	43	13.79	30.29	16.15	14.33	1.82
LBB102-1035	94631	14	15.72	79.20	16.07	16.29	1.55	S32	30428	44	14.67	25.35	16.15	14.96	1.82
LBB102-1035	94631	15	10.00	64.49	16.20	12.55	2.03	S32	30428	45	15.09	68.38	16.15	15.85	1.82
LBB102-1035	94631	16	12.49	65.18	16.17	14.15	1.91	S32	30428	46	14.23	85.23	16.15	15.38	1.82
LBB102-1035	94631	17	15.78	54.19	16.13	16.21	1.77	S32	30428	47	14.19	46.49	16.15	14.98	1.82
LBB102-1035	94631	18	15.90	63.51	16.13	16.34	1.77	S32	30428	48	13.67	56.14	16.19	14.78	1.98
LBB102-1035	94631	19	16.25	5.39	16.13	16.26	1.77	S32	30428	49	9.65	83.53	16.10	12.77	1.66
LBB102-1035	94631	20	16.75	47.18	16.08	16.87	1.59	S32	30428	50	13.79	62.78	16.13	14.95	1.78
LBB102-1035	94631	21	14.95	70.30	16.08	15.77	1.59	S32	30428	51	13.00	64.03	16.11	14.46	1.69
LBB102-1035	94631	22	10.07	79.20	16.08	12.79	1.59	S32	30428	52	14.00	66.19	16.10	15.13	1.66
LBB102-1035	94631	23	15.94	80.38	16.12	16.43	1.73	S32	30428	53	14.46	85.33	16.25	15.52	2.18

Table C3 Apatite fission track lengths for all samples analysed in this thesis

UBC	A2Z	Track	Angle				Dpar	UBC	A2Z	Track	Angle				Dpar
			Length (μm)	to c- axis	Lo calc (μm)	Lc calc (μm)					Length (μm)	to c- axis	Lo calc (μm)	Lc calc (μm)	
LBB102-1035	94631	24	12.86	49.08	16.12	14.09	1.73	S32	30428	54	12.12	89.66	16.25	14.09	2.18
LBB102-1035	94631	25	14.34	80.00	16.11	15.43	1.71	S32	30428	55	13.24	70.98	16.25	14.69	2.18
LBB102-1035	94631	26	14.28	38.96	16.11	14.91	1.71	S32	30428	56	13.83	84.54	16.27	15.13	2.26
LBB102-1035	94631	27	12.61	55.77	16.11	14.06	1.70	S32	30428	57	14.10	81.26	16.27	15.29	2.26
LBB102-1035	94631	28	12.88	28.46	16.15	13.53	1.83	S32	30428	58	14.89	68.77	16.27	15.72	2.26
LBB102-1035	94631	29	8.18	80.41	16.15	12.34	1.83	S32	30428	59	13.54	60.46	16.27	14.76	2.26
LBB102-1035	94631	30	12.54	69.45	16.13	14.23	1.75	S32	30428	60	14.72	20.09	16.09	14.92	1.62
LBB102-1035	94631	31	11.74	22.47	16.13	12.38	1.75	S32	30428	61	14.91	50.64	16.09	15.56	1.62
LBB102-1035	94631	32	14.71	46.13	16.16	15.36	1.86	S32	30428	62	12.52	71.02	16.18	14.24	1.96
LBB102-1035	94631	33	13.59	74.44	16.17	14.94	1.90	S32	30428	63	13.14	76.68	16.18	14.67	1.96
LBB102-1035	94631	34	13.61	71.58	16.14	14.93	1.79	S32	30428	64	14.66	63.45	16.15	15.53	1.85
LBB102-1035	94631	35	15.13	51.54	16.15	15.73	1.82	S32	30428	65	15.02	55.79	16.14	15.70	1.80
LBB102-1035	94631	36	13.87	52.88	16.24	14.87	2.14	S32	30428	66	9.74	59.87	16.09	12.29	1.61
LBB102-1035	94631	37	15.13	8.15	16.15	15.16	1.83	S32	30428	67	12.89	38.12	16.16	13.83	1.87
LBB102-1035	94631	38	14.98	37.04	16.06	15.42	1.53	S32	30428	68	13.77	84.46	16.13	15.10	1.76
LBB102-1035	94631	39	14.79	56.02	16.13	15.54	1.76	S33	30429	1	14.86	21.39	16.15	15.06	1.85
LBB102-1035	94631	40	14.96	31.60	16.07	15.32	1.57	S33	30429	2	13.63	74.04	16.15	14.96	1.85
LBB102-1035	94631	41	10.46	74.46	16.07	12.99	1.57	S33	30429	3	13.60	60.17	16.15	14.79	1.85
LBB102-1035	94631	42	15.58	49.79	16.22	16.03	2.07	S33	30429	4	13.67	56.54	16.21	14.79	2.04
LBB102-1035	94631	43	15.55	73.33	16.14	16.16	1.79	S33	30429	5	13.70	52.47	16.21	14.74	2.04
LBB102-1035	94631	44	11.33	57.65	16.13	13.26	1.75	S33	30429	6	13.13	79.10	16.17	14.68	1.91
LBB102-1035	94631	45	13.15	56.37	16.26	14.44	2.21	S33	30429	7	12.43	50.89	16.17	13.84	1.91
LBB102-1035	94631	46	15.57	55.58	16.13	16.07	1.76	S33	30429	8	9.76	77.49	16.17	12.61	1.91
LBB102-1035	94631	47	14.19	57.88	16.13	15.16	1.76	S33	30429	9	13.68	81.98	16.17	15.03	1.91
LBB102-1035	94631	48	14.36	65.25	16.13	15.35	1.76	S33	30429	10	12.78	32.41	16.17	13.58	1.92
LBB102-1035	94631	49	15.13	64.45	16.21	15.85	2.06	S33	30429	11	11.99	58.79	16.13	13.71	1.77
LBB102-1035	94631	50	15.87	53.90	16.09	16.27	1.61	S33	30429	12	13.95	72.96	16.13	15.15	1.77
LBB102-1035	94631	51	11.78	59.57	16.16	13.59	1.88	S33	30429	13	16.95	42.06	16.14	17.01	1.80
LBB102-1035	94631	52	15.76	57.87	16.21	16.22	2.05	S33	30429	14	12.15	68.30	16.14	13.97	1.80
LBB102-1035	94631	53	14.20	56.48	16.21	15.14	2.05	S33	30429	15	14.09	47.79	16.13	14.93	1.76
LBB102-1035	94631	54	14.78	69.28	16.21	15.65	2.05	S33	30429	16	14.10	7.71	16.09	14.14	1.64
LBB102-1035	94631	55	15.67	83.28	16.17	16.26	1.92	S33	30429	17	15.76	28.93	16.09	15.96	1.64
LBB102-1035	94631	56	8.48	56.88	16.13	11.84	1.77	S33	30429	18	14.72	54.42	16.16	15.47	1.89
LBB102-1035	94631	57	16.14	58.68	16.13	16.48	1.76	S33	30429	19	12.66	68.99	16.14	14.30	1.80
LBB102-1035	94631	58	11.09	47.25	16.15	12.83	1.83	S33	30429	20	13.92	44.49	16.11	14.75	1.68
LBB102-1035	94631	59	14.73	73.33	16.14	15.65	1.80	S33	30429	21	13.77	53.49	16.11	14.81	1.68
LBB102-1035	94631	60	15.91	59.12	16.10	16.33	1.67	S33	30429	22	13.09	65.04	16.15	14.53	1.82
LBB102-1035	94631	61	14.26	80.34	16.15	15.39	1.85	S33	30429	23	15.43	15.50	16.15	15.51	1.82
LBB102-1035	94631	62	14.03	63.91	16.19	15.12	1.98	S33	30429	24	16.00	27.54	16.11	16.15	1.69
LBB102-1035	94631	63	13.35	59.83	16.19	14.62	1.98	S33	30429	25	14.66	61.28	16.11	15.51	1.69
LBB102-1035	94631	64	12.49	64.82	16.12	14.14	1.73	S33	30429	26	9.00	31.92	16.18	10.79	1.95
LBB102-1035	94631	65	12.66	32.54	16.21	13.49	2.06	S33	30429	27	12.50	66.18	16.07	14.17	1.57
LBB102-1035	94631	66	14.39	35.16	16.21	14.92	2.06	S33	30429	28	11.47	85.63	16.07	13.69	1.57
LBB102-1035	94631	67	10.79	66.01	16.18	13.08	1.93	S33	30429	29	14.86	27.05	16.14	15.16	1.80
LBB102-1035	94631	68	15.17	80.03	16.03	15.95	1.43	S33	30429	30	14.26	70.82	16.14	15.33	1.80
LBB102-1035	94631	69	15.49	69.03	16.11	16.11	1.68	S33	30429	31	11.86	68.85	16.14	13.80	1.80
LBB102-1035	94631	70	16.31	29.48	16.15	16.43	1.84	S33	30429	32	10.01	72.01	16.14	12.68	1.80
LBB102-1035	94631	71	12.34	64.41	16.15	14.04	1.84	S33	30429	33	14.24	37.66	16.14	14.85	1.80
LBB102-1035	94631	72	10.21	79.78	16.17	12.88	1.90	S33	30429	34	14.47	33.48	16.10	14.95	1.67
LBB102-1035	94631	73	12.88	80.51	16.16	14.53	1.87	S33	30429	35	12.92	49.26	16.14	14.14	1.80
LBB102-1035	94631	74	14.08	68.06	16.10	15.20	1.66	S33	30429	36	10.30	60.24	16.15	12.66	1.83
LBB102-1035	94631	75	13.04	81.16	16.12	14.64	1.72	S33	30429	37	14.06	71.96	16.15	15.22	1.83
LBB102-1035	94631	76	12.27	60.08	16.14	13.92	1.79	S33	30429	38	12.43	70.52	16.15	14.17	1.83
LBB102-1035	94631	77	15.18	38.26	16.14	15.60	1.79	S34	30430	1	13.95	22.36	16.21	14.27	2.06
LBB102-1035	94631	78	14.30	28.80	16.11	14.72	1.68	S34	30430	2	11.68	42.65	16.21	13.09	2.06
LBB102-1035	94631	79	9.94	54.33	16.11	12.28	1.68	S34	30430	3	9.65	65.77	16.17	12.36	1.92
LBB102-1035	94631	80	9.81	59.72	16.13	12.33	1.78	S34	30430	4	14.21	25.04	16.14	14.56	1.81
LBB102-1035	94631	81	11.66	41.34	16.20	13.04	2.02	S34	30430	5	11.28	89.80	16.16	13.58	1.86
LBB102-1035	94631	82	14.11	55.90	16.17	15.08	1.90	S34	30430	6	14.91	89.52	16.16	15.80	1.86
LBB102-1035	94631	83	14.70	32.99	16.10	15.13	1.67	S34	30430	7	13.56	52.27	16.16	14.64	1.86
LBB102-1035	94631	84	16.56	35.21	16.10	16.68	1.67	S34	30430	8	14.77	69.38	16.13	15.65	1.77

Table C3 Apatite fission track lengths for all samples analysed in this thesis

UBC	A2Z	Track	Angle				Dpar	UBC	A2Z	Track	Angle				Dpar
			Length (μm)	to c- axis	Lo calc (μm)	Lc calc (μm)					Length (μm)	to c- axis	Lo calc (μm)	Lc calc (μm)	
LBB102-1035	94631	85	13.37	57.63	16.18	14.60	1.95	S34	30430	9	10.89	45.31	16.13	12.63	1.77
LBB102-1035	94631	86	8.03	70.50	16.19	12.14	1.99	S34	30430	10	12.32	53.11	16.11	13.81	1.69
LBB102-1035	94631	87	14.49	50.92	16.23	15.27	2.11	S34	30430	11	14.78	79.48	16.25	15.70	2.18
LBB102-1035	94631	88	11.53	63.92	16.20	13.51	2.00	S34	30430	12	12.71	69.77	16.25	14.34	2.18
LBB102-1035	94631	89	10.89	55.89	16.20	12.93	2.00	S34	30430	13	14.63	48.27	16.25	15.33	2.18
LBB102-1035	94631	90	13.44	77.37	16.16	14.86	1.86	S34	30430	14	13.04	38.85	16.13	13.97	1.75
LBB102-1035	94631	91	9.69	61.16	16.09	12.29	1.64	S34	30430	15	11.44	70.54	16.10	13.55	1.66
LBB102-1035	94631	92	9.46	61.12	16.13	12.16	1.76	S34	30430	16	11.71	80.58	16.15	13.81	1.82
LBB102-1035	94631	93	14.21	65.25	16.15	15.25	1.85	S34	30430	17	13.42	63.91	16.15	14.73	1.82
LBB102-1035	94631	94	13.21	80.99	16.10	14.74	1.65	S34	30430	18	10.51	64.40	16.15	12.87	1.82
LBB102-1035	94631	95	13.84	75.00	16.18	15.10	1.93	S34	30430	19	8.31	68.25	16.08	12.23	1.60
LBB102-1035	94631	96	14.57	44.17	16.13	15.22	1.75	S34	30430	20	11.85	72.74	16.18	13.84	1.94
LBB102-1035	94631	97	16.66	66.06	16.18	16.85	1.94	S34	30430	21	15.75	89.96	16.18	16.32	1.94
LBB102-1035	94631	98	13.92	83.55	16.09	15.19	1.61	S34	30430	22	16.19	73.80	16.18	16.57	1.94
LBB102-1035	94631	99	15.53	70.33	16.09	16.14	1.61	S34	30430	23	15.37	15.82	16.11	15.46	1.68
LBB102-1035	94631	100	13.66	69.78	16.20	14.94	2.03	S34	30430	24	13.92	43.92	16.15	14.74	1.85
LBB102-1035	94631	101	12.21	62.37	16.09	13.92	1.62	S7	30407	1	14.16	32.47	16.10	14.68	1.66
LBB102-1035	94631	102	16.52	11.71	16.09	16.54	1.62	S7	30407	2	10.67	80.25	16.10	13.17	1.66
LBB102-1035	94631	103	13.74	28.58	16.09	14.24	1.62	S7	30407	3	14.16	89.78	16.10	15.34	1.66
LBB102-1035	94631	104	11.39	58.51	16.09	13.32	1.62	S7	30407	4	10.75	35.27	16.10	12.16	1.66
LBB102-1035	94631	105	15.30	38.36	16.24	15.69	2.14	S7	30407	5	11.00	37.18	16.10	12.42	1.66
LBB102-1035	94631	106	13.77	80.60	16.20	15.08	2.02	S7	30407	6	6.75	77.60	16.23	12.35	2.11
LBB102-1035	94631	107	12.08	72.92	16.20	13.98	2.02	S7	30407	7	6.63	55.31	16.10	11.59	1.66
LBB102-1035	94631	108	13.29	63.70	16.14	14.64	1.81	S7	30407	8	14.09	31.33	16.57	14.60	3.33
LBB102-1035	94631	109	16.09	39.66	16.13	16.33	1.78	S7	30407	9	13.05	67.31	16.30	14.53	2.38
LBB102-1035	94631	110	13.83	75.88	16.14	15.10	1.81	S7	30407	10	12.41	45.59	16.15	13.69	1.82
LBB102-1035	94631	111	14.17	73.04	16.14	15.29	1.81	S7	30407	11	12.03	39.02	16.15	13.23	1.82
LBB102-1035	94631	112	10.76	81.12	16.14	13.23	1.81	S7	30407	12	11.49	59.94	16.15	13.41	1.82
LBB102-1035	94631	113	14.59	53.88	16.22	15.38	2.10	S7	30407	13	14.68	45.75	16.15	15.33	1.82
LBB102-1035	94631	114	15.91	81.64	16.09	16.41	1.61	S7	30407	14	6.25	80.22	16.28	12.35	2.29
LBB102-1035	94631	115	9.06	55.70	16.18	11.90	1.96	S7	30407	15	10.48	44.54	16.28	12.33	2.29
LBB102-1035	94631	116	15.63	60.60	16.08	16.15	1.59	S7	30407	16	12.93	82.64	16.27	14.57	2.25
LBB102-1035	94631	117	10.61	44.37	16.10	12.41	1.65	S7	30407	17	16.12	50.62	16.19	16.42	1.97
LBB102-1035	94631	118	14.71	75.32	16.16	15.64	1.87	S7	30407	18	13.77	7.91	16.19	13.82	1.97
LBB102-1035	94631	119	15.25	56.87	16.14	15.86	1.79	S7	30407	19	13.96	61.23	16.24	15.05	2.16
LBB102-1035	94631	120	12.33	55.30	16.18	13.87	1.96	S7	30407	20	14.19	62.89	16.24	15.22	2.16
LBB102-1035	94631	121	13.67	70.06	16.18	14.95	1.96	S7	30407	21	14.36	81.99	16.18	15.45	1.94
LBB102-1035	94631	122	11.47	34.83	16.17	12.67	1.91	S7	30407	22	11.15	42.97	16.28	12.73	2.30
LBB102-1035	94631	123	10.32	64.80	16.16	12.76	1.87	S7	30407	23	15.12	22.46	16.09	15.31	1.62
LBB102-1035	94631	124	10.80	26.99	16.14	11.83	1.81	S7	30407	24	15.11	57.86	16.30	15.78	2.37
LBB102-1035	94631	125	12.82	87.41	16.14	14.52	1.81	S7	30407	25	13.06	57.96	16.30	14.40	2.37
LBB102-1035	94631	126	13.63	48.17	16.17	14.61	1.92	S7	30407	26	13.50	52.01	16.16	14.60	1.88
LBB102-1035	94631	127	13.08	65.12	16.10	14.52	1.66	S7	30407	27	13.04	63.08	16.16	14.47	1.88
LBB102-1035	94631	128	15.29	48.12	16.19	15.80	1.97	S7	30407	28	8.90	48.23	16.16	11.52	1.86
LBB102-1035	94631	129	11.35	66.56	16.20	13.44	2.03	S7	30407	29	12.77	82.87	16.29	14.48	2.33
LBB102-1035	94631	130	12.48	46.43	16.20	13.76	2.03	S7	30407	30	10.98	65.34	16.29	13.19	2.33
LBB102-1035	94631	131	13.58	34.83	16.09	14.27	1.62	S7	30407	31	14.59	71.79	16.31	15.55	2.42
LBB102-1035	94631	132	14.75	15.04	16.09	14.87	1.62	S7	30407	32	9.84	16.66	16.25	10.54	2.18
LBB102-1035	94631	133	14.24	71.36	16.20	15.32	2.00	S7	30407	33	14.54	44.17	16.12	15.20	1.73
LBB102-1035	94631	134	15.24	75.09	16.19	15.97	1.99	S7	30407	34	11.26	86.98	16.31	13.56	2.39
LBB102-1035	94631	135	13.10	72.96	16.18	14.62	1.96	S7	30407	35	13.61	67.70	16.23	14.89	2.11
LBB102-1035	94631	136	13.73	58.29	16.15	14.85	1.85	S7	30407	36	8.98	80.99	16.23	12.67	2.11
LBB102-1035	94631	137	14.55	76.81	16.17	15.55	1.91	S7	30407	37	13.33	50.66	16.44	14.45	2.87
LBB102-1035	94631	138	13.97	34.81	16.11	14.58	1.68	S7	30407	38	11.99	56.78	16.44	13.67	2.87
LBB102-1035	94631	139	12.32	48.37	16.16	13.70	1.87	S7	30407	39	15.31	83.45	16.19	16.04	1.99
LBB102-1035	94631	140	14.60	46.05	16.13	15.27	1.76	S7	30407	40	14.46	50.41	16.19	15.24	1.99
LBB102-1035	94631	141	15.02	86.88	16.25	15.87	2.18	S7	30407	41	15.50	77.29	16.22	16.14	2.08
LBB102-1035	94631	142	13.94	75.41	16.25	15.16	2.18	S7	30407	42	15.27	38.85	16.33	15.68	2.46
LBB102-1035	94631	143	6.58	50.34	16.21	11.29	2.04	S7	30407	43	14.01	38.15	16.26	14.69	2.23
LBB102-1035	94631	144	15.47	14.59	16.14	15.54	1.80	S7	30407	44	12.90	68.92	16.26	14.45	2.24
LBB102-1035	94631	145	14.76	48.23	16.14	15.42	1.80	S7	30407	45	14.50	76.56	16.26	15.52	2.24

Table C3 Apatite fission track lengths for all samples analysed in this thesis

UBC	A2Z	Track	Angle				Dpar	UBC	A2Z	Track	Angle				Dpar
			Length (μm)	to c- axis	Lo calc (μm)	Lc calc (μm)					Length (μm)	to c- axis	Lo calc (μm)	Lc calc (μm)	
LBB102-1035	94631	146	8.53	79.11	16.14	12.40	1.80	S7	30407	46	14.35	62.38	16.31	15.32	2.41
LBB102-1035	94631	147	13.18	77.22	16.12	14.70	1.74	S7	30407	47	13.76	53.61	16.39	14.80	2.68
LBB102-1940	94632	1	13.67	58.85	16.18	14.82	1.95	S7	30407	48	13.47	36.95	16.25	14.24	2.18
LBB102-1940	94632	2	12.61	14.09	16.18	12.84	1.95	S7	30407	49	11.99	55.33	16.25	13.64	2.18
LBB102-1940	94632	3	15.24	31.99	16.22	15.56	2.09	S7	30407	50	10.33	49.22	16.25	12.38	2.18
LBB102-1940	94632	4	17.07	65.76	16.23	17.12	2.11	S7	30407	51	13.94	24.55	16.18	14.31	1.93
LBB102-1940	94632	5	15.75	44.52	16.26	16.11	2.22	S7	30407	52	13.65	89.62	16.32	15.03	2.43
LBB102-1940	94632	6	13.55	69.05	16.20	14.87	2.03	S7	30407	53	14.51	51.72	16.19	15.29	1.98
LBB102-1940	94632	7	12.94	85.20	16.20	14.59	2.00	S7	30407	54	14.29	65.02	16.28	15.30	2.31
LBB102-1940	94632	8	15.52	49.03	16.22	15.98	2.08	S7	30407	55	12.19	44.99	16.07	13.52	1.57
LBB102-1940	94632	9	14.12	30.42	16.22	14.60	2.08	S7	30407	56	14.15	45.71	16.07	14.94	1.57
LBB102-1940	94632	10	11.02	67.23	16.08	13.24	1.58	S7	30407	57	13.71	50.92	16.27	14.72	2.26
LBB102-1940	94632	11	14.36	87.73	16.08	15.46	1.58	S7	30407	58	13.65	64.34	16.15	14.88	1.85
LBB102-1940	94632	12	13.30	48.86	16.18	14.40	1.95	S7	30407	59	13.61	56.27	16.15	14.74	1.85
LBB102-1940	94632	13	14.46	52.11	16.18	15.26	1.95	S7	30407	60	14.33	60.66	16.24	15.28	2.14
LBB102-1940	94632	14	12.97	57.86	16.18	14.34	1.95	S7	30407	61	14.75	82.87	16.13	15.70	1.77
LBB102-1940	94632	15	14.72	47.16	16.18	15.38	1.95	S7	30407	62	13.52	37.23	16.14	14.29	1.81
LBB102-1940	94632	16	13.15	77.40	16.14	14.68	1.79	S7	30407	63	14.72	39.26	16.22	15.25	2.08
LBB102-1940	94632	17	14.33	65.57	16.14	15.33	1.79	S7	30407	64	15.29	56.83	16.15	15.89	1.84
LBB102-1940	94632	18	15.88	16.15	16.14	15.95	1.79	S7	30407	65	12.66	73.09	16.15	14.35	1.84
LBB102-1940	94632	19	16.03	9.04	16.14	16.05	1.79	S7	30407	66	14.42	42.31	16.23	15.08	2.13
LBB102-1940	94632	20	13.60	69.97	16.14	14.91	1.79	S7	30407	67	11.23	47.73	16.41	12.94	2.74
LBB102-1940	94632	21	17.28	38.24	16.13	17.27	1.77	S7	30407	68	14.46	64.68	16.21	15.41	2.05
LBB102-1940	94632	22	14.05	81.13	16.19	15.26	1.98	S7	30407	69	14.01	24.89	16.21	14.38	2.05
LBB102-1940	94632	23	12.28	45.36	16.10	13.59	1.66	S7	30407	70	13.34	86.39	16.13	14.84	1.78
LBB102-1940	94632	24	13.98	88.99	16.10	15.23	1.66	S7	30407	71	13.43	83.51	16.17	14.89	1.91
LBB102-1940	94632	25	13.79	69.14	16.13	15.02	1.77	S7	30407	72	16.55	25.74	16.40	16.62	2.73
LBB102-1940	94632	26	14.02	42.81	16.16	14.79	1.87	S7	30407	73	13.84	74.18	16.24	15.09	2.14
LBB102-1940	94632	27	15.19	41.83	16.16	15.65	1.87	S7	30407	74	15.02	49.36	16.38	15.62	2.66
LBB102-1940	94632	28	14.74	56.58	16.18	15.51	1.96	S7	30407	75	14.95	53.48	16.37	15.62	2.61
LBB102-1940	94632	29	14.70	72.43	16.12	15.62	1.73	S7	30407	76	15.74	56.47	16.09	16.20	1.61
LBB102-1940	94632	30	16.32	30.19	16.17	16.45	1.91	S7	30407	77	12.19	64.86	16.21	13.95	2.05
LBB102-1940	94632	31	14.17	54.28	16.17	15.09	1.91	S7	30407	78	13.65	38.89	16.21	14.43	2.05
LBB102-1940	94632	32	15.45	19.55	16.17	15.58	1.90	S7	30407	79	6.47	63.16	16.45	11.85	2.88
LBB102-1940	94632	33	15.37	10.87	16.13	15.42	1.78	S7	30407	80	8.52	89.71	16.04	12.94	1.45
LBB102-1940	94632	34	15.15	37.07	16.13	15.56	1.77	S7	30407	81	6.29	76.66	16.04	12.25	1.45
LBB102-1940	94632	35	11.01	36.72	16.13	12.41	1.77	S7	30407	82	14.97	55.71	16.32	15.66	2.44
LBB102-1940	94632	36	14.92	69.46	16.10	15.74	1.66	S7	30407	83	13.15	58.70	16.32	14.48	2.44
LBB102-1940	94632	37	15.74	81.89	16.13	16.30	1.78	S7	30407	84	14.68	60.28	16.20	15.51	2.03
LBB102-1940	94632	38	13.47	61.46	16.23	14.73	2.11	S7	30407	85	12.29	43.68	16.15	13.55	1.84
LBB102-1940	94632	39	15.86	55.43	16.17	16.27	1.91	S7	30407	86	12.44	30.36	16.31	13.24	2.39
LBB102-1940	94632	40	6.88	72.81	16.20	11.95	2.00	S7	30407	87	11.47	68.70	16.20	13.55	2.00
LBB102-1940	94632	41	15.77	49.33	16.17	16.16	1.92	S7	30407	88	15.08	30.16	16.26	15.40	2.24
LBB102-1940	94632	42	14.36	62.43	16.16	15.32	1.88	S7	30407	89	12.27	63.39	16.29	13.98	2.34
LBB102-1940	94632	43	14.71	53.29	16.15	15.45	1.82	S7	30407	90	13.84	36.10	16.25	14.51	2.18
LBB102-1940	94632	44	12.19	63.25	16.15	13.92	1.85	S7	30407	91	13.75	68.71	16.13	14.99	1.76
LBB102-1940	94632	45	13.48	82.99	16.27	14.91	2.25	S7	30407	92	10.85	59.03	16.06	12.98	1.52
LBB102-1940	94632	46	14.27	86.03	16.20	15.41	2.01	S7	30407	93	13.84	52.60	16.34	14.84	2.51
LBB102-1940	94632	47	13.60	28.82	16.23	14.13	2.13	S7	30407	94	11.71	27.13	16.25	12.54	2.19
LBB102-1940	94632	48	14.06	66.43	16.20	15.17	2.00	S7	30407	95	12.51	67.45	16.13	14.19	1.77
LBB102-1940	94632	49	9.59	64.80	16.22	12.31	2.07	S7	30407	96	14.80	88.02	16.41	15.73	2.76
LBB102-1940	94632	50	14.05	65.06	16.13	15.15	1.75	S7	30407	97	13.35	27.52	16.23	13.89	2.13
LBB102-1940	94632	51	15.70	62.66	16.25	16.21	2.20	S7	30407	98	5.50	38.26	16.25	10.72	2.20
LBB102-1940	94632	52	14.67	37.46	16.20	15.18	2.02	S7	30407	99	15.00	44.50	16.36	15.55	2.59
LBB102-1940	94632	53	13.59	65.55	16.15	14.86	1.84	S7	30407	100	13.20	55.26	16.36	14.45	2.59
LBB102-1940	94632	54	15.58	51.80	16.15	16.05	1.84	S7	30407	101	12.32	84.73	16.32	14.21	2.44
LBB102-1940	94632	55	14.18	63.54	16.15	15.22	1.84	S7	30407	102	14.50	67.19	16.29	15.46	2.32
LBB102-1940	94632	56	14.17	79.00	16.15	15.33	1.84	S7	30407	103	7.04	31.05	16.18	10.44	1.93
LBB102-1940	94632	57	16.21	60.84	16.15	16.54	1.84	S7	30407	104	9.57	57.73	16.03	12.13	1.40
LBB102-1940	94632	58	15.38	57.30	16.21	15.96	2.05	S7	30407	105	14.86	51.66	16.25	15.54	2.20
LBB102-1940	94632	59	14.33	26.12	16.20	14.69	2.02	S7	30407	106	15.66	78.98	16.23	16.25	2.13

Table C3 Apatite fission track lengths for all samples analysed in this thesis

UBC	A2Z	Track	Angle				Dpar	UBC	A2Z	Track	Angle				Dpar
			Length (μm)	to c- axis	Lo calc (μm)	Lc calc (μm)					Length (μm)	to c- axis	Lo calc (μm)	Lc calc (μm)	
LBB102-1940	94632	60	15.06	27.08	16.20	15.33	2.02	S7	30407	107	5.99	52.21	16.27	11.39	2.27
LBB102-1940	94632	61	6.84	72.56	16.13	11.93	1.75	S7	30407	108	14.21	79.00	16.40	15.35	2.71
LBB102-1940	94632	62	16.22	83.84	16.18	16.60	1.94	S7	30407	109	10.70	62.17	16.21	12.95	2.04
LBB102-1940	94632	63	15.60	44.39	16.23	15.99	2.12	S7	30407	110	13.65	61.27	16.21	14.84	2.04
LBB102-1940	94632	64	15.39	35.07	16.16	15.72	1.88	S7	30407	111	12.97	62.03	16.28	14.41	2.28
LBB102-1940	94632	65	14.51	50.74	16.18	15.28	1.94	S7	30407	112	6.80	67.76	16.15	12.04	1.85
LBB102-1940	94632	66	13.68	74.75	16.09	15.00	1.64	S7	30407	113	15.34	58.52	16.15	15.94	1.85
LBB102-1940	94632	67	15.52	30.59	16.09	15.77	1.64	S7	30407	114	13.81	37.87	16.15	14.53	1.85
LBB102-1940	94632	68	13.45	64.58	16.13	14.75	1.77	S7	30407	115	15.06	37.41	16.31	15.49	2.40
LBB102-1940	94632	69	13.51	35.44	16.13	14.24	1.77	S7	30407	116	10.25	83.18	16.31	12.93	2.40
LBB102-1940	94632	70	14.60	83.36	16.13	15.60	1.77	S7	30407	117	13.46	83.12	16.25	14.90	2.20
LBB102-1940	94632	71	14.50	49.45	16.13	15.25	1.77	S7	30407	118	14.07	28.24	16.09	14.51	1.61
LBB102-1940	94632	72	15.95	65.03	16.13	16.38	1.77	S7	30407	119	14.45	58.74	16.09	15.34	1.61
LBB102-1940	94632	73	9.86	53.28	16.13	12.20	1.77	S7	30407	120	11.98	47.27	16.27	13.44	2.27
LBB102-1940	94632	74	14.27	49.66	16.15	15.09	1.85	S7	30407	121	13.37	49.29	16.24	14.45	2.14
LBB102-1940	94632	75	9.98	51.91	16.15	12.24	1.85	S7	30407	122	13.10	68.85	16.11	14.58	1.71
LBB102-1940	94632	76	15.36	43.47	16.17	15.80	1.92	S7	30407	123	15.80	86.77	16.30	16.35	2.37
LBB102-1940	94632	77	15.28	65.52	16.29	15.95	2.34	S7	30407	124	13.36	47.28	16.15	14.40	1.84
LBB102-1940	94632	78	7.96	67.23	16.29	12.05	2.34	S7	30407	125	14.04	20.00	16.25	14.30	2.19
LBB102-1940	94632	79	13.58	52.01	16.16	14.65	1.89	S7	30407	126	6.46	86.11	16.34	12.59	2.50
LBB102-1940	94632	80	17.30	33.54	16.25	17.29	2.19	S7	30407	127	14.34	56.10	16.21	15.24	2.06
LBB102-1940	94632	81	15.21	70.44	16.15	15.93	1.83	S7	30407	128	11.28	37.98	16.21	12.65	2.06
LBB102-1940	94632	82	14.85	48.20	16.20	15.49	2.02	S7	30407	129	14.09	66.47	16.32	15.19	2.43
LBB102-1940	94632	83	16.38	28.12	16.13	16.49	1.77	S7	30407	130	15.33	48.73	16.10	15.84	1.65
LBB102-1940	94632	84	13.69	68.86	16.13	14.95	1.77	S7	30407	131	14.44	80.07	16.54	15.50	3.22
LBB102-1940	94632	85	15.11	87.54	16.13	15.92	1.77	S7	30407	132	15.16	22.92	16.28	15.36	2.30
LBB102-1940	94632	86	14.54	70.74	16.13	15.51	1.77	S7	30407	133	14.16	80.14	16.06	15.32	1.52
LBB102-1940	94632	87	13.63	84.75	16.21	15.01	2.04	S7	30407	134	15.50	67.52	16.17	16.10	1.91
LBB102-1940	94632	88	13.96	71.38	16.20	15.15	2.01	S7	30407	135	15.00	53.16	16.29	15.65	2.33
LBB102-1940	94632	89	14.90	66.86	16.23	15.71	2.11	S7	30407	136	15.95	9.53	16.32	15.97	2.43
LBB102-1940	94632	90	15.87	70.33	16.23	16.35	2.11	S7	30407	137	14.56	63.57	16.32	15.46	2.43
LBB102-1940	94632	91	14.69	49.45	16.11	15.39	1.68	S7	30407	138	12.21	48.45	16.33	13.63	2.47
LBB102-1940	94632	92	15.00	45.06	16.12	15.55	1.74	S7	30407	139	12.77	44.51	16.33	13.92	2.47
LBB102-1940	94632	93	14.39	78.56	16.12	15.46	1.74	S7	30407	140	13.84	78.36	16.28	15.12	2.31
LBB102-1940	94632	94	14.45	51.20	16.09	15.24	1.61	S7	30407	141	14.83	57.29	16.53	15.58	3.17
LBB102-1940	94632	95	12.43	71.00	16.09	14.18	1.64	S7	30407	142	14.76	39.51	16.53	15.29	3.17
LBB102-1940	94632	96	11.80	63.27	16.16	13.67	1.89	S7	30407	143	13.85	30.99	16.13	14.39	1.77
LBB102-1940	94632	97	12.95	70.73	16.16	14.50	1.89	S7	30407	144	13.10	74.91	16.22	14.64	2.08
LBB102-1940	94632	98	12.38	58.65	16.16	13.97	1.86	U10-P05-06-1055	110307	1	12.82	28.38	16.00	13.48	1.30
LBB102-1940	94632	99	14.54	68.26	16.16	15.49	1.86	U10-P05-06-1055	110307	2	16.45	74.15	16.00	16.73	1.30
LBB102-1940	94632	100	12.83	73.86	16.22	14.46	2.07	U10-P05-06-1055	110307	3	11.68	59.49	16.09	13.53	1.61
LBB102-1940	94632	101	13.75	84.96	16.15	15.09	1.85	U10-P05-06-319	110304	1	11.76	86.67	16.56	13.87	3.27
LBB102-1940	94632	102	14.20	82.06	16.13	15.36	1.75	U10-P05-06-319	110304	2	16.56	13.97	16.28	16.58	2.31
LBB102-1940	94632	103	13.26	54.83	16.12	14.48	1.72	U10-P05-06-319	110304	3	15.41	71.99	16.52	16.07	3.16
LBB102-1940	94632	104	14.13	43.15	16.23	14.88	2.12	U10-P05-06-319	110304	4	15.80	35.37	16.52	16.06	3.16
LBB102-1940	94632	105	14.49	50.16	16.19	15.26	1.98	U10-P05-06-319	110304	5	15.56	32.94	16.37	15.83	2.62
LBB102-1940	94632	106	13.37	55.76	16.12	14.57	1.72	U10-P05-06-319	110304	6	14.79	36.33	16.48	15.26	3.02
LBB102-1940	94632	107	13.77	34.17	16.12	14.41	1.72	U10-P05-06-319	110304	7	14.18	69.60	16.46	15.27	2.94
LBB102-1940	94632	108	12.99	71.41	16.26	14.54	2.23	U10-P05-06-319	110304	8	12.57	36.14	16.38	13.53	2.65
LBB102-1940	94632	109	13.05	67.03	16.19	14.53	1.98	U10-P05-06-319	110304	9	14.58	57.47	16.41	15.41	2.75
LBB102-1940	94632	110	14.44	76.16	16.20	15.48	2.00	U10-P05-06-319	110304	10	14.36	79.99	16.52	15.45	3.14
LBB102-1940	94632	111	13.73	64.31	16.09	14.93	1.64	U10-P05-06-319	110304	11	13.72	56.38	16.48	14.82	3.00
LBB102-1940	94632	112	14.38	70.87	16.27	15.41	2.26	U10-P05-06-319	110304	12	14.17	25.54	16.48	14.54	3.00
LBB102-1940	94632	113	14.52	58.11	16.27	15.38	2.26	U10-P05-06-319	110304	13	13.95	79.56	16.63	15.19	3.55
LBB102-1940	94632	114	15.64	76.07	16.22	16.23	2.08	U10-P05-06-319	110304	14	15.96	51.20	16.40	16.31	2.72
LBB102-1940	94632	115	14.22	87.29	16.15	15.38	1.84	U10-P05-06-319	110304	15	14.62	46.57	16.56	15.30	3.28
LBB102-1940	94632	116	13.78	74.72	16.22	15.06	2.09	U10-P05-06-319	110304	16	13.69	73.51	16.52	14.99	3.15
LBB102-1940	94632	117	13.85	53.81	16.09	14.87	1.63	U10-P05-06-319	110304	17	14.74	40.45	16.61	15.29	3.46
LBB102-1940	94632	118	12.74	77.88	16.22	14.43	2.09	U10-P05-06-319	110304	18	14.71	56.55	16.48	15.49	3.00
LBB102-1940	94632	119	13.13	53.10	16.22	14.36	2.09	U10-P05-06-319	110304	19	13.31	85.77	16.52	14.82	3.13
LBB102-1940	94632	120	13.60	80.77	16.18	14.98	1.96	U10-P05-06-319	110304	20	15.87	0.51	16.52	15.87	3.15

Table C3 Apatite fission track lengths for all samples analysed in this thesis

UBC	A2Z	Track	Angle				Dpar (μm)	UBC	A2Z	Track	Angle				Dpar (μm)
			Length (μm)	to c- axis	Lo calc (μm)	Lc calc (μm)					Length (μm)	to c- axis	Lo calc (μm)	Lc calc (μm)	
LBB102-1940	94632	121	14.57	66.22	16.29	15.49	2.34	U10-P05-06-319	110304	21	15.47	74.12	16.48	16.12	3.02
LBB102-1940	94632	122	8.14	45.78	16.22	11.35	2.10	U10-P05-06-319	110304	22	14.54	89.86	16.41	15.58	2.75
LBB102-1940	94632	123	15.37	31.57	16.13	15.66	1.75	U10-P05-06-319	110304	23	14.41	36.42	16.48	14.96	3.02
LBB102-1940	94632	124	14.58	34.56	16.14	15.06	1.81	U10-P05-06-319	110304	24	14.21	37.11	16.44	14.82	2.86
LBB102-1940	94632	125	14.36	15.22	16.14	14.50	1.81	U10-P05-06-319	110304	25	8.78	45.31	16.44	11.42	2.87
LBB102-1940	94632	126	15.66	70.63	16.24	16.22	2.15	U10-P05-06-319	110304	26	12.22	64.11	16.52	13.96	3.13
LBB102-1940	94632	127	13.75	25.84	16.20	14.18	2.02	U10-P05-06-319	110304	27	11.99	67.44	16.30	13.86	2.38
LBB102-1940	94632	128	15.24	30.73	16.16	15.54	1.86	U10-P05-06-319	110304	28	14.64	75.36	16.58	15.60	3.35
LBB102-1940	94632	129	15.51	43.07	16.12	15.91	1.74	U10-P05-06-319	110304	29	16.03	44.15	16.45	16.31	2.91
LBB102-1940	94632	130	16.41	35.35	16.12	16.55	1.74	U10-P05-06-319	110304	30	14.74	65.10	16.54	15.60	3.23
LBB102-1940	94632	131	13.41	43.68	16.13	14.36	1.77	U10-P05-06-319	110304	31	13.77	28.44	16.34	14.27	2.51
LBB102-1940	94632	132	13.38	83.85	16.11	14.86	1.71	U10-P05-06-319	110304	32	14.95	71.14	16.41	15.77	2.74
LBB102-1940	94632	133	12.29	60.53	16.18	13.94	1.94	U10-P05-06-319	110304	33	12.38	0.65	16.21	12.38	2.06
LBB102-1940	94632	134	14.29	57.70	16.13	15.22	1.76	U10-P05-06-319	110304	34	14.99	57.64	16.39	15.69	2.68
LBB102-1940	94632	135	13.30	73.78	16.26	14.75	2.22	U10-P05-06-319	110304	35	13.65	60.68	16.51	14.84	3.11
LBB102-1940	94632	136	14.32	49.25	16.26	15.12	2.23	U10-P05-06-319	110304	36	15.40	62.14	16.45	16.01	2.89
LBB102-1940	94632	137	16.41	54.31	16.05	16.65	1.47	U10-P05-06-319	110304	37	14.04	77.70	16.51	15.24	3.11
LBB102-1940	94632	138	11.69	64.31	16.11	13.62	1.69	U10-P05-06-319	110304	38	12.54	30.05	16.52	13.31	3.16
LBB102-1940	94632	139	15.23	64.50	16.09	15.91	1.62	U10-P05-06-319	110304	39	13.74	57.07	16.62	14.84	3.51
LBB102-1940	94632	140	12.28	55.60	16.08	13.84	1.60	U10-P05-06-319	110304	40	13.52	51.99	16.43	14.61	2.82
LBB102-1940	94632	141	15.72	35.70	16.16	16.00	1.89	U10-P05-06-319	110304	41	13.56	46.79	16.43	14.54	2.82
LBB102-1940	94632	142	14.57	85.30	16.14	15.59	1.81	U10-P05-06-319	110304	42	15.18	19.32	16.49	15.33	3.04
LBB102-1940	94632	143	13.31	48.84	16.22	14.40	2.08	U10-P05-06-319	110304	43	12.96	82.83	16.38	14.59	2.66
LBB102-1940	94632	144	15.56	56.04	16.10	16.07	1.65	U10-P05-06-319	110304	44	16.64	55.92	16.40	16.81	2.72
LBB102-1940	94632	145	13.99	55.32	16.20	14.99	2.01	U10-P05-06-319	110304	45	15.34	87.36	16.40	16.06	2.71
LBB102-1940	94632	146	11.92	32.37	16.20	12.91	2.01	U10-P05-06-319	110304	46	14.48	89.71	16.62	15.54	3.51
LBB102-1940	94632	147	14.46	46.03	16.20	15.17	2.01	U10-P05-06-319	110304	47	14.73	70.82	16.44	15.63	2.85
LBB102-1940	94632	148	14.04	63.77	16.16	15.13	1.88	U10-P05-06-319	110304	48	15.36	64.56	16.38	16.00	2.66
LBB102-1940	94632	149	13.33	61.34	16.16	14.63	1.88	U10-P05-06-319	110304	49	14.74	8.04	16.33	14.78	2.49
LBB102-3050	94633	1	15.81	40.76	16.23	16.12	2.13	U10-P05-06-319	110304	50	14.18	58.75	16.43	15.16	2.83
LBB102-3050	94633	2	14.78	76.80	16.13	15.69	1.75	U10-P05-06-319	110304	51	12.73	59.09	16.41	14.20	2.76
LBB102-3050	94633	3	15.06	29.01	16.18	15.36	1.93	U10-P05-06-319	110304	52	14.99	80.07	16.52	15.84	3.13
LBB102-3050	94633	4	15.45	66.59	16.18	16.07	1.94	U10-P05-06-319	110304	53	14.86	68.46	16.42	15.70	2.79
LBB102-3050	94633	5	14.73	36.34	16.18	15.21	1.94	U10-P05-06-319	110304	54	15.18	73.59	16.51	15.93	3.10
LBB102-3050	94633	6	13.99	68.64	16.18	15.14	1.94	U10-P05-06-319	110304	55	13.81	40.10	16.33	14.58	2.49
LBB102-3050	94633	7	14.45	52.25	16.07	15.26	1.57	U10-P05-06-319	110304	56	13.38	48.59	16.51	14.45	3.11
LBB102-3050	94633	8	14.65	51.80	16.13	15.39	1.76	U10-P05-06-319	110304	57	15.15	61.59	16.50	15.84	3.09
LBB102-3050	94633	9	14.53	72.25	16.13	15.51	1.76	U10-P05-06-319	110304	58	15.19	44.05	16.50	15.68	3.09
LBB102-3050	94633	10	14.13	16.28	16.27	14.30	2.27	U10-P05-06-319	110304	59	15.07	33.19	16.55	15.43	3.24
LBB102-3050	94633	11	13.96	45.13	16.17	14.79	1.92	U10-P05-06-319	110304	60	14.70	54.93	16.40	15.47	2.71
LBB102-3050	94633	12	14.42	67.22	16.20	15.41	2.03	U10-P05-06-319	110304	61	14.65	29.11	16.48	15.02	3.02
LBB102-3050	94633	13	13.32	22.47	16.20	13.72	2.03	U10-P05-06-319	110304	62	12.98	68.33	16.42	14.50	2.78
LBB102-3050	94633	14	14.57	53.15	16.11	15.35	1.70	U10-P05-06-319	110304	63	14.20	48.70	16.33	15.03	2.49
LBB102-3050	94633	15	12.75	89.36	16.20	14.48	2.00	U10-P05-06-319	110304	64	14.59	20.52	16.37	14.81	2.61
LBB102-3050	94633	16	14.58	28.41	16.17	14.94	1.90	U10-P05-06-319	110304	65	14.30	73.92	16.38	15.38	2.64
LBB102-3050	94633	17	15.28	61.20	16.17	15.92	1.90	U10-P05-06-319	110304	66	14.64	89.28	16.49	15.64	3.05
LBB102-3050	94633	18	11.70	54.25	16.22	13.43	2.07	U10-P05-06-319	110304	67	13.58	79.37	16.54	14.96	3.22
LBB102-3050	94633	19	14.59	78.22	16.26	15.58	2.21	U10-P05-06-319	110304	68	11.38	28.21	16.43	12.33	2.83
LBB102-3050	94633	20	16.47	27.45	16.14	16.56	1.81	U10-P05-06-319	110304	69	15.28	29.62	16.33	15.56	2.48
LBB102-3050	94633	21	15.10	48.92	16.18	15.68	1.96	U10-P05-06-319	110304	70	14.88	78.47	16.35	15.76	2.55
LBB102-3050	94633	22	15.99	77.95	16.17	16.45	1.90	U10-P05-06-319	110304	71	14.83	75.87	16.40	15.72	2.72
LBB102-3050	94633	23	14.20	64.70	16.13	15.24	1.77	U10-P05-06-319	110304	72	16.49	48.84	16.51	16.68	3.11
LBB102-3050	94633	24	11.99	33.78	16.25	13.02	2.19	U10-P05-06-319	110304	73	15.76	51.19	16.37	16.17	2.60
LBB102-3050	94633	25	15.95	65.99	16.20	16.39	2.03	U10-P05-06-577	110306	1	12.98	56.60	16.19	14.33	1.99
LBB102-3050	94633	26	15.47	46.90	16.14	15.92	1.80	U10-P05-06-577	110306	2	14.30	28.77	16.19	14.72	1.97
LBB102-3050	94633	27	12.84	62.69	16.26	14.33	2.24	U10-P05-06-577	110306	3	14.30	77.67	16.19	15.40	1.97
LBB102-3050	94633	28	15.46	61.84	16.26	16.04	2.24	U10-P05-06-577	110306	4	13.57	58.72	16.21	14.75	2.04
LBB102-3050	94633	29	14.87	75.54	16.26	15.74	2.24	U10-P05-06-577	110306	5	14.00	39.84	16.20	14.71	2.00
LBB102-3050	94633	30	14.23	52.65	16.18	15.11	1.96	U10-P05-06-577	110306	6	13.23	24.86	16.22	13.71	2.09
LBB102-3050	94633	31	14.42	26.43	16.07	14.77	1.55	U10-P05-06-577	110306	7	13.76	50.81	16.22	14.75	2.09
LBB102-3050	94633	32	14.15	83.11	16.07	15.33	1.55	U10-P05-06-577	110306	8	12.83	82.32	16.28	14.51	2.30

Table C3 Apatite fission track lengths for all samples analysed in this thesis

UBC	A2Z	Track	Angle				Dpar	UBC	A2Z	Track	Angle				Dpar
			Length (μm)	to c- axis	Lo calc (μm)	Lc calc (μm)					Length (μm)	to c- axis	Lo calc (μm)	Lc calc (μm)	
LBB102-3050	94633	33	11.21	70.45	16.07	13.41	1.55	U10-P05-06-577	110306	9	15.97	79.96	16.28	16.44	2.30
LBB102-3050	94633	34	14.90	25.24	16.27	15.16	2.26	U10-P05-06-577	110306	10	15.98	56.81	16.17	16.36	1.92
LBB102-3050	94633	35	14.19	61.46	16.27	15.20	2.26	U10-P05-06-577	110306	11	13.42	57.75	16.22	14.64	2.09
LBB102-3050	94633	36	13.92	75.47	16.27	15.15	2.26	U10-P05-06-577	110306	12	14.55	68.35	16.22	15.50	2.09
LBB102-3050	94633	37	16.35	32.85	16.28	16.49	2.31	U10-P05-06-577	110306	13	13.59	83.05	16.22	14.98	2.09
LBB102-3050	94633	38	15.19	47.10	16.19	15.72	1.97	U10-P05-06-577	110306	14	12.84	61.80	16.22	14.32	2.09
LBB102-3050	94633	39	12.11	42.31	16.24	13.39	2.15	U10-P05-06-577	110306	15	14.24	46.84	16.22	15.03	2.09
LBB102-3050	94633	40	9.83	71.33	16.20	12.56	2.01	U10-P05-06-577	110306	16	12.99	83.34	16.22	14.61	2.09
LBB102-3050	94633	41	12.53	66.84	16.20	14.19	2.01	U10-P05-06-577	110306	17	13.22	44.91	16.22	14.25	2.09
LBB102-3050	94633	42	14.90	67.09	16.20	15.71	2.01	U10-P05-06-577	110306	18	13.69	74.59	16.22	15.00	2.09
LBB102-3050	94633	43	13.88	22.29	16.13	14.21	1.78	U10-P05-06-577	110306	19	14.40	41.94	16.30	15.06	2.37
LBB102-3050	94633	44	14.62	85.55	16.15	15.62	1.82	U10-P05-06-577	110306	20	14.08	21.04	16.25	14.36	2.19
LBB102-3050	94633	45	14.35	64.29	16.15	15.33	1.82	U10-P05-06-577	110306	21	13.07	52.46	16.25	14.31	2.19
LBB102-3050	94633	46	14.26	45.77	16.15	15.02	1.82	U10-P05-06-577	110306	22	13.23	65.55	16.25	14.62	2.19
LBB102-3050	94633	47	11.33	61.60	16.15	13.34	1.82	U10-P05-06-577	110306	23	14.97	65.58	16.22	15.75	2.08
LBB102-3050	94633	48	12.43	37.24	16.08	13.46	1.59	U10-P05-06-577	110306	24	13.28	44.56	16.18	14.29	1.94
LBB102-3050	94633	49	15.16	55.09	16.26	15.78	2.21	U10-P05-06-577	110306	25	13.31	65.77	16.21	14.68	2.06
LBB102-3050	94633	50	12.54	48.41	16.16	13.86	1.87	U10-P05-06-577	110306	26	14.64	81.50	16.21	15.62	2.06
LBB102-3050	94633	51	15.02	59.17	16.16	15.73	1.87	U10-P05-06-577	110306	27	13.97	27.59	16.21	14.41	2.06
LBB102-3050	94633	52	12.74	74.04	16.23	14.40	2.13	U10-P05-06-577	110306	28	13.91	81.72	16.17	15.17	1.92
LBB102-3050	94633	53	14.91	36.90	16.15	15.36	1.83	U10-P05-06-577	110306	29	13.44	54.84	16.17	14.61	1.92
LBB102-3050	94633	54	15.00	74.14	16.15	15.82	1.83	U10-P05-06-577	110306	30	6.94	72.64	16.12	11.96	1.74
LBB102-3050	94633	55	15.45	43.95	16.13	15.88	1.78	U10-P05-06-577	110306	31	14.00	56.24	16.27	15.01	2.26
LBB102-3050	94633	56	13.82	72.58	16.13	15.07	1.78	U10-P05-06-577	110306	32	14.26	75.91	16.23	15.37	2.13
LBB102-3050	94633	57	15.03	39.81	16.14	15.50	1.81	U10-P05-06-577	110306	33	13.73	47.98	16.26	14.68	2.21
LBB102-3050	94633	58	15.05	58.23	16.19	15.74	1.98	U10-P05-06-577	110306	34	12.27	56.26	16.29	13.85	2.32
LBB102-3050	94633	59	14.50	71.57	16.09	15.49	1.63	U10-P05-06-577	110306	35	16.43	27.64	16.29	16.53	2.32
LBB102-3050	94633	60	12.30	80.74	16.26	14.18	2.23	U10-P05-06-577	110306	36	14.32	81.52	16.29	15.43	2.32
LBB102-3050	94633	61	14.87	31.29	16.26	15.24	2.23	U10-P05-06-577	110306	37	12.74	80.40	16.29	14.45	2.32
LBB102-3050	94633	62	12.71	69.53	16.23	14.34	2.11	U10-P05-06-577	110306	38	16.47	53.11	16.29	16.69	2.32
LBB102-3050	94633	63	6.41	87.85	16.23	12.05	2.11	U10-P05-06-577	110306	39	16.11	85.53	16.29	16.54	2.32
LBB102-3050	94633	64	13.76	62.91	16.16	14.94	1.86	U10-P05-06-577	110306	40	13.96	67.89	16.20	15.12	2.00
LBB102-3050	94633	65	12.96	84.10	16.05	14.60	1.50	U10-P05-06-577	110306	41	15.80	50.57	16.26	16.19	2.23
LBB102-3050	94633	66	11.54	22.84	16.05	12.23	1.50	U10-P05-06-577	110306	42	14.19	63.55	16.20	15.22	2.02
LBB102-3050	94633	67	13.91	71.12	16.15	15.11	1.85	U10-P05-06-577	110306	43	14.09	75.50	16.27	15.26	2.27
LBB102-3050	94633	68	14.78	73.77	16.17	15.68	1.90	U10-P05-06-577	110306	44	14.67	64.07	16.27	15.54	2.27
LBB102-3050	94633	69	13.63	74.10	16.18	14.96	1.94	U10-P05-06-577	110306	45	15.61	65.41	16.17	16.16	1.92
LBB102-3050	94633	70	12.48	83.27	16.18	14.30	1.95	U10-P05-06-577	110306	46	13.33	40.59	16.15	14.23	1.84
LBB102-3050	94633	71	13.88	66.80	16.20	15.06	2.02	U10-P05-06-577	110306	47	8.78	61.01	16.23	12.03	2.11
LBB102-3050	94633	72	15.13	39.03	16.13	15.57	1.76	U10-P05-06-577	110306	48	14.52	61.51	16.30	15.42	2.38
LBB102-3050	94633	73	13.18	30.12	16.13	13.83	1.76	U10-P05-06-577	110306	49	15.12	58.47	16.30	15.79	2.38
LBB102-3050	94633	74	16.63	34.04	16.14	16.73	1.80	U10-P05-06-577	110306	50	14.26	55.44	16.21	15.17	2.05
LBB102-3050	94633	75	15.49	47.06	16.14	15.94	1.80	U10-P05-06-577	110306	51	15.15	84.18	16.21	15.94	2.05
LBB102-3050	94633	76	16.16	55.29	16.13	16.48	1.76	U10-P05-06-577	110306	52	13.61	63.07	16.28	14.84	2.28
LBB102-3050	94633	77	12.94	58.87	16.20	14.34	2.02	U10-P05-06-577	110306	53	12.60	40.06	16.28	13.67	2.28
LBB102-3050	94633	78	12.76	77.59	16.20	14.44	2.00	U10-P05-06-577	110306	54	15.39	42.85	16.22	15.82	2.07
LBB102-3050	94633	79	10.97	31.43	16.15	12.16	1.82	U10-P05-06-577	110306	55	16.57	58.63	16.22	16.77	2.07
LBB102-3050	94633	80	4.83	63.14	16.22	11.31	2.10	U10-P05-06-577	110306	56	14.98	55.81	16.28	15.67	2.28
LBB102-3050	94633	81	13.29	74.61	16.20	14.75	2.00	U10-P05-06-577	110306	57	12.66	66.23	16.21	14.27	2.05
LBB102-3050	94633	82	14.84	72.31	16.18	15.71	1.93	U10-P05-06-577	110306	58	14.33	70.40	16.21	15.37	2.05
LBB102-3050	94633	83	13.48	81.59	16.16	14.91	1.89	U10-P05-06-577	110306	59	14.24	60.85	16.26	15.23	2.23
LBB102-3050	94633	84	10.79	87.46	16.19	13.28	1.99	U10-P05-06-577	110306	60	13.74	53.80	16.16	14.79	1.87
LBB102-3050	94633	85	15.00	64.99	16.08	15.76	1.60	U10-P05-06-577	110306	61	13.05	82.81	16.16	14.65	1.87
LBB102-3050	94633	86	14.49	68.18	16.08	15.46	1.60	U10-P05-06-577	110306	62	16.74	55.38	16.26	16.88	2.23
LBB102-3050	94633	87	16.15	78.32	16.22	16.55	2.10	U10-P05-06-577	110306	63	12.92	24.57	16.20	13.44	2.03
LBB102-3050	94633	88	11.93	55.65	16.14	13.61	1.79	U10-P05-06-577	110306	64	13.15	49.07	16.13	14.29	1.76
LBB102-3050	94633	89	11.70	54.28	16.26	13.43	2.23	U10-P05-06-577	110306	65	13.43	58.14	16.13	14.65	1.76
LBB102-3050	94633	90	14.07	47.84	16.06	14.92	1.52	U10-P05-06-577	110306	66	13.66	66.34	16.32	14.91	2.43
LBB102-3050	94633	91	13.92	76.42	16.14	15.16	1.80	U10-P05-06-577	110306	67	14.76	78.56	16.29	15.69	2.32
LBB102-3050	94633	92	12.60	42.64	16.13	13.75	1.75	U10-P05-06-577	110306	68	12.92	42.60	16.28	13.98	2.31
LBB102-3050	94633	93	14.62	55.15	16.20	15.41	2.00	U10-P05-06-577	110306	69	12.38	61.46	16.26	14.02	2.24

Table C3 Apatite fission track lengths for all samples analysed in this thesis

UBC	A2Z	Track	Angle				Dpar	UBC	A2Z	Track	Angle				Dpar
			Length (μm)	to c- axis	Lo calc (μm)	Lc calc (μm)					Length (μm)	to c- axis	Lo calc (μm)	Lc calc (μm)	
LBB102-3050	94633	94	14.45	65.71	16.17	15.41	1.91	U10-P05-06-577	110306	70	7.80	65.66	16.38	11.98	2.65
LBB102-3050	94633	95	12.08	51.68	16.17	13.62	1.90	U10-P05-06-577	110306	71	11.22	85.49	16.25	13.53	2.18
LBB102-3050	94633	96	15.20	75.24	16.17	15.95	1.90	U10-P05-06-577	110306	72	11.94	43.50	16.15	13.30	1.82
LBB102-3050	94633	97	14.44	55.49	16.15	15.30	1.82	U10-P05-06-577	110306	73	13.82	85.22	16.31	15.13	2.42
LBB102-3050	94633	98	13.55	54.24	16.18	14.67	1.94	U10-P05-06-577	110306	74	13.47	84.34	16.18	14.91	1.93
LBB102-3050	94633	99	13.62	41.64	16.13	14.47	1.75	U10-P05-06-577	110306	75	15.32	53.30	16.31	15.88	2.41
LBB102-3050	94633	100	14.75	61.05	16.17	15.57	1.92	U10-P05-06-577	110306	76	14.07	39.95	16.23	14.77	2.12
LBB102-3050	94633	101	13.97	45.18	16.15	14.80	1.82	U10-P05-06-577	110306	77	13.90	76.79	16.23	15.15	2.12
LBB102-3050	94633	102	15.19	41.45	16.09	15.65	1.62	U10-P05-06-577	110306	78	13.64	44.80	16.23	14.55	2.12
LBB102-3050	94633	103	15.35	70.56	16.09	16.02	1.62	U10-P05-06-577	110306	79	13.33	36.65	16.32	14.13	2.45
LBB102-3050	94633	104	15.05	81.50	16.16	15.88	1.86	U10-P05-06-577	110306	80	14.63	84.56	16.32	15.63	2.45
LBB102-3050	94633	105	15.59	52.75	16.08	16.06	1.60	U10-P05-06-577	110306	81	13.46	40.31	16.28	14.32	2.28
LBB102-3050	94633	106	3.79	88.97	16.08	11.41	1.60	U10-P05-06-577	110306	82	14.83	70.72	16.28	15.69	2.28
LBB102-3050	94633	107	14.23	75.34	16.07	15.34	1.57	U10-P05-06-577	110306	83	14.07	83.97	16.28	15.28	2.31
LBB102-3050	94633	108	11.28	54.90	16.13	13.16	1.78	U10-P05-06-577	110306	84	14.41	48.33	16.28	15.17	2.31
LBB102-3050	94633	109	14.43	66.55	16.13	15.41	1.78	U12-P05-16-1303	110303	1	13.11	85.81	16.05	14.69	1.49
LBB102-3050	94633	110	13.85	34.48	16.19	14.48	1.99	U12-P05-16-1303	110303	2	14.61	77.48	16.29	15.59	2.34
LBB102-3050	94633	111	12.84	51.10	16.19	14.12	1.99	U12-P05-16-1303	110303	3	10.81	86.67	16.10	13.29	1.67
LBB102-3050	94633	112	15.93	36.95	16.18	16.18	1.95	U12-P05-16-1303	110303	4	13.47	55.76	16.27	14.64	2.25
LBB102-3050	94633	113	16.16	39.62	16.16	16.38	1.87	U12-P05-16-1303	110303	5	12.73	43.78	16.27	13.87	2.25
LBB102-3050	94633	114	13.58	68.12	16.13	14.88	1.77	U12-P05-16-1303	110303	6	10.75	54.76	16.27	12.81	2.25
LBB102-3050	94633	115	13.90	60.31	16.13	14.99	1.77	U12-P05-16-1303	110303	7	10.59	74.36	16.34	13.07	2.50
LBB102-3050	94633	116	15.25	37.29	16.21	15.64	2.05	U12-P05-16-1303	110303	8	14.04	21.35	16.34	14.33	2.50
LBB102-3050	94633	117	12.77	34.10	16.21	13.62	2.05	U12-P05-16-1303	110303	9	14.19	40.40	16.20	14.87	2.03
LBB102-3050	94633	118	13.28	48.51	16.16	14.37	1.89	U12-P05-16-1303	110303	10	13.16	39.03	16.26	14.06	2.22
LBB102-3050	94633	119	14.92	78.36	16.16	15.79	1.89	U12-P05-16-1303	110303	11	10.05	68.94	16.26	12.66	2.22
LBB102-3050	94633	120	14.94	73.78	16.13	15.78	1.76	U12-P05-16-1303	110303	12	13.57	46.85	16.28	14.54	2.29
LBB102-3050	94633	121	13.54	66.02	16.23	14.83	2.12	U12-P05-16-1303	110303	13	13.22	64.53	16.28	14.61	2.29
LBB102-3050	94633	122	13.63	84.02	16.16	15.01	1.86	U12-P05-16-1303	110303	14	8.42	66.10	16.33	12.11	2.46
LBB102-3050	94633	123	12.65	65.02	16.16	14.25	1.86	U12-P05-16-1303	110303	15	14.02	32.56	16.30	14.57	2.35
LBB102-3050	94633	124	15.54	4.70	16.20	15.55	2.00	U12-P05-16-1303	110303	16	14.90	22.78	16.30	15.12	2.35
LBB102-3050	94633	125	14.55	66.19	16.17	15.48	1.91	U12-P05-16-1303	110303	17	12.84	53.87	16.30	14.18	2.35
LBB102-3050	94633	126	7.85	71.42	16.17	12.12	1.91	U12-P05-16-1303	110303	18	9.57	61.21	16.18	12.22	1.94
LBB102-3050	94633	127	14.25	41.41	16.24	14.93	2.14	U12-P05-16-1303	110303	19	14.21	76.11	16.28	15.34	2.30
LBB102-3050	94633	128	16.49	22.02	16.26	16.55	2.22	U12-P05-16-1303	110303	20	13.57	66.66	16.12	14.86	1.72
LBB102-3050	94633	129	13.71	74.92	16.26	15.02	2.22	U12-P05-16-1303	110303	21	14.71	34.44	16.12	15.16	1.72
LBB102-3050	94633	130	13.47	68.88	16.26	14.82	2.22	U12-P05-16-1303	110303	22	14.43	74.16	16.41	15.46	2.76
LBB102-3050	94633	131	11.44	31.30	16.22	12.51	2.07	U12-P05-16-1303	110303	23	13.80	23.26	16.22	14.16	2.09
LBB102-3050	94633	132	12.38	47.93	16.22	13.73	2.07	U12-P05-16-1303	110303	24	14.09	78.52	16.33	15.27	2.47
LBB102-3050	94633	133	13.47	36.16	16.22	14.22	2.07	U12-P05-16-1303	110303	25	12.47	45.53	16.33	13.73	2.47
LBB102-3050	94633	134	14.70	76.74	16.24	15.64	2.15	U12-P05-16-1303	110303	26	14.41	56.00	16.33	15.28	2.47
LBB102-3050	94633	135	15.02	20.45	16.24	15.19	2.15	U12-P05-16-1303	110303	27	13.74	57.48	16.26	14.85	2.21
LBB102-3050	94633	136	15.25	57.67	16.07	15.87	1.56	U12-P05-16-1303	110303	28	15.55	55.36	16.26	16.06	2.21
LBB102-3050	94633	137	14.50	68.89	16.07	15.47	1.56	U12-P05-16-1303	110303	29	13.63	86.21	16.26	15.01	2.24
LBB102-3050	94633	138	15.37	62.17	16.07	15.99	1.56	U12-P05-16-1303	110303	30	7.59	35.66	16.24	10.76	2.17
LBB102-3050	94633	139	8.88	36.31	16.22	10.94	2.10	U12-P05-16-1303	110303	31	13.24	56.34	16.24	14.50	2.15
LBB102-3050	94633	140	14.14	89.05	16.22	15.33	2.10	U12-P05-16-1303	110303	32	16.24	73.19	16.24	16.60	2.15
LBB102-3050	94633	141	14.07	41.31	16.22	14.80	2.10	U12-P05-16-1303	110303	33	4.46	46.10	16.24	10.74	2.15
LBB102-3050	94633	142	12.92	64.21	16.15	14.41	1.82	U12-P05-16-1303	110303	34	14.90	36.37	16.11	15.35	1.69
LBB102-3050	94633	143	14.68	57.46	16.15	15.48	1.83	U12-P05-16-1303	110303	35	12.63	85.83	16.11	14.40	1.69
LBB102-3050	94633	144	16.34	57.76	16.19	16.61	1.99	U12-P05-16-1303	110303	36	14.09	32.19	16.30	14.62	2.36
LBB102-3050	94633	145	15.59	13.54	16.22	15.65	2.09	U12-P05-16-1303	110303	37	11.92	42.49	16.30	13.26	2.36
LBB102-3050	94633	146	14.49	42.53	16.20	15.13	2.02	U12-P05-16-1303	110303	38	13.89	45.19	16.30	14.74	2.36
LBB102-3050	94633	147	13.30	62.35	16.12	14.63	1.74	U12-P05-16-1303	110303	39	12.99	37.81	16.34	13.90	2.51
LBB102-3050	94633	148	14.87	67.44	16.13	15.70	1.75	U12-P05-16-1303	110303	40	13.43	70.36	16.18	14.80	1.94
LBB102-3050	94633	149	14.28	42.39	16.13	14.98	1.75	U12-P05-16-1303	110303	41	13.73	53.07	16.18	14.77	1.94
LBB102-3050	94633	150	12.11	59.27	16.13	13.80	1.75	U12-P05-16-1303	110303	42	13.02	85.37	16.18	14.64	1.94
LBB102-3050	94633	151	14.11	47.09	16.20	14.94	2.01	U12-P05-16-1303	110303	43	14.16	62.76	16.29	15.19	2.34
LBB102-3050	94633	152	16.96	20.34	16.15	16.98	1.82	U12-P05-16-1303	110303	44	13.96	65.52	16.29	15.09	2.34
LBB102-3050	94633	153	14.90	68.57	16.23	15.72	2.12	U12-P05-16-1303	110303	45	14.68	79.54	16.29	15.64	2.34
LBB102-3050	94633	154	14.67	81.13	16.18	15.64	1.93	U12-P05-16-1303	110303	46	14.68	75.41	16.23	15.63	2.11

Table C3 Apatite fission track lengths for all samples analysed in this thesis

UBC	A2Z	Track	Angle					UBC	A2Z	Track	Angle				
			Length (μm)	to c- axis	Lo calc (μm)	Lc calc (μm)	Dpar (μm)				Length (μm)	to c- axis	Lo calc (μm)	Lc calc (μm)	Dpar (μm)
LBB102-3050	94633	155	15.35	57.75	16.23	15.94	2.13	U12-P05-16-1303	110303	47	13.87	71.39	16.23	15.09	2.11
LBB102-3900	94634	1	12.99	42.81	16.15	14.03	1.83	U12-P05-16-1303	110303	48	14.12	63.87	16.23	15.18	2.11
LBB102-3900	94634	2	14.43	80.44	16.20	15.49	2.00	U12-P05-16-1303	110303	49	7.91	67.77	16.30	12.05	2.36
LBB102-3900	94634	3	8.27	63.05	16.20	12.00	2.00	U12-P05-16-1303	110303	50	12.20	50.01	16.36	13.66	2.58
LBB102-3900	94634	4	12.96	8.21	16.19	13.04	1.98	U12-P05-16-1303	110303	51	15.81	25.40	16.36	15.96	2.58
LBB102-3900	94634	5	12.99	42.86	16.19	14.04	1.98	U12-P05-16-1303	110303	52	15.89	34.84	16.36	16.12	2.58
LBB102-3900	94634	6	13.49	77.34	16.21	14.89	2.06	U12-P05-16-1303	110303	53	13.74	38.71	16.36	14.49	2.58
LBB102-3900	94634	7	12.85	64.29	16.14	14.36	1.81	U12-P05-16-1303	110303	54	14.61	52.71	16.34	15.38	2.52
LBB102-3900	94634	8	12.51	45.15	16.03	13.75	1.42	U12-P05-16-1303	110303	55	12.45	20.67	16.34	12.91	2.52
LBB102-3900	94634	9	14.31	27.07	16.16	14.69	1.87	U12-P05-16-1303	110303	56	14.64	23.13	16.34	14.90	2.52
LBB102-3900	94634	10	12.16	43.07	16.09	13.44	1.61	U12-P05-16-1303	110303	57	12.46	34.94	16.34	13.41	2.52
LBB102-3900	94634	11	13.37	51.74	16.24	14.50	2.14	U12-P05-16-1303	110303	58	15.38	18.37	16.34	15.50	2.52
LBB102-3900	94634	12	14.55	60.04	16.27	15.42	2.27	U12-P05-16-1303	110303	59	11.44	52.92	16.36	13.22	2.59
LBB102-3900	94634	13	13.58	64.43	16.27	14.84	2.27	U12-P05-16-1303	110303	60	11.89	58.69	16.36	13.65	2.59
LBB102-3900	94634	14	13.17	60.73	16.10	14.52	1.65	U12-P05-16-1303	110303	61	14.41	36.26	16.36	14.96	2.59
LBB102-3900	94634	15	13.64	68.92	16.10	14.92	1.65	U12-P05-16-1303	110303	62	15.76	81.49	16.36	16.32	2.59
LBB102-3900	94634	16	14.93	18.45	16.12	15.08	1.74	U12-P05-16-1303	110303	63	15.94	7.67	16.31	15.95	2.41
LBB102-3900	94634	17	13.99	45.42	16.18	14.82	1.96	U12-P05-16-1303	110303	64	15.56	84.57	16.31	16.20	2.41
LBB102-3900	94634	18	12.90	67.75	16.11	14.44	1.71	U12-P05-16-1303	110303	65	13.47	67.10	16.33	14.80	2.48
LBB102-3900	94634	19	12.41	65.25	16.11	14.09	1.71	U12-P05-16-1303	110303	66	14.68	36.37	16.33	15.17	2.48
LBB102-3900	94634	20	14.10	50.90	16.14	14.99	1.81	U12-P05-16-1303	110303	67	13.21	69.85	16.33	14.66	2.48
LBB102-3900	94634	21	12.68	81.55	16.31	14.42	2.41	U12-P05-16-1303	110303	68	14.59	82.19	16.37	15.60	2.61
LBB102-3900	94634	22	13.98	81.58	16.31	15.22	2.41	U12-P05-16-1303	110303	69	13.21	31.35	16.25	13.89	2.20
LBB102-3900	94634	23	13.95	32.48	16.31	14.51	2.41	U12-P05-16-1303	110303	70	14.65	30.70	16.25	15.05	2.20
LBB102-3900	94634	24	16.41	62.29	16.31	16.68	2.41	U12-P05-16-1303	110303	71	9.67	50.12	16.25	11.98	2.20
LBB102-3900	94634	25	14.34	88.82	16.31	15.45	2.41	U12-P05-16-1303	110303	72	16.03	16.78	16.19	16.09	1.98
LBB102-3900	94634	26	13.11	55.12	16.31	14.39	2.41	U12-P05-16-1303	110303	73	6.65	70.72	16.22	11.86	2.07
LBB102-3900	94634	27	13.78	51.44	16.31	14.78	2.41	U12-P05-16-1303	110303	74	14.01	64.12	16.22	15.11	2.07
LBB102-3900	94634	28	13.73	48.27	16.31	14.69	2.41	U12-P05-16-1303	110303	75	12.59	31.72	16.22	13.41	2.07
LBB102-3900	94634	29	12.81	47.57	16.31	14.02	2.41	U12-P05-16-1303	110303	76	7.30	78.73	16.36	12.13	2.58
LBB102-3900	94634	30	14.28	31.18	16.15	14.75	1.82	U12-P05-16-1303	110303	77	14.68	70.02	16.36	15.59	2.58
LBB102-3900	94634	31	13.87	43.42	16.15	14.69	1.82	U12-P05-16-1303	110303	78	13.69	83.74	16.22	15.05	2.08
LBB102-3900	94634	32	13.63	89.35	16.15	15.02	1.82	U12-P05-16-1303	110303	79	12.25	38.75	16.37	13.38	2.63
LBB102-3900	94634	33	10.83	76.88	16.15	13.24	1.82	U12-P05-16-1303	110303	80	15.78	20.76	16.21	15.89	2.05
LBB102-3900	94634	34	13.52	45.72	16.15	14.48	1.82	U12-P05-16-1303	110303	81	13.96	45.31	16.21	14.79	2.05
LBB102-3900	94634	35	11.96	67.85	16.15	13.84	1.82	U12-P05-16-1303	110303	82	13.94	66.37	16.21	15.09	2.05
LBB102-3900	94634	36	15.05	58.77	16.15	15.74	1.82	U12-P05-16-1303	110303	83	14.11	89.84	16.21	15.31	2.05
LBB102-3900	94634	37	14.35	27.19	16.04	14.73	1.46	U12-P05-16-1303	110303	84	14.27	75.05	16.21	15.37	2.05
LBB102-3900	94634	38	14.23	82.85	16.04	15.38	1.46	U12-P05-16-1303	110303	85	13.72	54.67	16.21	14.79	2.05
LBB102-3900	94634	39	13.28	78.96	16.04	14.77	1.46	U12-P05-16-1303	110303	86	15.73	25.29	16.21	15.89	2.05
LBB102-3900	94634	40	14.80	75.34	16.04	15.70	1.46	U12-P05-16-1303	110303	87	14.67	8.51	16.21	14.71	2.05
LBB102-3900	94634	41	16.12	82.50	16.22	16.54	2.09	U12-P05-16-1303	110303	88	15.93	44.43	16.25	16.24	2.20
LBB102-3900	94634	42	12.45	86.61	16.22	14.29	2.09	U12-P05-16-1303	110303	89	14.36	26.75	16.25	14.72	2.20
LBB102-3900	94634	43	14.34	30.19	16.13	14.78	1.78	U12-P05-16-1303	110303	90	14.45	26.20	16.30	14.79	2.36
LBB102-3900	94634	44	14.78	79.09	16.29	15.70	2.33	U12-P05-16-1303	110303	91	13.75	86.09	16.22	15.09	2.09
LBB102-3900	94634	45	14.86	50.50	16.29	15.52	2.33	U12-P05-16-1303	110303	92	11.79	89.37	16.22	13.89	2.09
LBB102-3900	94634	46	15.42	2.32	16.29	15.42	2.33	U12-P05-16-1303	110303	93	12.86	73.61	16.14	14.48	1.79
LBB102-3900	94634	47	13.70	80.20	16.29	15.04	2.33	U12-P05-16-1303	110303	94	14.43	84.39	16.14	15.50	1.79
LBB102-3900	94634	48	14.20	32.09	16.29	14.70	2.33	U12-P05-16-1303	110303	95	12.65	76.55	16.27	14.37	2.25
LBB102-3900	94634	49	14.55	71.27	16.19	15.52	1.98	U12-P05-16-1303	110303	96	12.46	60.47	16.30	14.05	2.36
LBB102-3900	94634	50	14.72	86.28	16.19	15.68	1.98	U12-P05-16-1303	110303	97	15.75	22.44	16.26	15.88	2.22
LBB102-3900	94634	51	14.89	74.11	16.12	15.75	1.73	U12-P05-16-1303	110303	98	11.51	78.76	16.32	13.68	2.44
LBB102-3900	94634	52	14.55	25.11	16.12	14.86	1.73	U12-P05-16-1303	110303	99	13.79	89.94	16.32	15.12	2.44
LBB102-3900	94634	53	13.69	80.58	16.12	15.04	1.73	U12-P05-16-1303	110303	100	10.35	49.95	16.23	12.42	2.13
LBB102-3900	94634	54	14.11	36.51	16.20	14.73	2.01	U12-P05-16-1303	110303	101	14.42	51.51	16.24	15.23	2.14
LBB102-3900	94634	55	15.32	39.02	16.20	15.72	2.01	U12-P05-16-271	110301	1	11.64	80.41	16.52	13.77	3.16
LBB102-3900	94634	56	14.48	38.40	16.20	15.05	2.01	U12-P05-16-271	110301	2	13.55	55.26	16.52	14.69	3.13
LBB102-3900	94634	57	15.94	49.65	16.16	16.29	1.88	U12-P05-16-271	110301	3	13.56	89.69	16.46	14.97	2.93
LBB102-3900	94634	58	14.15	72.63	16.18	15.28	1.96	U12-P05-16-271	110301	4	15.33	85.00	16.36	16.06	2.59
LBB102-3900	94634	59	14.71	56.86	16.18	15.50	1.95	U12-P05-16-271	110301	5	15.47	73.10	16.33	16.11	2.48
LBB102-3900	94634	60	14.57	72.24	16.15	15.54	1.83	U12-P05-16-271	110301	6	7.64	64.09	16.30	11.91	2.38

Table C3 Apatite fission track lengths for all samples analysed in this thesis

UBC	A2Z	Track	Angle				Dpar	UBC	A2Z	Track	Angle				Dpar
			Length (μm)	to c- axis	Lo calc (μm)	Lc calc (μm)					Length (μm)	to c- axis	Lo calc (μm)	Lc calc (μm)	
LBB102-3900	94634	61	15.79	63.23	16.15	16.27	1.83	U12-P05-16-271	110301	7	13.33	57.54	16.57	14.58	3.31
LBB102-3900	94634	62	14.43	67.45	16.15	15.42	1.83	U12-P05-16-271	110301	8	12.30	71.26	16.57	14.10	3.31
LBB102-3900	94634	63	12.77	79.80	16.20	14.46	2.00	U12-P05-16-814	110302	1	13.69	48.90	16.39	14.67	2.67
LBB102-3900	94634	64	15.18	57.86	16.18	15.82	1.93	U16-H07-34-537	107009	1	16.15	59.74	16.47	16.49	2.96
LBB102-3900	94634	65	14.81	68.02	16.15	15.66	1.84	U16-H07-34-537	107009	2	16.00	23.66	16.50	16.12	3.09
LBB102-3900	94634	66	13.40	38.70	16.22	14.23	2.08	U16-H07-34-537	107009	3	15.60	82.42	16.50	16.22	3.09
LBB102-3900	94634	67	15.21	63.06	16.22	15.89	2.08	U16-H07-34-537	107009	4	13.59	87.37	16.49	14.99	3.03
LBB102-3900	94634	68	11.74	72.99	16.17	13.77	1.90	U16-H07-34-537	107009	5	17.89	37.59	16.52	17.76	3.15
LBB102-3900	94634	69	15.86	23.81	16.08	15.99	1.60	U16-H07-34-537	107009	6	10.69	71.30	16.56	13.09	3.30
LBB102-3900	94634	70	14.28	39.83	16.08	14.93	1.60	U16-H07-34-537	107009	7	15.43	19.90	16.61	15.56	3.45
LBB102-3900	94634	71	16.50	33.64	16.19	16.62	1.97	U16-H07-34-537	107009	8	15.57	76.47	16.45	16.19	2.91
LBB102-3900	94634	72	12.88	74.53	16.19	14.50	1.97	U16-H07-34-537	107009	9	14.08	21.79	16.60	14.37	3.43
LBB102-3900	94634	73	13.19	74.52	16.19	14.69	1.97	U16-H07-34-537	107009	10	14.55	34.56	16.52	15.04	3.13
LBB102-3900	94634	74	15.48	74.19	16.19	16.12	1.97	U16-H07-34-537	107009	11	10.26	75.32	16.58	12.88	3.37
LBB102-3900	94634	75	14.85	84.61	16.19	15.76	1.97	U16-H07-34-537	107009	12	16.05	2.66	16.53	16.05	3.19
LBB102-3900	94634	76	15.40	35.58	16.19	15.74	1.97	U16-H07-34-537	107009	13	15.10	64.62	16.42	15.83	2.79
LBB102-3900	94634	77	12.63	50.35	16.19	13.96	1.97	U16-H07-34-537	107009	14	14.62	67.68	16.57	15.54	3.33
LBB102-3900	94634	78	13.38	62.87	16.15	14.69	1.85	U16-H07-34-537	107009	15	14.44	54.51	16.56	15.28	3.28
LBB102-3900	94634	79	14.84	79.29	16.15	15.74	1.85	U16-H07-34-537	107009	16	13.50	85.70	16.48	14.93	2.99
LBB102-3900	94634	80	12.88	68.33	16.15	14.43	1.85	U16-H07-34-537	107009	17	13.57	67.31	16.55	14.86	3.24
LBB102-3900	94634	81	13.33	54.18	16.18	14.52	1.95	U16-H07-34-537	107009	18	13.68	67.80	16.45	14.94	2.88
LBB102-3900	94634	82	14.09	68.61	16.18	15.21	1.95	U16-H07-34-537	107009	19	14.32	69.55	16.50	15.36	3.08
LBB102-3900	94634	83	17.91	17.91	16.18	17.87	1.95	U16-H07-34-537	107009	20	12.63	49.08	16.50	13.93	3.08
LBB102-3900	94634	84	5.90	65.39	16.12	11.59	1.73	U16-H07-34-537	107009	21	13.96	78.38	16.58	15.19	3.35
LBB102-3900	94634	85	14.96	63.86	16.12	15.73	1.73	U16-H07-34-537	107009	22	12.29	77.90	16.58	14.15	3.35
LBB102-3900	94634	86	13.30	56.45	16.24	14.54	2.15	U16-H07-34-537	107009	23	14.24	38.74	16.57	14.87	3.32
LBB102-3900	94634	87	10.58	67.29	16.24	12.97	2.15	U16-H07-34-537	107009	24	17.06	30.16	16.60	17.08	3.42
LBB102-3900	94634	88	12.02	61.53	16.14	13.78	1.79	U16-H07-34-537	107009	25	15.52	53.80	16.18	16.02	1.94
LBB102-3900	94634	89	14.64	54.90	16.14	15.42	1.79	U16-H07-34-537	107009	26	13.40	52.23	16.20	14.53	2.00
LBB102-3900	94634	90	12.93	29.97	16.14	13.62	1.79	U16-H07-34-537	107009	27	14.16	39.74	16.58	14.83	3.37
LBB102-3900	94634	91	13.48	50.80	16.17	14.56	1.91	U16-H07-34-537	107009	28	14.84	7.09	16.49	14.87	3.05
LBB102-3900	94634	92	12.48	70.66	16.14	14.21	1.80	U16-H07-34-537	107009	29	13.63	56.08	16.19	14.75	1.98
LBB102-3900	94634	93	11.58	65.71	16.11	13.57	1.71	U16-H07-34-537	107009	30	16.96	21.91	16.51	16.98	3.11
LBB102-3900	94634	94	13.89	59.10	16.10	14.97	1.65	U16-H07-34-537	107009	31	10.14	26.34	16.51	11.30	3.12
LBB102-3900	94634	95	13.65	64.73	16.17	14.89	1.92	U16-H07-34-537	107009	32	14.05	64.23	16.52	15.14	3.13
LBB102-3900	94634	96	12.35	72.32	16.14	14.14	1.79	U16-H07-34-537	107009	33	14.60	68.26	16.63	15.53	3.52
LBB102-3900	94634	97	14.39	77.30	16.17	15.45	1.92	U16-H07-34-537	107009	34	14.23	44.07	16.49	14.97	3.03
LBB102-3900	94634	98	15.44	60.14	16.20	16.02	2.02	U16-H07-34-537	107009	35	13.53	87.93	16.57	14.96	3.31
LBB102-3900	94634	99	15.89	30.49	16.18	16.08	1.96	U16-H07-34-537	107009	36	13.41	40.18	16.42	14.28	2.78
LBB102-3900	94634	100	15.28	68.70	16.16	15.97	1.86	U16-H07-34-537	107009	37	14.19	62.68	16.50	15.21	3.08
LBB102-3900	94634	101	13.66	50.48	16.16	14.68	1.86	U16-H07-34-537	107009	38	14.38	59.73	16.56	15.31	3.29
LBB102-3900	94634	102	12.15	71.05	16.18	14.00	1.96	U16-H07-34-537	107009	39	14.75	42.72	16.49	15.33	3.04
LBB102-3900	94634	103	14.92	35.06	16.18	15.34	1.96	U16-H07-34-537	107009	40	14.63	23.12	16.50	14.89	3.06
LBB102-3900	94634	104	12.84	69.43	16.15	14.42	1.84	U16-H07-34-537	107009	41	14.46	70.21	16.38	15.46	2.66
LBB102-3900	94634	105	15.36	80.63	16.21	16.07	2.04	U16-H07-34-537	107009	42	14.76	70.95	16.38	15.65	2.66
LBB102-3900	94634	106	13.37	89.10	16.21	14.86	2.04	U16-H07-34-537	107009	43	15.71	9.98	16.53	15.74	3.18
LBB102-3900	94634	107	12.14	65.86	16.21	13.93	2.04	U16-H07-34-537	107009	44	15.29	66.45	16.14	15.96	1.79
LBB102-3900	94634	108	14.49	43.68	16.21	15.15	2.04	U16-H07-34-537	107009	45	15.19	16.69	16.14	15.30	1.79
LBB102-3900	94634	109	13.78	78.34	16.16	15.08	1.89	U16-H07-34-537	107009	46	14.29	26.89	16.14	14.67	1.79
LBB102-3900	94634	110	15.91	84.39	16.11	16.41	1.71	U16-H07-34-537	107009	47	14.75	49.40	16.23	15.43	2.12
LBB102-3900	94634	111	13.41	63.74	16.17	14.72	1.90	U16-H07-34-537	107009	48	14.77	42.80	16.23	15.35	2.12
LBB102-3900	94634	112	13.46	57.79	16.17	14.67	1.90	U16-H07-34-537	107009	49	15.60	67.89	16.54	16.17	3.20
LBB102-3900	94634	113	13.91	70.65	16.24	15.11	2.14	U16-H07-34-537	107009	50	15.02	68.97	16.49	15.80	3.05
LBB102-3900	94634	114	12.12	55.19	16.16	13.73	1.87	U16-H07-34-537	107009	51	13.85	39.36	16.65	14.59	3.59
LBB102-3900	94634	115	8.27	44.26	16.16	11.30	1.89	U16-H07-34-537	107009	52	13.69	82.93	16.58	15.04	3.35
LBB102-3900	94634	116	15.15	43.63	16.11	15.65	1.70	U16-H07-34-537	107009	53	14.67	27.42	16.53	15.00	3.17
LBB102-3900	94634	117	13.15	82.06	16.11	14.71	1.70	U16-H07-34-537	107009	54	15.41	87.44	16.72	16.11	3.85
LBB102-3900	94634	118	12.33	64.02	16.11	14.03	1.70	U16-H07-34-537	107009	55	14.37	19.90	16.59	14.59	3.39
LBB102-3900	94634	119	16.00	89.42	16.09	16.47	1.62	U16-H07-34-537	107009	56	15.61	54.45	16.45	16.09	2.90
LBB102-3900	94634	120	15.68	51.47	16.09	16.12	1.62	U16-H07-63-976	107005	1	14.42	64.25	16.43	15.38	2.83
LBB102-3900	94634	121	13.59	46.00	16.09	14.54	1.62	U16-H07-63-976	107005	2	13.07	57.52	16.47	14.40	2.96

Table C3 Apatite fission track lengths for all samples analysed in this thesis

UBC	A2Z	Track	Angle				Dpar	UBC	A2Z	Track	Angle				Dpar
			Length (μm)	to c- axis	Lo calc (μm)	Lc calc (μm)					Length (μm)	to c- axis	Lo calc (μm)	Lc calc (μm)	
LBB102-3900	94634	122	13.94	36.56	16.19	14.60	1.98	U16-H07-68-247	117801	1	14.69	50.40	16.23	15.40	2.12
LBB102-3900	94634	123	12.56	46.45	16.14	13.82	1.79	U16-H07-68-247	117801	2	14.38	67.36	16.23	15.38	2.12
LBB102-3900	94634	124	13.10	15.61	16.17	13.34	1.92	U16-H07-68-247	117801	3	14.29	53.16	16.23	15.16	2.12
LBB102-3900	94634	125	12.90	87.29	16.09	14.57	1.62	U16-H07-68-247	117801	4	13.19	61.89	16.23	14.55	2.12
LBB102-3900	94634	126	13.20	27.03	16.09	13.75	1.62	U16-H07-68-247	117801	5	13.38	73.82	16.23	14.80	2.12
LBB102-3900	94634	127	12.80	83.80	16.09	14.50	1.62	U16-H07-68-247	117801	6	13.19	50.51	16.23	14.35	2.12
LBB102-3900	94634	128	13.61	49.61	16.09	14.63	1.62	U16-H07-68-247	117801	7	14.10	56.15	16.23	15.07	2.12
LBB102-3900	94634	129	12.43	71.71	16.17	14.19	1.91	U16-H07-68-247	117801	8	14.26	83.88	16.23	15.40	2.12
LBB102-3900	94634	130	13.44	54.56	16.09	14.60	1.64	U16-H07-68-247	117801	9	13.96	60.84	16.23	15.04	2.12
LBB102-3900	94634	131	14.41	30.65	16.09	14.85	1.64	U16-H07-68-247	117801	10	13.08	34.27	16.23	13.87	2.12
LBB102-3900	94634	132	13.11	62.08	16.18	14.50	1.93	U16-H07-68-247	117801	11	13.57	72.79	16.23	14.91	2.12
LBB102-3900	94634	133	15.23	62.66	16.20	15.90	2.01	U16-H07-68-247	117801	12	12.17	51.72	16.26	13.68	2.22
LBB102-3900	94634	134	12.57	83.67	16.09	14.36	1.61	U16-H07-68-247	117801	13	14.76	48.28	16.26	15.42	2.22
LBB102-3900	94634	135	13.50	55.00	16.21	14.65	2.05	U16-H07-68-247	117801	14	14.64	50.09	16.26	15.36	2.22
LBB102-3900	94634	136	14.00	80.33	16.18	15.23	1.96	U16-H07-68-247	117801	15	13.63	77.22	16.26	14.98	2.22
LBB102-3900	94634	137	13.99	60.57	16.13	15.06	1.76	U16-H07-68-247	117801	16	12.69	72.89	16.26	14.36	2.22
LBB102-3900	94634	138	14.04	80.73	16.12	15.25	1.73	U16-H07-68-247	117801	17	13.07	60.96	16.26	14.46	2.22
LBB102-3900	94634	139	12.93	75.99	16.12	14.54	1.73	U16-H07-68-247	117801	18	14.67	65.96	16.26	15.56	2.22
LBB102-3900	94634	140	11.81	62.67	16.12	13.67	1.73	U16-H07-68-247	117801	19	13.28	58.37	16.26	14.56	2.22
LBB102-3900	94634	141	13.27	65.83	16.16	14.65	1.86	U16-H07-68-247	117801	20	15.65	48.98	16.26	16.07	2.22
LBB102-3900	94634	142	14.67	83.47	16.16	15.65	1.86	U16-H07-68-247	117801	21	14.71	27.22	16.26	15.03	2.22
LBB102-3900	94634	143	14.25	47.84	16.16	15.05	1.86	U16-H07-68-247	117801	22	14.29	52.30	16.39	15.15	2.70
LBB102-3900	94634	144	14.81	41.30	16.09	15.36	1.62	U16-H07-68-247	117801	23	13.21	49.32	16.22	14.34	2.09
LBB102-3900	94634	145	15.28	21.91	16.12	15.45	1.73	U16-H07-68-247	117801	24	14.11	67.53	16.22	15.21	2.09
LBB102-3900	94634	146	13.15	83.84	16.12	14.71	1.73	U16-H07-68-247	117801	25	12.89	39.09	16.22	13.86	2.09
LBB102-3900	94634	147	11.26	71.05	16.12	13.45	1.73	U16-H07-68-247	117801	26	12.03	76.49	16.22	13.98	2.09
LBB102-3900	94634	148	13.33	82.46	16.23	14.82	2.11	WB-04C-720	107003	1	14.60	72.31	16.27	15.56	2.27
LBB102-3900	94634	149	11.79	49.24	16.33	13.36	2.47	WB-04C-720	107003	2	14.58	64.06	16.26	15.48	2.21
LBB102-3900	94634	150	14.40	54.38	16.33	15.25	2.47	WB-04C-720	107003	3	16.77	59.19	16.23	16.91	2.13
LBB102-3900	94634	151	13.93	70.14	16.16	15.12	1.88	WB-04C-720	107003	4	14.90	26.16	16.32	15.18	2.43
LBB102-3900	94634	152	15.37	21.57	16.26	15.53	2.22	WB-04C-720	107003	5	14.61	42.16	16.35	15.22	2.56
LBB102-3900	94634	153	14.10	41.48	16.13	14.82	1.76	WB-04C-720	107003	6	12.94	70.63	16.38	14.50	2.65
LBB102-3900	94634	154	15.34	81.23	16.19	16.06	1.99	WB-04C-720	107003	7	12.66	43.67	16.34	13.82	2.50
LBB102-3900	94634	155	10.62	60.00	16.19	12.85	1.99	WB-04C-720	107003	8	13.96	86.00	16.38	15.22	2.64
LBB102-3900	94634	156	12.44	67.27	16.19	14.14	1.99	WB-04C-720	107003	9	16.02	15.66	16.31	16.08	2.41
LBB102-3900	94634	157	13.41	42.45	16.14	14.33	1.80	WB-04C-720	107003	10	14.52	52.09	16.31	15.31	2.41
LBB102-3900	94634	158	10.93	44.84	16.14	12.64	1.80								
LBB102-3900	94634	159	13.78	34.62	16.25	14.43	2.20								
LBB102-3900	94634	160	14.56	61.79	16.16	15.45	1.87								
LBB102-3900	94634	161	14.09	70.81	16.11	15.23	1.71								
LBB102-3900	94634	162	12.70	36.14	16.18	13.63	1.94								
LBB102-3900	94634	163	13.39	52.48	16.18	14.53	1.94								
LBB102-3900	94634	164	11.80	78.05	16.18	13.85	1.94								
LBB102-3900	94634	165	14.47	75.39	16.07	15.49	1.55								
LBB102-3900	94634	166	13.29	43.03	16.28	14.26	2.30								
LBB102-3900	94634	167	14.33	83.68	17.06	15.44	5.04								
LBB102-3900	94634	168	14.17	42.22	16.26	14.89	2.24								
LBB102-3900	94634	169	15.07	47.22	16.26	15.63	2.24								
LBB102-3900	94634	170	13.21	73.74	16.26	14.70	2.24								
LBB102-3900	94634	171	11.28	84.86	16.26	13.57	2.24								
LBB102-3900	94634	172	12.63	17.49	16.26	12.96	2.24								
LBB102-3900	94634	173	13.64	32.67	16.04	14.27	1.45								
LBB102-3900	94634	174	12.85	30.90	16.04	13.59	1.45								
LBB102-3900	94634	175	11.68	68.20	16.18	13.67	1.95								
LBB102-3900	94634	176	14.36	84.89	16.18	15.46	1.95								
LBB102-3900	94634	177	15.43	50.94	16.18	15.93	1.95								
LBB102-3900	94634	178	15.39	38.66	16.18	15.77	1.95								
LBB102-3900	94634	179	13.89	56.49	16.18	14.94	1.95								
LBB102-3900	94634	180	15.79	42.24	16.18	16.12	1.95								
LBB102-3900	94634	181	12.08	78.54	16.18	14.03	1.95								
LBB102-3900	94634	182	11.64	33.29	16.16	12.73	1.87								

Appendix D U-Pb dating analytical techniques

CA-TIMS procedures at the PCIGR are modified from Mundil et al. (2004), Mattinson (2005) and Scoates and Friedman (2008). After rock samples have undergone standard mineral separation procedures zircons are handpicked in alcohol. The clearest, crack- and inclusion-free grains are selected, photographed and then annealed in quartz glass crucibles at 900°C for 60 hours. Annealed grains are transferred into 3.5 mL PFA screwtop beakers, ultrapure HF (up to 50% strength, 500 mL) and HNO₃ (up to 14 N, 50 mL) are added and caps are closed finger tight. The beakers are placed in 125 mL PTFE liners (up to four per liner) and about 2 mL HF and 0.2 mL HNO₃ of the same strength as acid within beakers containing samples are added to the liners. The liners are then slid into stainless steel Parr™ high pressure dissolution devices, which are sealed and brought up to a maximum of 200°C for 8-16 hours (typically 175°C for 12 hours). Beakers are removed from liners and zircon is separated from leachate. Zircons are rinsed with >18 MΩ.cm water and subboiled acetone. Then 2 mL of subboiled 6N HCl is added and beakers are set on a hotplate at 80°-130°C for 30 minutes and again rinsed with water and acetone. Masses are estimated from the dimensions (volumes) of grains. Single grains are transferred into clean 300 mL PFA microcapsules (crucibles), and 50 mL 50% HF and 5 mL 14 N HNO₃ are added. Each is spiked with a ²³³⁻²³⁵U-²⁰⁵Pb tracer solution (EARTHTIME ET535), capped and again placed in a Parr liner (8-15 microcapsules per liner). HF and nitric acids in a 10:1 ratio, respectively, are added to the liner, which is then placed in Parr high pressure device and dissolution is achieved at 240°C for 40 hours. The resulting solutions are dried on a hotplate at 130°C, 50 mL 6N HCl is added to microcapsules and fluorides are dissolved in high pressure Parr devices for 12 hours at 210°C. HCl solutions are transferred into clean 7 mL PFA beakers and dried with 2 mL of 0.5 N H₃PO₄. Samples are

loaded onto degassed, zone-refined Re filaments in 2 mL of silicic acid emitter (Gerstenberger and Haase, 1997).

Isotopic ratios are measured a modified single collector VG-54R or 354S (with Sector 54 electronics) thermal ionization mass spectrometer equipped with analogue Daly photomultipliers. Analytical blanks are 0.2 pg for U and 1 pg for Pb. U fractionation was determined directly on individual runs using the EARTHTIME ET535 mixed $^{233-235}\text{U}$ - ^{205}Pb isotopic tracer and Pb isotopic ratios were corrected for fractionation of 0.23%/amu, based on replicate analyses of NBS-982 reference material ad the values recommended by Thirlwall (2000). Data reduction employed the excel-based program of Schmitz and Schoene (2007). Standard concordia diagrams (Figure D1) were constructed and regression intercepts, weighted averages calculated with Isoplot (Ludwig, 2003). Unless otherwise noted all errors are quoted at the 2 sigma or 95% level of confidence. Isotopic dates are calculated with the decay constants $\lambda_{238}=1.55125\text{E-}10$ and $\lambda_{235}=9.8485\text{E-}10$ (Jaffey et al., 1971) and are presented in Table D1. EARTHTIME U-Pb synthetic solutions are analysed on an on-going basis to monitor the accuracy of results.

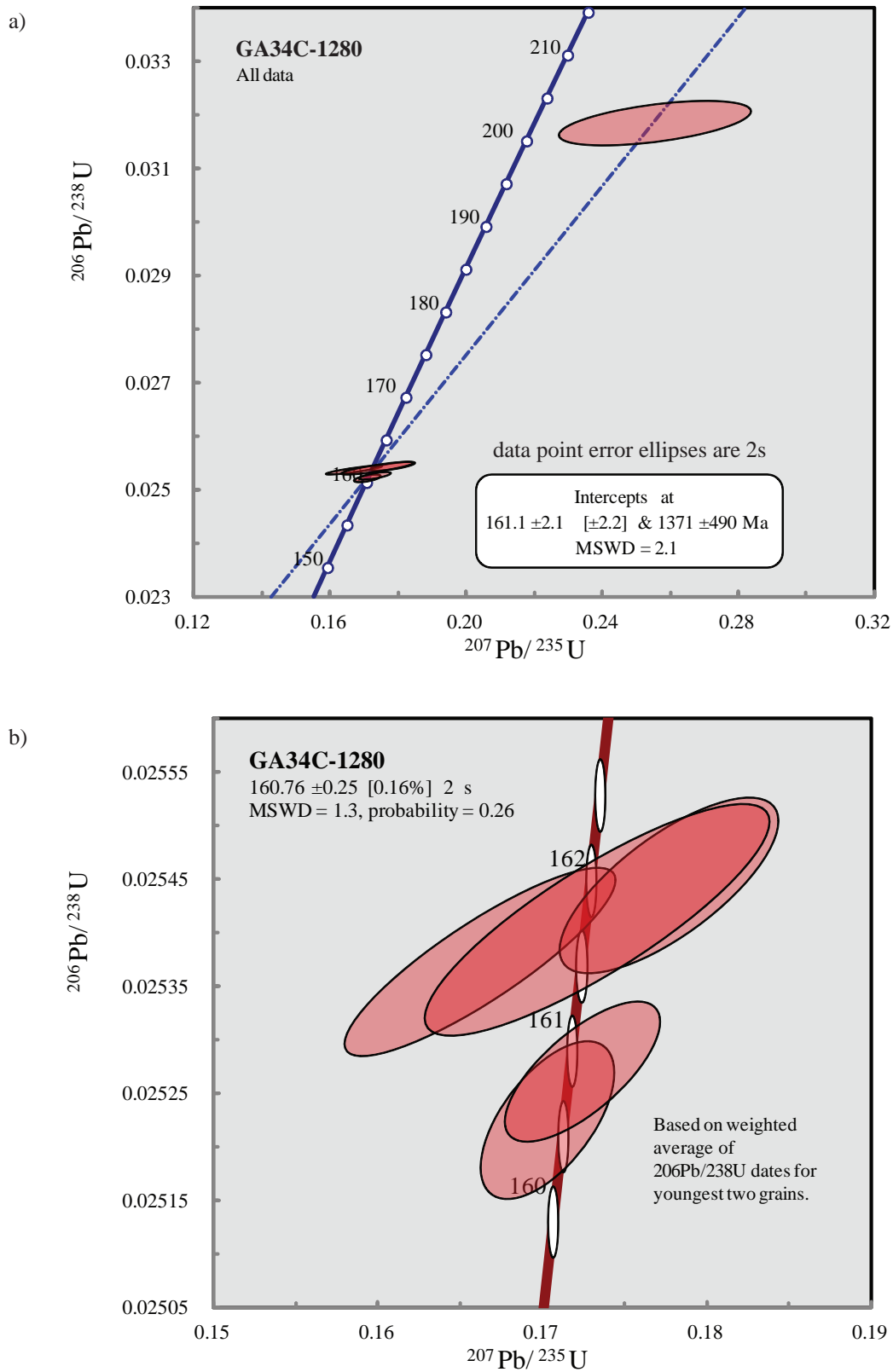


Figure D1 Concordia plots for lamprophyre dike GA-34C-1280 zircons dated with CA-TIMS U-Pb dating. (a) All zircons dated (n=6). (b) Close up of zircons with similar U-Pb ages (n=5). The age of the dike, 160.76 \pm 0.25 Ma, is based on the weighted average of the 2 youngest grains. Data error ellipses are shown at 2s.

Table D1 U-Th-Pb isotopic data

Sample	Wt. mg	Compositional Parameters								Radiogenic Isotope Ratios								Isotopic Ages					
		U	Th	Pb	²⁰⁶ Pb*	mol %	Pb*	Pb _c	²⁰⁶ Pb	²⁰⁸ Pb	²⁰⁷ Pb	²⁰⁷ Pb	²⁰⁶ Pb	corr.	²⁰⁷ Pb	²⁰⁷ Pb	²⁰⁶ Pb						
		ppm	U	ppm	x10 ⁻¹³ mol	²⁰⁶ Pb*	Pb _c	(pg)	²⁰⁴ Pb	²⁰⁶ Pb	²⁰⁶ Pb	% err	²³⁵ U	% err	²³⁸ U	% err	coef.	²⁰⁶ Pb	±	²³⁵ U	±	²³⁸ U	±
		(c)	(d)	(c)	(e)	(e)	(e)	(e)	(f)	(g)	(g)	(h)	(g)	(h)	(g)	(h)		(i)	(h)	(i)	(h)	(i)	(h)
GA34C																							
A	0.004	82	0.777	2.9	0.3027	91.85%	4	2.21	227	0.246	0.049	1.824	0.170294	1.957	0.025	0.237	0.602	146.00	42.77	159.67	2.89	160.60	0.38
B	0.004	42	0.748	1.6	0.1548	88.79%	3	1.61	165	0.230	0.048	3.802	0.166192	4.045	0.025	0.282	0.871	74.62	90.34	156.11	5.85	161.53	0.45
C	0.004	56	0.858	2.1	0.2270	92.15%	4	1.59	235	0.280	0.051	2.880	0.177779	3.069	0.025	0.265	0.735	226.06	66.56	166.15	4.70	161.97	0.42
D	0.004	82	0.394	3.8	0.4271	89.20%	2	4.26	171	0.143	0.058	8.537	0.255453	9.049	0.032	1.047	0.534	535.57	186.82	231.00	18.70	202.17	2.08
E	0.003	27	0.772	1.1	0.0924	87.71%	2	1.06	151	0.247	0.049	4.680	0.173326	4.971	0.025	0.348	0.848	170.01	109.26	162.30	7.46	161.77	0.55
F	0.002	86	0.885	3.3	0.2175	89.74%	3	2.05	180	0.283	0.049	2.092	0.172439	2.238	0.025	0.213	0.713	171.08	48.82	161.53	3.34	160.88	0.34

(a) A, B etc. are labels for fractions composed of single zircon grains or fragments; all fractions annealed and chemically abraded after Mattinson (2005) and Scoates and Friedman (2008).

(b) Nominal fraction weights estimated from photomicrographic grain dimensions, adjusted for partial dissolution during chemical abrasion.

(c) Nominal U and total Pb concentrations subject to uncertainty in photomicrographic estimation of weight and partial dissolution during chemical abrasion.

(d) Model Th/U ratio calculated from radiogenic ²⁰⁸Pb/²⁰⁶Pb ratio and ²⁰⁷Pb/²³⁵U age.

(e) Pb* and Pb_c represent radiogenic and common Pb, respectively; mol % ²⁰⁶Pb* with respect to radiogenic, blank and initial common Pb.

(f) Measured ratio corrected for spike and fractionation only. Mass discrimination of 0.23%/amu based on analysis of NBS-982; all Daly analyses.

(g) Corrected for fractionation, spike, and common Pb; up to 1 pg of common Pb was assumed to be procedural blank: ²⁰⁶Pb/²⁰⁴Pb = 18.50 ± 1.0%; ²⁰⁷Pb/²⁰⁴Pb = 15.50 ± 1.0%; ²⁰⁸Pb/²⁰⁴Pb = 38.40 ± 1.0% (all uncertainties 1-sigma). Excess over blank was assigned to initial common Pb with S-K model Pb composition at 161 Ma.

(h) Errors are 2-sigma, propagated using the algorithms of Schmitz and Schoene (2007) and Crowley et al. (2007).

(i) Calculations are based on the decay constants of Jaffey et al. (1971). ²⁰⁶Pb/²³⁸U and ²⁰⁷Pb/²⁰⁶Pb ages corrected for initial disequilibrium in ²³⁰Th/²³⁸U using Th/U [magma] = 3.

(j) Corrected for fractionation, spike, and blank Pb only.